THE UNIVERSITY *of* EDINBURGH

This thesis has been submitted in fulfilment of the requirements for a postgraduate degree (e.g. PhD, MPhil, DClinPsychol) at the University of Edinburgh. Please note the following terms and conditions of use:

- This work is protected by copyright and other intellectual property rights, which are retained by the thesis author, unless otherwise stated.
- A copy can be downloaded for personal non-commercial research or study, without prior permission or charge.
- This thesis cannot be reproduced or quoted extensively from without first obtaining permission in writing from the author.
- The content must not be changed in any way or sold commercially in any format or medium without the formal permission of the author.
- When referring to this work, full bibliographic details including the author, title, awarding institution and date of the thesis must be given.

Compartment Fire Analysis
for
Contemporary Architecture

Agustín Héctor Majdalani

Doctor of Philosophy

The University *of* Edinburgh

2014

Compartment Fire Analysis
for
Contemporary Architecture

by

Agustín Héctor Majdalani

This thesis has been supervised by

Prof. José Luis Torero

©Agustin Hector Majdalani, 2014

To Flor, Pedro, Lucas, and Jaime

Declaration

This thesis and the work described within have been completed solely by Agustín Héctor Majdalani at the BRE Centre for Fire Safety Engineering at the University of Edinburgh, under the supervision of Prof. José Luis Torero. Where others have contributed or other sources are quoted, references are given.

Agustín Héctor Majdalani,

May 2014

Table of Contents

Preface

This thesis was developed and written in the context of the following definition of the *Contemporary Fire Safety Engineer – A Creative Engineer with a Holistic Approach*:

Several years ago, Harmathy set the basis to define a contemporary fire safety engineer under the following statement:

> "It is extremely important to realize that fire safety is not something to be 'added on' after the completion of the plans for a building. To be really effective the problem of fire safety must be considered from the beginning of the architectural design".[1]

Fire Safety Engineering is a knowledge-based discipline where the most effective engineer is the one that understands the building. Given that fire safety effects every component of building design, the fire engineer is not the person with detailed understanding of the scientific underpinning of a component or the meticulous code consultant that knows all interpretations of the code; it is the individual that has the most comprehensive and complete understanding of the integrity of the problem. The *contemporary or creative fire safety engineer* is, therefore, the person that uses scientific knowledge and creativity to enable a solution that meets the requirements of all other sectors of the building design but at the same time delivers the *intentions* of the code.

The *conventional* fire protection engineering approach, based on the sole application of codes and standards without analysing the holistic picture further than just classifying a particular building under a prescribed *type* of construction, has become ineffective when applied to contemporary architecture. Contemporary architecture is typically very different in nature to the conventional structures (or parts of them) that served as the design basis for the tests whose results established standardised solutions and/or criteria in search of a reasonably conservative approach. The

building of the 21st century cannot be classified, thus, cannot be code compliant. The building of the 21st century is a prototype, thus, needs to be understood. In this context, it is obvious that codes and standards are not *the* tool but just *one* tool – in complement with scientific knowledge and creativity – for the resourceful *contemporary or creative fire safety engineer.*

Progress towards achieving state of the art fire safety cannot come until it is clearly understood what the fire engineer's role needs to be today and for the near future; i.e., defining the profession's real *identity* and *scope of practice*, as a result of the advance in science but also as a function of the evolution and consequent needs of the society. This evolution is clearly reflected in other professions such as architecture and civil engineering, which resolve the essential task of adapting the environment to the evolving societal needs. From here, the importance of the role of fire engineering serving these professions while always fulfilling its main objective of safety. The professional identity of the *contemporary or creative fire safety engineer* is therefore that of the knowledge-based integrator.

One Problem, not 'The problem'…

It is important to always approach the fire problem not only holistically but also in perspective and within its context. A fire safety engineer – or a team of such engineers depending on the size of the project – cannot be conceived working in isolation: he/she or they must understand and consider the scopes of other disciplines, and that the fire problem and safety more generally, albeit very important, is not the only issue to be resolved. The different fields altogether must be conscious that each speciality serves as an individual but correlated design component attainable for the designer (typically an architect) to conceive safe, functional, economical, attractive, and sustainable buildings, in a random order of importance.

The following quotes by those who could be regarded as the very first *fire engineers* prove that they forged, practised, and promoted this view:

"Admittedly, structural fire protection is not the only aspect of the fire problem and, under certain conditions, it may even become an insignificant aspect. This is always the case, for example, when the contents of a building rather than the building itself comprise the primary object of fire protection. Even further, frequently the fire problem is quite insignificant in comparison with other problems connected with the functioning of the building under normal service conditions. It is obvious, therefore, that in a proper design of a building all aspects of its performance must be given due consideration."[2]

Tibor Z. Harmathy, 1972

A New Look at Compartment Fires

"A modern building is a machinery of multiple functions. Defence against fire is one of the functions of this machinery."[1]

Tibor. Z. Harmathy, 1976

Design of Buildings for Life Safety – Part II

"There are many constraints on the design of a building; fire safety is one important, but small aspect which cannot be allowed to dominate." [3]

Margaret Law, 1986

Translation of Research into Practice: Building Design

Acknowledgements

I would like to thank everyone who shared with me, in one way or another, this fascinating research and life experience.

First of all to Flor, for being the very best partner in this life journey. With her limitless and lovely energy, she turns every challenge we face together into an attractive and fun adventure. To our sons Pedro, Lucas, and Jaime for their naturally sincere and unconditional loving support, and at the same time for being my true instructors. And of course to Estela for being an essential and happy player in this entire story.

To José Luis Torero, for his huge generosity offering me what I always regarded (and now confirm) as the opportunity of a lifetime. Thanks for shattering my ordinary plans back in 2008, inspiring me, teaching me, and being my mentor since then.

To Adam Cowlard, for his immense and inestimable task of trying to kill my enduring written Spanglish, and proposing magic changes in the arrangement to make this otherwise tar flow with less viscosity. His brilliant and lunatic sarcasm – always disclosing fundamental truths – was vital to keep my mental sanity no only during the writing process but also during all this time together.

To Cecilia Abecassis Empis, for her inexhaustible willingness and capacity to help, always in her typical warm-hearted way.

To my parents, for their lifelong emotional and ongoing support. To my sisters, for being each of them an essential part of my life, and very especially to Sole, for the exquisite touch of her drawings.

To Braulio, for his eternal friendship.

To my office mates, Adam Bittern, Steffen Kahrman, and Ryan Hilditch for the long and nice hours burnt in that quasi-cubic room, a true every-day reminder of the architecture associated to the *classic compartment fire framework* in the pleasant but

horribly designed (if at all) JM Building. And of course, to the fifth musketeer of the 1.2 room, Cristian Maluk not only for being a beginning-to-end buddy – and of course for calibrating my TSCs with his new version of R2E2 (formally H-TRIS) – but also for being my IT (with basically everything that needed to be plugged into a wall socket) and thesis design consultant.

To Jaime Cadena Gomez, for his invaluable collaboration modelling with FDS and interpreting the otherwise just colourful outputs.

To Nicholas Groth Merrild, for his priceless devotion and creativity to build the small-scale test compartment and install, wire, codify, remove, fix and reinstall tirelessly every single device over and over again during an entire summer break.

To Michal Krajcovic, for his paramount help and involvement during my lab phase.

To Juan Hidalgo Medina, for his generous aid in simplifying my life in the lab.

To Stephen Welch, for helping me with his sharp scientific insight and experimental experience.

To Guillermo Rein, for the enthusiasm he injected me during the initial phases of the PhD.

To Dougal Drysdale, for sharing his experience, knowledge, bibliography collection, and time to witness experiments and give his invaluable point of view.

To Pedro Reszka, for convincing me of plunging into this blessed madness at an advanced age.

To BRE and the BRE Trust, for the funding of my studentship, and special thanks to Debbie Smith, for her genuine interest on my research and continuous full support along these years.

And finally to Edinburgh, for being such a fantastic, beautiful, and loyal city, embracing this whole adventure…

Nomenclature

Related to the fuel, fire and heat losses

R = burning rate, rate of decomposition, or weight loss of the fuel, kg/s

R'' = burning rate per unit floor area, kg/s.m^2

$\dot{m}_F$ = mass loss rate, kg/s (equal to the burning rate, R, when all the mass produced is burnt)

$\bar{\dot{m}}_F$= average mass loss rate, kg/s

L = fuel load, kg

L'' = fire load per unit floor area or fire load density, kg/m^2

f = fuel thickness, m

D = equivalent fire diameter, m (in Figure 3-3 Thomas refers to the compartment's depth as D although in this nomenclature the latter is referred as H_5), m

A_f = surface area of the fuel, m^2

$\tilde{t}$ = dimensionless time, dimensionless

t = actual time, s

τ = characteristic time, s, or duration of (fully-developed) fire, s (or h)

$\dot{Q}$ = total heat release rate (by the fire) in the compartment, kW

$\dot{Q}_{PUA}$ = total heat release rate (by the fire) in the compartment per unit area, kW/m^2

$\bar{\dot{Q}}_{MAX}$ = maximum averaged theoretical ventilation-limited heat release rate, kW

$\dot{Q}_{in}$ = enthalpy entering the control volume with the reactants per unit time, kW

$\dot{Q}_{out}$ = enthalpy leaving the control volume with the products per unit time, kW

$Y_{O2,\infty}$= ambient oxygen concentration

ΔH_{CO2} = heat of combustion per kilogram of oxygen consumed, kJ/kg_{O2}

H_F = height of flame, m

Related to the fluid (gases) and fluid flow

m = mass of fluid, kg

V = volume of fluid, m^3

g = acceleration due to gravity, m/s^2

g' = reduced gravity, m/s^2

$\vec{F}$ = force applied by the fluid; weight of fluid, N

$F_i = F_y$ = gravitational force (in the 'y' direction) per unit volume or buoyancy force, N/m^3

γ = specific weight of fluid, N/m^3

ρ_i = generic density of fluid, kg/m^3

$\rho_a = \rho_2$ = density of ambient air, kg/m^3

$\rho_g = \rho_1$ = density of combustion gases, kg/m^3

μ_i = generic dynamic viscosity of fluid, Pa.s

μ_a = dynamic viscosity of ambient air, Pa.s

μ_g = dynamic viscosity of combustion gases, Pa.s

ν_a = kinematic viscosity of ambient air, m^2/s

c_p = specific heat capacity of fluid (ambient air and combustion gases), kJ/kg.K

$T_g = T_1$ = temperature of combustion gases, K or C

$\bar{T}_g$ = average temperature of combustion gases, K or C

$T_{g\text{-}MAX}$ = maximum temperature of combustion gases, K or C

$\bar{T}_{g-MAX}$ = maximum average temperature of combustion gases, K or C

$T_a = T_2$ = temperature of ambient air, K or C

T_L = temperature of lower (internal) layer, K or C

ΔT = temperature difference (combustion gases vs. ambient air), K or C

T_F = characteristic temperature of flame, K or C

T_{CD} = characteristic conduction temperature, K or C

T_{CV} = characteristic convection temperature, K or C

θ_b = temperature of combustion gases (recorded at ¼ of the compartment height above the centre of the floor in the CIB Tests), C

θ_c = temperature of combustion gases (recorded at ½ of the compartment height above the centre of the floor in the CIB Tests), C

u_i = generic (actual) characteristic (maximum) velocity of fluid in any direction, m/s (the terminology *u* does not imply horizontal direction in this case)

$\tilde{u}_i$ = generic dimensionless velocity of fluid, dimensionless

U_i = generic characteristic velocity of fluid, m/s

$\bar{u}_i$ = average (over inflow/outflow area) generic characteristic velocity of fluid, m/s

u_{in} = maximum inflow (i.e.; brought about by the hydrostatic ΔP in a stack-driven motion) horizontal velocity of ambient air, m/s

$\bar{u}_{in}$ = average inflow velocity of ambient air, m/s

$u_{in\text{-}fire\text{-}entrainment}$ = maximum natural entrainment (i.e.; brought about naturally by the fire plume in a turbulence-driven motion) horizontal velocity of ambient air, m/s

$u_{in\text{-}comb}$ = maximum inflow combined (i.e.; brought about by the fire (turbulence + inertia driven motion) plus the hydrostatic ΔP (stack-driven motion)) horizontal velocity of ambient air, m/s

u_{out} = maximum outflow (i.e.; brought about by the hydrostatic ΔP in a stack-driven motion) horizontal velocity of combustion gases, m/s

$\bar{u}_{out}$ = average outflow velocity of combustion gases, m/s

$u_{out\text{-}comb}$ = maximum outflow combined (i.e.; brought about by the fire (turbulence + inertia driven motion) plus the hydrostatic ΔP (stack-driven motion)) horizontal velocity of combustion gases, m/s

v = velocity component of fluid in the 'y' (vertical) direction, m/s

$v_{fire,MAX}$ = maximum vertical velocity of fire plume (i.e.; brought about by the fire in an inertia-driven motion), m/s

$v_{out\text{-}comb}$ = idem $u_{out\text{-}comb}$ but in the vertical direction, m/s

P = pressure, Pa

P_{ext} = atmospheric (external) pressure profile, Pa

P_{int} = internal (compartment) pressure profile, Pa

ΔP = pressure differential, Pa

$\Delta \tilde{P}_i$ = generic pressure differential, Pa

ΔPi = generic actual (maximum) pressure differential, Pa

ΔP_c = generic characteristic pressure differential, Pa

P_i = static pressure (internal energy per unit volume – associated to the fluid's state), Pa

$P_i/\rho_i\, g$ = static pressure head, m

$P_{hydrostatic} = h_i\, \rho_i\, g$ = hydrostatic pressure or gravitational potential (potential energy per unit volume – associated to the fluid's elevation), Pa

h_i = hydrostatic pressure head, m

$P_{hydrodynamic} = ½\, u_i^2\, \rho_i$ = hydrodynamic pressure (kinetic energy per unit volume – associated to the fluid's motion), Pa

$u_i^2/2g$ = hydrodynamic pressure head, m

E = energy per unit volume, Pa ($J/m^3 = N.m/m^3 = N/m^2 = Pa$)

Ψ = total or energy pressure head, m

$\dot{m}_\iota$ = generic mass flow rate, kg/s

$\dot{m}_{in}$= mass flow rate of ambient air into the compartment, kg/s

$\dot{m}_{out}$ = mass flow rate of combustion gases out of the compartment, kg/s

$\dot{m}_{in}^*$ = minimum mass flow rate of ambient air into the compartment estimated after Φ^*, kg/s (this is equal to $\bar{\dot{m}}_{in-MAX}$)

$\bar{\dot{m}}_{in-MAX}$ = maximum averaged theoretical buoyancy driven mass flow rate of ambient air into the compartment, kg/s

C = air inflow proportionality constant, dimensionless (≠ to calibration factor from Appendix A)

$\dot{V}$ = volumetric flow rate through an orifice, m^3/s

$\dot{V}_i$ = generic volumetric flow rate, m^3/s

Fr = Froude number, dimensionless

Re = Reynolds number, dimensionless

Related to the compartment

W = width of compartment, m

$\tilde{x}_i$ = generic dimensionless length, dimensionless

x_i = generic actual (maximum) length, m

H_i = generic characteristic length, m

H_1 = height of ceiling, m

H_2 = height of smoke layer, m

$H_3 = H$ = height of opening, m

$H_{3\text{-}in}$ = height of inflow opening, m ($\approx N$ or H_N)

$H_{3\text{-}out}$ = height of outflow opening, m

$H_4 = H_D$ = height of 'clean' or 'cold' layer, m

H_5 = depth of compartment, m (in Figure 3-3 Thomas refers to it as D instead)

$N = H_N$ = height of neutral plane, m

z = evaluated height over/under the neutral plane, m

h_{up} = height of the (lower edge of the) upper door, m

h_{down} = height of the (upper edge of the) lower door, m

A_i = generic cross-sectional area of the orifice (i.e., compartment opening), or area over which the pressure is evaluated, m^2

A_w = area of ventilation opening, m^2

A_{in} = area of inflowing ambient air, m^2

A_{out} = area of outflowing combustion gases, m^2

W_w = width of opening, m

$\phi = A_w\sqrt{H}$ = *ventilation factor* or parameter, $m^{5/2}$

A_F = area of compartment's floor, m^2

A_T = area of compartment's internal surfaces (excluding A_w and A_F) through which heat is being transferred, m^2

$\frac{A_W\sqrt{H}}{A_T}$ = *opening factor*, $m^{1/2}$

$\frac{A_T}{A_W\sqrt{H}}$ = *inverse opening factor*, $m^{-1/2}$

d = diameter of flow source (holes drilled in the pipes), m

c_d = orifice flow coefficient or discharge coefficient, dimensionless

k_b = effective thermal conductivity of solid compartment boundaries, W/m.K

ρ_b = density of solid compartment boundaries, kg/m^3

c_b = specific heat capacity of solid compartment boundaries, J/kg.K

$k\rho c$ = thermal inertia, $J^2/m^4.K^2.s$

δ_b = characteristic thickness of solid compartment boundaries, m

k_b/δ_b = thermal conduction heat transfer coefficient, W/K

h_T = total heat transfer coefficient, W/m^2.K

T_b = equilibrium interior surface temperature of solid compartment boundaries, K

F = intensity of radiation per unit area or downward heat transfer flux, kW/m^2

$\dot{Q}_b$ = heat losses through the solid compartment boundaries, kW

Related to the instruments' calibration

P_s = stagnation pressure, Pa

P_o = total pressure, Pa

$\Delta P_{Pitot\text{-}Simple}$ = pressure differential measured with a simple *Pitot* tube, Pa

$\Delta P_{Pitot\text{-}Static}$ = pressure differential measured with a *Pitot*-static tube, Pa

ΔP_{probe} = pressure differential measured with a *McCaffrey* probe, Pa

K = factor (for the pressure probes calibration) function of the Reynolds number, dimensionless

h_c = average convection heat transfer coefficient (or average convective factor) (radiant panel calibration tests), W/m^2.K

$h_{c,fire}$ = average convection heat transfer coefficient (fire tests), W/m^2.K

h_k = average conduction heat transfer coefficient, W/m^2.K

h_{eff} = effective heat transfer coefficient (radiant panel calibration tests), W/m^2.K

h_{fire} = effective heat transfer coefficient (fire tests), W/m^2.K

$h_{charact}$ = average characteristic convective heat transfer coefficient, W/m^2.K

L = vertical length of calibration assembly (TSC + Ceraboard), m

$L_{charact}$ = characteristic length, m

ρ_s = density of TSC's stainless steel plate, Kg/m^3

δ_s = thickness of TSC's stainless steel plate, m

c_s = specific heat capacity of TSC's stainless steel plate, J/Kg·K

k_s = thermal conductivity of TSC's stainless steel plate, W/m·K

k_a = thermal conductivity of air, W/m·K

α = thermal diffusivity of air, m^2/s

β = volumetric thermal expansion coefficient of air, K^{-1}

ν = kinematic viscosity of air, m^2/s

A_s = surface area of TSC's stainless steel plate, m^2

m_s = mass of the TSC's stainless steel plate, kg

ε_s = emissivity of TSC's stainless steel plate, dimensionless

T_s = temperature of TSC's stainless steel plate, C or K

T_f = 'film' temperature, C or K

σ = Stefan-Boltzmann constant, W/m^{2}K^4

C = calibration corrective (or conduction) factor of TSC's stainless steel plate, dimensionless ($\neq$ to air inflow proportionality constant from Chapter 4)

$t_{r,calibration}$ = time constant of the device (calibration tests), s

$t_{r,fire}$ = time constant of the device (fire tests), s

$\dot{Q}_{inc}$ = incident heat flux to the TSC's stainless steel plate, W

$\dot{Q}_{TSC}$ = total incident heat flux to the TSC's stainless steel plate, W

$\dot{Q}_{fire}$ = total incident heat flux from the compartment fire to the TSC's stainless steel plate, W

$\dot{Q}_{rad}$ = radiative portion of the incident heat flux from the compartment fire to the TSC's stainless steel plate, W

B_i = Biot number, dimensionless

R_a = Rayleigh number, dimensionless

R_{aL} = Rayleigh number averaged over the calibration assembly length L, dimensionless

Pr = Prandtl number, dimensionless

Nu = Nusselt number, dimensionless

Nu_L = Nusselt number averaged over the calibration assembly length L, dimensionless

Related to Harmathy's Doctrine

$\bar{q}_E$ = Harmathy's overall penetration heat flux, kW/m^2

H^* = Harmathy's *potential for destructive spread* or *normalized heat load*, s$^{1/2}$.K

μ-factor = Harmathy's *potential for convective spread*, dimensionless

$\bar{q}_E\,\tau$ = Harmathy's *(overall) heat load*, kJ/m^2

Φ = Harmathy's ventilation parameter, kg/s

Φ^* = Harmathy's minimum ventilation parameter, kg/s

G = fire load, kg

G_e = 'equivalent' design fire load, kg (equal to G only if the combustibles consist entirely of cellulosics)

A_F = area of compartment's floor, m^2

Abstract

Understanding the relevant behaviour of fire in buildings is critical for the continued provision of fire safety solutions as infrastructure continually evolves. Traditionally, new and improved understanding has helped define more accurate classifications and correspondingly, better prescriptive solutions. Among all the different concepts emerging from research into fire behaviour, the *compartment fire* is probably the one that has most influenced the evolution of the built environment. Initially, compartmentalization was exploited as a means of reducing the rate of fire spread in buildings. Through the observations acquired in fires, it was concluded that reducing spread rates enabled safe egress and a more effective intervention by the fire service. Thus, different forms of compartmentalization permeated through most prescriptive codes. Once fire behaviour within a compartment was conceptualized on the basis of scientific principles, the *compartment fire framework* became a means to establish, under certain specific circumstances, temperatures and thermal loads imposed by a fire to a building. This resulted not only in improved codes but also in a scientifically based methodology for establishing the thermal input from which to assess structural performance.

The last decades have however seen an evolution of the built environment away from compartmentalization while the *classic compartment fire framework* has remained. Within this framework, while *Regime I* corresponds to the idealised experimental setups adopted by many of the researchers, the usually ignored *Regime II* is characteristic of open spaces and volumes, typical of contemporary architecture. This research project commences, through a review of classic literature by those regarded as the *fathers* of fire safety engineering, by revisiting the knowledge underpinning this seminal approach, and initiating the discussion of its continued relevance and applicability to an increasingly non-compartmentalised built environment.

Compartment fires are extremely complex processes. Nevertheless, when treating the theoretical problem with sufficient accuracy, simple mathematical approaches can be extremely informative and serve as the background to more complex methodologies. In this context, the project introduces the problem of the compartment fire in its full

complexity before discussing some simplifications typically assumed when representing the actual problem for design purposes.

Further, despite the detailed experimental and theoretical background behind analytical formulations in the *classic compartment fire framework*, their development is revisited to establish the extent to which they can be applied. In this way, the range of validity of the *classic framework* is characterized, clarifying the limitations of existing design methods based on this framework, and identifying the areas where further research and extension is necessary.

Given the importance of counting on simple analytical formulations at the early design stage when dealing with atypical architectural designs in today's fire safety practice, an elementary theoretical *compartment fire framework* is elaborated with the aim of enveloping traditional as well as contemporary architectural layouts. This gave way to the development of a new set of *regime of behaviour* definitions, in addition to – and falling in-between – the classic *Regime I* and *Regime II* fully-developed compartment fire behaviours.

With the aim of filling this gap of knowledge empirically and characterizing these additional behaviours, a series of small and large-scale tests are presented. The results demonstrate complex behaviours that cannot be described in terms of the *classic framework*. This evidences the great need to conduct research that provides physical insight into the dynamics of a fire in spaces that deviate from the small quasi-cubic enclosure – the natural consequence of compartmentalization – that was typically adopted throughout the original work that resulted in the data which validated the *classic compartment fire framework*.

Overall, this project aims to inform and encourage the discussion of the existence of a *broader compartment fire framework*, where the historical *Regimes I* and *II* are limiting cases of a vaster fire behaviour which is intimately linked to the geometry of the compartment, the ventilation conditions, and the available fuel. While the *classic compartment fire framework* is still a robust tool, it is only one piece in the puzzle of approaching and resolving the fire problem in a building in a holistic way. The

relevance of this discussion is apparent in face of contemporary architecture and infrastructure.

1 Chapter 1: Introduction

1.1 Contemporary Architecture

The historical evolution of architecture shows that, from the 1920s to 1980s, a period of pioneering fire research in the built environment, open volumes and large interconnected compartments were not the exception of the avant-garde, but already a common and key element in mainstream architecture:

> "If the Renaissance marks the beginning of our (the architecture) discipline, its maturity and current constitution have been achieved during the refoundation of the discipline in the 1920s. In this sense our (the architecture) discipline is Modern architecture…key watershed within the development of the discipline as we understand and practice it today."[4]

One of the fundamental principles of Modern architecture is the expression of volume rather than mass, which in practical constructive terms means large and flexible volumes avoiding compartmentation, and lots of light through multiple large openings [5]. This criterion led to a fundamental change in the build environment, which P. Schumacher describes as follows:

> "The key conceptual shift that best encapsulates the radicality of architecture's refoundation as Modern architecture is perhaps the conceptual re-orientation from edifice to space."[4]

As a consequence of this alteration introduced at the beginning of the 20th Century, the present architectural network is comprised by a wide range of compartment sizes and shapes extending all the way from pre-Modernist (e.g. Classic) to Contemporary (e.g. Parametricism) architecture, and going through Modernist (e.g. International Style) and post-Modernist (e.g. Deconstructivism) architecture styles.

Nevertheless, probably owing to the non-critical mass of such interior layouts during the early phases of fire research, and to the practical necessity in search of simple characterisation on the other, the bulk of the research in compartment fires was – and still is – based in single and relatively small compartments, with a few conceptual exceptions [6]. Thus, most of the past and present scientific knowledge which is applied to fire safety engineering in contemporary architecture, comes from this idealised configuration.

Therefore, the switch from edifice to space is materialised today – more than ever – in spaces very different to those used in the past to characterise compartment fires. It is evident, hence, that **the fire problem in the built environment has changed** posing a strong challenge to the current scientific knowledge and evidencing, in many cases, a lack of consistency in the engineering methodologies [7] based on this knowledge and intended as generalised prediction and design tools applicable indiscriminately to every space composition.

A new look at fires in the built environment must be taken, in light of the critical fact that the present environment is far removed the simplistic, idealised forms on which most engineering tools are based, and that its form will not "stand still and wait until radically new solutions have been theorized, developed, tested and evaluated"[4].

1.2 The Importance of Simplified Design Methodologies

Fire safety engineering has fundamentally two capital fields of application: the *built* and the *wild* environments. In the built environment, the foundation of any design, whether prescriptive or performance based, is the definition of the design fire or fire environment. Performance based design in particular requires the explicit prediction / representation of the fire environment as the starting point of a design.

Defining the time evolution of all relevant variables (temperatures, velocities, species, etc.) is the initial challenge that a Fire Engineer faces when attempting to quantify the performance of a system and all countermeasures introduced to mitigate the impact of a fire. Decades of research have focused on the different processes linked to the characterization of a fire environment and numerous engineering

methods have been developed to enable engineers to quantify the performance of a design. This is particularly true when focusing on the evolution of a fire within buildings.

The evolution of a fire within a building is characterized by the coupling between the building and the combustion process. The environment resulting from the interaction of building and combustion can then be used to establish its influence on egress, countermeasures (detection and suppression) or on structural behaviour. Each component of a fire safety strategy is drastically different from the others therefore the evaluation of the performance of each component needs to be done in a manner consistent with the specific processes involved. A comprehensive assessment of the evolution of a fire and its interactions with people and buildings has long been recognised as an intractable problem. And while in recent years complex computational tools have been developed for all aspects of a fire strategy, it is still necessary, for the purpose of design, to develop simplified methods that allow an effective but manageable design process.

A common mechanism to simplify the design process is to separate the different components of the problem by linking specific processes to specific characteristic times within a fire timeline. For example, the characteristic timescales associated to egress and the activation of countermeasures are relatively small, therefore the assessment of their performance will emphasize the understanding of the earlier phases of a fire, i.e. fire growth time and time to flashover. In contrast, when addressing structural behaviour, growth and flashover occur within time scales that are much smaller than those required to significantly affect the mechanical strength of structural systems, thus the focus has been on fully-developed fires.

While a similar analysis could be done for each process, this research project focuses on the interaction between a fire and the structure. The dissertation emphasises the pertinence of simplified methodologies for defining the fire environment as the basis of a design – specifically those related to the *classic compartment fire framework* – and revisits the knowledge underpinning this framework analysing its applicability to increasingly non-compartmentalised contemporary architecture.

1.3 The Development of the Compartment Fire Concept

Countless experimental and theoretical studies on compartment fires have been completed throughout the last century. This literature review intends to list the most relevant ones in relation to the project's aims and scope. However, realising that referencing the totality of the available sources in the subject is an impossible task, a succinct review of that deemed particularly pertinent to this work is presented next. For further sources related directly or indirectly to this subject of study, the reader is guided to references [8], [9] and [10].

1.3.1 Pre-Fire Dynamics

The understanding of the thermal interaction between a fire and a structure has been explored since the late 19th century, but soon after WWI, fire research in the built environment started gaining relevance. Bisby *et al.* [8] provide a comprehensive review of the associated literature. In an effort to understand the fire behaviour in enclosures and the consequent fire damage to the structure – from Ingberg [11] in the 1920s to Kawagoe [12] in the 1940s and 1950s – the attention was drawn mainly to analysing the temperatures of the gases, T_g, and duration of the fire, τ. The main achievement of these earlier stages of research was the definition of the *standard temperature vs time curve* [11] as a general description of the fire environment in enclosures. This enabled structural engineers to establish methods to protect structural systems from a fire. Thus, achieving a *fire-structure proximity* situation was the first obvious necessity in the study of structural reaction to thermal loads, and setting 'tight' *enclosure fires* has been the natural reaction towards this end. To this extent, the research was focused in single small rooms with usually multiple ventilation openings [11][12][13], in an attempt to to reproduce habitual scenarios.

Acknowledging the complexity of the confined fire problem demonstrated by the results of this pioneering work, from the late 1950s to 1990, the fire research community took a step back in search of the understanding and further characterisation of the basic physical and chemical processes involved in the study of room fires [14][15]. In this period, a series of seminal studies authored by the *fathers* of fire safety science provided the foundations for our current engineering methods.

1.3.2 Important Breakthroughs

When burning freely in an open environment, most fuels lose c. 30% of their energy by radiation from the flame to the surroundings while the remnant is lost by convection in the buoyant plume [16]. For the same fuel burning in the same free conditions, the burning rate, R, is simply proportional to its exposed area, A_f.

$$R \propto A_f \qquad \textbf{Equation 1-1}$$

However, if the burning fuel is enclosed in a compartment, this alters the free burning behaviour. The hot convected fire gases trapped below the compartment's ceiling exchange heat with the structure and with the fuel below. Additionally, the radiation from the flame heats the surrounding walls which in turn re-radiate the fuel bed. This intensification of the heat exchange processes increases consequently the burning rate, R. The enclosure effect on the burning rate is clearly shown by Drysdale [16] in the following figure:

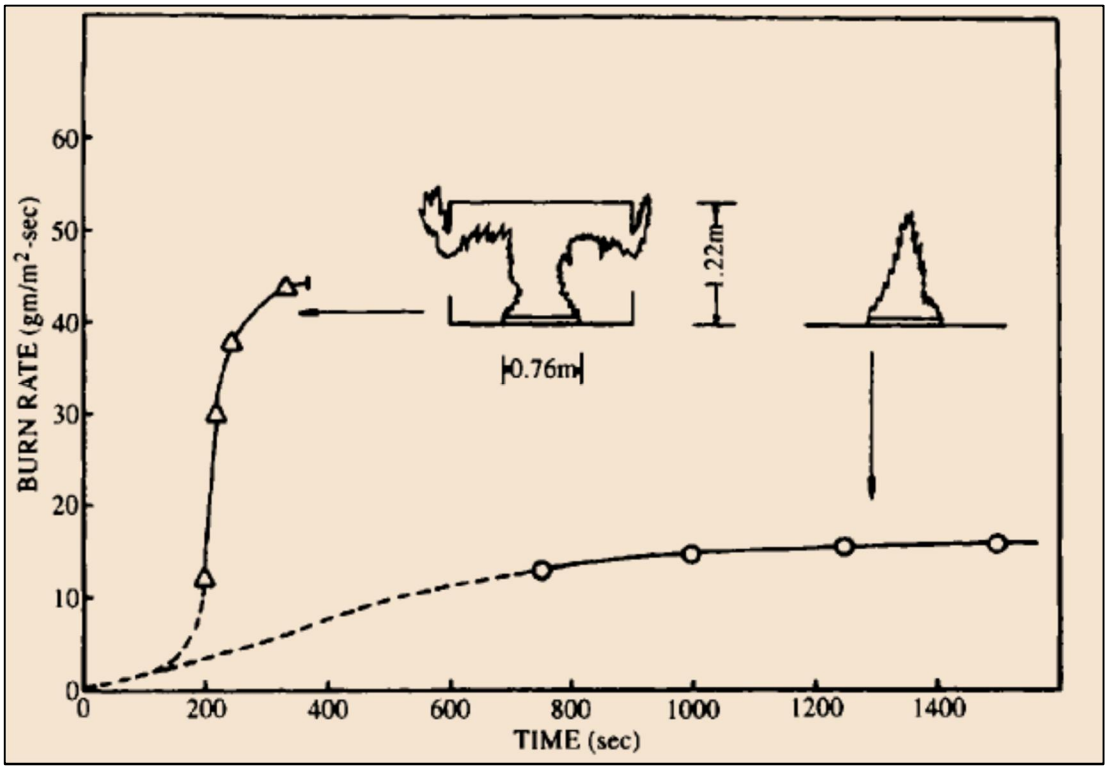

Figure 1-1: The effect of enclosure on the rate of burning of a slab of PMMA (Friedman, 1975) Figure 9.2 from Reference [16]

Although air had unrestricted access around the fuel in these experiments [16], the hood above the burning slab deflected the flames increasing the heat feedback to the fuel and, thus, increasing the burning rate in comparison to the free burning case. Drysdale explains [16] that the compartment effect in the burning rate is "quite general although its magnitude depends on the nature of the fuel and the size of the compartment".

1.3.2.1 Ventilation and Burning Rate

These confinement effects in the burning rate were first reported by Kawagoe and co-workers in 1958 [12][17] – based on work done previously by Fujita [18] – reporting the first known theoretical study on the mechanisms of an enclosed fire, together with the results of many large and reduced scale tests in small compartments carried out in Japan for a decade. Their main goal was to find a method to establish the fire duration, τ, in order to analyse the fire severity in buildings. In this work,

they found the average maximum temperature within the compartment, $\bar{T}_{g-MAX}$, to be quite uniform. Most importantly though, they were the first to introduce the empirical relationship between the burning rate, *R*, and what is now defined as the *ventilation parameter* or *ventilation factor*, $A_w\sqrt{H}$. They found that during the period that they defined as active combustion (i.e., that of full involvement of the present combustibles) the burning rate, *R*, was a strong function of the size and shape of the compartment's ventilation opening, and not coupled to the fuel load, *L* (through the fuel's exposed surface area, A_f), as it is the case in fires in the open. Their experimental results correlated very well with the following relationship:

$$R = 5.5A_w\sqrt{H} \quad [kg/\text{min}] \qquad \vee \qquad R = 0.09A_w\sqrt{H} \quad [kg/\text{sec}] \qquad \textbf{Equation 1-2}$$

Where A_w and *H* are the area (in m^2) and height (in m) of the ventilation opening, respectively, and the combination $A_w\sqrt{H}$ was defined as the *ventilation parameter* or *ventilation factor*. Kawagoe is, then, the first to intuitively establish the concept of the compartment fire [12] by coupling the compartment interaction with the burning rate. Today, this remains one of, if not the most important findings in the area of compartment fire dynamics.

The tendency towards a linear relationship between burning rate, *R*, and *ventilation parameter* was further confirmed by other authors. Ptchelintzev published in 1958 [19] data which showed a slightly different constant of proportionality to that of Kawagoe (assuming window heights of the order of 1 m), nevertheless, confirming the tendency.

In their studies, Simms *et al.* [14] used models to measure the both the temperature, T_g, and the duration of fires, τ, in compartments of three different sizes with various fire loads and ventilation configurations (adjustable openings located centrally in all four sides), as well as full-scale compartments [15]. The results were found to be similar in both reduced and full-scale tests. They found that the fire was divided in three well-defined periods – fire growth, full involvement, and decay – and that the burning rate, *R*, in the period of full involvement was independent of fuel load, *L*,

and dependent only on the inflow of air into the compartment, $\dot{m}_{in}$. In addition, the results showed that the maximum temperature reached, T_g, increased with the air inflow but was independent of the fire load, L. In a similar way, Gross and Robertson [20] experimented in three geometrically similar enclosures using various sizes of wood cribs as the fuel. Horizontal or vertical openings were centered on one side of the compartment extending across the entire wall. The data – temperatures, concentration of CO, CO_2, and O_2, burning rate – were correlated in terms of a normalised ventilation parameter and, once more, the latter was found to be proportional to it.

1.3.2.2 Thomas' Two Regimes

Using Simms *et al.* experiments [14][15] in combination with Hinkley *et al.* flow pattern studies in roof vented model compartments [21][22][23], Philip Thomas' early studies during the 1960s [24][25][26][27][28] concluded [29] that there were at least *two regimes* of behaviour in the fully-developed stage of compartment fires i.e. that of full room involvement in which all exposed combustible surfaces are burning [16]. This demarcation holds great significance today due to its strong implications for fire safety design in contemporary architecture. The following figure shows the results obtained for these experiments measuring the burning rate of wooden cribs in small-scale enclosures:

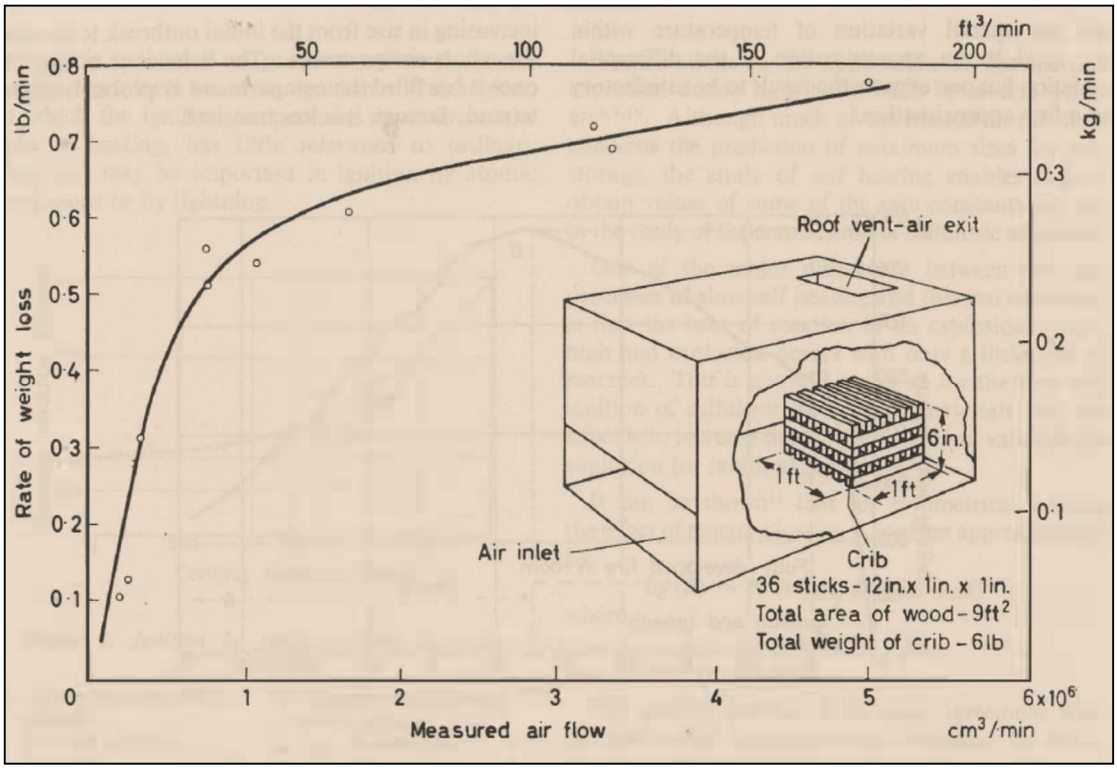

Figure 1-2: Simms *et al.* [21][22] [24] **and Hinkley's** [23] **experimental results from 1959-60**

Thomas *et al*. observed that, at low air flows the rate of burning, *R*, has a linear dependency on the air flow, $\dot{m}_{in}$, confirming what Fujita [18] and Kawagoe [12] had found some years before. Contrary, at high air flows the burning rate reaches an almost constant value which appeared proportional to the surface area of the fuel, A_f. These distinct burning behaviours where defined [29] as the low ventilation regime or *Regime I*, and the high ventilation regime or *Regime II*.

In further studies, Thomas and Nilsson [30] described what they defined as a third regime controlled by the crib porosity instead. This last regime is consequence of a specific crib configuration where the wooden burning surfaces are shielded from the environment within the compartment and consequently the rate of burning is relatively insensitive to the thermal environment. Thus, it should be avoided in tests if searching for data representing real fuels in actual fire situations.

In short, for fully-developed compartment fires, a total of three main regimes of fire behaviour could be identified according to the variables involved. These are:

- *Regime I*, or window controlled, where the opening is small and the average burning rate is determined by the size and geometry of the vent.

- *Regime II*, or fuel surface area controlled, where the opening is large and the burning rate is defined by the location, size, and distribution of the fuel.

- *Regime III*, or porosity controlled, is a regime in which the burning rate is controlled by the crib's structure.

The following photos exhibit *Regime I* and *II* as they can be observed in a simple small-scale laboratory test:

1-1 **1-2**

Photo 1-1: Reduced-scale *Regime I* or *ventilation-controlled* fully-developed fire (small opening) and Photo 1-2: Reduced-scale *Regime II* or *fuel-controlled* fully-developed fire (large opening).

As will be elaborated later (Section 1.4.2.1), Thomas firmly believed that the extensive collaborative international experimental programme that was taking place necessitated more in depth analysis of the resulting data. He considered this essential in order to truly reveal the extent of the wealth of knowledge that had been captured in these tests. It was in exactly this spirit that he furthered his understanding of the two regimes.

1.3.2.2.1 Equilibrium Burning Rate Theory

As a consequence of the observed small and large window regimes of behaviour, Thomas showed [28] – by means of a qualitative theory – that for the former the fire load per unit window area, L/A_w, and for the latter the fuel thickness, f, were more important than other factors in determining the duration of fully-developed fires, τ, and thus, their severity. The relevance of said theory relies on the fact that it explicitly provided a foundation for further research and fire technologists dealing directly with the practical evaluation of fire-resistance requirements.

As it will be set out below, Thomas' theory for the *quasi-steady burning rate of a fully-developed fire* [28][29] reveals how the duration of a compartment fire, τ, depends – for any given amount of fuel, L – on the burning rate, R, with special emphasis on the role of the window openings. Through it, Thomas was able to explain the effects on the burning rate as a result of changing the fuel surface, A_f, and/or the ventilation conditions, which otherwise were not fully explained based on empirical observations.

The theory is rooted in the effect that the heat transfer has on the rate of decomposition of the fuel explored by Margaret Law and, vice versa, in the effect that the rate of decomposition has on the heat transfer, explored by Heselden [31][28].

In her experiments [32], Margaret Law placed pieces of wood in front of a radiant source recording their weight loss, R. Her data (Figure 1-3) showed that the rate of weight loss was almost constant and was little affected by the piece of wood being enclosed in an inert atmosphere such as nitrogen, if allowance were made for the presence or absence of the extra heat from the flame.

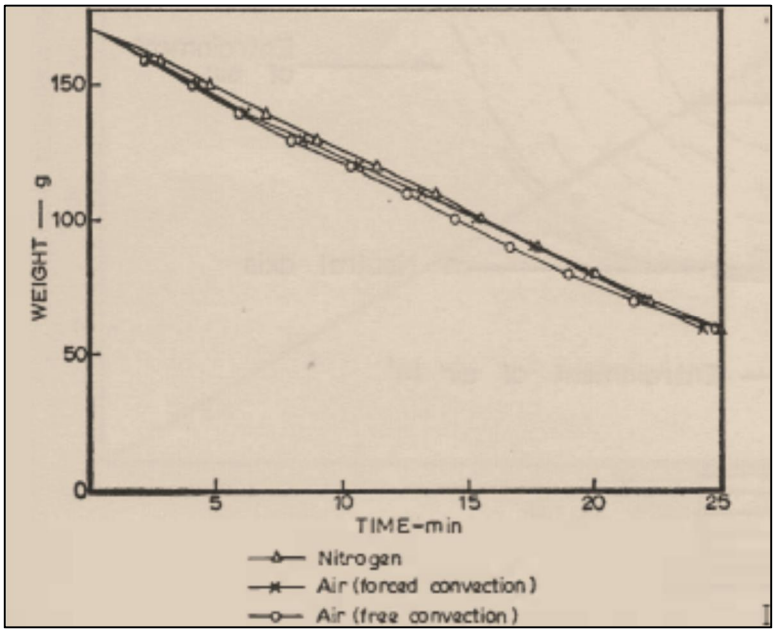

Figure 1-3: Decomposition of wood by radiant heat (Figure 6 from reference [29]**)**

Increasing the intensity of the radiation, *F*, by moving the piece of wood nearer the source increased the rate of decomposition, *R*. The results for different levels of radiant intensity were plotted by Law as follows:

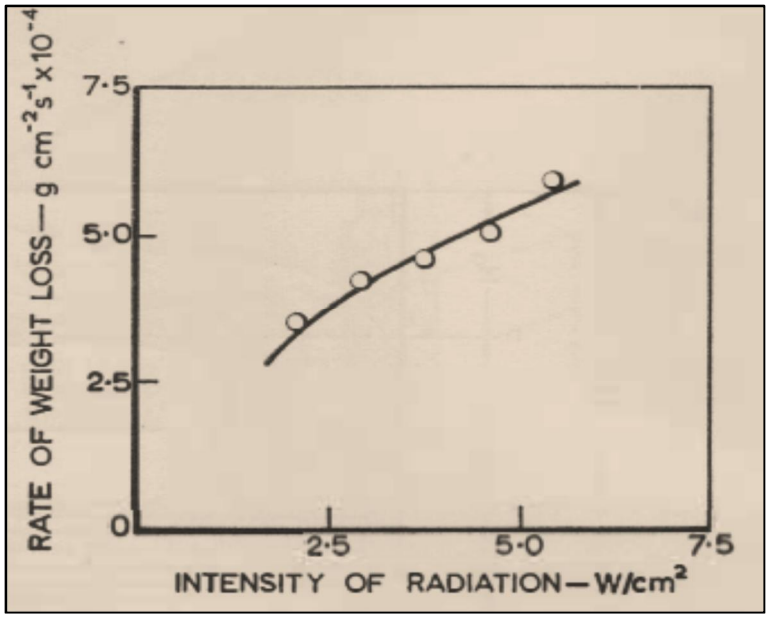

Figure 1-4: Rate of weight loss per unit area (Figure 7B from reference [29]**)**

In his experiments [31][28], Heselden used a simulated fuel bed in a model room with a small window to provide data on rate of heat release promoted by burning town gas. A calibrated calorimeter was placed so as to measure the downward heat flux, *F*, in a horizontal plane just above the burner, as it is depicted in the following figure:

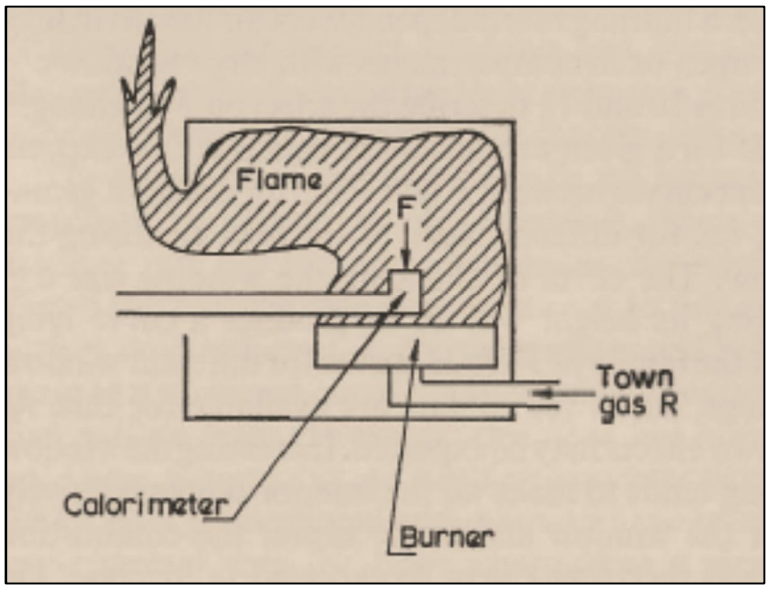

Figure 1-5: Compartment configuration in Heselden experiments (Figure 1(i) from reference [28]**)**

Heselden injected town gas at various controlled rates, *R*, and measured the heat transfer rate, *F*, at various points within the compartment.

Assuming that the form of the relationship between *R* and *F* in these two different sets of experiments was similar (i.e. neglecting the difference in the emissivity of the burning wood flames in comparison to that from the burning town gas flames), Thomas [28] inserted the results from both experiments into a single graph – simplifying the problem not only by using gas experiments to generalize a wood behaviour, but also by decoupling the compartment effects and then reintroducing them – obtaining what he defined as the *quasi-steady burning rate of a fully-developed fire in the* compartment. This theory is depicted in the following figure:

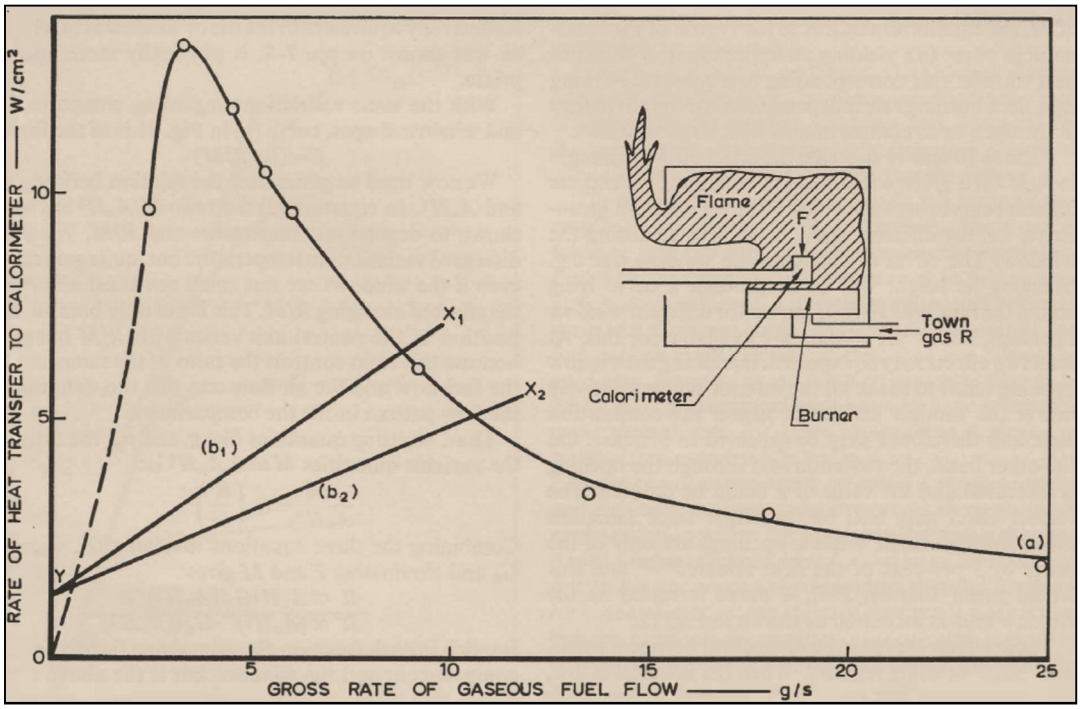

Figure 1-6: Relation between Heat Transfer and Gross Rate of Gaseous Fuel Flow (Figure 9 from reference [29]**)**

The dependence of the gross heat transfer, *F*, to the calorimeter on the flow rate of town gas, *R* – i.e., Heselden's results – is shown as Curve (*a*) in Figure 1-6; whereas the Curves (b_n) come from Law's results and represent an idealized relation between the heat transfer, *F*, and the decomposition rate of the solid fuel into gaseous fuel, *R*, for two given fuel surface areas (Curve b_2 shows an increase in the fuel surface area).

The equilibrium rate of burning is given by the intersections of the two heat transfer characteristics; these are:

Curve (*a*): Heselden's curve reproduces the feedback produced by a given arbitrary flow of fuel. When the town-gas flow, *R*, was reduced in proportion to the window width, the heat transfer to the fuel, *F*, was largely unaltered and was therefore, at least in the region on the RHS of the curve, largely a function of the burning rate to air ratio, $\frac{R}{\dot{m}_{in}}$ (see Figure 1-7) more than on the burning rate, *R*, alone ($\frac{R}{\dot{m}_{in}}$ vs. *F)* (see Figure 1-6). This effect is clarified after the following figure:

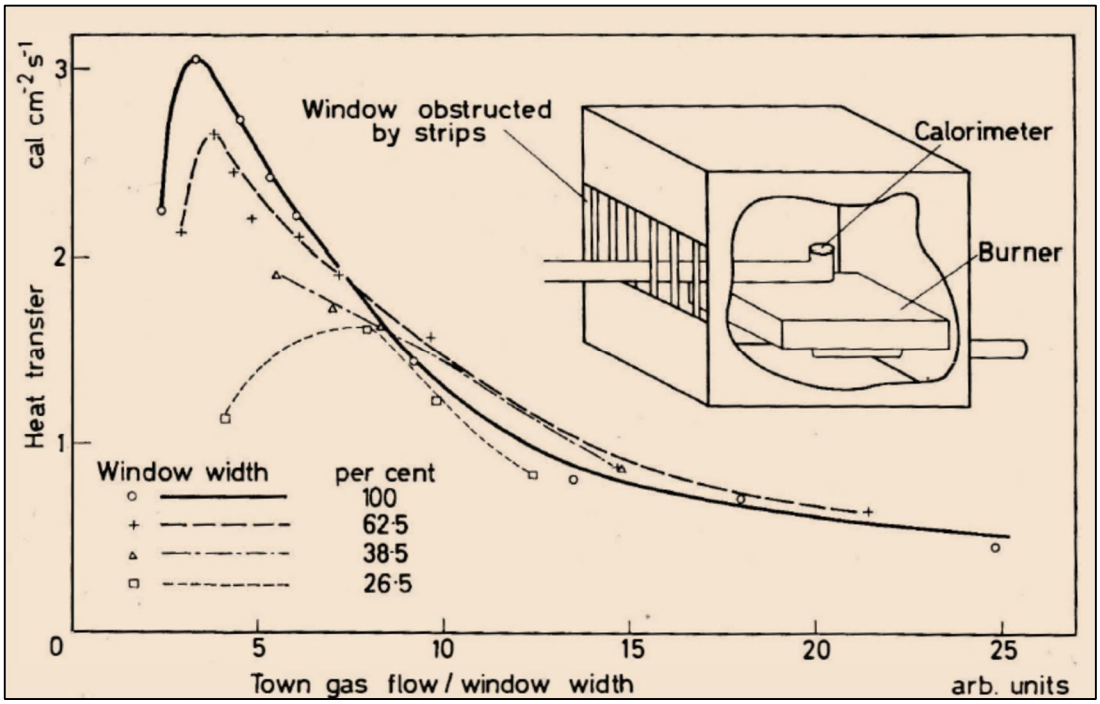

Figure 1-7: Correlation of effect of different fuel and air flows (Figure 2 from reference [28]**)**

This curve – i.e., Curve (*a*) in Figure 1-6 – also depends on the thermal properties of the walls (i.e. $k\rho c$). Thomas' interpretation of the falling branch – namely the *negative feedback* – points to either or both of the following effects:

- Lower temperatures being produced by extra fuel not being burnt but taking up heat (heat balance effect), and/or
- The combustion zone moving away from the fuel towards and out of the window with less heat being fed back to the fuel as the burning rate, *R*, increases.

These two effects are further generalized in that, changes in the amount of fuel load, *L*, will change the mixing pattern of flow in that compartment and alter the position of the combustion zone so that the distribution of heat flux (and therefore the heat flux rate) to any one point are changed. If the change is positive (i.e. the fuel is in excess) the position of the combustion zone will move towards the opening and some

fuel will not burn in the compartment taking up heat and reducing the thermal feedback to the solid fuel.

Curve (*b*): Law's curve reproduces the thermal decomposition characteristic of the fuel bed (*R* vs. *F*). This curve depends on the burning rate, *R*, alone, and is independent of the thermal properties of the walls.

In general, Curve (*b*) has two intersections with Curve (*a*) denoting equilibria but – according to Thomas – only the higher one is stable, and represents the *quasi-steady burning rate of a fully-developed fire* in the compartment.

1.3.2.2.1.1 The effect of increasing the fuel surface, A_f, without changing the size or geometry of the window

For a given thermal condition, extending the fuel surface area, A_f, and keeping the same fuel load, *L*, might be thought to increase its rate of decomposition, *R*; and thus, the extra fuel, being unable to burn inside, might burn outside as a taller diffusion flame. Nevertheless, Thomas – after Heselden's experiments [28] – explains that this only happens if the windows are large (i.e., within *Regime II*), but does not happen to any large extent when the windows are small (i.e., within *Regime I*). Therefore, he declares that the factors which compensate for this effect of increased surface, A_f, can be explained using *the quasi-steady burning rate of a fully-developed fire theory* as follows: if the fuel surface area is increased, Curve (*a*) will in principle be unaltered – i.e., equilibria will move always along Curve (*a*) – but Curve (b_2) will replace curve (b_1) in Figure 1-6. Thus the equilibrium value of the burning rate, *R*, is increased from X_1 to X_2 in the same figure, a smaller proportional increase than that expected if considering the surface area increase without this theory; i.e., the increase expected when moving horizontally (i.e., same value on the ordinate axis representing the same thermal condition, *F*) from Curve (b_1) to Curve (b_2) ignoring any intersection with Curve (*a*).

1.3.2.2.1.2 The effect of changing the airflow, $\dot{m}_{in}$, without changing the size or geometry of the window

Idealizing Figure 1-6 the following figure is obtained:

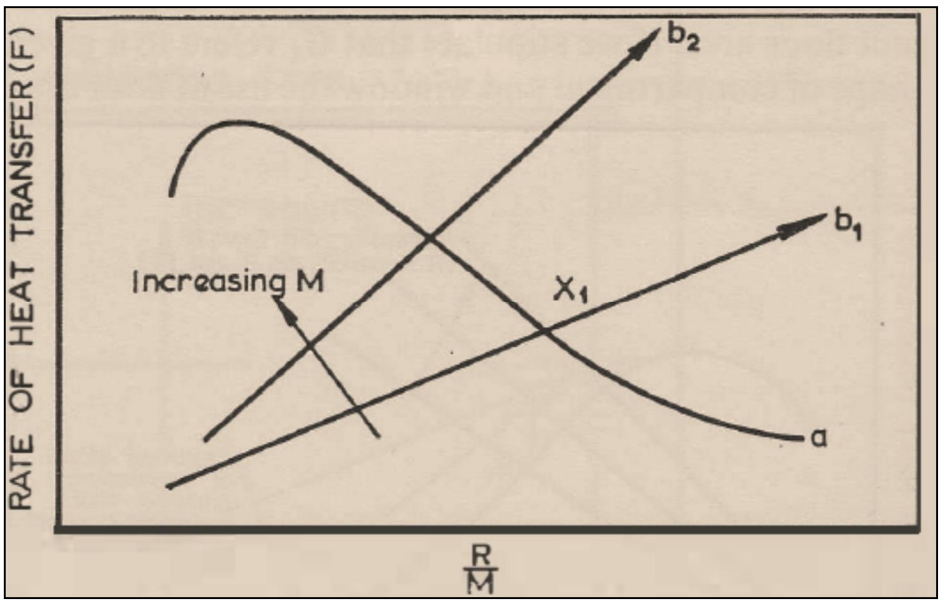

Figure 1-8: Effect on equilibrium value of *R/M* (idem $\frac{R}{\dot{m}_{in}}$ in the present nomenclature) of increasing *M* (idem $\dot{m}_{in}$ in the present nomenclature) (Figure 11 from reference [29]**)**

Using this figure, Thomas explains [29] that the effect of increasing the air flow, $\dot{m}_{in}$, for a given size of window will be to raise Curve (b_1) to a new Curve (b_2), since – according to Law [32] – the burning rate, *R*, is constant for a constant heat flux, *F*, no matter the atmosphere nor the convection mode (forced/natural) in which the combustion takes place. Thus, the physical relationship between the burning rate, *R*, and the heat flux, *F*, (in this case the proportional line) will not change by increasing the airflow, $\dot{m}_{in}$,. As such, the gradient of the strait line (b_n) will increase if the inflow of air into the compartment, $\dot{m}_{in}$, increases, as the burning rate, *R*, and the heat flux to the fuel, *F*, stay constant. Analytically:

$$r\left(gradient\right)=\frac{F}{\left(R/\dot{m}_{in}\right)}=F\left(\frac{\dot{m}_{in}}{R}\right) \quad \Rightarrow \quad r \propto \dot{m}_{in} \qquad \textbf{Equation 1-3}$$

In sum, increasing the air flow, $\dot{m}_{in}$, without changing the window size tends to move the equilibrium conditions denoted by point X_1 towards lower values of $\frac{R}{\dot{m}_{in}}$ in accordance with experimental results.

1.3.2.2.1.3 The effect of changing the window size (e. g. changing its height)

Increasing the window size involves not only an increase in the air inflow, $\dot{m}_{in}$, but also a change in geometry and therefore in flow pattern. So, at least two effects may be expected following this theory:

- Increasing the window opening tends to make all the interior points relatively nearer the window and hence nearer the combustion zone and therefore the heat transfer rate, *F*, may be expected to increase, or
- The radiation loss through the opening is increased and the heat transfer rate, *F*, could be reduced.

Thomas explains [29] how the former effect may well be the larger since radiation losses through small window openings are only of the order of 5% of heat released and this would mean that an [F *vs* $\frac{R}{\dot{m}_{in}}$] curve is raised as the window area is increased as shown in the following figure:

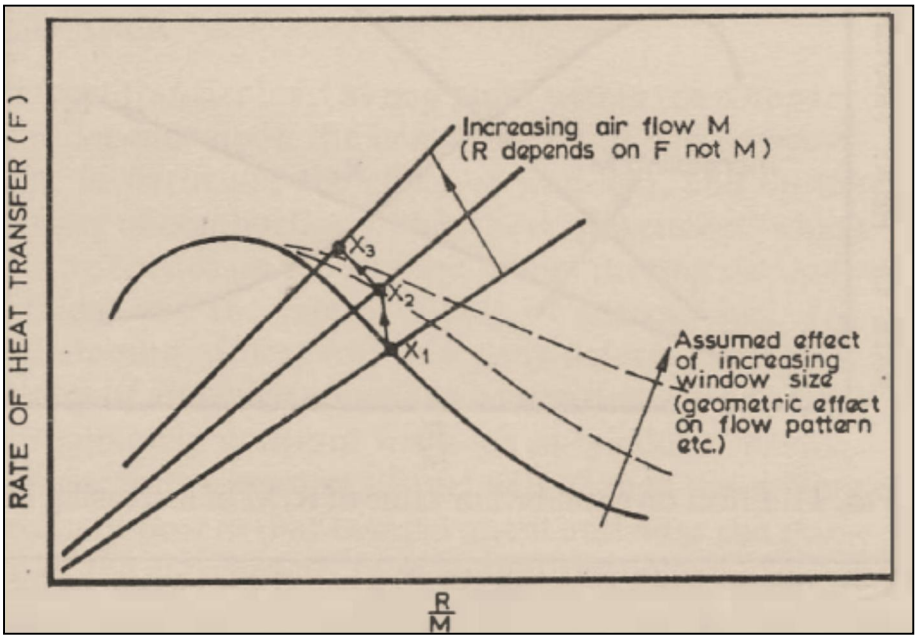

Figure 1-9: Effects on equilibrium *X* of increases of window opening size and air flow (Figure 12 from reference [29]**)**

Figure 1-9 summarises Thomas' *quasi-steady burning rate of a fully-developed fire* qualitative theory, and sets the basis to define the second regime of behaviour and consequent demarcation between the latter and *Regime I*.

1.3.2.2.2 Definition of High Ventilation Regime

After analysing all these effects under his theory, Thomas realized that all of them sharpened the distinction between the *small* and *large* opening regimes; i.e., *Regime I* and *Regime II*, respectively.

For example, following the explanation in Section 1.3.2.2.1.2, Thomas noted that continually increasing the air inflow into the compartment, $\dot{m}_{in}$, without changing the window shape or size, would tend to move the equilibrium to the region of the maximum in Curve (*a*) (Figure 1-8), yielding an approximately constant heat transfer rate, *F*, corresponding to a constant burning rate, *R*. In other words, a burning rate, *R*, independent of the air flow, $\dot{m}_{in}$, as in fires in the open or in compartments with large windows.

Further, as it was seen in Section 1.3.2.2.1.3, when the window opening is increased, the heat transfer rate, *F*, is expected to increase too, moving the equilibrium to the top of the *F* curve in Figure 1-9.

And finally, Thomas explains [29] that when the fire load, *L*, is low, the burning rate, *R*, at a given heat transfer rate, *F*, is lower than when the fire load is high. This, taken to Figure 1-9, moves the equilibrium once more to the top of the *F* curve.

Therefore, following this theory it is clearly seen how the *high ventilation* regime (i.e., *Regime II*) is in fact a regime characterized by a large opening in relation to the amount of fuel, *L*.

1.3.2.2.3 Demarcation between Regimes

This section depicts how Thomas finds the demarcation between fires controlled either by the ventilation (i.e., *Regime I* fires) or by the fuel (i.e., *Regime II* fires), and discusses how the difference in the burning behavior influences the duration of the fire, τ.

The following figure shows some experimental points for a series of large scale experiments [29] carried out in compartments 7.7 meters wide, 3.7 meters deep, and 3.0 meters high with two window openings, where wood cribs evenly distributed over the floor covering about 1/3 or 2/3 of the floor area were burnt:

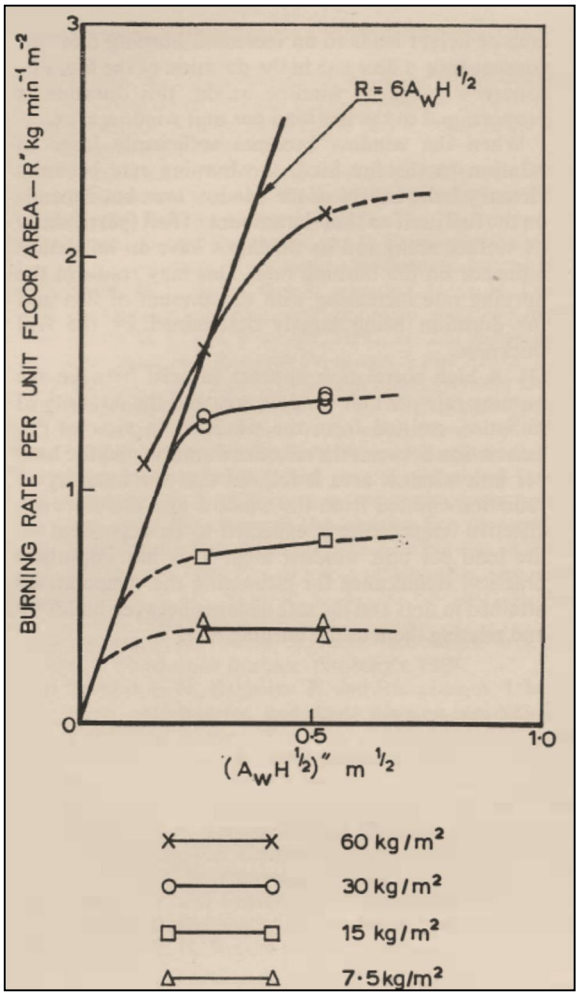

Figure 1-10: Burning rate data for a compartment 7.7 x 3.7 x 3.0 (m) (Figure 13 from reference [29]**)**

The diagonal line represents the equation for the burning rate, *R*, in a *Regime I* fire. It is important to note that Thomas' constant of proportionality in this equation is 6.0 [29] in contrast to Kawagoe's 5.5 [12]. Thomas further explains [29] that the ordinates of the horizontal asymptotes of the three lowest curves (i.e., where they touch and are equal to the diagonal line) are given by:

$$R''\left[\frac{kg}{s.m^2}\right]=\frac{L''\left[\frac{kg}{m^2}\right]}{\tau\,[s]}$$ **Equation 1-4**

Where R'' is the burning rate per unit floor area, L'' is the fire load per unit floor area (fire load density) and τ is a time which is dependent on the properties of the fuel bed design, especially the fuel thickness, f, and surface area, A_f.

This means that the burning rate, R, would be equal to:

$$R\left[\frac{kg}{s}\right]=\frac{L''\left[\frac{kg}{m^2}\right]A_F\left[m^2\right]}{\tau\,[s]}$$ **Equation 1-5**

or

$$R\left[\frac{kg}{\min}\right]=\frac{L''\left[\frac{kg}{m^2}\right]A_F\left[m^2\right]}{\tau\,[s]}60\left[\frac{s}{\min}\right]$$ **Equation 1-6**

Where A_F is the floor area.

Thus, equating both burning rates per floor area (ventilation-controlled with fuel-controlled) in their intersection point, the demarcation between fires controlled by ventilation and fuel is obtained as follows:

$$6\,A_w\sqrt{H}=60\frac{L''A_F}{\tau}$$ **Equation 1-7**

$$A_w\sqrt{H}=10\frac{L}{\tau}$$ **Equation 1-8**

$$\frac{L}{A_w\sqrt{H}}=\frac{\tau}{10}$$ **Equation 1-9**

Where L is the total amount of fuel in kg.

Summarizing, it follows that if:

$$\frac{L}{A_w\sqrt{H}} > \frac{\tau}{10} \quad \Rightarrow ventilation-controlled \qquad \textbf{Equation 1-10}$$

$$\frac{L}{A_w\sqrt{H}} < \frac{\tau}{10} \quad \Rightarrow fuel-controlled \qquad \textbf{Equation 1-11}$$

This demarcation emphasizes Thomas' conclusion – after his *equilibrium burning rate theory* – that the *high ventilation* or *fuel-controlled* regime (i.e., *Regime II*) is a regime characterized by a large opening in relation to the amount of fuel, *L*.

Diagrammatically, the demarcation would appear as follows:

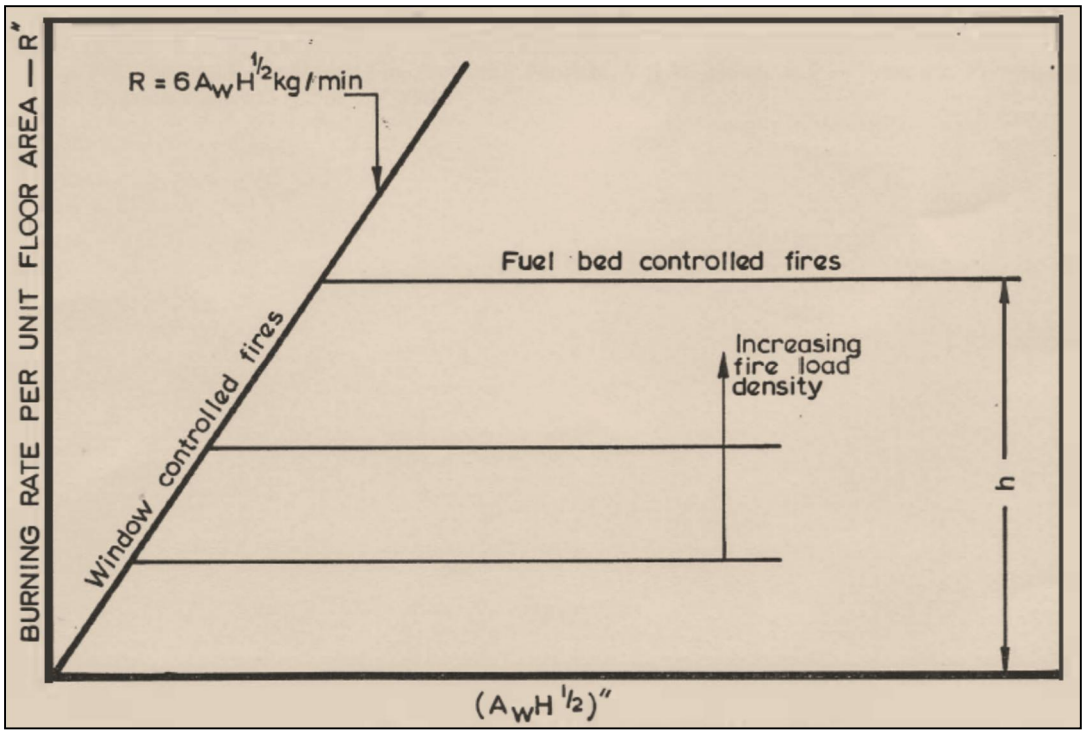

Figure 1-11: Burning rates of fully-developed fires (Figure 14 from reference [29]**)**

Additionally, Thomas demonstrates [29] that for a given window height, *H*, (e.g. 1.8 m), there is an association between the effective duration, τ, and the fire load per unit window area, L/A_w. This is to say:

$$\frac{L}{A_w} = 0.2\,\tau$$ **Equation 1-12**

This means that, for a narrow range of window height, the duration, τ, is proportional to the fire load per unit window area, L/A_w:

$$\frac{L}{A_w} \propto \tau$$ **Equation 1-13**

Concluding, this demarcation exhibits the following relevant differences:

Small Windows: an increase in window area, A_w, or height, H, leads to an increased burning rate, R, and consequently a decrease in the duration of the fire, τ ($\tau = L/R$). For a narrow range of window height, H, this duration, τ, is proportional to the fire load per unit window area, L/A_w.

$$R = f\left(A_w\sqrt{H}\right) \;\therefore\; \tau = f\left(\frac{L}{R}\right) \;\wedge\; \tau = f\left(\frac{L}{A_w}\right)_{H\approx 1.8}$$ **Equation 1-14**

Large Windows: when the window becomes sufficiently large in relation to the fire load, L, the burning rate, R, becomes virtually independent of the window area, A_w, but depends on the fuel itself so that the amount of fuel – particularly its surface area, A_f, and its thickness, f – have an important influence on the burning rate, R. This may result in the burning rate, R, increasing with the amount of fuel, L, and the duration, τ, being largely determined by the fuel thickness.

$$R = f\left(A_f\right) \;\therefore\; \tau = f\left(f\right)$$ **Equation 1-15**

In summary, in regards to determining the duration, τ, of fires, Thomas' theory shows that for small and large windows the fire load per unit window area, L/A_w, and fuel thickness, f, respectively, are more important than other factors.

1.3.2.2.4 Mechanisms of Burning and External Flaming

It was traditionally believed that in *Regime I* fires, the inflow of fresh air set an upper limit to the oxidation reactions towards reaching the necessary stoichiometric relation. This led to this regime being termed *ventilation-limited* in relation to the burning mode, and support the reason behind external flaming as simply being that the fuel gases, unable to burn in an oxygen starved internal atmosphere, burn outside once they encounter and mix with fresh air.

Nevertheless, after analysing several compartment burnout tests, Thomas' [29] and Harmathy's [2][33] theoretical developments revealed that in *Regime I* fires, the ratio of the rate of inflow air to the rate of volatile production was higher than the stoichiometric air requirement for the combustion of typical wood.

This fact led Harmathy [2] to refer to poorly vented fires (i.e., *Regime I* fires) as *ventilation-controlled* fires replacing the classic *ventilation-limited* expression, basing his argument on the fact that the rate of air inflow literally controls – and not limits – the rate of burning in an indirect way: by being instrumental in regulating the rate of heat supply to the fuel. Harmathy's mechanism of burning model [2] states that the rate of the decomposition reactions (i.e. the pyrolysis rate) is largely controlled by the rate of heat supply to the decomposing fuel. In the case of cellulosic materials, the primary source of heat is the combustion of charcoal, the rate of which is controlled by the rate of flow of air enveloping the charring surfaces; i.e., the rate of oxygen transport to the wood surface.

Following this model, the *burning mode* (refer to Table 5-3) is therefore defined after the ability of the air inflow into the compartment to reach the decomposing fuel surfaces: compartment fires burning in a *fuel-controlled mode* are those were the air inflow is unrestricted from flooding and enveloping the charring surfaces and thus the generation of heat is *controlled* by the fuel supply, while compartment fires burning in a *ventilation-controlled mode* are be those were the air inflow is restricted from reaching the charring surfaces and hence the generation of heat is *controlled* by the air supply to the decomposing fuel.

Thomas [27] explained that in *Regime I* situations, the maximum velocity head of air is proportional to the height of the opening, *H*, while the maximum velocity head of the fuel gases is proportional to the square of the ratio of the burning rate to the opening area, $\left(\frac{R}{A_w}\right)^2$. He stated that if the latter was large compared to the former, combustion could not further occur within the compartment and there would be insufficient heat received by the fuel to sustain the combustion process. Therefore, considerations of mixing place an upper limit on the ratio of these two maximum velocity heads and hence on the burning rate inside the compartment, which in turn will promote the typically observed external flaming in *Regime I* fires. As a matter of fact, Thomas explanation is the only theoretical clue to the empirical relationship found by Kawagoe (Equation 1-2) that describes the burning rate, *R*, in a *Regime I* fire:

$$\frac{\left(\frac{R}{A_w}\right)^2}{H} = \text{upper limit} \qquad \Rightarrow \qquad R \propto A_w\sqrt{H} \qquad \textbf{Equation 1-16}$$

As it can be evidenced by Photo 1-1 and Photo 1-2 in Section 1.3.2.2, both regimes can experience external flaming depending on the mixing and flow conditions. In what concerns to *Regime II*, if external flaming occurs to any extent this effect is simply founded on the high momentum of the burning mixture that carry the flames outside.

In this way, the *burning mode* is function of the rate of transport of air into the fire base or fuel bed, while the *external flaming* is function of the mixing and flow (momentum) conditions. To this extent, in small compartments classic *Regime I* fires are those experiencing restricted air supply (i.e. *ventilation-controlled* burning mode) and external flaming due to poor mixing conditions, while classic *Regime II* fires are those supplied by un unrestricted air flow (i.e. *fuel-controlled* burning mode) and – if to any extent – external flaming due to a high momentum burning mixture.

1.3.3 The Geometrical Basis of these Breakthroughs

As observed above, the basis of these critical breakthroughs was a significant body of experimental work. Of particular relevance was Thomas' ground breaking work during the 1960s [25][26][27][28]. To this extent, the simplest and most extreme configuration of a small compartment with a single opening was typically selected as the best possible choice to be analysed and modelled. As a result of testing under this specific configuration, the three different fire stages (growth, full-development, decay) were identified, the first separated from the latter two by a unique phenomenon defined as *flashover*. Moreover, it was recognised that – under these conditions – the fully-developed stage was the most critical one in terms of structural damage and, thus, specific research attention was given to it [34] in search of further characterisation.

Before these tests, most experiments had been made in cubical or near cubical-shaped compartments. Although still reduced in size, these tests emphasized the relevance of different compartment shapes. So far, the attention was given to try to understand the cause-effect relations between the numerous variables present in a compartment fire (assessing conservative fire resistance requirements), and not trying to predict the characteristics of an actual (non-laboratory) fire by extrapolation of fires in unrealistic, artificial, laboratory configurations [35].

During the 1970s and 1980s, in an attempt to predict the general fire behaviour and its consequences in actual buildings – Harmathy [2][36][1] adapted the single opening laboratory compartment to a more realistic communicated system of (small) compartments.

The bulk results of the research in compartment fires completed throughout these decades was put together in what is today known as the *classic compartment fire framework*. Special attention must be given to the fact that reduced size – although varied shapes – compartments were tested, in contrast to the architectural context presented in Section 1.1.

1.4 Bringing the Compartment Fire Framework to Engineering Practice

1.4.1 Overview

During the 1970s Thomas and co-workers – after the well-known international programme coordinated by CIB (Conseil International du Batiment) [34] (see Section 3.2) – investigated and reported the relationship of the main factors which influence the behaviour of fully-developed fires in compartments – i.e., mean burning rates, mean temperatures and mean intensity of radiation – as well as the relative importance of the compartment shape and scale. Some relationships were derived empirically and some by theoretical considerations of the heat balance in the compartment. The more than 400 small-scale tests ran in – single and rectangular – compartments of up to 6 x 6 x 1.5 m height dimensions open on one side, were performed by 8 different laboratories around the globe.

Thomas' research in compartment fires continued for another decade [30][37][38][39][40][41][42][43][44], extending and formalising the experimental database into a series of engineering expressions that characterised the maximum temperature within a compartment, $T_{g\text{-}MAX}$, and, given a fuel load, L, the potential duration of the a fully-developed fire, τ. His formulation de-emphasizes time and provides a worst case time invariant temperature regime for the fire until total burn-out of the fuel.

Tewarson's studies [45][46] on both char and non-char formation materials (cellulosic, alcohol and oil, respectively) were assessed in two geometrically similar enclosures having 1:2:1 aspect ratios with sides of 0.5 and 1 m, respectively. The ventilation was provided by two openings located in the long dimension walls of the enclosure. He investigated the formation of combustion gases (CO, CO_2 and O_2) giving an expression to estimate the ventilation parameter for the most dangerous gas concentration.

At this point research bifurcates, while Petterson *et al.* [47] extend the empirical data base by re-emphasizing the time evolution of the fire, Emmons *et al.* [48] and McCaffrey *et al.* [49] refine Thomas's formulation by further describing the different processes and adding more experimental data. It is important to note that only Petterson *et al.* [47] emphasize the time evolution of the fire while all others focus on the worst case condition.

Of notable importance are the studies by Harmathy *et al.* [2], Law *et al.* [50][51][52] and Tanaka *et al.* [53][54][55][56][57] who attempted to translate the acquired knowledge into design methodologies with an emphasis on structural performance.

Tibor Harmathy's extensive review of fully-developed fires published in 1972 [2] was based on hundreds of small-scale and full-scale compartment burnout tests conducted by Kawagoe [12], Gross and Robertson [20], Butcher and co-workers [58][59], and many others [60][61], as well as on his own theoretical interpretation of these tests, which in turn had evolved from previous theoretical studies performed by Kawagoe [12][17], Thomas *et al*. [29], Pettersson, Magnusson and Thelandersson [62][63][64][47], and others [65]. He introduced the concept of a critical ventilation parameter and regime (i.e., Harmathy's *Critical Regime*) that defined the break-point between the two regimes previously found by Thomas *et al*. [29], and proposed a model for the mechanism of burning of fully-developed fires [33]. Harmathy's review of compartment fires and interpretation of the fire problem set the basis for his transcendent engineering approach and contribution to fire safety, compiled into an integral doctrine [6][66] that characterises and deals with the fire severity in the compartment of origin as well as the fire spread beyond it.

Numerous complementary studies were conducted in this period providing refinements and extensions to the existing methods but always accentuating the validity of the fundamental approach initiated by Kawagoe [12] and mainly focused on scenarios corresponding to Thomas' *Regime I*.

1.4.2 Thomas and Harmathy – Contrasting in Unison

Philip Thomas' and Tibor Harmathy's contribution to fire research and its application to fire engineering is too vast to be fully presented here, but their most significant contribution in the topic of *fully-developed compartment fires*, a legacy which will always remain crucial to the whole fire safety engineering community, is summarized next.

While both instrumental in the development of compartment fire theory, their contributions are particularly relevant and thus the subject of special focus here due to their transformation of their theoretical contributions and empirical interpretations into practical form for designers to utilise. Their doctrines, still relevant today, are a corner stone of fire safety design. A full comprehension of their own unique engineering interpretation and application is essential to assess its utilization in the design of contemporary architecture.

Both authors exposed substantial differences in certain aspects of the approaches taken to model compartment fires mathematically. These differences gave place to an invaluable and long held debate which has enlightened not only the aspects in question but many others in this complex problem. Nevertheless, given the poor reproducibility of such a complex phenomena, their views on the problem of compartment fires was not only sufficiently accurate in relation to the reproducibility described, but also not that far apart as the historical debate tends to suggest.

The two pioneers also took different approaches to conveying their work to those who would utilise it. Once again though, the deeper philosophies that drove them in these processes appear very much in unison.

1.4.2.1 Thomas' Legacy

Thomas' legacy in fully-developed fires is not quite framed in an organized methodology which can be followed in a step by step design process. Instead, it is a compilation of valuable empirical and theoretical correlations backed with helpful concepts that provides the designer with a great deal of freedom but, at the same

time, demands substantial fundamental knowledge in order to be able to assess the applicability of and link between the correlations selected for a given situation.

The aim of the present section is not to list Thomas' tens of correlations, but to expose his general approach to the fire problem, from the broad concepts to his always enlightening views – although sometimes controversial – on particularly relevant matters.

1.4.2.1.1 Within the Framework: Fire Severity

Thomas was of the idea that research in fully-developed fires was mainly applicable to predict fire severity [39], stating the following:

> "Mathematically expressed, theoretically based design for fire safety is possible at present in almost exclusively the one field, structural design." [67]

Therefore, all his initial efforts in the topic of fully-developed fires were directed towards reducing the data to simple form correlations to predict the fire protection requirements of structural elements. In this way, having the fuel content, L, information on the ventilation openings, A_w and H, and the compartment surface area, A_T, it was possible to obtain the fire resistance requirements. As an example, he showed [34] that the fire resistance required of protected steel columns was proportional to $\frac{L}{\sqrt{A_W A_T}}$, and explained that this correlation eliminates the effect of shape but nevertheless has a variable coefficient of proportionality depending on the compartment tested (or to be analysed).

Thomas further extended this expression [68] to emphasize the role of the openings and the shape of the compartment, variables which were not considered – at that stage and following Ingberg's concepts – by many fire codes. He, thus, showed that the fire resistance required for confining a fire throughout its whole duration or 'burn out' (i.e., considering the cooling effects of the decay period of the fire) was in effect

proportional to $\frac{L}{A_F}\left(\frac{A_F}{\sqrt{A_W A_T}}\right)$, where the shape of the compartment is implicit in the ratio $\frac{A_W A_T}{A_F^2}$. Thomas, hence, considered Ingberg's classic relation between $\frac{L}{A_F}$ and fire resistance, a particular case of a (his) more general relation; i.e., where $\sqrt{A_w A_T} = A_F$.

1.4.2.1.2 Beyond the Framework: Other Fire Problems

Recognizing that the confinement of a fully-developed fire was relevant to life safety in large buildings where rapid evacuation is not possible [34], Thomas still believed [39] that fire problems beyond those directly related to the prediction of fire resistance (i.e., those related to the fire severity) fell outside the theory of fully-developed fires, and regarded them as secondary features of compartment fires. After analysing some of these 'secondary' problems – for example, flames emerging from an opening posing threats outside the compartment – Thomas concludes that once departed from the original objective of designing fire resistance "…the theory of fully-developed compartment fires requires considerable development to provide an adequate base for the other fire problems."

This last conclusion is a clear indicator of the *classic compartment fire framework*'s original goal and consequently its greatest limitation.

In regards to the differences that might exist in approaching the 'primary' vs. 'secondary' problems with the *classic compartment fire framework*, of especial relevance is the fact that Thomas [68] agrees with Kawagoe's proportionality factor between the burning rate, *R*, and the *ventilation parameter*, $A_w\sqrt{H}$, (see Equation 1-2) only when predicting fire resistance but not for other problems like, for example, estimating the length of flames emerging from windows.

Further, in recognising the limitations of the *classic compartment fire framework* to provide only passive fire protection design, Thomas addresses the topic of active fire protection. In doing so, he presents a model [69] which shows how to trade off one

against the other towards the optimum combination, arguing that fire resistance and sprinklers are not freely interchangeable due to the fact that they serve different functions.

1.4.2.1.3 Regulatory Structure

Thomas research in fully-developed compartment fires targeted "the fire technologist responsible for the protection of structures and the prediction of fire-resistance requirements which form the basis of advice to those formulating legislation or regulations", as he claimed [34]. In regards to the latter, he believed the following:

> "Statutory building control is of fundamental importance in providing passive fire protection in a highly organized urban community… it is necessary to examine critically the basis for this control and its economic justification to make sure that the protection provided is commensurate with what is now required. Too much fire protection is expensive, too little is dangerous." [34]

He therefore believed in an explicit rational approach to fire safety, proposing [67] to include calculation methods into the codes as an alternative to the existing rules or requirements for tests. The typical objection to the limitation of the calculation methods – for example, that they apply only to structural elements and not entire building structures, and that some are restricted to exposure to fire on one side only – he left clear that also applied to the rule and test requirement methodology, with the latter having even the further limitation of hardly coping with future developments in the built environment.

Nevertheless, before rational control can be accomplished – he stated [34] – "knowledge of the effect of various parameters on the development of fire in buildings is required". Therefore, he was also aware of the difficult task that is gathering that knowledge. For example, Thomas was of the idea [67] that in practical terms one may not need full fire protection if the situation – e.g. rapid arrival of fire

brigade or the absence of life risk in small readily evacuated buildings – allowed for it (in those cases he proposes for example control over the flammability of materials). But recognizing that there was no way of quantifying such relaxations on a scientific basis, he simply proposed to seek for correlations of life and property loss with a given design or regulatory requirement, and assist these with scientific knowledge – for example by expressing fire severity in terms of $\frac{L}{\sqrt{A_W A_T}}$ – in order to have a clearer picture of the potential situation and propose solutions accordingly.

So in summary, he made clear his desire for the removal of arbitrary commands of regulations, but also exposed the difficulties in replacing them with objective performance criteria and satisfactory design procedures [67].

1.4.2.1.4 Research & Education

To overcome these difficulties Thomas proposes [67] to focus in research and education. He urges to increase the efficiency of fire research by better balancing the abundant data with analysis and interpretation of it, and believed it was important to encourage the public availability of data, especially from expensive full-scale experiments (a pioneering statement in today's open sourcing tendency).

In regards to the growing field of education in fire safety at that time, Thomas was of the idea that both professional engineers and architects must be prepared to understand better the basic problems and principles of designing for fire safety, dissuading them from the 'rule book' approach. He stated the following:

> "The architect must do more than simply seek to use the 'approved' materials with no understanding…. as long as basic principles are not expressed in the courses (in fire safety), then education is a catalogue of regulatory prohibition and will soon be out of date." [67]

Leading the CIB working group W14, he pushed firmly towards this goal.

1.4.2.1.5 Fire Testing, Modelling and the Future

Thomas believed [67] that the ties between the combustion and building aspects of fire research were weak at that time in Europe (unlike in Japan). This is to say there was a lack of connection between research, testing, regulation and application. He exposes – as an example of this lack of communication – the virtual absence of a combustion and heat transfer analysis of any fire testing furnace until W14 encouraged the need for harmonization between different furnaces and laboratories.

Thomas also stressed that only when the physical and theoretical models of fire behaviour were better understood could fire tests be developed satisfactorily and the role of the test in the assessment of a hazard could be properly defined. He was of the idea that fire testing only partially helps in the assessment of a hazard. In this regard, Thomas was eager that a methodology of the prediction of the time scale of fire development in buildings was in urgent need, not only to grade risk satisfactorily but also to understand the relationship between fire testing and fire hazard.

In what refers to modelling, Thomas recognized the increasing importance of the interaction between the latter and fire testing, defining it as "a landmark in the development of the subject of fire safety" [44]. He strongly believed [44] that the understanding of fires that they had at that time was sufficient to provide a framework for the design of new and assessment of old fire tests. In this sense, he suggested [70] that those fire tests that could not be understood in terms of a model – when applied to a simple material – must be rejected. Unfortunately, this view was refused by the community.

In terms of the future of fire tests, Thomas announced [70] that fire tests – in addition to the typical goal of providing data for the regulatory process – "were beginning to be seen as having to provide data for productive modelling as well". And for productive modelling he referred to that applied in the design of buildings:

> "Modelling provides the engineer and the architect with a technique for designing buildings and processes to be safe and for providing a technique for the authority to assess that

> safety (...) For this, the model requires information and here we do have a major problem (…) Modelling the gas phase connects the fire world with the furnace world, the meteorological world, the oceanographic world, etc., but obtaining information that can be used to include the boundary conditions (…) will be virtually the sole responsibility of those in the fire community. In short, the development of tests will be increasingly geared to providing information for use in models." [70]

1.4.2.1.6 Summary of Thomas' Approach

Thomas believed that the classic fully-developed compartment fire framework – in the developed stages it was at that time – was solely applicable to analyse the fire severity and consequent fire resistance requirements of structural elements. For this reason, he considered that the approach to all the other fire problems needed to be tailored to the individual case, using all the available scientific knowledge at hand in the selection – and modification if applicable – of any set of correlations or models developed.

In regards to the regulatory structure, which mainly consisted at that time of simple rules based on tests – he made clear his desire to remove the arbitrary rules, but also was aware of the difficulty in replacing these with objective performance criteria and satisfactory design procedures.

To overcome this difficulty, Thomas fervently supported the idea of reinforcing the scientific or fundamental research, and at the same time develop solid educational programmes in fire safety, not only for professional engineers and architects but also for regulators and code writers.

He finally believed in a tight feedback between fire modelling and fire testing, where one helps better (or ideally fully) understand the other and vice-versa. In this way, he foresaw the role of fire testing not only feeding the physical modelling (e.g. fire

resistance tests or fire tests methods used to evaluate different and particular aspects of an element's performance), but also feeding the sub-models beneath mathematical modelling, from the simplest to the most complicated computer-based CFD existent today. And of course, believed that models – again from the simplest correlation to that simulating the most complex interaction of variables – were an essential tool in the design of fire safety in buildings.

1.4.2.2 Harmathy's Legacy

1.4.2.2.1 Philosophy

In 1976 Tibor Harmathy believed [36] that advances in fire science were consistently outpaced by the emergence of newer problems that tended to make the risk of fire higher than ever before. He raised examples such as the increasing popularity of high-rise buildings, the use of large and undivided areas in commercial and office buildings, and the introduction of a multitude of plastics to replace wood or metal both in furniture and in building components.

Similar problems are still being faced by the fire safety community, with the addition of newer construction materials, sometimes in combination with large and non-conventional volumes as part of the contemporary architectural trend.

In order to address those 'new' problems, Harmathy proposed to take a 'new look' at the fire problem, instead of trying to adapt conventional solutions to those new and varied conditions. His idea was that the conventional solutions (discussed in section 1.4.2.2.1.1), once believed to serve the objective of fire safety reasonably well had become ineffective. Subsequently, he established what he called a new system of defence against fire, which he developed during the succeeding years of active research. His doctrine is summarized in the following sections.

1.4.2.2.1.1 Conventional Philosophy vs. Harmathy's Philosophy

The conventional fire safety philosophy or solutions Harmathy refers to are those developed at the beginning of the 20th Century, namely passive (e.g. compartmentation) and active (e.g. sprinklers) fire protection features and devices.

But specifically, he referred to this philosophy's fundamental approach, compartmentation, and the two postulates on which this approach is still founded today:

- *Fire severity*
- *Fire spread*

His conviction was that both postulates were inaccurate and that therefore, the fire safety provided by the fire resistant compartmentation of buildings at that time was fallacious. Very little has changed since then in terms of compartmentation and fire testing (i.e. *ratings*), therefore, Harmathy's conviction should be reconsidered in light of the last three decades of "progress" in fire safety. Accordingly, his reasons and explanations for holding such a strong belief are summarized – for the most literally – in the following sections.

1.4.2.2.1.1.1 Conventional fire severity vs. Harmathy's potential for destructive spread (H^*)

The conventional philosophy, under the influence of Ingberg's concept [11], assumes that the severity of compartment fires depends solely on the fire load density, *L"*; i.e. the mass of combustibles per unit floor area, $\frac{L}{A_F}$ (refer to correlations in section 1.4.2.1.1). This concept, developed at the beginning of the 20th Century, claims that the destructive potential of compartment fires is proportional to the specific fire load, and that the fire resistance requirement for compartment boundaries should also be allocated in proportion to the specific fire load [71][36].

On the other hand, Harmathy characterises the *severity* of fires [72] as:

> "The term *fire severity* has different connotations for different researchers. Some look upon fire severity as characterizing the fire itself, others as characterizing the destructive potential of the fire with respect to the confining boundaries.

> The interpretation of fire severity in strict scientific terms comes naturally from an analysis of the heat balance for post-flashover compartment fires. If opportunely conducted, the analysis will yield a number of descriptors which are capable of fully characterizing the fire process, including the nature of the fire itself and the destructive potential of the fire with respect to the compartment boundaries."

Harmathy provided three of these descriptors [72], and recommended that they were referred to as *fire severity parameters*. These are:

- Overall penetration flux, $\bar{q}_E$ [kW/m^2], i.e. heat flux penetrating the compartment boundaries, averaged spatially over all boundary surfaces, and temporally over the period of full fire development.
- Duration of fully-developed fire, τ [s],
- Average temperature of compartment gases, $\bar{T}_g$ [K] (average *fire temperature* as defined in reference [72]), averaged spatially over the compartment volume and temporally over the period of full development.

Later, on a closer examination into these parameters Harmathy revealed [72] that of the three, two, either $\bar{T}_g$ and τ or $\bar{q}_E$ and τ, were sufficient for unequivocally characterizing the fire process. The interesting distinction he pointed out was that:

- if $\bar{T}_g$ and τ are selected, the characterization is done from the point of view of the fire itself, whereas
- if $\bar{q}_E$ and τ, are chosen, the effect of the fire on the compartment boundaries – in other words its destructive potential – is emphasized.

Harmathy was concerned, in this occasion, primarily with design for fire safety; thus, he believed that characterizing the fire by the two parameters $\bar{q}_E$ and τ seemed to be more appropriate [72] in this sense.

After this interpretation of *fire severity*, namely Harmathy's *destructive spread potential*, it is clear why he – in reference to Ingberg's fire load concept [11] – believed and literally stated that:

> "Considering only the fire load is, in itself, grossly misleading" [36]

Therefore, it becomes clear that Harmathy did not agree with the way the traditional philosophy treated the problem of the *destructive spread potential*, under the classic and invalid concept of a fire severity – and consequent fire resistance – only considered as proportional to the fire load density, *L"*.

1.4.2.2.1.1.2 Conventional fire spread vs. Harmathy's potential for convective spread (μ-factor)

With respect to the mechanisms of fire spread, Harmathy states [36] that the method of conducting and evaluating fire endurance tests implies the claim that spread occurs either by:

- excessive heat conduction through a boundary element followed by ignition of combustibles in an adjacent compartment, or
- structural failure of a boundary element followed by penetration of the flames into the neighbouring spaces.

This means that the two mechanisms of fire spread implied by the conventional fire protection philosophy – namely heat conduction through, or structural failure of, the compartment boundaries [36] – fall under the *destructive spread potential*. In this sense, the conventional philosophy assesses the spread of fire by means of requiring that all compartment boundaries exhibit a specified *fire resistance*, that is to say, proven ability to resist heat conduction and structural damage for specified periods [66]. Contrary to this traditional philosophy, Harmathy believes [36] that the flames are driven by pressure differences from one space to another, either:

- horizontally through doors left open by the escaping tenants, or vertically through ducts, shafts, openings in ceilings, and
- by flames issuing from windows then jumping to the floor above.

He referred to this fire spread mode as the *convective spread potential*. The difference in these two conceptions – i.e. the traditional vs. Harmathy's – is illustrated in the following figure:

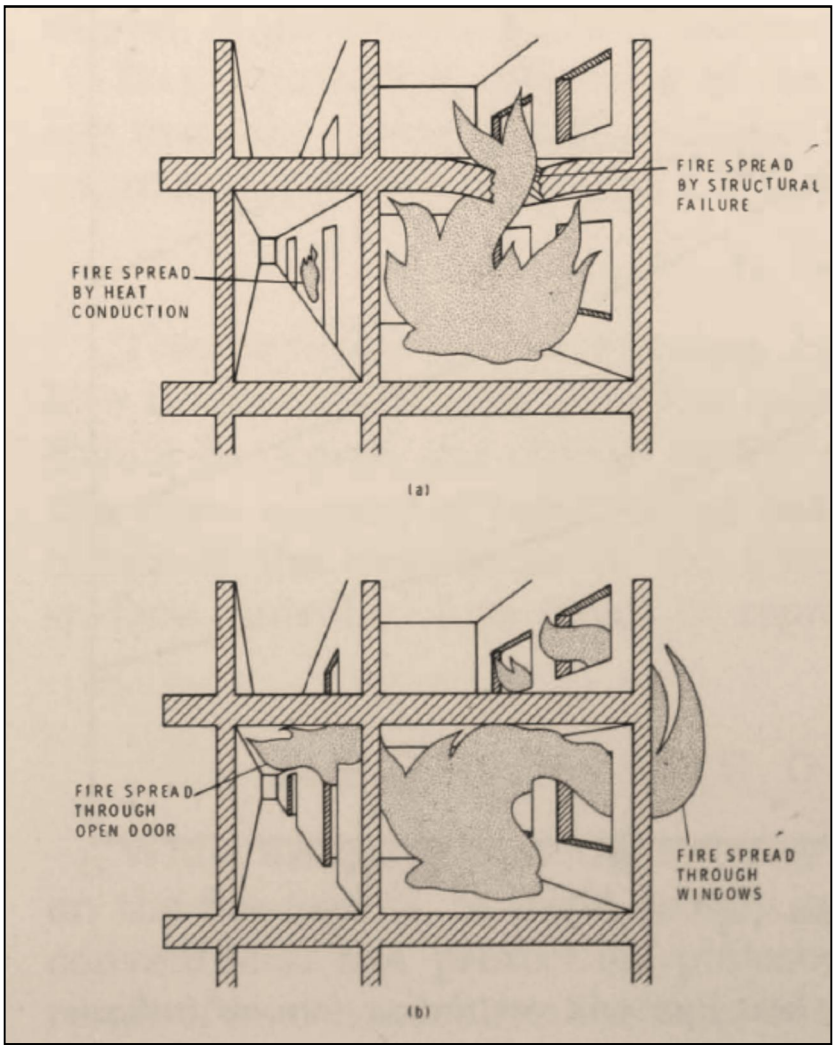

Figure 1-12: Mechanisms of fire spread: (a) assumed mechanisms, (b) actual mechanisms (Figure 5 from reference [36]**)**

Summarizing so far, Harmathy believed that the traditional philosophy was concerned mainly with the problem of *destructive spread potential*, giving relatively little attention to the spread of fire by convection or *convective spread potential*. Moreover, he added [6] that on top of this crudeness, the attention to the destructive spread was given "in an antiquated way", clearly referring to Ingberg's fire load concept [11] with which he didn't agree [36] as already discussed in the previous section (section 1.4.2.2.1.1.1).

1.4.2.2.1.1.3 Conventional 'fire resistance' vs. Harmathy's 'flame spread resistance'

In relation to the precedent sections 1.4.2.2.1.1.1 and 1.4.2.2.1.1.2, Harmathy [6] argued that the conventional concept of 'fire resistant' compartmentation assumes that the compartments in a building are perfectly isolated from each other and from the rest of the building, therefore also assuming that fire spreads through the traditionally believed mechanisms – as previously seen – of excessive heat conduction and/or successive failure of the compartment boundaries. Following this, he explained [6] that if these boundaries were 'fire resistant' under the conventional approach definition, this view would claim that excessive heat conduction or failure will not occur keeping the size of the fire within acceptable limits; i.e., contained in the compartment of origin. Contrary to this belief, in Harmathy's mind this idea of perfectly isolated compartments was a crude abstraction [35], founding this statement in the fact that compartments are always communicated with other inside or outside spaces through communication paths (e.g. open doors and broken windows), and that these serve as routes along which the fire can spread by convection, this is, by the advance of flames and hot gases.

Consequently, the confronting fire spread conceptions depicted in Figure 1-12, brought up the argument of the traditionally defined 'fire resistance' vs. Harmathy's *flame spread resistance* definition discussed in a separate publication [73].

Regardless of this interpretation debate, due to the fact that Harmathy believed in the spread mechanisms depicted in Figure 1-12(b), he therefore concluded that compartment boundaries were rarely able to prevent the spread out of the space of

origin and, thus, may become exposed to fire on both sides. For this reason, he argues [73] that the *true fire resistance* of key building components must be judged on their ability to withstand fire exposure from two sides and not just from one. To this extent, he introduced a different procedure to be applied to *key structural components* [74], and a practical way to assess the fire resistance (in rigor, *flame spread resistance* in Harmathy's doctrine) of the *dividing elements* [6] (explained in detail in section 1.4.2.2.2.2).

In such manner, sections 1.4.2.2.1.1.1, 1.4.2.2.1.1.2 and 1.4.2.2.1.1.3, make clear the reasons by which Harmathy believed that the two postulates of *fire severity* and *fire spread* – on which the conventional fire safety philosophy and its most fundamental feature, compartmentation, is founded – were inaccurate and, therefore, concluded that the fire resistant compartmentation of buildings was "largely illusory" [36] using his own words. The following table summarizes the difference between both approaches:

Table 1-1: Traditional Fire Protection Philosophy vs. Harmathy's Fire Safety Doctrine

Traditional Philosophy		**Harmathy's Doctrine**	
Concept	**Characterization/Mode**	**Concept**	**Characterization/Mode**
Fire Severity	Characterized as Proportional to the Fire Load Density (Ingberg's concept)	*Destructive spread potential*	Characterized through combination of the *fire severity parameters* (e.g. $\bar{q}_E\,\tau$)
Fire Spread	Excessive heat conduction through, or failure of boundary	*Convective spread potential*	Flames and hot gases escaping through doors, ducts, shafts, and windows

1.4.2.2.1.2 Numerical Characterization: Basis of Harmathy's Fire Safety Design

Before envisioning Harmathy's complete 'new' doctrine in fire safety design (section 1.4.2.2.2), it is essential to understand the foundations on which this doctrine and associated approaches are grounded. To this extent, it is explained next how Harmathy characterized both *destructive* and *convective* spread potentials by finding the way to quantify them, such that they could be comparable.

1.4.2.2.1.2.1 Characterizing the potential destructive spread (H^*) - severity

A notable conception proposed by Harmathy [72] and presented already in section 1.4.2.2.1.1.1 was the possibility of characterizing the severity of enclosure fires by a single parameter; i.e. by permanently combining the product of $\bar{q}_E$ and τ as the measure and unique quantifier of *fire severity* in terms of potential for *destructive* spread. The idea was that this product could be recognized as quantifying the total heat absorption per unit surface area of the compartment boundaries during the period of full fire development, irrespective of the temperature history of the fire gases. He referred to it as the overall *heat load*, $\bar{q}_E\,\tau$ [kJ/m^2], on the compartment.

He also made very clear that although the *heat load* can describe the relative severity of fires in a given enclosure, it cannot be used to compare fire severities in different enclosures. A good example presented [6] to explain this fact, is the case of two compartments, one lined with high thermal inertia ($k\rho c$) materials and, opposite, the other lined with low thermal inertia materials. In order to drive the same amount of heat per unit surface area – i.e. the same *heat load*, $\bar{q}_E\,\tau$ – on the boundaries of both enclosures, a much more severe fire (i.e. more energy) is needed in the latter case. This is why, in order to allow for fire severity comparisons of differently lined enclosures, the sole consideration of the *heat load* is not sufficient. To circumvent this issue, Harmathy introduced [6] the concept of *normalized heat load*, H^*, as the heat load referred to the thermal inertia; i.e., the ratio of the heat load to the thermal inertia. The correspondent equation for H^* is then:

$$H^* = \frac{\bar{q}_E\,\tau}{\sqrt{k\rho c}} \qquad \textbf{Equation 1-17}$$

In this way, the *normalized heat load*, H^*, allows for a way to compare the effects of different fires (i.e. different average heat release rates, $\bar{Q}$), on different compartments (i.e., size, shape and ventilation openings, all of these variables accounted for in the *heat load*, $\bar{q}_E\,\tau$), with different lining materials (i.e., different *thermal inertia*, $k\rho c$).

Details on how this value is used in Harmathy's design process are presented in section 1.4.2.2.2.2.

1.4.2.2.1.2.2 Characterizing the potential convective spread (μ-factor)

Harmathy introduced a factor to characterize the potential for convective spread [6], the *μ-factor*, that can be determined once the *fire severity parameters* are calculated. He simply defined it as the following ratio:

$$\mu = \frac{\text{rate of heat evolution outside the compartment}}{\text{total rate of heat evolution from fuel}} \qquad \textbf{Equation 1-18}$$

Details on how this value is used in Harmathy's design process are presented in section 1.4.2.2.2.3.

1.4.2.2.2 Doctrine

Now that Harmathy's elementary panorama of the fire problem has been covered in detail in the previous sections, the backbone where his proposed 'new doctrine' in the design for fire safety relies on can be foreseen.

In a paper presented at the International Symposium Fire Safety of Concrete Structures, in San Juan de Puerto Rico: "Fire Severity: Basis of Fire Safety Design" [6], Harmathy states that the design for fire safety has two well defined components, which are directly equivalent to his definition of *severity* (or *destructive spread potential*) and understanding of the mechanisms of *spread* (or *convective spread potential*) of fires, in contraposition to the conventional philosophy (see Table 1-1). These are:

- countering the *destructive spread potential* of fire, and

- countering its *convective spread potential*.

As a consequence, Harmathy's doctrine is based on four fundamental approaches to overcome both spread potentials. To account for the *destructive spread potential* of a fire, the doctrine relies on:

- reducing the fire severity (Section 1.4.2.2.2.1), and
- the use of fire-resistant compartment boundaries (Section 1.4.2.2.2.2).

In addition, to account for the *convective spread potential* of a fire, the doctrine relies on two proposed methods. These are:

- the *fire isolation* method (Section 1.4.2.2.2.3), and
- the *fire drainage* method (Section 1.4.2.2.2.4).

Hence, Harmathy's entire dogma stands on these four 'columns' – listed above – which are reported in detail in the following sections.

1.4.2.2.2.1 Reducing the fire severity

Pertinent to Harmathy's concepts:

> "The simplest way of improving fire safety is to reduce its destructive potential in the fire cell (space on fire) by ensuring that the fire, if it occurs, will be fuel-surface-controlled, in other words, by using large window areas whenever possible." [1]

This first approach is based on the previous findings by Harmathy that the fully developed period of fuel-surface controlled (i.e. *Regime II*) fires in compartments with typical residential or office occupancy fuel load, is not expected to be longer than 30 minutes [73][74] – typically around 20 minutes [2][36] – and that almost any non-combustible compartment element is capable of resisting the spread of fire for at least 30 minutes [1]. Thus, under the circumstances of a small compartment layout,

Harmathy's own theoretical interpretation of the results of many burnout tests conducted by other researchers [12][20][58][59][60][61], is that it is possible to replace fire resistance requirements with ventilation requirements. He stated the following,

> "The designer is entitled to decide whether to choose between buildings built with small windows and heavy fire-rated walls and floors, and buildings with large windows and lighter non-combustible, non-fire-rated elements". [1]

In addition to relying on the ventilation to reduce the severity, Harmathy proposed to consider designing relatively low ceilings [75], with the intention of decreasing the heat release rate inside the compartment after forcing the flames – to a given extent – to burn outside. He nevertheless realized that this measure creates an increased danger of vertical flame spread along the building façade and, therefore, proposed a method for overcoming this danger through what he called [76][36][1][6][77][66] and patented [78] *flame deflectors* (these are explained in section 1.4.2.2.2.3.3 as part of the strategy to counteract the convective spread potential).

Summarising this appeal, Harmathy suggested to reduce the fire severity by correctly selecting the compartment and openings dimensions, in what he referred to as a *defensive design approach* [75] – as opposed to an *offensive approach* which relies solely in fire protection devices. The basis of the *defensive approach* is committed to decisions made at the architectural design stage, with the objective of not only reducing the fire severity but also minimizing the cost impact of the entire fire protection strategy. This step, however, is the first step in this doctrine towards preventing the spread of fire from the origin compartment to neighboring spaces. The additional steps – namely the use of fire resistant boundaries, the *fire isolation method* and the *fire drainage method* – are detailed in sections 1.4.2.2.2.2, 1.4.2.2.2.3 and 1.4.2.2.2.4, respectively.

It is important to note, once more, that this theoretical approach [75] to reducing the fire severity by means of the ventilation, was developed on the basis of small compartments burnout tests [58][59] but was never validated for large compartments.

1.4.2.2.2.2 Use of fire resistant compartment boundaries

As introduced in section 1.4.2.2.1.2.1, Harmathy quantified the destructive potential of a compartment fire through what he defined as the *normalized heat load* (see Equation 1-17) on the compartment boundaries. Thus, obtaining information on the *normalized heat load* is one of the aims of Harmathy's design process. This consisted of selecting those compartment boundaries which, in standard fire resistance tests, have been proved to be capable of withstanding a *calculated normalized heat load*. To this extent, he performed a series of numerical studies to determine the normalized value of the heat load applied in the course of standard fire tests to various constructions made from the most commonly used building materials. The following figure shows the results of these studies [6]:

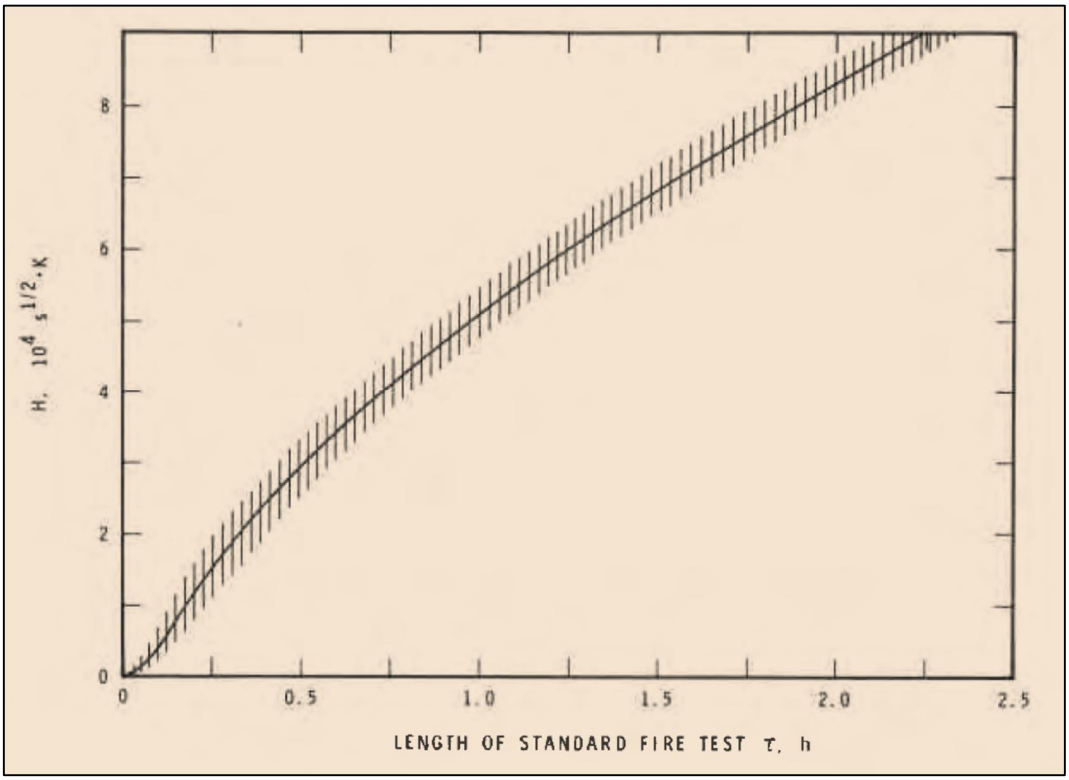

Figure 1-13: The heat load imposed (i.e., H = H^* in the present nomenclature) in constructions in standard fire tests (Fig. 7 from reference [6]**)**

In this graph, the abscissa axis, τ, is interpreted as the period of satisfactory performance in a standard fire test (i.e., the length of fire test in hours), and the lined area reflects the spread due to the differences in the thermal inertia of the materials. Consequently, after calculating the design value of H^* with Equation 1-17 and entering this value in the graph along the ordinate axis (H instead of H^* in this graph due to the present nomenclature), the fire resistance requirement, τ, is found by reading the correspondent value along the abscissa axis. Once more, τ represents the required time of satisfactory performance in a standard fire test; i.e., the classic concept of *fire resistance*.

In this way, Harmathy found a practical way to relate the *normalized heat load* to the abundant results available on the standard fire resistance test, when assessing the fire resistance (or better *flame spread resistance*) of the *dividing* (i.e. secondary in structural terms) and some *key* structural elements. Nevertheless, he emphasised that

extra precautions were necessary with some other *key elements* of the building, clearly referring to those structural elements whose performance cannot be obtained after estimations based on the conventional one-sided exposure standard test results; i.e., those structural elements that could potentially be exposed to fire on both sides. For these *key elements*, he proposed to analyse their specific performance through a different calculation technique [73][74][71].

Finally in this regard, it is important to note that Harmathy admitted [6] that the *overall heat load concept* – i.e. the permanent combination of the product of $\bar{q}_E$ and τ as the measure and unique quantifier of *fire severity* in terms of *potential for destructive spread* – is applicable to reinforced and pre-stressed concrete compartment boundaries and possibly many other types, but is definitely not applicable to unprotected steel constructions.

1.4.2.2.2.3 The fire isolation method

Before seeing the details of this method, it is important to note that although Harmathy described how to characterize quantitatively the *convective fire spread* by means of the *μ-factor* (see section 1.4.2.2.1.2.2), he also emphasized [6] that there was not yet an established method on how to use this value in fire safety design. He simply proposed [6] as an acceptable approach, to require extra measures of countering the *convective spread* of fires (as those described in the following subsections 1.4.2.2.2.3.1, 1.4.2.2.2.3.2, and 1.4.2.2.2.3.3) whenever the value exceeded the suggested specified limit of 0.4, but mainly urged to the use of common sense when assessing the danger of fire spread in each particular situation. As an example of common sense considerations, he illustrated the following scenario [6]:

> "It is obvious that the danger of fire spread is more severe if uncombusted volatiles have a means of entering the inside of a building, for example by a corridor, than if they leave through windows to the outside atmosphere. In high-rise buildings, there is an increased danger that the volatiles will enter the corridors, because the pressure drop in the lower

> storeys during the heating season is directed away from the outside shell of the building toward the major shafts."

With the issue of the lack of a formal method to deal with the *μ-factor* clarified, the *fire isolation* method can now be fully described. The essence of this method is to cut off the two main routes of *convective fire spread* – these are, open doors and broken windows – shown in Figure 1-12(b). To this extent, Harmathy [1] proposed different mechanisms, devices and features which are described next.

1.4.2.2.2.3.1 Self-closing doors

Harmathy argues that due to the large pressure differences that may arise between the fire room and the adjacent non-fire area, it could be difficult – or even impossible – to open the typical hinged doors connecting both spaces. Therefore, he proposes weight-operated, self-closing sliding doors that would technically require less force to open at any pressure difference. This door is depicted in Figure 1-14:

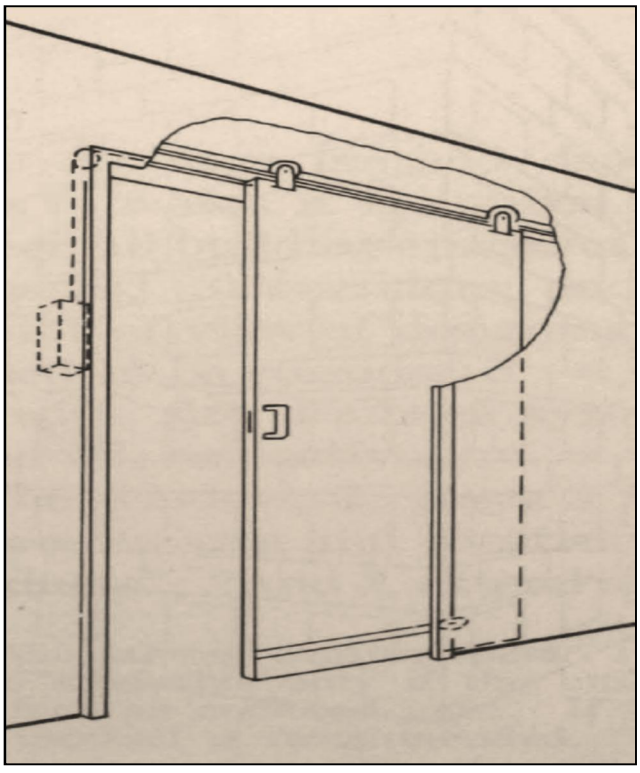

Figure 1-14: Self-closing sliding door (Figure 8 in reference [1]**)**

He also added that these doors must provide at least 30 'real' minutes fire resistance – i.e., not in the sense specified by the fire test standards, but following his duration estimations [73][74][2][36][1] – in order to withstand a compartment burnout, preventing the spread of flames and also preventing or substantially reducing the spread of smoke.

1.4.2.2.2.3.2 Continuous balconies & Open corridors

The main advantage of these architectural features is to avoid the flames climbing vertically from story to story along the facade of the building. Nevertheless, Harmathy was of the opinion [1] that:

> "Unfortunately, their use is rarely considered nowadays even for residential buildings, because they cut down the natural daylight reaching the interior, substantially increase the building costs, and may produce aesthetically undesirable effects."

1.4.2.2.2.3.3 Flame deflectors

The flame deflectors he describes [76][78] are simple devices which could provide the same degree of protection as continuous balconies and open corridors at – he declared – "substantially lower costs and without the aforementioned drawbacks". His description [1] of these devices is the following:

> "… light metal panels mounted above each window and held in a vertical position by a fusible fastening device. They fall down to assume a horizontal position when activated by flames issuing from the window below. Covered with baked-on enamel, or furnished with bronzed, imprinted surfaces, the deflectors may be consciously applied to the building as decorative elements."

Figure 1-15 shows the device:

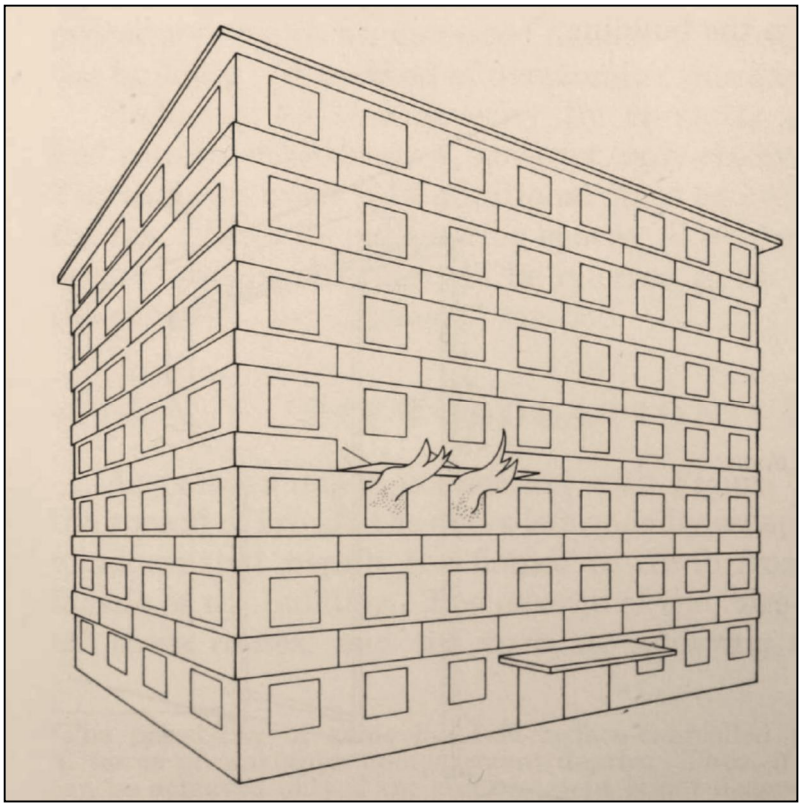

Figure 1-15: Flame deflectors in operation (Figure 9 in reference [1]**)**

Rounding up over this method, Harmathy claimed [1] that it was especially suitable for well-compartmented buildings, using examples of such building like hotels, apartment buildings, and some office buildings. He nevertheless explained that the method was not meant to protect the occupants of the fire compartment but all the other occupants of the building, insisting in that the method not only diminishes the hazard of structural failure but also those of smoke inhalation and reduced visibility due to smoke. Moreover, he even came up with a saving figure – estimated in around 1.5 percent of the building cost – associated with the use of these devices, remarking that the economic analysis only considers the capital costs, and nothing related to insurance premiums or the inhabitants' higher sense of security.

1.4.2.2.2.4 The fire drainage method

1.4.2.2.2.4.1 Introduction

The *fire drainage method* developed by Harmathy [66] claims that if a fire occurs, smoke and fire will be confined to the room of origin and a small section of the corridor adjacent to it. Harmathy also explained [66] that the system can be designed to operate without the use of water and electric energy.

1.4.2.2.2.4.2 Basic description of the method

Contrary to the *fire isolation* method, Harmathy manifests [1] that the *fire drainage* method is applicable to poorly compartmented high-rise buildings. The concept behind this method is to render the fire relatively harmless, by using its own energy in three different ways [1]:

- to draw air into the fire cell in quantities that ensure fuel-surface-controlled conditions (i.e., short fire duration and relatively low fire temperature) and, therefore, relatively low heat load on the cell,
- to keep the pressure in the fire cell below the pressure levels prevailing in the neighbouring spaces, thus hindering the spread of flames and smoke,
- to remove the flames and smoke from the fire cell in a safe and organized manner.

Harmathy explained that the technical details of accomplishing the *fire drainage* method depends on the type of building space to which the method is applied. In this sense, he classified the different building spaces into four different groups:

- rooms,
- uncompartmented spaces,
- corridors, and
- shafts (staircases, elevator shafts, etc.).

In Harmathy's opinion, only the first three groups needed to be considered when designing fire safety measures. And he finally emphasized that, because the fire drainage system was not sensitive to the input information related to the characteristics of the fire, the design could be based on a set of nominal – although realistic – data.

The following figure extracted from reference [1] shows an example of a building equipped with such system:

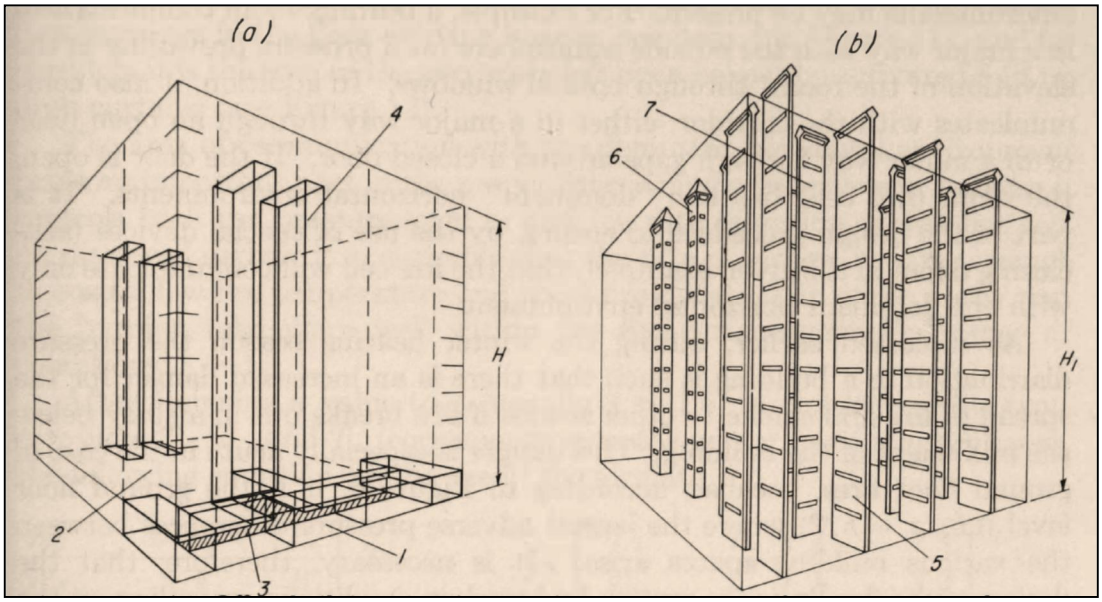

Figure 1-16: Example of a building equipped with a Fire Drainage System (Figure 13 from reference [1]**) (a) Office building and its constituent spaces, 1 – fire rooms on each story, 2 – uncompartmented space on each story, 3 – T-shaped corridor on each story, 4 – shafts. (b) Fire drainage system for the exemplified office building, 5 – six ducts serving the rooms (five on each story, 6 – ten ducts serving the uncompartmented spaces, 7 – two ducts serving the corridors. Additionally, there are access gates on the ducts on each story near the ceiling level, and release gates at the top of each duct.**

1.4.2.2.2.5 Summary of Harmathy's Doctrine

Harmathy's doctrine of designing buildings for fire safety basically relied in two components: design to cope with the spread of fire by destruction of the fire compartment boundaries (*destructive spread potential*), and design to cope with the

fire spread by convection (*convective spread potential*); i.e. by the advance of flames and hot gases out of the compartment of origin. Harmathy was of the idea that the traditional philosophy prescribed fire safety measures only to cope with the former – i.e., ignoring the latter – and, on top of this, in an antiquated way rooted in Ingberg's *L"* vs. fire severity relationship. He believed [66] that building code developers – once aware of the inefficiency of the supposedly 'fire resistant' compartments – prescribed additional requirements (to those ineffective and specifically referred to fire resistance) as 'patches' in an effort to combat the spread of fire through buildings, instead of going back to the beginning and addressing the problem more rationally and holistically.

In his approach to fire safety, Harmathy managed to quantify the destructive potential of a compartment fire through the introduction of the *normalized heat load* concept. In this way, countering the destructive spread potential of a fire in his doctrine consists of selecting those compartment boundaries (secondary and some key structural elements) which, in standard fire resistance tests, have been proved to be capable of withstanding the calculated *normalized heat load* [6]. With certain relevant key structural components, a different calculation technique [73][74][71] is available to analyse their specific performance.

In regards to accounting for the convective potential, Harmathy quantified it through the design value of what he called the *μ-factor*. In the absence of an agreed-upon tolerance level, it is up to the designer (with strong background in fire safety engineering) to establish the need for countermeasures. These could be either or all of the following: self-closing doors, flame deflectors and/or fire drainage.

All in all, Harmathy's doctrine supports the idea that certain aspects of fire safety that traditionally where established by the code, could now be provided by a qualified building designer.

The following table summarizes the main characteristics of Harmathy's doctrine:

Table 1-2: Summary of Harmathy's Fire Safety Doctrine

Concept	Characterization/Mode	Quantification	Countermeasures
Destructive spread potential	Characterized through combination of the *fire severity parameters* (e.g. $\bar{q}_E\ \tau$)	*Normalized heat load (H^*)* *Double-fire exposure technique*	**Defensive approach** (reduce fire severity) **Fire** ('flame spread') **resistant boundaries**
Convective spread potential	Flames and hot gases escaping through doors, ducts, shafts, and windows	*μ-factor*	**Fire Isolation Method** ▪ Self-closing doors ▪ Flame deflectors ▪ Open corridors ▪ Open balconies **Fire Drainage Method**

1.4.3 Summary

After going through Thomas' and Harmathy's interpretation and application of the *classic compartment fire framework* – for the most forged by them – it comes clear that while they had some differences, they agreed upon the most important concepts of the discipline and had the same vision towards the future of it.

They both were scientific researchers (not practitioners) and as such, they exposed – and long argued on – several scientific differences like, for example, considerations on the thermal feedback [79] and derivation of the relationship between the burning rate and the air inflow into a compartment in the fully-developed stage [80].

They both were focused on the translation of research into practice; i.e., on providing the building designer with practical information, and agree upon the idea (the same as Margaret Law [81]) that the designer is not so much interested in the behaviour of the fire itself but on the consequences that behaviour might have on the building (e.g., fire severity and other fire-related problems). Nevertheless, they also had evident differences in their design approaches: while Thomas provided separate simple correlations more prone to be used towards the structural impact of the fire and performance of the building, Harmathy went a step further in providing a methodology that in principle simplifies the design process to the designer, and that addresses more than just the fire severity.

They both agree on the importance of making the most (i.e., related to actual fire behaviour in the best way possible) of the extensive database gathered on past fire tests results: Thomas (and Margaret Law [81]) through the concept of 'effective fire resistance', while Harmathy through the concept of 'normalized heat load' [6].

But the most transcendental resemblance between these two *fathers* of fire safety engineering is their conceptual approach to the discipline. They both believed and made considerable effort in providing a rational framework in contrast to listed regulations. Their views on this matter provided the founding basis to the actual performance based design approach. Thomas declared:

> "…Control based on objective assessment rather than on long-term accumulation of experience also permits more rapid assimilation of new and improved building methods and materials." [34]

And further to this declaration set the goal of the W14 working body – as its active convenor – as that of "prescribing more rationally the levels of protection to meet the objectives like in the chemical and atomic energy industries."[67].

Following the same line, Harmathy was a true believer that the advances in fire science already at that time "…made it possible that decisions on certain aspects of

fire safety, traditionally made by writers of building codes, can now be made by the building designer."[6]. He summarised:

> "An organized society is inconceivable without a system of laws which, if necessary, restrict the freedom of the individual in the interest of the community. History has proved, however, that the progress of mankind is best served if restrictions are kept to a minimum and the individual is left with a great degree of freedom in finding his own approach to the solution of problems. Competition of ideas is the essence of progress." [82]

And coined the concept – today referred to by many code writers (e.g. NFPA) – that regulations are the minimum indispensable or absolutely necessary in the interest of public safety and not the maximum, pushing the idea of going beyond the level of safety attainable by simple code compliance (implying savings and not extra expenditures).

In addition to the closeness in the rational framework concept, they agreed on the relevance and benefits of including fire engineering from the very beginning of any given project. Thomas and Harmathy stated, in this regard and respectively, the following:

> "The main practical design problem is to exploit the appreciation of the fire problem so that fire safety is considered at the earliest stage of planning a building, rather than something to be introduced when the building is near final approval or even in some cases after it has been built." [67]

> "It is extremely important to realize that fire safety is not something to be "added on" after the completion of the plans for a building. To be really effective the problem of fire

> safety must be considered from the beginning of the architectural design. Real progress toward achieving fire safety cannot come until it is clearly understood that the time when a building was regarded as a passive mass for providing shelter, passed a long time ago. A modern building is a machinery of multiple functions. Defense against fire is one of the functions of this machinery." [1]

It is therefore evident that their similarities – especially in the vision of the discipline – stand out as being more important than the technical differences they exhibited in addressing certain specific scientific problems.

Their legacy – being concepts, correlations and methods – is an extremely valuable endeavour which not only can still be used for design purposes provided it is used within their true range of validity, but also can serve as the foundations for a comprehensive approach to contemporary fire safety engineering, supported with further theoretical and experimental research.

1.5 Forward to the Modern Day

In 1998 the SFPE Task Group on Fire Exposures to Structural Elements chaired by Prof. J.G. Quintiere started to develop the SFPE Engineering Guide for Fire Exposure to Structural Elements that was finally published in 2004 [7]. This guide provides a comprehensive review of the different methods – models and correlations – used in the calculation of how fires thermally affect structures. This guide was followed in 2011 with the SFPE Engineering Standard on Calculating Fire Exposures to Structures [83] developed by SFPE Standards-Making Committee on Calculating Fire Exposures to Structures chaired by J. K. Richardson. The SFPE Engineering Standard draws on the information of SFPE Engineering Guide to provide a method that enables the engineer to establish the evolution of the thermal boundary condition for a structure subject to a fire. Given a well-defined set of boundary conditions, the evolution of the transient temperature distribution of a structure can be established by means of a heat conduction analysis [29][34][2][83][36][1][75][84]. These

temperature distributions are then used as inputs for a structural analysis that determines the performance of a structural system in fire [84][85]. There are other methods available in the literature [86][87][88][89][90], nevertheless, not as comprehensive as the SFPE Guide and Standard together.

Peatros and Beyler [91] studied the effects of natural and forced ventilation on full-scale compartment fires, using wood cribs, diesel and polyurethane slabs. They reported a linear proportionality between the burning rate and the reduced oxygen concentration at the flame base, as well as what they referred to as a *well-mixed* condition in all the tests comprising forced ventilation.

Kumar and Sharma [92] studied the effects of cross ventilation on the burning rate and gas temperatures in compartments with ventilation opening located in opposite walls, and compared the results to those found in single ventilation compartments. The experiments were conducted in a fire clay brick compartment of size 2.55 x 2.0 m in floor area and 1.50 m internal height with. The temperatures found in cross ventilation conditions were found to be higher than those in single ventilation conditions.

Several other studies [10] have been recently carried out at the University of Maryland by various authors in small-scale cubic compartments burning heptane in various ventilation configurations. Various results and comparisons to zone and field models were reported.

In parallel to the development of correlations, design methods, and zone models, significant advances in the development of Computational Fluid Dynamics (CFD) models for fire applications have been reported. These field models allow a significant level of refinement – after solving the fundamental conservation laws in three dimensions – that enables a much more detailed treatment of the thermal boundary conditions for the structure. Successful applications have populated the literature in the last 10 years [93][94]. CFD has a fundamental role in enabling better understanding of the physical processes [95] but it is recognized that there are still many uncertainties in the models. In what concerns the use of CFD for design, the

utilization of the models can be too complex to be practical for main stream design and the drastic differences between solid and gas phase time scales do not necessarily justify the level of precision brought by the utilization of CFD [96].

1.6 Preliminary Observations and Conclusions

Summarising, essentially four streams of research – in Japan lead by Kawagoe *et al.*, in the UK lead by Thomas *et al.*, in Sweden lead by Pettersson *et al.*, and in North America lead by Harmathy *et al.* – set the physical basis and behavioural trend for the conceptual *classic compartment fire framework*, still used today. While numerous studies have been conducted after these seminal studies, the framework still remains.

Kawagoe *et al.* [12] made the initial breakthrough linking burning rate in a compartment to ventilation. Thomas [29] added the most significant advance on this theory showing that, while this relationship is true for a range of conditions, (*Regime I*), there is a second set of conditions (*Regime II*) whose fire dynamics were never deciphered as comprehensively. While *Regime I* corresponded to the typical, idealised experimental setups so many of the researchers adopted, *Regime II* is characteristic of open spaces and volumes, typical of 20th Century architecture and continually increasing in prevalence to the present day.

Two of the early pioneers, Thomas and Harmathy, provided unique interpretation and application of the *classic compartment fire framework*. While Thomas provided separate simple correlations more prone to be used towards the structural impact of the fire and performance of the building, Harmathy went a step further in providing a methodology that in principle simplifies the design process to the designer, and that addresses more than just the fire severity. Both realised though that the real benefit of their contributions was in their utilisation for transcending regulation based fire safety engineering and thus, they are also the forefathers of performance based design. Both were careful however to acknowledge the limitations of their methodologies and insist that practitioners utilising them be fully aware of their theoretical and experimental basis.

Finally, both championed the continued research and translation to extend the relevance and range of application of the compartment fire framework to keep step with contemporary architecture.

1.7 Aims – Scope of Project

This research project addresses the current applicability limitations of the *classic compartment fire framework*, through a review of classic literature and standing theory on which existing design methodologies are based.

Through the consideration of potential framework extensions and some recent small and large-scale experiments presented, this dissertation aims to evidence the areas where further research is necessary, and initiate the discussion towards the introductions of a new look at the fire problem in the contemporary built environment.

1.8 Chapters Overview

Chapter 2: The Compartment Fire Framework

Chapter 2 introduces the problem of *the compartment fire* in its full complexity before discussing some simplifications typically assumed when representing or simulating the actual problem. The simplified expressions of the flow model that lies beneath the *classic compartment fire framework* are developed first, followed by the derivation of the resultant characteristic velocities in representative fire scenarios.

Chapter 3: Range of Validity of the Compartment Fire Framework - Empirical Design Limitations

Chapter 3 presents a detailed background of the CIB Programme – decisive in the development of the *classic compartment fire framework* – on which many design methodologies are based still to this day. More recent large-scale tests are also presented together with other empirical methodologies to contrast and discuss some of the most relevant empirical results from the CIB Programme, and clarify the limitations of those existing design methods based on the *classic compartment fire framework*.

Chapter 4: Range of Validity of the Compartment Fire Framework - Theoretical Design Limitations

Chapter 4 consists of a review of the classic and typical assumptions which are a direct consequence of the simplifications introduced to the *flow model* presented in Chapter 2, and form the basis of many existing theoretical design methodologies. In doing so, this chapter aims to clarify the theoretical limitations of said methodologies and the areas where further research is necessary.

Chapter 5: Filling the Gaps with Theory

Chapter 5 presents an elaborated – though based on simple analytical formulations – theoretical *compartment fire framework*, inclusive of the *classic* one, and aiming to broaden the envelope of applicability to encompass and enable the design of contemporary architectural layouts. Through the exploration of the range of combinations of characteristic length scales, a scaling analysis is used to identify the governing flow mechanisms within, into and out of the compartment, and thus establish a more complete set of *regime of behaviour* definitions.

Chapter 6: Filling the Gaps with Experiments

After exploring the *classic compartment fire framework* simplifications (Chapter 2), its range of validity and associated design limitations (Chapters 3 and 4), and after attempting to encompass the present-day layouts with simple analytical formulations (Chapter 5), it is evidenced that a range of potential regimes of behaviours – particularly relevant in contemporary architecture layouts – is not characterized by the *classic framework* leaving an open gap. Chapter 6 presents a series of small and large-scale tests designed to start filling empirically this gap of knowledge, towards a *comprehensive compartment fire framework*.

Chapter 7: Overall Conclusions

The most relevant specific conclusions arrived and discussed at each of the previous chapters are summarized and listed in this final chapter, together with the more general conclusions presented from a practical perspective.

2 Chapter 2: The Compartment Fire Framework

2.1 Introduction

T.Z. Harmathy [79] observed that:

> "Fires are extremely complex processes involving hundreds of identifiable and incidental variables, so any attempt to model them mathematically will invariably be poor."

Nevertheless, when treating the theoretical problem with sufficient accuracy, simple mathematical approaches can be extremely informative and frequently serve as the background to much more complex computer-based methodologies [97]. In this context, the present chapter briefly introduces the problem of the compartment fire in its full complexity before discussing some simplifications typically assumed when representing or simulating the actual problem.

The *flow model* stands as the *classic compartment fire framework* backbone and most notable simplification, thus, the general expressions beneath it are developed first, followed by the application of these to representative scenarios in order to derive the resultant characteristic velocities in each – key in the understanding of the *compartment fire framework* and instrumental in any attempt to extend it.

2.2 Complexity Overview of Compartment Effects

Before discussing the flow model and the simplifications involved, the following section briefly presents the complexity brought about by the introduction of the compartment to a fire scenario, discussing the interactive, circular nature of the problem linking the combustion, gas flow and energy exchanges.

In open or natural fires, once the combustion process of a condensed fuel (i.e. solid or liquid) is triggered and a flame is ignited, the fuel is gasified at a rate – the so-called burning rate, R – that is determined by the heat supply to the fuel bed. This energy supply comes from the flame's heat feedback and other heat sources like, for example, the oxidation of char in the case of cellulosic fuels. The heat generated by

the fire results in buoyant entrainment of air. This entrainment delivers oxidizer towards the fuel, and the relative quantities of fuel and oxidizer define the location and characteristics of the flame.

As introduced briefly in relation the burning rate and basic behaviour (Section 1.3.2), the presence of a compartment alters the relationship between the fire and its environment: heat exchange between the surrounding solids (walls/ceiling), hot gas layer, fuel and the flames occurs, as well as variations in the pressure fields that drive the air entrainment into the compartment and ultimately into the fire base and along the fire plume.

Walls receive heat from the fire and as they heat up, they enhance the heat feedback which potentially results in an enhanced burning rate. Further, the walls surrounding the fire restrict the surface area for entrainment and, thus, change the pressure field. Depending on the position and number of walls, the pressure field can be changed creating privileged entrainment and potentially tilting the flames with the consequent variation in the heat exchange process. Further, if a ceiling above the pool fire is introduced, the plume will be deflected creating a ceiling jet that will heat up the ceiling, which will feedback heat to the fuel bed and, thus, will also potentially affect the burning rate. Moreover, the air entrainment into the deflected flame is reduced by limiting the vertical dimension, thus, affecting the pressure field that will potentially change the nature of the plume [98].

If the geometry allows for hot combustion products accumulation in the upper end of the compartment, this further reduces the plume entrainment area, once more changing the pressure field and affecting the characteristics of the flames. Thus, the nature of this accumulation depends on the size and characteristics of the fire but also on the geometry of the compartment. Finally, if the compartment (i.e. walls and ceiling) fully encloses the fire tightly, the evident boundary-fire proximity will have an important impact on both the fire evolution and the compartment, due to the enhanced heat transfer exchange between them. The magnitude of the openings, the dimensions of the compartment, and the thermal properties of the inner surfaces will

define the nature of the fire and its evolution in time. In short, enclosures tend to conserve heat and restrict air supply [25].

2.3 The Model Simplification

2.3.1 Introduction

Models are intended to represent or simulate some aspects of reality. It is common for them to hypothesize and assume simplifications in order to overcome the typical complexity inherent in real problems and instead focus on generating solutions of sufficient accuracy with respect to the problem being addressed.

The mathematical modelling of compartment fires started by developing engineering correlations like, for example, that from Kawagoe [12] (Equation 1-2), and went all the way to computer-based models that consider and solve the interaction of many variables. The latter – in its more comprehensive and complex version – is based on solving the conservation equations for mass, species, energy and momentum to different control volumes. In order of complexity, field models solve the equations in every cell within the computational domain, while two-zone models and one-zone models solve them (without considering the momentum equation) for a few relatively large, and a single control volume, respectively.

With ventilation being amongst the most important variables in a compartment fire, an extremely basic explanation of how to obtain simple expressions for vent flows is presented here. These flows can be obtained in a simplified way by modelling the energy conservation in the control volume of interest. This derivation process serves to further expose the assumptions adopted behind the simplified theoretical zone model used to describe the velocities and consequent volumetric and mass flow rates of fresh air entering, $\dot{m}_{in}$, and hot gases exiting, $\dot{m}_{out}$, a compartment in fire (Section 2.3.4).

2.3.2 Energy Conservation in a Control Volume

The *principle of conservation of energy* is crucial in setting out any theoretical problem regarding a compartment in fire. *Bernoulli's Principle* can be derived from the former, which states that in a steady flow the sum of all forms of mechanical

energy in a fluid along a streamline is the same at all points on that streamline. This requires that the sum of kinetic energy and potential energy remain constant. If the fluid is flowing out of a reservoir – in this case a compartment – the sum of all forms of energy is the same on all streamlines because in a reservoir the energy per unit volume, E, is the same everywhere. This means that an increase in the velocity, u_i, of the fluid (kinetic energy) occurs simultaneously with a decrease in the static pressure, P_i (internal energy), or a decrease in the fluid's potential energy [99].

Thus, by applying the *principle of conservation of energy* to a flowing fluid assuming no viscosity and an incompressible fluid – incompressible meaning that even though the pressure varies, the density remains constant along a streamline; i.e. there are no deformations of the fluid particles –*Bernoulli's Equation* is derived with the help of the following sketch:

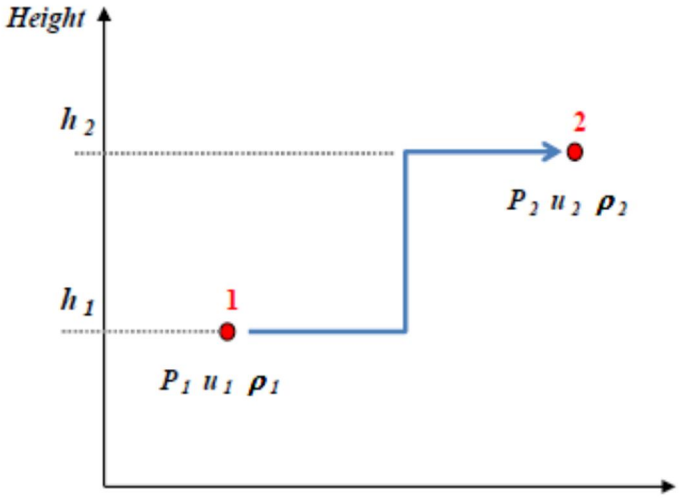

Figure 2-1: The *Bernoulli Principle* sketched

$$P_i + \frac{1}{2} u_i^2 \rho_i + g\, \rho_i\, h_i = const. \qquad \textbf{Equation 2-1}$$

Or simply,

$$P_1 + \frac{1}{2} u_1^2 \rho_1 + g\, \rho_1\, h_1 = P_2 + \frac{1}{2} u_2^2 \rho_2 + g\, \rho_2\, h_2 \qquad \textbf{Equation 2-2}$$

Where,

P_i = static pressure (internal energy per unit volume – associated to the fluid's state), Pa

$½\ u_i^2\ \rho_i$ = hydrodynamic pressure (kinetic energy per unit volume – associated to the fluid's motion), Pa

$h_i\ \rho_i\ g$ = hydrostatic pressure or gravitational potential (potential energy per unit volume – associated to the fluid's elevation), Pa

Equation 2-2 gives the *theoretical net energy balance* of an incompressible fluid at any point along its flow path, and expresses the relationship between the pressure, P_i, and velocity, u_i, within an incompressible fluid flow [99]. This relationship is fundamental at the time of expressing the inflow of fresh air into, $\dot{m}_{in}$, and the outflow of hot gases out of, $\dot{m}_{out}$, the compartment. These mass flow rate expressions are further developed in the next section (Section 2.3.3).

Further, the hydrostatic pressure or gravitational potential is the pressure exerted by the weight of a column of gas or liquid [99]. Fiscally, this would be the force applied by its mass (i.e., its weight) divided by the area over which the force is applied:

$$P_{hydrostatic,i} = \frac{\vec{F}}{A_i} = \frac{mg}{A_i} = \frac{(V\rho_i)g}{A_i} = \frac{(h_i A_i)\rho_i g}{A_i} = g\ \rho_i h_i \qquad \textbf{Equation 2-3}$$

Where,

$\vec{F}$ is the force applied by the fluid – its weight (typically in N);

m is the mass of the fluid (typically in kg);

g is the acceleration due to gravity (typically in m/s^2);

V is the volume of the fluid (typically in m^3);

ρ_i is the density of the fluid (mass per unit volume, typically in kg/m^3);

h_i is the given height at which the pressure difference is assessed (typically in m);

A_i is the area over which the pressure is assessed (typically in m^2);

$P_{hydrostatic,i}$ is the hydrostatic pressure difference (typically in Pascals).

Finally, the constant in the *Bernoulli Equation* can be normalized so, instead of pressures in Pascals, the equation represents *heads* in meters, a very commonly used term in fluid mechanics and by extension in assessing compartment fire phenomena. *Pressure head* represents the energy of a fluid due to the pressure exerted on its container, and it is mathematically expressed as:

$$\Psi = \frac{E}{g\,\rho_i} = \frac{E}{\gamma}$$ **Equation 2-4**

Where,

Ψ is total or energy pressure head (length, typically in m);

E is fluid total energy per unit volume (force per unit area, typically in Pa);

ρ_i is the density of the fluid (mass per unit volume, typically in kg/m^3);

g is acceleration due to gravity (rate of change of velocity, typically in m/s^2);

γ is the specific weight (force per unit volume, typically in N/m^3).

Therefore, a common approach to represent the *Bernoulli Principle* (Equation 2-1) is in terms of *total head or energy head*, Ψ, obtaining the following equation:

$$\Psi = \frac{E}{g\,\rho_i} = \frac{P_i}{g\,\rho_i} + \frac{u_i^2}{2g} + h_i$$ **Equation 2-5**

Where,

$P_i/\rho_i\,g$ = static pressure head, m

$u_i^2/2g$ = hydrodynamic pressure head, m

h_i = hydrostatic pressure head, m

2.3.3 General Expressions

The first attempt to model the fluid mechanics of a compartment in fire was presented by Kawagoe in 1958 [12]. His model assumed that the temperature inside the burning compartment was uniform and that the air inflow and gas outflow through the opening were induced by a static pressure field created by the difference in temperature and density between the uniformly hot inner gases and the uniformly cold outer atmosphere. Kawagoe elaborated [12] the pressure and velocity profiles at the opening plane based on the *principle of energy conservation* in the moving fluids, by means of the *Bernoulli Equation*.

The following sketch depicts the situation of a compartment interior (1) fully filled with stagnant hot gases at a certain uniform temperature, T_g, and density, ρ_g, and connected to the also stagnant exterior ambient atmosphere (2) at a lower temperature, T_a, and thus higher density, ρ_a, through an opening (3). Due to a mass balance demand, the hot gas layer flowing out through the upper part of the opening forces the cold external air to flow in through the lower part of it.

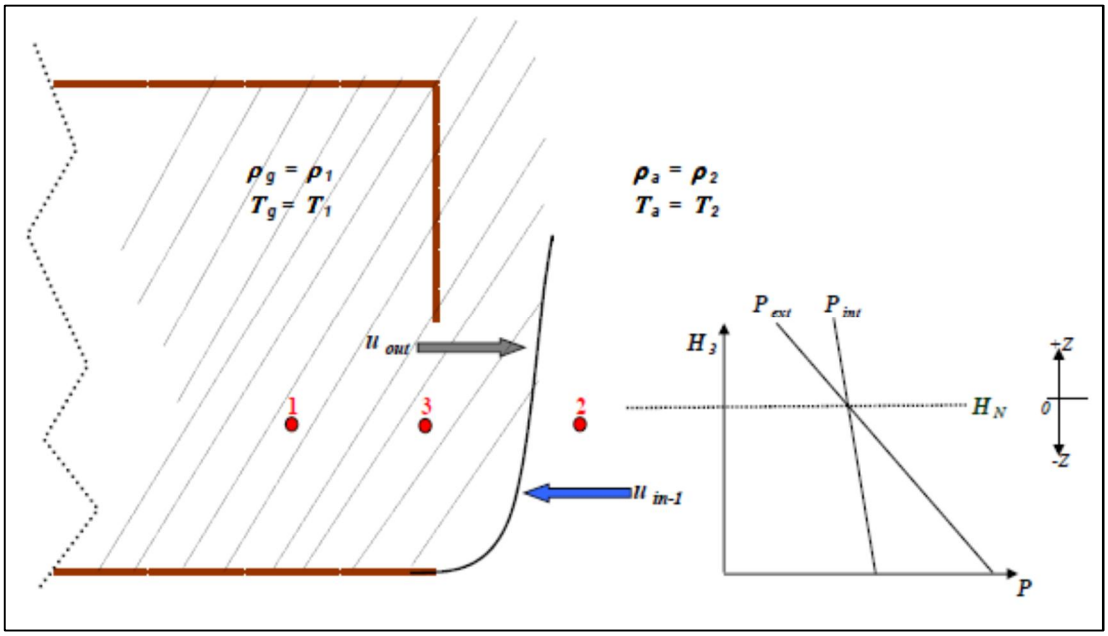

Figure 2-2: Compartment fire sketch for Bernoulli application

Figure references:

***H* = H_3 = opening height**
***N* = H_N = neutral plane height**
P_{ext} = atmospheric (external) pressure profile
P_{int} = internal pressure profile
$T_a = T_2$ = ambient (external) temperature
$T_g = T_1$ = gas (internal) temperature
$\rho_a = \rho_2$ = ambient (external) density
$\rho_g = \rho_1$ = gas (internal) density

Therefore, applying *Bernoulli* at a given height in an interior (1) and exterior (2) point – i.e. no velocities in either of them – this situation can be described as:

$$P_1 + g\,\rho_1\,h_1 = P_2 + g\,\rho_2\,h_2$$ **Equation 2-6**

Being $h_1 = h_2$, we obtain the final expression for the *hydrostatic* pressure difference, between the ideal compartment interior in post-flashover conditions filled with hot gases, and the exterior ambient atmosphere:

$$\Delta P_{hydrostatic} = P_1 - P_2 = g\left(\rho_2 - \rho_1\right)h = g\left(\rho_a - \rho_g\right)h$$ **Equation 2-7**

Next, the *hydrodynamic* pressure difference is the pressure difference caused by a static pressure head, P_i, across an opening at a given height, where a volume of fluid goes from being at rest to having a velocity, u_i.

Again, applying *Bernoulli* at a given height in the same sketch, in an interior/exterior point (1 or 2; i.e. with no velocity) and a point in the opening (3; i.e. with velocity), gives the following:

$$P_1 + g\,\rho_1\,h_1 = P_3 + \frac{1}{2}u_3^2\rho_3 + g\,\rho_3\,h_3 \qquad \textbf{Equation 2-8}$$

Taking into account that being $h_1 = h_3$ and $\rho_1 = \rho_3$, the final expression for the hydrodynamic pressure difference at a given height above the neutral pressure plane, between this compartment in fire and the external atmosphere, is:

$$\Delta P_{hydrodynamic} = P_1 - P_3 = \frac{1}{2}u_3^2\rho_3 = \frac{1}{2}u_{out}^2\,\rho_g \qquad \textbf{Equation 2-9}$$

When a fluid is put into motion, the hydrostatic pressure is fully converted into hydrodynamic pressure and, therefore, they must be equal. Thus,

$$\Delta P_{hydrostatic} = \Delta P_{hydrodynamic} \qquad \textbf{Equation 2-10}$$

This is the physical concept beneath the vent flows induced in the situation of a heated compartment; i.e., when almost stagnant masses of hot and cold gases reach the opening plane connecting the compartment with the external atmosphere. The concept defines the *ventilation mode* of the compartment fire, one of the most relevant variables in defining the whole fire problem. Therefore, combining Equation 2-7, Equation 2-9, and Equation 2-10:

$$g\left(\rho_a - \rho_g\right)h_i = \frac{1}{2}u_{out}^2\,\rho_g \qquad \textbf{Equation 2-11}$$

Working out the velocity of the exiting hot gases at that given height, h_i, the following expression is obtained:

$$u_{out} = \sqrt{2g\left(\frac{\rho_a - \rho_g}{\rho_g}\right)h_i} \qquad \textbf{Equation 2-12}$$

This would be for an upper vent above the neutral pressure plane, H_N, at a height h_i, and at an assumed positive flow out.

For a lower vent at a different height h_i – this time below the neutral pressure plane and at an assumed positive flow in – a similar expression is obtained:

$$\Delta P_{hydrostatic} = \Delta P_{hydrodynamic} \qquad \textbf{Equation 2-13}$$

$$g\left(\rho_a - \rho_g\right)h_i = \frac{1}{2}u_{in}^2\,\rho_a \qquad \textbf{Equation 2-14}$$

$$u_{in} = \sqrt{2g\left(\frac{\rho_a - \rho_g}{\rho_a}\right)h_i} \qquad \textbf{Equation 2-15}$$

The coordinate system could be defined so that the flow into the enclosure is negative and vice versa.

Summarizing, from basic fluid mechanics and the application of the *Bernoulli Principle* to the flow through an orifice (in this case represented by the compartment's opening), Kawagoe [12] expressed the velocity of flow through said opening in terms of the hydrostatic pressure as:

$$u_i = \sqrt{\frac{2\Delta P_{hydrostatic}}{\rho_i}} \qquad \textbf{Equation 2-16}$$

In 1967, Thomas *et al*. [29] further elaborated Kawagoe's theoretical static pressure field model finding expressions for the volumetric, $\dot{V}$, and mass, $\dot{m}$, flow rates. These were expressed as:

$$\dot{V}_i = c_d A_i \; u_i = c_d A_i \sqrt{\frac{2\Delta P_{hydrostatic}}{\rho_i}} \qquad \textbf{Equation 2-17}$$

$$\dot{m}_i = \rho_i \dot{V}_i = \rho_i c_d A_i \sqrt{\frac{2\Delta P_{hydrostatic}}{\rho_i}} = c_d A_i \sqrt{2\Delta P_{hydrostatic} \;\; \rho_i} \qquad \textbf{Equation 2-18}$$

Where A_i is the cross-sectional area of the opening (m^2), ρ_ι is the density of the intervening fluid, and c_d is an appropriate discharge coefficient for the opening (dimensionless). The latter is indeed a correction factor generally known as the *orifice flow coefficient* as used in pipe flow analysis, which primarily accounts for the decrease in the cross-section (*vena contracta* in orifice flow) but also takes some account of the acceleration and the friction between the two streams.

2.3.4 Characteristic Scenarios

Now that the general expressions for velocity, u_i, pressure difference, ΔP, and mass flow, $\dot{m}_\iota$, have been derived, they can further be applied to the different forms of the quasi-steady layer model in order to express the resultant velocities for a selection of characteristic scenarios.

2.3.4.1 One-Layer or *Regime I* Scenario

The first case treated is basically what Kawagoe described in the first theoretical flow model [12] depicted previously in Figure 2-2, and reproduced here for clarity:

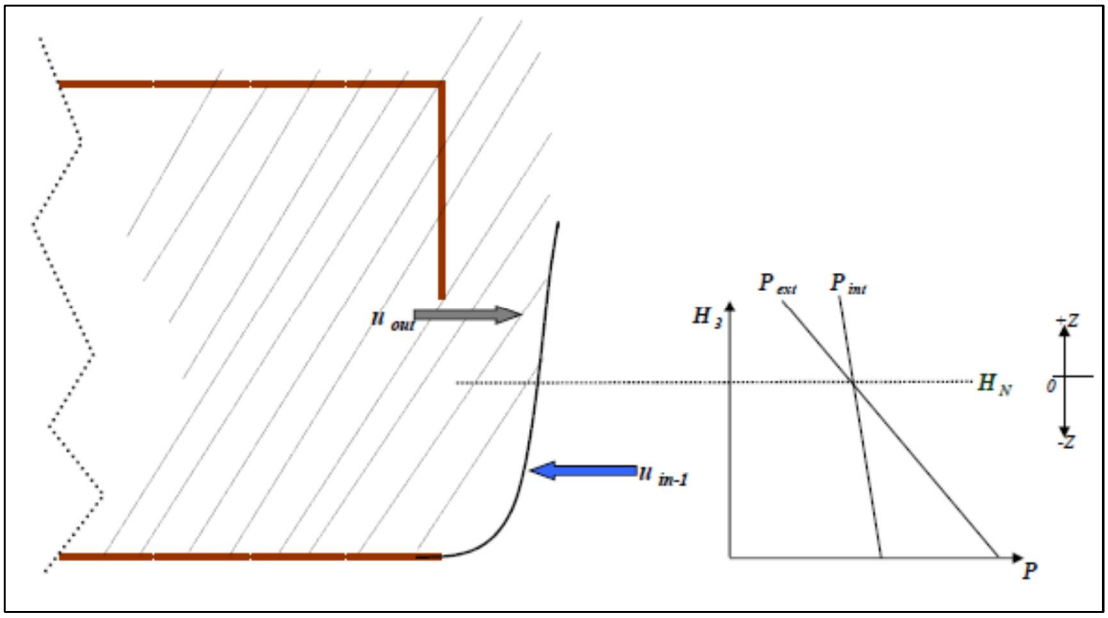

Figure 2-3: Classic One-layer Case

Figure references:

Same as references in Figure 2-2, plus
H_D = clean layer height (cero in this case)

In this case, the hot layer reaches the floor level giving as a result a single-layer condition – the so-called one-layer flow model.

Assuming that the gases – cold air and hot products of combustion – are frictionless, incompressible, and motionless inside and outside the compartment but flowing in the surroundings of the opening, the *principle of conservation of energy* can be applied to either layer of flowing fluid – by means of the *Bernoulli Equation* – to find the expressions for the pressure differences and velocities associated to these pressure gradients, as it was made clear in the previous section (Section 2.3.3).

Thus, using the expression for the *hydrostatic* pressure difference deducted before (Equation 2-7), above the neutral pressure plane, H_N, along the entire characteristic length z – i.e., along the outflow height $0 < z < (H_3 - H_N)$ – the maximum pressure difference would be:

$$\Delta P_{up,MAX} = g\left(\rho_a - \rho_g\right)\left(H_3 - H_N\right)$$ **Equation 2-19**

Below H_N, there is one characteristic length – i.e., along the inflow height $0 < z_1 < (H_N - H_D)$ – along which there is a linear pressure difference that causes entrainment of fresh air. Being $H_D = 0$, the maximum pressure difference below the neutral plane would be:

$$\Delta P_{low-1,MAX} = g\left(\rho_a - \rho_g\right)H_N$$ **Equation 2-20**

Therefore, it comes clear that, after assuming uniform temperatures in both inner layers and outer atmosphere, the resulting pressure profile is a function of the correspondent height; in other words, its magnitude is different at each given height.

Now, using the expression for the *hydrodynamic* pressure difference deduced before (Equation 2-9), the expression for the exit gas velocity, u_{out}, can be worked out as:

$$u_{out} = \sqrt{\frac{2\Delta P}{\rho_g}}$$ **Equation 2-21**

In an analogous way, the expression for the inflow air velocity below the neutral plane, u_{in}, is worked out as:

$$u_{in} = \sqrt{\frac{2\Delta P}{\rho_a}}$$ **Equation 2-22**

Equalizing the *hydrostatic* and *hydrodynamic* pressure differences at the opening, the expression for the maximum exit gas velocity – above the neutral plane – and for the maximum inflow air velocity – below the neutral plane – are obtained:

$$u_{out,MAX} = \sqrt{2g\left(\frac{\rho_a - \rho_g}{\rho_g}\right)\left(H_3 - H_N\right)}$$ **Equation 2-23**

$$u_{in-1,MAX} = \sqrt{2g\left(\frac{\rho_a - \rho_g}{\rho_a}\right)H_N}$$ **Equation 2-24**

So far, the model solely describes the situation of a fully and uniformly heated enclosure in connection to and contrasted against a uniform temperature external atmosphere, where there are two different maximum characteristic velocities caused by the hydrostatic pressure field. This case is representative of what Thomas *et al.* [34] defined as *Regime I* fully-developed fire behaviour.

2.3.4.2 *Regime II* Scenario

Further, in the same publication Thomas *et al.* [34] defined a different regime of behaviour: *Regime II*. In this case, the compartment does not allow for a hot layer build-up or gas accumulation. Therefore, being that there is no pressure differential field, those velocities which are a function of the characteristic length *z* do not exist. Schematically, this is represented as follows:

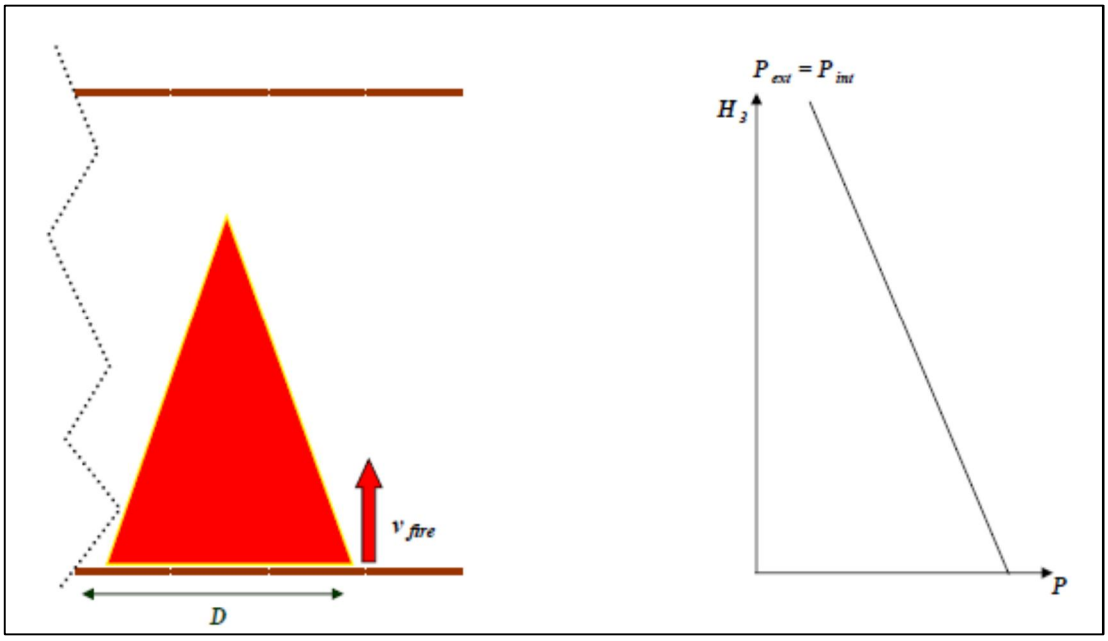

Figure 2-4: Characteristic Velocity in a Fully-Vented Compartment Situation (idem Open Fire Situation)

The only characteristic velocity in this representative configuration is the maximum fire entrainment velocity; i.e., that powered by the pressure difference created by the fire itself. The characteristic length in this case is then the fire diameter, *D*, so that the maximum pressure difference is expressed as:

$$\Delta P_{fire,MAX} = g\left(\rho_a - \rho_g\right)D \qquad \textbf{Equation 2-25}$$

Therefore, the maximum fire entrainment velocity can be expressed as:

$$v_{fire,MAX} = \sqrt{2g\left(\frac{\rho_a - \rho_g}{\rho_a}\right)D} \qquad \textbf{Equation 2-26}$$

One of the underlying assumptions in Harmathy's 1972 extensive review of fully-developed compartment fires [2] was the flow model and consideration of these two regimes of behaviour.

2.3.4.3 Two-Layer Scenario

In 1975, the flow model was further refined by Prahl and Emmons [48] who added a second uniform cold layer beneath the uniformly hot gas layer located at ceiling level, in what is known as the *quasi-steady two-layer model*. This final version of the theoretical flow model – which was further adapted for each of the different stages that typically describe the evolution of a compartment fire in the literature [100][90] – is the one used still to this day. In this case, the opening size and location with respect to the ceiling level allow for the build-up of a hot gas layer beneath the ceiling:

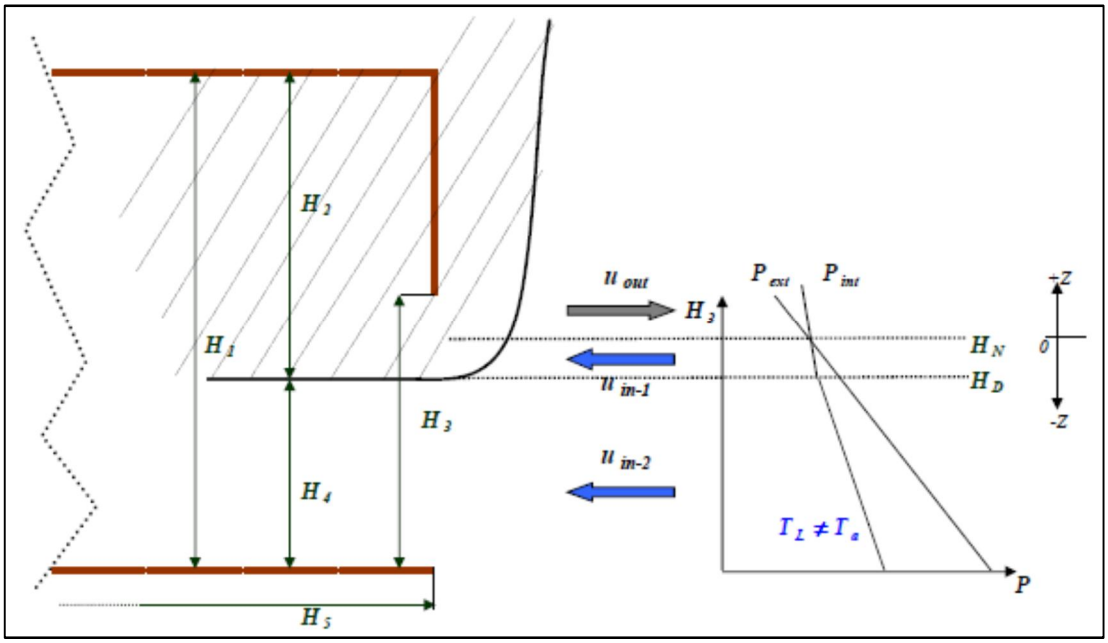

Figure 2-5: The Two-Layer Classic Model Case

Figure references:

H_1 = ceiling height
H_2 = smoke layer height
$H = H_3$ = opening height
$H_4 = H_D$ = clean layer height
H_5 = compartment depth (≈ compartment width)
$N = H_N$ = neutral plane height
P_{ext} = atmospheric (external) pressure profile
P_{int} = internal pressure profile
T_a = ambient (external) temperature
T_L = lower layer (internal) temperature

For this case, above the neutral pressure plane, H_N, along the entire characteristic length z – i.e., along the outflow height $0 < z < (H_3 - H_N)$ – the maximum pressure difference would be once more:

$$\Delta P_{up,MAX} = g\left(\rho_a - \rho_g\right)\left(H_3 - H_N\right) \qquad \textbf{Equation 2-27}$$

But now, below H_N there are two different characteristic lengths instead along which there is a linear pressure difference that causes entrainment of fresh air. These are:

z_1 – where $0 < z_1 < (H_N - H_D)$ – and the maximum pressure difference would be:

$$\Delta P_{low-1,MAX} = g\left(\rho_a - \rho_g\right)\left(H_N - H_D\right) \qquad \textbf{Equation 2-28}$$

and z_2 – where $(H_N - H_D) < z < H_N$ – and the maximum pressure difference would be:

$$\Delta P_{low-2,MAX} = g\left(\rho_a - \rho_g\right)H_D \qquad \textbf{Equation 2-29}$$

These pressure differentials lead to the following expressions for the maximum characteristic velocities in this case:

$$u_{out,MAX} = \sqrt{2g\left(\frac{\rho_a - \rho_g}{\rho_g}\right)\left(H_3 - H_N\right)} \qquad \textbf{Equation 2-30}$$

$$u_{in-1,MAX} = \sqrt{2g\left(\frac{\rho_a - \rho_g}{\rho_a}\right)\left(H_N - H_D\right)} \qquad \textbf{Equation 2-31}$$

$$u_{in-2,MAX} = \sqrt{2g\left(\frac{\rho_a - \rho_g}{\rho_a}\right)H_D} \qquad \textbf{Equation 2-32}$$

Therefore, it can be seen that in this general two-layer case (assuming the lower layer temperature, T_L, different to the ambient temperature, T_a), there are three different maximum velocities caused by the hydrostatic pressure field: a maximum exit velocity, $u_{out,MAX}$, and two different maximum inflow velocities, $u_{in-1,MAX}$ and $u_{in-2,MAX}$. These are the only velocities derived from the classic two-layer model.

2.3.4.4 Modified Two-Layer Scenario

Harmathy pointed out in 1980 [101] that the fire plume played a role by influencing the final pressure distribution (and thus, the final velocities). Therefore, a fourth velocity – powered by the pressure difference created by the fire itself – needs to be accounted for in the model. For this velocity – the same as in a *Regime II* situation – the characteristic length is the fire diameter, *D*, so that the maximum pressure difference can be expressed (same as Equation 2-25) as:

$$\Delta P_{fire,MAX} = g\left(\rho_a - \rho_g\right)D \qquad \textbf{Equation 2-33}$$

Therefore, the maximum fire entrainment velocity can be expressed (same as Equation 2-26) as:

$$v_{fire,MAX} = \sqrt{2g\left(\frac{\rho_a - \rho_g}{\rho_a}\right)D} \qquad \textbf{Equation 2-34}$$

In summary, in the general case of this modified theoretical two-layer model, there are four different characteristic velocities that define the air and hot gases motion, and consequent mass and volumetric flow rates in a compartment fire situation.

The four velocities are listed again for clarity:

$$u_{out,MAX} = \sqrt{2g\left(\frac{\rho_a - \rho_g}{\rho_g}\right)\left(H_3 - H_N\right)} \qquad \textbf{Equation 2-30}$$

$$u_{in-1,MAX} = \sqrt{2g\left(\frac{\rho_a - \rho_g}{\rho_a}\right)\left(H_N - H_D\right)} \qquad \textbf{Equation 2-31}$$

$$u_{in-2,MAX} = \sqrt{2g\left(\frac{\rho_a - \rho_g}{\rho_a}\right)H_D} \qquad \textbf{Equation 2-32}$$

$$v_{fire,MAX} = \sqrt{2g\left(\frac{\rho_a - \rho_g}{\rho_a}\right)D} \qquad \textbf{Equation 2-34}$$

Schematically, this situation is represented as follows:

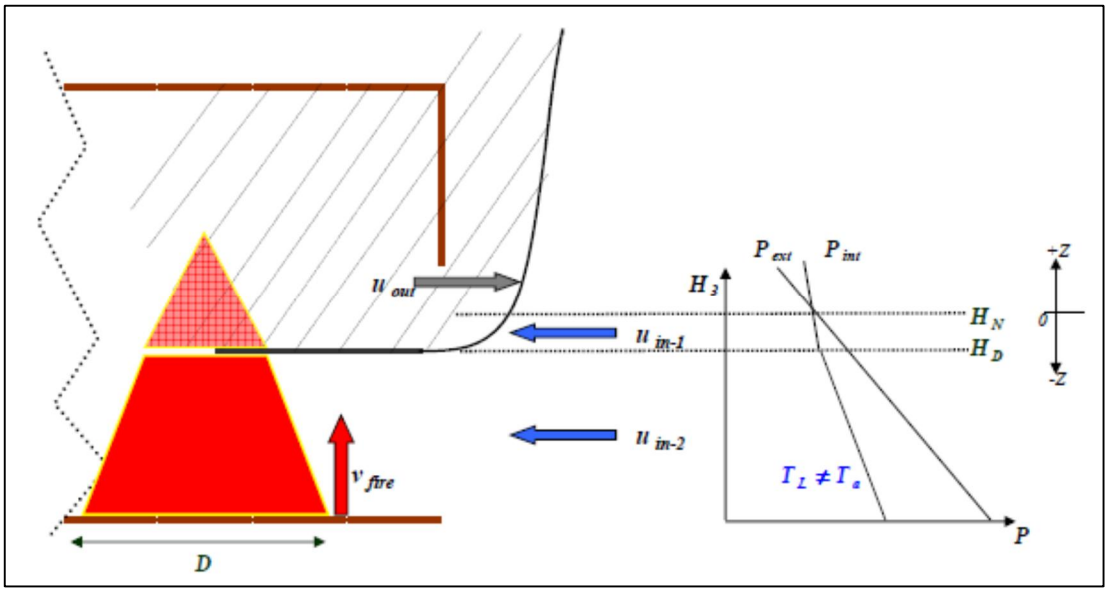

Figure 2-6: Characteristic Velocities in the Modified Two-Layer Model ($T_L \neq T_a$)

Furthermore, the conditions in a compartment fire could be such that the lower (cold) layer could be assumed to be at the same temperature as the exterior atmosphere; i.e., $T_L = T_a$. This is a case derived from the previous one, so it is treated in this same section.

In this case, the maximum inflow velocities, $u_{in\text{-}1,MAX}$ and $u_{in\text{-}2,MAX}$, will be exactly the same, giving as a result a total of three characteristics velocities: $u_{out,MAX}$, $u_{in\text{-}1,MAX}$ and $v_{fire,MAX}$. Schematically, this is represented as follows:

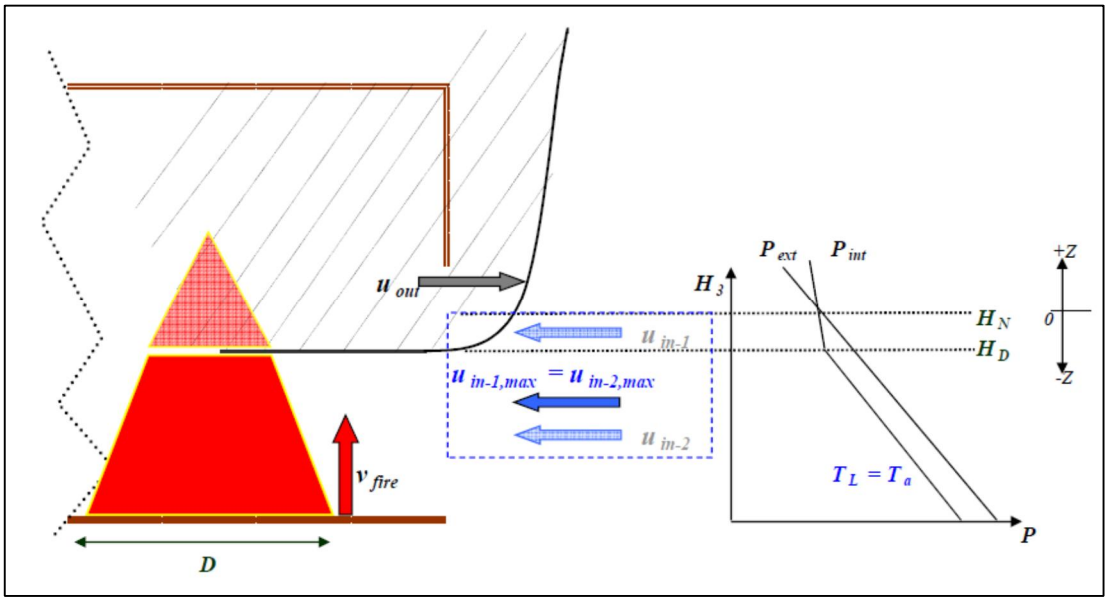

Figure 2-7: Characteristic Velocities in the Modified Two-Layer Model (T_L=T_a)

The three velocities for this case are listed – once again – for clarity:

$$u_{out,MAX} = \sqrt{2g\left(\frac{\rho_a - \rho_g}{\rho_g}\right)(H_3 - H_N)} \quad \textbf{Equation 2-30}$$

$$u_{in-1,MAX} = \sqrt{2g\left(\frac{\rho_a - \rho_g}{\rho_a}\right)(H_N - H_D)} \quad \textbf{Equation 2-31}$$

$$v_{fire,MAX} = \sqrt{2g\left(\frac{\rho_a - \rho_g}{\rho_a}\right)D} \quad \textbf{Equation 2-34}$$

2.4 Preliminary Conclusions

The characteristic velocities of the gases – triggered by the compartment and the fire independently – were evidenced through one and two-layer modelling for the generality of the most representative compartment fire scenarios, and a comprehensive modified two-layer model was presented. The latter included four different characteristic velocities which – depending on the case – can either take up relevance or be disregarded. For example, the resultant characteristic velocities in

single and small compartments with a single vertical opening (i.e., a typical *laboratory compartment* like those used in the CIB Programme [34]) during the period of full development, were shown to be typically those from either Figure 2-3 (*Regime I*) or Figure 2-4 (*Regime II*). These two could be taken as limiting cases from the comprehensive two-layer case, as they take the form of a single either hot or cold layer when modelled.

In real architectural conditions – i.e., situations such as multiple openings, wind, cross-drafts, far-from-cubic small or large compartments – the modified two-layer model needs to be accounted for.

Thus, it has been demonstrated that by taking a simplified preliminary approach, this model can be used to analyse the effects that the confinement has on the intervening fluids' motion (i.e. the *flow pattern*), prior to determining the resultant system's *ventilation mode* for several representative configurations. This extension to the *classic compartment fire framework* is further developed and analysed in Chapter 5: Filling the Gaps with Theory.

3 Chapter 3: Range of Validity of the Compartment Fire Framework: Empirical Design Limitations

3.1 Introduction

Despite the detailed *experimental* background behind analytical formulations in the *classic compartment fire framework*, it is important to revisit their development to establish the extent to which they can be applied.

The present chapter presents a detailed background of the well-known CIB Programme [34] – decisive in the development of the *classic compartment fire framework* – on which many design methodologies are based still to this day. In addition, more recent large-scale tests [102][103][104][105][106] are presented together with other empirical methodologies to contrast and discuss some of the most relevant empirical results from the CIB Programme, and clarify the limitations of those existing design methods based on the *classic compartment fire framework*.

3.2 The CIB Experiments

3.2.1 Temperatures

Two series of large-scale experiments provide the initial set of data used to develop the Compartment Fire framework: those by Kawagoe [12] and those of the CIB Programme [34]. The latter, comprising over 400 experiments, also summarizes Kawagoe's experiments therefore will be used to describe the nature of the tests.

In the late 1960s and early 1970s, an international co-operative programme of large-scale tests was coordinated by the laboratories participating in Working Party W14 of the Conseil International du Batiment (CIB), designed to investigate the factors which influence the behaviour of fully-developed fires in compartments. Thomas and Heselden were tasked with compiling and analysing information on compartment fires gathered from eight different laboratories around the world. The results and conclusions of this extensive study were reported and published in 1972 [34].

The shape of the compartments used in the CIB Programme was rectangular, designated by a three figure code representing the three principal dimensions of width, depth and height (where all dimensions are normalized by the height). Thus, a 211 compartment measured 2 units wide, 1 unit depth and 1 unit height. The four shapes of compartment examined were 211, 121, 221, and 441. The overall scale of the compartment was taken as the compartment height, and scales of 0.5, 1, and 1.5 meter were employed. Therefore, the larger compartment size was 6 m x 6 m x 1.5 m height.

The data obtained through these experiments are mainly burning rates, R, and average compartment temperatures, θ_c, as per the reference notation [34]. The temperatures were recorded by only two thermocouples placed at ¼ and ¾ of the compartment height above the centre of the floor (θ_b and θ_c respectively, as per the nomenclature of reference [34]). As pointed out by Thomas and Heselden [34], in some cases, the lower thermocouple was laid inside the wood cribs that were used as fuel resulting in a measurement bias for the average temperature and, thus, its recordings were removed from the final data set. The data obtained from each test were recorded in a standardized report form showing mean values of temperatures over periods when the fuel weight was falling from 80 to 55 per cent and from 55 to 30 per cent of the initial fuel weight. The 80/30 period was subsequently chosen as representing the period of steady burning of the fire, excluding the period at the beginning when the fire was growing in size and intensity and the period at the end when charcoal was burning. Therefore, the mean values calculated over this 80/30 period recorded by a single high-centered thermocouple were those used by Thomas and Heselden to analyse what they judged and defined as the average ceiling temperatures, denoted by θ_c in the reference [34].

Although the CIB data for average temperatures vs. the *inverse opening factor*, $\frac{A_T}{A_W\sqrt{H}}$, presented significant scatter, Thomas and Heselden [34] drew a best-fit line through one of the fuel configuration data sets (i.e. the (2,1) crib configuration,

meaning 20 mm thick sticks spaced 20 mm apart) obtaining as a result the very well-known plot presented in Figure 3-1.

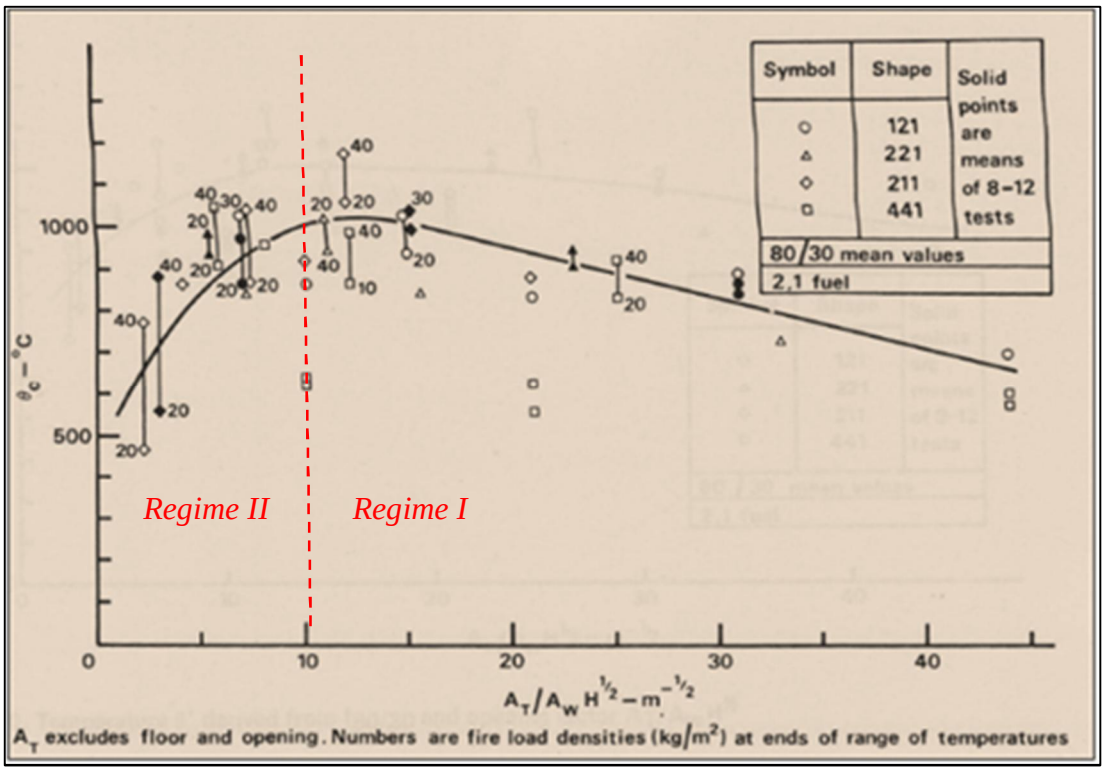

Figure 3-1: Average compartment temperature for the CIB Tests (2,1 configuration), extracted from [34]

Similar graphs for other fuel crib configurations were presented by Thomas and Heselden [34] but because the (2,1) configuration resulted in higher average temperatures, the data of Figure 3-1 is generally used for design analysis. It is important to emphasize that the data shows reasonable scatter in the region that represents *Regime I* conditions (approximately defined as those values with the abscissa > 10) but the scatter is very large for *Regime II* region. In the latter case, factors such as aspect ratio, nature of the fuel and scale were shown by the authors to have a significant effect on the resulting temperatures.

Moreover, the apparent low temperature tendency seen under *Regime II* conditions in Figure 3-1 – which sometimes serve as the justification to force a 'cooler' fire after

designing well-ventilated enclosures – is challenged when drawing best-fit lines through the different fuel configuration data sets from the CIB programme [34], as shown in the following figure:

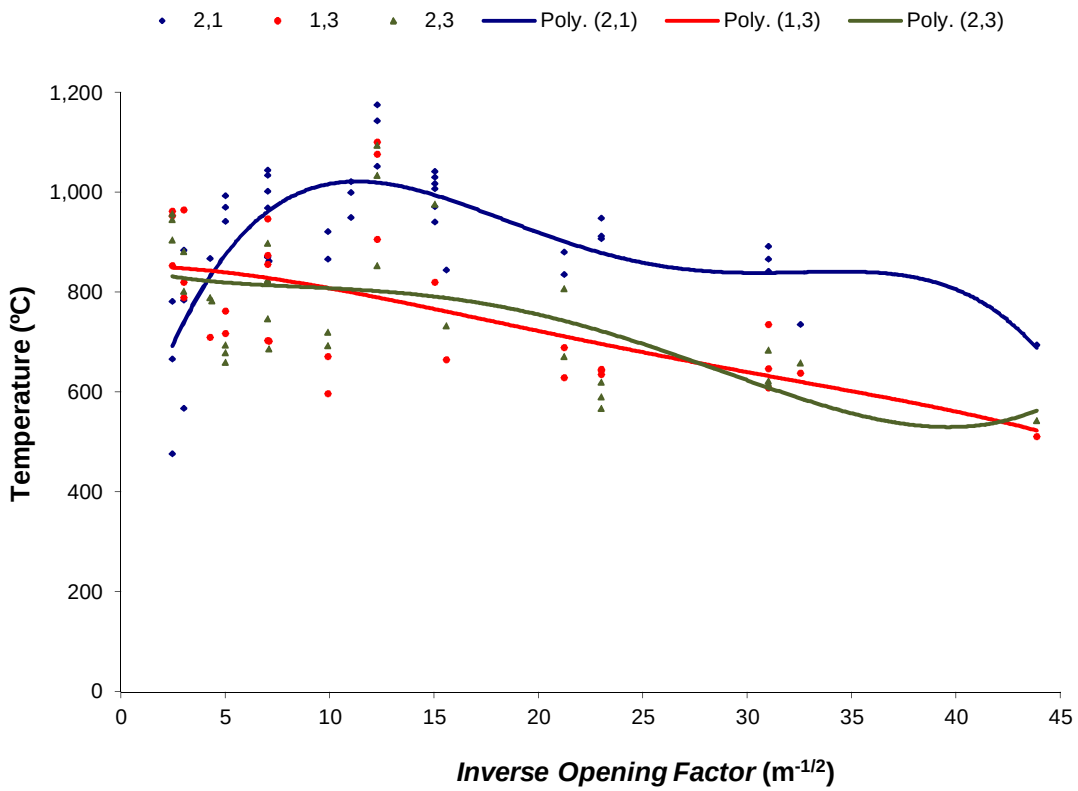

Figure 3-2: Average compartment ceiling temperature for the CIB Tests for crib configurations 2,1 - 1,3 and 2,3, together with their correspondent best-fit lines drawn as 4th grade polynomials.

Figure 3-2 shows that although the (2,1) crib configuration effectively presents the higher overall temperature recordings, the tendency for crib configurations (1,3) and (2,3) is to find higher temperatures as the *opening factor* is increased or the *inverse opening factor* is decreased. Therefore, it is important to emphasize two conclusions from here. Firstly, the fact that the temperatures do not necessarily fall when switching from a *Regime I* to a *Regime II* behaviour and, secondly, that the crib configuration has a significant impact on the time-averaged highest temperatures.

3.2.2 Burning Rates

The weight of the fuel was obtained throughout each test either by weighing the whole compartment or by weighing the floor separately. The same as with the temperature, the fuel weight values were recorded and reported in the standardized report form at two-minute intervals, together with rates of burning averaged over the 80/30 period chosen as representing the period of steady burning of the fire. The CIB data for the so-called normalized burning rate, $\frac{R}{A_W\sqrt{H}}\sqrt{\frac{D}{W}}$, versus the *inverse opening factor*, $\frac{A_T}{A_W\sqrt{H}}$, had less scatter and presented a rather smoother tendency than the temperature data seen previously. Once more, Thomas and Heselden [34] drew best-fit lines through the different fuel configuration data sets, obtaining the following graph for the (2,1) crib configuration:

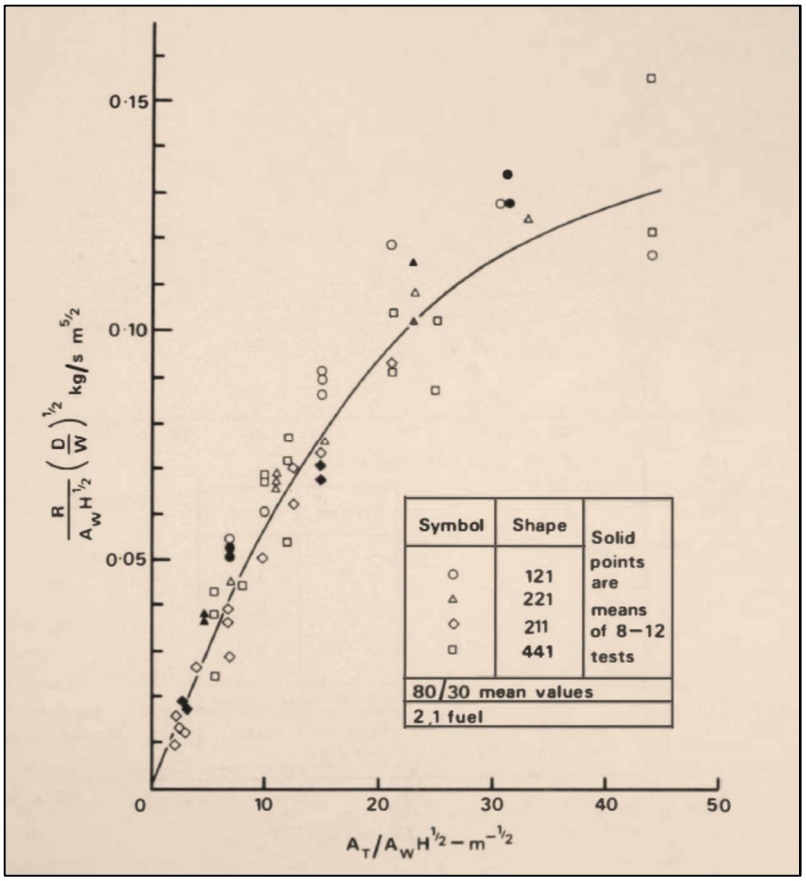

Figure 3-3: Normalized burning rate vs. *inverse opening factor* (taken from reference [34]**)**

As the *inverse opening factor*, $\frac{A_T}{A_w\sqrt{H}}$,was not sufficient as a parameter to account for all the effects of shape, the ratio, $\frac{R}{A_w\sqrt{H}}$ **,** was multiplied by the term $\sqrt{\frac{D}{W}}$ (i.e. ratio of the enclosure's depth to width to the one-half power) because it was found to bring data for different shapes together.

In their analysis, Thomas and Heselden [34] state that the presence of the *ventilation factor*, $A_w\sqrt{H}$, in the denominator of both terms makes these graphs (for every crib configuration) inadequate for discussing the region where the terms are proportional to each other, i.e. in the large opening regime (*Regime II*). They explained [34] that the data were plotted this way only to show that the value of $\frac{R}{A_w\sqrt{H}}$ conventionally assumed to be constant and in the range of 0.08-0.1 according to Kawagoe [12] and

various other authors [2][19], not only was not so, but also its apparent asymptotic value was approximately twice this originally thought constant value.

> "The conventional relationship $R = 0.09\,A_w\sqrt{H}$ is a gross approximation. Any asymptote to the maximum value is perhaps twice this but it is reached at values of $\frac{A_T}{A_{w\sqrt{H}}}$ far higher than have been conventionally used in experiments though they may be appropriate to large area buildings."

Moreover, these $\frac{R}{A_w\sqrt{H}}$ *vs* $\frac{A_T}{A_w\sqrt{H}}$ correlations where obtained in experimental compartments that had low thermal capacity boundaries and therefore an almost constant heat loss coefficient. This meant that the peak temperatures reached in the fully developed stage were virtually independent of the fire duration. The situation is different where a transient heat transfer coefficient is expected, i.e., in the presence of thicker solid boundaries with greater thermal capacity. Under these circumstances, as the heat transfer coefficient decreases, the peak temperatures increase, thus, these will be higher the longer the fire duration. This means, therefore, that the $\frac{R}{A_w\sqrt{H}}$ *vs* $\frac{A_T}{A_w\sqrt{H}}$ correlation is intimately linked to the peak temperatures obtained under the same conditions (i.e., *ventilation factor*, $A_w\sqrt{H}$, compartment size, type, etc.). For this reason, the authors left clear [34] that to predict the duration in large-scale fires where a transient heat transfer coefficient is expected, it is essential to know how the relationships between $\frac{R}{A_w\sqrt{H}}$ and $\frac{A_T}{A_w\sqrt{H}}$ change with the different temperature correlations. Hence, as the data cannot be applied indiscriminately to every compartment configuration, the authors concluded that the answer to the fire duration in large-scale fires must be speculated from theoretical grounds instead.

From the previous paragraphs, it can be concluded that, if this graph is to be used as a gross estimate of the burning rate, R (and hence duration, τ) from a previously

estimated *inverse opening factor*, $\frac{A_T}{A_w\sqrt{H}}$, it must be done only for the region of low ventilation conditions (or *Regime I*), and for compartments with similar characteristics to those used in the CIB tests; i.e., small compartments especially with low thermal capacity and a single ventilation opening.

3.3 Non-Uniformity of Temperature

Following the observations of the CIB studies, Stern-Gottfried *et al*. [107] reviews the test literature in an attempt to establish if the assumption of homogeneous temperature distribution within the compartment is valid through the available data. The data compiled shows that for smaller, cubic compartments the assumption of a homogeneous temperature distribution is robust but it breaks down with the size of the compartment but in particular when the aspect ratio deviates from the cubic compartment.

Additionally, Drysdale [16] explains that most of our knowledge of the behaviour of compartment fires comes from experiments with near-cubical compartments, with characteristic dimensions ranging from 0.5 m to 3 m which of course are very different in shape and size compared with typical spaces in modern commercial buildings [105].

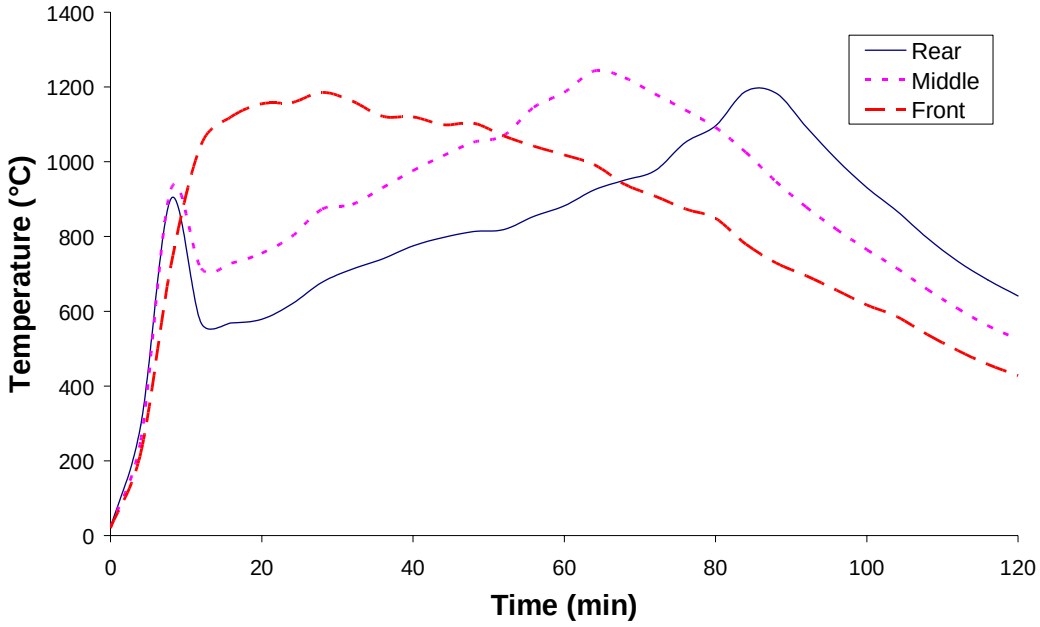

Figure 3-4: Temperature distributions for the Natural Fire safety Concept Tests [90]

In 1999 and the Natural Fire Safety Concept 2 test series at Cardington [105] included a much greater spatial resolution of instrumentation. The eight tests were conducted in a room 12 m x 12 m x 3 m with uniformly spaced fuel load packages distributed across the floor. Sixteen thermocouple trees containing four thermocouples each were placed on a uniform grid in the compartment to record the gas temperatures, shown in Figure 3-4. The tests were conducted with various combinations of fuel type, ventilation distribution, and interior lining material. The tests had liquid fuel channels connecting the fuel packages so that ignition and the subsequent burning could be as uniform as possible.

The Cardington experiments intended to test two types of compartment insulation; "insulating" and "highly insulating". However, after Test 1, the "highly insulating" material was placed on the ceiling for all remaining tests, creating an intermediate level of insulation. The fuel packages were either just wood cribs or a combination of wood and plastic cribs. The ventilation openings were either fully open on the front of the enclosure or fully open on the front and back. As shown in Figure 3-4 there is a significant evolution in space and time of the temperature. The evolution in

time is mostly related to the time lag between heating in the gas phase and the heating of the compartment, thus is related to the level of insulation. This had been previously extensively studied by Pettersson *et al*. [47] when developing the parametric fire curves, nevertheless the Natural Fire Safety Concept tests were the first where the insulation was systematically varied. The evolution in space was observed but not studied in detail due to the restricted amount of instrumentation.

A different form of temperature distribution was reviewed and reported by Clifton [108] who describes fires that spread through a large compartment generating spatial and temporal distributions as a consequence not only of stratification but also of the progression of the fire through the compartment. Clifton [108] emphasizes a simple framework to model these fires and only presents a limited set of experimental data to validate the analytical approach. While the data is coarse and limited it does indicate drastic spatial and temporal temperature evolutions throughout the compartment. An earlier study concerning the 1959 St. Lawrence Burn project [109] was recently reported by Gales [110] where compartments of dimensions 11.2 m x 12.8 m and 13 m x 9 m respectively were exposed to a propagating fire, showing once again significant spatial and temporal temperature distributions.

3.4 Other Empirically Based Methods

Several methods for predicting fire exposures – i.e., time-average gas temperatures, $\bar{T}_g$, burning rates, *R*, and fire duration, τ – were developed during the past half century, and all falling within the *classic compartment fire framework*. The most relevant in terms of defining the framework were probably those developed by Harmathy (already seen in Chapter 1), Law, Lie, Tanaka, Magnusson and Thelandersson, Babrauskas, and Ma and Makelainen [7]. These simple methods were developed for the fully-developed stage, thus their main limitation is implicit behind the conditions necessary to arrive to that stage; i.e., they should be used in relatively small compartments containing a fairly uniform fuel distribution which would allow for a full fire involvement. Another limitation inherited from the CIB tests configuration, is that they are only applicable to compartments with vertical openings subject to natural ventilation.

A thorough comparison between the predictions obtained applying these methods against the CIB [34] and the Cardington [105] data, as well as a contrasts between the predictions obtained with the CIB method against the Cardington data, is presented in reference [7]. This publication gives a clear picture of the empirical limitations of the *classic compartment fire framework* when utilized – using any of the methods derived from its roots – under any set of conditions.

3.5 The Dalmarnock Fire Tests

The Dalmarnock Fire Tests, which provide the greatest instrumentation density to date, were conducted in a real high-rise apartment building in Glasgow, UK [106]. The two tests conducted had a realistic fuel load of typical furnishings. The compartment was 4.75 m x 3.50 m x 2.45 m, containing 20 thermocouple trees, each with 12 thermocouples (placed 0, 0.05, 0.1, 0.2, 0.3, 0.4, 0.6, 0.8, 1.0, 1.3, 1.6 and 2 m from the ceiling). The Dalmarnock experimental results are given in Figure 3-5. Ignition occurred in the waste-paper basket adjacent to the sofa. Two tests were conducted, Test One was allowed to progress to burn-out while the second test was manually suppressed immediately after flashover. Thus only Test One is of interest here.

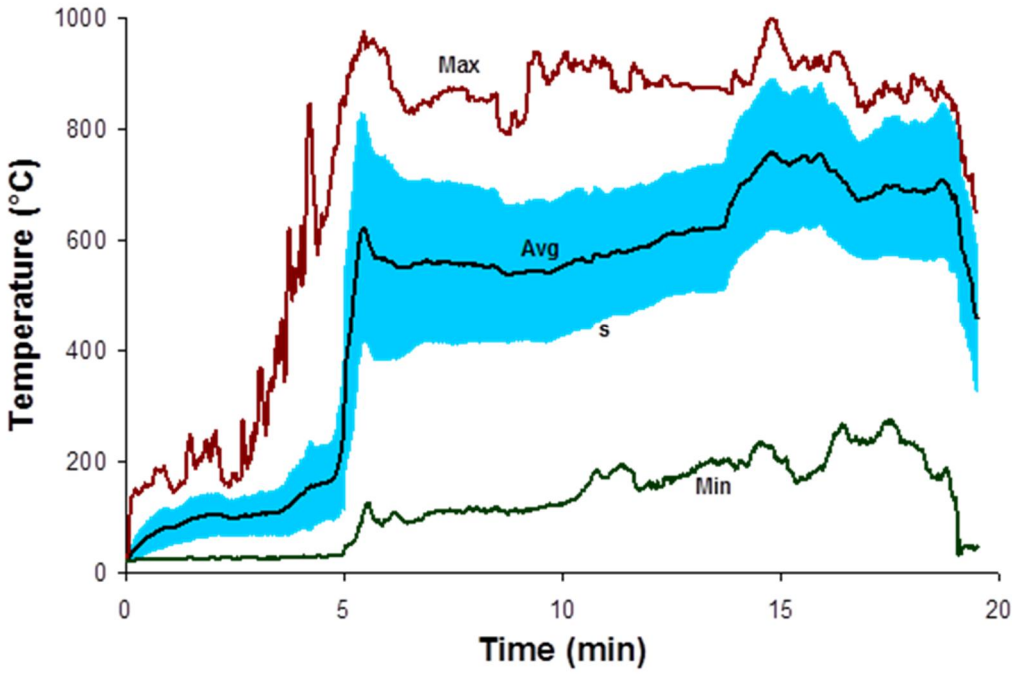

Figure 3-5: Experimental results of Dalmarnock Test One [106] **showing the compartment average, maximum and minimum temperatures, and the standard deviation. Flashover occurred at 5 min and the fully developed lasted until suppression at 19 min.**

The fundamental observation of the Dalmarnock Test One is that the temperature distributions, even for a small compartment, show very large variations in space and time. All it takes is to provide sufficient instrumentation density to spatially resolve the temperature fields. In particular, this is important if the compartment is large enough and the fire is allowed to travel through the compartment. In the Natural Fire Safety Concept tests the compartment was large but all fires were ignited simultaneously. In Dalmarnock the fire was allowed to propagate, nevertheless, the compartment was fairly small. In the study by Clifton [108] one series of experiments was reported where the compartment was large (44 m x 34 m) and the fire was allowed to propagate nevertheless the data has poor resolution and only a single experimental condition is reported. A similar situation occurs with the St. Lawrence Burns Project where only two tests were reported and limited data is available.

3.6 Preliminary Conclusions

After revisiting the development of the most important formulations resulting from the *classic compartment fire framework*'s empirical background, the range of validity of the framework becomes clearer, exposing the limitations of some of the existing design methods and typical assumptions based on the erroneous interpretation of the CIB Programme results.

Due to the fact that (*i*) the highest temperatures found in the CIB Programme [34] fell arguably within *Regime I*, (*ii*) this regime has been historically assumed to be more severe than *Regime II*. This was especially remarked after Harmathy's theoretical studies [2] on the fire severity (Section 1.4.2.2.2). Therefore, with the intention of maintaining conservatism in design, (*iii*) fully-developed fires were *solely* understood and described as *Regime I* fires with the following typical characteristics:

- a stagnant hot layer reaching the floor level;
- uniform temperatures throughout the fire compartment; and
- a ventilation-controlled fire with external flaming, due to lack of oxygen.

Finally, in terms of the burning rate, and in a similar fashion to the temperature controversy, (*iv*) because the (2,1) crib configuration in the CIB Programme [34] resulted in lower normalized burning rates, $\frac{R}{A_W\sqrt{H}}\sqrt{\frac{D}{W}}$, Figure 3-3 is also arguably recommended for design considerations under the claim that lower burning rates give longer predicted burning durations. Other empirically derived methods – which also form the foundations of the *classic compartment fire framework* – based on the actual or very similar configurations from the CIB Programme, expose obviously similar limitations in their estimations of fire severity.

Contrasting Figure 3-1 against Figure 3-2 puts into question the belief that the highest temperatures will always occur in *Regime I*; i.e., statement *(i)*. Regarding

statement *(ii)*, although valid for small compartments [75], the concept of *Regime I* being more severe than *Regime II* has not necessarily been validated for large and open compartment layouts, as evidenced by those described in the St. Lawrence Burn project [109] or in the Natural Fire Safety Concept test series at Cardington [105].

In respect to *(iii)*, the misconception of assuming *Regime I* characteristics as representative of *every* fully-developed or post-flashover fire thus, accepting them as the general rule for every architectural design, came from automatically extending the validity of the theoretical [2] and experimental compartment fire studies [34] to all compartment designs. The large variations in the temperature distribution found in the Dalmarnock fire tests [106] have shown that, even for small compartments, the assumption that *every* fully-developed fire behaves following a pure *Regime I* behaviour with the typical characteristics listed above is, at least, misleading. Further, an important finding in the CIB Programme [34] was that high values of the enclosure's depth to height ratio produced non-uniform temperatures horizontally and large windows non-uniformity vertically, with the ceiling temperatures typically being the maximum temperatures found in an enclosure fire. These conditions could easily trigger a regime of behaviour different to the classic *Regime I* (refer to Chapter 5). In this way, the physical nature of *Regime II* is particularly relevant when defining the fire safety approach in contemporary architecture design. Moreover, rather than simply burning simultaneously throughout the compartment, fires have also been observed to travel as flames spread [111] producing, subsequently, significant ventilation changes which in turn could affect the fire's regime of behaviour.

In connection with *(iv)*, as explained in Section 3.2.2, this graph must not be used under any circumstances for large ventilation conditions (or *Regime II*) – i.e., within the region where the line is straight showing a proportional relationship between both variables – or for compartments with different characteristics (materials, size, openings, etc.) to those used in the CIB tests.

In summary, the abbreviated limitations listed below help characterize the *classic compartment fire framework*'s range of validity:

(i). In small and large compartments, the tendency for the peak temperature to decline in more ventilated conditions cannot be taken as definite before more research is completed.

(ii). In small compartments *Regime I* appears to be more severe than *Regime II*. Nevertheless, this tendency was not validated for large compartments.

(iii). In small and large compartments, fully-developed fires do not always behave as a classic *Regime I* fire (the characteristics typically used to describe post-flashover compartments). They could behave following a *Regime II* behaviour or even as an entirely different regime definition.

(iv). For most compartment configurations (type, size, ventilation, aspect ratio, etc.), it is not appropriate to rely on the CIB Programme empirical correlations nor on other classic compartment fire methods derived from the same research roots to estimate the fire exposure; i.e., temperatures, burning rates, and consequent fire durations.

4 Chapter 4: Range of Validity of the Compartment Fire Framework: Theoretical Design Limitations

4.1 Introduction

Despite the detailed *theoretical* background behind analytical formulations in the *classic compartment fire framework*, it is important to revisit their development to establish the extent to which they can be applied. The *framework* was mainly developed to provide a means by which structural fire resistance could be defined, thus the principle correlations contained within it and derived here, establish relationships between air inflow, the subsequent generation of heat, and the distribution of heat between compartment gas phase and the structure itself.

At each stage, the parameters of interest – namely, air inflow, heat generation, temperatures, and burning rates – can be shown to be principally a function of the compartment ventilation represented, under certain conditions, by the opening characteristics; i.e., a function of either the *opening factor*, $\frac{A_w\sqrt{H}}{A_T}$, or the *ventilation factor*, $A_w\sqrt{H}$. What is also apparent is that this is only possible through assumptions only valid for and resulting from a limited variability of these ventilation characteristics.

This chapter aims therefore to present a review of the classic and typical assumptions which are a direct consequence of the simplifications introduced to the flow model in Chapter 2 (Section 2.3), and form the basis of many existing theoretical design methodologies, and in doing so, clarifies their theoretical limitations and the areas where further research is necessary.

4.2 The Theoretical Maximum Mass Flow Rate

A description of the successive steps that will end with the derivation of the maximum (averaged) buoyancy driven mass flow rate, $\overline{\dot{m}}_{in-MAX}$ – typically assumed in design situations when relying on the classic framework – is presented next.

Applying the *principle of conservation of energy* to non-viscous and incompressible (i.e., constant density) fluids – i.e., *Bernoulli's Equation* – the first step is to find an expression for the averaged inflow, $\bar{u}_{in}$ and outflow, $\bar{u}_{out}$, velocities. For that, the variable inflow and outflow velocities (Equation 2-15 and Equation 2-12, respectively) need to be integrated over the inflow and outflow areas – i.e., along the correspondent height h_i or z – respectively. Due to the fact that these induced velocities vary as the square root of the distance from the neutral axis ($z - N$) or ($N - z$), their mean velocities would equal 2/3 of their maximum expressions. Thus, the outflow mean velocity, $\bar{u}_{out}$, would be:

$$\bar{u}_{out} = \frac{2}{3}\sqrt{2g\left(\frac{\rho_a - \rho_g}{\rho_g}\right)(z - N)} \qquad \textbf{Equation 4-1}$$

And the inflow mean velocity, $\bar{u}_{in}$, would be:

$$\bar{u}_{in} = \frac{2}{3}\sqrt{2g\left(\frac{\rho_a - \rho_g}{\rho_a}\right)(N - z)} \qquad \textbf{Equation 4-2}$$

With the help of Equation 2-18, the generic expression for the averaged mass flow rate would be:

$$\bar{\dot{m}}_i = \rho_i c_d A_i \bar{u}_i \qquad \textbf{Equation 4-3}$$

where the generic area, A_i, is equal to the width of the opening, W_w, multiplied by its height. This means that both the outflow and inflow areas, respectively, would be:

$$A_{out} = W_w(z - N) \quad \longrightarrow \quad A_{in} = W_w(N - z) \qquad \textbf{Equation 4-4}$$

Therefore, the expressions for the averaged mass flow rates – considering that $z = H$ and $z = 0$ for the total outflow and inflow heights, respectively – are:

$$\overline{\dot{m}}_{out} = \frac{2}{3} c_d \rho_g W_w \sqrt{2g\left(\frac{\rho_a - \rho_g}{\rho_g}\right)} (H - N)^{3/2}$$ **Equation 4-5**

and

$$\overline{\dot{m}}_{in} = \frac{2}{3} c_d \rho_a W_w \sqrt{2g\left(\frac{\rho_a - \rho_g}{\rho_a}\right)} N^{3/2}$$ **Equation 4-6**

In both cases, dividing and multiplying by $H^{3/2}$ will give as a result:

$$\overline{\dot{m}}_{out} = \frac{2}{3} c_d \rho_g \left(A_w \sqrt{H}\right) \sqrt{2g\left(\frac{\rho_a - \rho_g}{\rho_g}\right)} \left(1 - \frac{N}{H}\right)^{3/2}$$ **Equation 4-7**

$$\overline{\dot{m}}_{in} = \frac{2}{3} c_d \rho_a \left(A_w \sqrt{H}\right) \sqrt{2g\left(\frac{\rho_a - \rho_g}{\rho_a}\right)} \left(\frac{N}{H}\right)^{3/2}$$ **Equation 4-8**

Following the *principle of conservation of mass*, both expressions can be equated to arrive at an expression for the relative neutral plane height or ratio (*N*/*H*). This brings the implicit assumption of considering that the mass flow produced by the burning object inside the room, $\dot{m}_F$, is negligible if compared to the amount of air, $\dot{m}_{in}$, and hot gases, $\dot{m}_{out}$ – entering and leaving the enclosure, respectively – in every time step.

$$\frac{N}{H} = \frac{1}{1 + \left(\frac{T_g}{T_a}\right)^{1/3}}$$ **Equation 4-9**

Finally, replacing this ratio in the expression for the mass flow rate into the enclosure, the following very well know equation is obtained:

$$\overline{\dot{m}}_{in} = \frac{2}{3} c_d \rho_a \left(A_w \sqrt{H}\right) \sqrt{2g} \sqrt{\frac{T_a \Delta T}{T_g^2}} \left(1 - \frac{1}{1 + \left(\frac{T_g}{T_a}\right)^{1/3}} \right)^{3/2}$$ **Equation 4-10**

This equation implies that the ratio $\frac{\overline{\dot{m}}_{in}}{A_w \sqrt{H}}$ is a function *only* of the temperatures; i.e.:

$$\frac{\overline{\dot{m}}_{in}}{A_w \sqrt{H}} = f\left(\frac{T_g}{T_a}\right)$$ **Equation 4-11**

Plotting this function (Figure 4-1), it appears clear that this ratio – sometimes called the *wall vent flow factor* – is insensitive to absolute temperature ratios greater than 2, being almost constant and equal to 0.5:

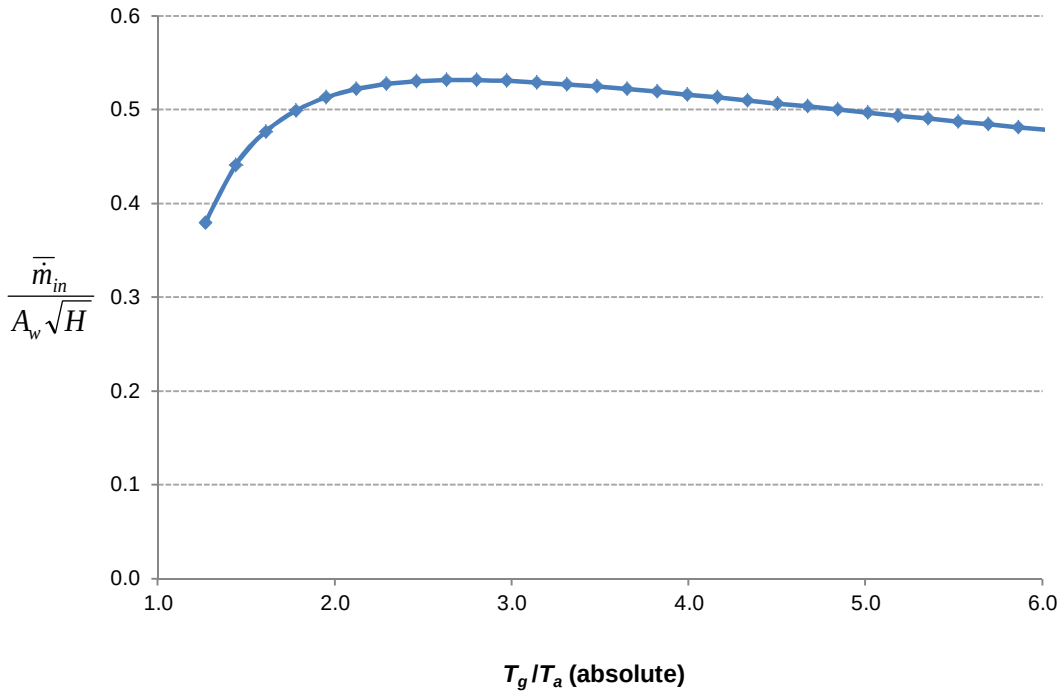

Figure 4-1: Average Vent Flows (normalised by the *ventilation factor*) *vs* Absolute Temperature Ratio

In summary, this means that what in theory is the maximum mass flow rate of air through a single vertical vent, could be approximated as:

$$\overline{\dot{m}}_{in-MAX} \approx 0.5 A_w \sqrt{H} \qquad \textbf{Equation 4-12}$$

It should be borne in mind that to arrive to this theoretical conclusion, the assumptions taken were as follows:

- The inside temperature, T_g, is assumed to be uniformly distributed over the entire volume;
- T_g it is at least twice T_a in absolute values (Kelvin). In practice, doubling an ambient temperature of 20ºC (or 293 K) means having an inside temperature of 313ºC (or 586 K);
- The mass produced inside the enclosure per time step or mass loss rate, $\dot{m}_F$, is assumed to be negligible. This corresponds to the *conservation of mass* assumption, where the mass loss rate is found to fall typically between 1 to 10% of the mass flow rates through the vent [100]. It is important to note that $\dot{m}_F$ differs from the burning rate, R, in situations where there are unburnt fuel gases.
- The air and hot gases are assumed to be non-viscous and incompressible (i.e. constant density) fluids. This corresponds to the *conservation of energy* assumption; and
- The hot gases are assumed stagnant (stationary, i.e. no vertical accelerations) within the entire enclosure, except near the window where there is a small zone at ambient temperature, T_a, causing what is known as a 'chimney effect'.

In addition to the assumptions listed above, it is pertinent to recall Harmathy's statement in regards to the flow pattern described by the model:

> "… the pattern of flow of air and fire gases is often quite different from that assumed in the classic model, that leads to the modeling of compartment fires perfectly isolated from the rest of the building and communicating with a calm exterior atmosphere through a single vertical opening." [101]

It is evident that Equation 4-12 is not only limited to situations where all these assumptions are indeed applicable, but also to situations where the inflow of air into the compartment in fire could be regarded as only hydrostatically driven; i.e., where the effects of wind, cross-drafts, mechanical ventilation, and inertial effect can expressly be disregarded.

Therefore, the flow of air into the compartment is not only shown to be a direct function of the ventilation characteristics, but more importantly, can only be derived in this form based on assumptions resulting from and valid for a very specific range of conditions.

4.2.1 Classic vs. Real World Flow Conditions

In relation to the last statement in the last paragraph of the above section (Section 4.2), the present sub-section presents some important observations made by Harmathy [6] on the effect of ventilation.

In order to explore the effect of ventilation on the potentials for destructive, H^*, and convective spread, μ, Harmathy performed a series of calculations [6] on compartment fires of non-charring and cellulosic fuels. The graphical results of these calculations are depicted in the following figures:

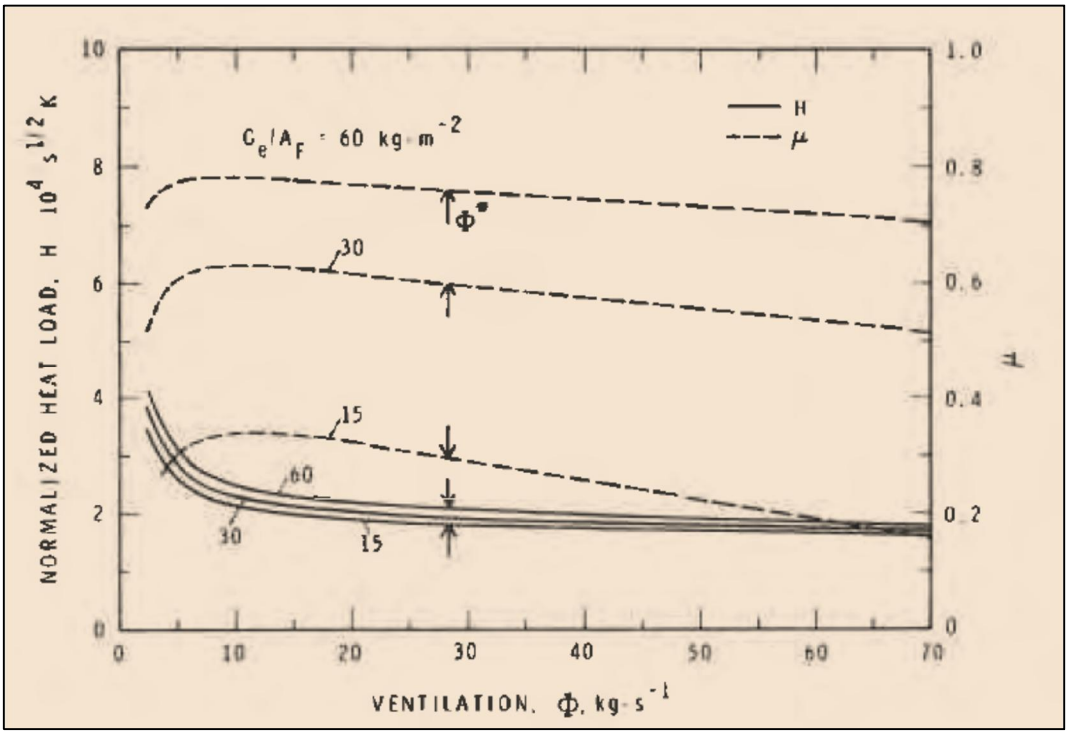

Figure 4-2: The effect of ventilation on the potential for destructive spread and convective spread, with compartment fires involving non-charring fuels in pool configuration (Figure 4 in reference [6]**)**

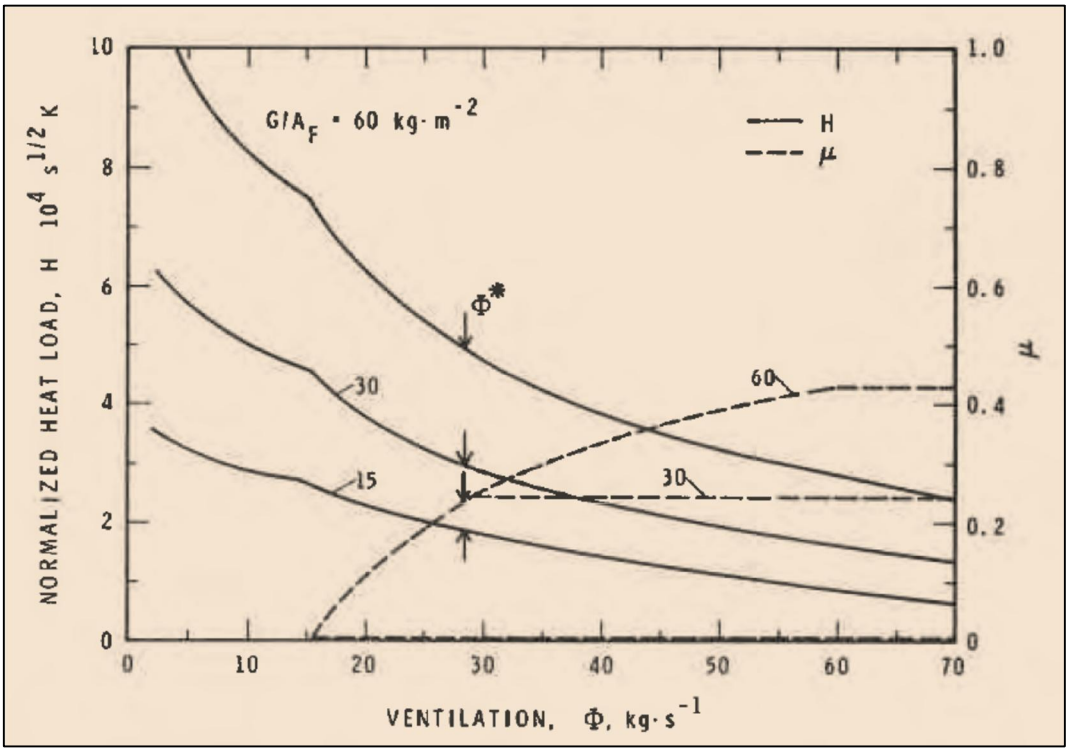

Figure 4-3: The effect of ventilation on the potential for destructive spread and convective spread, with compartment fires involving cellulosics (Figure 6 in reference [6]**)**

Harmathy defined his ventilation parameter as:

$$\Phi = \rho_a \sqrt{g}\left(A_w \sqrt{H}\right) \qquad \textbf{Equation 4-13}$$

He proposed Φ instead of the classic $A_w\sqrt{H}$ on the basis that the former offers the advantage that it helps to eliminate dimensional constants from some equations, and thus the annoyance of converting these constants when changing dimensional systems.

The following observations were made by the author for non-charring fuels [6]:

> "(i) The destructive spread potential of pool fires (as represented by H^*), is not a strong function of the fire load, because with an increase in the fire load an increasing portion of the fuel energy is released outside the fire compartment. Thus the danger of storing large amounts of pool-forming

> materials in a compartment lies not so much in the damage that the fire can cause to the compartment itself, as in the damage that it can bring about in the surrounding building spaces.
>
> (ii) Both the destructive spread potential, H^*, and the convective spread potential, μ, decrease slightly with increasing ventilation."

And the subsequent for charring fuels [6]:

> "(i) The destructive spread potential of cellulosic fires (as represented by H^*) is, under real-world fire conditions, usually much higher than that for fires of non-charring materials, and is a strong function of the fire load. At any fire load, it decreases rapidly with increasing ventilation.
>
> (ii) The convective spread potential (as represented by the μ-*factor*) comes nowhere near that characterizing non-charring fires. It is also a strong function of the fire load and increases with increasing ventilation."

In these graphs, the arrows show the minimum value that the ventilation parameter for the given compartment, Φ, can assume; i.e., Φ^*. This minimum value is calculated under the assumption that the compartment communicates only with a single environment; i.e. under the classic flow conditions. Real-world compartments typically communicate with more than one environment making the flow conditions draft modified. Under this situation cross-drafts may develop – as depicted in Figure 4-4 – potentially increasing the ventilation of the compartment by a factor of five (according to Harmathy [6][35]) in comparison to the classic, draft-free flow conditions. This means that the flow rate of air, $\dot{m}_{in}^*$ – estimated with Φ^* – can be regarded as the minimum that can occur in real-world fires [6].

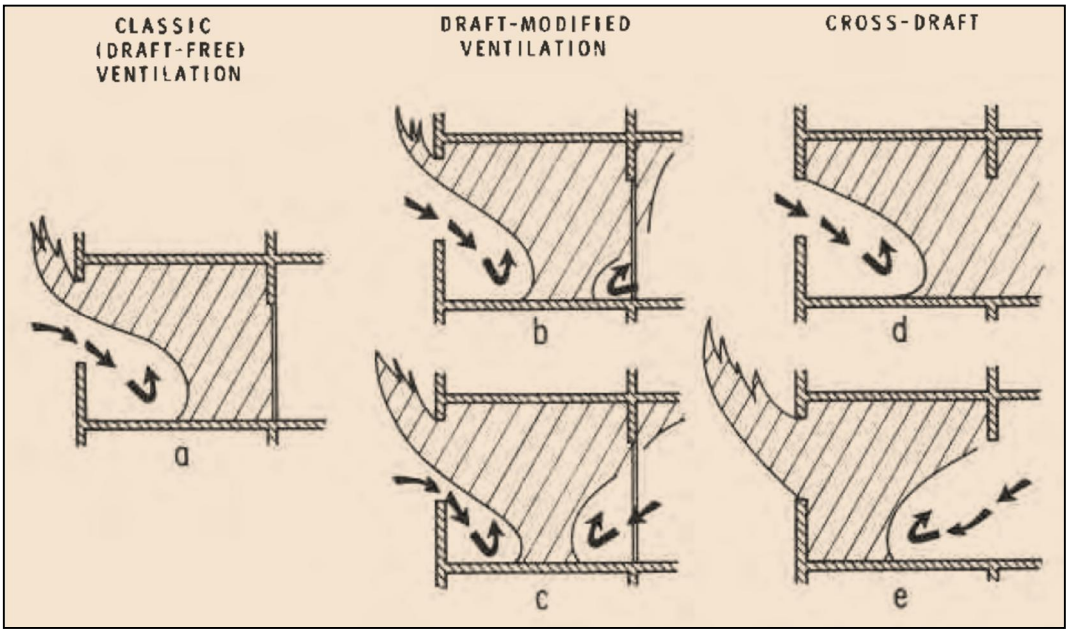

Figure 4-4: Classic and draft-modified ventilations (Figure 2 in reference [6]**)**

Therefore, in what concerns to non-charring fuels, Φ^* could be regarded as a design parameter appropriate to find conservative estimates for H^* and μ. With regards to charring fuels – taking into account that the fire load in residential and office buildings predominantly consists of this type of fuels – Φ^* could still be used to find conservative estimates for H^*. Nevertheless, the most crucial observation made by Harmathy for these fuels is the fact that as far as the convective spread potential (μ-*factor*) is concerned, Φ^* is not acceptable as a conservative design value. This is because under drafty conditions μ can assume much higher values than those pertaining to Φ^*. Noticing this concerning issue, Harmathy recommended [6] that when contemplating measures for countering the convective spread of fire, a higher value of Φ ($\Phi = 5\,\Phi^*$), be selected as input for the design.

Based on Harmathy's declaration [71][77][6] that the convective spread potential far outweighs the destructive spread potential, the fact that it is still usual to assume for design purposes that the ventilation of the compartment is determined by the dimensions of the ventilation opening – i.e. using the non-conservative design value of $\Phi = \Phi^*$ – is for the least immensely concerning in terms of fire safety design.

Once the defence against the convective spread is overwhelmed and the fire spreads uncontrolled to subsequent compartments, then the defence against the destructive spread potential is bypassed, leading to a multi-compartment fire scenario that has not been designed for and thus implies and unforeseen and unpredictable outcome.

4.3 The Theoretical Maximum Heat Release Rate

Following the above theoretically derived maximum (averaged) buoyancy driven mass flow rate, $\overline{\dot{m}}_{in-MAX}$, the maximum averaged theoretical *ventilation-controlled heat release rate*, $\overline{\dot{Q}}_{MAX}$ – that can occur within the enclosure under quasi-steady conditions – could be expressed as:

$$\overline{\dot{Q}}_{MAX} = \overline{\dot{m}}_F \ \Delta H_{fuel} = \frac{\overline{\dot{m}}_{in-MAX}}{\left(\overline{\dot{m}}_{in-MAX} / \overline{\dot{m}}_F\right)} \Delta H_{fuel} = \overline{\dot{m}}_{in-MAX} \left(\frac{\Delta H_{fuel}}{r_{air}}\right) = \\ = 0.5 A_w \sqrt{H} \left(\frac{\Delta H_{fuel}}{r_{air}}\right) \qquad \textbf{Equation 4-14}$$

Using an *air heat of combustion*, $\left(\frac{\Delta H_{fuel}}{r_{air}}\right)$, of 3,000 kJ/kg$_{air}$ – which represents the more or less constant heat release rate per unit mass of air consumed with unlimited air supply found for most gases, liquids, and solids [112] – the previous expression results in approximately:

$$\overline{\dot{Q}}_{MAX} \approx 1{,}500 \ A_w \sqrt{H} \qquad \textbf{Equation 4-15}$$

Therefore, this would be the *theoretical maximum heat release rate* that can evolve within a compartment fire, in situations where the assumptions listed in Section 4.2 are still applicable with the further addition of assuming unlimited air for combustion; i.e., a combustion efficiency of 100%.

After deriving the theoretical maximum mass flow rate and consequent maximum heat release rate, it is important to remark that these *classic* (i.e., single vertical opening and *Regime I* behaviour) fires to which all these assumptions apply, are by no means common compartment fires. There are usually additional openings between

the fire compartment and the surrounding building and/or the external environment, which will produce completely different pressure profiles – even sometimes further incremented by the effect of the wind – leading to results quite different to those predicted by the theoretical model which, in this regard, would tend to fall on the non-conservative side. Outside the validity of the fundamental assumptions the theoretical link between air inflow, heat release rate, and *ventilation factor* does not exist.

4.4 The Theoretical Maximum Temperature

4.4.1 Context

The temperature evolution within a building enclosure is defined by a compendium of complex processes occurring simultaneously. Fuel is pyrolysed at a rate determined by the characteristics of the material and the net heat exchange between the fuel, the fire, the enclosure, the exterior environment and gas phase (hot and cold). The fuel mixes with oxidizer flowing through the compartment leading to a combustion reaction whose characteristics are defined by the relative quantities of fuel and oxidizer (local stoichiometry) as well by heat exchange with the enclosure and the exterior environment. The heat generated by the combustion reaction is partially lost at the openings, partially transferred to the enclosure and to a minor extent fed back to the fuel. The relative importance of all these terms defines the energy accumulated in the compartment and thus its temperature evolution. The resulting gas-phase temperature, T_g, will most likely be a function of all three spatial coordinates and time (x,y,z,t) and the consequence of complex heat and mass transfer processes. The characteristic time scales of combustion, flow and heat transfer can be very different, thus significant simplifications are potentially possible. Given the complexity of the processes, an *a priori* assessment of the possible simplifications is not possible without a detailed quantification of each term.

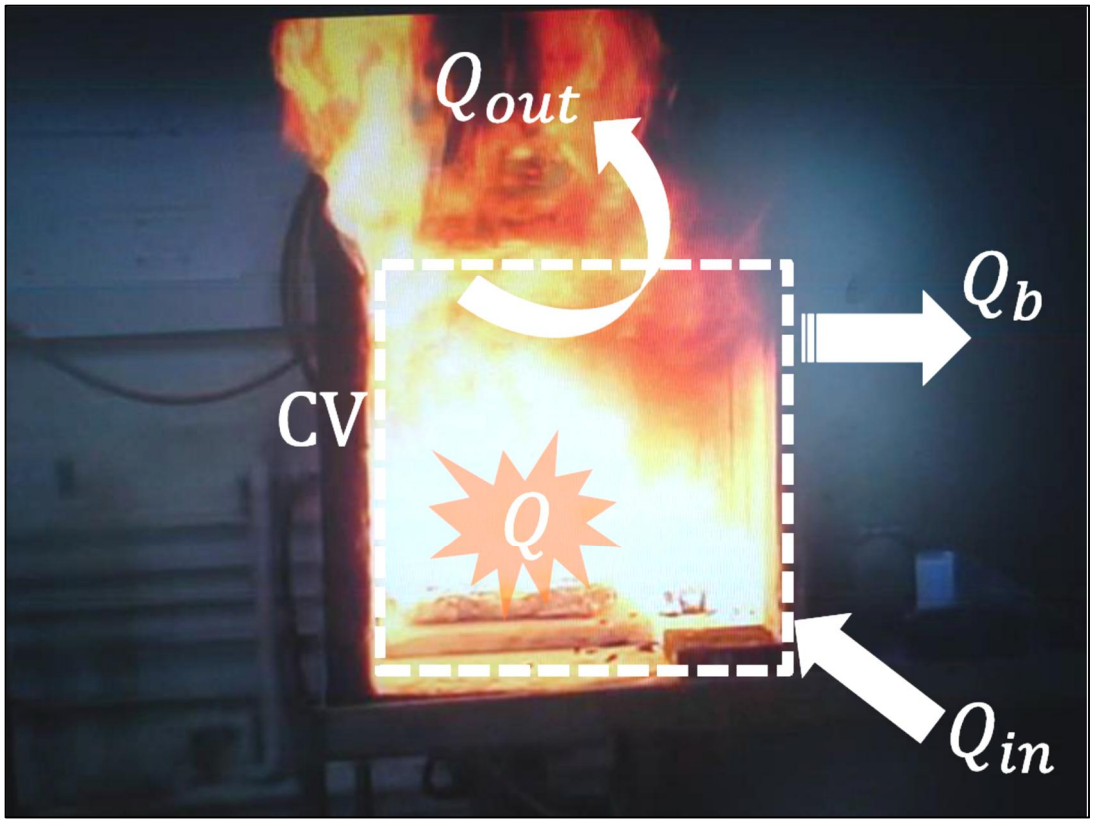

Figure 4-5: The Classic Compartment Fire Framework

The principle behind the *classic compartment fire framework* is that characteristic time scales for combustion are very short thus energy is assumed to be released as a function of reactant supply, i.e. oxygen in the case of a *ventilation-controlled* reaction and fuel in the case of a *fuel-controlled* reaction. The characteristic time for heating of the enclosure is extremely long compared to all gas phase processes, therefore the gas phase can be assumed to be quasi-steady. The characteristic time for fuel pyrolysis is comparable to that of solid heating therefore a single characteristic time describes both. The burning rate will attain steady state conditions at the same time as the enclosure reaches thermal equilibrium with the gas phase. Under those circumstances a maximum gas phase temperature will be achieved (and maintained) beyond the transient heating of the enclosure. The steady state condition implies a constant heat transfer to the walls, a constant generation of heat, and a constant flow of heat out of the enclosure. The main consequence of this approach is that the geometry of the enclosure (dimensions, aspect ratio and openings) defines

the relative importance of each term and therefore the value of the equilibrium gas phase temperature ($T_{g\text{-}MAX}$ (x,y,z)). Thomas explores all three parameter spaces emphasizing the role of each of them [29][34][113].

In compartments, following a similar explanation as above, depending on the circumstances – i.e. ultimately depending on the overall rate of transport of air (refer to Section 1.3.2.2.4) – the generation of heat is either controlled by fuel supply (*fuel-controlled*) or air supply to the decomposing fuel (*ventilation-controlled*). This distinction is important in that it determines the form the energy source takes when introduced in the energy equation. Nevertheless, it does not eliminate the need to resolve the transport processes that bring fuel and oxidizer towards the reaction zone. As introduced in Section 1.3.2.2, Thomas *et al.* [29] describe the role of transport by establishing two limit regimes, *Regime I* and *Regime II*. Harmathy [2], offers a similar discussion proposing a different terminology for the former (ventilation-controlled instead; refer to section 1.3.2.2.4) but identical concepts.

Thomas *et al.* [29] describe *Regime I* as the case where the vents are small enough that they allow for the compartment to fill with smoke. In this case – according to Harmathy's burning model [33] – at steady-state, the rate of entry of air controls the rate of pyrolysis (or so-called burning rate), and the mixture of volatiles, air and combustion products within the compartment is far from ideal for gas-phase reactions. Thus, a significant amount of the energy released by combustion occurs outside the compartment and the flow field within the enclosure is dominated by thermal expansion of the gases allowing the assumption that momentum within the enclosure is negligible. Momentum and mass is only exchanged at the openings therefore it can be characterized by static pressure differentials across the openings. If a fixed fraction of the energy released is lost through the openings, then the maximum temperature distribution ($T_{g\text{-}MAX}$ (x,y,z)) will only be a function of the equilibrium heat exchange with the enclosure and the heat generated, where the heat generated is directly related to the mass flow of oxygen through the vents. Given the reduced optical depth and low velocities, a linearized approximation for total heat transfer is acceptable. This enables not only the formulation of heat exchange

through the walls by simple expressions [7][96] but also the expression of the burning rate as a direct function of the gas phase temperature. As Thomas *et al.* [29] and Harmathy [2] pointed out, the equilibrium temperature, and consequently all other characteristic values, are defined by the relative magnitude of the three main terms of the energy equation: heat generation, heat transfer to the enclosure and heat losses through the vents. The relative values are therefore strongly dependent on the geometry of the compartment. While the validity of the framework extends to all geometries that comply with the assumptions, the resulting values are defined by the complex heat and mass transfer processes that remained unresolved. All unresolved processes are substituted by experimental values; therefore, the quantitative values extracted from experimentation are only applicable for the characteristic geometries reported in the tests.

In the case where the vents are sufficiently large, the smoke evacuates the enclosure with little resistance allowing for the fire to draw air. If the pressure differentials generated by the fire dominate over the static pressure differentials, the combustion products are expelled from the enclosure as fast as air is drawn into the enclosure. Complex heat and mass transfer processes dominate over this regime that Thomas *et al.* [4] labelled *Regime II*. No simple theoretical analysis can be defined for *Regime II*. Characteristic heat transfer times are short and soot concentrations are low; therefore – as summarized in Section 3.6 – heat exchange from the fire to the structure was deemed to be less severe than for *Regime I* [29]. Harmathy [36] presents a theoretical argument for the lower severity of *Regime II* showing that the large velocities and vent size result in a major fraction of the heat being expelled through the vents, a decreased net heat accumulation in the enclosure and lower gas phase temperatures. Quantification of the actual heat transfer to the structure and the fuel is highly dependent on the geometry of the enclosure and extrapolation is extremely difficult under these circumstances. If quantification of the environment is desired, *Regime II* needs to be avoided.

4.4.2 Analysis

A compartment will be used as a control volume to describe the mechanisms by which energy can be transferred in and out of the control volume resulting in temperature distributions within the compartment. Friction work will be neglected and the volume of the compartment will be assumed constant. The energy conservation equation for the fixed control volume of Figure 4-5 can be represented [114] as:

$$\frac{dQ_{CV}}{dt} = \dot{Q}_{in} - \dot{Q}_{out} + \dot{Q} - \dot{Q}_b \qquad \textbf{Equation 4-16}$$

Where $\dot{Q}_{in}$ is the enthalpy entering the control volume with the reactants per unit time, $\dot{Q}_{out}$ is the enthalpy leaving the control volume with the products per unit time, $\dot{Q}_b$ represents the heat losses to the enclosure boundaries and $\dot{Q}$ the total heat release rate within the enclosure by the fire. To understand better the role of each term it is useful to normalize Equation 4-16 by the heat release rate.

$$\frac{1}{\dot{Q}}\frac{dQ_{CV}}{dt} = 1 + \frac{\dot{Q}_{in}}{\dot{Q}} - \frac{\dot{Q}_{out}}{\dot{Q}} - \frac{\dot{Q}_b}{\dot{Q}} \qquad \textbf{Equation 4-17}$$

Given that the addition of mass into the enclosure associated to the fuel's mass loss rate, $\dot{m}_F$, is negligible in comparison to the air mass inflow, $\dot{m}_{in}$, and gas mass outflow rates, $\dot{m}_{out}$, (estimated between 1% and 10% [100] or at most between 16% [2] and 18% [29]), the rate of change of mass within the control volume can be considered close to zero (i.e. $\frac{dm_{CV}}{dt} \approx 0$), therefore the transient term of the conservation of mass equation can be neglected resulting in:

$$\dot{m}_{in} = \dot{m}_{out} = \dot{m}_i \qquad \textbf{Equation 4-18}$$

Given the significant temperature differences between the reactants and products it is possible to establish that $\frac{\dot{Q}_{in}}{\dot{Q}} \ll \frac{\dot{Q}_{out}}{\dot{Q}}$. This simplification is not necessary for the

rest of the analysis but it will be retained here for consistency with the original presentation. Simple scaling analysis establishes that the characteristic heating time for the solid walls is at least two orders of magnitude longer than that of the combustion products allowing to assume quasi-steady conditions in the gas phase, i.e. $\frac{1}{\dot{Q}}\frac{d\dot{Q}_{CV}}{dt} \approx 0$. On the basis of these simplifications Equation 4-17 can be rewritten as:

$$1 = \frac{\dot{Q}_{out}}{\dot{Q}} + \frac{\dot{Q}_b}{\dot{Q}}$$ **Equation 4-19**

It is important to note that until this point no strong assumptions have been made and Equation 4-19 can be satisfied by any enclosure subject to a fire. What follows is a series of assumptions that enable the transformation of Equation 4-19 into a set of very simple expressions that serve to characterise the enclosure fire under *Regime I* conditions. The assumptions are:

1. The heat release rate is defined by the complete consumption of all oxygen entering the compartment and its subsequent transformation into energy, $\dot{Q} = \dot{m}_i Y_{O_2,\infty} \Delta Hc_{O_2}$. Where the ambient oxygen concentration is given by $Y_{O_2,\infty}$ and the heat of combustion per kilogram of oxygen consumed is given by ΔHc_{O_2}. This assumption not only eliminates the need to define the oxygen concentration in the outgoing combustion products but also eliminates the need to resolve the oxygen transport equation within the compartment. Implicitly this assumption limits the analysis to scenarios where the chemistry is fast enough to consume all oxygen transported to the reaction (or intense pyrolysis [33]) zone, although the mixing conditions of volatiles, air and combustion products (and not the stoichiometric air requirement [33]) still do not allow for the complete combustion of all the volatiles produced within the boundaries of the compartment. It is important to add that if the heat of combustion is assumed to be an invariant then the level of

completeness of the combustion process is assumed to be independent of the compartment.

2. Radiative losses through the openings are assumed to be negligible [29] therefore $\dot{Q}_{out}$ is treated as an advection term. Harmathy [2] provides an estimate for the radiative losses of approximately 3% of the total energy released.

3. There are no gas or solid phase temperature spatial distributions within the compartment. The gas-phase equilibrium temperature is therefore defined by a single value, $T_{g\text{-}MAX}$, and the equilibrium surface temperature of all solid surfaces also by a single value, T_b. $\dot{Q}_{out}$ and $\dot{Q}_b$ can then be strongly simplified. If the specific heat of the gases, c_p, is assumed to be a constant, then $\dot{Q}_{out} = \dot{m}_i c_p T_{g-MAX}$. $\dot{Q}_b$ can be simplified in several manners depending on the objectives of the simplification. The simplifications associated to $\dot{Q}_b$ require more detail and are addressed later.

4. Mass transfer through the openings is governed by static pressure differences, therefore a simple orifice plate expression can be used to evaluate the mass flow of air through the openings, $\dot{m}_{in} = C A_w \sqrt{H}$, where A_w and H are the opening area and height, respectively, and C is a constant that amalgamates all other constants including the orifice plate coefficient and gravity. It is important to note that this assumption requires all velocities within the compartment to be negligible. Different values of the constant were derived by Harmathy [2][101] and calculated by Thomas [34] for different experimental conditions.

The classical approach is to define $\dot{Q}_b$ as conduction losses through the boundaries of the compartment. While more complex formulations are possible, a simple steady-state approximation will be used to quantify conductive losses:

$$\dot{Q}_b = A_T \, k_b \frac{\left(T_{g-MAX} - T_a\right)}{\delta_b} \qquad \textbf{Equation 4-20}$$

Where A_T is the area through which heat is being transferred, k_b an effective thermal conductivity of the compartment boundaries, δ_b a characteristic thickness of the boundaries and T_a the ambient temperature. It is important to note that this approximation is quite coarse in that it assumes the temperature difference between the interior and the exterior of the compartment boundaries ($T_{g\text{-}MAX} - T_a$) as the maximum possible value; i.e., T_a does not rise due to heat transfer through the walls, therefore the resulting heat transfer to the boundaries is maximized and the compartment temperature is minimized as a consequence of these maximal heat losses. While this approximation might not be conservative – depending on the perspective – it is useful to establish the relationship between the gas-phase temperature, $T_{g\text{-}MAX}$, the air intake, $\dot{m}_{in}$, and the compartment geometry. Substituting Equation 4-20 into Equation 4-19 and solving for the steady-state gas-phase temperature the following expression is obtained:

$$T_{g-MAX} = \left(\frac{1 + \frac{T_a}{T_{CD}}}{1 + \frac{T_F}{T_{CD}}} \right) T_F \qquad \textbf{Equation 4-21}$$

Where $T_F = Y_{O_{2,\infty}} \Delta H c_{O_2} / c_p$ is a characteristic flame temperature and $T_{CD} = \frac{C Y_{O_{2,\infty}} \Delta H c_{O_2}}{(k_b/\delta_b)} \left(\frac{A_W \sqrt{H}}{A_T} \right)$ is a characteristic conduction temperature. It is important to note that under the present assumptions all terms of Equation 4-21 are constant with the exception of the classic *opening factor* $\left(\frac{A_W \sqrt{H}}{A_T} \right)$ and the thermal conduction heat transfer coefficient (k_b/δ_b), both properties of the compartment.

An alternative approach to define the heat transfer through the walls is by means of a convective boundary condition. In this case heat transfer through the walls can be described by:

$$\dot{Q}_b = A_T h_T \left(T_{g-MAX} - T_b \right) \qquad \textbf{Equation 4-22}$$

Where h_T is a total heat transfer coefficient and T_b the interior surface temperature of the compartment boundaries. Once again, this is a very simple expression that establishes a different form of the steady-state gas-phase temperature:

$$T_{g-MAX} = \left(\frac{1 + \frac{T_w}{T_{CV}}}{1 + \frac{T_F}{T_{CV}}} \right) T_F \qquad \textbf{Equation 4-23}$$

Where $T_{CV} = \frac{CY_{O_{2,\infty}} \Delta Hc_{O_2}}{h_T} \left(\frac{A_w \sqrt{H}}{A_T} \right)$ is a characteristic convection temperature. While both expressions (Equation 4-21 and Equation 4-23) are very similar and depend on the *opening factor* $\left(\frac{A_w \sqrt{H}}{A_T} \right)$, Equation 4-23 also depends on a gas phase parameter which is the total heat transfer coefficient, h_T. This only becomes interesting when the asymptotic conditions are attained.

If $\frac{T_a}{T_{CD}}$ << 1 and $\frac{T_F}{T_{CD}}$ << 1 (i.e., large *opening factor* and insulating walls) then Equation 4-21 results in:

$$T_{g-MAX} = T_F \qquad \textbf{Equation 4-24}$$

If $\frac{T_a}{T_{CD}}$ >> 1 and $\frac{T_F}{T_{CD}}$ >> 1 (i.e., small *opening factor* and non-insulating walls) then Equation 4-21 results in:

$$T_{g-MAX} = T_a \qquad \textbf{Equation 4-25}$$

Similarly, if $\frac{T_w}{T_{CV}}$ << 1 and $\frac{T_F}{T_{CV}}$ << 1 (i.e., very large *opening factor* and weak total convective heat transfer) then Equation 4-23 results in:

$$T_{g-MAX} = T_F \qquad \textbf{Equation 4-26}$$

But if $\frac{T_W}{T_{CV}}$ >> 1 and $\frac{T_F}{T_{CV}}$ >> 1 (i.e., very small *opening factor* and strong total convective heat transfer) then Equation 4-23 results in:

$$T_{g-MAX} = T_b \qquad \textbf{Equation 4-27}$$

It is important to note that the asymptotic values associated with Equation 4-21 (i.e., Equation 4-24 and Equation 4-25) directly relate the gas phase temperature to the two hard limits, the ambient, and characteristic flame temperatures, T_a and T_F respectively. Therefore, this equation is very useful when addressing the evolution of the gas phase temperature as a function of the *opening factor*. In the work by Thomas *et al.* [29] it is stated that the quantitative values of $T_{g\text{-}MAX}$ will be dependent on the conduction heat transfer coefficient (k_b/δ_b) and that a conservative characteristic value can be taken for testing leading to a conservative empirical evolution of $T_{g\text{-}MAX}$ as a function of only the *opening factor*. Figure 4-6 shows the plot extracted from reference [34] where the right hand side of the curve shows the evolution of $T_{g\text{-}MAX}$ as a function of the *inverse opening factor*, $\frac{A_T}{A_W\sqrt{H}}$. Extrapolation of the trend in this region in both directions will lead towards the asymptotic values defined by Equation 4-24 and Equation 4-25. The asymptotic limit defined by Equation 4-24 will not be attained. Towards the left of the maximum temperature (Figure 4-6) the conditions are representative of *Regime II* which does not comply with the assumptions of this analysis and therefore deviates from the trends defined by Equation 4-21 and the asymptotic limit defined by Equation 4-24.

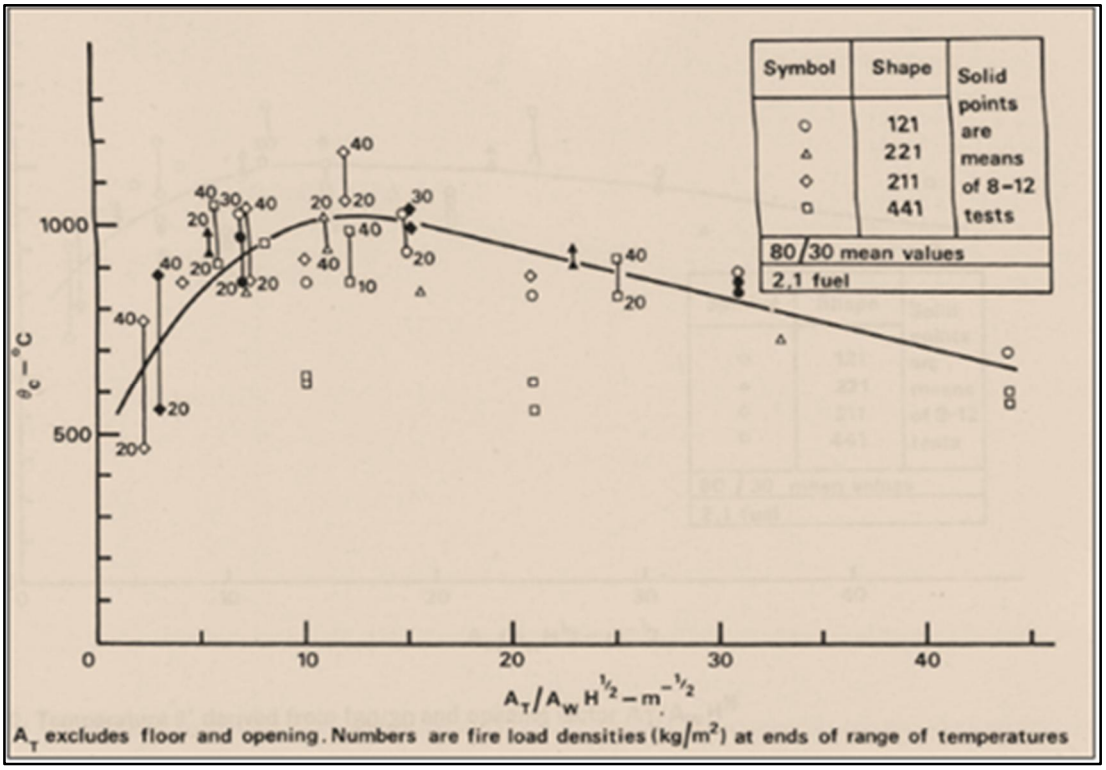

Figure 4-6: Average compartment temperature for the CIB Tests (2,1 configuration), extracted from [34] **(identical to Figure 3-1)**

Finally, Kawagoe [12] established from Equation 4-20 – and from the fact that the burning rate is proportional to the heat transfer rate to any of the boundaries of the compartment – that the burning rate is proportional to $A_w\sqrt{H}$.

In contrast to Equation 4-21, Equation 4-23 has a different asymptotic term for the case where heat transfer between the gas and compartment is high. In this case the gas-phase and wall temperatures are the same (as represented by Equation 4-27). This observation is significant in that it focuses on the temperature of the structure and indicates that given the right heat transfer conditions, the thermal characteristics of the structure can dominate the minimum temperature of the gas-phase and the balance of the two right hand terms of Equation 4-19.

In summary, the compartment fire framework allows, by means of several strong assumptions, a representation of the maximum steady-state temperature, $T_{g\text{-}MAX}$, of a compartment simply as a function of the *opening factor*, $\frac{A_W\sqrt{H}}{A_T}$, and the burning

rate, *R*, as proportional to the *ventilation factor*, $A_w\sqrt{H}$. Those assumptions are consistent with *Regime I*, and while remaining within these assumptions, simple expressions (Equation 4-21 and Equation 4-23) can be used to link $T_{g\text{-}MAX}$ to the *opening factor*. Outside the validity of the fundamental assumptions the theoretical link between temperature, burning rate and *opening* or *ventilation factor* does not exist.

4.5 Preliminary Conclusions

Taking over from the preliminary conclusions arrived to in the previous chapter (Section 3.6) – and after revisiting in this instance the development of the most important theoretical formulations from the *classic compartment fire framework*, the range of validity of the framework is further disclosed, exposing once more the limitations of some of the existing design methods and typical assumptions.

From a design perspective different approaches can be followed. Code based restrictions on vent and compartment size can be imposed to avoid either regime. As it has been uncovered in Chapter 1 and summarised in Section 3.6, through Thomas' and Harmathy's work it is generally implied that *Regime I* is more severe than *Regime II* (albeit never truly quantified); therefore, building design can be done under the quantifiable worst case conditions of *Regime I*. In other words, the building geometry can be such that *Regime I* fires are a possible outcome and structural design is done to withstand the thermal load of such fires. Alternatively, an even more conservative approach can be followed which is to quantify *Regime I* as a worst case condition but require building characteristics consistent with *Regime II* while restricting those consistent with *Regime I*. A final approach was strongly advocated by Harmathy [36][1] – still implicit in some current regulations [115] – who encouraged designers to increase venting as an effective means to reduce fire proofing. The following quote is extracted from Reference [1]:

> "The simplest way of improving fire safety is to reduce its destructive potential in the 'fire cell' (space on fire) by ensuring that the fire, if it occurs, will be fuel-surface-

> controlled (i.e., *Regime II*), in other words, by using large window areas, whenever possible, it becomes possible to replace fire resistance requirements with ventilation requirements. This means that the designer is entitled to decide whether to choose between buildings built with small windows and heavy fire-rated walls and floors, and buildings with large windows and lighter non-combustible, non-fire-rated elements."

Whatever approach is followed, it was recognized that this is only valid within the context of the specific geometries studied [34][2].

An important point regarding the differences between *Regime I* and *Regime II* is highlighted by Harmathy [36]. The mechanisms linking compartment temperature and burning rate are only valid for *Regime I* and not for *Regime II*, in particular, the inverse relationship between the maximum average gas phase temperature ($T_{g\text{-}MAX}$) and the duration of the fire, τ. In Reference [36] Harmathy indicates:

> "The conclusion reached so far is that well-ventilated fires, i.e., fuel-surface controlled fires, not only burn at lower temperatures (in general), but also are very short. The common belief that compartment fires are either short and hot or long and relatively cool is, therefore, completely wrong."

This observation seems to have been forgotten and it has become common to describe both regimes as being defined by the same interaction of physical processes [116] without remembering that *Regimes I* and *II* are two extremes of the real range of behaviour and are the result of neglecting different processes and having the remaining ones interacting in a very specific manner.

In summary, the *Classic Compartment Fire Framework* is a robust representation of the behaviour of a fire in an enclosure. It allows, by means of several strong assumptions consistent with *Regime I*, a representation of the principle parameters by

simple expressions, typically functions of either the *opening factor* or the *ventilation factor*. There is no fundamental weakness in the approach but the quantitative results are intimately linked to the geometry of the compartment (size, vent size, aspect ratio) and the single vertical opening configuration. The geometry will define if the conditions are consistent with the assumptions of the analysis but most importantly, it will establish the relative magnitude of the heat flow in and out of the enclosure (terms in Figure 4-5), which in turn defines the equilibrium temperature. Currently, the relative distribution is not defined in an analytic way but by means of experimental values. Extrapolation of these experimental values requires geometrical consistency. The SFPE Engineering Guide for Fire Exposure to Structural Elements [7] addresses this issue as early as the Executive Summary, nevertheless it addresses the influence of the geometry on the validity of the different methodologies employed in terms that are relevant only to *Regime I* fires, in other words as a function of the *opening factor*, $\frac{A_W\sqrt{H}}{A_T}$. The ventilation configuration will define the pressure profiles and consequent flow conditions which, in turn, will affect the energy balance and overall fire behaviour. It was inferred – in Sections 4.2, 4.2.1, and 4.3 – that the *classic* ventilation configuration (i.e., single vertical opening) is by no means a common architectural configuration, which implies that certain conditions predicted by the theoretical model could be misleading if this fact is not expressly accounted for.

To conclude and round-up the range of validity *empirical* and *theoretical* analysis (i.e., Chapters 3 and 4), a fire in a contemporary building could potentially fall either under a different *regime* definition, and/or under the so-called *Traveling Fire* [111] definition. Therefore, further experimentation – in small and large scale – and research is required to define the *Classic* C*ompartment Fire Framework*'s range of validity, while aiding to understand the widespread compartment fire behaviour thoroughly. This will allow extending the underlying theory towards a more general one that contemplates large volume enclosures and other contemporary arrangements. This conclusion opens the analyses of the following Chapters 5 and 6.

5 Chapter 5: Filling the Gaps with Theory

5.1 Introduction

In today's fire safety practice, when dealing with atypical designs, it is becoming more and more common to adopt engineering decisions or approaches based on the general and particular performance of said designs and design features, respectively, when subjected to different theoretical fire scenarios. It is for this reason that simple analytical formulations are so valuable.

Thus, this chapter presents an elaborated theoretical *compartment fire framework* entirely developed by the author, inclusive of the *classic* one, and aiming to broaden the envelope of applicability to encompass and enable the design of contemporary architectural layouts. Through the exploration of the range of combinations of characteristic length scales, a scaling analysis is used to identify the governing flow mechanisms within, into and out of the compartment, and thus establish a more complete set of *regime of behaviour* definitions.

It is important to emphasize beforehand that analytical formulations should be treated with great care; their theoretical and/or practical background needs to be understood to ensure their appropriate use and extension. While the numerical aspects of analytical formulations are generally very simple, the understanding of fire dynamics required to be able to use them correctly can be extensive. Improper use of these calculations can lead to misinterpretations and to decisions in the design process that could fall on the non-conservative side. The desired practicability should not overcome their accuracy.

5.2 The Fluid Motion

5.2.1 Conservation of Momentum

The characteristics of a fire change as fuel and the manner in which air is delivered, from this point termed the *ventilation mode*, changes. Fuel delivery changes with the fuel type and as the area burning changes, but also its transport will be affected by the flow field induced by buoyancy. In fire situations, the fuel injection velocity

tends to be negligible [117][118] thus transport of gaseous fuel from the fuel surface to the flame is controlled by natural convection. Furthermore, natural convection will also affect heat transfer from the flame to the fuel, affecting the burning rate. Natural convection will also control the supply of oxidizer to the reaction. The role of natural convection is therefore a key element when determining the characteristics of a fire. In this context, confinement will affect natural convection and therefore will strongly affect the nature of the fire. The confinement's influence can be characterised by determining the system's *ventilation mode* through the description of the fluid motion.

A simple way of approaching this topic is to apply Newton's *Second Law of Motion*. This Law states that "the rate of change of momentum (per unit volume) is equal to the summation of the applied forces (per unit volume)". The forces acting on the volume in this case are, the external body force applied by gravity (i.e. the buoyancy force), and the internal forces applied by the viscous and pressure stresses that appear when a fluid is brought into motion. Therefore, making use of the *Navier-Stokes Equation* in vectorial form this can be depicted as:

$$\rho_i \frac{Du_i}{Dt} = -\nabla P_i + \mu_i \nabla^2 u_i + \frac{1}{3}\mu_i \; grad\left(\nabla . u_i\right) + F_i \qquad \textbf{Equation 5-1}$$

Where ρ_i, u_i, P_i, μ_i and F_i are the generic density, velocity, pressure, dynamic viscosity and external force, respectively.

The left hand side of Equation 5-1corresponds to the rate of change of momentum, i.e. the inertial force per unit volume, and the terms on right hand side are the applied forces per unit volume, i.e. the pressure force, the viscous force due to the shear stresses (i.e. the rate of stress), the viscous force due to the deformation (i.e. the rate of deformation or rate of strain), and the buoyancy force, respectively.

When assuming an incompressible fluid (i.e., no deformation), the fourth term in Equation 5-1 disappears since the divergence of the vector field velocity, ∇u_i, equals zero, i.e.:

$$\nabla u_i = \frac{\delta u}{\delta x} + \frac{\delta v}{\delta y} + \frac{\delta w}{\delta z} = 0$$ **Equation 5-2**

Thus, Equation 5-1 reduces to:

$$\rho_i \frac{Du_i}{Dt} = -\nabla P_i + \mu_i \nabla^2 u_i + F_i$$ **Equation 5-3**

The gravitational force per unit volume or buoyancy force, F_i, acts through the centre of gravity, thus, its only component is the vertical one, F_y. Gravitational forces are only significant when there are density differences; i.e., when $\Delta\rho \neq 0$. Given the existence of a density difference between the ambient air and the combustion gases in the vicinity of the heat source – namely the *near field* surrounding the fire – this results in the gravitational force not only being relevant but also the flow system main driver. It is defined as:

$$F_y = \rho_a g$$ **Equation 5-4**

where g is the acceleration due to gravity, and ρ_a the density of the ambient air.

When natural convection is the main driver of fluid motion, far away from the fire source – namely the *far field* – where the density differences are sufficiently small (i.e. $\Delta\rho \approx 0$), it can be assumed that $\rho_a \approx \rho_g$, where ρ_g is the density of the combustion gases. However, as stated before, when expressing the buoyancy force, F_y, this assumption does not apply [100]. This is known as the *Boussinesq approximation* which expresses that while the difference in inertia between the two fluids is negligible, gravity is still sufficiently strong to make the specific weight between them substantially different; i.e., $\rho_a g \neq \rho_g g$.

According to this approximation, in the *far field* where the velocities, u_i, are zero, Equation 5-3 can be simplified to:

$$0 = -\nabla P_i + \rho_g g$$ **Equation 5-5**

This means that when the fluid is at rest describing a stratified flow case, the hydrostatic solution to the *Navier-Stokes Equation* (Equation 5-3) shows that the gravitational force, $\rho_g\, g$, is balanced by a vertical pressure gradient, ∇P_i. This applies when the only body force acting is the gravitational force and when considering a flow with no free surface, as it is in this case.

This hydrostatic balance (i.e., $\rho_g\, g = \nabla P_i$) can be subtracted from the dynamical relation – this is, the *Navier-Stokes Equation* applied to the *near field* where the fluid is not any more at rest – reducing the problem to either:

(1) one with no body forces (i.e., $F_i = 0$), as long as the local pressure is measured relative to the undisturbed hydrostatic pressure which would occur with equilibrium under gravity at the point considered [119], or

(2) one with no pressure gradient (i.e., $\nabla P_i = 0$), as long as the pressure term is replaced by the buoyancy force that would have been present under hydrostatic equilibrium, $\rho_g\, g$.

Taking the second approach, Equation 5-5 can be substituted in the *near field*, i.e., into Equation 5-3, giving as a result the following dynamic equation:

$$\rho_a \frac{Du_i}{Dt} = -\rho_g g + \mu_a \nabla^2 u_i + \rho_a g \qquad \textbf{Equation 5-6}$$

Rearranging,

$$\rho_a \frac{Du_i}{Dt} = \mu_a \nabla^2 u_i + g\left(\rho_a - \rho_g\right) \qquad \textbf{Equation 5-7}$$

The third term in this equation shows a *resultant buoyancy force* – referred from now as buoyancy force for simplicity – which is relative to that found under hydrostatic equilibrium. Dividing now Equation 5-7 by ρ_a gives,

$$\frac{Du_i}{Dt} = \nu_a \nabla^2 u_i + g\left(\frac{\rho_a - \rho_g}{\rho_a}\right)$$ **Equation 5-8**

Where ν_a is the kinematic viscosity of the ambient air, and the last term is the so-called *reduced gravity*, *g'*. This shows that under *Boussinesq* flow circumstances, the only sensible way that acceleration due to gravity, *g*, enters the equation of motion is in this term.

The relative importance of the inertial, pressure, and viscous forces – first, second, and third term in Equation 5-6, respectively – all triggered by the buoyancy force F_y, will therefore determine the flow pattern (i.e., the system's ventilation *mode*) and consequent *regime of behaviour* of any chosen fire situation or characteristic compartment fire scenario.

5.2.1.1 Scale Analysis Applied to the Generic (2D) Fluid Motion

The generic dimensionless relations will now be generated to fit in Equation 5-7 and generalise said flow pattern towards the analysis of selected characteristic scenarios. These ratios are defined as:

$$\tilde{u}_i = \frac{u_i}{U_i}$$ **Equation 5-9**

$$\tilde{x}_i = \frac{x_i}{H_i}$$ **Equation 5-10**

$$\tilde{t} = \frac{t}{\tau}$$ **Equation 5-11**

$$\Delta\tilde{P}_i = \frac{\Delta P_i}{\Delta P_c}$$ **Equation 5-12**

Where $\tilde{u}_i$, $\tilde{x}_i$, $\tilde{t}$, and $\Delta\tilde{P}_i$ are the generic *dimensionless* velocity, length, time, and pressure, respectively; u_i, x_i, t, and ΔP_i are the generic *actual* velocity, length, time,

and pressure, respectively; and finally U_i, H_i, τ, and ΔP_c are the generic *characteristic* velocity, length, time, and pressure, respectively.

The dominant characteristic time, τ, will be extracted from all the multiple characteristic times possible as:

$$\tau = \frac{H_i}{U_i}$$ **Equation 5-13**

Whereas the generic characteristic pressure, ΔP_c, is that extracted from the dominant generic characteristic velocity, U_i, as:

$$\Delta P_c = \rho_a U_i^2$$ **Equation 5-14**

With these generic dimensionless relations and Equation 5-7 at hand, it is now possible to analyse and further classify a range of characteristic fire scenarios that range from the open to the fully-enclosed configuration.

The usual way to assess this is through a *scale analysis* with which the magnitude of the individual terms can be approximated and compared in the same circumstances, ignoring those which are relatively small. The original differential equation – Equation 5-7 in this case – can be then simplified by removing those terms which have a negligible effect on the integrated solution. The essential difficulty in applying this method is defining the characteristic lengths that define the scale of each term and ultimately that of the system, in order to decide what physical forces are negligible and which are the drivers in a given flow situation.

Equation 5-7 is re-written for clarity:

$$\rho_a \frac{Du_i}{Dt} = \mu_a \nabla^2 u_i + g\left(\rho_a - \rho_g\right)$$ **Equation 5-7**

And presented in differential form:

$$\rho_a\left(\frac{\delta u}{\delta t}+u\frac{\delta u}{\delta x}+v\frac{\delta u}{\delta y}\right)=\mu_a\left(\frac{\delta^2 u}{\delta x^2}+\frac{\delta^2 u}{\delta y^2}\right)+g\left(\rho_a-\rho_g\right) \qquad \textbf{Equation 5-15}$$

Each of the terms in Equation 5-7 (or Equation 5-15) can be approximated with the correspondent characteristic property, as shown in Table 5-1:

Table 5-1: Approximated terms in Equation 5-7

Inertial force (per unit volume)	**Viscous force** (per unit volume)	**Buoyancy force** (per unit volume)
$\rho_a\frac{U_i^2}{H_i}$	$\mu_a\frac{U_i}{H_i^2}$	$g\left(\rho_a-\rho_g\right)$

Where – as it will be seen in more detail in the following sections – the generic characteristic length, H_i, is different in each fire situation depending on the circumstances of the particular case analysed.

5.2.2 The Open Fire

Generally, the problem of an open or free burning pool fire has *one* fundamental characteristic length scale symbolising the fire size. The fire size can typically be represented either by the fuel bed's equivalent diameter or by the flame height. Figure 5-1 depicts the open fire situation:

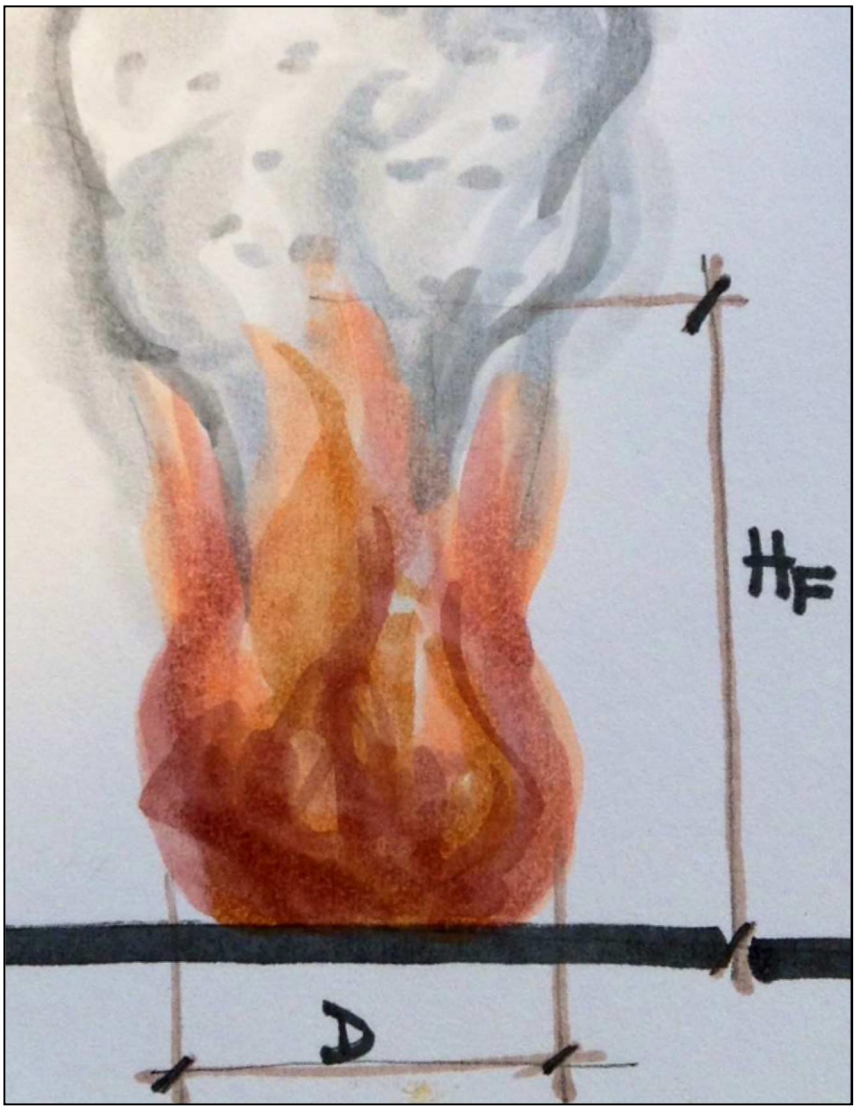

Figure 5-1: Characteristic lengths in an Open Fire

Figure references:

***H_F* = flame height (e.g. 1~3 m)**
***D* = equivalent diameter of fire (e.g. 3~4 m)**

Extensive literature [100][16] has demonstrated that both length scales – D and H_F – are related for different fire configurations, thus, this guarantees that in the end there is only *one* fundamental length scale (i.e., $H_i = H_F = D$), which in this case will be represented by the fire's equivalent diameter, D.

Knowing the characteristic length, D, the principle of *conservation of momentum* (per unit volume) can be applied with the force terms approximated (as per Table

5-1), to analyse their relative magnitude and thus characterise the fluid motion. Further, the dominant velocity in an open fire situation is the vertical velocity, *v*, which is that depicted in Figure 2-4; i.e., $v_{fire,MAX}$ (Equation 2-34). Thus, the force terms approximated for this case are represented in Table 5-2 as:

Table 5-2: Force Terms Approximated for the Open Fire Case

Inertial force (per unit volume)	**Viscous force** (per unit volume)	**Buoyancy force** (per unit volume)
$\rho_a \frac{v^2}{D}$	$\mu_a \frac{v}{D^2}$	$g\left(\rho_a - \rho_g\right)$

The order of magnitude of the buoyancy term will be:

$$g\left(\rho_a - \rho_g\right) = O\left(10^1\right) O\left(10^0\right) = O\left(10^1\right) \qquad \textbf{Equation 5-16}$$

Assuming no viscous forces as a first approximation, the buoyancy term equals the inertia term which will have the same order of magnitude; i.e., $O(10^1)$. Then, the expression to obtain the velocity's maximum order of magnitude can be obtained by working the velocity out from the equality statement as:

$$\frac{\rho_a v^2}{D} = g\left(\rho_a - \rho_g\right) \quad \Rightarrow \quad v_{fire,MAX} = \sqrt{g\left(\frac{\rho_a - \rho_g}{\rho_a}\right) D} \qquad \textbf{Equation 5-17}$$

Thus, disregarding the viscosity, the vertical velocity will be at maximum of the order:

$$v_{fire,MAX} = \sqrt{O(10^1)\,O(10^0)\,O(10^0)} = O(10^0)^* \qquad \textbf{Equation 5-18}$$

We can now substitute this maximum velocity in the viscous term, to analyse what its maximum order of magnitude would be if accounted for:

$$\mu_a \frac{v}{D^2} = \frac{O(10^{-6})\,O(10^0)}{O(10^0)} = O(10^{-6}) \qquad \textbf{Equation 5-19}$$

When comparing all three terms, it is clear that the viscous forces are negligible and, thus, the *a priory* assumption of ignoring them is now validated. Therefore, the buoyancy force leads to the inertial force, creating an upward flow with vertical accelerations within and in the immediate surroundings of the fire plume.

Summarizing this case, the gasified fuel and air are transported towards each other by a combination of buoyancy and viscous forces (the latter negligible in relative terms), so that combustion occurs in the zone where they mix. In addition, the difference in density – given by the difference in temperature – between the hot products of combustion and the cold surrounding air, will make the combustion gases rise upwards as a result of the buoyancy force. The resultant buoyancy force can generate turbulence if the length scale is large enough, and in the case of fires beyond a candle flame, this always results in turbulent upward flows, generally referred to as the *fire* or *buoyant plume*. Moreover, air is entrained not only into the flame zone providing the oxygen for the combustion of the fuel, but also – once more due to a combination of buoyancy and viscous forces – along the entire fire plume envelope mixing up with the hot rising gases. If present, turbulence will enhance air entrainment by a combination of natural convection and friction. This cold air entrainment dilutes the combustion products, increasing progressively the plume's volume and decreasing its temperature and velocity as a function of height.

---

* Assuming the nondimensionalised density of the order 10^0 ($\Delta\rho/\rho_a \approx 1$) means that the *Boussinesq approximation* can no longer be applied. This is correct, since the maximum velocity is found in the proximities of the fire; i.e., in the *near field*, where the density difference ($\Delta\rho$) is significant and of the order of ρ_a.

This description characterizes the typical buoyant (generally turbulent) entrainment mode of cold air into an upward moving stream of hot gases where, in sum, the resultant buoyant flow determines the structure of the flames, the energy released, and the transport of the combustion products upwards in consequential order. Because in a free pool this mode of air entrainment is physically unrestricted and exceeds the requirements for fuel consumption, the limiting reactant is the fuel and, thus, can be labelled as a *fuel-controlled* fire in terms of its *burning mode* (see Section 5.2.3.1). It appears clear, therefore, how relevant the fuel's characteristics are in natural fires – in particular its type, amount, L, and surface area exposed, A_f.

5.2.3 The Confined Fire

5.2.3.1 Burning Regimes

In this dissertation, compartment fires are proposed to be classified into different *regimes of behaviour* – or simply *regimes* – which arise as a combination of *ventilation* and *burning modes* or mechanisms. As introduced above, the *ventilation mode* defines the principle gas flow driver within, into and out of the compartment. *Burning mode* defines the limiting factor for combustion; i.e., rate of production of fuel or the rate of air supply to the decomposing fuel (refer to Section 1.3.2.2.4). The proposed set of *regimes of behaviour* and their respective *burning* and *ventilation modes* are listed in Table 5-3 as:

Table 5-3: Regimes of Behaviour

Ventilation Mode / Burning Mode	***Fire*** (*turbulence driven*) ***Induced***	***Fire*** (*turbulence + inertia driven*) ***& Compartment*** (*stack driven*) ***Induced***	***Compartment*** (*stack driven*) ***Induced***
Fuel-controlled (unrestricted air transport)	*Regime A**	*Regime C***	*Regime E §***
Ventilation-controlled (restricted air transport)	*Regime B §***	*Regime D §***	*Regime F**

Table references:

*** Historically defined as *Regime II* (here *Regime A*) & *Regime I* (here *Regime F*)** [29]
**** Newly defined**
§ Derived from the Regime with the same Ventilation Mode

The '*§*' symbol in Table 5-3 designates a *derived* regime, i.e. a regime that shares the majority of the characteristics as the regime with an identical *ventilation mode,* but has one or more significant differences so as to warrant a separate classification. For example *Regime B* is a derivation of *Regime A*, *Regime D* of *Regime C*, and *Regime E* of *Regime F*. These classifications will be referred to and developed in the following section (Section 5.2.3.2) by addressing a set of representative cases in

detail. These cases aim to provide an envelope encompassing the envisaged range of characteristic behaviours.

Further, it is important to note that the *burning mode* defines a general tendency for the actual *burning rate* with respect to that in an open fire – assuming same fuel load density, *L"* – but does not take into account the thermal feedback effect which would depend on each compartment configuration. In other words, *fuel*-controlled and *ventilation*-controlled *burning modes* generally tend to give similar and lower *burning rates*, respectively, than an open fire burning condition *before* the thermal feedback is computed into the analysis.

The presence of a compartment introduces numerous characteristic length scales that need to be considered when establishing the mechanisms controlling the nature of a fire within it. Figure 5-2 represents a schematic that illustrates some of the potential length scales in a two dimensional framework. It is clear that a third dimension could potentially introduce numerous other length scales, nevertheless for simplicity, the problem will be discussed as two dimensional.

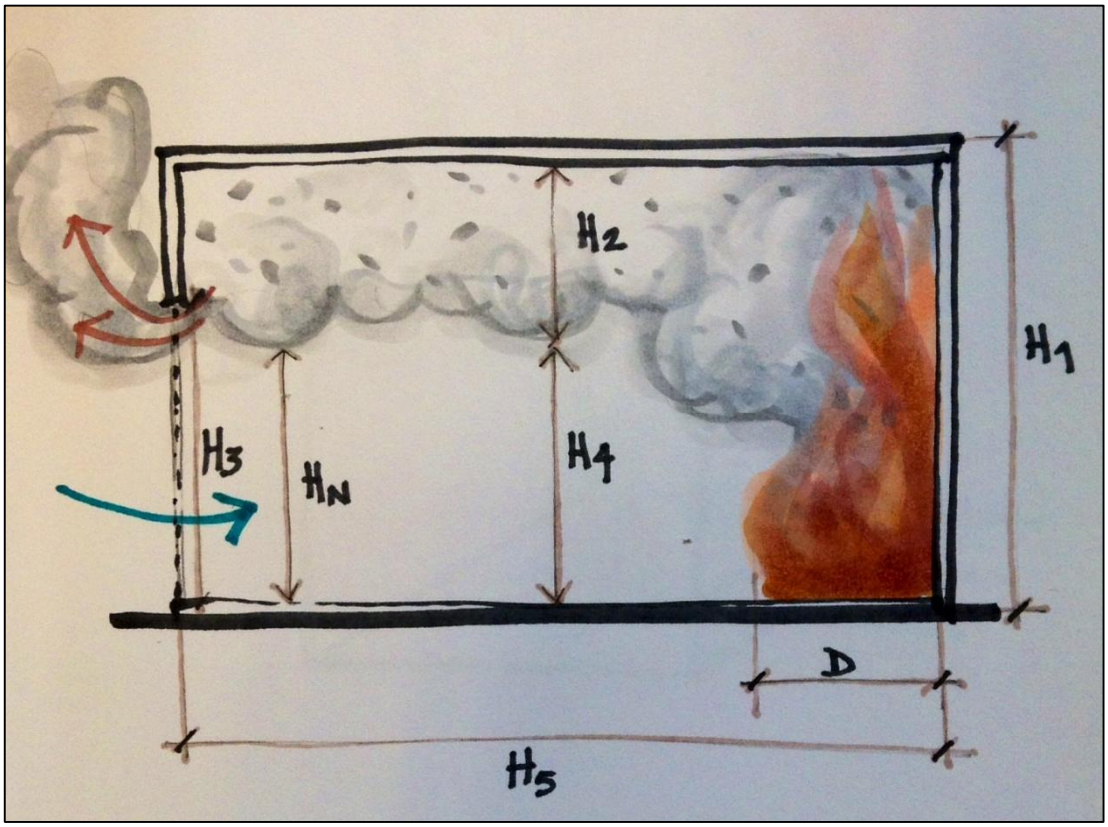

Figure 5-2: Characteristic Lengths in a Compartment Fire

Figure references:

***H_1* = ceiling height**
***H_2* = smoke layer height**
***H_3* = opening height**
***H_4* = *H_D* = clean layer height**
***H_5* = compartment depth (≈ compartment width)**
***N* = *H_N* = neutral plane height**
***D* = equivalent diameter of a fully-developed fire**

The extent to which the confinement influences the main characteristics of a fire will be exposed in the following section (Section 5.2.3.2) as different cases that range from small to large enclosed volumes. Each case is associated to a different characteristic (or extreme) compartment configuration and scenario. For each particular case, a scaling analysis – aided with information on the characteristic or dominant velocities taken from the modified two-layer model previously presented (Section 2.3.4.4) – will help characterise (1) the *flow pattern* and assist in defining (2) the *ventilation mode*. Also, the (3) *burning mode* and consequent (4) *regime* (refer to Table 5-3) will be further defined. Finally, a characteristic (5) *burning rate*

and (6) *heat exchange rate* will also be described. All these parameters are assumed as representative of a fully-developed stage where no time scale is introduced in the analysis; i.e., they are assumed at a peak steady-state condition to run the analysis on the conservative side.

5.2.3.2 Representative Cases

Most experimental studies conducted in real scale compartments dealt with cubic volumes of the order of 4 m x 4 m x 4 m [34], therefore this will be taken as the reference compartment (*Case 1* in Table 5-4). Many studies have been reported [58][59] using smaller compartments of similar cubic nature. For the purpose of this exercise these scaled-down studies will be treated also as *Case 1*, where the horizontal length scale, $H_{5,}$ is of the order of the vertical one, H_1, and of the characteristic fire diameter, D (i.e., $H_1 \approx H_5 \approx D$ – refer to Figure 5-2).

For convenience three other extreme cases are defined as follows: *Case 2* corresponds to a compartment with a height much greater than the characteristic horizontal length scale and characteristic fire diameter (i.e., $H_1 >> H_5 \approx D$); *Case 3* corresponds to the opposite scenario where the horizontal characteristic length scale is much larger than the height (i.e., $H_5 >> H_1 \approx D$); and finally, *Case 4* corresponds to a very large volume compartment (i.e., $H_1 \approx H_5 >>$ D). The four characteristic cases are summarised in the following table:

Table 5-4: Characteristic Cases

Ceiling Height (H_1) / *Floor Area Size (H_5 x H_5)*	***SHORT*** (e.g. 4 m)	***TALL*** (e.g. 20 m)
SMALL (e.g. 4 m x 4 m)	***Case 1***: $H_1 \approx H_5 \approx D$	***Case 2***: $H_1 >> H_5 \approx D$
LARGE (e.g. 20 m x 20 m)	***Case 3***: $H_5 >> H_1 \approx D$	***Case 4***: $H_1 \approx H_5 >>$ D

Additionally, for the following scaling analysis, *Cases 1* to *3* will be divided into *(a)* large opening, and *(b)* small opening, while *Case 4* will instead be divided into *(a)* vented, and *(b)* not vented, for reasons that will be explained at the relevant stage of each analysis. In some situations, a combination of *Cases* (*a)* and *(b)* – labelled as *Case (ab)* – is introduced for further comprisal of the analysis. The following table summarises the representative diagrams for each of the characteristic cases:

Table 5-5: Diagram Summary

TALL	***Case 2***: $H_1 >> H_5 \approx D$	***Case 2(b)***	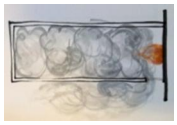	***Case 4: $H_1 \approx H_5 >>$ D***	***Case 4(ab)***	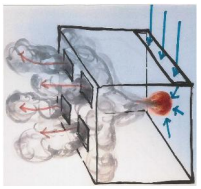
		Case 2(ab)	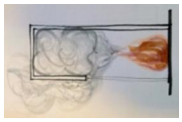		***Case 4(a)***	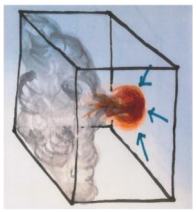
		Case 2(a)	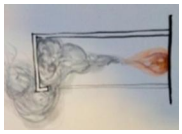			
SHORT	***Case 1***: $H_1 \approx H_5 \approx D$	***Case 1(b)***	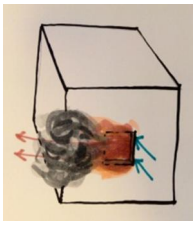	***Case 3: $H_5 >> H_1 \approx D$***	***Case 3(b)***	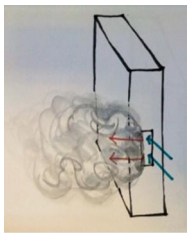
		Case 1(a)	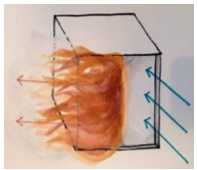		***Case 3(ab)***	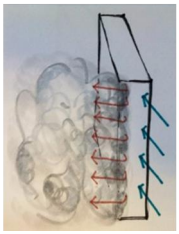
					Case 3(a)	
	SMALL			**LARGE**		

Knowing the characteristic length scale, H_i, and the dominant velocity, U_i, in each characteristic scenario, the principle of *conservation of momentum* (per unit volume) is applied in the same fashion as it was done for the open fire case in Section 5.2.2 – with the force terms approximated (refer to Table 5-1), to analyse their relative magnitude and thus characterise the *flow pattern* and define the *ventilation mode*. These, as stated above, are the first and second steps in the case analysis, followed by the definition of the *burning mode* and consequent *regime of behaviour* (refer to Table 5-3), and description of the *burning rate* and *heat exchange rate*.

5.2.3.2.1 Case 1(a): Small + Short + Large Opening

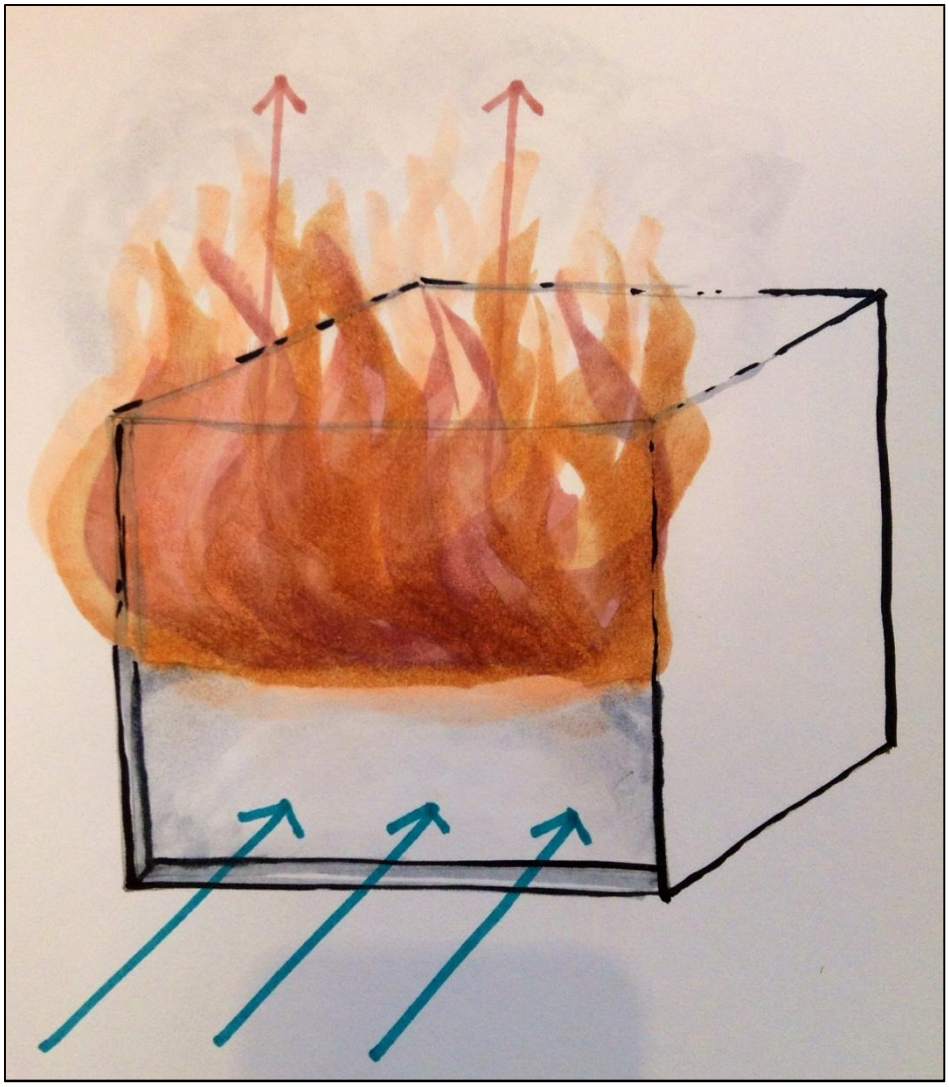

Figure 5-3: Case 1(a)

$$\text{Particular ities} \begin{cases} H_1 \approx H_5 \approx D \rightarrow (\text{fully} - \text{developed fire}) \\ H_1 \approx H_3 \rightarrow (\text{large opening}) \\ H_1 \approx H_4 \quad \vee \quad H_2 \approx 0 \rightarrow (\text{no hot gas layer built - up}) \end{cases}$$

In scaling terms, the order of magnitude of the buoyancy term will be:

$$g\left(\rho_a - \rho_g\right) = O\left(10^1\right) O\left(10^0\right) = O\left(10^1\right) \qquad \textbf{Equation 5-20}$$

Assuming no viscous forces as a first approximation, the buoyancy term equals the inertia term which will have the same order of magnitude: $O(10^1)$. Further, being that the dominant velocity in this case is that from Figure 2-4; i.e., $v_{fire,MAX}$ (Equation 2-34) like in an open fire situation, the expression to obtain the velocity's maximum order of magnitude can be obtained by working the velocity out from the equality statement as:

$$\frac{\rho_a v^2}{D} = g\left(\rho_a - \rho_g\right) \qquad \Rightarrow \qquad v_{fire,MAX} = \sqrt{g\left(\frac{\rho_a - \rho_g}{\rho_a}\right) D} \qquad \textbf{Equation 5-21}$$

Thus, disregarding the viscosity, the vertical velocity will be at maximum of the order:

$$v_{fire,MAX} = \sqrt{O\left(10^1\right) O\left(10^0\right) O\left(10^0\right)} = O\left(10^0\right) \qquad \textbf{Equation 5-22}$$

If the viscous force was to be taken into account, the characteristic length, H_i, in this case will take the form of the fire diameter D. Then, using the maximum velocity estimated above, the term would be at maximum of the order:

$$\frac{\mu_a v_{fire,MAX}}{D^2} = \frac{O\left(10^{-6}\right) O\left(10^0\right)}{O\left(10^1\right)} = O\left(10^{-7}\right) \qquad \textbf{Equation 5-23}$$

In a similar fashion to the open fire case, when comparing all three terms, it is clear that since the viscous forces are negligible – and thus the *a-priory* assumption of

ignoring them is validated for this case too – the buoyancy force leads to the inertial force, creating an upward flow with vertical accelerations within the compartment.

Philip Thomas [29] described this case in the following way:

> "If the accelerations are large, the pressure gradients become small and there are only small inflows (…) termed entrainment."

In summary, when small compartments have large openings, the air drawn into the fire zone will be determined by natural cold entrainment (i.e., a natural fire-induced or turbulence-driven *ventilation mode*) into an upward moving hot stream of gas driven by the buoyancy force created by the temperature – and thus density – difference between the flame and the ambient atmosphere surrounding the fire. Due to the reduced compartment geometry and large opening, no hot layer accumulation is viable and, thus, no stack-induced entrainment (i.e., induced by the hydrostatic pressure difference, namely compartment-induced) could be achieved. In terms of the *burning mode*, the fire in this case will be fuel-controlled, behaving almost like in the open with a *burning rate* equal or close to that expected in an exterior fire. This case is the historically termed *Regime II* [29] behaviour (renamed as *Regime A* in Table 5-3), where the available airflow for combustion is unrestricted (i.e., fuel-controlled) and purely fire-induced (i.e., drawn by the fire itself in the typical turbulence-driven fashion). The good mixing of volatiles with fresh air allows for a good combustion process and consequent high temperature combustion products giving as a result an intense *heat exchange rate* with the target. This, in turn, can potentially enhance the *burning rate* through the thermal feedback from the heated inner surfaces, and that coming from a potentially tilted flame that bends when encountering the ceiling.

5.2.3.2.2 *Case 1(b): Small + Short + Small Opening*

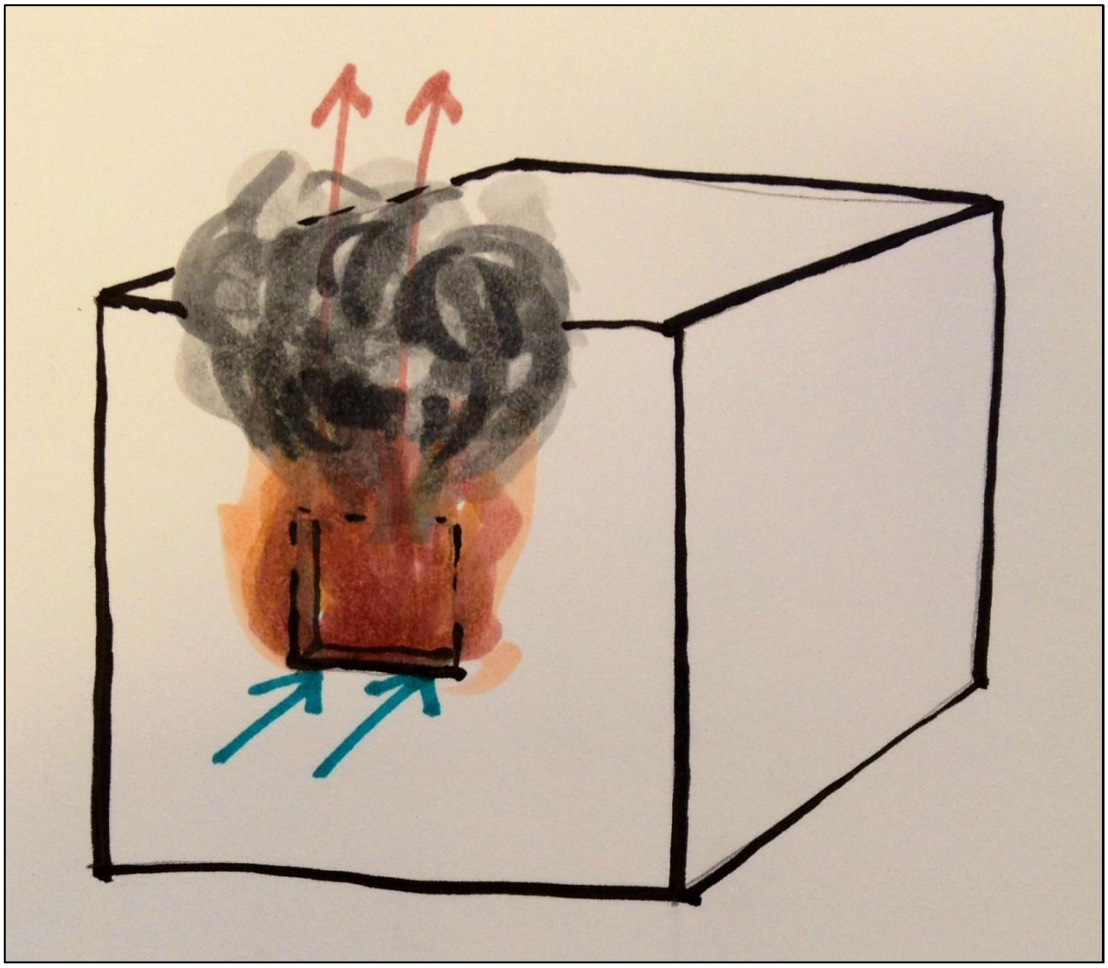

Figure 5-4: Case 1(b)

$$\text{Particularities} \begin{cases} H_1 \approx H_5 \approx D \rightarrow (\text{fully} - \text{developed fire}) \\ H_1 >> H_3 \rightarrow (\text{small opening}) \\ H_1 \approx H_2 \quad \vee \quad H_4 \approx 0 \rightarrow (\text{hot gas layer almost at floor level}) \end{cases}$$

Similarly to the previous case, the order of magnitude of the buoyancy term will be:

$$g\left(\rho_a - \rho_g\right) = O\left(10^1\right) O\left(10^0\right) = O\left(10^1\right) \qquad \textbf{Equation 5-24}$$

This would be the case of a single uniform hot layer inside the compartment (Figure 2-3). As there are no vertical velocities within the compartment, the buoyancy force

exerted by the hot gas layer on the compartment is converted straightaway into a pressure force. By combining Equation 5-14 and the inertial force term approximated from Table 5-1, the pressure force term can be approximated as:

$$\rho_a \frac{U_i^2}{H_i} \quad \wedge \quad \Delta P_c = \rho_a U_i^2 \quad \Rightarrow$$

$$\Rightarrow \quad \textit{pressure force term approx.} = \frac{\Delta P_c}{H_i} \qquad \textbf{Equation 5-25}$$

The characteristic length related to the pressure term in this case will be the smoke layer height ($H_i \approx H_1 \approx H_2$), so by making the buoyancy term equal to the pressure term (there is no viscosity force in the vertical equation since there is no vertical velocity), the following expression describing the characteristic hydrostatic pressure difference, ΔP_c, is obtained:

$$\frac{\Delta P_c}{H_2} = g\left(\rho_a - \rho_g\right) \qquad \Rightarrow \qquad \Delta P_c = g\left(\rho_a - \rho_g\right) H_2 \qquad \textbf{Equation 5-26}$$

Thus, the characteristic presure would be at maximum of the order:

$$\Delta P_c = g\left(\rho_a - \rho_g\right) H_2 = O\left(10^1\right) O\left(10^0\right) O\left(10^0\right) = O\left(10^1\right) \qquad \textbf{Equation 5-27}$$

The dominant velocities in this case will therefore be the horizontal inflow and outflow velocities, u_{in} and u_{out} respectively, triggered by the hydrostatic pressure difference between the compartment and the ambient atmosphere. Disregarding the horizontal viscous forces as a first approximation, the pressure force will be fully converted into inertial force; thus, equating both terms will allow scaling the maximum horizontal outflow velocity as:

$$\frac{\rho_g u_{out}^2}{H_2} = \frac{\Delta P_c}{H_2} \qquad \Rightarrow \qquad u_{out} = \sqrt{\frac{\Delta P_c}{\rho_g}} = \sqrt{\frac{O\left(10^1\right)}{O\left(10^0\right)}} = O\left(10^0\right) \qquad \textbf{Equation 5-28}$$

The inflow and outflow velocities are related by the *continuity equation*; i.e., by the principle of *conservation of mass*, which expresses that the rate of entrained air,

$\dot{m}_{in}$ – in this case into the compartment – must equal the rate of expelled gases, $\dot{m}_{out}$, from the compartment. Both mass flow rates can be expressed as:

$$\dot{m}_{in} = A_{in}\, u_{in}\, \rho_a = W_w\, H_{3\text{–}in}\, u_{in}\, \rho_a \qquad \textbf{Equation 5-29}$$

$$\dot{m}_{out} = A_{out}\, u_{out}\, \rho_g = W_w\, H_{3\text{–}out}\, u_{out}\, \rho_g \qquad \textbf{Equation 5-30}$$

with A_{in} and A_{out} being the inflow and outflow opening areas, respectively, W_w being the opening width, and $H_{3\text{-}in}$ and $H_{3\text{-}out}$ being the inflow and outflow heights of the opening, respectively. Assuming equal densities (*Boussinesq approximation*) and that the inflow height, $H_{3\text{-}in}$ ($\approx N$ or H_N), is some percentage x of the total window height H_3 (equivalent to the ratio of the neutral plane height, N, to the total window height, H_3), it is found that:

$$W_w\left(xH_3\right)u_{in}\,\rho_a = W_w\left[\left(1-x\right)H_3\right]u_{out}\,\rho_g \qquad \textbf{Equation 5-31}$$

Rearranging,

$$u_{in} = \left(\frac{1-x}{x}\right)u_{out} \qquad \textbf{Equation 5-32}$$

Given that in this case x is always < 0.5 (i.e., inflow area < outflow area), it is found that $u_{\text{in}} > u_{\text{out}}$. For example, assuming x as 1/3 gives as a result an inflow velocity which is twice the outflow velocity, and assuming x as 1/10 gives a multiplying factor of 9. Being that the outflow velocity was of the order 10^0, assuming the limiting situation of an extremely reduced inflow area will give an inflow velocity of the order 10^1 (i.e., 10^0 multiplied by a factor of around 10). With these estimations, both the inflow and outflow viscous force terms can further be scaled and see if the assumption of disregarding them still holds. Because there is inflow along the height N, and outflow along the height ($H_3 - N$), these are the characteristic length to be taken. Thus, the viscous force terms would be at maximum of the order:

$$\frac{\mu_a u_{in}}{N^2} = \frac{O(10^{-6})\,O(10^{1})}{O(10^{0})} = O(10^{-5})$$ **Equation 5-33**

$$\frac{\mu_g u_{out}}{(H_3 - N)^2} = \frac{O(10^{-6})\,O(10^{0})}{O(10^{0})} = O(10^{-6})$$ **Equation 5-34**

It becomes clear, once more, that both viscosity terms can be neglected and, hence, the assumption of disregarding them *a priori* is acceptable.

Therefore, in this case the buoyancy force is balanced by the hydrostatic pressure difference created by the stack of hot smoke accumulated under the ceiling. These pressure differences are responsible for the horizontal velocities of the inflow air and outflow gases that give place to the *flow pattern* sometimes described as the 'chimney effect'.

Philip Thomas [29] described this case as follows:

> "If the window openings are small, we have small vertical accelerations and the buoyancy is balanced by a pressure gradient which causes horizontal flows."

In summary, as the opening is reduced, the process by which the air is drawn into the compartment changes from a fire-induced *ventilation mode* (i.e., turbulence-driven/entrainment mode) to a compartment-induced mode (i.e., stack-driven/stack mode). This transition is a consequence of the enhanced enclosure effects: the loses through the opening are reduced, creating a fairly constant spatial temperature field within the compartment that essentially prompts it to act as a chimney, drawing air into the fire zone in a stack-driven motion. In terms of the *burning mode*, the fire is now ventilation-controlled, since the restricted rate of air inflow now controls the rate of pyrolysis by regulating the rate of heat supply to the charring fuel. This case is the historically termed *Regime I* [29] behaviour (*Regime F* in Table 5-3), where the available (restricted) air for combustion is all drawn in a stack-driven fashion. Due to the fact that in small compartments the maximum gas temperatures occur at

relatively low ventilation conditions, the large volume of hot combustion products accumulated under the ceiling allow for an intense *heat exchange rate* between these and the structure. This, in turn, can potentially enhance the *burning rate* through thermal feedback from both the heated inner surfaces, and the hot gas layer.

5.2.3.2.3 Case 2(a): Small + Tall + Large Opening

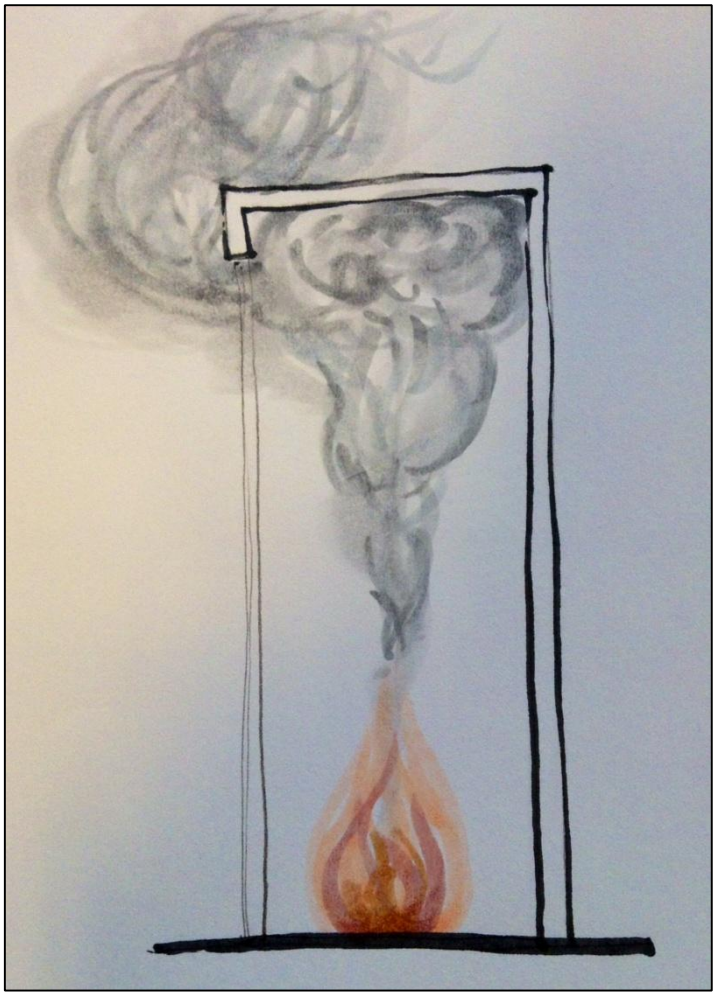

Figure 5-5: Case 2(a)

$$\text{Particular ities} \begin{cases} H_1 >> H_5 \approx D \rightarrow (\text{fully} - \text{developed fire}) \\ H_1 \approx H_3 \rightarrow (\text{large opening}) \\ H_1 \approx H_4 \quad \vee \quad H_2 \approx 0 \rightarrow (\text{no hot gas layer buit - up}) \end{cases}$$

In this particular case of a configuration with extremely large openings of the size of the full compartment height for instance, the *flow pattern* will be that of the buoyant force transforming purely into inertial force (i.e., the pattern of an open fire), the *ventilation mode* will purely be naturally fire-induced (i.e., turbulence-driven

because no hot layer accumulation is allowed), and the fire will burn following a *fuel-controlled mode* with a *burning rate* potentially enhanced only by the thermal feedback from the surrounding heated walls, giving as a result, a *Regime II* behaviour (*Regime A* in Table 5-3), similar to that presented under ***Case 1(a)***. The *thermal impact* on the lower structure could be significant after the close flame-walls radiative heat transfer, as much as the upper impact will be insignificant due to the extensive dilution of the products of combustion accumulated there (if any), and the considerable distance to the flame.

5.2.3.2.4 Case 2(ab): Small + Tall + Large Opening

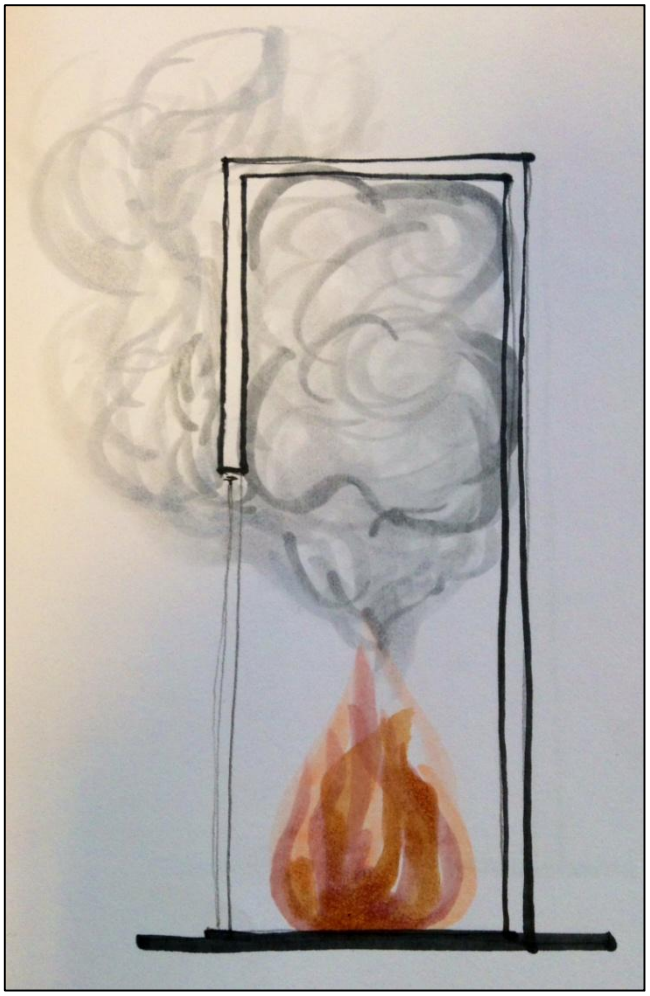

Figure 5-6: Case 2(ab)

$$\text{Particularities} \begin{cases} H_1 >>> H_5 \approx D \rightarrow (\text{fully} - \text{developed fire}) \\ H_1 > H_3 \rightarrow (\text{still large opening}) \\ H_1 > H_2 \rightarrow (\text{still large hot gas layer built} - \text{up}) \\ H_4 \approx H_2 \rightarrow (\text{equally large cold and hot layers} (\sim 10\text{m})) \end{cases}$$

Same as in the previous cases, the order of magnitude of the buoyancy term will be:

$$g\left(\rho_a - \rho_g\right) = O\left(10^1\right)O\left(10^0\right) = O\left(10^1\right)$$ **Equation 5-35**

This particular case could either be that shown in Figure 2-6 ($T_L \neq T_0$), or in Figure 2-7 ($T_L = T_0$) in Section 2.3.4.4. This means that there are velocities in both horizontal and vertical directions. Nevertheless, it is still not known which component of the velocity is the dominant one. By analysing the upward stream assuming no viscous forces in this direction for the time being, the buoyancy term can be equated to the inertial term – which will have the same order of magnitude of 10^1 – and work out the maximum vertical velocity, $v_{fire,MAX}$, as:

$$\frac{\rho_a v^2}{D} = g\left(\rho_a - \rho_g\right) \quad \Rightarrow \quad v_{fire,MAX} = \sqrt{g\left(\frac{\rho_a - \rho_g}{\rho_a}\right)D}$$ **Equation 5-36**

This is clearly the same as Equation 2-34, although taking into account that when dealing with maximum orders of magnitudes, some constants – like the ½ associated to the inertial energy force – turn irrelevant for the analysis and are thus ignored.

Thus, disregarding the viscosity, the vertical fire plume velocity will be at maximum of the order:

$$v_{fire,MAX} = \sqrt{O\left(10^1\right)O\left(10^0\right)O\left(10^0\right)} = O\left(10^0\right)$$ **Equation 5-37**

If the viscous force was to be taken into account, the characteristic length H_i in this case will take again the magnitude of the fire diameter D. Then, using the maximum velocity estimated above, the upward viscosity term would be at maximum of the order:

$$\frac{\mu_a v_{fire,MAX}}{D^2} = \frac{O\left(10^{-6}\right)O\left(10^0\right)}{O\left(10^1\right)} = O\left(10^{-7}\right)$$ **Equation 5-38**

Once more, the ruling out of the vertical viscous term from the analysis appears realistic given its low relative weighting relevance.

Assuming steady-state conditions, when the plume encounters the smoke layer, all its inertial energy is converted into pressure energy extinguishing the vertical velocity. On the other hand, the condition in the accumulated and stagnant hot layer was already that of its buoyancy force being converted into pressure force. So this implies a situation where the buoyancy force – which was fully converted into inertial force in the upward moving stream – is now converted into pressure force that adds up to the pressure already built-up by the buoyancy of the former hot layer stack. This gives as a result, a characteristic pressure term expressed as follows:

$$\Delta P_c = \rho_a v_{fire,MAX}^2 + g\left(\rho_a - \rho_g\right)H_2 \qquad \textbf{Equation 5-39}$$

This means that the maximum ΔP – i.e., the characteristic pressure difference, ΔP_c – would be of the order of:

$$\Delta P_c = O\left(10^0\right)O\left(10^0\right) + O\left(10^1\right)O\left(10^0\right)O\left(10^1\right) = O\left(10^2\right) \qquad \textbf{Equation 5-40}$$

Now, analysing the horizontal outflow velocity triggered by this resultant pressure difference, $u_{out\text{-}comb}$, and assuming for now no viscous forces, it is seen that the maximum order of magnitude of said velocity would be:

$$\rho_g u_{out-comb}^2 = \Delta P_c \qquad \Rightarrow \qquad u_{out-comb} = \sqrt{\frac{\Delta P_c}{\rho_g}} = \sqrt{\frac{O\left(10^2\right)}{O\left(10^0\right)}} = O\left(10^1\right) \quad \textbf{Equation 5-41}$$

Making use of the *conservation of mass*, this maximum outflow velocity can be related to the maximum inflow velocity into the compartment, as it was done before. In this case, assuming a neutral plane, *N*, located around the middle height of the compartment will imply that both (i.e., inflow and outflow) velocities will be of the same order of magnitude. Therefore,

$$u_{in-comb} = O\left(10^1\right) \qquad \textbf{Equation 5-42}$$

With these velocity estimations, we can further scale both the inflow and outflow viscous force terms as,

$$\frac{\mu_a u_{in-comb}}{N^2} = \frac{O(10^{-6})O(10^1)}{O(10^2)} = O(10^{-7})$$ **Equation 5-43**

$$\frac{\mu_g u_{out-comb}}{(H_3 - N)^2} = \frac{O(10^{-6})O(10^1)}{O(10^1)} = O(10^{-6})$$ **Equation 5-44**

and rule them out due to their low relative importance in scaling terms.

The maximum orders of magnitude of the three characteristic velocities – $v_{fire,MAX}$, $u_{in\text{-}comb}$ and $u_{out\text{-}comb}$ – (conceptualised in either Figure 2-6 or Figure 2-7) correspondent to this particular case, can now be compared:

$$\{ u_{out-comb} = O(10^1) \} \approx \{ u_{in-comb} = O(10^1) \} > \{ v_{fire,MAX} = O(10^0) \}$$ **Equation 5-45**

Therefore, in this case both horizontal and vertical velocities are relevant in the defining the overall *flow pattern*. The buoyancy force gives as a result an upward stream (plume) which, once it encounters the hot layer, converts all its inertial energy into pressure energy. Further, this combined pressure energy (given by (*i*) the buoyancy = inertia of the rising plume *plus* (*ii*) the buoyancy = pressure of the stagnant hot layer) is responsible for the outflow of gases and resultant inflow of ambient air. Thus, the air inflow into the fire zone is brought about not only by the compartment acting as a 'chimney', but also by the enhanced pressure difference brought about by the rising fire plume after encountering the smoke layer. This implies the following equation:

$$u_{in-comb} = u_{in} + u_{in-plume-effect}$$ **Equation 5-46**

The increase in the inflow velocity, $u_{in\text{-}plume\text{-}effect}$, is in straight relation and of the same order of magnitude as $v_{fire,MAX}$.

It is interesting, in this regard, to compare the maximum order of magnitude of the characteristic velocity in a natural entrainment *ventilation mode*, $u_{in\text{-}fire\text{-}entrainment}$, against the maximum order of magnitude of the velocity obtained after a combined entrainment *ventilation mode*, $u_{in\text{-}comb}$, like that occurring under this configuration.

The horizontal mass flow rates entrained by the fire around its envelope in a natural situation can be expressed as:

$$\dot{m}_{entrainment} = 2\pi\left(\frac{D}{2}\right)H_4\, u_{in-fire-entrainment}\,\rho_a \qquad \textbf{Equation 5-47}$$

The air entrained is 'pumped' upwards by the fire into the fire plume. This mass flow rate can be expressed as:

$$\dot{m}_{plume} = \pi\left(\frac{D}{2}\right)^2 v_{fire,MAX}\;\rho_g \qquad \textbf{Equation 5-48}$$

By means of *continuity* (or *conservation of mass*), both expressions can be equated and, assuming equal densities (*Boussinesq* approximation), it is found that:

$$u_{in-fire-entrainment} = v_{fire,MAX}\left(\frac{D}{4H_4}\right) = O\left(10^0\right)\left[\frac{O\left(10^0\right)}{O\left(10^1\right)}\right] = O\left(10^{-1}\right) \qquad \textbf{Equation 5-49}$$

This means that the horizontal maximum natural entrainment velocity, $u_{in\text{-}fire\text{-}entrainment}$, is one order of magnitude lesser than the vertical maximum fire plume velocity estimated before, $v_{fire,MAX}$ (Equation 5-37):

$$u_{in-fire-entrainment} = O\left(10^{-1}\right) \quad < \quad v_{fire,MAX} = O\left(10^0\right) \qquad \textbf{Equation 5-50}$$

This is in good agreement with the typical assumption taken in the *ideal* or *weak plume theory* [100] that the horizontal entrainment velocity is around 15% of the upward plume velocity. The comparison of this natural entrainment velocity to that resulting from the combined entrainment effect found in this scenario, exhibits the following inequality:

$$u_{in-fire-entrainment} = O\left(10^{-1}\right) \quad << \quad u_{in-comb} = O\left(10^1\right) \qquad \textbf{Equation 5-51}$$

This means that the combined entrainment effect could potentially bring air at a velocity 2 orders of magnitude higher than that naturally driven by the fire alone.

In summary, in the reduced floor area to height ratio compartment configuration (H_1 >>> H_5) that allows for a significant hot gas accumulation underneath the ceiling, the air drawn into the compartment will be driven by both the fire itself (i.e., turbulence and inertia driven) and by the stack of hot gas that, when reaching the upper part of the opening and escaping, creates a horizontal pressure gradient that induces extra inflows – in addition to the turbulence and inertia fire-driven entrainment – through the lower part of the opening (i.e., stack-driven). The combined *ventilation mode* implies a larger air inflow than that brought about either by the fire or by the hydrostatic pressure difference independently. In regards to the *burning mode*, this is fuel-controlled due to the fact that the incoming air flows freely through the entire lower regions of the compartment where the majority of the fuel is usually located. Given the fact that there is a double-induced air inflow – i.e. a combination of both fire and compartment-induced *ventilation mode* – combined with a fuel-controlled *burning mode*, this regime is different from the historically defined ones and, thus, is proposed to be termed as *Regime C* (refer to Table 5-3) [30]. In small compartments with tall ceilings and relatively large openings, fires will tend to produce large amounts of diluted and, thus, low temperature products of combustion. This means, in principle, a hot gas layer with (*i*) a typically weak *thermal impact* on the upper structure – although the thermal impact on the lower structure could be significant due to the close flame-walls radiative heat transfer – and (*ii*) a low energy *feedback* to the distant combustibles located at floor level with the consequent weak influence on the *burning rate* from this perspective. Nevertheless, the same as for both cases 1, the *burning rate* in a fire-wall proximity configuration could potentially be enhanced by the thermal feedback from the heated solids to the fuel.

Finally, a singular observation after Equation 5-51 is exposed next: the air impinging on the charring surfaces at a higher velocity than the naturally entrained by the fire can potentially increase the *burning rate* beyond the maximum burning rate found in natural or open conditions, making this situation burn in a combined fuel/ventilation-control *burning mode*; i.e., the *burning rate* would be both a function of the fuel *and* the ventilation. This *burning mode* is different to that found under *Regime C* which is purely fuel-controlled, and different to that found under *Regime D* which is purely

ventilation-controlled (refer to Table 5-3). Falling somewhere in between both, thus, this behaviour is defined here as a *special Regime C*.

5.2.3.2.5 Case 2(b): Small + Tall + Small Opening

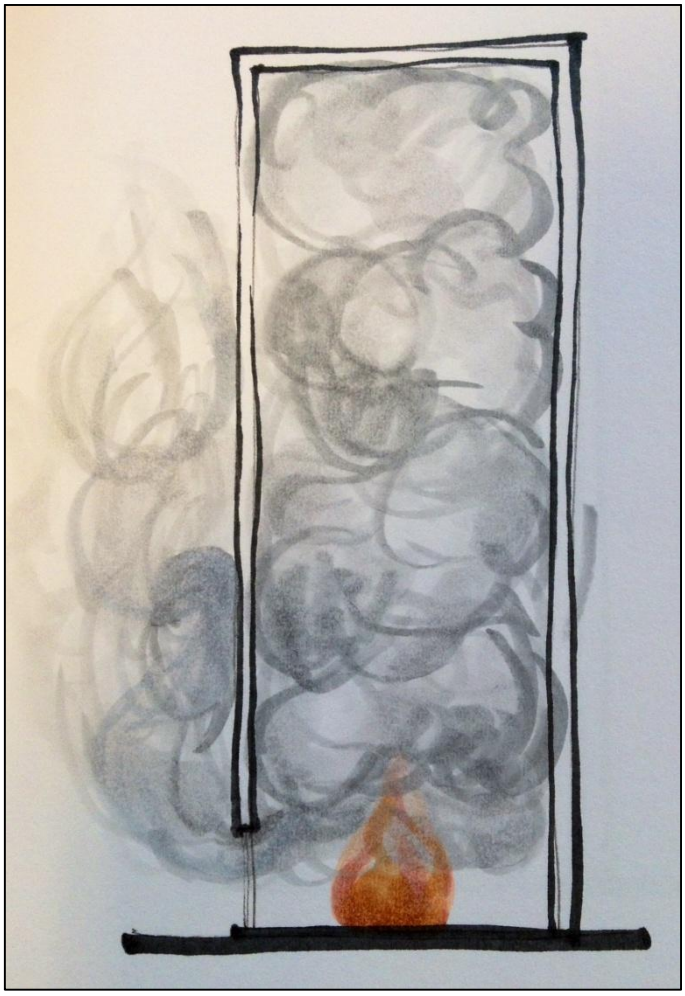

Figure 5-7: Case 2(b)

$$\text{Particularities} \begin{cases} H_1 >>> H_5 \approx D \rightarrow (\text{fully} - \text{developed fire}) \\ H_1 >>> H_3 \rightarrow (\text{small opening}) \\ H_1 \approx H_2 \quad \vee \quad H_4 \approx 0 \rightarrow (\text{hot gas layer almost at floor level}) \end{cases}$$

This would be the case of a single uniform and stagnant hot layer inside the compartment (refer to Figure 2-3) where there are no vertical velocities, therefore,

the flow behaves in a similar way to that presented in ***Case 1(b)***. This implies that the buoyancy force exerted by the hot gas layer on the compartment is converted straightaway into pressure force. The characteristic length – i.e., the smoke layer height ($H_i \approx H_1 \approx H_2$) – in this case is one order of magnitude greater than in ***Case 1(b)***, so the characteristic pressure would now be at maximum of the order:

$$\Delta P_c = g\left(\rho_a - \rho_g\right) H_2 = O\left(10^1\right) O\left(10^0\right) O\left(10^1\right) = O\left(10^2\right) \qquad \textbf{Equation 5-52}$$

The dominant velocities in this case are, once more, the horizontal inflow and outflow velocities, u_{in} and u_{out} respectively, triggered by the hydrostatic pressure difference between the compartment and the ambient atmosphere. Disregarding again the horizontal viscous forces (assumption that has been – and can be in this case too – shown to be appropriate), the maximum horizontal outflow velocity would now be of the order:

$$\frac{\rho_g u_{out}^2}{H_2} = \frac{\Delta P_c}{H_2} \qquad \Rightarrow \qquad u_{out} = \sqrt{\frac{\Delta P_c}{\rho_g}} = \sqrt{\frac{O\left(10^2\right)}{O\left(10^0\right)}} = O\left(10^1\right) \qquad \textbf{Equation 5-53}$$

Assuming the limiting situation of an extremely reduced inflow area will give an inflow velocity one order of magnitude greater than the outflow velocity (by means of following the same procedure as in ***Case 1(b)***; i.e., from Equation 5-29 to Equation 5-32). This means that:

$$u_{in} = O\left(10^2\right) \qquad \textbf{Equation 5-54}$$

It can clearly be seen that this case tends to ***Case 1(b)***, where the buoyancy force is only balanced by the hydrostatic pressure difference created by the stack of hot gases accumulated under the ceiling, forcing the compartment to act following the *flow pattern* of a 'chimney'. Thus, the horizontal inflow and outflow velocities are driven solely by the hydrostatic pressure difference. The same conclusions as in ***Case 1 (b)*** apply to this case: the *ventilation mode* would be compartment-induced (i.e., stack-driven) and the *burning mode* would be ventilation-controlled due to the fact that the fresh air drawn into the compartment is restricted (by the low hot gas layer exiting)

from freely flooding completely the fuel bed. Thus, this is a pure *Regime F behaviour* (refer to Table 5-3), with further similar *burning rates* (potentially enhanced by thermal feedback from both the heated inner surfaces, and the low hot gas layer), and an intense *heat exchange rate* and consequent heat impingement to the structure.

An alternative to this case could be a *Regime E behaviour* – referred as ***Case 2(b)'*** in Table 5-3 **–** where the only difference is that, given the reduced size of the floor area, the stack-driven inflow is such (not only in excess of the stoichiometric needs as explained in Section 1.3.2.2.4, but also in terms of the good mixing with the fuel vapours) that is capable of unrestrictedly flooding the entire lower compartment area where the fuel is located, turning the *burning mode* into a fuel-control instead.

5.2.3.2.6 *Case 3: Introductory Note*

It was observed in various tests [104][102][103][120] that in this kind of compartment configuration, once a fire is fully-developed, preferential burning near the opening occurs as a consequence of the oxygen starvation (and/or probably poor mixing between available oxygen and the vaporised fuel) at the rear of the compartment. Once the near-opening fuel is consumed, the fire progresses slowly back towards the rear of the compartment. Continuing with the same nomenclature rationale as above, the near-opening fully-developed fire is analysed under the 'large opening case' as ***Case 3(a)***, while the rear fully-developed fire will be treated as ***Case 3(ab)*** as a 'large opening case' too. In addition, case 3 is completed with ***Case 3(b)*** covering the 'small opening case'.

5.2.3.2.7 *Case 3(a): Large + Short + Large Opening*

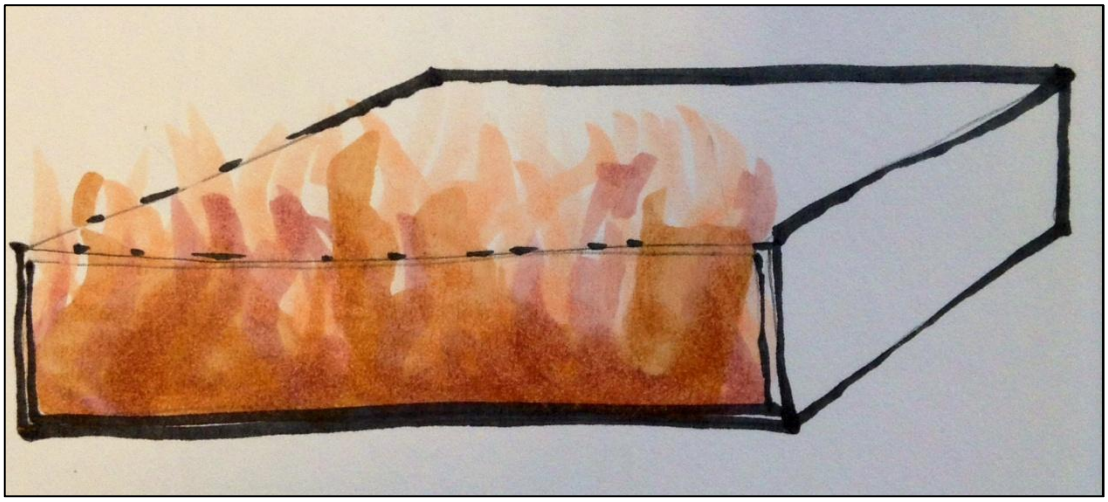

Figure 5-8: Case 3(a)

$$\text{Particularities} \begin{cases} H_5 >>> H_1 \approx D \rightarrow (\text{localized post - flashover fire}) \\ H_1 \approx H_3 \rightarrow (\text{large opening}) \\ H_1 \approx H_4 \quad \vee \quad H_2 \approx 0 \rightarrow (\text{no hot gas layer built - up}) \end{cases}$$

This case is almost exactly as ***Case 1(a)*** where, given that the fire is located next to the compartment's full height large opening, the *ventilation mode* will purely be naturally fire-induced (i.e., turbulence-driven). The only significant difference with said case is that the fire, will instead burn following a ventilation-controlled *burning mode* due to the fact that the air is restricted from reaching the fuel occupying the back of the compartment. Thus, this gives as a result, a *Regime B behaviour* (refer to Table 5-3 – differs from the *Regime A* pertinent to ***Case 1(a)***) with a *burning rate* potentially enhanced only by the thermal feedback from the heated lateral walls. Finally, the *thermal impact* on the ceiling could be significant after the direct flame impingement.

5.2.3.2.8 Case 3(ab): Large + Short + Large Opening

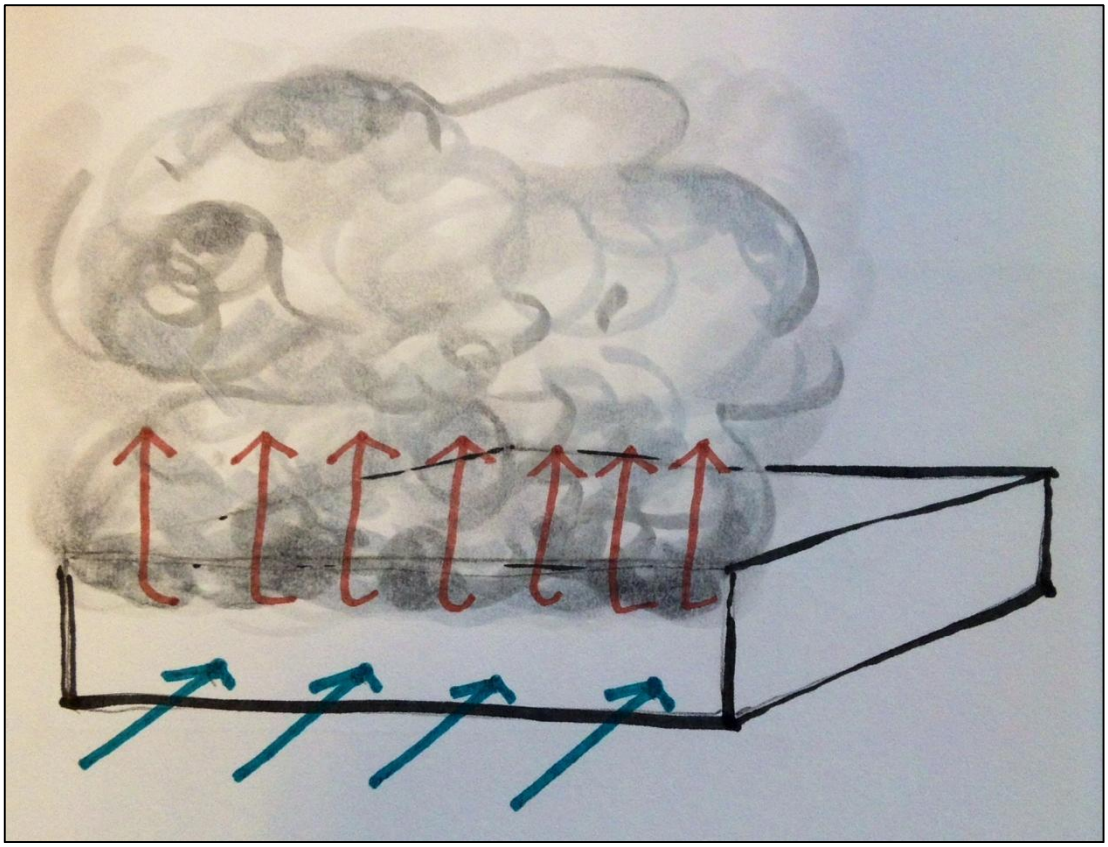

Figure 5-9: Case 3(ab)

$$\text{Particularities} \begin{cases} H_5 >>> H_1 \approx D \rightarrow (\text{localized post - flashover fire}) \\ H_1 \approx H_3 \rightarrow (\text{large opening}) \\ H_4 > H_2 \quad (\text{significant hot gas layer built - up}) \end{cases}$$

This case is similar to ***Case 2(ab)*** in that the buoyancy force is balanced by the hydrostatic pressure difference created by the hot gases accumulated under the ceiling, but also gives as a result vertical pressure accelerations within the compartment. The dominant velocities in this case are, therefore, both the horizontal inflow and outflow velocities plus the vertical velocity (see Figure 2-6 or Figure 2-7). Thus, the air inflow is brought about not only by the compartment acting as a 'chimney', but also by the enhanced pressure difference brought about by the rising

fire plume after encountering the smoke layer. As seen before, this gives as a result a characteristic pressure with the following expression:

$$\Delta P_c = \rho_a v_{fire,MAX}^2 + g\left(\rho_a - \rho_g\right)H_2 \qquad \textbf{Equation 5-55}$$

In this case, the maximum ΔP or characteristic ΔP_c would be of the order of:

$$\Delta P_c = O\left(10^0\right)O\left(10^0\right) + O\left(10^1\right)O\left(10^0\right)O\left(10^0\right) = O\left(10^1\right) \qquad \textbf{Equation 5-56}$$

This pressure term will give a horizontal outflow velocity, $u_{out\text{-}comb}$ – triggered by the resultant pressure difference – of the following order of magnitude:

$$\rho_g u_{out-comb}^2 = \Delta P_c \qquad \Rightarrow \qquad u_{out-comb} = \sqrt{\frac{\Delta P_c}{\rho_g}} = \sqrt{\frac{O\left(10^1\right)}{O\left(10^0\right)}} = O\left(10^0\right) \quad \textbf{Equation 5-57}$$

Using the *conservation of mass* and assuming a neutral plane, *N*, located around the middle height of the compartment (same assumption as in ***Case 2(ab)***), the combined (i.e., brought about by the fire plus the hydrostatic ΔP) inflow velocity will be of the same order of magnitude; i.e.:

$$u_{in-comb} = O\left(10^0\right) \qquad \textbf{Equation 5-58}$$

In regards to the vertical velocity, the buoyancy term can be equated to the inertial term and the maximum vertical velocity, $v_{fire,MAX}$, can be worked out from that equation:

$$\frac{\rho_a v_{fire,MAX}^2}{D} = g\left(\rho_a - \rho_g\right) \qquad \Rightarrow \qquad v_{fire,MAX} = \sqrt{g\left(\frac{\rho_a - \rho_g}{\rho_a}\right)D} \qquad \textbf{Equation 5-59}$$

This velocity is, again, the same as that developed in Section 2.3.4.4 (Equation 2-34) as $v_{fire,MAX}$, taking into account that when dealing with maximum orders of magnitudes, some constants – like the ½ associated to the inertial energy force – turn irrelevant for the analysis and are thus ignored. It maximum order of magnitude will therefore be:

$$v_{fire,MAX} = \sqrt{O(10^0)\,O(10^1)\,O(10^0)} = O(10^0) \qquad \textbf{Equation 5-60}$$

The vertical and horizontal viscous forces were disregarded in an assumption that has been shown (e.g. in ***Case 2(ab)***) to be appropriate, given the low relative impact they have in the momentum equation that describes the *flow pattern*.

The maximum orders of magnitude of the three characteristic velocities – $v_{fire,MAX}$, $u_{in\text{-}comb}$ and $u_{out\text{-}comb}$ – (conceptualised in either Figure 2-6 or Figure 2-7) correspondent to this particular case, can now be compared:

$$\left\{ u_{out-comb} = O(10^0) \right\} \approx \left\{ u_{in-comb} = O(10^0) \right\} \approx \left\{ v_{fire,MAX} = O(10^0) \right\} \qquad \textbf{Equation 5-61}$$

It can be seen again that in this case both horizontal and vertical velocities are relevant in the defining the overall *flow pattern*.

Equation 5-49 is used to compare the magnitude of the combined inflow (i.e., fire *plus* compartment) against the natural entrainment inflow (i.e., the fire alone without the plume impinging on an accumulated hot layer):

$$\begin{aligned} &\left\{ u_{in-fire-entrainment} = v_{fire,MAX}\left(\frac{D}{4H_4}\right) = O(10^0)\left[\frac{O(10^0)}{O(10^1)}\right] = O(10^{-1}) \right\} \\ &< \quad \left\{ u_{in-comb} = O(10^0) \right\} \end{aligned} \qquad \textbf{Equation 5-62}$$

This means that the combined entrainment effect could potentially bring air at a velocity 1 order of magnitude higher than that naturally driven by the fire alone.

In summary, in regards to the *ventilation mode*, as there are large openings, the air drawn into the fire zone will be naturally fire-induced (i.e. turbulence-driven), but due to the large compartment geometry and its configuration, that still allows for a hot layer to accumulate under the ceiling, stack-induced entrainment (i.e., induced by the hydrostatic pressure difference) can also be achieved enhanced by the additional pressure difference generated by the fire plume after impinging the hot smoke layer. In terms of the *burning mode*, the fire in this case could either be (*i*) fuel-controlled with the *burning rate* equal or close to that expected in an exterior fire which, falling

under a *Regime C behaviour* (refer to Table 5-3), where the available airflow for combustion is completely unrestricted; or (*ii*) ventilation-controlled due to the fact that the fuel located at the rear is air-restricted, falling this time under a *Regime D behaviour* (***Case 3(ab)'*** in Table 5-3). In both cases, the reduced flame entrainment area will typically mean less diluted (i.e., high temperature and high soot concentration) combustion products, that lead to high radiation and an intense *heat exchange rate* along the flame impingement area of the structure. This radiation from the upper hot and sooty gas layer can, in turn, enhance the *burning rate* through thermal feedback to the virgin fuel, together with the feedback coming from a potentially tilt flame spreading horizontally along the ceiling.

5.2.3.2.9 Case 3(b): Large + Short + Small Opening

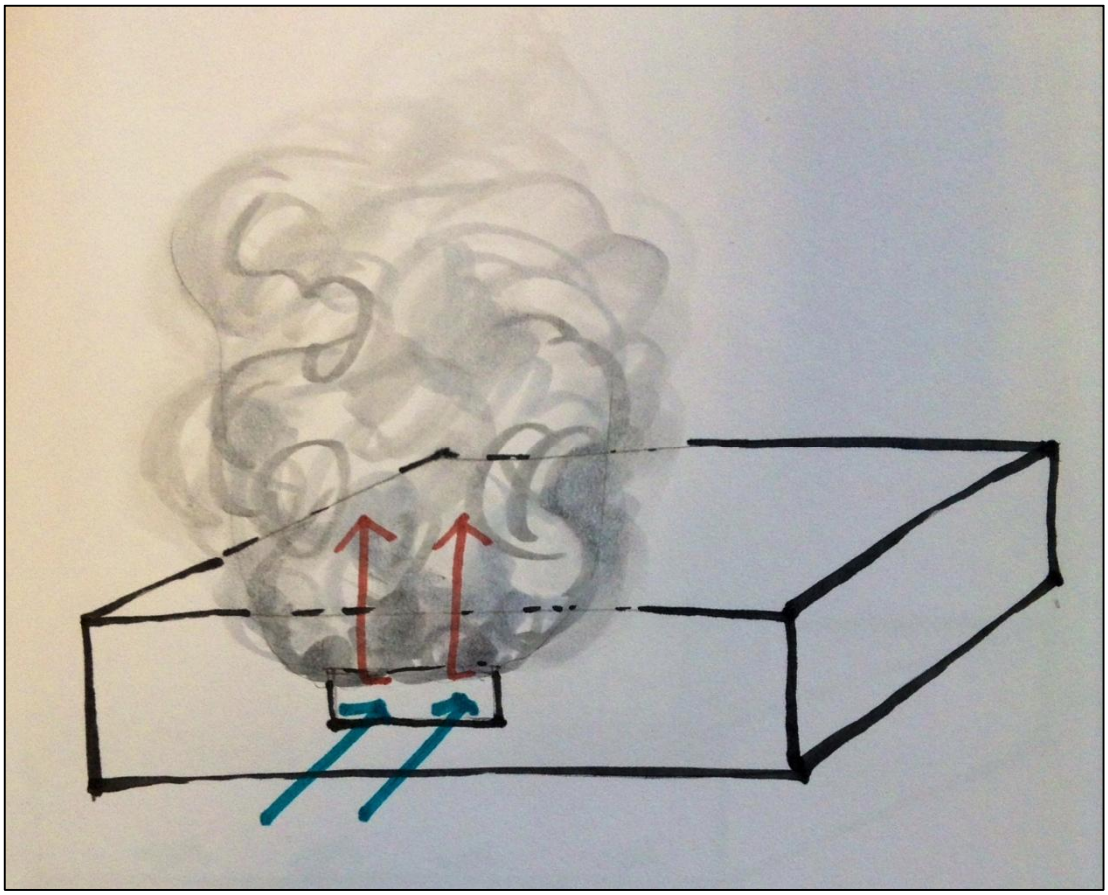

Figure 5-10: Case 3(b)

$$\text{Particularities} \begin{cases} H_5 >>> H_1 \approx D \rightarrow (\text{localized post - flashover fire}) \\ H_1 >>> H_3 \rightarrow (\text{small opening}) \\ H_1 \approx H_2 \quad \vee \quad H_4 \approx 0 \rightarrow (\text{hot gas layer almost at floor level}) \end{cases}$$

Once more, this would be the case of a single uniform and stagnant hot layer inside the compartment (Figure 2-3) where there are no vertical velocities, so the flow will behave in a similar way to that presented in ***Case 1(b)*** and ***Case 2(b)***. This implies that the buoyancy force exerted by the hot gas layer on the compartment is only balanced by the hydrostatic pressure difference that exists between this hot layer and the exterior atmosphere (at the opening plane). The pressure differential forces the compartment to act as a 'chimney' in regards to the inflow of cold air and outflow of hot gases. Thus, the characteristic pressure term would now be at maximum of the order:

$$\Delta P_c = g(\rho_a - \rho_g) H_2 = O(10^1)\, O(10^0)\, O(10^0) = O(10^1) \qquad \textbf{Equation 5-63}$$

The dominant velocities in this case are again both horizontal inflow and outflow velocities, triggered by the hydrostatic pressure difference. Assuming no viscous forces acting (for the same reasons verified in ***Cases 1(a)*** and ***1(b)***), the maximum horizontal outflow velocity would now be of the order:

$$\frac{\rho_g u_{out}^2}{H_2} = \frac{\Delta P_c}{H_2} \qquad \Rightarrow \qquad u_{out} = \sqrt{\frac{\Delta P_c}{\rho_g}} = \sqrt{\frac{O(10^1)}{O(10^0)}} = O(10^0) \qquad \textbf{Equation 5-64}$$

Assuming the limiting situation of an extremely reduced inflow area (refer to procedure proposed from Equation 5-29 to Equation 5-32), this means that the maximum horizontal inflow velocity would now be of the order:

$$u_{in} = O(10^1) \qquad \textbf{Equation 5-65}$$

In summary, this case also tends to ***Case 1(b)***, where the 'chimney' *flow pattern* brings a compartment-induced (i.e., stack-driven) *ventilation mode*, and the *burning mode* would be ventilation-controlled due to the fact that the fresh air drawn into the

compartment is restricted (by the low hot gas layer exiting) from freely flooding completely the fuel bed. Thus, this is a pure *Regime F behaviour* (refer to Table 5-3), with further similar *burning rates* (potentially enhanced by thermal feedback from both the heated inner surfaces, and the low hot gas layer), and an intense *heat exchange rate* and consequent heat impingement to the structure.

5.2.3.2.10 *Case 4: Introductory Note*

In all the previous cases the analysis was divided into large and small openings but always assuming the hot gas layer reaching the ventilation opening, thus, forcing the hydrostatic pressure to convert into hydrodynamic pressure giving motion to the hot fluid exiting the compartment and causing, in turn, horizontal cold (air) inflows. In very large and tall compartments like an atrium, it is more reasonable to assume that the hot layer exits the compartment through an upper vent, than assuming it will exit through a hypothetical lower vent where the inflow is coming from. In addition, it is also reasonable to assume that the lower vent is always large leaving no practical meaning to the small opening case analysis (i.e., ***Case 4(b)***). Therefore, in factual terms, it is more legitimate to present a non-cleared case versus a cleared smoke situation (e.g. natural venting system in place), instead of the previous large versus small opening comparison.

5.2.3.2.11 Case 4(a): Large + Tall + (Large Opening) + Non-Cleared

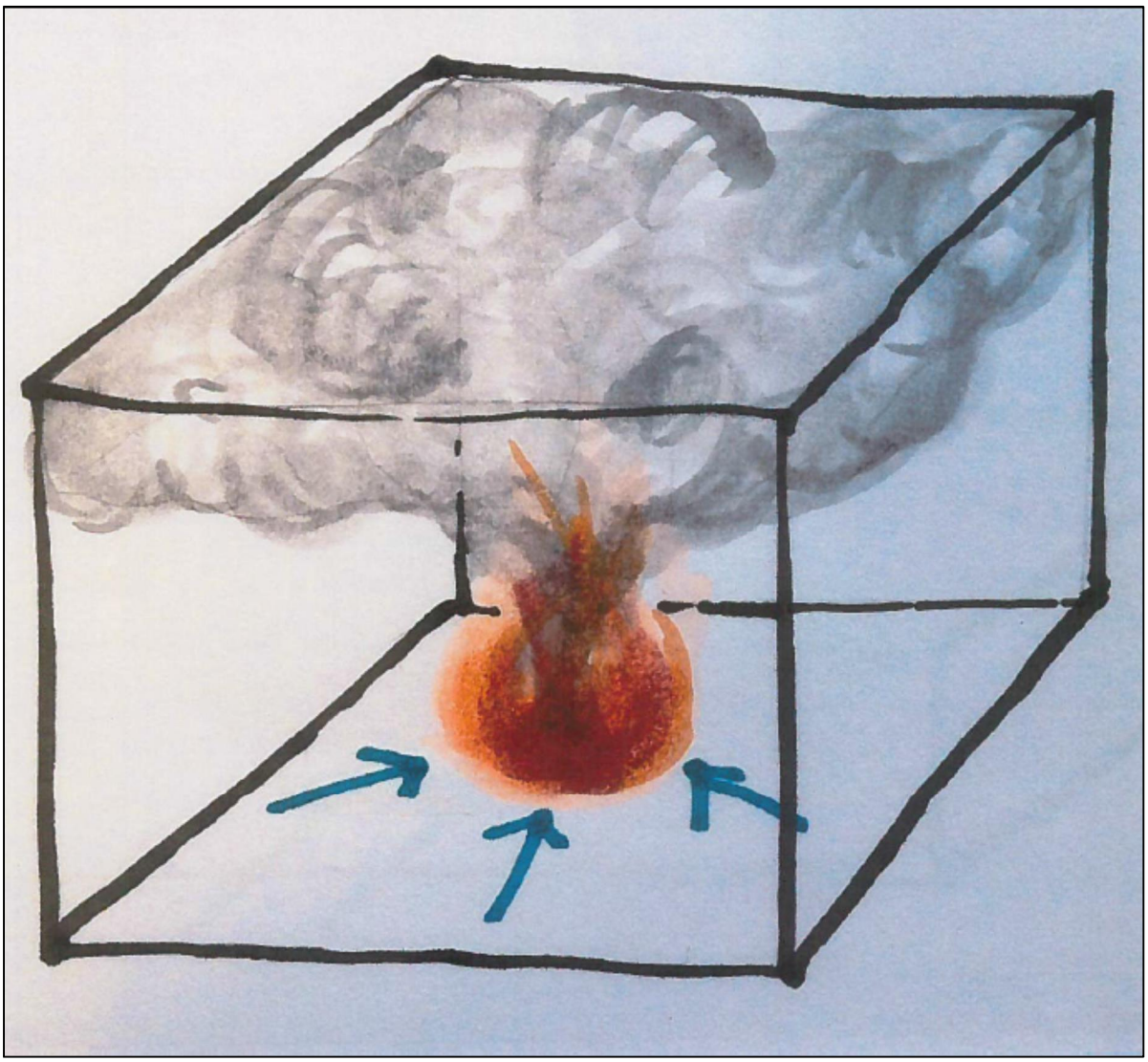

Figure 5-11: Case 4(a)

$$\text{Particularities} \begin{cases} H_1 \approx H_5 >>> D \rightarrow (\text{localized fire}) \\ H_1 > H_3 \rightarrow (\text{still large opening}) \\ H_1 > H_2 \rightarrow (\text{still large hot gas layer built}-\text{up}) \\ H_4 \approx H_2 \rightarrow (\text{equally large cold and hot layers}\,(\sim 10\text{m})) \end{cases}$$

In the particular case of an extremely large compartment volume with large openings connecting with multiple adjoining interior spaces, and where the flames will most probably never reach the ceiling, the *flow pattern* will be that of an open fire. Therefore, this case tends to ***Case 1(a)*** and ***Case 2(a)*** where the pressure and viscous forces are negligible, and the buoyant force purely converts into inertial force giving as a result vertical accelerations around the fire plume.

The *ventilation mode* will purely be naturally fire-induced (i.e., turbulence-driven), but in this case not because of the absence of a hot layer accumulated under the ceiling – in fact, there is significant accumulation – but because under this hypothetical scenario the large volume accumulated is not allowed to exit the compartment. The hot gas layer trapped under the ceiling is not able to convert its hydrostatic pressure (in contrast to that from the ambient atmosphere) into hydrodynamic pressure since there are no exit paths (e.g. openings) through which the gases can flow. Therefore, triggering of the stack induced flow is not possible. In addition, the fire will burn following a *fuel-controlled mode* as there is no air inflow restriction at all. This gives, as a result, a *Regime A* (refer to Table 5-3) behaviour.

Given the considerable dilution of the products of combustion – as a consequence of the abundant entrainment along the entire plume envelope – their temperature will be reduced as well as their soot concentration. This makes the *thermal impact* on the upper structure insignificant, in the same way the typical flame-boundaries remoteness does not allow for an intense *thermal impact* on the lower part of the compartment either. Hence, the *burning rate* will not be affected by the thermal feedback and, thus, will be close to ambient values.

5.2.3.2.12 Case 4(ab): Large + Tall + (Large Opening) + Cleared

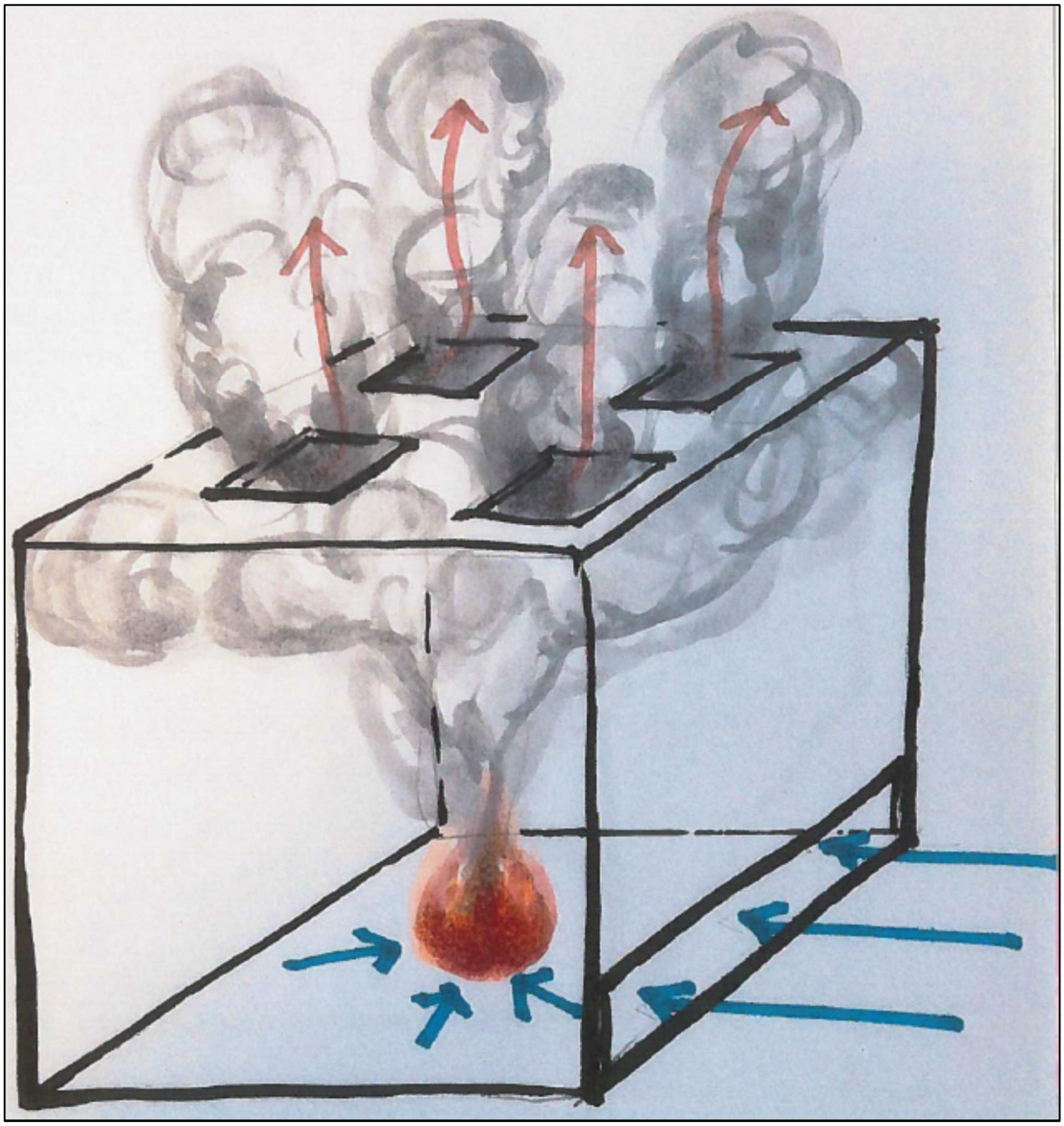

Figure 5-12: Case 4(ab)

$$\text{Particularities} \begin{cases} H_1 \approx H_5 >>> D \rightarrow (\text{localized fire}) \\ H_1 > H_3 \rightarrow (\text{still large opening}) \\ H_1 > H_2 \rightarrow (\text{still large hot gas layer built}-\text{up}) \\ H_4 > H_2 \rightarrow (\text{equally large cold and hot layers}\,(\sim 10\text{m})) \end{cases}$$

Similar to ***Cases 2(ab)*** and ***3(ab)***, in this situation the buoyancy force is balanced by the hydrostatic pressure difference created by the hot gases accumulated under the ceiling, but also by the vertical pressure accelerations that exists within the compartment in the proximity of the fire plume. Thus, the air inflow is brought about not only by the compartment acting as a 'chimney' (i.e., stack-driven), but also by the fire itself (i.e., turbulence and inertia driven). In the same way as in the analogous cases, the upward stream is analysed assuming no viscous forces – an assumption shown to be appropriate e.g. in ***Case 2(ab)*** – so the buoyancy term can be equated to the inertial term to work out the maximum vertical velocity:

$$\frac{\rho_a v_{fire,MAX}^2}{D} = g\left(\rho_a - \rho_g\right) \qquad \Rightarrow \qquad v_{fire,MAX} = \sqrt{g\left(\frac{\rho_a - \rho_g}{\rho_a}\right)D} \qquad \textbf{Equation 5-66}$$

This vertical fire plume velocity, $v_{fire,MAX}$, will be at maximum of the order:

$$v_{fire,MAX} = \sqrt{O\left(10^1\right)O\left(10^0\right)O\left(10^0\right)} = O\left(10^0\right) \qquad \textbf{Equation 5-67}$$

Assuming steady-state conditions in this ceiling vented situation, when the plume encounters the smoke layer, all its inertial energy is converted into pressure energy as the vertical velocity is extinguished. This gives, as a result, a pressure term with the following expression:

$$\Delta P_c = \rho_a v_{fire,MAX}^2 + g\left(\rho_a - \rho_g\right)H_2 \qquad \textbf{Equation 5-68}$$

Thus, the maximum or characteristic ΔP_c in this case would be of the order of:

$$\Delta P_c = O\left(10^0\right)O\left(10^0\right) + O\left(10^1\right)O\left(10^0\right)O\left(10^0\right) = O\left(10^1\right) \qquad \textbf{Equation 5-69}$$

The maximum order of magnitude of the vertical outflow velocity triggered by this resultant pressure difference, $v_{out\text{-}comb}$, (disregarding the viscous forces for the reasons already stated in the previous cases), would therefore be:

$$\rho_g v_{out-comb}^2 = \Delta P_c \qquad \Rightarrow \qquad v_{out-comb} = \sqrt{\frac{\Delta P_c}{\rho_g}} = \sqrt{\frac{O(10^1)}{O(10^0)}} = O(10^0)$$ **Equation 5-70**

After the principle of *conservation of mass*, this vertical maximum outflow velocity can be related to the horizontal maximum inflow velocity into the compartment. In atrium fire situations like those represented by this case, equipped with a natural ventilation system, it is common to assume that the inflow area bringing fresh air into the atrium is larger than the exhaust area at ceiling level. This implies that the outflow velocity will be greater than the inflow velocity. Assuming that the difference is one order of magnitude (assumption that can later be reassessed), this means that:

$$u_{in-comb} = O(10^{-1})$$ **Equation 5-71**

Therefore, the maximum orders of magnitude of the three characteristic velocities – $v_{fire,MAX}$, $u_{in\text{-}comb}$ and $v_{out\text{-}comb}$ – correspondent to this particular case, can now be compared:

$$\left\{ v_{out-comb} = O(10^0) \right\} > \left\{ u_{in-comb} = O(10^{-1}) \right\} < \left\{ v_{fire,MAX} = O(10^0) \right\}$$ **Equation 5-72**

It becomes clear, thus, that the vertical velocities are more important than the horizontal ones in an atrium fire situation like the one depicted under this representative case, nevertheless, both are relevant in the defining the overall *flow pattern*.

Equation 5-49 is used once more to compare the magnitude of the combined inflow (i.e., fire *plus* compartment) against the natural entrainment inflow (i.e., the fire alone without the plume impinging on an accumulated hot layer):

$$\left\{ u_{in-fire-entrainment} = v_{fire,MAX}\left(\frac{D}{4H_4}\right) = O(10^0)\left[\frac{O(10^0)}{O(10^1)}\right] = O(10^{-1}) \right\} \approx \left\{ u_{in-comb} = O(10^{-1}) \right\} \quad \textbf{Equation 5-73}$$

This shows that the combined entrainment effect could potentially bring more air than the natural fire entrainment only in the presence of a significant hot gas layer depth, H_2, accumulated under the ceiling, which would imply a larger $v_{out\text{-}comb}$ and therefore a larger $u_{in\text{-}comb}$.

In summary, in regards to the *ventilation mode*, when the large volume of diluted (i.e., low temperature and soot concentration) gases accumulated under the tall ceiling of this large compartment configuration are vented, the pressure exerted on the upper part of the compartment is hydro-dynamically balanced by horizontal inflows that will drive fresh air in stack-induced entrainment. In addition, air will be drawn into the fire zone by the fire itself in a fire-induced (i.e., turbulence plus inertia-driven) entrainment fashion. This combined entrainment could be either weak or strong depending basically on the hot gases layer depth accumulated under the ceiling and the designed vented and inflow areas. In regards to the *burning mode*, the fire in this case will be fuel-controlled as there is no possible air inflow restriction. Thus, this case falls under a *Regime C behaviour* (refer to Table 5-3), where the available airflow for combustion is completely unrestricted (i.e., fuel-controlled) and dually induced by the fire and the hydrostatic pressure difference. Same as in ***Case 4(a)***, the *thermal impact* of the diluted gas layer accumulated under the ceiling on the structure is insignificant, as it is the thermal impact of the flames in the remote boundaries at lower levels. This makes the *burning rate* similar to that in ambient conditions, virtually unaffected by the thermal feedback from the boundaries or upper gas layer.

5.3 Preliminary Conclusions

In addition to the classic and historically defined ***Cases 1(a)*** and ***(b)***, ten additional cases (including the 'prime' cases) were analysed covering many characteristic fire

scenarios. The results obtained in terms of their *regime of behaviour* are summarized in the following table:

Table 5-6: Different cases and their regimes of behaviour

Ventilation Mode / **Burning Mode**	***Fire*** (*turbulence driven*) ***Induced***	***Fire*** (*turbulence + inertia driven*) ***& Compartment*** (*stack driven*) ***Induced***	***Compartment*** (*stack driven*) ***Induced***
Fuel-controlled (unrestricted air transport)	***Regime A***	***Regime C***	***Regime E***
	Case 1(a) *Case 2(a)* *Case 4(a)*	*Case 2(ab)* *Case 3(ab)* *Case 4(ab)*	*Case 2(b)'*
Ventilation-controlled (restricted air transport)	***Regime B***	***Regime D***	***Regime F***
	Case 3(a)	*Case 3(ab)'*	*Case 1(b)* *Case 2(b)* *Case 3(b)*

It can clearly be seen that most extreme cases termed as *(a)* (very large openings) and *(b)* (very small openings), tend to the classic *Regime II* or *Regime I* behaviours, respectively (i.e., *Regimes A and F*, respectively, in Table 5-6).

The most important finding is that all the other cases examined fall somewhere in between *(a)* and *(b)*. In practical terms this means they represent compartments which are far from small and cubic and with realistic ventilation, ergo, fire scenarios

that exemplify real contemporary buildings. Thus real compartments must tend to different *regimes of behaviour* than those represented by the classical framework definitions. The majority fall under a regime which could be thought of, in principle, as a comprehensive combination of the classic ones. This regime is termed *Regime C*.

Following the flow scaling analysis assessed in the different cases, it appears clear that the viscous forces do not have much relevance in any representative fire scenario. This means, therefore, that the *flow pattern* is either:

- a function of the ratio between the inertial force and the buoyancy force (i.e., a function of the *Froude number*) when in *Regime A*,
- a function of the ratio between the pressure force and the buoyancy force when in *Regime F*, or
- a function of the inertial, buoyancy and pressure forces all together when in the comprehensive *Regime C*.

Depicting this concept in an *x*-*y*-*z* coordinate system, where *x* represents the pressure force, *y* the inertial force, and *z* the buoyancy force, the three different regimes would stand graphically as follows:

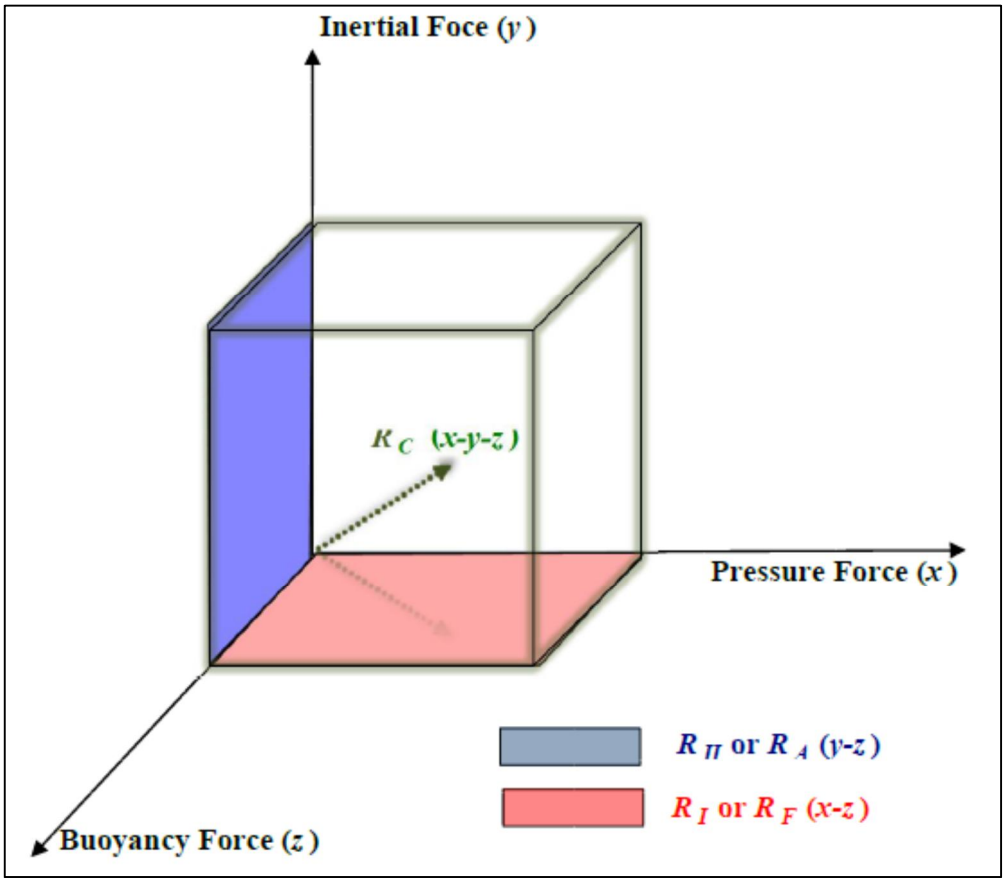

Figure 5-13: Different Regimes of Behaviour

Figure 5-13 clearly shows that both historical *Regimes I* (i.e., *Regime F*) and *II* (i.e., *Regime A*) are limiting cases of a broader compartment fire behaviour – and thus a broader theory underneath – whose relevance is apparent in relation to contemporary architecture and infrastructure. It becomes clear once more, that further experimentation and research is in need to understand the widespread behaviour thoroughly.

6 Chapter 6: Filling the Gaps with Experiments

6.1 Introduction

After exploring the *classic compartment fire framework* range of validity and examining the associated design limitations in Chapters 3 and 4, and after the attempt in Chapter 5 to encompass the present-day layouts with simple analytical formulations, it was evidenced that the *classic framework* only characterizes the two end-rope extreme *regime behaviours*, excluding the range of potential in-between behaviours. This leaves an open gap particularly relevant in contemporary architecture layouts.

The present chapter presents a series of small – designed, constructed, ran, and analysed by the author – and large-scale tests created to start filling empirically these gaps of knowledge, towards a *comprehensive compartment fire framework*.

6.2 Small-Scale Experiments

6.2.1 Idealized Conditions

Sharing the same observation enunciated by Harmathy during the late 1970s – which still apply to these days more than thirty years later:

> "Building fires are generally modeled as phenomena confined to a single compartment, perfectly isolated from the rest of the building and communicating with, i.e. receiving air from and discharging hot fire gases to, a calm atmosphere through openings, namely broken windows or open doors. Such **'***classic'* fires are by no means common. There are usually some secondary routes of communication between the fire compartment and the surrounding building spaces, and thus, owing to pressure differences which prevail in a building during a fire and which are sometimes augmented by wind, the pattern of flow of air and fire gases is often quite different from that assumed in the classic model." [35]

Yet, Harmathy also pointed out [35] that restricting the studies of compartment fires to the *classic case* was, on the one hand, a practical necessity at that time, but on the other hand, it was purely meant to understand the cause-effect relations between the numerous variables present in a compartment fire, and not the prediction of the characteristics of a fire under such non-real conditions.

Therefore, the main justification for performing experimentation as part of this research under the *classic case*'s idealized conditions, was to reproduce both classic *Regimes I* and *II* (i.e., *Regimes F* and *A*, respectively, as per Table 5-3) in order to understand in depth the fundamental physical characteristics of the two contrasting behaviours that gave way to the *classic compartment fire framework* several years ago [29], while re-clarifying the coupling between different variables and the occurring phenomena in each regime through high resolution, state-of-the-art instrumentation, combined with Computational Fluid Dynamics (CFD) modelling.

6.2.1 Experimental and Modeling Aim and Goals

While reproducing the classic regimes of behaviour and assessing the main variables interactions, the *aim* of the small-scale experiments and modelling was to establish the true extent to which the *classic compartment fire framework* could be applied; i.e., to reconfirm the framework's range of validity and analyse its suitability beyond the boundaries where it was originally conceived, in relation to the theory developed in Chapter 5.

To this extent, the *main goal* was to assess the accuracy of the simple theoretical hydraulic model suggested by Kawagoe [12] and further developed by Thomas [29] for fully-developed fires. This was done, firstly, by examining the gas temperature distribution in detail and, secondly, by studying the role the fire plume played in characterizing the flow pattern; i.e., in the movement of air and hot gases in and out of the compartment.

Consequential goals of these experiments and modeling were (*i*) finding the break-point region between *Regime I* and *Regime II* (i.e., *Regime F* and *Regime A*, respectively, as per Table 5-3) and, thus, gaining a better understanding of the

boundaries of both regimes of behaviour; and (*ii*) evaluate the thermal insult from the flames and hot layer to the interior of the compartment boundaries in each regime as a measure of the fire severity [72].

While the experimental results helped mainly with the *quantitative* characterization of the different regimes of behaviour, the modelling – by means of the fire simulation tool FDS – helped in the *qualitative* understanding of the system of interest. At the same time, it cooperated towards the validation of the results obtained allowing, ultimately, for the uncertainty quantification.

6.2.2 Experimental Setup

The description of the post-flashover compartment fire system chosen is divided in: surroundings and geometry, ventilation, fuel load, and finally the variables of interest and the instrumentation in place to measure and record them.

6.2.2.1 Surroundings and Geometry

The experiments took place at the Rushbrook Laboratory of the University of Edinburgh during the period of September to December 2012. This made it necessary to record the initial atmospheric temperature in case large variations occurred, finding an average of 20°C and only slight variations that translated into a 2°C standard deviation. Within the laboratory the experimental setup was located under an extraction hood to assure the safety of the personnel during the tests by capturing the combustion gases. No other relevant elements influenced the surroundings of the system.

The geometry of the system was defined by a small-scale compartment built with 5 cm thick Ceraboard 115 board that provided high thermal insulation (0.07 W/m·K @ 300°C). The compartment (Figure 6-1) comprised a total internal volume of 0.71 m^3, measuring 820 mm wide, 1060 mm deep, and 820 mm high. All the fixed joints (ceiling, floor, left and right walls) were sealed using FireCement sealant to assure air and gas tightness. The rear of the compartment had a single upward sliding door while the front had two – an upper and lower moving upwards and downwards,

respectively – sliding doors to provide the compartment with different natural ventilation configurations.

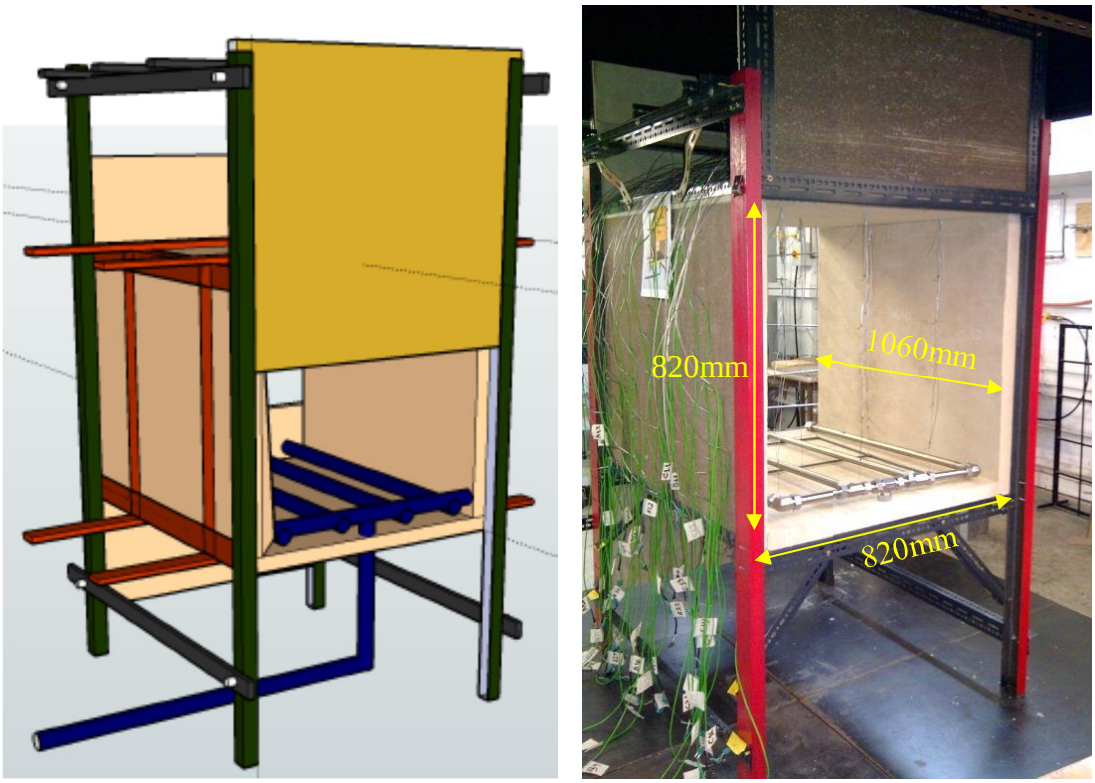

Figure 6-1: Design sketch (left) vs. actual experimental compartment (right) with main internal dimensions

6.2.2.2 Ventilation

Given that the compartment's front and rear doors were adjustable, it was possible to set different opening configurations that allowed for the evaluation of different ventilation mechanisms. The height of the front opening, H (or H_3), was the only dimension varied given its greater relevance in the *ventilation factor* or *parameter*, $A_w\sqrt{H}$. To simplify the nomenclature, the latter is represented by ϕ. Thus,

$$\phi = A\sqrt{H} = (WH)\sqrt{H} = W^1 H^{1.5} \qquad \textbf{Equation 6-1}$$

As uncovered by Equation 6-1, changes in the height of the opening, *H*, will have a greater impact on the *ventilation parameter*, ϕ, than changes in the width dimension, *W*, given that the former is to the power of 1.5. The relation between *H* and *W*, and the fact that compartment fires are typically characterized by a hot gas layer underneath the ceiling and a cold air layer next to the floor, led to positioning the ventilation opening in all configurations centred on the compartment's front plane. Thus, both the inflow and outflow flow patterns were altered in the same way in each experimental configuration.

These considerations led to establishment of six different opening configurations comprehending a compartment fully opened at both front and rear ends (ϕ_1), fully opened at the front and closed at the rear (ϕ_2), and four additional configurations where the rear opening remained fully closed while the front opening was decreased 20% of its total area in each consecutive setting (ϕ_3 - ϕ_6). These configurations are summarized in the following table:

Table 6-1: Experimental Opening Configurations

Opening Configuration (ϕ_n)	Front Window Opening	Rear Window Opening
ϕ_1	100%	100%
ϕ_2	100%	0%
ϕ_3	80%	0%
ϕ_4	60%	0%
ϕ_5	40%	0%
ϕ_6	20%	0%

6.2.2.3 Fuel Load

In order to reproduce a fire area representative of a fully-developed stage, a gas fuel distributor was installed covering the entire compartment's floor. The distributor consisted of four stainless steel pipes equally distributed along the floor area. Each of the pipes had 30 uniformly distributed 2 mm diameter holes drilled along the entire length, giving a total of 120 downward facing holes to introduce the gas fuel into the compartment. All the pipes within the compartment were covered with ceramic fibre paper – a lightweight refractory material processed from a blend of alumna-silica fibres – in order to minimize the heat radiation from them to the compartment. The pipes were fed with propane gas from a pressurized storage vessel and ignited by manual operation, allowing for 120 burners equally distributed next to floor level. The combustion products were expected to be clear with negligible soot formation inside the compartment, minimizing any radiation correction error to the thermocouples' temperature readings.

In order to prescribe a constant heat release rate, $\dot{Q}$, in each system configuration, fixed flows of propane were defined to feed the pipe arrangement. The selected values were 0.5, 1.0 and 1.5 g/s, which in terms of $\dot{Q}$ per unit floor area – assuming a combustion efficiency of 90% – would correspond approximately to 24, 48 and 72 kW/m^2, respectively.

In order to obtain a flow pattern as similar as possible to that obtained when burning solid cellulosic fuels (e.g. wood cribs) in natural fires, momentum-dominated flames (i.e., jet flames) were avoided and in turn buoyancy-dominated flames were forced. This was achieved by positioning the pipe distributor holes facing downwards. In this way, the relative importance of the buoyancy to the inertia of the flame – exposed by the non-dimensional *Froude number* – was assured by killing the propane flow velocity and in turn its momentum, giving as a result, buoyancy-driven turbulent diffusion flames. [16]

$$Fr = \frac{v^2}{gd}$$ **Equation 6-2**

In Equation 6-2, *Fr* is the Froude number, *v* is the flow (vertical) velocity, *g* is the acceleration due to gravity, *d* is the diameter of the flow source. This ratio shows that with a negligible upwards flow velocity (after ignition) a low *Froude number* was guaranteed giving flames falling in the buoyancy-dominated regime.

It is important to note that the fact of using a constant flow of propane for each modelling and experimental run, necessary forced a constant volatile supply equivalent to what would have been the volatile production in the pyrolysis process of cellulosic material combustion. This means that, when the CFD modelling and experiments were set to a constant propane flow, any variations in the air inflow (by means of changing the compartment opening for example) did not affect the volatile production, as would have happened in a cellulosic material fire due to the related changes in the oxygen transportation to the charring surfaces, and the consequent heat rate evolved in the solid [33].

6.2.2.4 Instrumentation

The compartment was equipped with several instruments and equipment measuring and recording the most relevant variables in a compartment fire. Table 6-2 presents the experimental instruments, the measured/recorded variables, and the range and accuracy of the measurements.

Table 6-2: Instrumentation & Measured Variables

Instrumentation/equipment	Measured Variables	Measuring range	Accuracy
Type K thermocouples	Gas Temperatures	0°C to 1,000°C	±1.5°C (min) ±3.5°C (max)
Think skin calorimeters	Incident Heat Flux to interior surfaces	0 kW/m^2 to 200 kW/m^2	±10%
McCaffrey probes connected to pressure transducers	Pressure Distribution on front opening and consequent flow velocities along it	Re>500	±7%
Thermal (IR) camera recorder	Neutral Plane position	variable	visual

Figure 6-2 presents the instruments and their location within the system. Each type of instrument used in the experiments is described in the following sub-sections, detailing their purpose and spatial arrange within the experimental compartment.

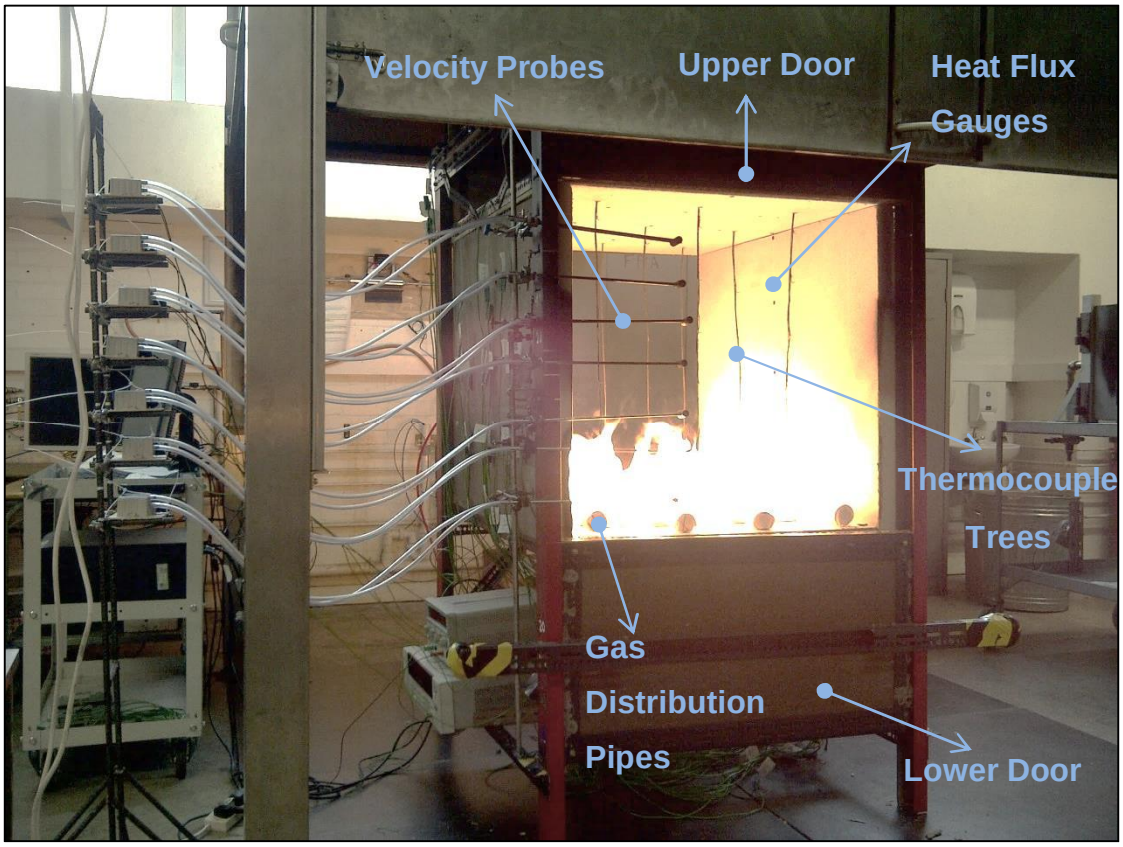

Figure 6-2: Instrumentation in the Small-scale Experiments

6.2.2.4.1 Gas Temperatures

The temperature of the gases was recorded by fifty-four K-type thermocouples, arranged in nine vertical arrays or 'trees' distributed evenly in a 3 x 3 fashion from ceiling to floor. This distribution gave, as a result, a good spatial resolution in regards to the inner gas temperatures achieved in each experimental run configuration.

The coding used to name each thermocouple was based on the following criteria: the three *lines* that ran from the front to the back of the compartment were named as lines A to C, respectively; the three *columns* that ran from left to right of the compartment were named as columns 1 to 3, respectively; and finally the six *levels* that ran from floor to ceiling of the compartment were named as 1 to 6, respectively. This ended up giving a 3 character code to each thermocouple – i.e., a letter followed by two numbers – which gives the exact location of each of them. For example,

thermocouple A23 was that located in *line* A, *column* 2, *level* 3. This spatial arrangement is presented graphically in Figure 6-3.

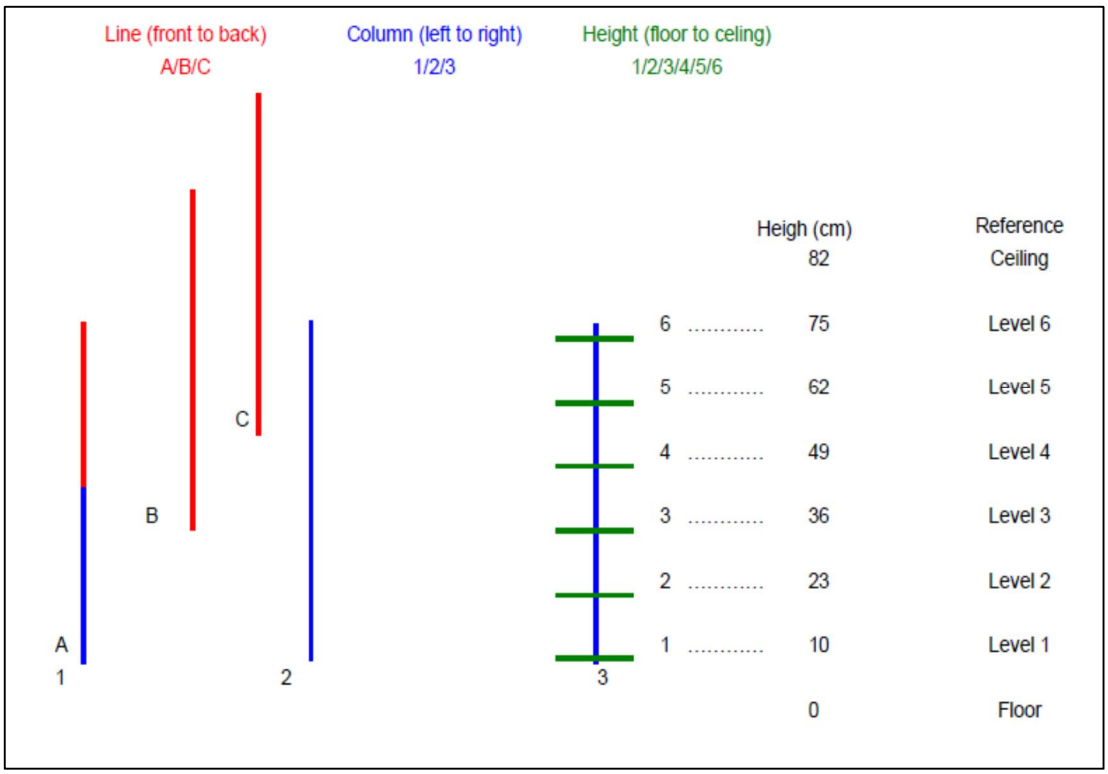

Figure 6-3: Thermocouple Coding

The thermocouples had a horizontal separation (parallel to the opening plane) of 27 cm and a vertical separation of 13 cm, with the bottom ones (level 1) located 10 cm above the compartment's floor. Additionally, the peripheral ones were located 15 cm from the side walls and 20 cm from the front and rear doors. This separation distances are summarized in Figure 6-4.

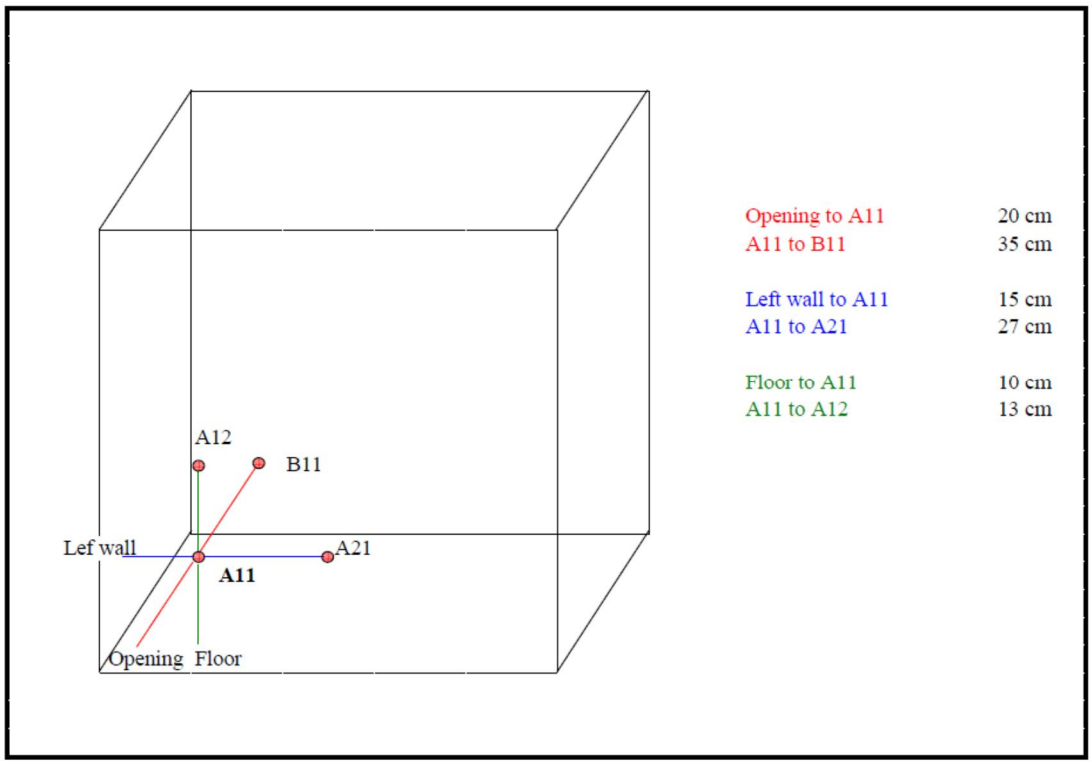

Figure 6-4: Thermocouple Spatial Arrangement

Welch *et al*. [121] pointed out that errors in local temperature measurements in – especially large – post-flashover fires are compromised by the uncertainty known as the *radiation error*. This was stated after showing that remote radiation may influence the thermocouple measurement with their proposed model. The authors explained that a thermocouple placed in a hot gas layer may receive a lower radiation than the one implied by the local gas temperature due to the influence of remote and cool surroundings such as a cold layer. The acting of additional sources of radiation gives as a result slightly lower recorded temperatures than the true gas temperature. In other words, the solid metal thermocouple tip re-radiates heat to the cooler surroundings (i.e., radiation loss), while this re-radiation energy loss mode is not viable in the gas surrounding the thermocouple. Contrary, in the lower layer, a temperature higher than the real local gas temperature can often be measured due to the influence of radiation emanating from the flames and/or the hot gas layer in the compartment which can be 'seen' by the thermocouple.

The authors also explain that the effect in both cases will tend to be more pronounced when heat transfer is dominated by radiation, which is normally the case in post-flashover fires. Therefore, because these small-scale experiments aim to represent the post-flashover stage, the temperature error correction by radiation was effectively done following the Welch *et al*. method (for further details on this calibration, refer to Appendix A).

This being said, in terms of temperature analysis within the scope of these experiments, average gas layer temperatures are generally useful approximations towards these small-scale experiments' main goal; i.e. assessing the accuracy of the simple hydraulic model. To this end, as the authors point out, whilst local gas temperatures might not be well represented by thermocouple measurements, values which are averaged over the whole fire region seem to provide a very good approximation to the average gas temperatures.

6.2.2.4.2 Incident Heat Flux

Forty-five thin skin calorimeters (TSC) were installed in a 2-D uniform mesh distribution along the inner compartment surfaces to measure the incident heat flux to the internal walls, floor, and ceiling. The distribution is depicted in the following figure:

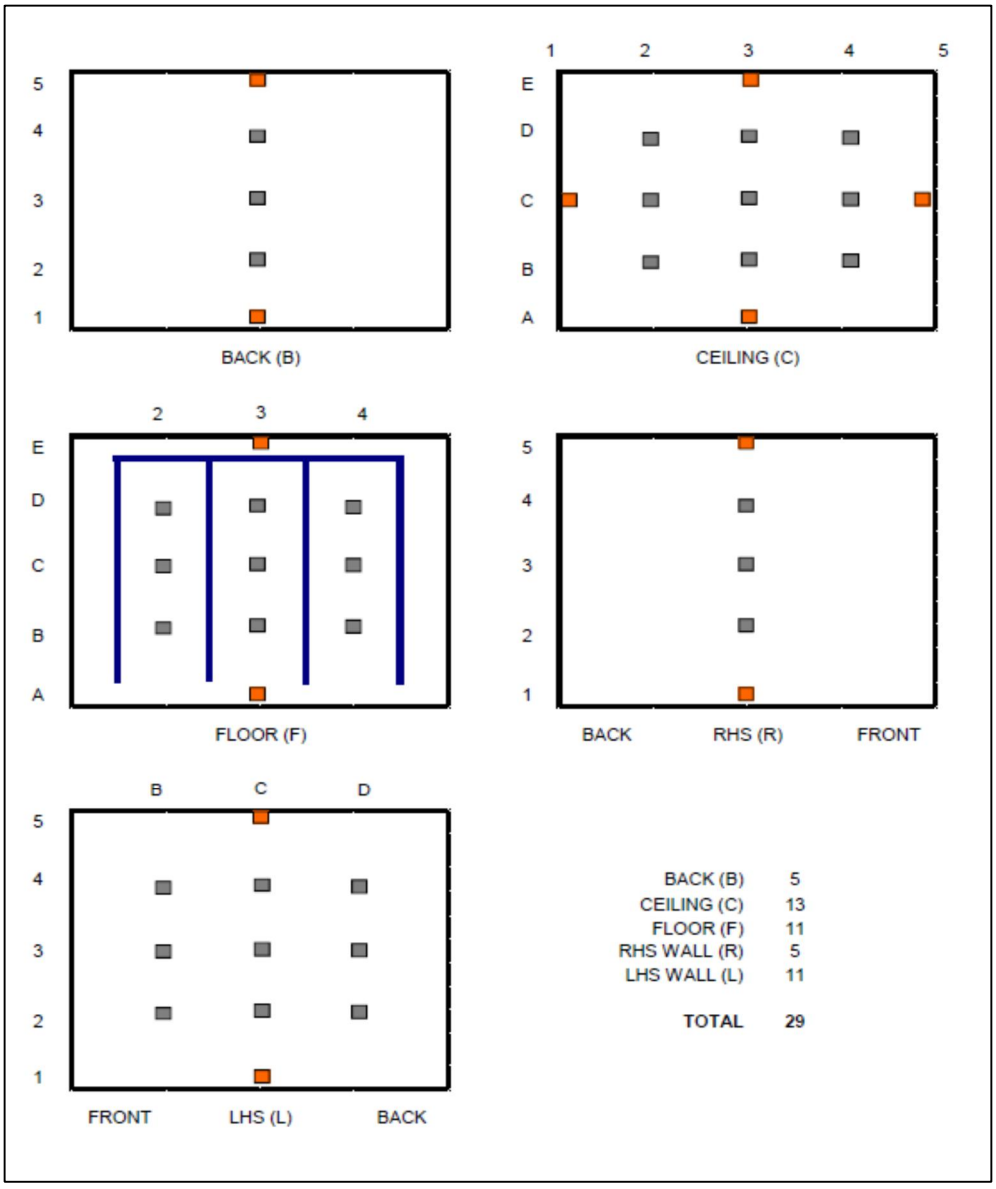

Figure 6-5: TSC 2-D arrangement and Distribution

The orange squares highlight those TSC which virtually shared the same location although in different planes (i.e., touching each other on one side), and the blue lines represent the gas distributor on the floor. Each plane was represented by a single letter (between brackets) so that each TSC was coded after its position, with the plane letter in first place followed either by a single number, or another letter and a number depending on which plane they were located. The TSC coding is depicted in the following figure:

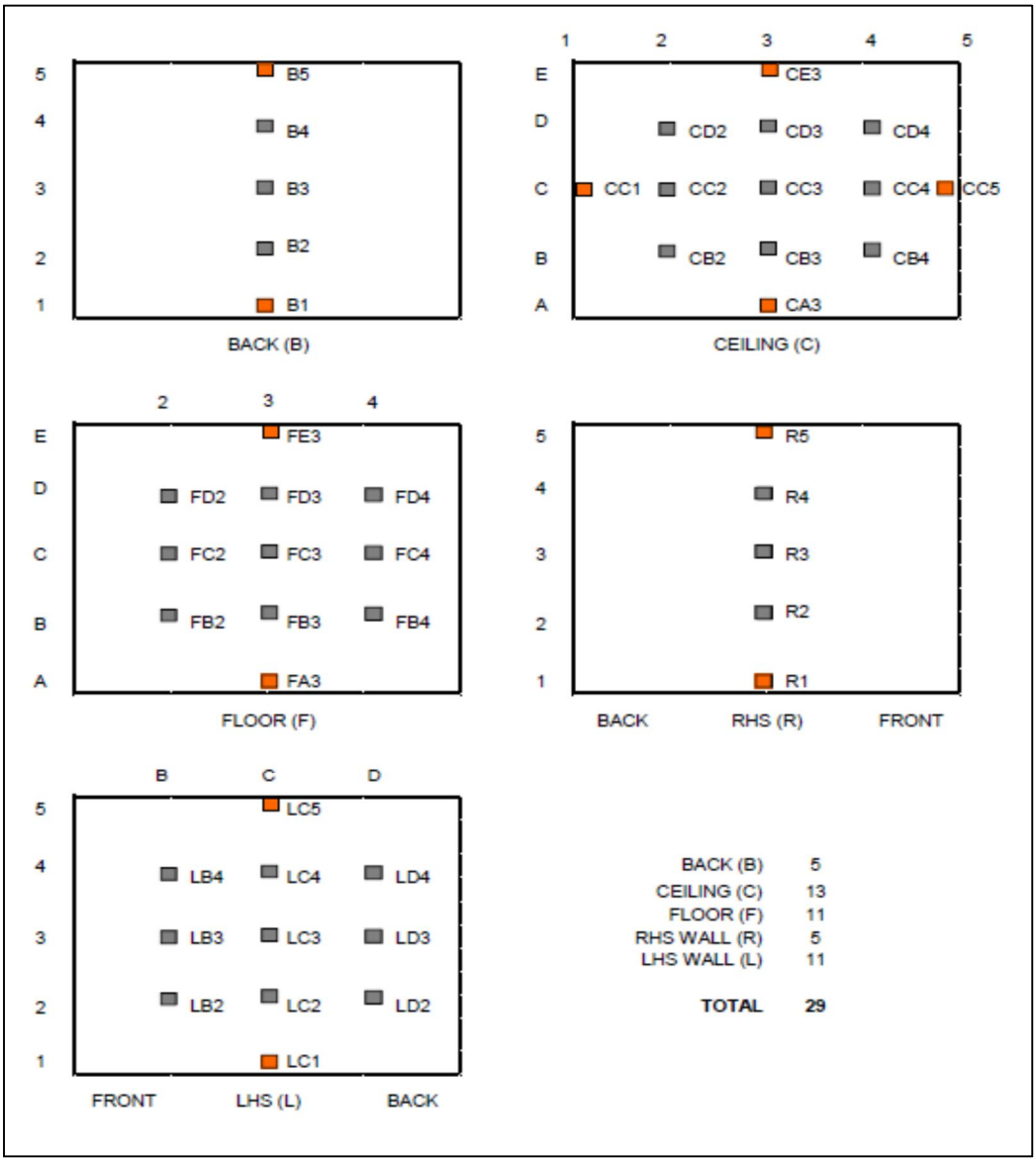

Figure 6-6: TSC Coding

Opposite facing TSCs (i.e., located on opposite planes) had exactly the same location allowing to record the effects in a 'mirror' fashion way. For example, LC3 was located at exactly the same 2-D coordinates as R3, on the LHS and RHS walls, respectively.

A calibration approach was selected in order to characterize the three dimensional heat transfer mode in a calibration assembly representative of the actual test

configuration, and obtain after it the wanted incident heat flux in the compartment's internal surfaces (for further details on this calibration, refer to Appendix A).

6.2.2.4.3 Pressure Difference (velocity & mass flow)

Changes in the pressure and velocity profiles at the opening plane of the compartment were measured using bi-directional pressure probes, with head outer diameter 17.0 mm, head length 32.0 mm, and pipe internal diameter 15.8 mm. These so-called *McCaffrey probes* [122] were logged on pressure transducers which recorded the hydrodynamic pressure difference at each time step. Different numbers of probes (depending on the opening size) were distributed vertically and evenly on the front opening plane, leaving a safe distance from the edges to avoid any edge effect that could affect the flow readings. For the full opening configuration, six probes were located along a vertical line, 250 mm from the left wall of the compartment, and at distances of 100, 230, 360, 490, 620, 750 mm from the compartment's floor (Photo 6-1):

Photo 6-1: Bi-directional probes distribution for the 100% opening configuration (ϕ_1)

In regards to the gas velocity estimation using this method, an accurate value of the gas density, ρ_g, must be used in each calculation. As demonstrated by Welch *et al*. [121], an ambient gas temperature, T_a, should be used in the calculation of the *inflow* velocity from measured pressure difference, and not the local thermocouple temperature which might have departed significantly from ambient due to the *radiation error*. In regards to the *outflow* velocities calculations, Welch *et al*. state the following:

> "The best estimates of local gas temperatures need to be used, otherwise the computed velocities will also be compromised by radiation errors, though the dependence is only to a half power of the temperature". [121]

Nevertheless, as noted before, the authors also point out that whilst local gas temperatures, T_g, might not be well represented by thermocouple measurements, values which are averaged over the whole fire region seem to provide a very good approximation to the average gas temperatures. Thus, average gas temperature values at each correspondent layer height were used towards *outflow* velocities estimations with sufficient accuracy within the experiments' main aim.

A bi-directional probe works in the same way as a *Pitot-static* tube; i.e., it is designed to measure the hydrodynamic pressure difference at the opening of a compartment, where the hydrostatic pressure is converted to hydrodynamic pressure. The only difference between a *Pitot-static* tube and a bi-directional probe is that the latter measures a slightly higher pressure than the former. The reason for this is that the positive end of the bi-directional probe measures the total pressure (simple Pitot pressure or stagnation pressure), while the negative end measures a slightly smaller pressure than the static instead [122][49]. Therefore, the probes must be calibrated to obtain the exact empirical value for the so-called *k factor*, which depends on the probe head geometry (Refer to Appendix A).

6.2.2.4.4 Neutral Plane & Smoke Interface Position

The neutral plane position, H_N or simply N (Figure 5-2), was assessed in each run by means of the values obtained from the pressure probes, while the smoke interface position, H_4 or H_D (Figure 5-2), was estimated using an infrared (IR) camera fixed at a height equal to half the height of the opening, which recorded each experimental run displaying the three dimensional thermal field.

Figure 6-7 shows an example of the six different probes layout in relation to the front opening frame (i.e., upper and lower edges), with negative and positive values separated by the estimated neutral plane position, H_N:

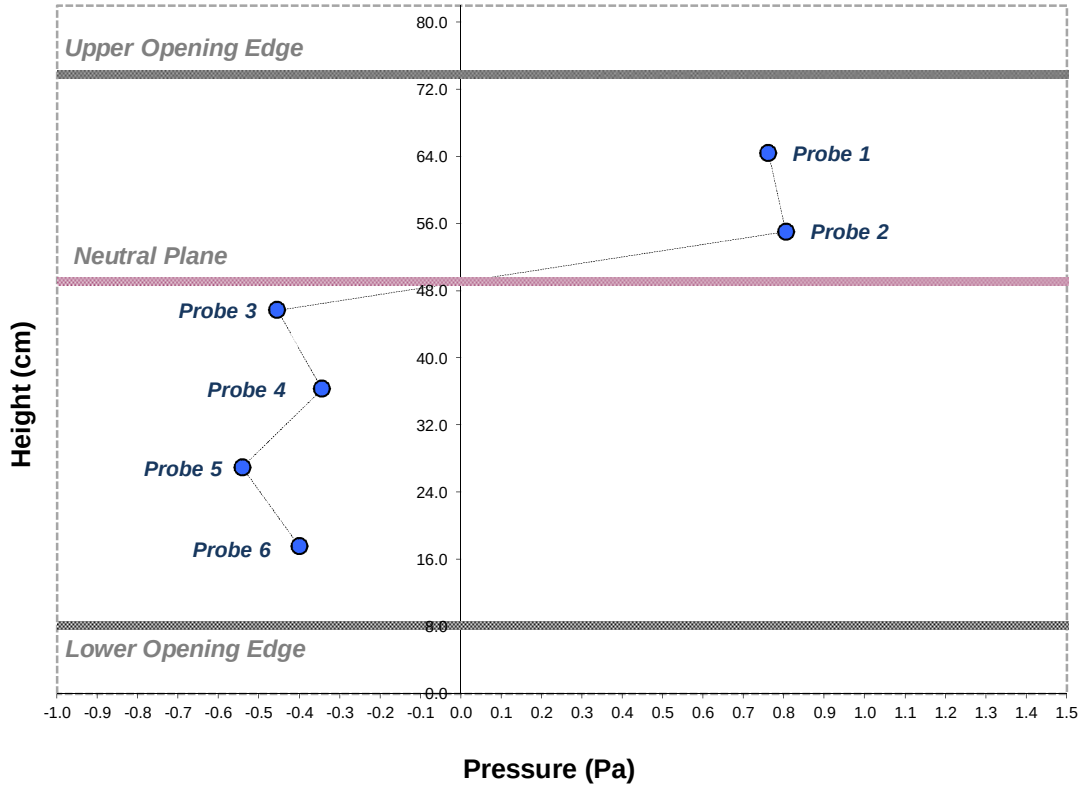

Figure 6-7: Pressure probes locations with respect to the opening edges and the neutral plane position in the 80% - 1.5 g/s run

And Figure 6-8 is a snapshot of the thermal field showing the smoke interface position, H_D, at a determined time during one of the experimental runs, making evident the difficulty to have accurate and consistent visual measurements of the hot gas layer height.

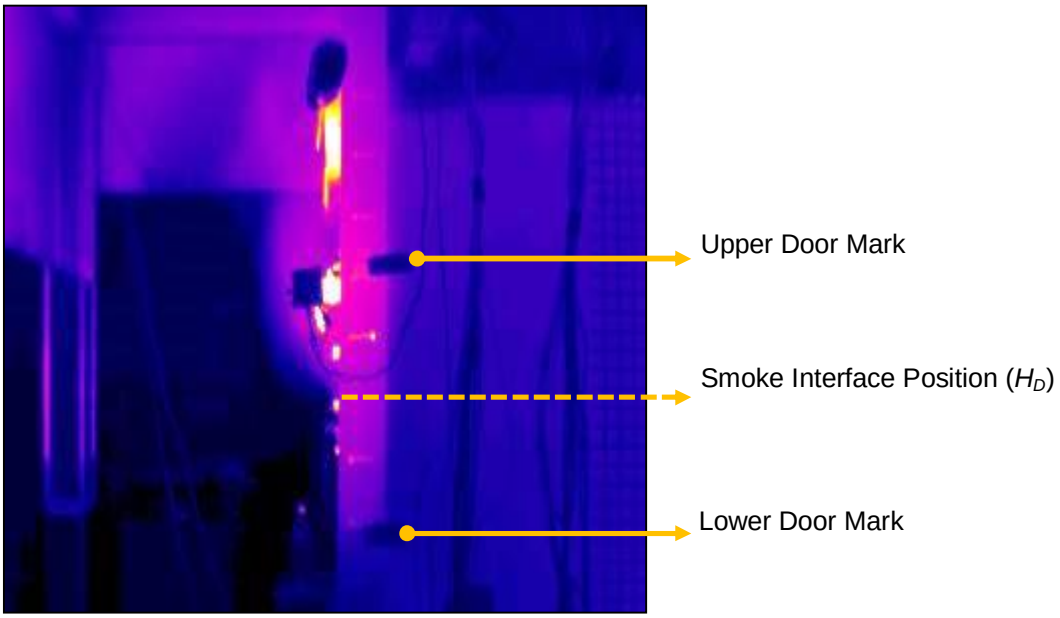

Figure 6-8: Thermal image showing the smoke interface in the ϕ_5 (40% - 1.0 g/s) run experimental procedure

The experimental procedure is intended to register the fire behaviour as it goes from a fairly 'wild or natural' setting (open fire, opening configuration ϕ_1), to the opposite extreme case of a ventilation-controlled post-flashover compartment fire (*Regime I*, opening configurations ϕ_6, ϕ_5 and probably ϕ_4), passing through the fuel-controlled post-flashover situation (*Regime II*, opening configurations ϕ_2 and probably ϕ_3) in its trajectory from one extreme to the other. So the whole idea is to twist the problem: instead of following the typical trend of a real fire that breaks windows as it develops trying to find its way out, a free fire is triggered and will gradually be constrained by limiting the ventilation until the very special case of a *classic Regime I compartment post-flashover fire* is encountered. This is the smoother way to add complexity to the problem as it develops, and not the other way round.

Every test strictly followed a time-coordinated routine procedure in order to obtain a consistent bulk of pre-processed information which enabled a sound analysis once this information was post-processed, calibrated/corrected, and contrasted. Due to the large amount of data recorded by the single Agilient Datalogger which was handling all the thermocouples and thin-skin calorimeters, the sampling frequency was around

0.2 Hz; i.e., a data recorded line (consisting of a data point for each sensor) every 5 seconds.

A single run consisted of a constant fuel flow – or burning rate, R – and a constant opening configuration, ϕ_n, lasting for a certain period of time (around 40 minutes) ensuring that steady-state conditions were reached. Three different propane flows were selected for each of the six opening configurations, giving a total of eighteen combinations tested. These are listed in the following table:

Table 6-3: Experimental design based on *ventilation factor* and propane mass flow

Opening Configuration (ϕ_n)	Opening area		Propane mass flow (g/s)
	Front	Back	
ϕ_1	100%	100%	0.5 1.0 1.5
ϕ_2	100%	0%	
ϕ_3	80%	0%	
ϕ_4	60%	0%	
ϕ_5	40%	0%	
ϕ_6	20%	0%	

6.2.3 Modelling Setup

The model selected to perform the simulations of the 18 combinations tested (Table 6-3) was the Fire Dynamics Simulator (FDS). FDS – as most Computational Fluid Dynamic (CFD) models – solves the *Navier-Stokes equations* in a particular way

suited for thermally driven flows [123]. The main characteristics of the FDS model and the way it solves these flows is that the acoustic effects of possible high *Mach number* flows is suppressed by decomposing the total pressure of the system into two components: a perturbation component that responds to the changes of the system and a background pressure of the compartment as a whole. These characteristics have made FDS one of the most popular models to aid the design of fire in the build environment.

6.2.3.1 Surroundings and Geometry

The surroundings of the compartment were modelled through the definition of the boundary conditions of the simulation domain, given by the atmospheric temperature and pressure which were input in FDS as recorded in the experimental tests. However, given the limitations on computational resources the simulation domain could not comprehend the same volume as the Rushbrook Laboratory, implying that a smaller domain was defined in which the compartment was located. Given that no official guidelines exist to define an optimal domain extension in relation to the characteristic lengths involved in the fire phenomenon, three different type of domains were defined: a tight domain close to the solid boundaries of the compartment; an extension of this domain on the axis perpendicular to the opening plane; and finally the former tight domain (mesh 1) with the addition of a coarse mesh (mesh 2). The extensions and volumes of these domains are presented in Table 6-4, setting the tight domain as the default domain for all simulations, while the others were used for specific comparisons.

Table 6-4: Domain extensions for the CFD modelling

Type of domain		Range of domain per axis			Volume (m^3)
		X **(m, m)**	***Y*** **(m, m)**	***Z*** **(m, m)**	
Tight		0.00, 1.64	0.00, 1.64	0.00, 1.64	4.4
Extended domain		0.00, 1.64	-1.00, 1.64	-0.50, 2.00	10.8
Additional coarse mesh	**Mesh 1**	0.00, 1.68	0.00, 1.64	0.00, 1.68	13.2
	Mesh 2	0.00, 1.68	-3.04, 0.00	0.00, 1.68	

Once the domain was defined, the next step to specify the surroundings consisted on defining the grid size for each of the domains presented and establishing the simulation time. The information related to grid size and simulation time is presented in detail in Table 6-5. Since in FDS all nodes of a particular mesh must be uniform cubes, the grid size was defined by the size of the arista of each node. These sizes allowed for the calculation of the total number of nodes, which was a relevant task given that the parallelization options in FDS are limited and carry strong restrictions, making it necessary to run most of the simulations in a single processing thread.

Table 6-5: Grid size, number of nodes and simulation times

Type of domain		Grid size	Nodes	Simulation time	Computational time
Tight		2 cm	551,368	750 s	12 hours
		4 cm	68,921	200 s	3.5 hours
		8 cm	8,000		10 minutes
Extended domain		2 cm	1’353,000		30 hours
Additional coarse mesh	**Mesh 1**	2 cm	578,592		22 hours
	Mesh 2	8 cm	16,758		

The conventional domain with a grid size of 2 cm was the one chosen as the basis of analysis. Therefore, the 18 experimental runs were modelled under this domain extension for 750 seconds. This time was approximately equivalent to 25% of the experimental time during which post-flashover conditions were sustained at steady-state. The 100% simulation time was disregarded since the very beginning due to computational time constraints. All the other domain extension and grid size configurations were used for specific aspects of the analysis and were limited to 200 seconds of simulation time due to computational time restrictions too. The hardware used to carry out the simulation was a computer with Intel® Xeon® processor (3.46 GHz, 24 processing threads) and 196 GB of Random Access Memory (RAM) and a Red Hat operating system.

The geometry of the compartment was defined with the same dimensions of the experimental setup, but limited to just the box and not the supporting elements. The

material of the compartment was modelled in FDS as ceramic fibre sheets with specific heat of 0.9 (kJ/kg/K), with a conductivity specified as a ramp function depending on the temperature to achieve the response of the real material going from 0.07 W/m·K @ 300°C to 0.2 W/m·K @ 1,000°C and a density of 310 kg/m^3.

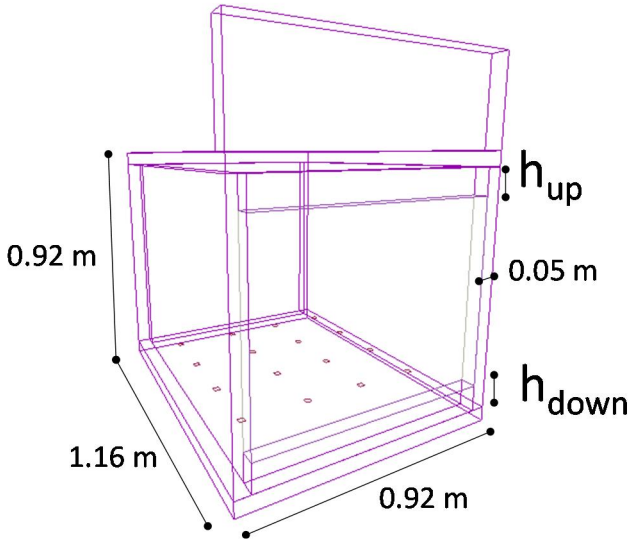

Figure 6-9: Geometrical representation in FDS of the experimental system

6.2.3.2 Ventilation and Fuel Load

The ventilation of the modelled compartment was defined exactly as the experimental one. The following table adds to each configuration the correspondent height of the upper, h_{up}, and lower doors, h_{down}:

Table 6-6: Modelling Configuration Based on Experimental Setup

Opening Configuration (ϕ_n)	Opening area		Compartment doors	
	Front	**Back**	h_{up} **(m)**	h_{down} **(m)**
ϕ_1	100%	100%	0	0
ϕ_2	100%	0%	0	0
ϕ_3	80%	0%	0.082	0.082
ϕ_4	60%	0%	0.164	0.164
ϕ_5	40%	0%	0.246	0.246
ϕ_6	20%	0%	0.328	0.328

The gas burners were modelled as holes on the floor from where propane gas flowed into the compartment giving a buoyancy-driven flame. Due to the computational mesh restrictions, the 2 mm holes of the original burners were not able to be reproduced. Therefore, the 120 holes were replaced by 16 square burners with a 2 cm^2 area each, which nevertheless supplied an equivalent heat release rate, $\dot{Q}$, achieved by fixing the propane mass flow and its combustion reaction. The latter was assumed to be an incomplete reaction solved by the mixture fraction model and defined by the heat of combustion (which had a value of 50,340 kJ/kg) and a soot yield of 10%. With the heat of combustion and the propane flows previously defined, the heat release rate per unit area, $\dot{Q}_{PUA}$, was defined and inputted in FDS as released by the 16 square burners.

6.2.3.3 Instrumentation

The instrumentation in FDS is defined as 'devices' which allow the user to record the desired measurements and include them in the simulation output. In these simulations, two groups of devices were defined.

The first group comprised instrumentation equivalent to that used in the experimental runs (thermocouples, heat flux gauges, and bi-directional probes). The devices were modelled following the correspondent manufacturers' parameters to achieve the best fit between the experimental measurements and the simulation output.

The second group comprised additional virtual devices that allowed for the gathering of extra information related to the fire dynamics of each configuration. They measured the gas linear velocity within the compartment and the mass flow rate through the opening area.

The velocity was measured by 44 devices that recorded the horizontal (perpendicular to the opening) and vertical (perpendicular to the floor) components of the gases' velocity inside the compartment at 4 different heights, as shown in Figure 6-10:

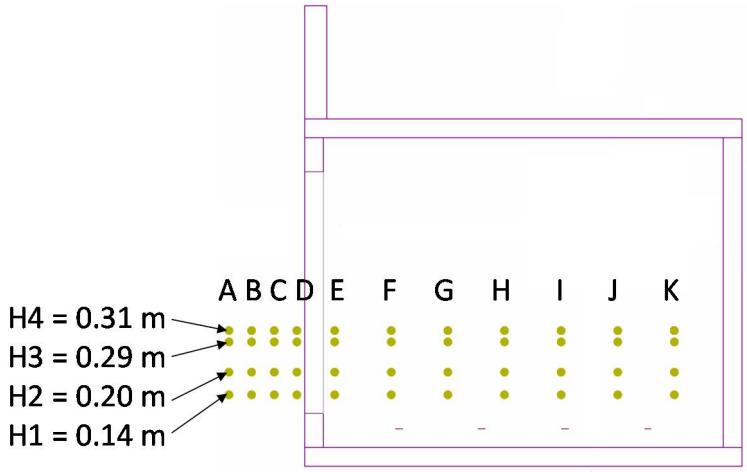

Figure 6-10: Gas linear velocity devices (11 monitor points at 4 different levels – i.e., 44 devices in total – denoted as A to K (or 1 to 11 in Section 6.2.4.3 figures))

And the mass flow throughout the opening was measured through devices that recorded the flow through a specific horizontal section or slice of the opening as shown in Figure 6-11:

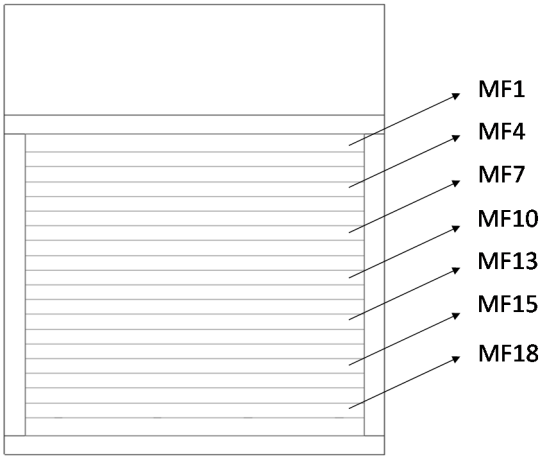

Figure 6-11: Mass flow rate devices

The number of mass flow rate devices varied with the ventilation configuration and ranged from 20 for ϕ_1 and ϕ_2, to 8 for the ϕ_6 configuration.

The results obtained with this set of virtual instrumentation, contrasted and compared against the experimental results, were key in helping fulfil the *main goal* of assessing the accuracy of the theoretical hydraulic model, as well as fulfilling the *consequential goal* of identifying the transition zone between the classic regimes of behaviour; i.e., *Regime I* and *Regime II*.

6.2.4 Relevant Results and Analysis

6.2.4.1 Temperature Analysis

The following three graphs – one for each propane flow – show the experimental time-averaged temperature recordings during a selected portion (of around 10 minutes) of the steady-state period representing the fully-developed or post-flashover stage:

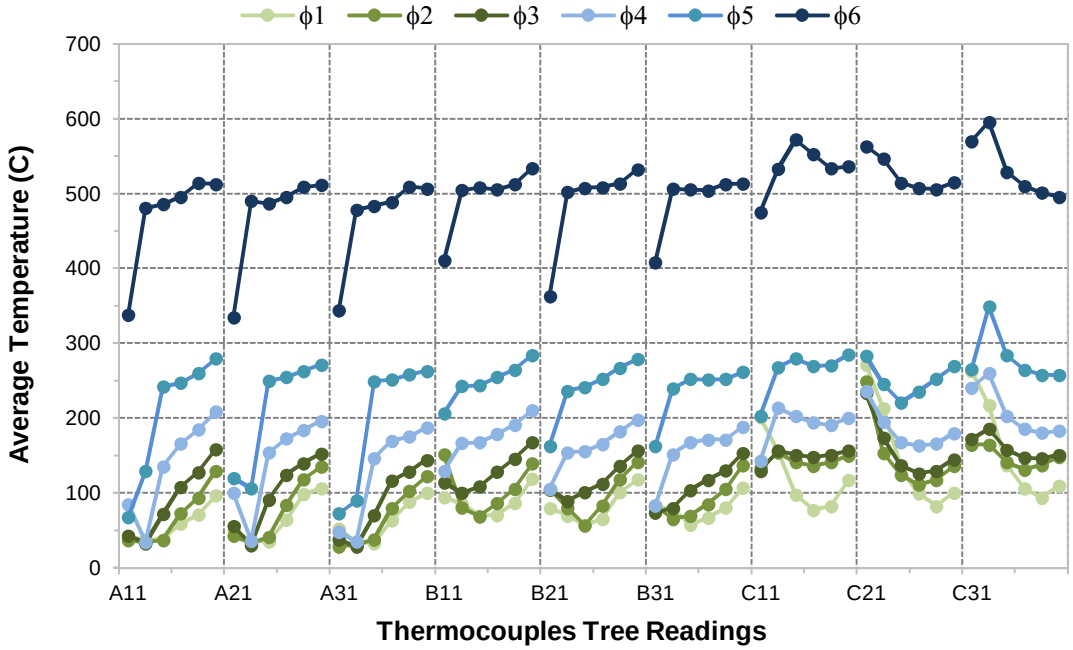

Figure 6-12: Time-averaged (over the steady-state period of fully-development) temperature readings for all 54 thermocouples in each opening configurations (0.5 g/s propane flow)

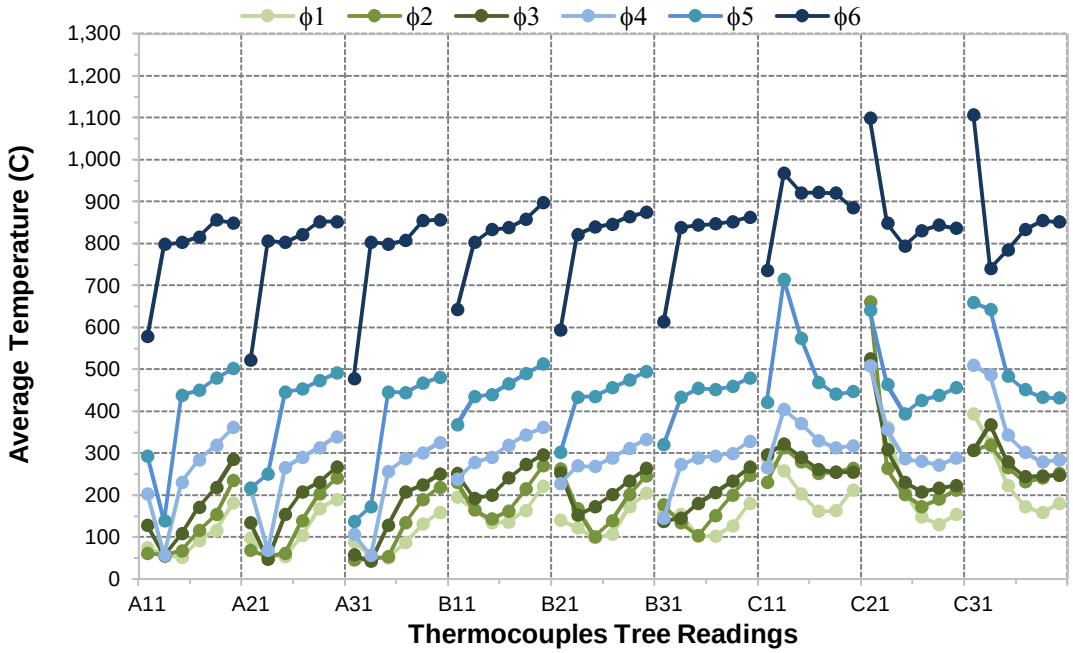

Figure 6-13: Time-averaged (over the steady-state period of fully-development) temperature readings for all 54 thermocouples in each opening configurations (1.0 g/s propane flow)

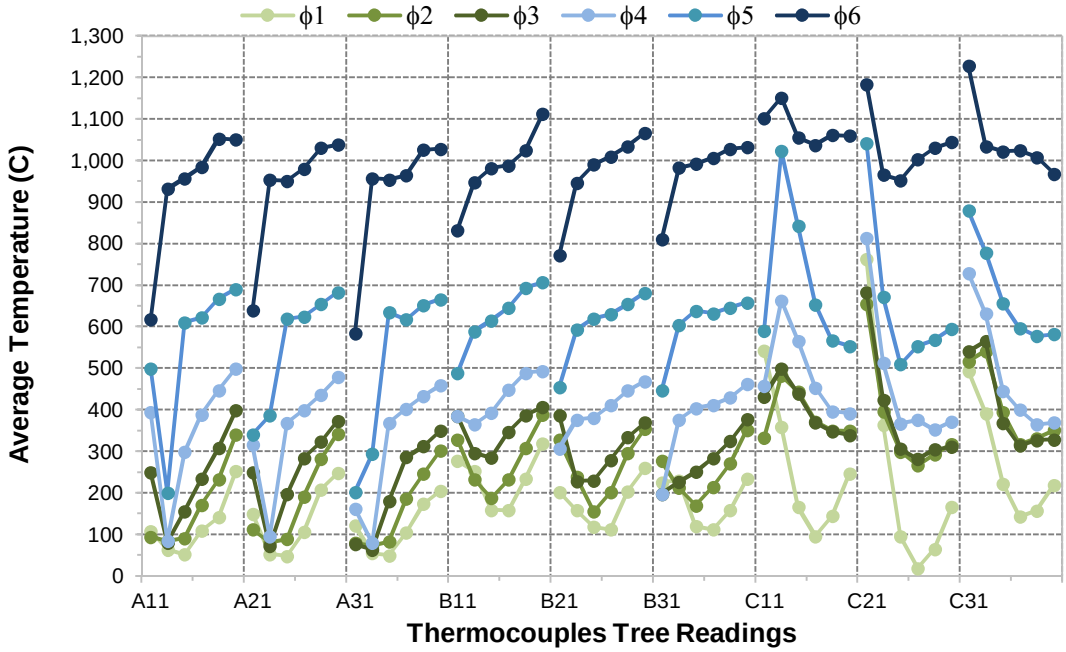

Figure 6-14: Time-averaged (over the steady-state period of fully-development) temperature readings for all 54 thermocouples in each opening configurations (1.5 g/s propane flow)

From Figure 6-12, Figure 6-13, and Figure 6-14, it can be observed that:

(A) there is a clear tendency towards a *uniform upper layer temperature* (represented by a horizontal dotted line in each thermocouple tree):

(i). as the ventilation opening is reduced; i.e., tending towards *Regime I*;

(ii). when moving further to the back of the compartment; i.e., from tree A to B and then C. Nevertheless, tree C experiences some flame (see bullet (C)) and flow (refer to the *back wall effect* in Section 6.2.4.4) effects in the lower thermocouples in almost all configurations, while trees A and B experience similar effects only in the larger opening configurations;

(iii). and as – quite surprisingly – the propane flow is reduced. It would have been more reasonable to expect more uniformity at higher heat release rates (represented by the propane flows), but evidently the turbulent flow and rocking flames played an important role (e.g., the *back wall effect* -

refer to Section 6.2.4.4) in breaking the layer uniformity, in contrast to the laminar and low kinetic energy flow condition typically present at low propane flows.

The following graphs show the time-average temperatures for each horizontal row layer. Each of these row layers comprises 3 thermocouples each: A11, A21, and A31 (labelled as Ai1); B11, B21, and B31 (labelled as Bi1); C11, C21, and C31 (labelled as Ci1); and so forth for each of the 6 layers:

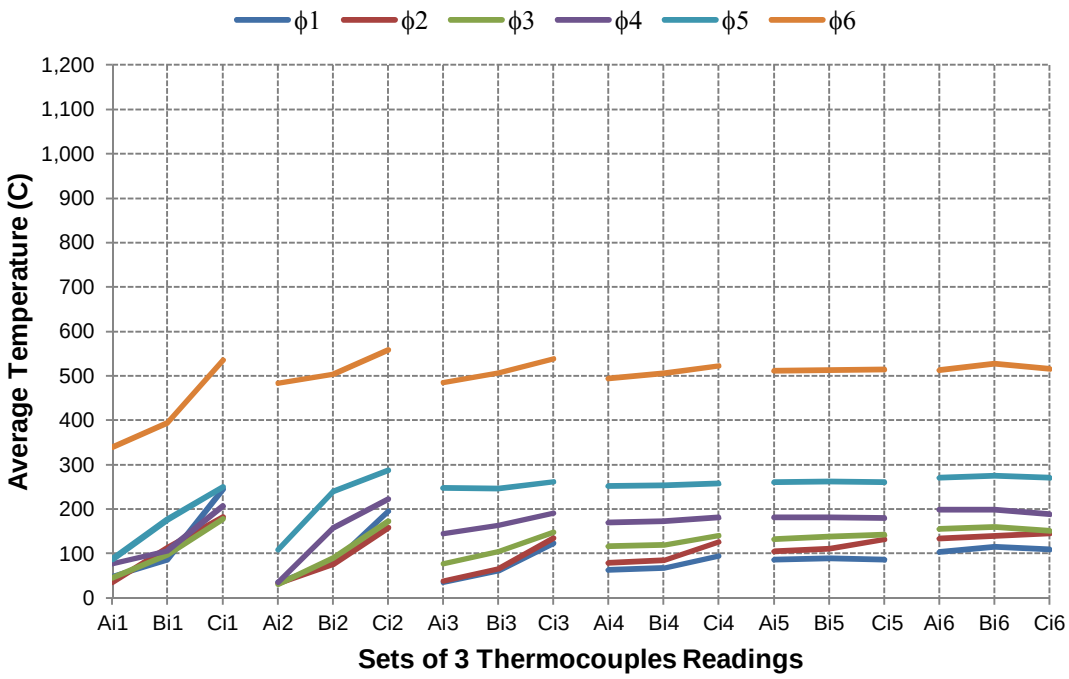

Figure 6-15: Time-averaged (over the steady-state period of fully-development) temperature readings for each horizontal row layer comprising 3 thermocouples each (0.5 g/s propane flow)

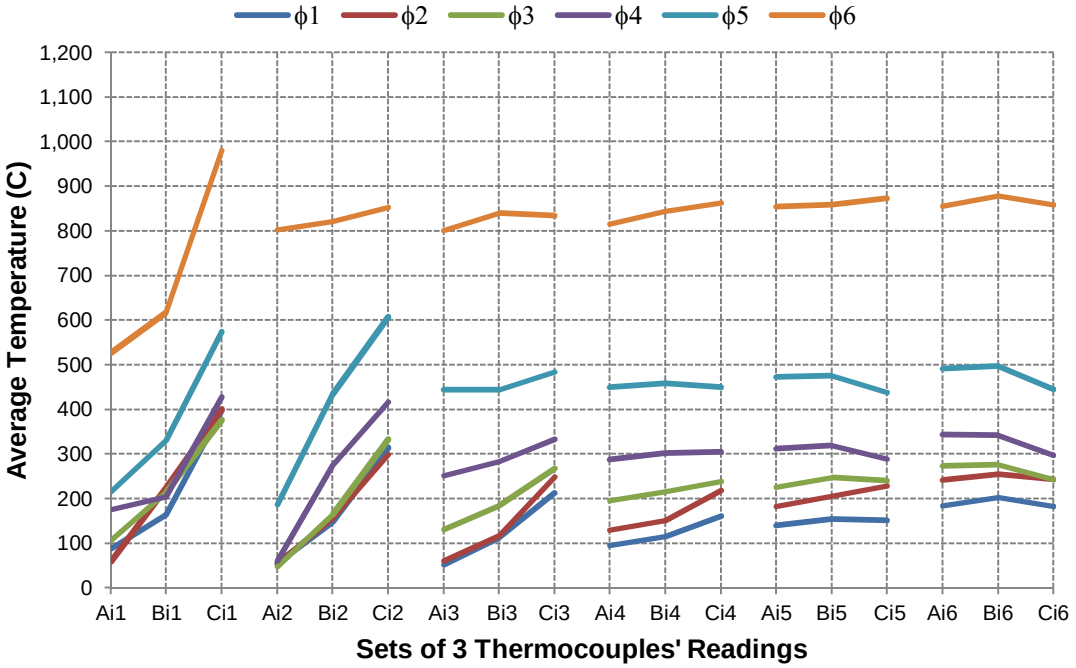

Figure 6-16: Time-averaged (over the steady-state period of fully-development) temperature readings for each horizontal row layer comprising 3 thermocouples each (1.0 g/s propane flow)

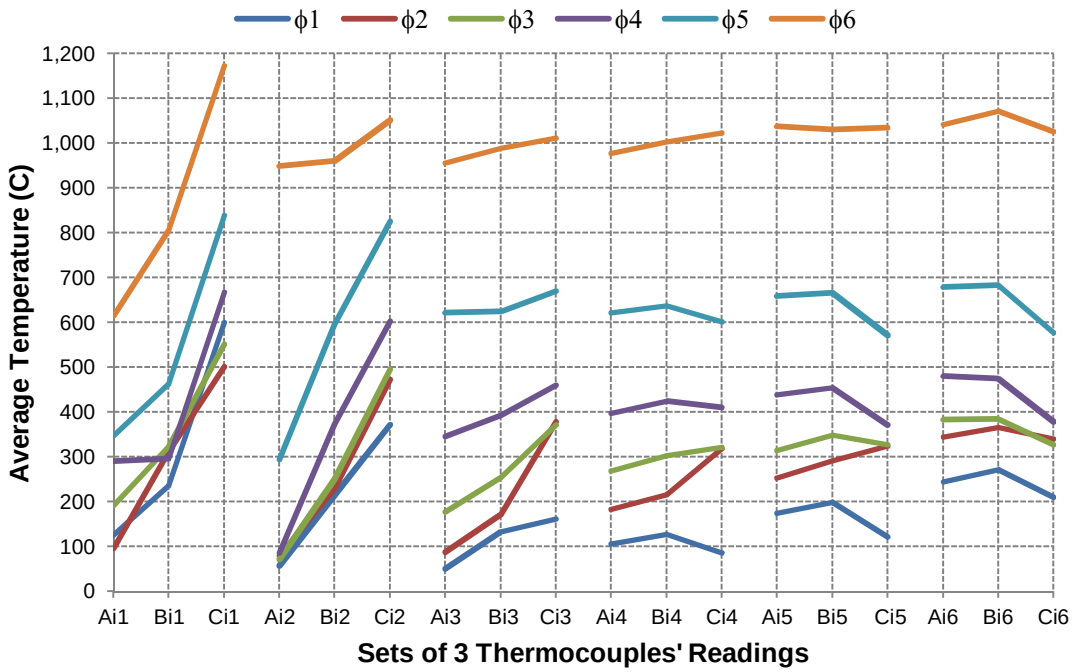

Figure 6-17: Time-averaged (over the steady-state period of fully-development) temperature readings for each horizontal row layer comprising 3 thermocouples each (1.5 g/s propane flow)

From Figure 6-15, Figure 6-16, and Figure 6-17, it can be observed that:

(B) there is an *increase in system's overall gas temperature*:

The first and most evident observation is that the general tendency for the system's temperature is to increase:

(i). as the ventilation opening is reduced (i.e., from ϕ_1 to ϕ_6), and

(ii). as the propane flow is increased (i.e., from 0.5 to 1.5 g/s).

This comes as no surprise, since the cause for (*i*) is an energy balance that effectively has less radiative and convective losses through the opening which altogether weight more than the increase in conductive losses through a larger internal solid boundary layer, and the cause for (*ii*) is the increased heat release rate of a larger fuel flow (the propane flow is actually replicating the heat release rate per unit area, $\dot{Q}_{PUA}$, as stated above).

(C) the flame *biases* the lower thermocouples readings:

The effect of increasingly taller buoyant flames as the propane flow was increased was recorded by the thermocouples readings in the lower layers. Due to the air inflow direction in configurations ϕ_2 to ϕ_6 (from front to back of the compartment through the single front opening), the flames tended to tilt backwards. This tilt flame effect is evidenced by the steep temperature gradient recorded by the bottom layers, especially in layers 1 and 2 during all 1.0 and 1.5 g/s propane flow runs. The thermocouples from these layers were either recording effectively the flame temperature when embedded in the flames (usually the middle and back rows, i.e. rows Bi1, Bi2 and Ci1, Ci2, respectively) or the gases in the near proximity of the flames (usually rows Ai1 and Ai2). This is the reason by which the maximum recorded temperature appears at the lower back of the compartment in what was observed and meant to be the 'cold' layer; i.e., these thermocouples where usually embedded in flames or extremely close to

them. This effect was taken into account in the analysis since it is not representative of the overall gas temperature where the focus was put on.

(D) the lower or 'cold' layer has a *positive temperature gradient*:

Looking at the lower layers – layers 1, 2 and 3 – a positive temperature gradient is evidenced in every opening configuration (ϕ_2 to ϕ_6). This 'cold' layer with a strong temperature variation in the inflow direction demonstrates that the cold air flooding the lower part of the compartment heats up as it travels deeper into the compartment.

6.2.4.1.1 Modelling Comparison

This subsection compares the time-averaged gas temperature results obtained in the experiments for each thermocouple against the time-averaged values output from the FDS modelling.

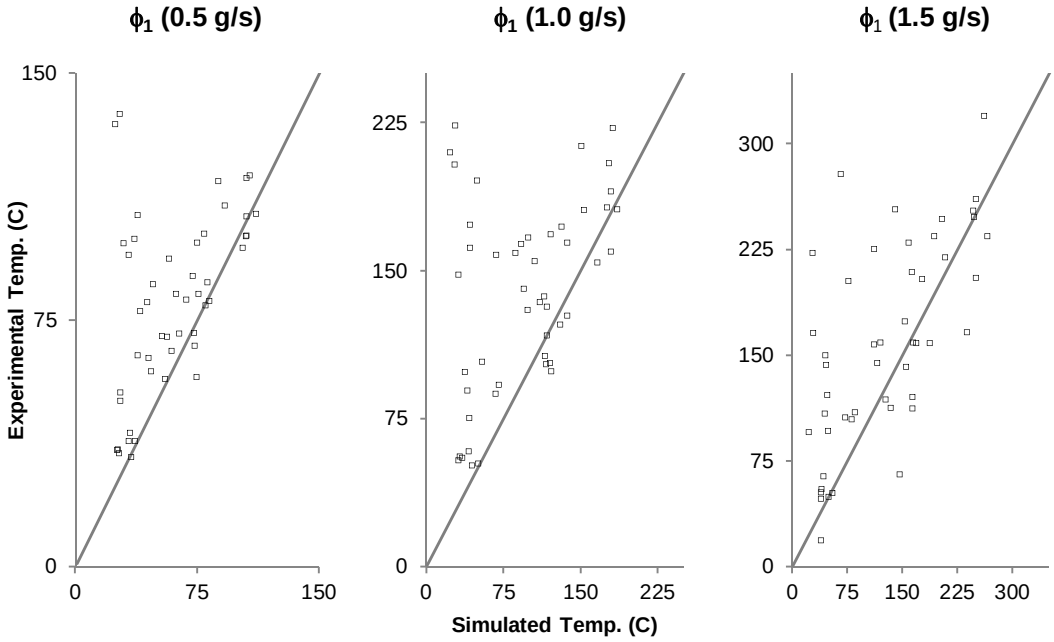

Figure 6-18: Time-averaged (over the steady-state period of fully-development) temperature results compared for the opening configuration ϕ_1

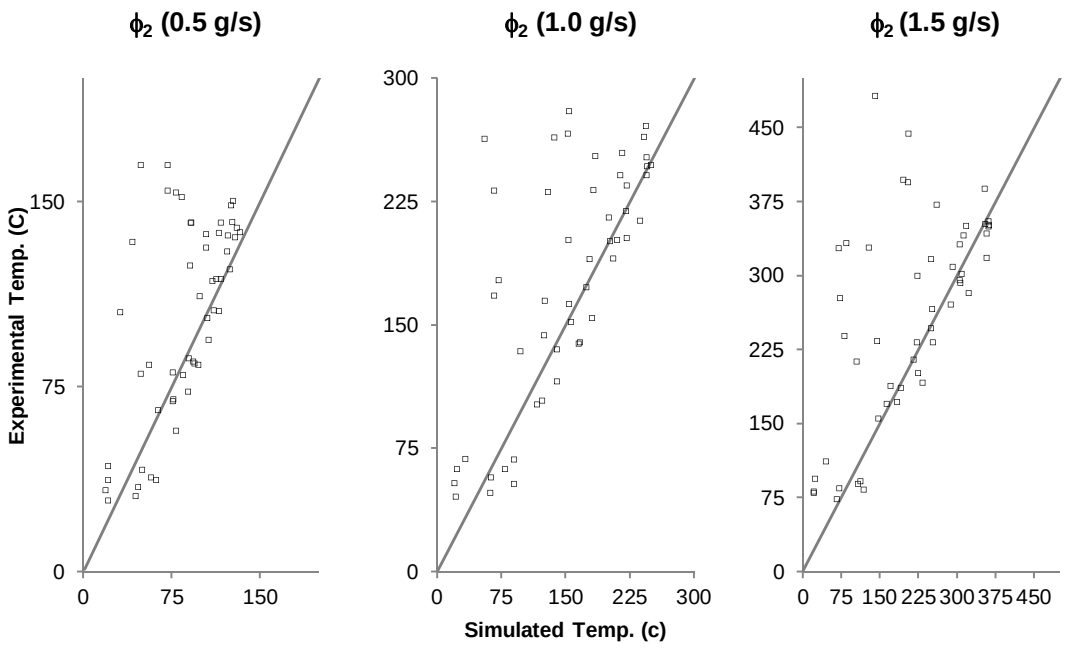

Figure 6-19: Time-averaged (over the steady-state period of fully-development) temperature results compared for the opening configuration ϕ_2

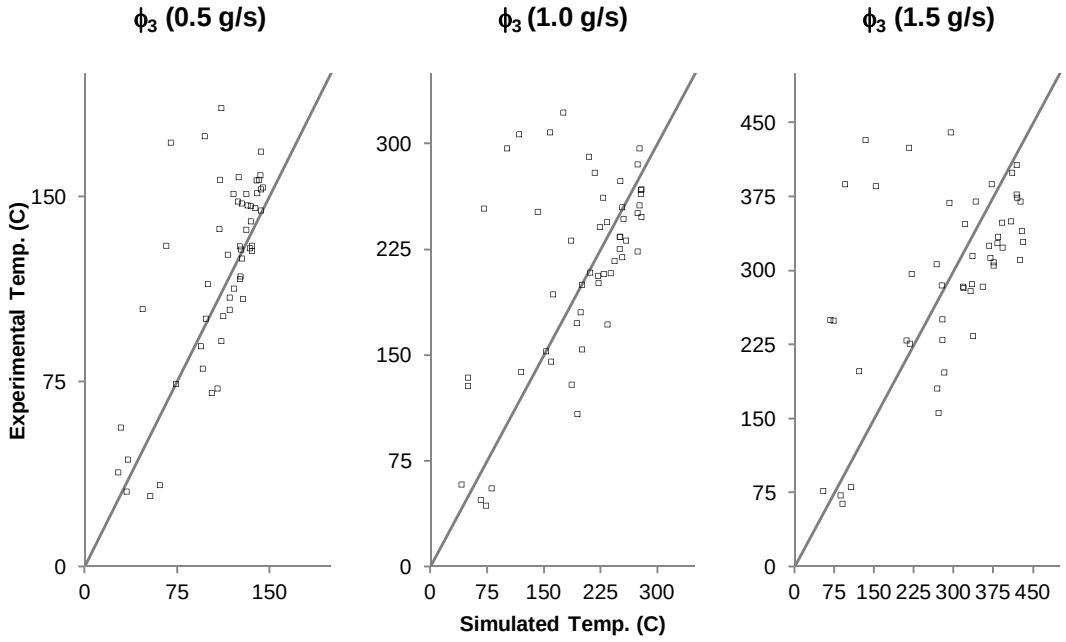

Figure 6-20: Time-averaged (over the steady-state period of fully-development) temperature results compared for the opening configuration ϕ_3

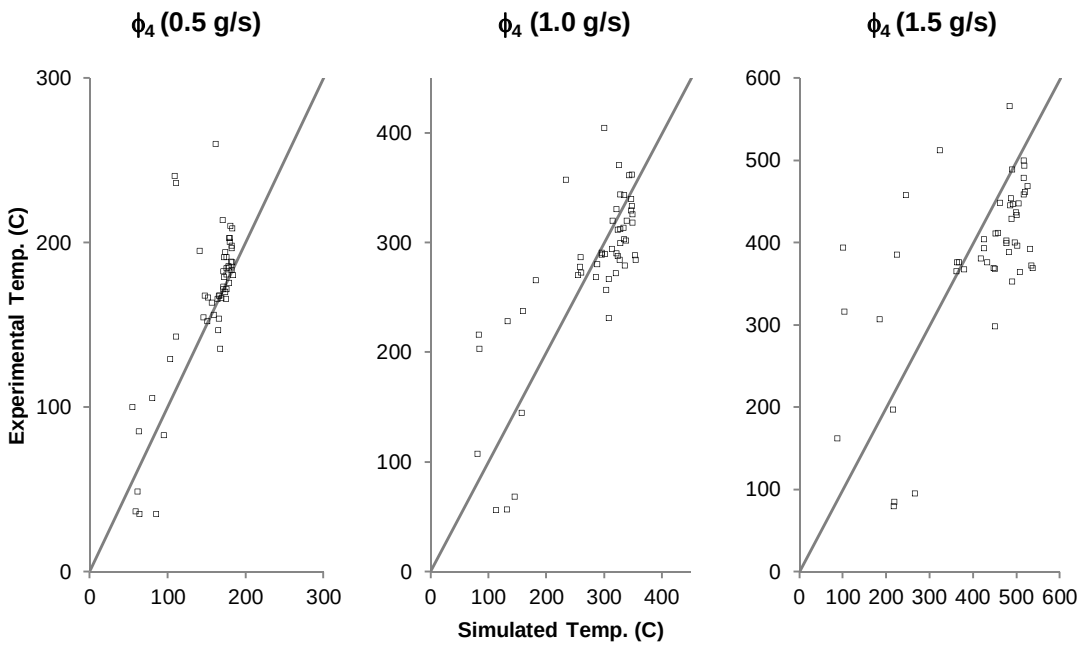

Figure 6-21: Time-averaged (over the steady-state period of fully-development) temperature results compared for the opening configuration ϕ_4

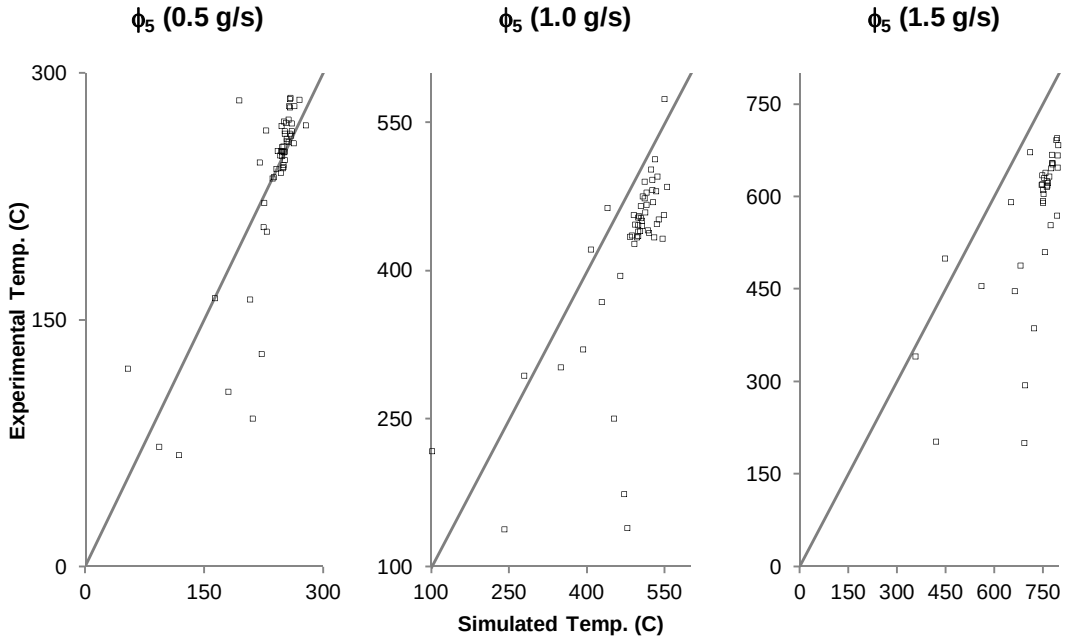

Figure 6-22: Time-averaged (over the steady-state period of fully-development) temperature results compared for the opening configuration ϕ_5

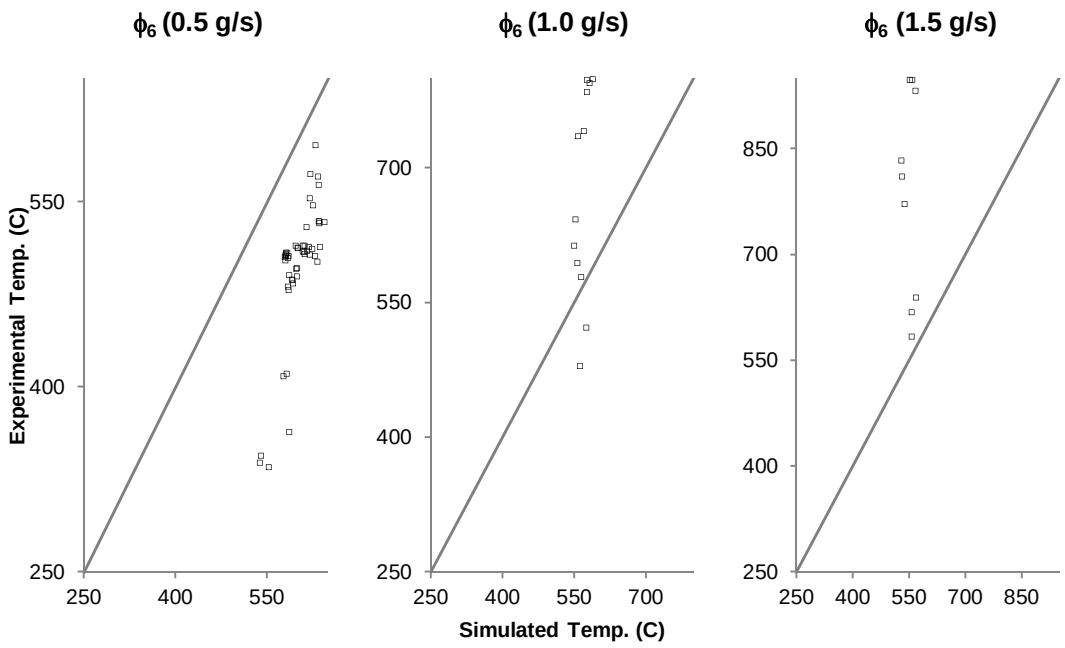

Figure 6-23: Time-averaged (over the steady-state period of fully-development) temperature results compared for the opening configuration ϕ_6

After these graphs, it comes clear that the smaller the opening configuration is – i.e., the more the compartment fire tends to a *Regime I* behaviour – the better FDS predicts the hot gas temperature readings. This means that when the upper hot layer is well-stirred giving as a result a more uniform temperature field, there is a better correspondence between the experimental and the modelled results. The turbulence appears to have a significant effect on said correspondence; i.e., there is a tendency for a better coincidence in the low propane flows. In this regard, configuration ϕ_6 – affected by the heaviest turbulent flow conditions – is the one with the worst data correspondence.

Summarizing, the more uniform the temperature field is (represented by a reduced opening configuration in this small compartment scenario) and the less turbulent the flow is (represented by a lower propane flow in this study), the better the coincidence between the experiments and the modelling. This is clearly observed when exposing the thermocouple error in the experimental vs. modelling recordings and comparing two limiting scenarios in the low propane flow:

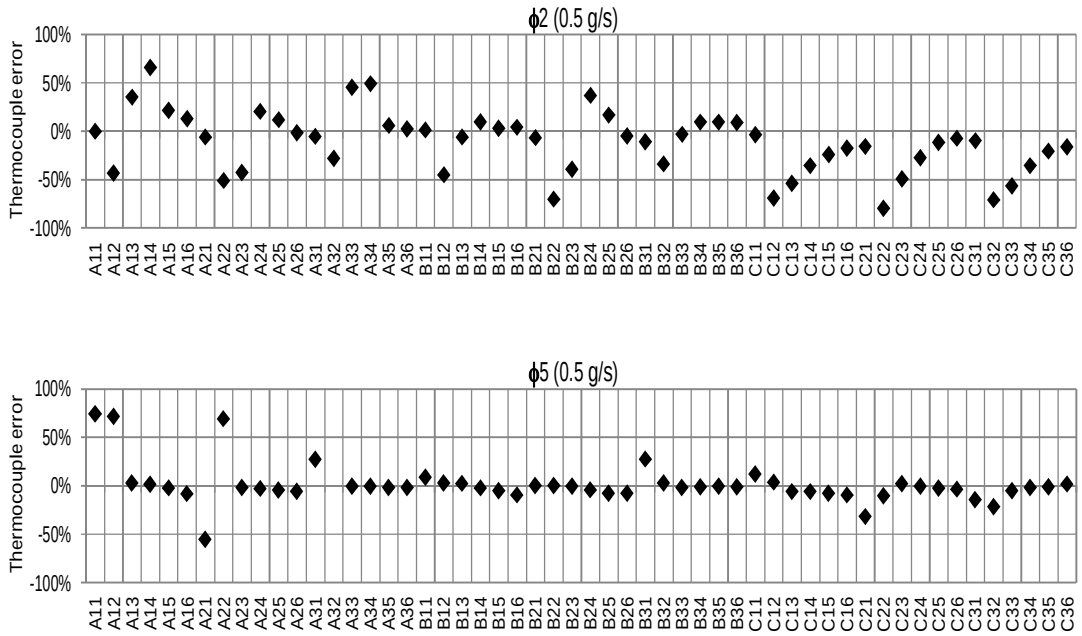

Figure 6-24: Experimental vs. modelling thermocouple reading error in two (ϕ_2 and ϕ_5) opening configurations with 0.5 g/s of propane flow

6.2.4.2 Flow Analysis

6.2.4.2.1 Velocities

The following figure shows the horizontal time-averaged velocities recorded by several bi-directional probes – the amount of probes installed depended on the size of the opening – at the opening plane during a selected portion (of around 10 minutes) of the steady-state period representing the fully-developed or post-flashover stage:

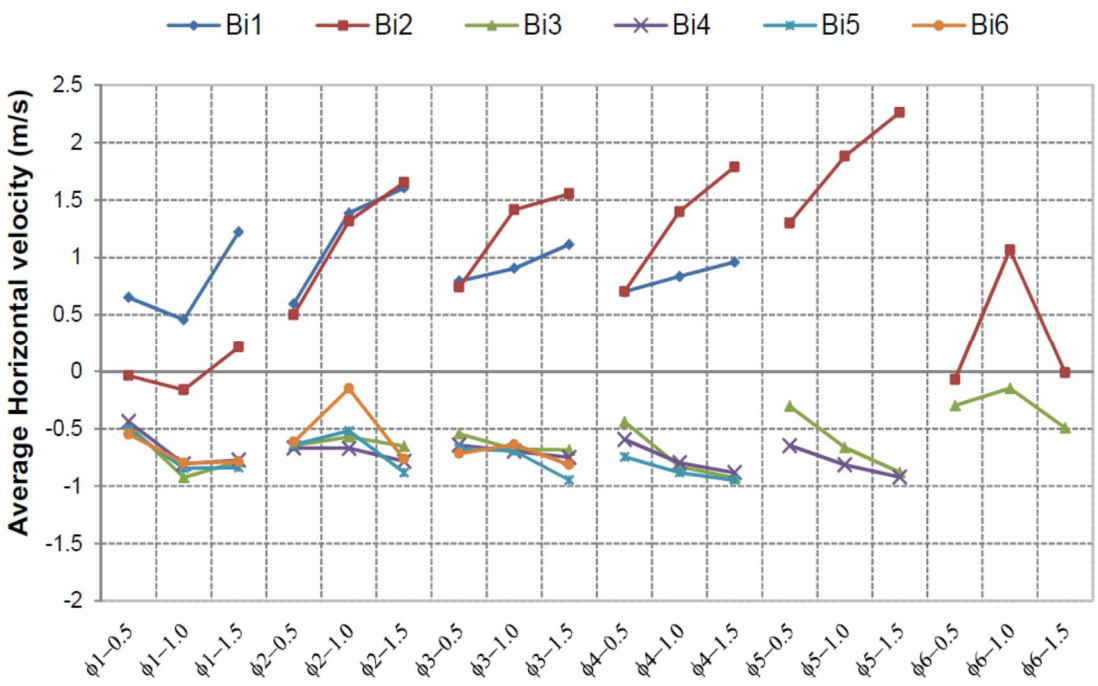

Figure 6-25: Time-averaged (over the steady-state period of fully-development) horizontal readings for each bi-directional probe located at the opening plane.

This graph clearly shows a tendency in all the opening configurations for the velocity to increase (in absolute value; i.e., positive and negative or outflow and inflow, respectively) as the propane flow – or heat release rate per unit area, $\dot{Q}_{PUA}$ – increases. It also gives an estimate of the location of the neutral plane, H_N. It is worth clarifying that the latter will coincide with the hot gas layer position, H_D, at the opening plane, but further into the compartment H_D stands below H_N. This 'chocking' (i.e., $H_D < H_N$ as depicted in Figure 2-5 and Figure 2-6) creates a depression in the lower part of the compartment that draws fresh air into the compartment achieving the natural mass balance.

Since the probes location usually changed from one opening configuration to the other, their outputs cannot be directly compared. This means that the same probe located in a different position with respect to the opening edges (given by the change in opening configuration) and with respect to the neutral plane (given by the change in the propane flow) is expected to give different readings. Having said this, the inflow velocities seem to stay in the tight range of 0.5 to 1.0 m/s in all experimental

configurations, while the outflow velocities range extensively from 0.5 to almost 2.5 m/s.

It is nevertheless important to note that due to the turbulent nature of the outflowing gases in contrast to the typically close-to-laminar nature of the inflowing air, the probes reading the outflow had a stronger noise – and therefore a much wider scatter – than those reading the inflow. The following figure exemplifies this effect, exposing the sensitivity of the probes readings to the flow turbulence:

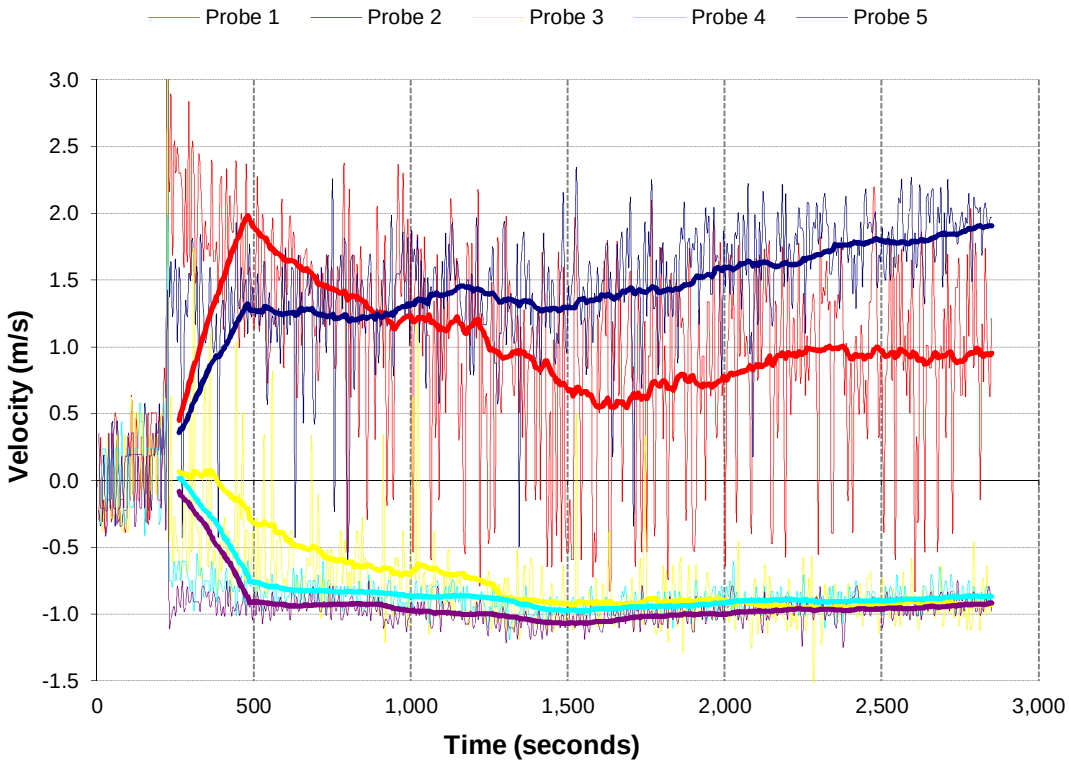

Figure 6-26: Outflow vs. inflow scatter in the velocity readings at the opening plane (ϕ_4, 1.5 g/s)

It is clear that the length scale of the turbulent outflow gas eddies was beyond the probes' diameter to accurately record the flow characteristics; i.e., the pressure difference and velocity at the opening plane. This implies that any estimation related to the mass or volumetric flow balance should only rely on the inflow data recorded.

6.2.4.2.1.1 Modelling Comparison

The following figure exposes the error in the readings when comparing the experimental to the modelled probes located exactly at the same spatial position:

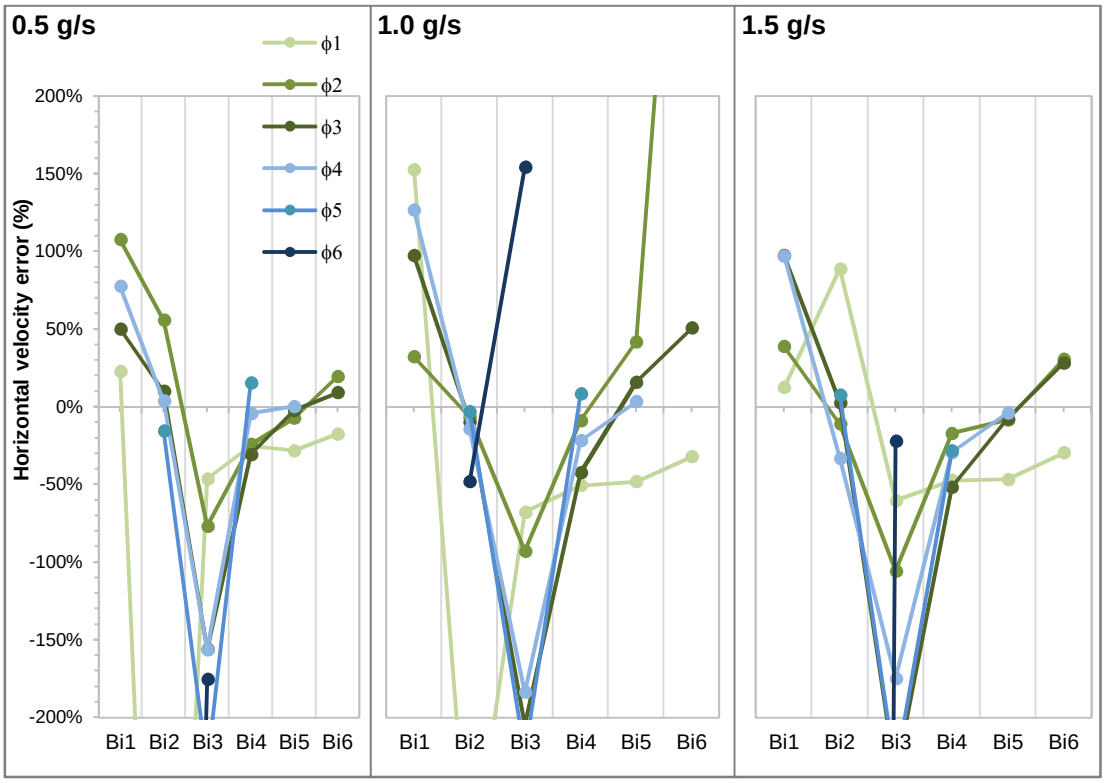

Figure 6-27: Experimental vs. modelling error in the velocity readings for every probe in all the experimental configurations

The massive errors found in the time-averaged velocity readings – especially in those probes which were closer to the neutral plane, H_N – exposes the complexity linked not only to the pressure and velocity readings (by this means) in experiments with turbulent flows, but also to any prediction or validation intended with a modelling tool.

6.2.4.2.2 Flow Turn-over Height

Going back to Figure 6-15, Figure 6-16, and Figure 6-17, it can be observed that as one moves upwards in the thermocouples layers in configurations ϕ_2 to ϕ_5 that at

some point – decreasing in layer as the openings are reduced and the propane flow increased – the positive gradient temperature (i.e., increasing from row A to C) peaks in row B instead and then changes sign decreasing from there on, exposing a 'hat' profile. This is effectively showing the turn-over height of the flow which also represents the neutral plane position, H_N.

Once the inflow air encounters the back wall after being heated along its way, it necessarily turns upwards before joining the exiting flow (refer to the *back wall effect* in Section 6.2.4.4). On its way out, the flow heats up towards the centre of the compartment before cooling down again as it reaches the opening. This shows that, while the in-coming flow temperature peaks at the back of the compartment, the out-coming flow temperature tends to peak towards the middle of the compartment, describing the typical hydraulic weir expected in small compartment fires.

Therefore, the change from a positive temperature gradient line (i.e., peaking in row C) to the 'hat' temperature profile (i.e., peaking in row B) evidences the height at which the inflow is converted into outflow, showing approximately which thermocouples layers fell beneath the neutral plane within the cold layer, and which ones fell above the neutral plane and were embedded in the hot layer.

The following table summarizes approximately which was the first layer embedded in the hot layer:

Table 6-7: First 'hot' or outflow thermocouple layer estimated after the turn-over method

First Outflow Layer			
Propane Flow	**0.5**	**1.0**	**1.5**
ϕ_1	5	5	4
ϕ_2	6	6	6
ϕ_3	6	5	5
ϕ_4	5	4	4
ϕ_5	5	4	4
ϕ_6	6	6	6

This means that, not only the layer shown in the table but also the layers above will be embedded in the exiting flow while the opposite happens for the layers beneath. For example, if the first outflow layer is shown to be 4, this means that the estimated neutral plane height falls somewhere between layers 4 and 3, with layers 4, 5 and 6 embedded in the outflowing gas layer, and layers 1, 2 and 3 embedded in the inflowing cold layer.

Interestingly, it can also be observed after these time-row-averaged temperature graphs (Figure 6-15, Figure 6-16, and Figure 6-17) that the turn-over height is also manifested in the double opposite opening case of configuration ϕ_1. A quite symmetrical temperature distribution – peaking towards the centre of the compartment – is observed in the upper layers, especially as the propane flow (or heat release rate per unit area) is increased and the fire demand for air (i.e., the pressure field) tends to neutralise any slight cross-flow that could have been present at the time of the experiment regardless of the practical efforts to prevent it. Strong cross-flows tend to push the flames and gases towards one of the openings – the

negative pressure opening – while the opposite opening – the positive pressure opening – serves as the inflow opening.

In regards to configuration ϕ_6, due to the strong turbulent hydraulic weir, almost the entire compartment volume – especially the upper layer – was flooded with flames (see Photo 6-2). This is the reason by which there is only a very small area at the upper of the compartment (around level 6) where the time-averaged temperature in row C was lower than in row B. In this case, therefore, this doesn't necessarily represent the flow turn-over point or neutral plane position.

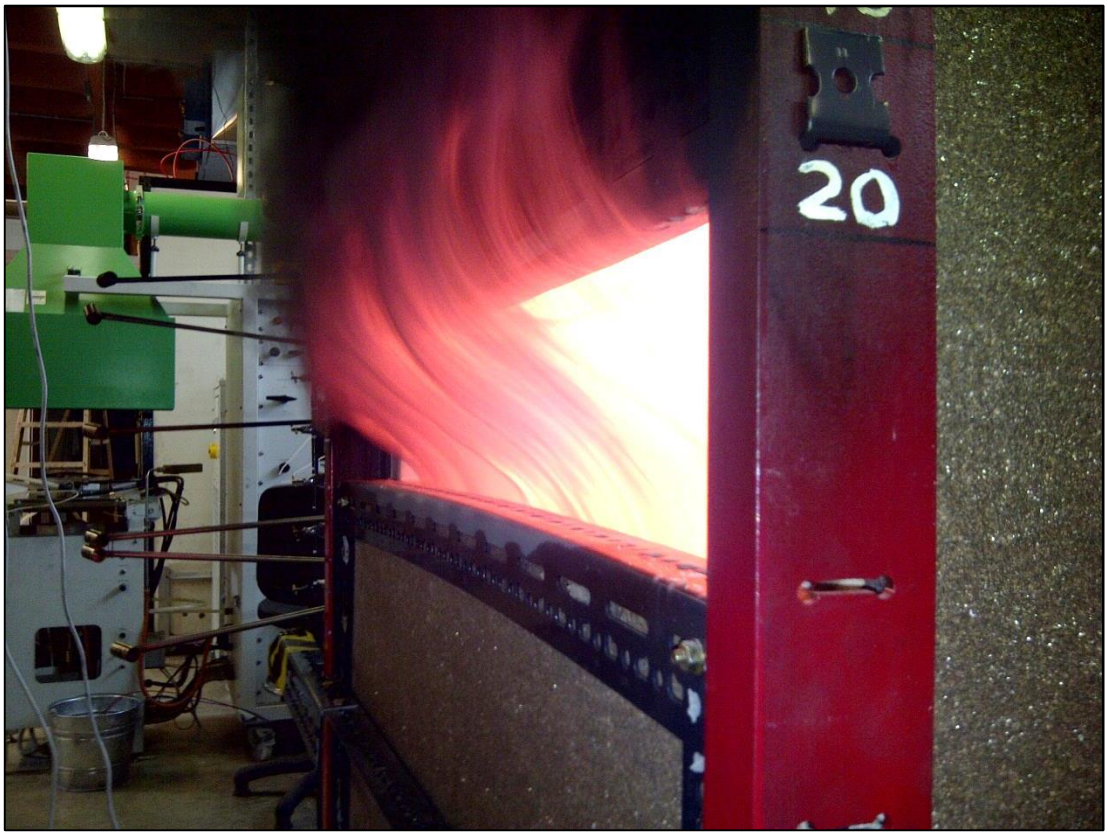

Photo 6-2: Compartment flooded with flames and strong hydraulic weir evidenced in the 20% opening configuration (ϕ_6, 1.5 g/s)

The neutral plane position estimates after the flow turn-over method can be compared to the recorded observations of the neutral plane position at the opening

during each experimental run (these are presented in Appendix B). The latter, relative to the thermocouple layers' height, are summarised in the following table:

Table 6-8: First 'hot' or outflow thermocouple layer estimated after observations

First Outflow Layer			
Propane Flow	**0.5**	**1.0**	**1.5**
ϕ_1	5	5	5
ϕ_2	5	5	5
ϕ_3	5	5	5
ϕ_4	4	4	4
ϕ_5	4	4	4
ϕ_6	4	4	4

After ruling out configuration ϕ_6 for the reasons explained above, it can be seen that there is quite a solid agreement between the turn-over method and what was observed in the laboratory during each of the experiments. The worst gross disagreement is a single layer height, equivalent to 13 cm.

6.2.4.2.3 Mass Flow Rates

The following figure shows the time-averaged mass flow rates – over the steady-state period of full fire development – obtained after the experiments (Section 6.2.2.4.3) and after the modelling (Section 6.2.3.3, Figure 6-11), and compares these results to the maximum theoretical limit, or maximum averaged buoyancy driven mass flow rate, $\bar{\dot{m}}_{in-MAX}$, derived in Section 4.2, which is typically assumed in design situations as a conservative estimate when relying on the classic framework (Equation 4-12):

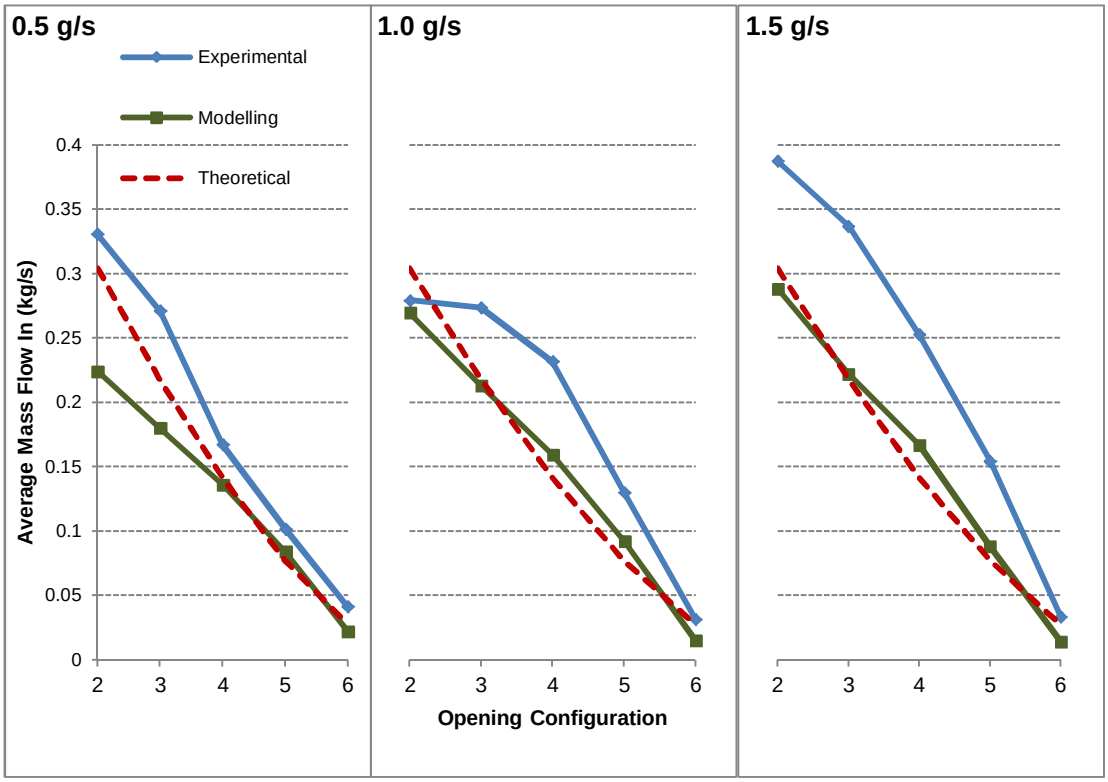

Figure 6-28: Time-averaged (over the steady-state period of fully-development) experimental, modelling and maximum theoretical mass flow rates compared

In order to obtain a clearer picture, the same results are presented this time normalized by the theoretical maximum limit; i.e., taking the later as the 100% boundary limit:

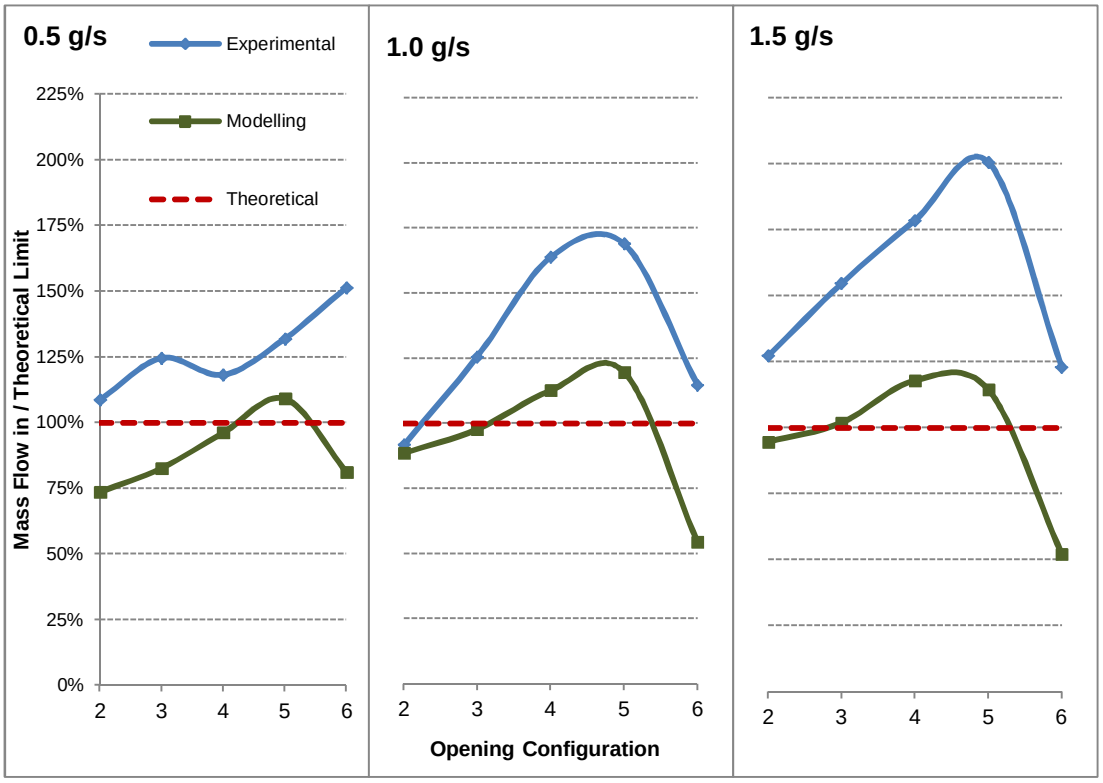

Figure 6-29: Time-averaged (over the steady-state period of fully-development) experimental and modelling mass flow rates normalized by the maximum theoretical limit

From these figures, it is seen that the theoretical air inflow upper limit is surpassed in almost every combination of propane flow and opening size in the experiments, as well as in several configurations in the modelling. The tendency to go beyond the limit appears to be stronger as the ventilation opening reduces and the propane flow increases; i.e., as clearer *Regime I* conditions are approached and attained. The exception is configuration ϕ_6, where it is not clear if the readings in both experiment and modelling were affected in some way by the strong turbulent nature of the flow giving non-realistic results, or if this is an indication that the theoretical model is effectively limited to extremely closed *Regime I* situations.

In any case, two clear conclusions can be drawn from these figures: the first one is that the significant differences between the experimental and modelling results expose – once more – the complexity and inaccuracies linked to the pressure, velocity, and mass flow readings (by this means) in experiments with turbulent

flows, and the sensibility of any predictions intended in this regard when modelling the complex fluid dynamics with a computational tool. And the second and more evident one, is that the maximum averaged buoyancy driven mass flow rate, $\bar{\dot{m}}_{in-MAX}$, derived in Section 4.2, cannot be taken as a conservative estimate for the generality of compartment fires.

6.2.4.3 Break-point Analysis

As the compartment's opening was reduced and the propane flow increased, the regime behaviour was expected to switch from a typical *Regime II* to a *Regime I* situation. The analysis of the break-point between these different behaviours was done in the computer modelled compartment making use of the 44 special devices (defined within the second group of instruments in Section 6.2.3.3) which recorded the horizontal (perpendicular to the opening) and vertical (perpendicular to the floor) components of the gas linear velocity within the compartment at 4 different heights (see Figure 6-10).

When searching for the clues that clarified the behavioural tendency towards one or the other regime, the following general characteristics and trends in regards to the velocity vectors were considered:

- *Regime I:* the accelerations (evidenced by the velocity vectors' enlargement) should be due to a compartment effect, thus, they should appear clear as from the compartment opening; i.e., as from its boundary. Therefore, there should be a tendency to find horizontal velocity vectors enlarging at the opening plane and tending to stay horizontal, only bending vertically once encountering the compartment's back wall, before turning horizontally again parallel to the ceiling in the outward direction. In summary, a C-shaped vector motion – increasing modulus as from the compartment's opening (or 'throttle') – should appear clear.

- *Regime II:* the accelerations in this case should be brought about by the fire and not by the compartment (i.e., by the opening). Therefore, there should be a tendency to find horizontal velocity vectors enlarging at the fire plume

boundary and quite immediately bending vertically as they entrain and join the uprising plume. The plume boundary could easily be at (or very close to) the opening plane because the fire tends to occupy the entire floor area in small compartments, so lots of care was taken in the analysis as this fact might bring some confusion when trying to identify the break-point, specifically when defining either the fire or the compartment as the responsible for the flow suction.

These different behaviours can be evidenced in an easy way when analysing the horizontal and vertical velocity components separately.

The following figures were chosen as representative of each of the regimes expected: *Regime II*, a transition regime, and *Regime I*, respectively:

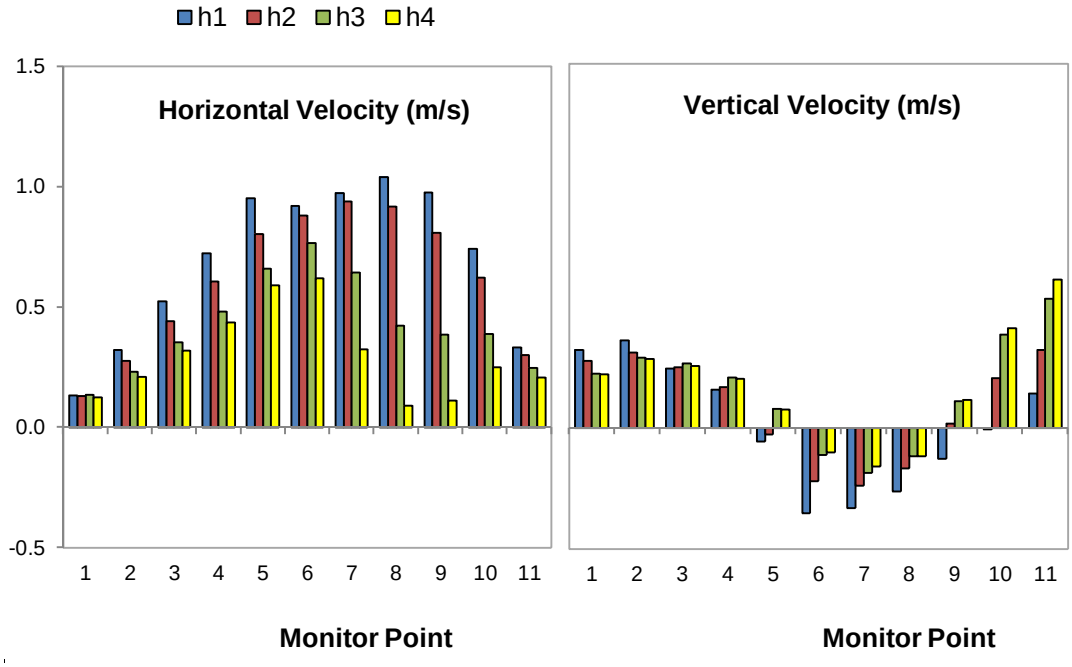

Figure 6-30: Velocity components (FDS modelling) for the 100% opening configuration (ϕ_2) and 1.0 g/s propane flow

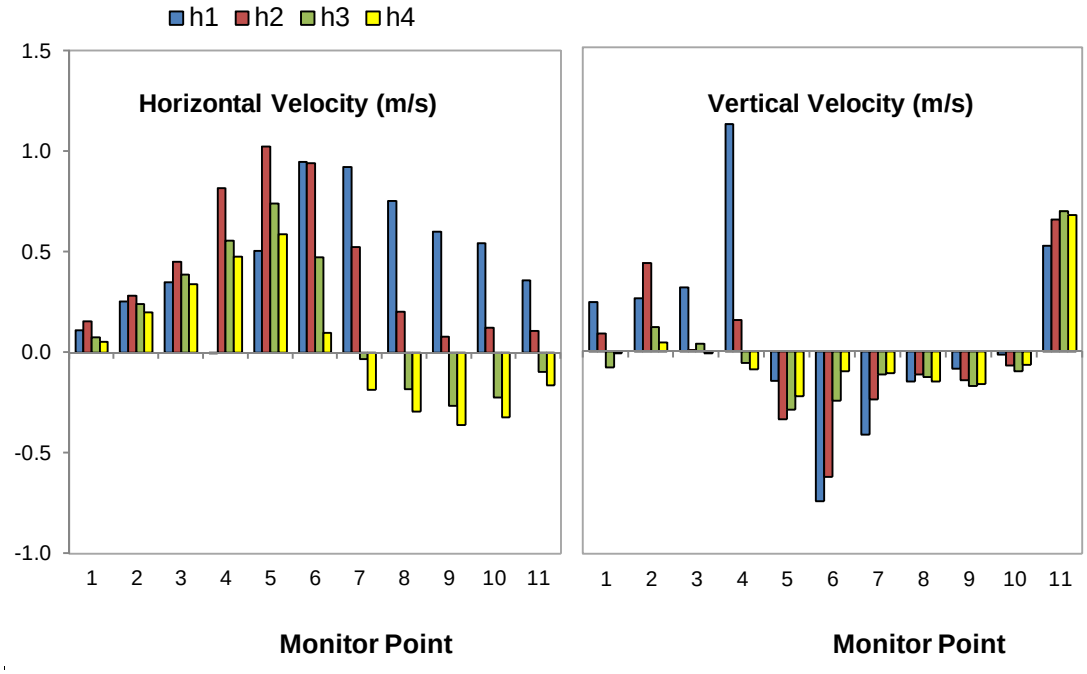

Figure 6-31: Velocity components (FDS modelling) for the 60% opening configuration (ϕ_4) and 1.0 g/s propane flow

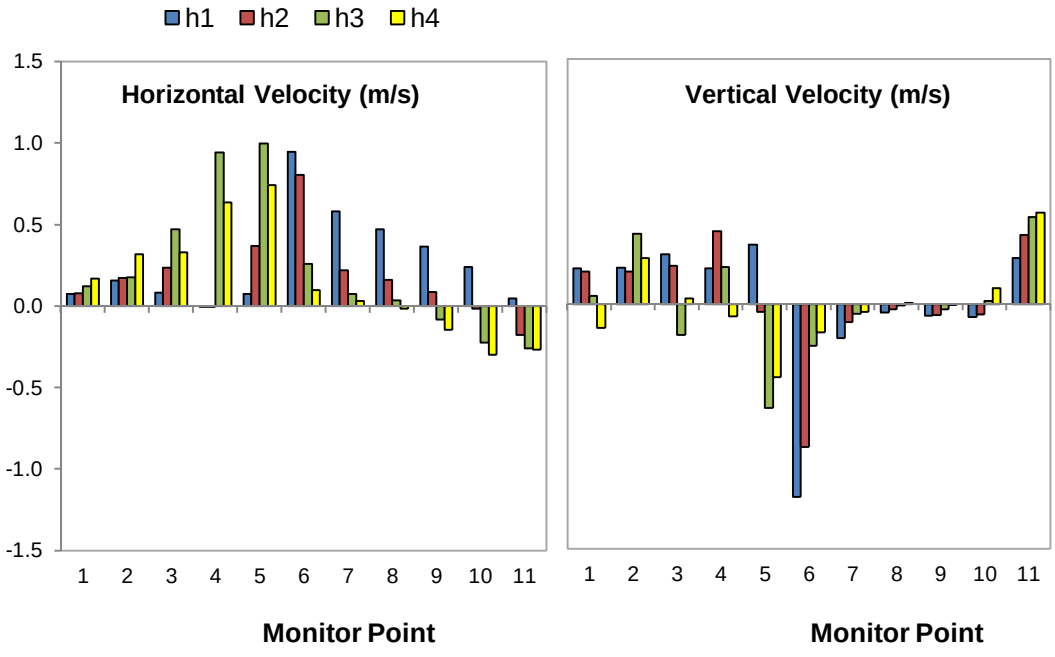

Figure 6-32: Velocity components (FDS modelling) for the 40% opening configuration (ϕ_5) and 1.0 g/s propane flow

Looking at the horizontal component of the velocity in the 3 figures, it can be seen how in Figure 6-30 – correspondent to a *Regime II* behaviour – the velocity at all heights increases smoothly (i.e., almost at a constant gradient) until it encounters the fire plume located between monitor points number 4 and 5 – coincident with the opening plane – while in Figure 6-31 and even more pronounced in Figure 6-32 – correspondent to a transition regime and a *Regime I* behaviour, respectively – there is a steep increase of the velocity as soon as the flow encounters the compartment opening.

Additionally, the horizontal components in the *Regime II* representative figure (Figure 6-30) are always positive, showing that all four monitor heights fell within the inflowing air. In the transition regime (Figure 6-31) as well as in *Regime I* (Figure 6-32), it can be clearly seen how the outflowing gases (represented by the negative horizontal velocity components) encounter the inflowing air (represented by the positive horizontal velocity components) in the typical 'chocked' flow situation found in fully-developed fires after to the fact that the neutral plane, H_N, is found always below the smoke layer height, H_D, beyond the opening and deep inside the compartment (refer to Section 2.3.4, and more specifically to Figure 2-5 and Figure 2-6).

Now looking at the vertical components of the velocity in the first situation of Figure 6-30, the suction effects of the fuel bed can be observed – as represented by the negative values 'pulling' the air downwards towards the fire base – approximately where the plume was located; i.e., between monitors 5 and 9. In configurations ϕ_4 and ϕ_5 (Figure 6-31 and Figure 6-32, respectively), significant downward velocities can be observed immediately after the opening plane. This was due to the fact that the lower opening edge height was not at floor level in these opening configurations, therefore, blocking the flow at some monitor heights and creating a turbulent eddy in the lower-inner part of the compartment next to the opening plane. Disregarding this effect, the transition regime (Figure 6-31) clearly shows a slight suction effect by the fuel bed (negative components between monitors 7 and 10 approximately) and an almost instant increase in the upward velocity as soon as the flow encounters the

back wall. At the same time, Figure 6-32 exhibits what Thomas [29] described in reference to what he defined as *Regime I* (refer to Section 5.2.3.2.2): there are virtually no vertical accelerations. The only vertical velocities that appear in this regime, and particularly well represented in this figure, are those that appear suddenly as the flow encounters the back wall, same as it happened in every configuration including those that fell with the transition regime and *Regime II*. This situation is described as the *back wall effect* and is explain in more detail in the following section (Section 6.2.4.4).

In summary, there was a general tendency in all three propane flows to find the openings configurations ϕ_1, ϕ_2, and ϕ_3 falling under the *Regime II* behaviour, configuration ϕ_4 falling under the transition regime, and configurations ϕ_5 and ϕ_6 falling under the *Regime I* behaviour. The full results are presented in Appendix B.

6.2.4.4 Pressure Analysis

The relevance of the *back wall effect* found in the previous analysis relies not only in the fact that it forces the flow to change direction but, more importantly, in that it has the potential to modify the pressure field and hence the characteristic flow velocity and consequent mass flow balance. This is to say, the stream that is forced upwards by the back wall will tend to push the smoke layer upwards at the back of the compartment, resulting in a deeper smoke layer at the front of it and at the opening plane. This gives as a result, an increased characteristic pressure term so that the air inflow (and combustion gases outflow) is brought about – in the limit behaviours – either by the compartment acting as a 'chimney' (i.e., purely compartment-driven or *Regime I*) or by turbulent entrainment (i.e., purely turbulence-driven or *Regime II*), both *ventilation modes* enhanced by pressure differences brought about by the deeper smoke layer built-up at the opening plane.

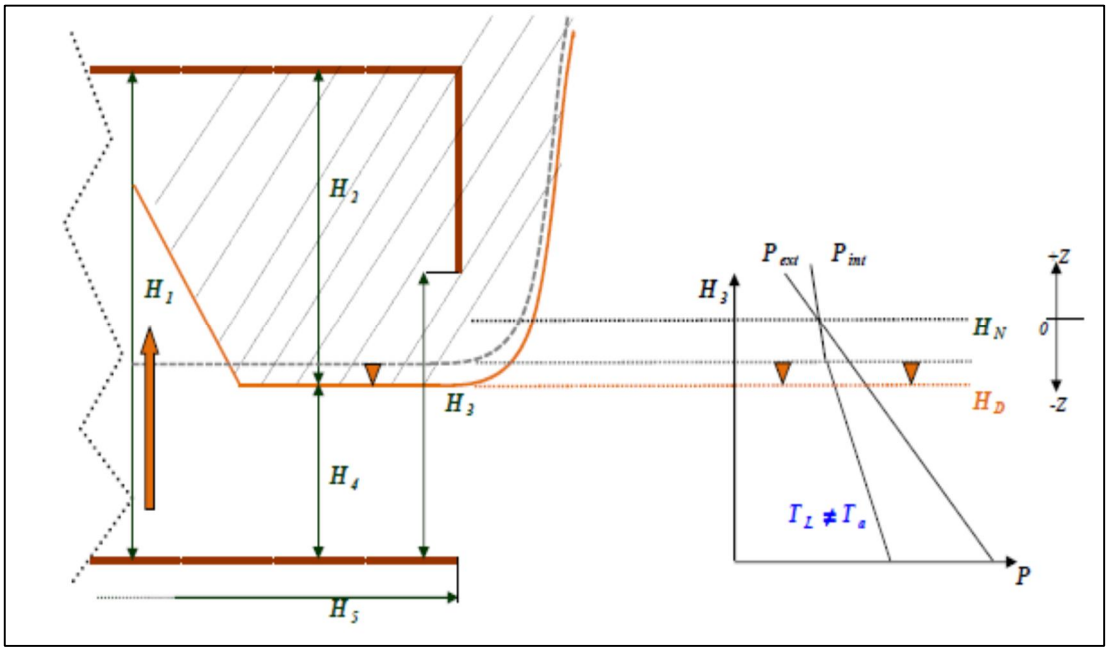

Figure 6-33: The back wall effect

The modifications introduced in the pressure field by a strong rising flow were first noticed by Harmathy in 1980 [101] and gave place to the modified two-layer scenario presented in Section 2.3.4.4, applied in some of the representative cases chosen in Chapter 5, Section 5.2.3.2 This scenario (Figure 2-6) attributes the entire pressure change responsibility to the rising plume, including (or ignoring) the effects of a flow forced in the upward direction after encountering the back wall with sufficient inertial force; i.e., the *back wall effect.*

Using Harmathy's empirically modified model [101], the following pressure and flow increases with respect to the classic model – i.e., two-layer scenario (Section 2.3.4.3) that gave rise to the maximum averaged buoyancy driven mass flow rate, $\bar{\dot{m}}_{in-MAX}$, derived in Section 4.2) – were obtained after a theoretical analysis of the small-scale experiments' results:

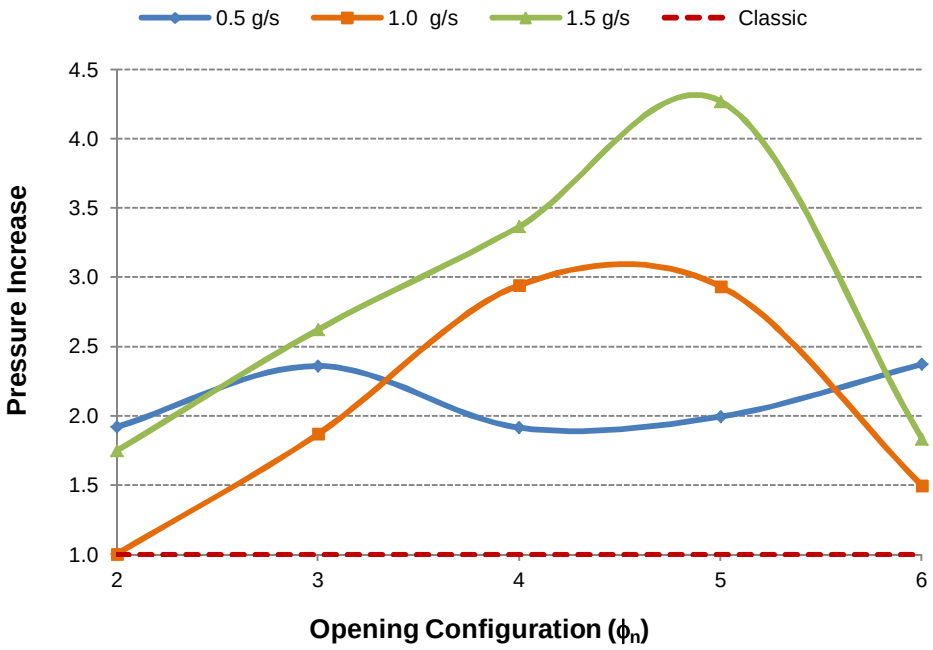

Figure 6-34: Pressure increase (in relation to the classic theoretical model) in the small-scale experiments using Harmathy's empirically modified model

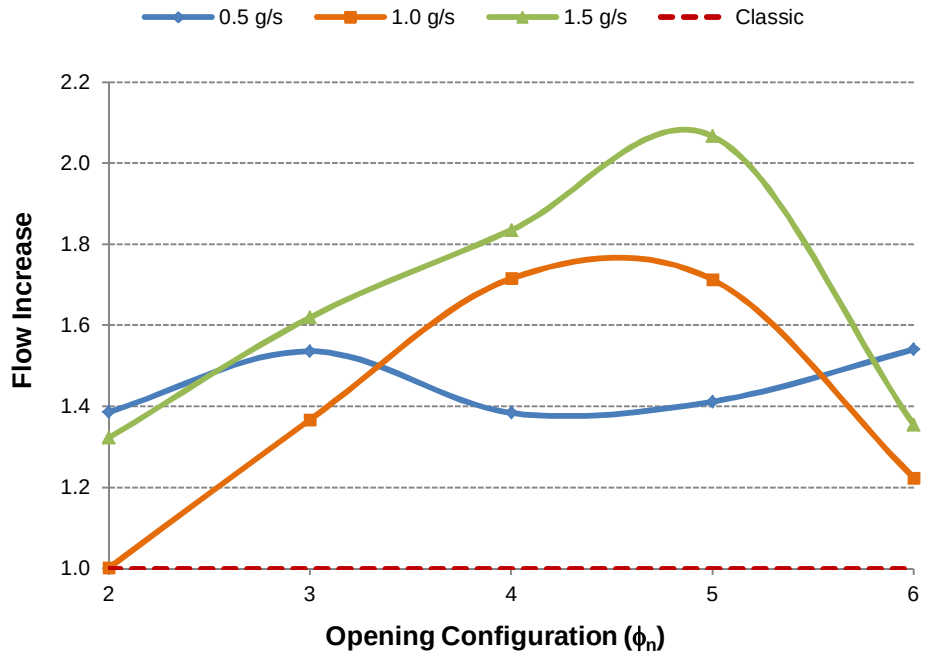

Figure 6-35: Flow increase (in relation to the classic theoretical model) in the small-scale experiments using Harmathy's empirically modified model

After the results presented in Figure 6-34 and Figure 6-35 – showing the same trend as that from Section 6.2.4.2.3 – it is evident that, due to the role the upward moving stream (either the fire plume or the forced back wall vertical flow, or both) plays, the factor of proportionality between the mass flow rate of air through the ventilation opening and the *ventilation parameter*, is sometimes higher than previously believed.

The graphs show a gross tendency (excluding ϕ_2 and ϕ_3 for 0.5 g/s) for the pressure and flow to increase as the opening is reduced. Once more, the exception is configuration ϕ_6, where it is not clear if the readings in the experiments were affected in some way by the strong turbulent nature of the flow giving non-realistic results, or if this is an indication that the theoretical model is effectively limited to extremely closed *Regime I* situations.

6.2.4.5 Heat Flux Analysis

The following graphs (Figure 6-36, Figure 6-37, Figure 6-38, and Figure 6-39 in the following pages in landscape orientation) show the average net heat flux impingement (in kW/m^2) during the selected steady-state period (of around 10 minutes) representing the fully-developed or post-FO conditions, recorded by the thin skin calorimeters (TSCs) installed on the inner surfaces of the experimental compartment.

The walls sensors (LHS image in these graphs) were grouped in vertical arrays while the floor and ceiling sensors (centre and RHS images in these graphs, respectively) were grouped in left-to-right arrays. In this way, a better picture of the average energy absorbed distribution along the compartment's boundaries for each opening configuration could be observed, and compared against the other opening configurations.

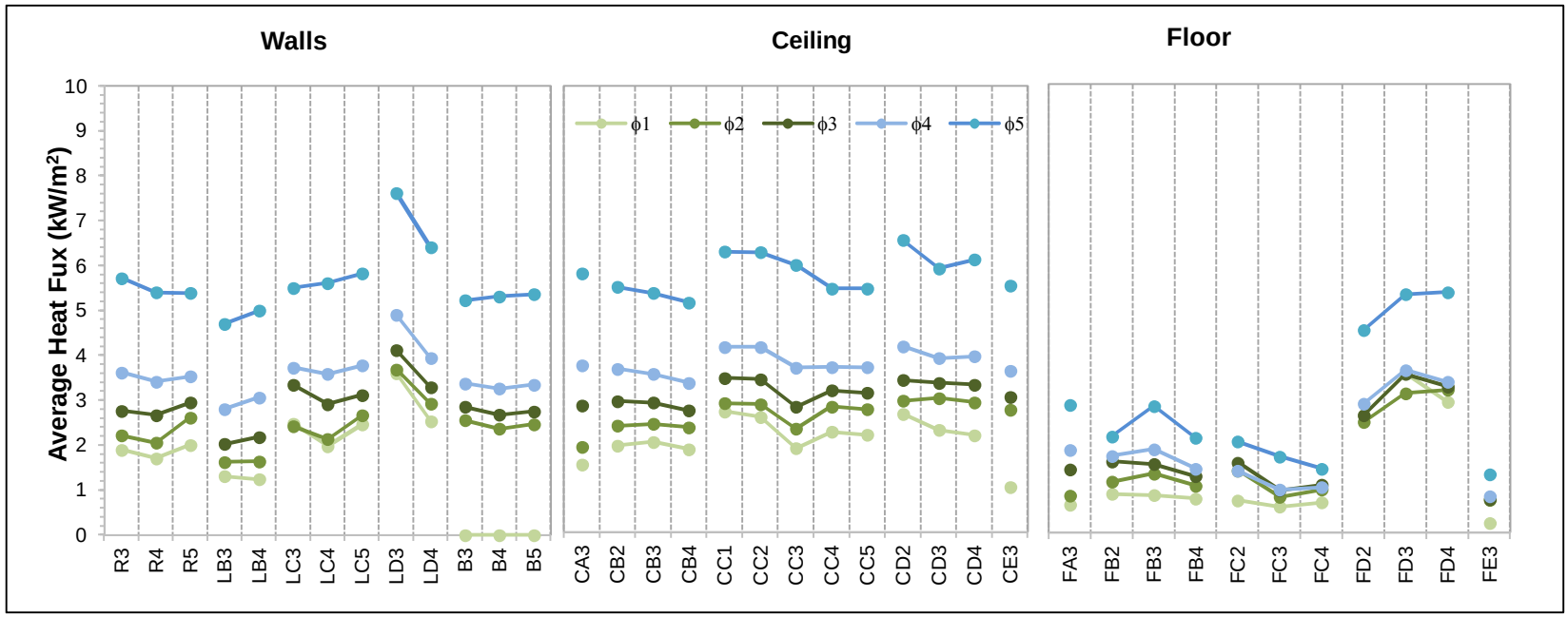

Figure 6-36: Time-averaged (over the steady-state period of fully-development) heat flux readings for all 45 TSC in each opening configurations (0.5 g/s propane flow)

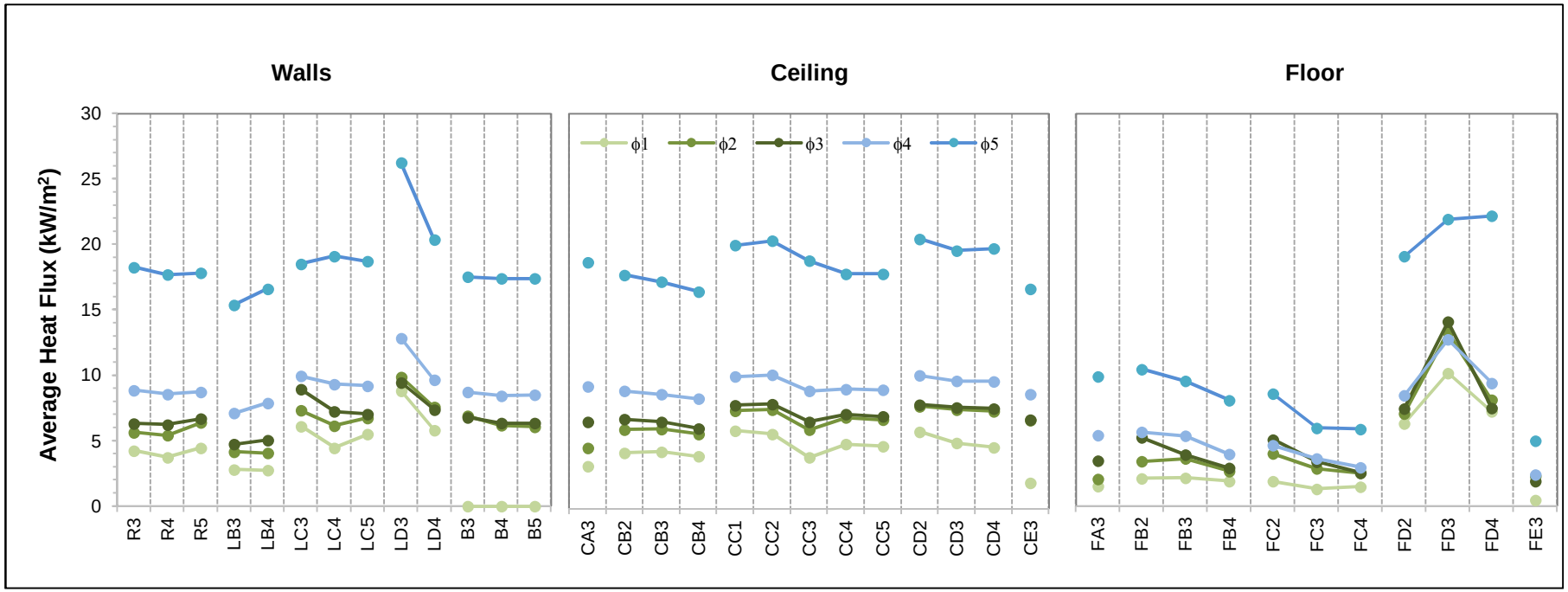

Figure 6-37: Time-averaged (over the steady-state period of fully-development) heat flux readings for all 45 TSC in each opening configurations (1.0 g/s propane flow)

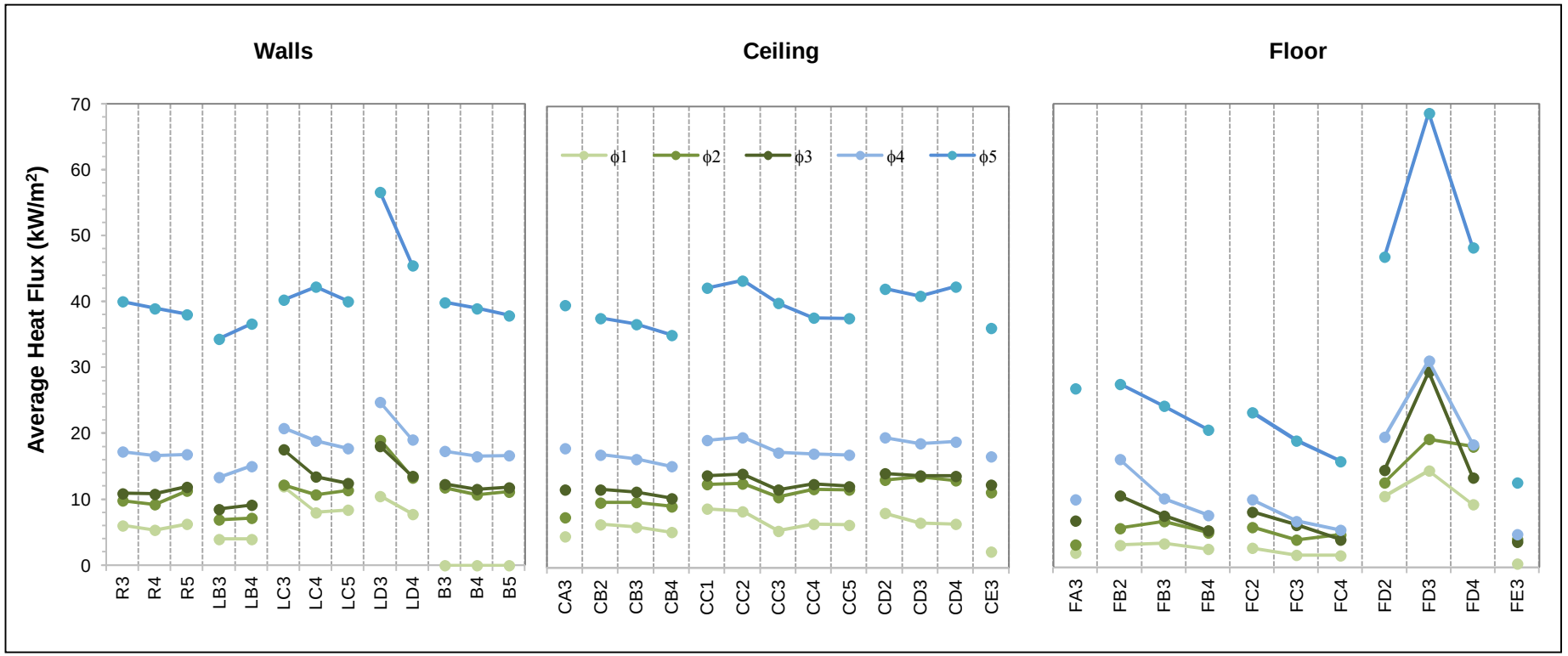

Figure 6-38: Time-averaged (over the steady-state period of fully-development) heat flux readings for all 45 TSC in each opening configurations (1.5 g/s propane flow)

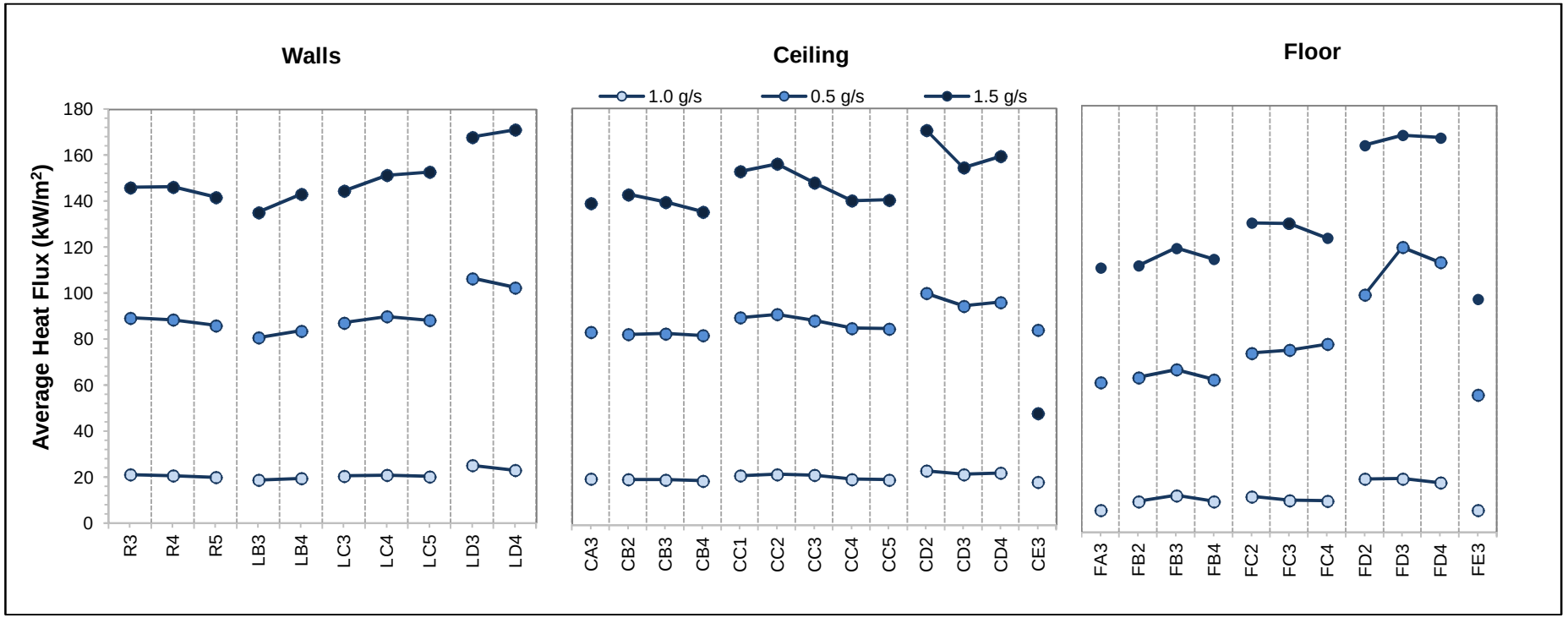

Figure 6-39: Time-averaged (over the steady-state period of fully-development) heat flux readings for all 3 propane flows in the ϕ_6 opening configurations

In regards to *side* and *back walls* of the compartment, the analysis presented comprises only the upper region in an effort to avoid the readings affected by the direct flame impingement in the lower region. This means that levels 1 and 2 from all 3 lateral walls – i.e., right, left, and back walls – were excluded from the analysis.

Looking at the averaged results recorded in configurations ϕ_1 to ϕ_6 along the steady-state period selected in all 3 propane flows, it can be seen that there is a quite homogeneous net heat flux impingement on the upper 3 levels of the compartment's inner surface. In addition, these values are in range with those recorded by the TSC calorimeters located on the *ceiling*. Altogether, this reconfirms that there is a tendency for a uniformly heated upper gas layer – as seen in the gas temeparature analysis in Section 6.2.4.1(A) – which in turn exchanges energy with the inner solid boundaries in the expected homogeneous distribution.

Looking at the *ceiling* average values in more detail, there is slight tendency in every opening configuration to experience a greater net heat flux impingement towards the back of the compartment, with the peak value found in the middle region. Once more, this is in agreement with what was reported in the flow (Turn-over height, Section 6.2.4.2.2) and pressure (*back wall effect*, Section 6.2.4.4) analyses where the middle row (i.e., row B) recorded the highest spatial and temporal average temperatures in the upper region of the compartment. Therefore, it becomes clear that in similar compartment configurations and under similar flow conditions (given by the compartment-opening size and shape, and by the $\dot{Q}_{PUA}$) the higher the gas temperature, the higher the net heat absorved by the inner surfaces will be, as expected.

The effects described above on the inner *walls* and *ceiling* surfaces were observed as being magnified as the propane flow was increased. This is to say, these observations apply to all three propane flows with similar tendency albeit greater average values. Nevertheless, it is important to note that – in all 3 propane flows – certain TSCs reported average values consistently higher than the overall wall averages, but these were observed to be recorded by those calorimeters – namelly the LD vertical array –

which typically experienced direct flame impingement. Furthermore, the averge results of opening configuration ϕ_6 were plotted separately in Figure 6-39 after they were found to be out of scale when compared to all other results (around 4 times the previous opening configuration (ϕ_5) average values).

In regards to the comopartment's *floor*, the results showed a tendency to a uniform heat flux impingement – although always in a lower value range than the upper portion of the compartment – along the entire horizontal surface. Same as it happened in a particualar area of the left wall (i.e., the LD array referenced in the previous paragraph), certain TSCs located on the floor reported average values consistently higher than the overall floor average. Once again, these out-of-range values were observed to be recorded by those calorimeters – namelly row FD – which typically experienced direct flame impingement due to the downward facing propane injection holes drilled in the piping array.

The flame impingement effect, therefore, was accounted for in the analysis as responsible for some distortion of the distribution of net energy absorbed in the areas specifically highlighted (i.e., LD array and FD row).

In general terms, as it can be observed from the ceiling and floor graphs in every opening and propane flow combination, there was a tendency to find longer flames in the back (especially left back corner) of the compartment. This was attributed to the following: (*i*) poorer air-fuel mixing conditions at the back of the compartemnt in comparisson to the front flames located closer to the opening plane; (*ii*) tilting of the front flames towards the back of the compartment by the inflowing air; and (*iii*) uneven propane pressure distribution in the pipes after the soot clogging of some of the drilled propane injection holes located towards the front of the compartment, due to the low surrounding temperatures found in this region where evidently soot burning temperatures were not achieved.

In summary, the heat flux analysis showed the same tendencies as the tempereature analysis, reconfirming the flow pattern and pressure field variations observed in the previous respective analyses.

6.3 Large-Scale Experiments

To respond to the need to better describe the special and temporal evolution of a fire that is allowed to progress in a large compartment a series of tests were conducted in 2013 at the Building Research Establishment in the UK. These tests are inscribed within a larger programme that looks to address fire scenarios for tall buildings, thus will be labelled the "Tall Building Tests."

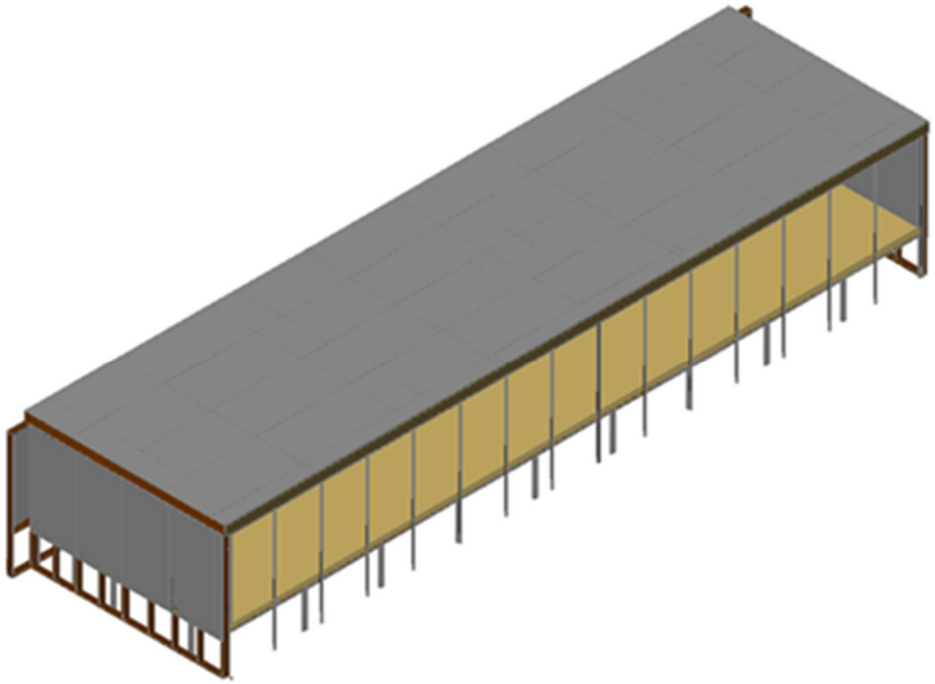

Figure 6-40: Schematic of the BRE large compartment constructed

Photo 6-3: Photograph of a characteristic gas burner test

A compartment of dimensions 5 m x 18 m x 2 m (Figure 6-40) was constructed and included 15 openings along the front (1.5 m high by about 1 m wide each) that can be opened or closed individually to allow varying ventilation in a systematic way. The tests are heavily instrumented including internal thermocouple trees spaced at 0.7 m in the x-direction, 0.6 m in the y-direction, and at 0.3, 0.6, 0.9, 1.2, 1.4, 1.6, 1.8, and 1.95m in the z-direction. There is also a thermocouple tree in the centre of each opening at z = 0.25, 0.5, 0.75, 1.0, and 1.25m. Outside there is also a thermocouple tree at around 0.4 m from the compartment and aligned with the centre of each opening. These trees have 12 thermocouples each which are spaced as follows: 0.25, 0.5, 0.75, 1.0, 1.25, 1.5, 1.75, 2.0, 2.25, 2.5, 2.75 and 3.0m. 100 thermocouples provide in-depth temperatures (at different depths) along a 3 m wide section of the back wall which is in-filled with non-flammable insulation. Heat flux gauges were placed on all 5 surfaces of the compartment evenly distributed. There are 45 on the floor (3 in x -direction, 15 in y-direction), 45 on the ceiling, 45 along the back wall (15 in y-direction, 3 in z-direction) and 15 (5 in the x-direction, 3 in the

z-direction) along each of the side walls. There are also heat flux gauges outside, opposite the centre of each opening, at different distances away from the compartment (in x-direction). Smoke obscuration is measured with 5 laser-receiver pairs in total, evenly spaced along the centre of the compartment. Bi-directional velocity probes allow characterizing the in-flow and out-flow of the compartment. There are 2 probes per opening (z = 0.225 m and z = 1.275 m of the opening height, respectively). There are 5 gas-sampling points evenly spaced along the ceiling of the compartment. The gas probes sample O_2, CO_2 and CO to establish completeness of combustion. Five cameras were used to film the compartment from different angles, including one camera at the centre of each of the side walls. An InfraRed camera was also used to film the compartment from the outside.

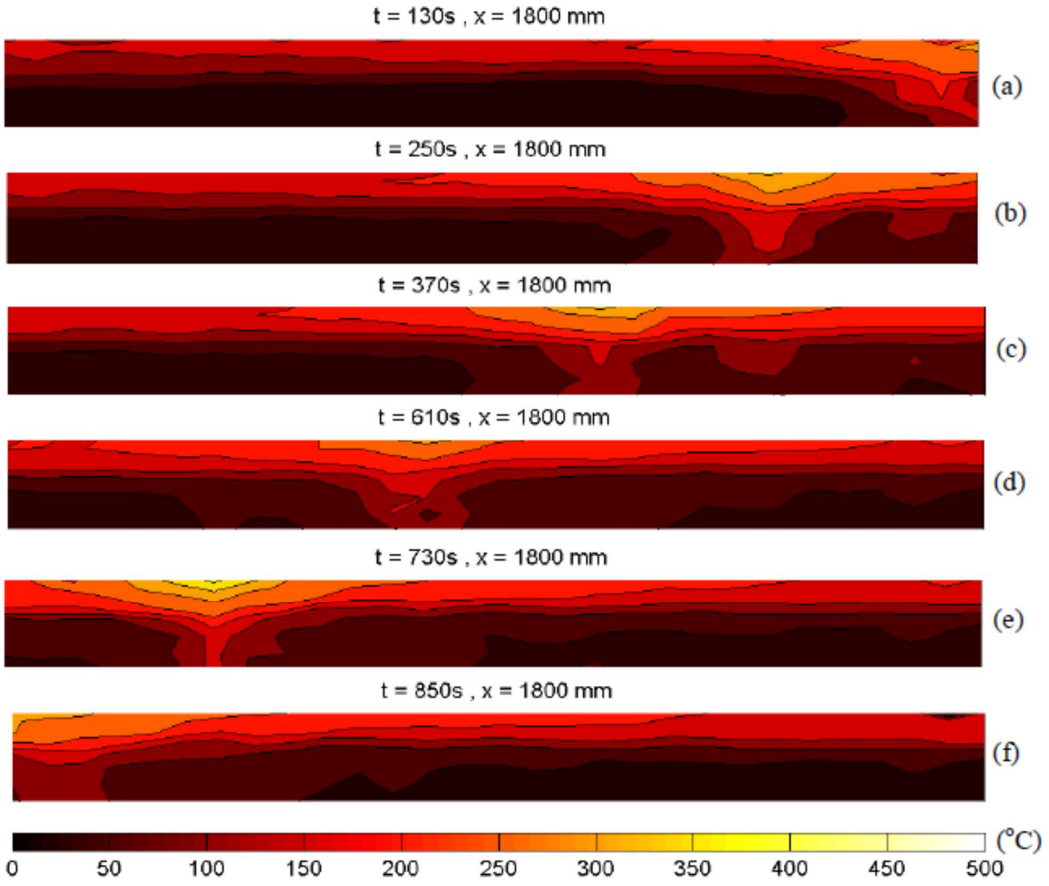

Figure 6-41: Temperature distributions along a plane 1800 mm from the rear wall and parallel to the open face (in between burners) – the openings were fully open allowing for the maximum evacuation of of smoke.

Two series of tests were conducted, a first series where a sequence of gas burners (12 propane burners, of 0.5 m x 0.5 m trays full of gravel, evenly spaced throughout the compartment in pairs of 2) was ignited progressing from one end of the compartment to the other. Ventilation and fire spread were varied to cover a range that allowed for spread both faster and slower than ventilation opening. The second series of tests was conducted with wood cribs covering the entire floor and ignited at one end. The ventilation was again varied. For the wood crib tests, the central staging area has been divided into 8 sections that can move up and down independently. These sat on load cell systems that enabled the measurement of mass loss. A photograph of a typical test is presented in Photo 6-3.

While the description of the experimental data is beyond the scope of this work, it is important to emphasize that the scale and data variety and resolution result in different observed behaviour that not only deviate from the compartment fire framework but that could potentially have a significant impact on the thermal boundary condition used to analyse structural behaviour. Furthermore, current detailed structural analysis requires a level of resolution that cannot be provided by the simple formulation of the compartment fire framework [96][116]. These tests provide a level of resolution that is more consistent with the needs of such analysis.

Figure 6-41 shows a series of representative data for an experiment using gas burners ignited in a sequential manner while the panels allowing air were opened fully. The fire is initiated with two burners (front and back – Photo 6-3) at the right hand side of the compartment. Initially, the ceiling jet propagates across the compartment with no significant accumulation of smoke but very rapidly it covers the entire compartment (<130 sec – Figure 6-41(a)). The smoke produced by the fire is fully evacuated allowing for the establishment of steady state conditions. The initial burners are turned-off as the next set is ignited and the temperatures once again reach steady-state conditions rapidly. A clear smoke layer can be seen in Figure 6-41(b). The smoke layer shows very similar temperatures to the ones observed in Figure 6-41(a).

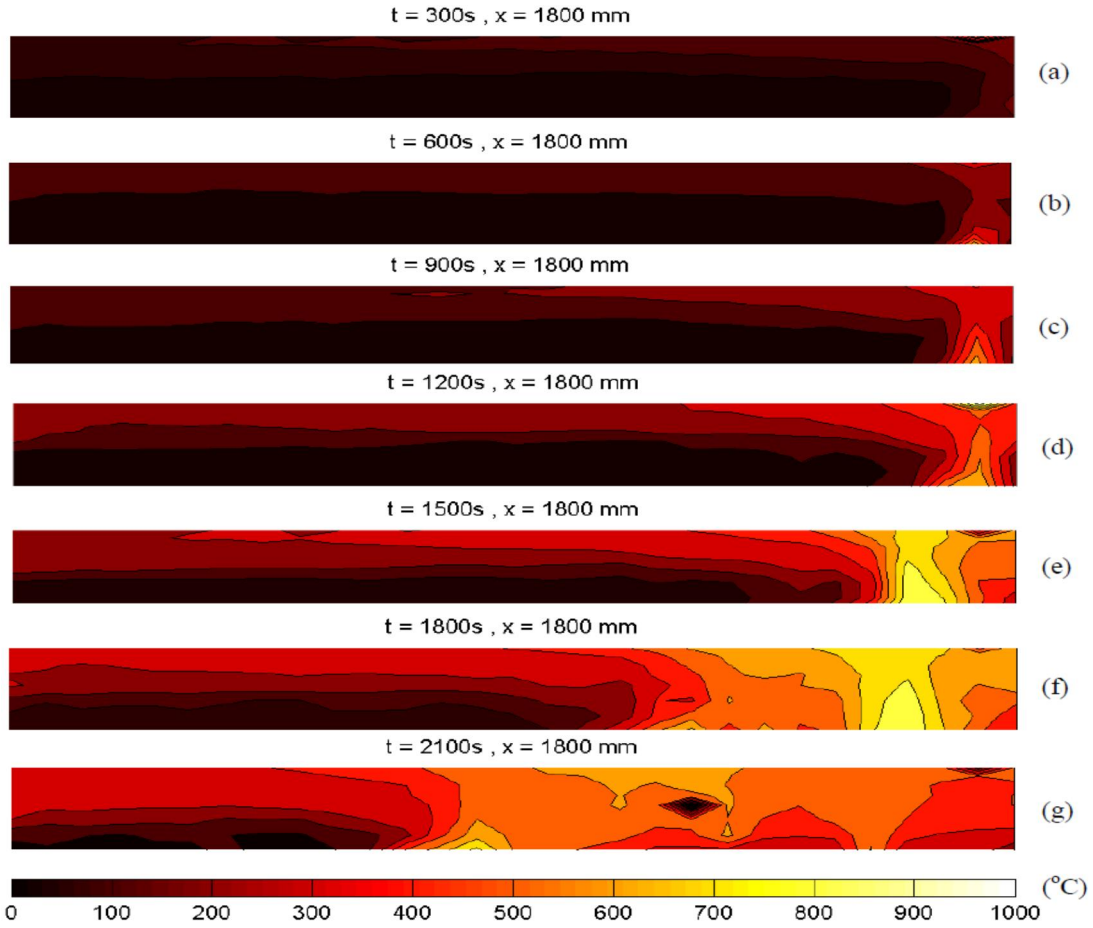

Figure 6-42: Temperature distributions along a plane 1800 mm from the rear wall and parallel to the open face – the openings were fully open allowing for the maximum evacuation of of smoke and the fuel were wood cribs.

This series of tests shows at each stage conditions very similar to those described by *Regime II*. These conditions reproduce themselves at each stage of the burning process and the characteristic times scales in the gas phase are short enough that quasi-steady conditions can be established at each stage of the propagation. The burners were ignited at rates consistent with spread rates of typical building fuels, therefore these observations could potentially be extrapolated to fires with realistic materials. While the conditions are similar to those of *Regime II* fires, the size of the compartment allows for the formation of gradients of temperature not only in the vertical direction but also in the directions parallel to the floor. The data has enough resolution to be able to provide an appropriate boundary condition for structures whose analysis requires spatial distribution.

The rate of ignition of the gas burners as well as the size and location of the openings were varied to establish other potential regimes. The rate of ignition of the burners as well as the size of the fire (i.e. number of burners) did not have a major impact on the nature of the fire in the compartment within the range of conditions studied. A clear smoke layer was rapidly established with the interface dependent mostly on the size of the fire indicating that the capacity of the open face to evacuate smoke exceeded the differences introduced by the changes to the fire. In contrast, as the vents were diminished in size or in number, smoke could not be evacuated and the quasi-steady nature of the process was lost leading to a complex and dynamic interaction between burners and smoke.

An experiment with wood cribs can be used as an example as it encompasses the full potential complexity of the dynamic interaction between the fire, the smoke and the compartment. Figure 6-42 presents temperature distributions within a plane (1800 mm deep) at different points in time. The fuel is wood cribs and the vents are fully open. The fire was ignited in the right hand corner and allowed to propagate. Initially the ceiling jet propagates across the compartment (Figure 6-42(a)) until a smoke layer is established (Figure 6-42(b)). Fire spread is very slow relative to the gas phase processes thus quasi-steady state conditions establish in a similar manner to those presented in Figure 6-41. As the fire continues to grow the temperature of the smoke layer starts to increase. An important aspect of this is that depending on the size of the fire and the amount of ventilation surface available, the rate at which conditions evolve in the vicinity of the fire is much different to the rate of evolution in the far field (left hand side Figure 6-42(c)). Furthermore, momentum-driven flows impinging on the walls start affecting the characteristics of the smoke layer (Figure 6-42(d)). At approximately 1500 seconds (Figure 6-42(e)) smoke layer temperatures on the right hand side of the compartment exceed 500^{o}C within approximately a third of the compartment. At this stage rapid ignition of the fuel through almost half of the compartment occurs in a manner that resembles a localized flashover (Figure 6-42(f)). The fire will continue to burn to the right of the flame front (Figure 6-42(g)) but the burning rate is maximum at the leading edge of the flame decreasing towards the right of the compartment. For the case where the vents were fully open, the

flames continue to spread towards the left of the compartment. Strong air entrainment from left to right and smoke evacuation behind the flame prevented any subsequent instantaneous ignition of the fuel.

The experimental sequence presented above is described only with the purpose of illustrating the complex dynamics of the fire within a large compartment. The different processes explained varied in their significance depending on the ventilation and it was very clear that the temperature distributions were a strong function of the geometry of the compartment. What is clear is that under these conditions the dynamics of the fire correspond to a complex mixture of the limit *Regimes I* and *II* described by Thomas *et al.* [29] and there is no relationship between the overall *opening factor*, $\frac{A_w\sqrt{H}}{A_T}$, and the temperatures or burning rates (refer to last paragraph in Section 4.4.2).

6.4 Preliminary Conclusions

As it was introduced at the beginning of this Chapter, the series of small and large-scale tests – the former supported by CFD modelling – were designated to better understand the *classic Regime I* and *Regime II* behaviours, and start to interpret the potential range of behaviours that exist between them.

To this extent, and in relation to the preliminary conclusions reached in Chapter 3 (Section 3.6), the small-scale tests have (*i*) shown that indeed the highest temperatures were achieved under the *Regime I* behaviour (Section 6.2.4.1) and, therefore, the highest heat fluxes found under this regime (Section 6.2.4.5) (*ii*) confirmed the long held view that *Regime I* is more severe than *Regime II* in small compartments. Nevertheless, regardless the tendency for the temperature uniformity of the upper layer found for small compartments, (*iii*) it was clearly observed that the temperatures could not be regarded as uniform throughout the entire compartment, not even when in a *Regime I* situation. In this regard, the large-scale tests (Section 6.3) have shown that a larger size of the compartment can allow for the formation of even larger gradients of temperature not only in the vertical direction but also in the

directions parallel to the floor. Therefore, after these empirical results it can be concluded that fully-developed fires in small and large compartments cannot be *solely* understood and described as *Regime I* fires and, moreover, they do not always behave as such.

In relation to the preliminary conclusions reached in Chapter 4 (Section 4.5), after analysing the break-point between the classic regimes (Section 6.2.4.3), studying the flow pattern in detail (Section 6.2.4.2.2), and contrasting the empirical and modelled mass flow rates against the theoretical limit given by the classic approach (Section 6.2.4.2.3), it can be concluded that the *Classic Compartment Fire Framework* is still a robust qualitative – though not quantitative – representation of the behaviour of a fire in an enclosure. The quantitative results are definitely intimately linked to the geometry of the compartment (size, vent size, aspect ratio) and the single vertical opening configuration.

Finally, in relation to the preliminary conclusions reached in Chapter 5 (Section 5.3), after studying the small-scale tests (Section 6.2.4.2.1) and modelling velocities (Section 6.2.4.3), and combining these observations with the increases in pressure and flow found (Section 6.2.4.4) – together with some qualitative observations from the large-scale tests – there is enough evidence to conclude that both historical *Regimes I* and *II* are limiting cases of a broader compartment fire behaviour. This is to say, compartment fires could definitely behave following any potential range of behaviours that exist between the *classic* behaviours, and this, once more, is intimately linked to the geometry of the compartment (size, aspect ratio), the ventilation conditions (vent size, quantity, wind, cross-flows, inertial effects), and available fuel (type, load).

7 Chapter 7: Overall Conclusions

The most relevant conclusions arrived and discussed at each of the previous chapters are summarized and listed below.

- Two of the early pioneers, Thomas and Harmathy, defined the *Classic Compartment Fire Framework*. Both realised that the real benefit of their contributions was the utilisation of said framework. Both were careful however to acknowledge the limitations of their methodologies and insisted that practitioners utilising them be fully aware of their theoretical and experimental basis. Finally, both championed continued research to extend the understanding and range of application of the *compartment fire framework* so as to keep step with contemporary architecture.

- The *Classic Compartment Fire Framework* remains as the most commonly used description of a fully developed compartment fire. While numerous studies have been conducted after the seminal studies that defined this framework, the framework still remains.

- Within the *Classic Compartment Fire Framework*, *Regime I* corresponds to the typical, idealised experimental setups adopted by many of the researchers, while *Regime II* is characteristic of open spaces and volumes, typical of contemporary architecture.

- A *modified* two-layer model was presented as a more generic way to represent fully-developed compartment fire scenarios. Through analysis of this model, it became evident that the flow models representative of the classic *Regime I* and *Regime II* conditions are limiting cases of a more comprehensive two-layer model.

- The *modified* two-layer model can be used to analyse the effects that the confinement has on the *flow pattern*, as a means of determining the resultant system's *ventilation mode* for a given compartment fire configuration.

- In contemporary architectural conditions – i.e., scenarios with multiple openings, wind, cross-drafts, and far-from-cubic small or large compartments – the *modified* two-layer model needs to be applied.

- Because (*i*) the highest temperatures found in the CIB Programme [34] fell within *Regime I*, (*ii*) this regime has been historically assumed to be more severe than *Regime II*. Therefore, with the intension of maintaining conservatism in design, (*iii*) fully-developed fires were described as *Regime I* fires:

    - Re (*i*), there is not sufficient evidence to establish that in small and large compartments, the tendency for the peak temperature is to decline as the ventilation increases.

    - Re (*ii*), in small compartments *Regime I* appears to be more severe than *Regime II*. Nevertheless, this tendency has not been established for large compartments.

    - Re (*iii*), in small and large compartments, fully-developed fires do not always behave as a classic *Regime I* fire despite the convention to assume these characteristics describing a post-flashover fire..

- The *Classic Compartment Fire Framework* is a robust representation of the behaviour of a fire in an enclosure. It allows, by means of several strong assumptions consistent with *Regime I*, a representation of the principle parameters by simple expressions, typically functions of either the *opening factor* or the *ventilation factor*. There is no fundamental weakness in the approach but the quantitative results are intimately linked to the geometry of the compartment (size, vent size, aspect ratio) and the single vertical opening configuration.

- In addition to the classic and historically defined cases (i.e., *Regime II* and *Regime I*, defined as *Cases 1(a)* and *(b)*, respectively, in this thesis) ten additional cases were analysed – covering many characteristic fire scenarios –

showing that most extreme cases (i.e., those with either very large or very small openings) tend to the classic *Regime II* or *Regime I* behaviour, respectively.

- All the other cases examined fall somewhere in between the *classic* regime behaviours (i.e., *Regime I* or *Regime II*). These cases represent fire scenarios that exemplify contemporary buildings showing – once more – that real compartments tend to different regimes of behaviour than those represented by the classic framework definitions.

- The existing data does not allow describing in sufficient detail the different regimes described above. In some cases, experimental data lacks resolution and in others, the experimental parameters are not varied in a comprehensive way. Therefore, a series of experiments (small and large scale) were conducted to complement the available data, allowing a more detailed description of all existing regimes.

- The small-scale tests results, together with some qualitative observations from the large-scale tests, have shown and empirically reconfirmed – in relation to the theoretical conclusions listed above – that:

    - Re (*i*), the highest temperatures were achieved under the *Regime I* behaviour.

    - Re (*ii*), correspondingly, the highest heat fluxes were found under this regime and confirm the long held view that *Regime I* is more severe than *Regime II* in small compartments.

    - Re (*iii*), it was clearly observed that the temperatures could not be regarded as uniform throughout the entire compartment, not even when in a *Regime I* situation. In addition, the large-scale tests have shown that a larger compartment size can allow for the formation of even larger gradients of temperature, not only in the vertical direction but also in the direction parallel to the floor. Thus, as previously

implied theoretically, it can be concluded and reconfirmed empirically that fully-developed fires in small and large compartments cannot be *solely* understood and described as *Regime I* fires.

- The *Classic Compartment Fire Framework* is still a robust qualitative – though not quantitative – representation of the behaviour of a fire in an enclosure. Quantitative results are linked to the geometry of the compartment (size, vent size, aspect ratio) and vertical opening configuration.

- Both historical *Regimes I* and *II* are limiting cases of a broader compartment fire behaviour. Compartment fires could definitely behave following any potential intermediate behaviour that exists between the *classic* behaviours.

The work presented re-establishes the range of applicability of the *Classic Compartment Fire Framework*. It suggests the existence of a broader theory underneath that is both important and extremely relevant to contemporary architecture and infrastructure. While the *classic framework* is a robust tool to approach the fire behaviour in small compartments in specific situations, this is only one piece in the puzzle of approaching and resolving the fire problem in a building in a holistic way, where the fire and surrounding architecture are in constant exchange.

Therefore, this work exemplifies the fact, forwarded in the preface, that a *fire safety engineer* must approach the fire problem initially from first principles, and must not blindly rely on methodologies or tools that could have been developed in a different context and, thus, are inappropriate for the situation to be solved, leading to misleading decisions resulting from a false sense of confidence. Codes, standards, and methodologies are just *tools* that serve – and not replace – the scientific knowledge and creativity of the *contemporary fire safety engineer*.

Appendix A: Small-Scale Experiments Instruments Calibration

A.1 Thermocouples Calibration Approach Selection

Welch *et al.* [121] pointed out that errors in local temperature measurements in – especially large – post-flashover fires are compromised by the uncertainty known as the *radiation error*. This was stated after showing with their proposed model that remote radiation may influence the thermocouple measurement. The authors explained that a thermocouple placed in a hot gas layer may receive a lower radiation than that implied by the local gas temperature due to the influence of remote and cool surroundings such as a cold layer giving, as a result, slightly lower recorded temperatures than the true gas temperature. In other words, the solid metal thermocouple tip re-radiates heat to the cooler surroundings (i.e.; radiation loss), while this re-radiation energy loss mode is not possible in the gas surrounding the thermocouple. Contrary, in the lower layer, a temperature higher than the real local gas temperature can often be measured due to the influence of radiation emanating from the flames and/or the hot gas layer in the compartment which can be 'seen' by the thermocouple. The authors also explain that the effect in both cases tends to be more pronounced when the heat transfer is dominated by radiation, which is normally the case in post-flashover fires.

Therefore, all the thermocouple data recorded in the small-scale experiments was corrected to eliminate the radiation error. The following figures (Figure A-1 to Figure A-216) show the results of the calibration for each test configuration. These graphs contrast the space-averaged original and corrected temperature for each of the 6 horizontal layers – layer 1 being the lowest and layer 6 being the highest – along the entire duration of the correspondent test, plus the associated error.

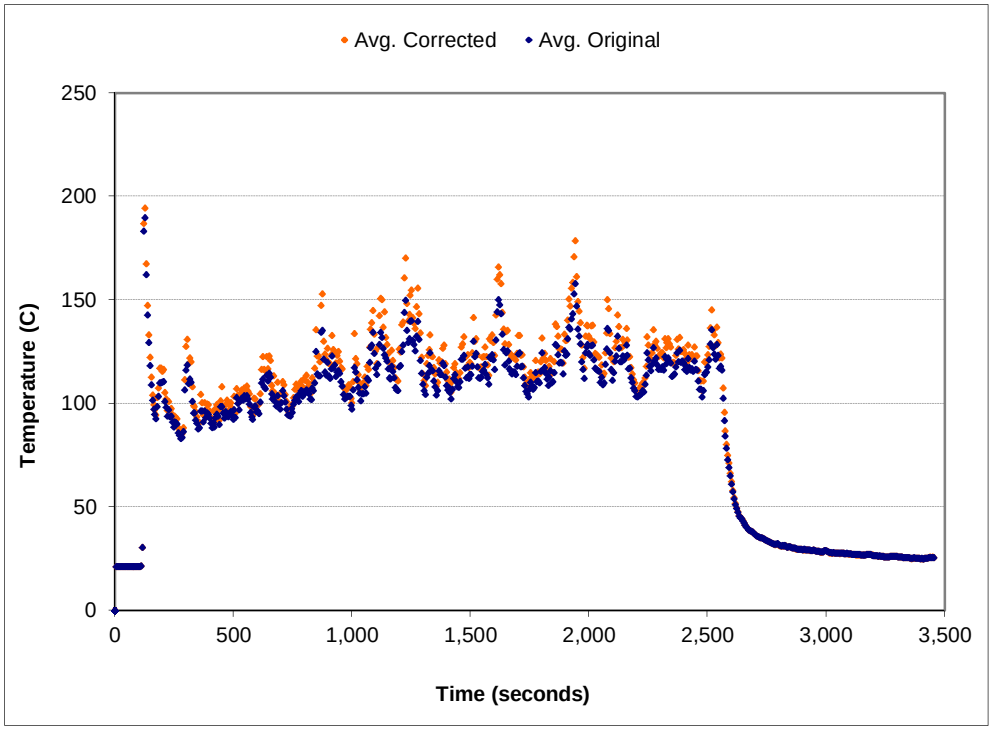

Figure A-1: Space-averaged (layer 1) temperature correction for the 0.5 g/s, ϕ_1 configuration

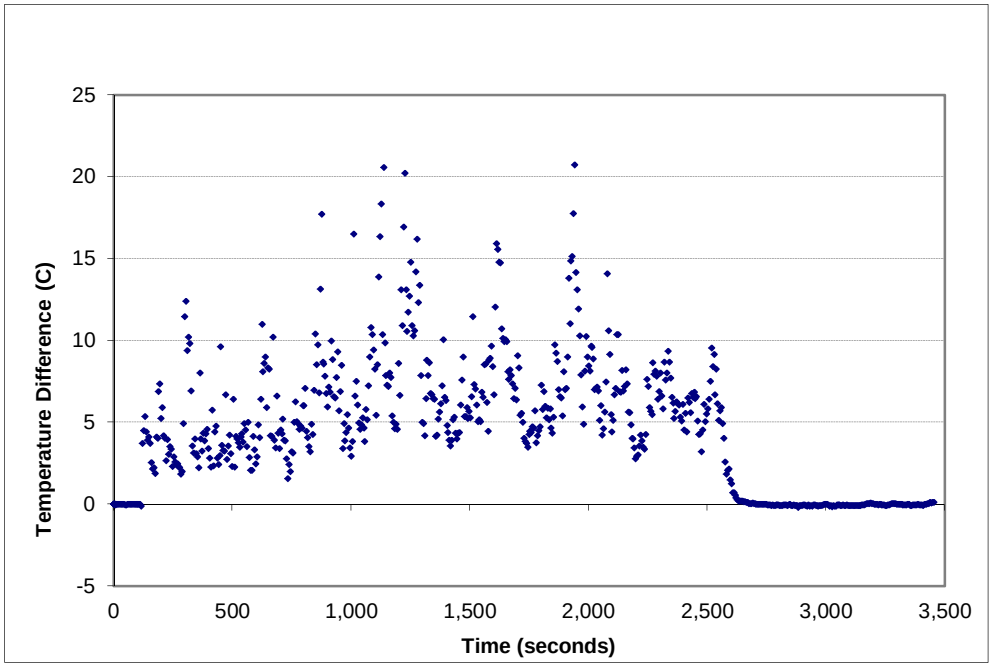

Figure A-2: Temperature error (layer 1) for the 0.5 g/s, ϕ_1 configuration

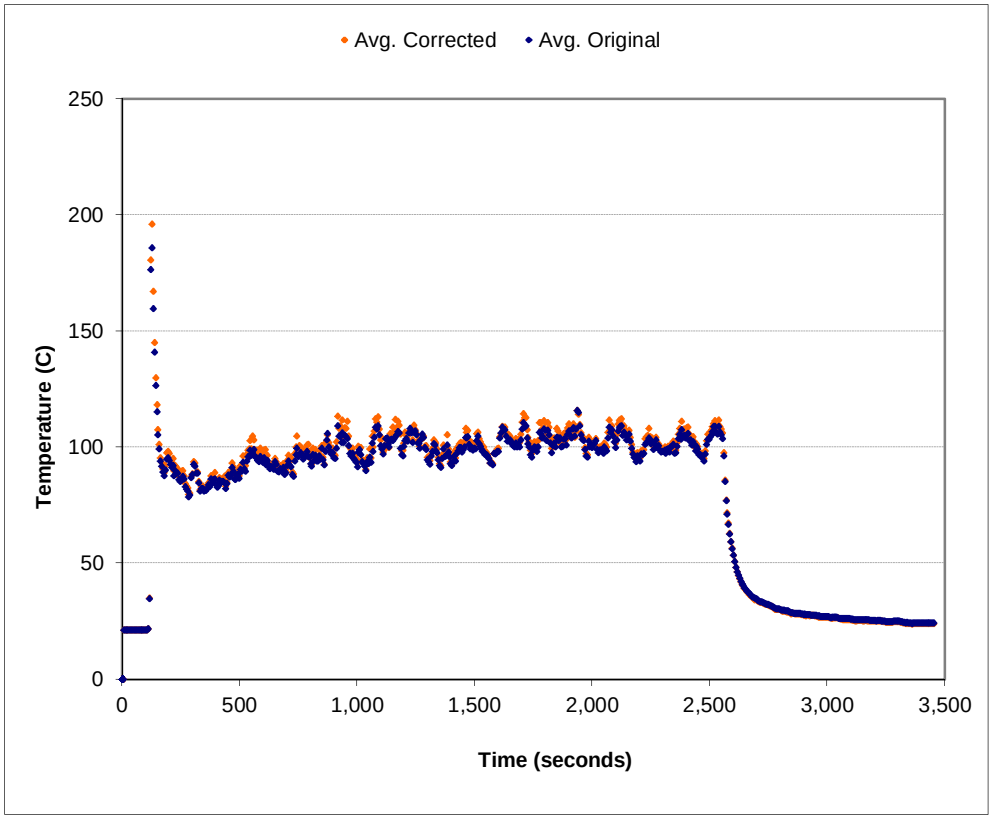

Figure A-3: Space-averaged (layer 2) temperature correction for the 0.5 g/s, ϕ_1 configuration

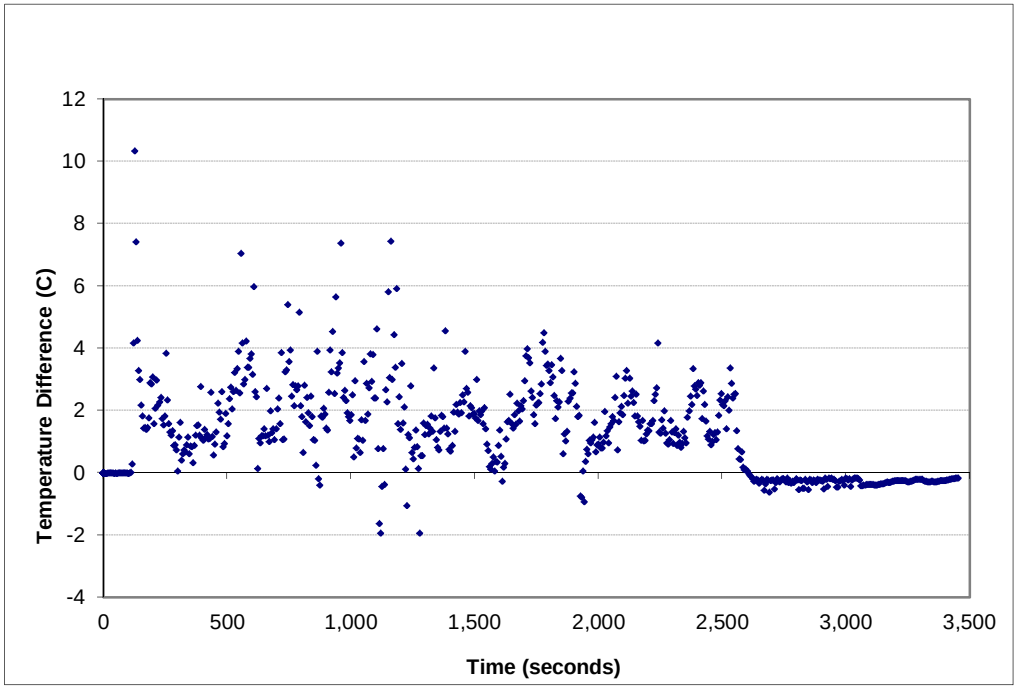

Figure A-4: Temperature error (layer 2) for the 0.5 g/s, ϕ_1 configuration

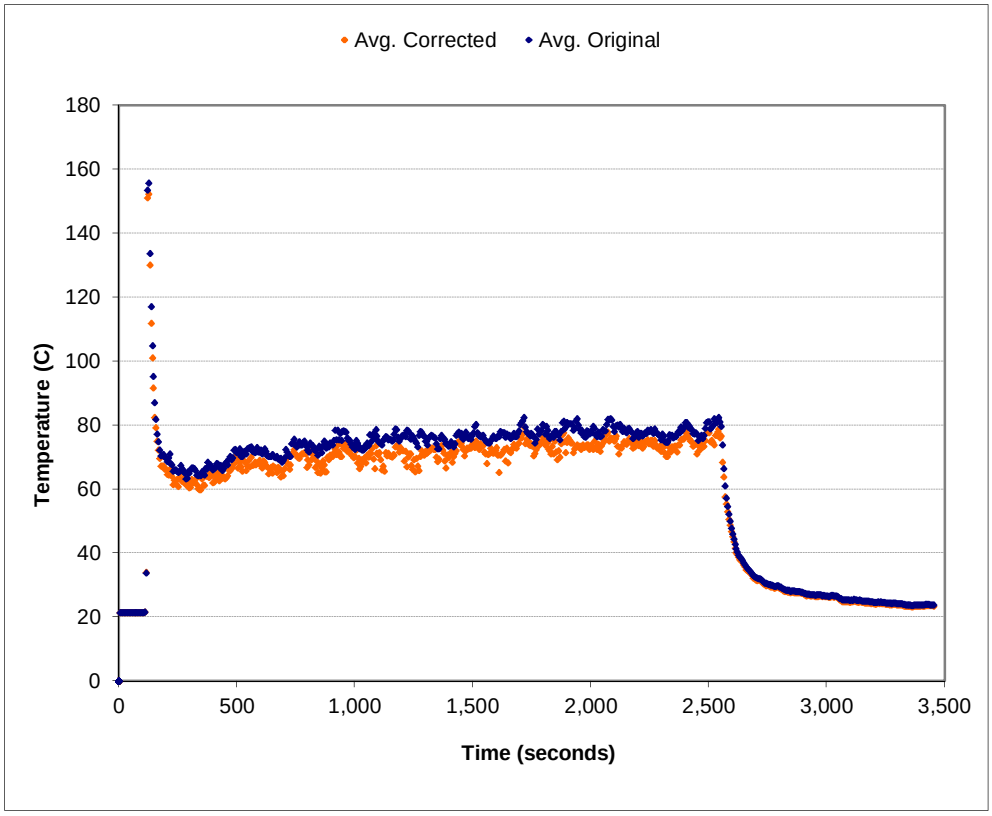

Figure A-5: Space-averaged (layer 3) temperature correction for the 0.5 g/s, ϕ_1 configuration

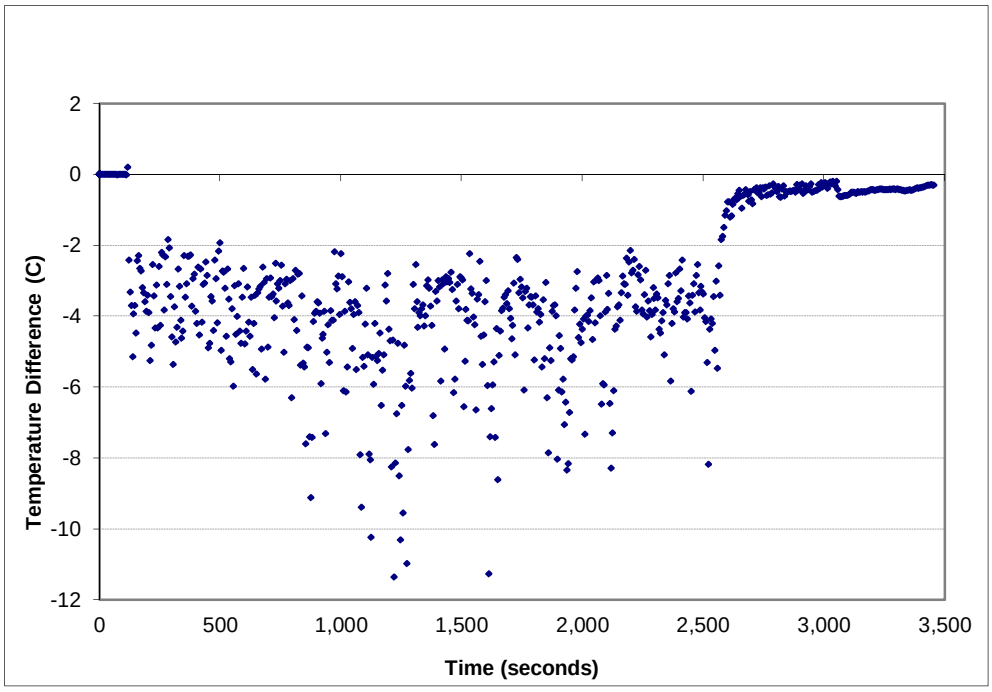

Figure A-6: Temperature error (layer 3) for the 0.5 g/s, ϕ_1 configuration

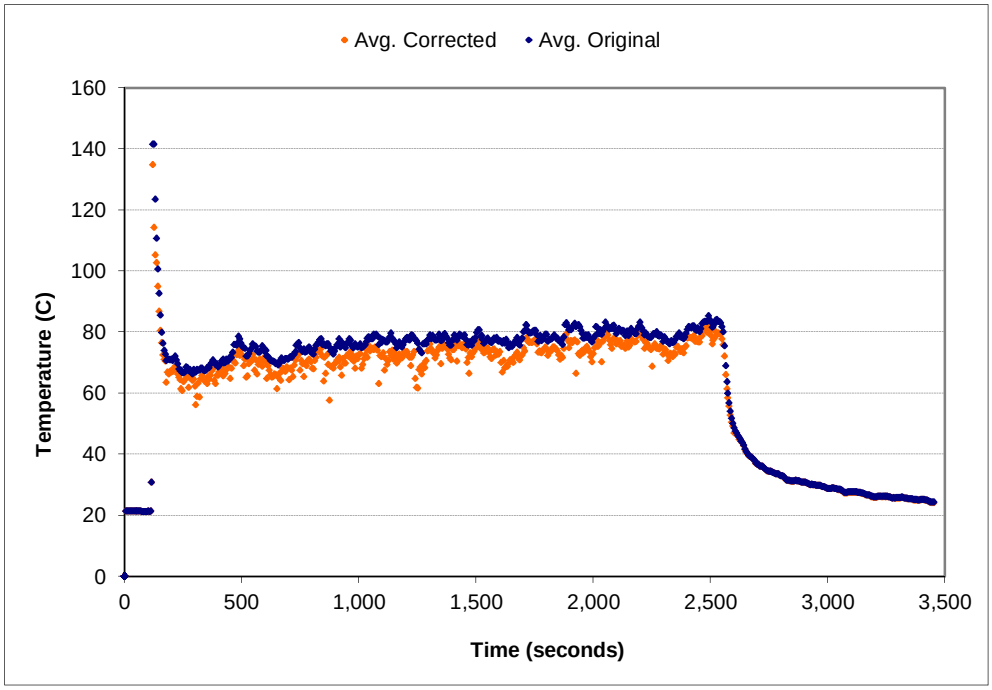

Figure A-7: Space-averaged (layer 4) temperature correction for the 0.5 g/s, ϕ_1 configuration

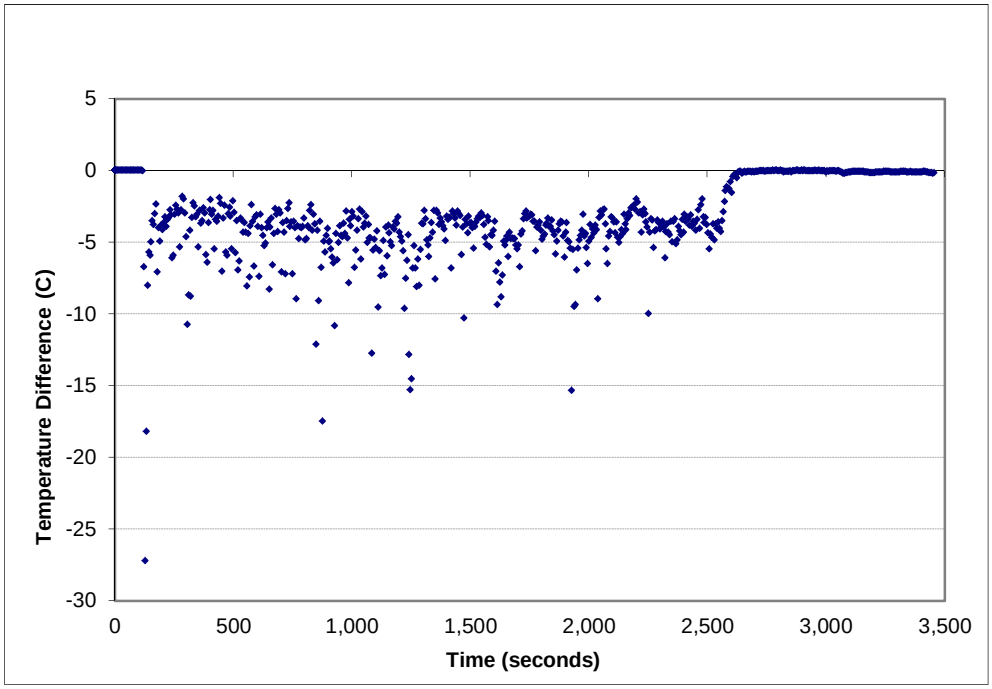

Figure A-8: Temperature error (layer 4) for the 0.5 g/s, ϕ_1 configuration

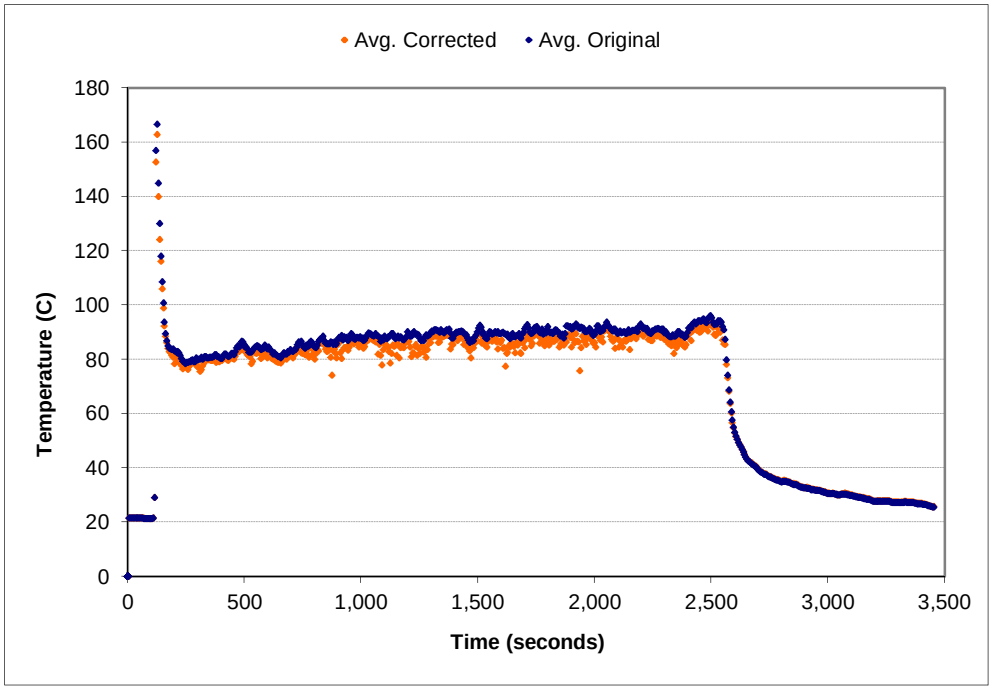

Figure A-9: Space-averaged (layer 5) temperature correction for the 0.5 g/s, ϕ_1 configuration

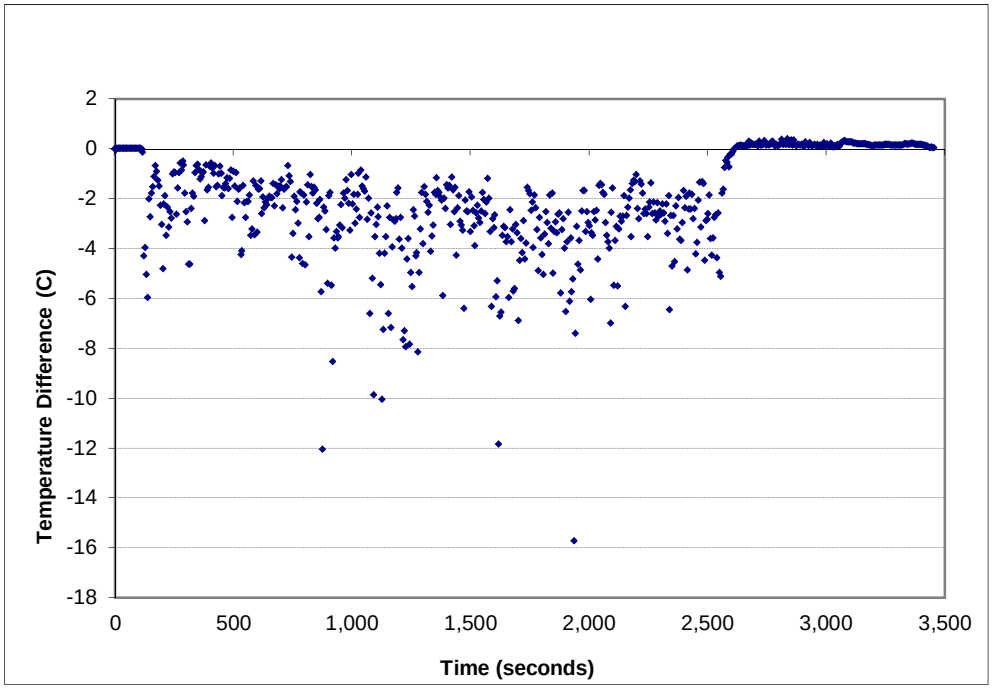

Figure A-10: Temperature error (layer 5) for the 0.5 g/s, ϕ_1 configuration

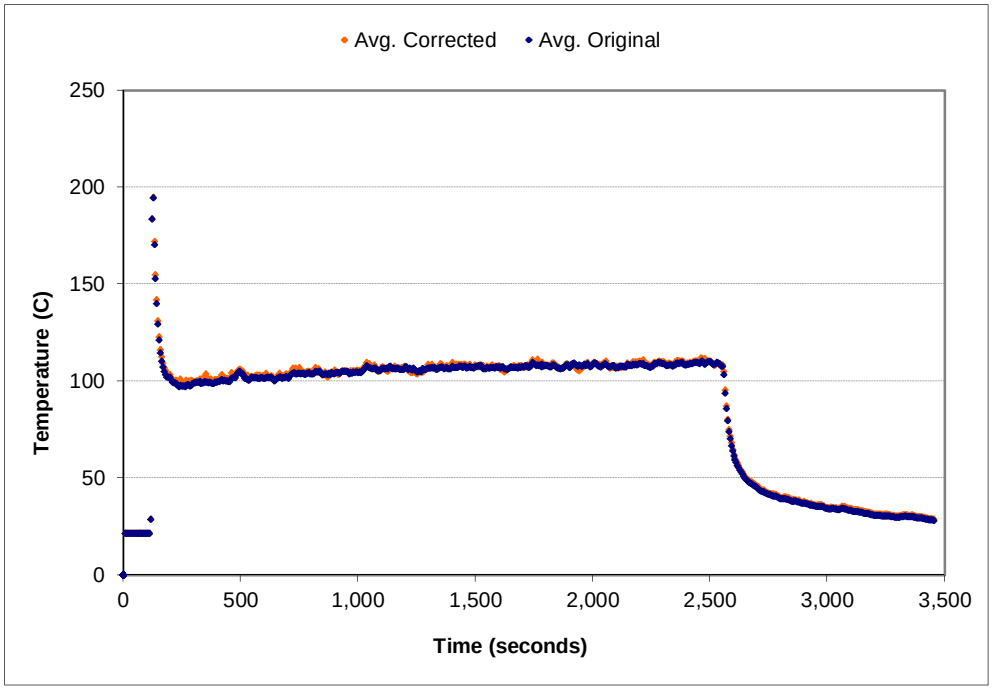

Figure A-11: Space-averaged (layer 6) temperature correction for the 0.5 g/s, ϕ_1 configuration

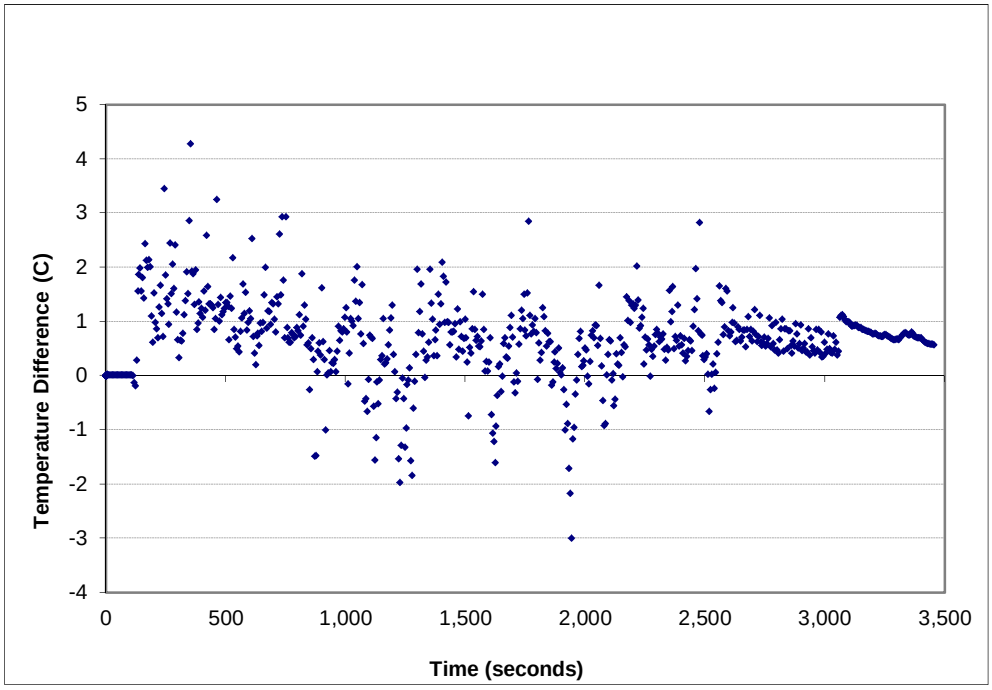

Figure A-12: Temperature error (layer 6) for the 0.5 g/s, ϕ_1 configuration

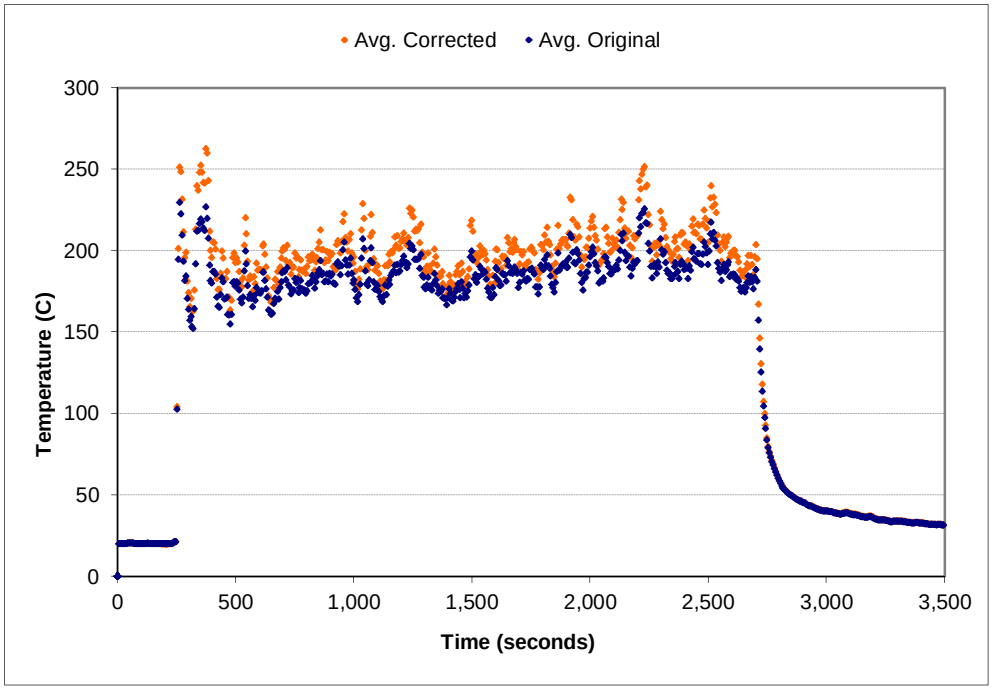

Figure A-13: Space-averaged (layer 1) temperature correction for the 1.0 g/s, ϕ_1 configuration

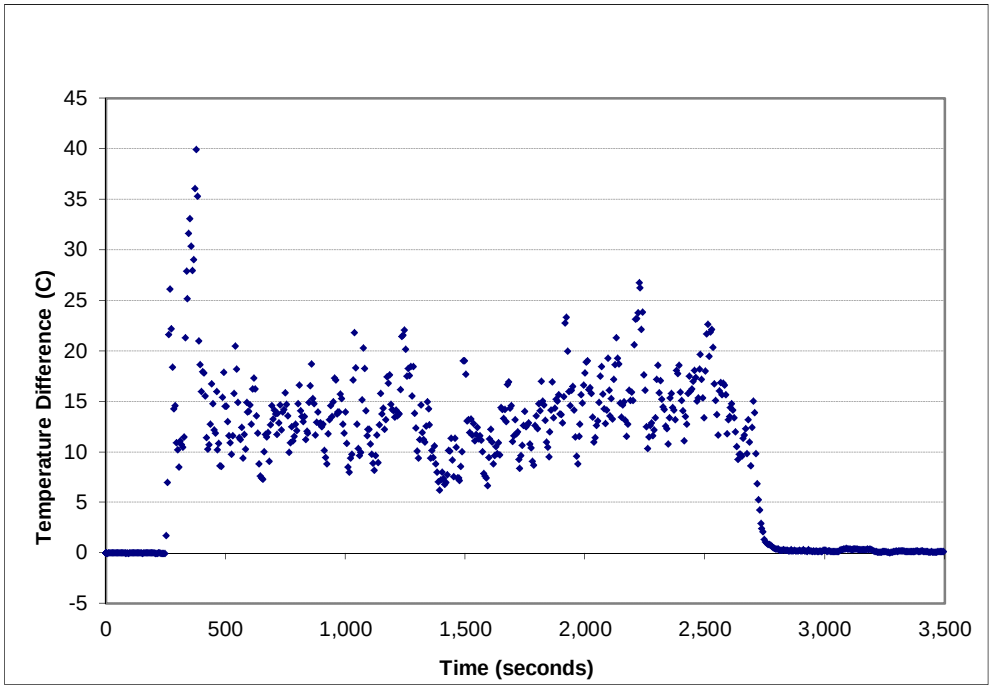

Figure A-14: Temperature error (layer 1) for the 1.0 g/s, ϕ_1 configuration

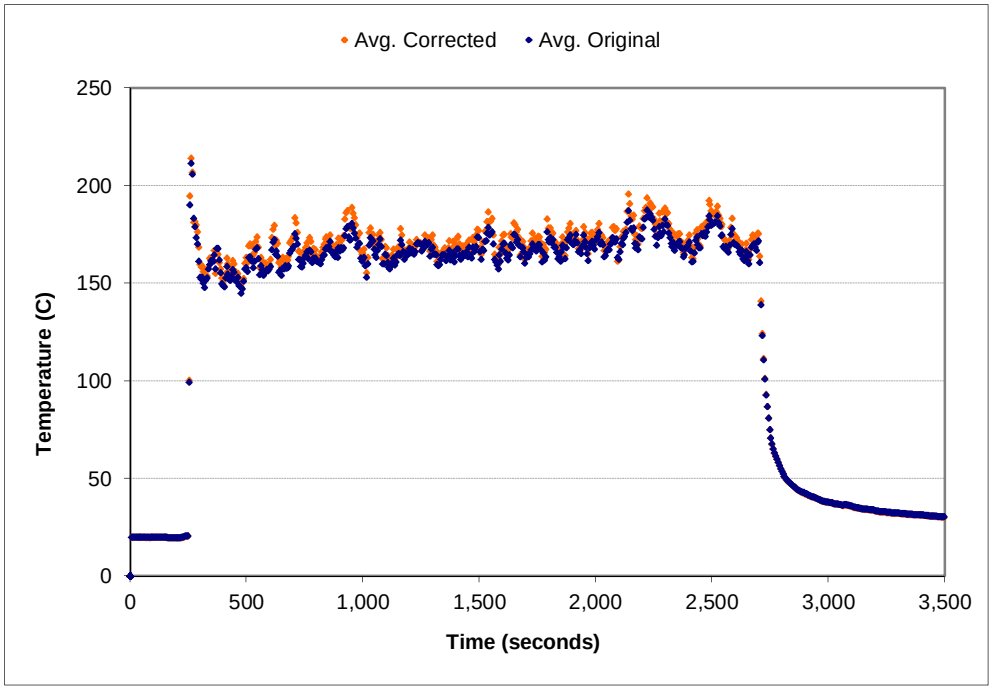

Figure A-15: Space-averaged (layer 2) temperature correction for the 1.0 g/s, ϕ_1 configuration

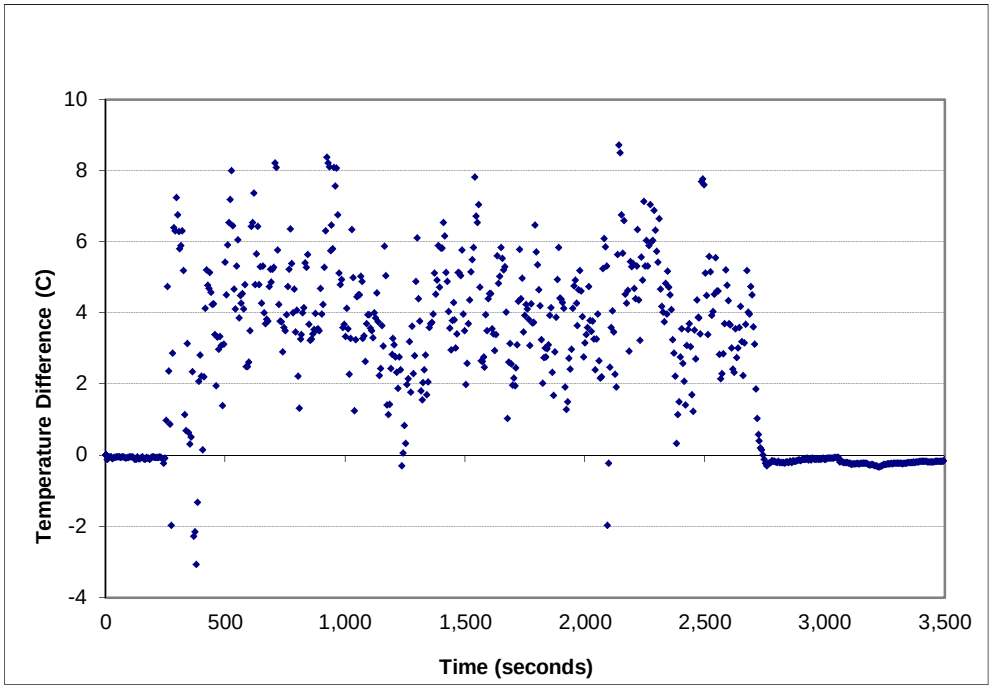

Figure A-16: Temperature error (layer 2) for the 1.0 g/s, ϕ_1 configuration

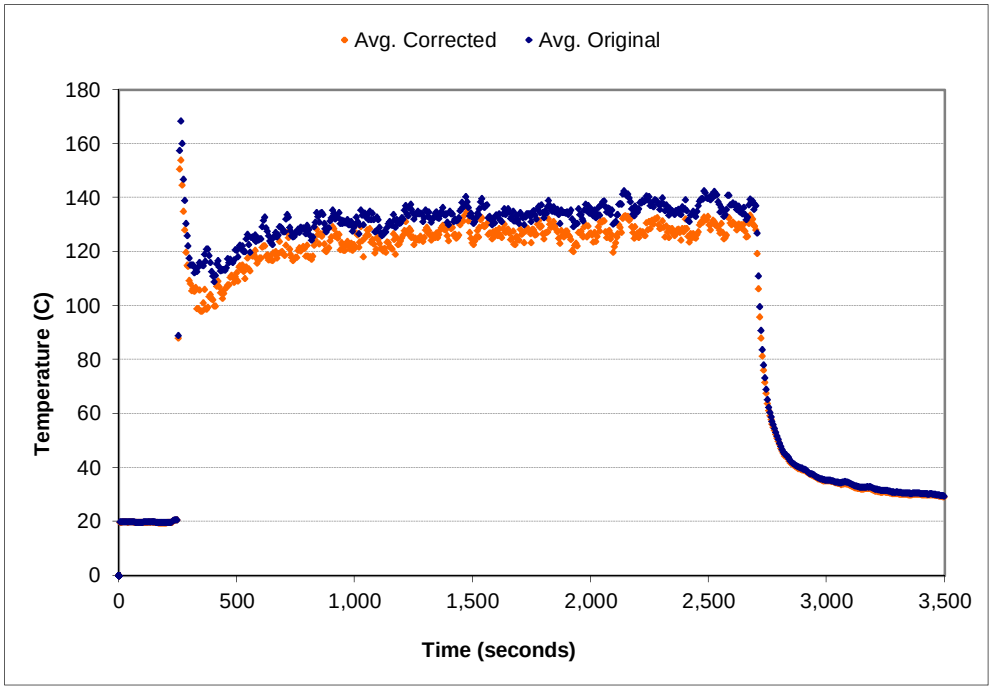

Figure A-17: Space-averaged (layer 3) temperature correction for the 1.0 g/s, ϕ_1 configuration

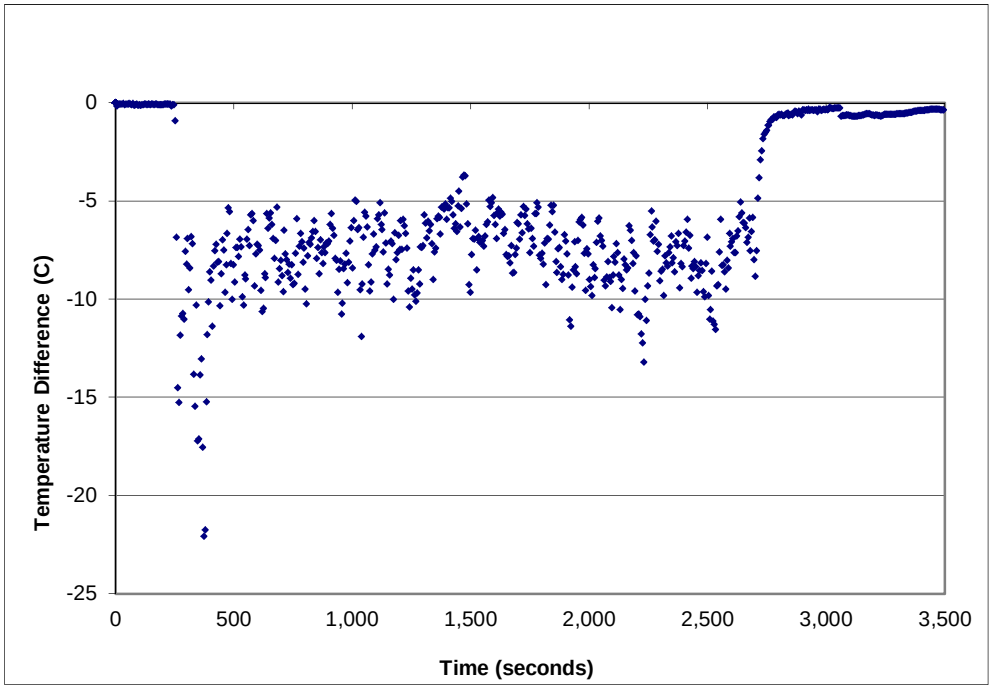

Figure A-18: Temperature error (layer 3) for the 1.0 g/s, ϕ_1 configuration

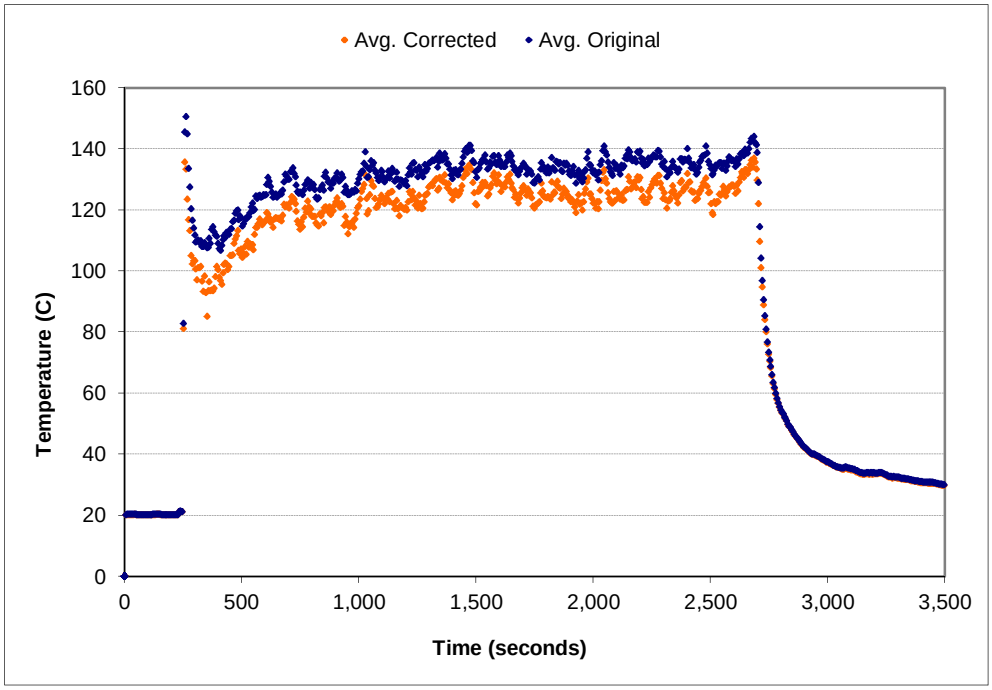

Figure A-19: Space-averaged (layer 4) temperature correction for the 1.0 g/s, ϕ_1 configuration

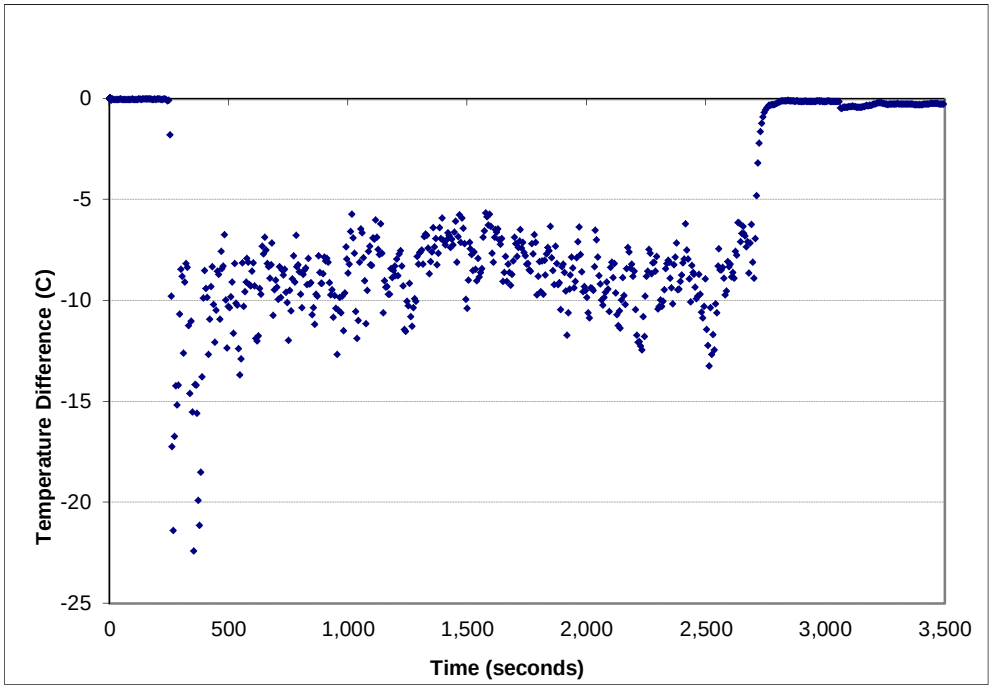

Figure A-20: Temperature error (layer 4) for the 1.0 g/s, ϕ_1 configuration

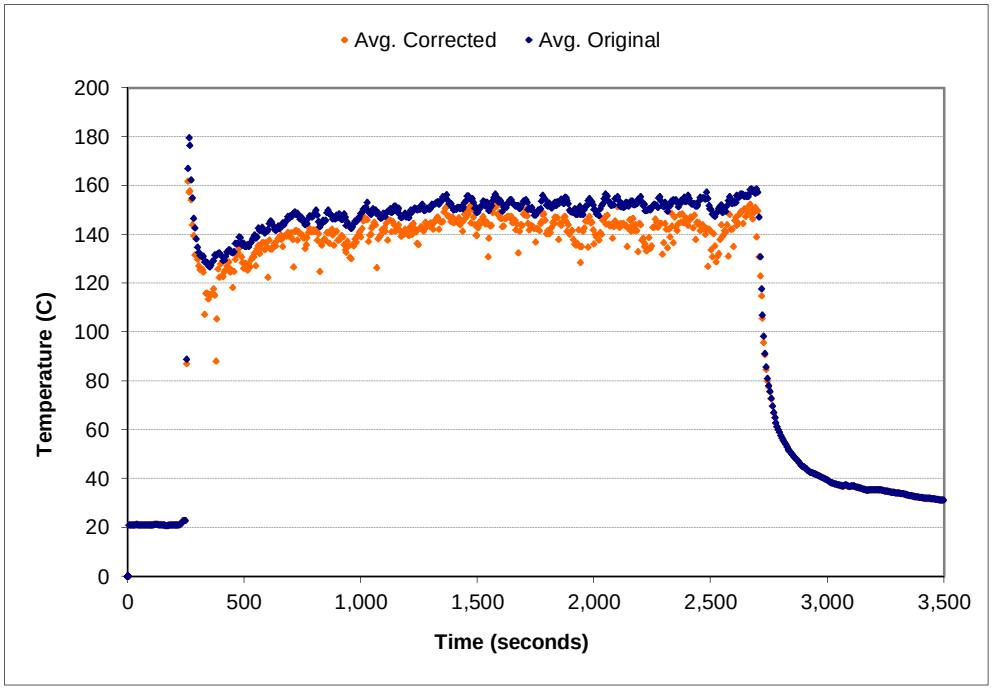

Figure A-21: Space-averaged (layer 5) temperature correction for the 1.0 g/s, ϕ_1 configuration

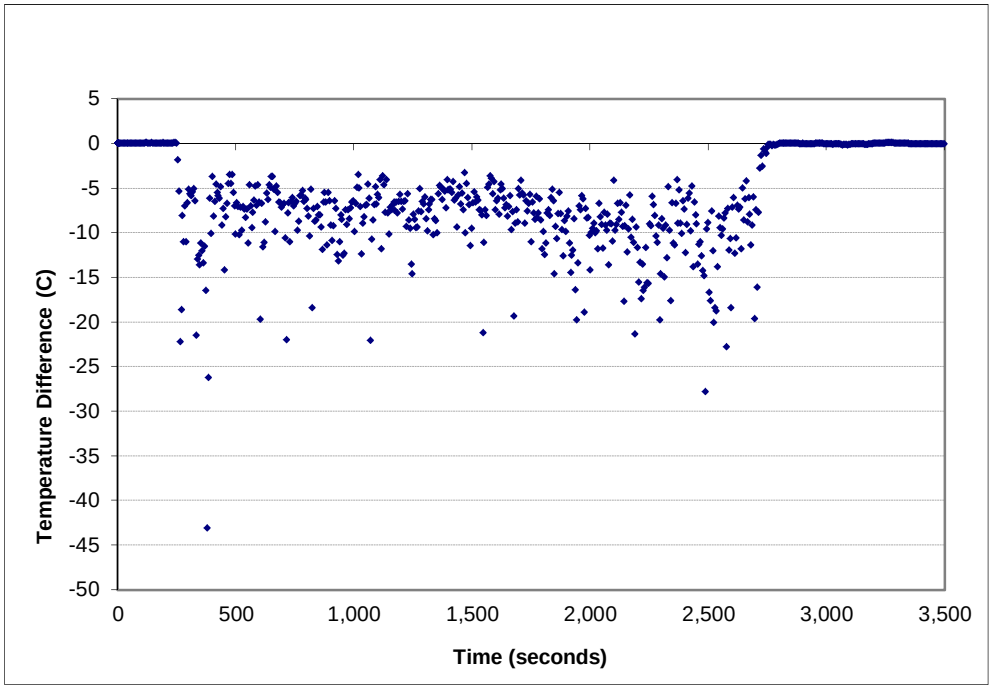

Figure A-22: Temperature error (layer 5) for the 1.0 g/s, ϕ_1 configuration

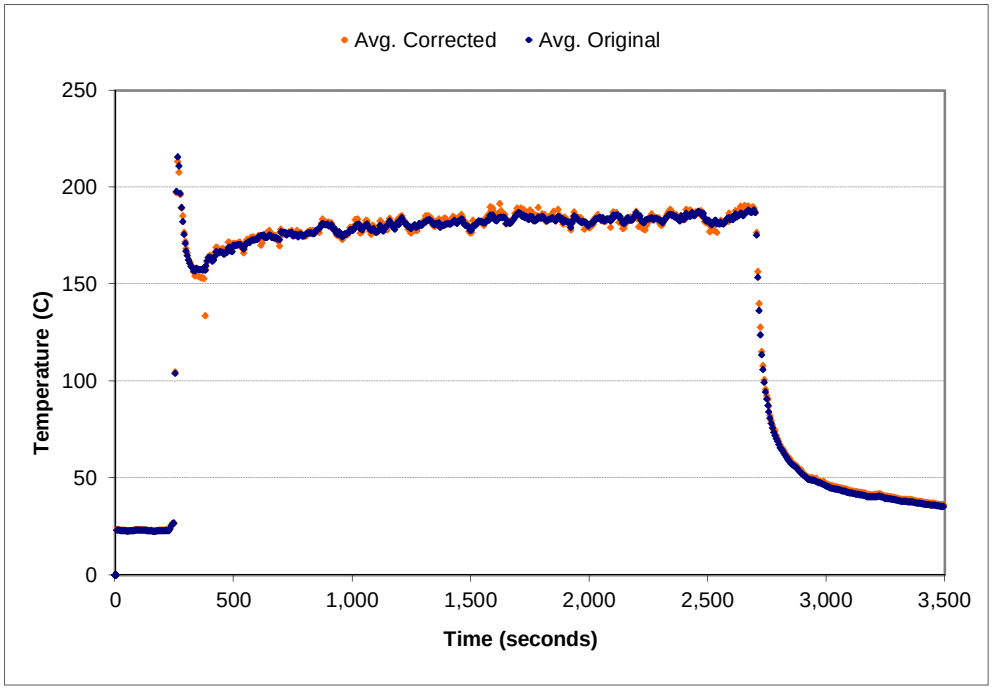

Figure A-23: Space-averaged (layer 6) temperature correction for the 1.0 g/s, ϕ_1 configuration

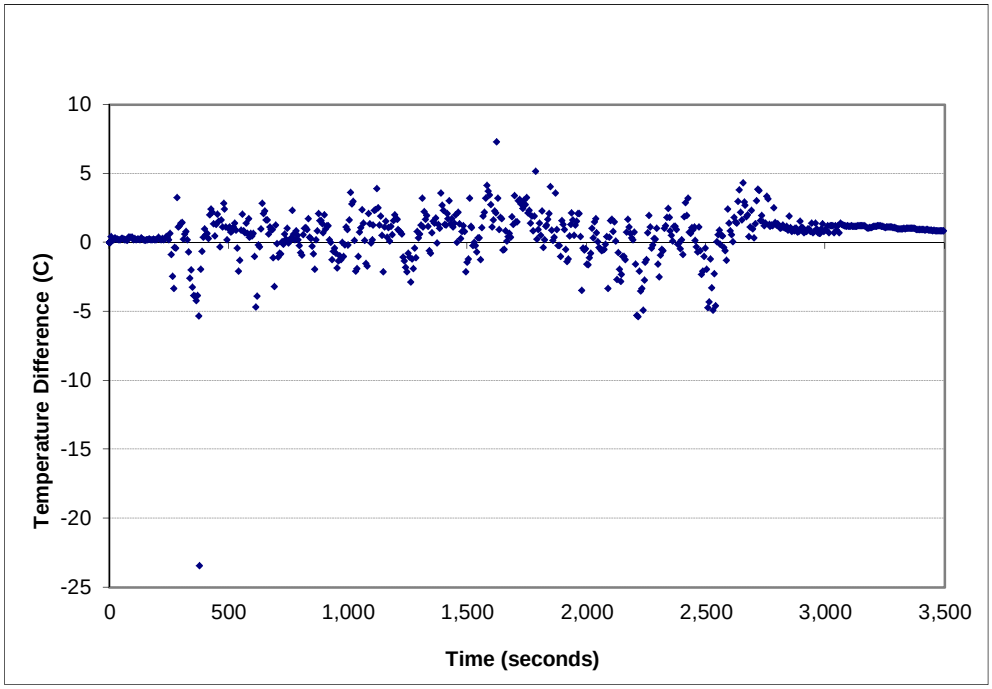

Figure A-24: Temperature error (layer 6) for the 1.0 g/s, ϕ_1 configuration

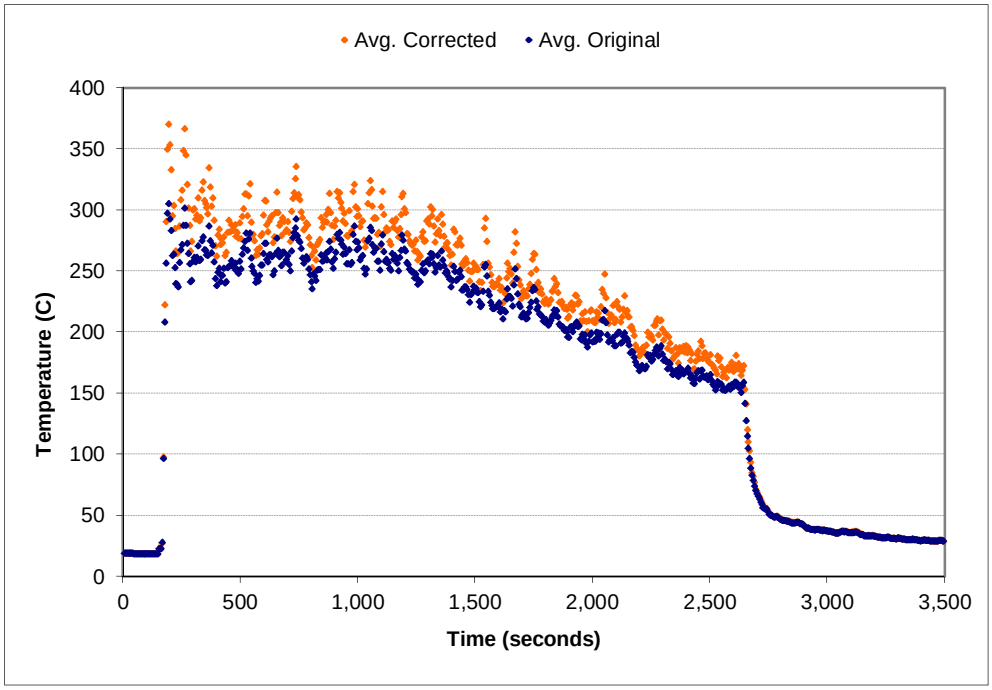

Figure A-25: Space-averaged (layer 1) temperature correction for the 1.5 g/s, ϕ_1 configuration

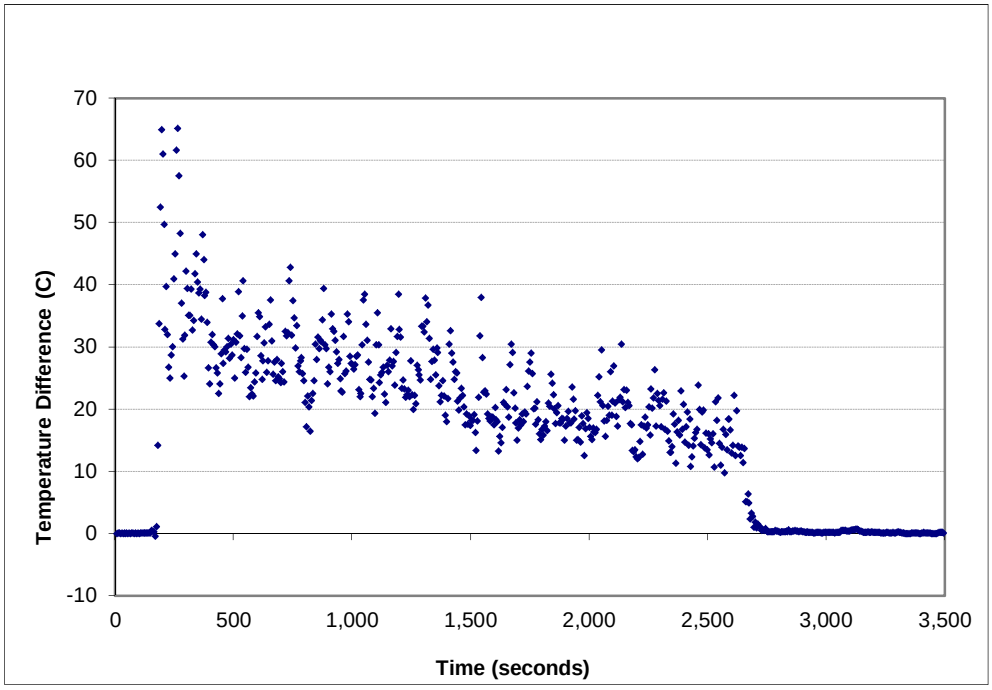

Figure A-26: Temperature error (layer 1) for the 1.5 g/s, ϕ_1 configuration

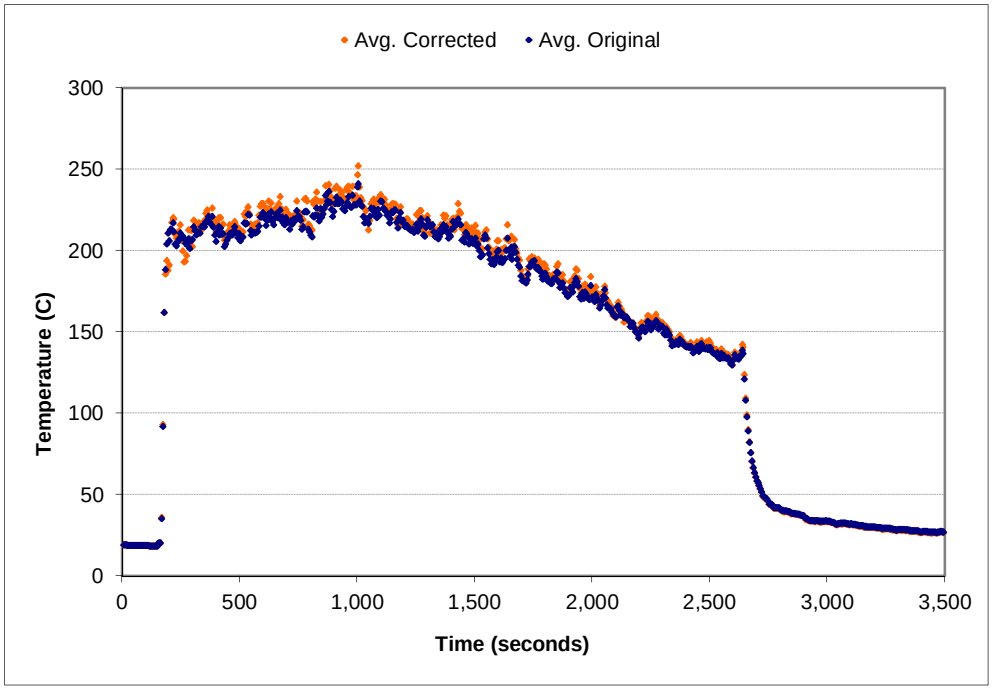

Figure A-27: Space-averaged (layer 2) temperature correction for the 1.5 g/s, ϕ_1 configuration

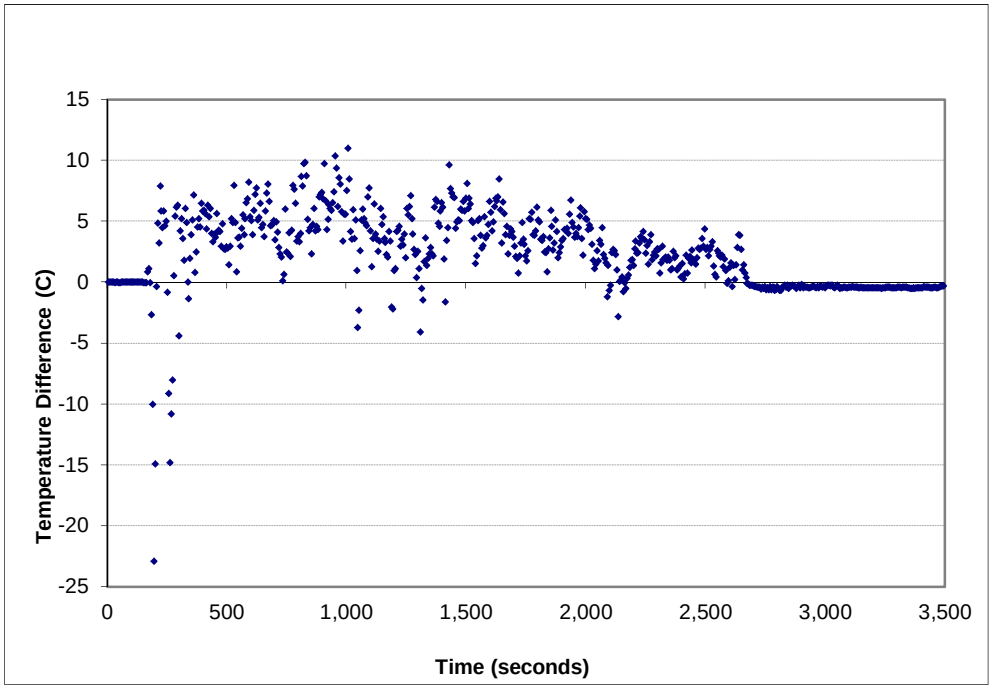

Figure A-28: Temperature error (layer 2) for the 1.5 g/s, ϕ_1 configuration

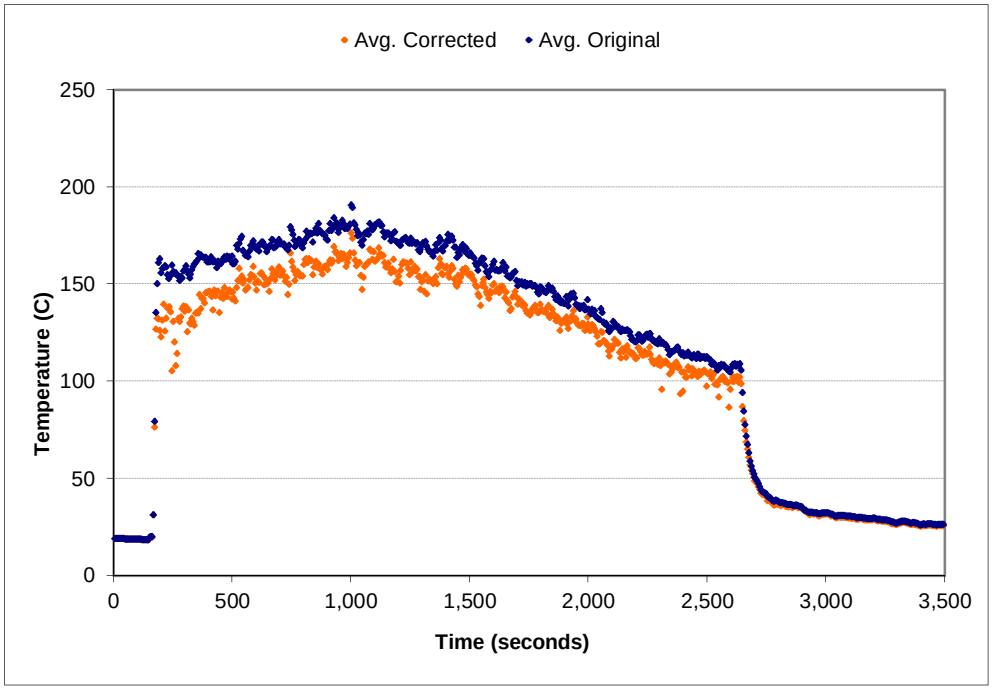

Figure A-29: Space-averaged (layer 3) temperature correction for the 1.5 g/s, ϕ_1 configuration

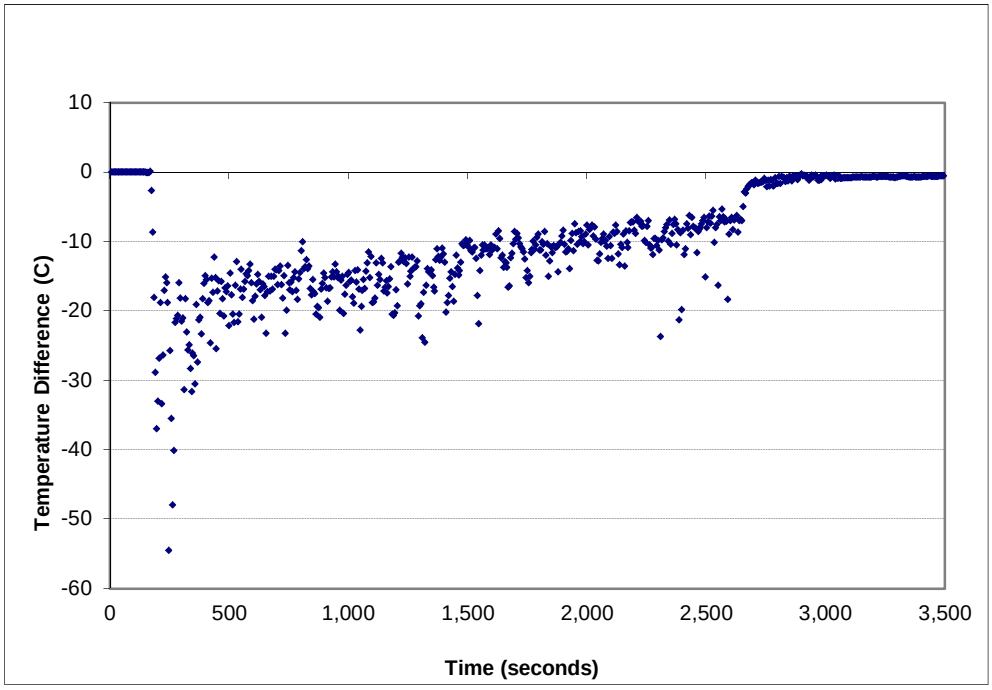

Figure A-30: Temperature error (layer 3) for the 1.5 g/s, ϕ_1 configuration

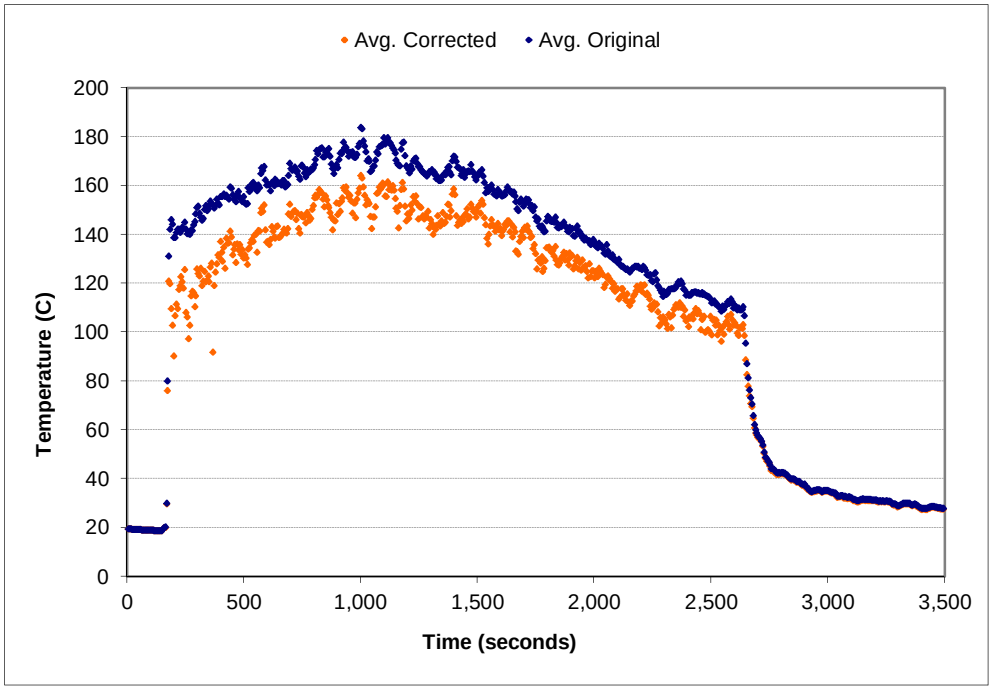

Figure A-31: Space-averaged (layer 4) temperature correction for the 1.5 g/s, ϕ_1 configuration

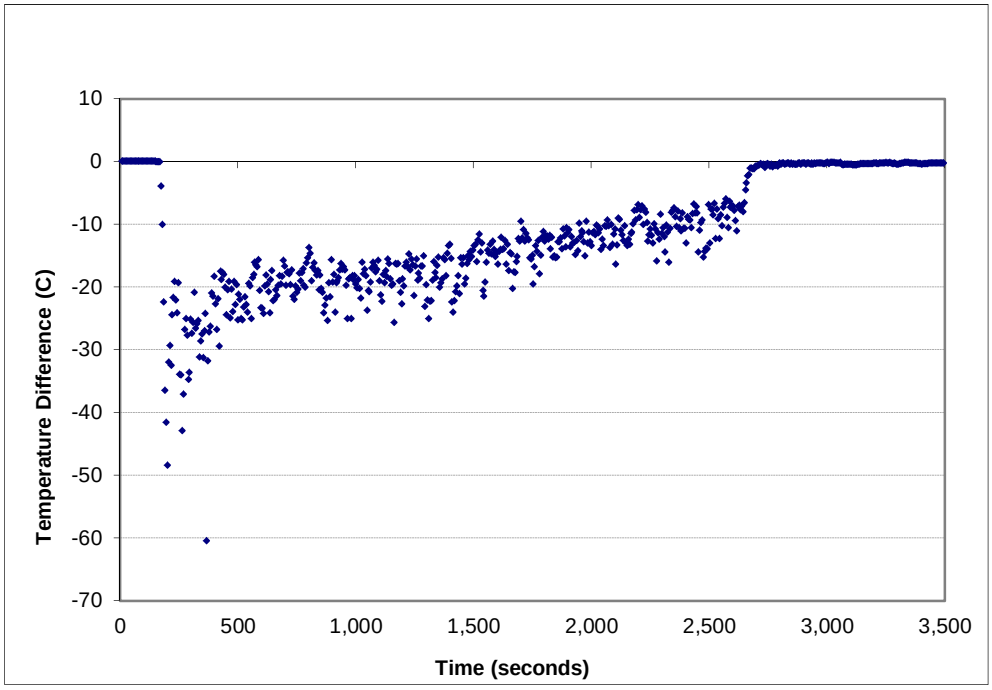

Figure A-32: Temperature error (layer 4) for the 1.5 g/s, ϕ_1 configuration

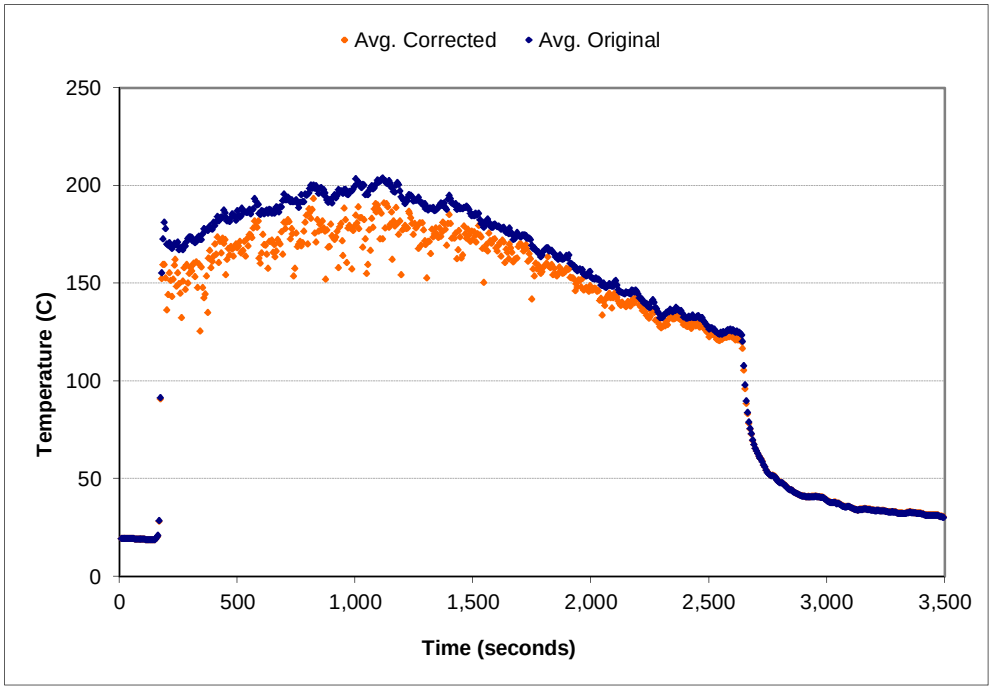

Figure A-33: Space-averaged (layer 5) temperature correction for the 1.5 g/s, ϕ_1 configuration

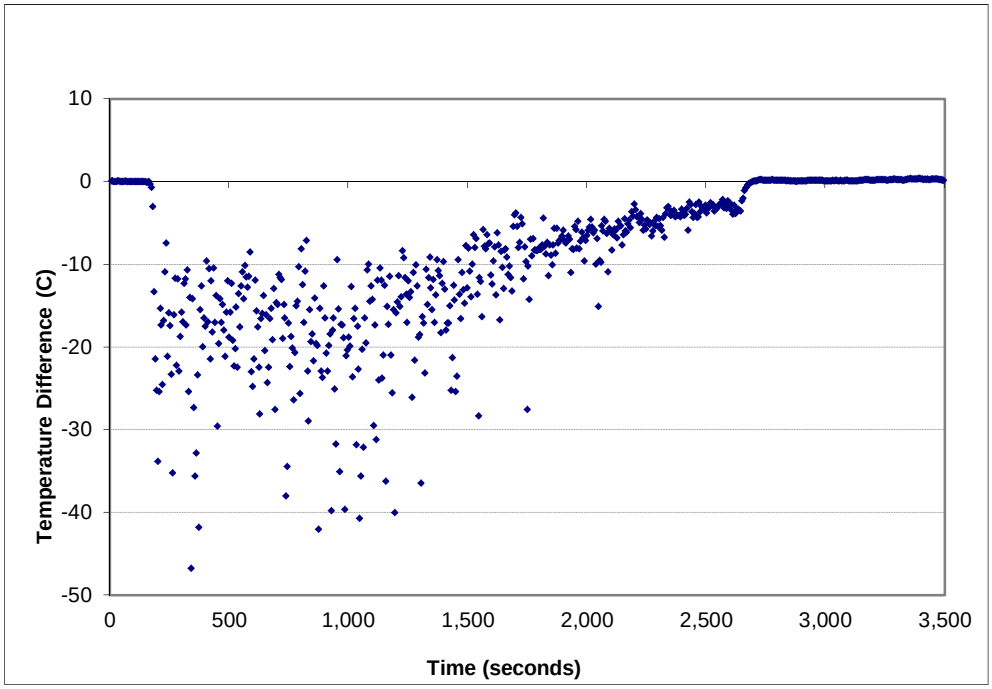

Figure A-34: Temperature error (layer 5) for the 1.5 g/s, ϕ_1 configuration

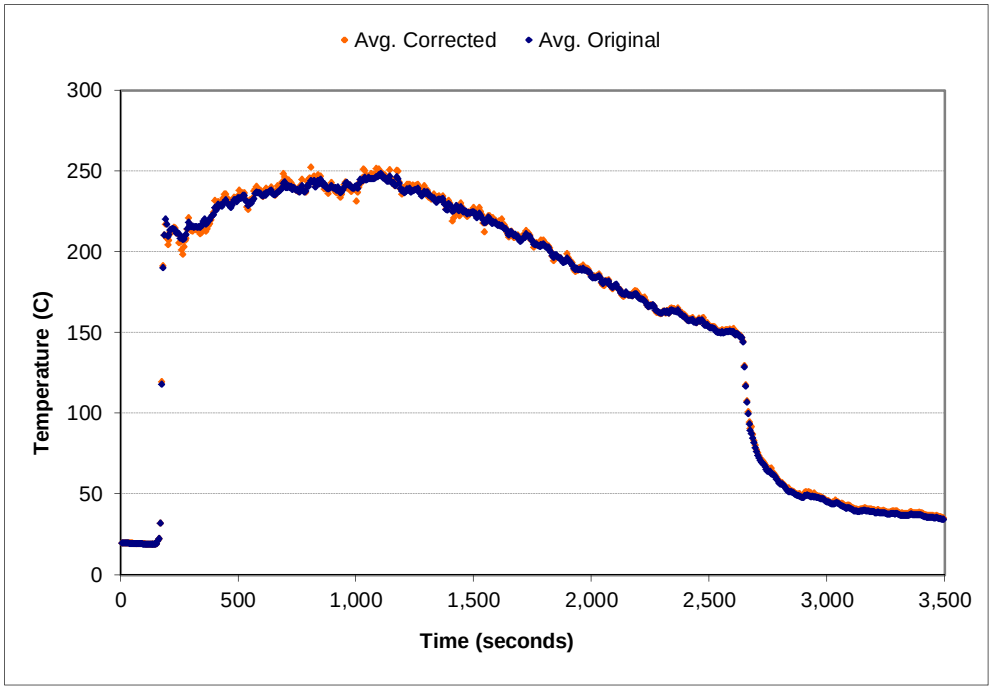

Figure A-35: Space-averaged (layer 6) temperature correction for the 1.5 g/s, ϕ_1 configuration

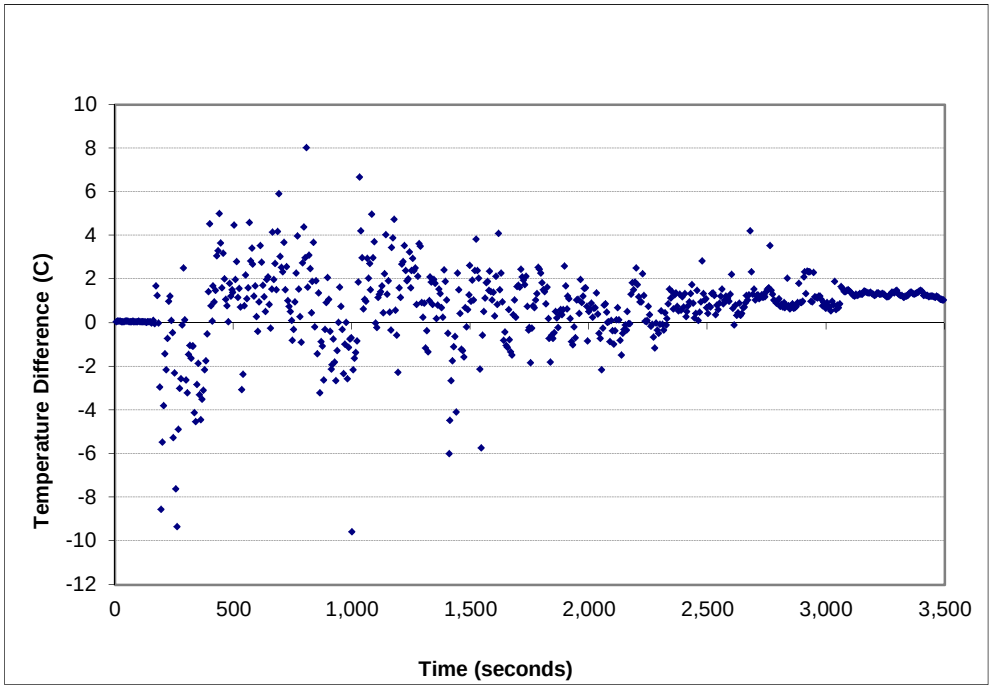

Figure A-36: Temperature error (layer 6) for the 1.5 g/s, ϕ_1 configuration

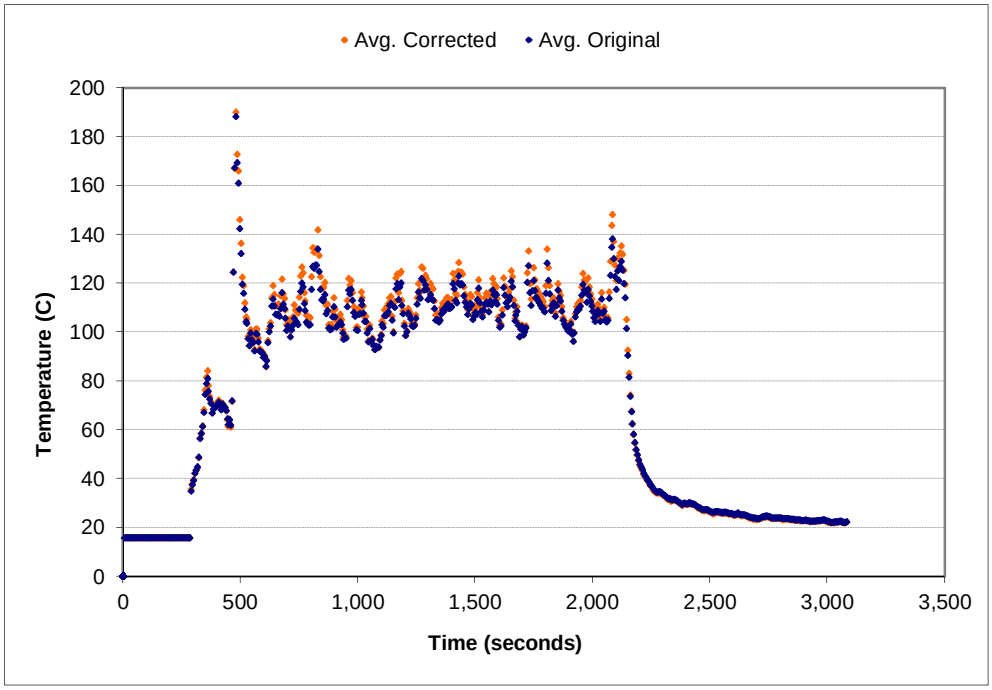

Figure A-37: Space-averaged (layer 1) temperature correction for the 0.5 g/s, ϕ_2 configuration

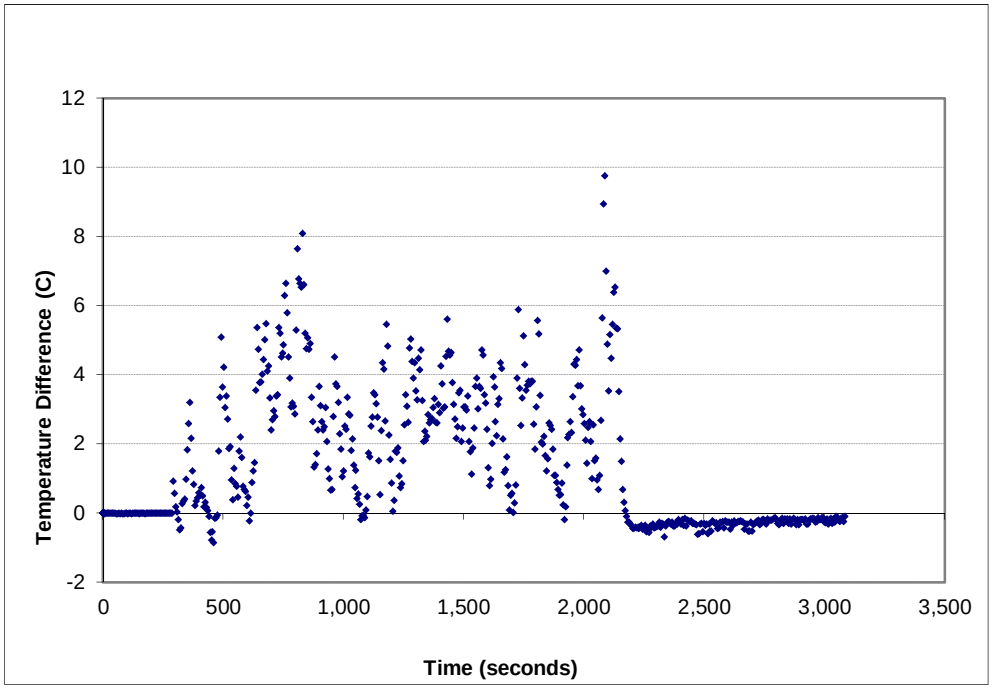

Figure A-38: Temperature error (layer 1) for the 0.5 g/s, ϕ_2 configuration

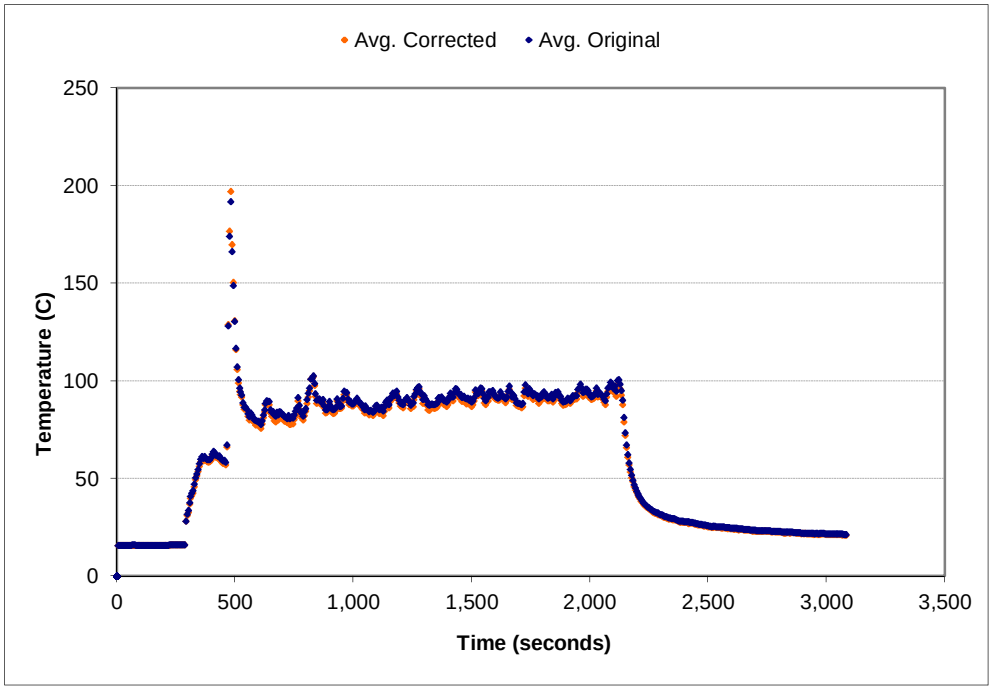

Figure A-39: Space-averaged (layer 2) temperature correction for the 0.5 g/s, ϕ_2 configuration

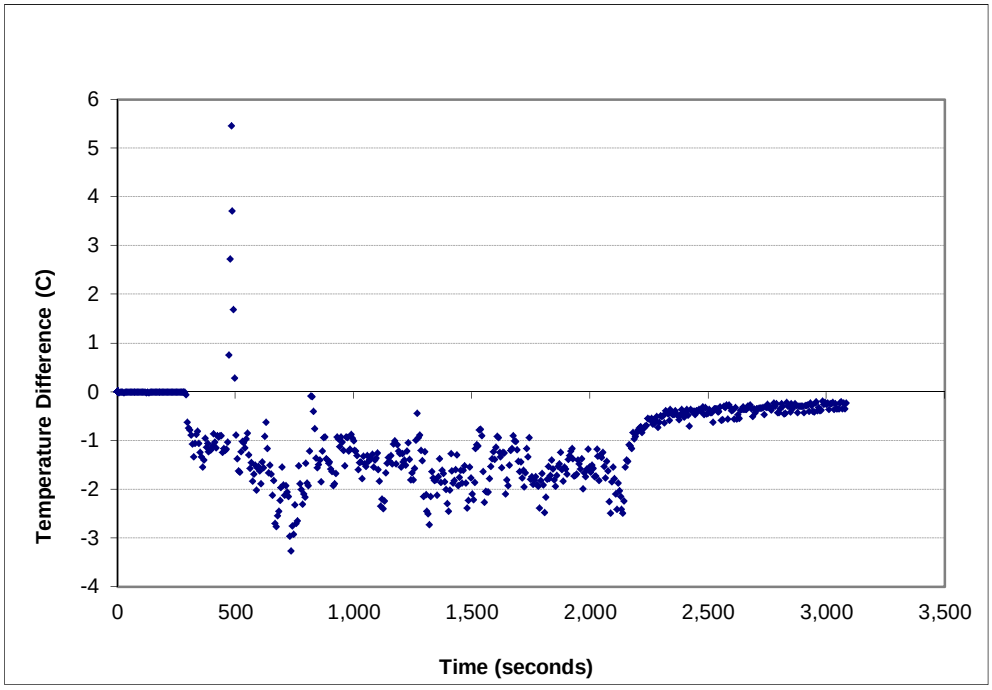

Figure A-40: Temperature error (layer 2) for the 0.5 g/s, ϕ_2 configuration

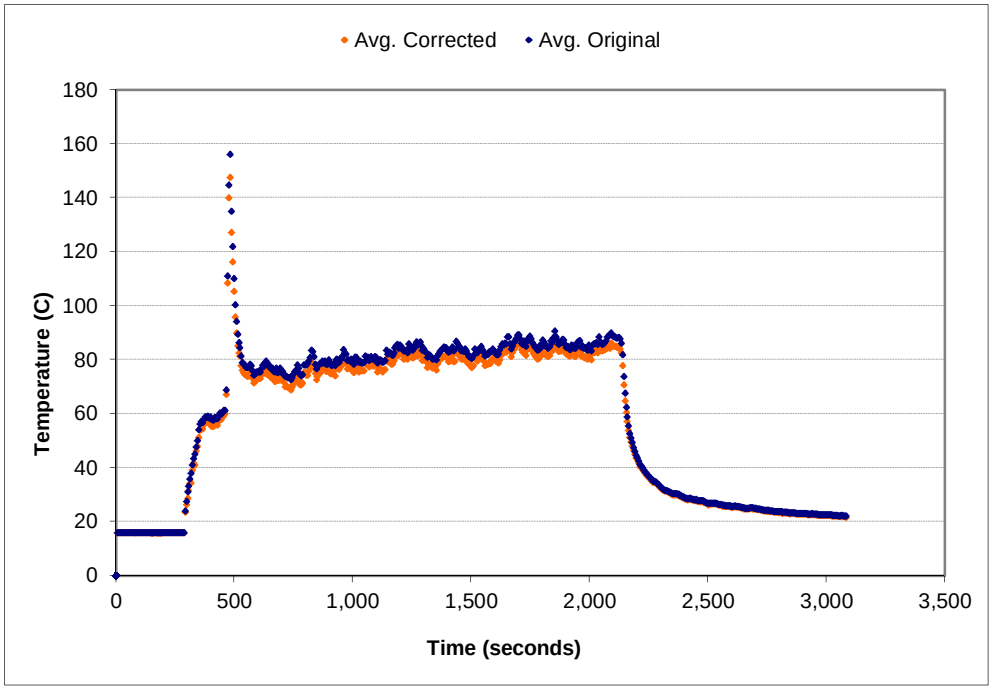

Figure A-41: Space-averaged (layer 3) temperature correction for the 0.5 g/s, ϕ_2 configuration

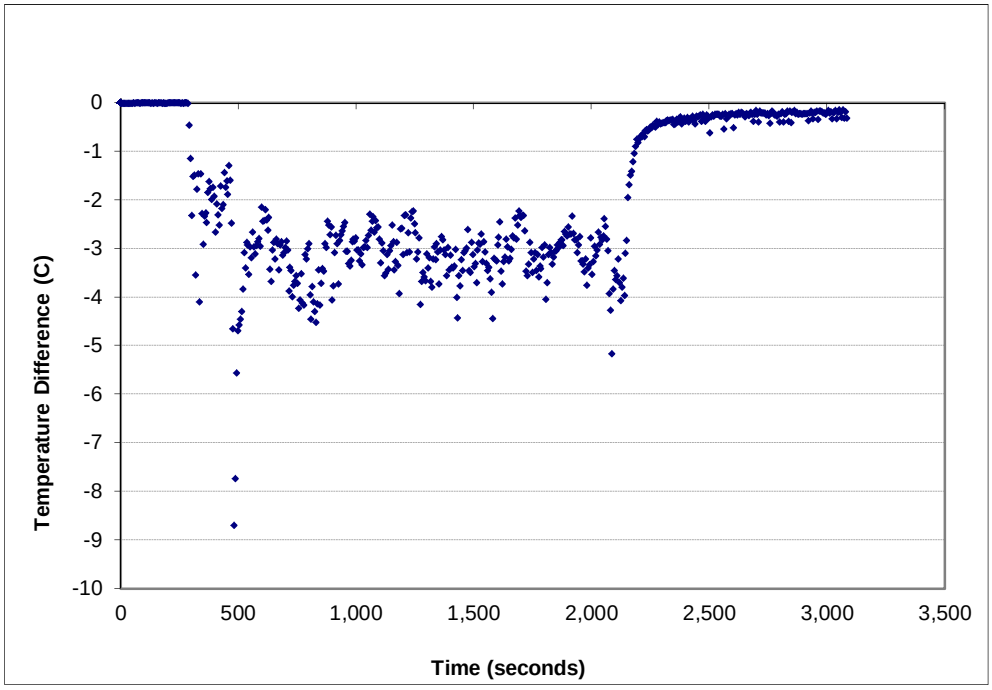

Figure A-42: Temperature error (layer 3) for the 0.5 g/s, ϕ_2 configuration

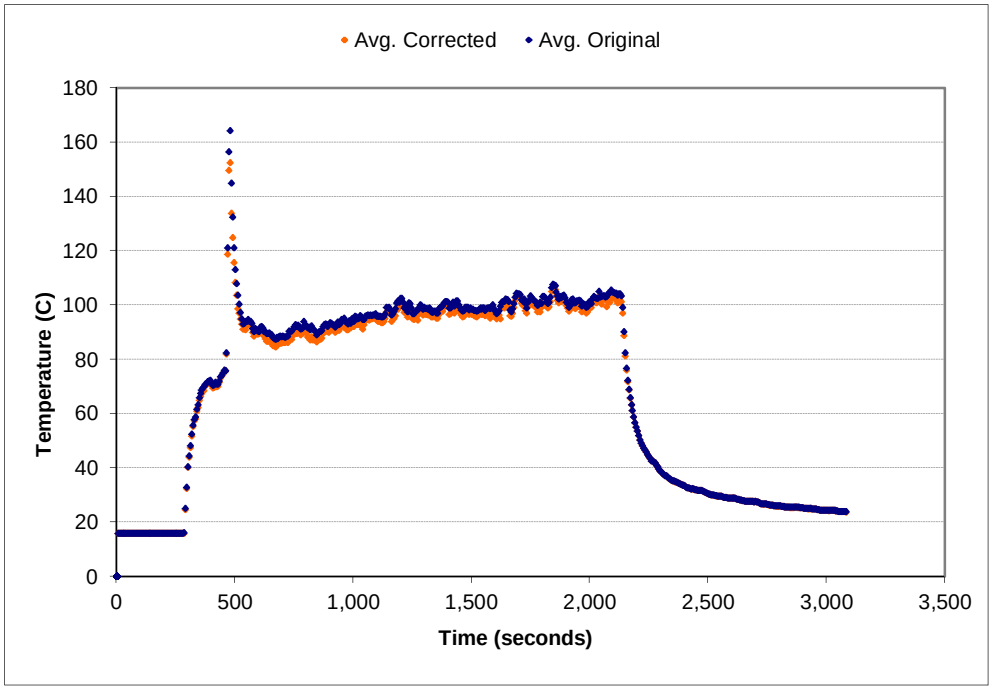

Figure A-43: Space-averaged (layer 4) temperature correction for the 0.5 g/s, ϕ_2 configuration

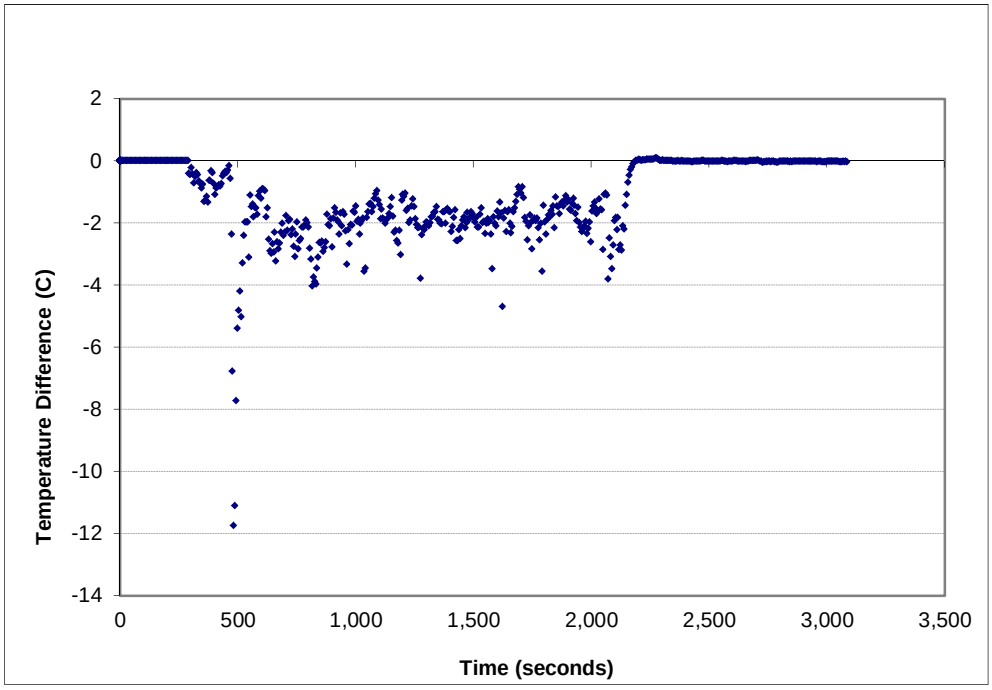

Figure A-44: Temperature error (layer 4) for the 0.5 g/s, ϕ_2 configuration

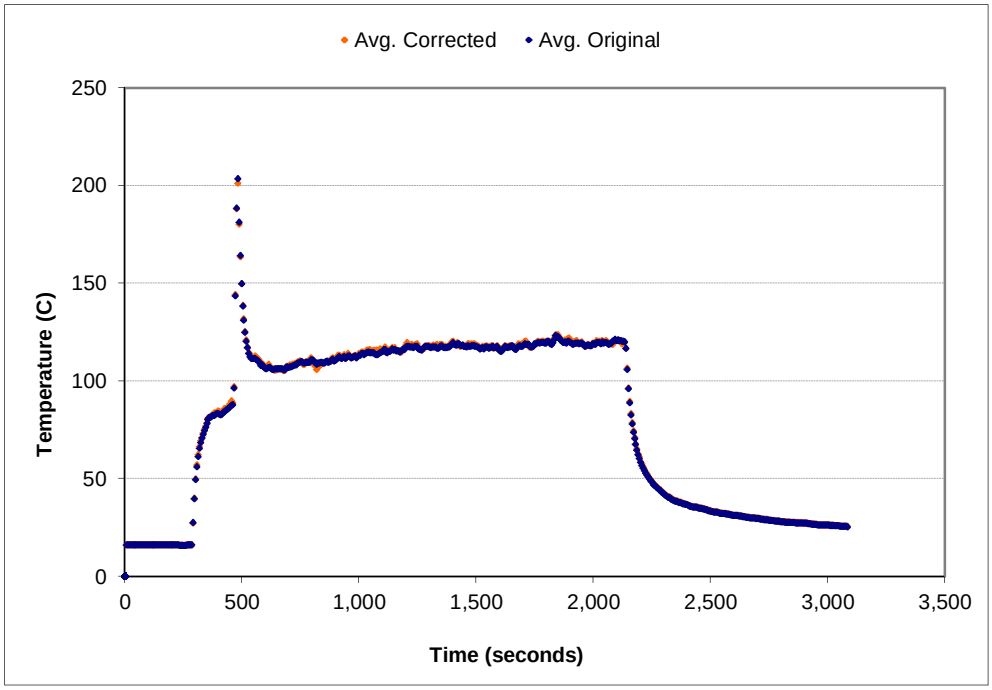

Figure A-45: Space-averaged (layer 5) temperature correction for the 0.5 g/s, ϕ_2 configuration

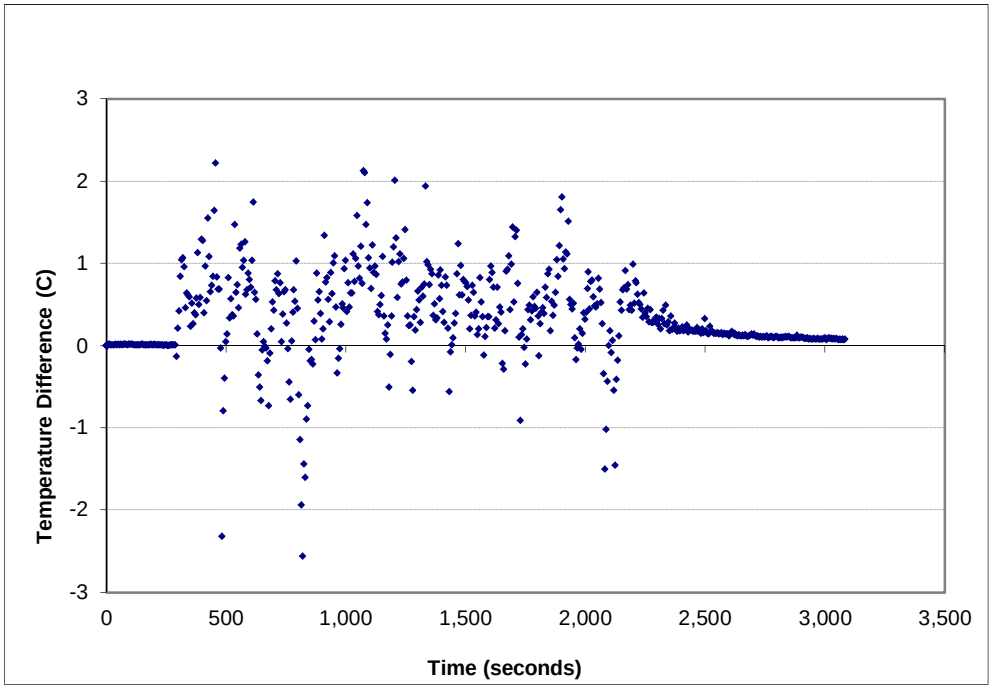

Figure A-46: Temperature error (layer 5) for the 0.5 g/s, ϕ_2 configuration

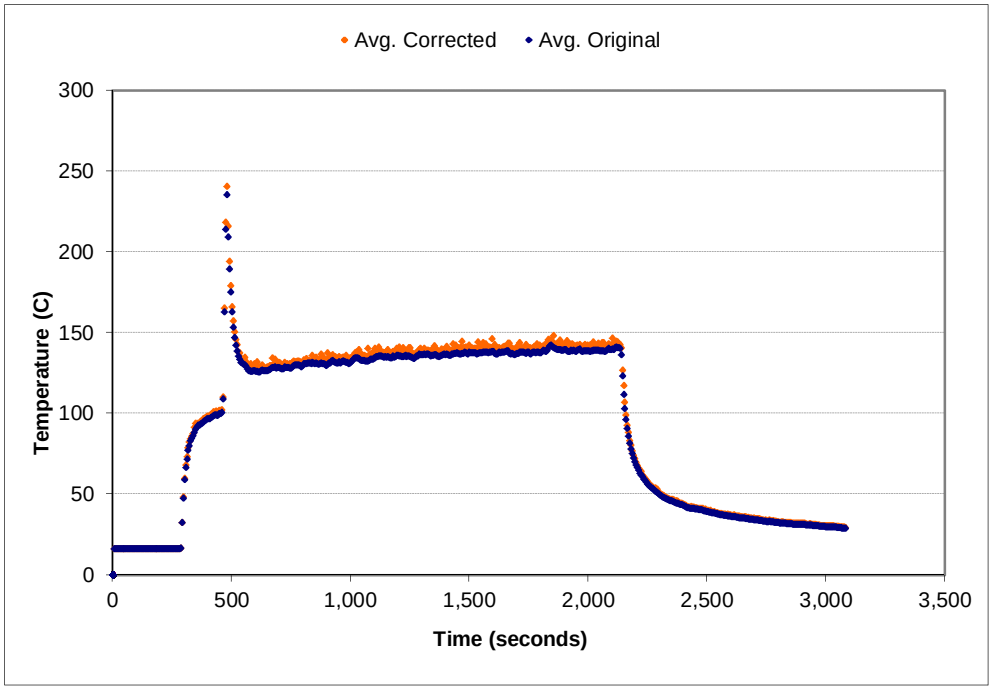

Figure A-47: Space-averaged (layer 6) temperature correction for the 0.5 g/s, ϕ_2 configuration

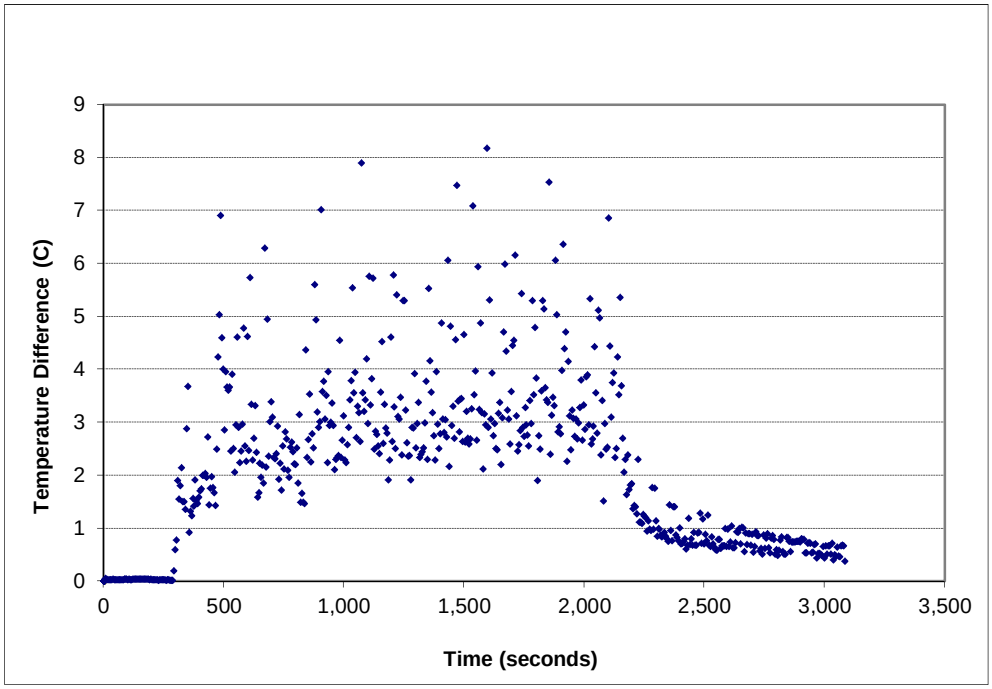

Figure A-48: Temperature error (layer 6) for the 0.5 g/s, ϕ_2 configuration

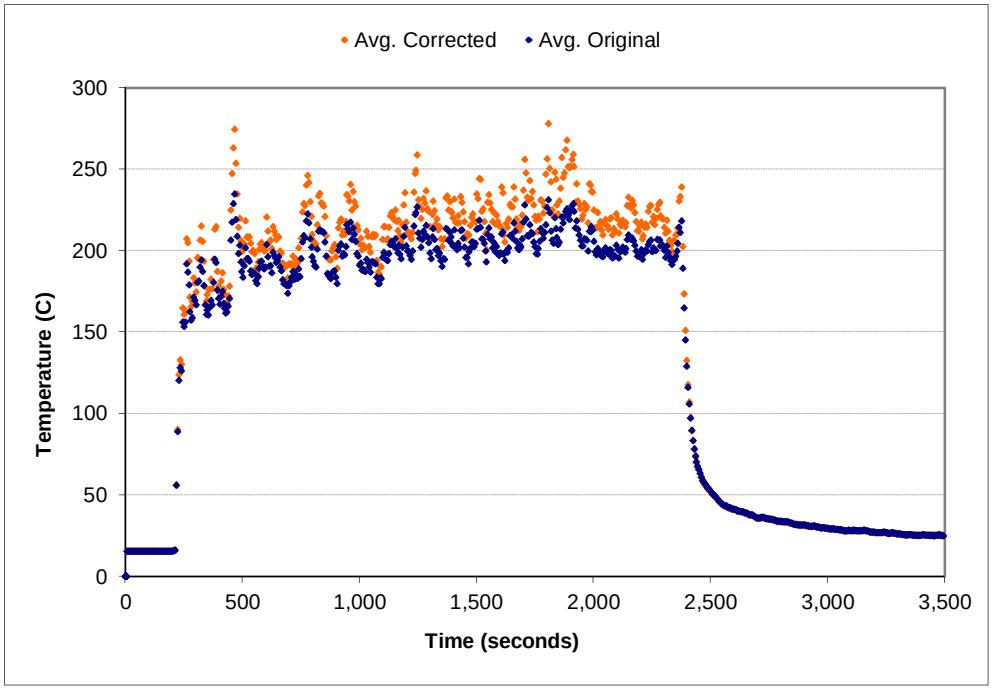

Figure A-49: Space-averaged (layer 1) temperature correction for the 1.0 g/s, ϕ_2 configuration

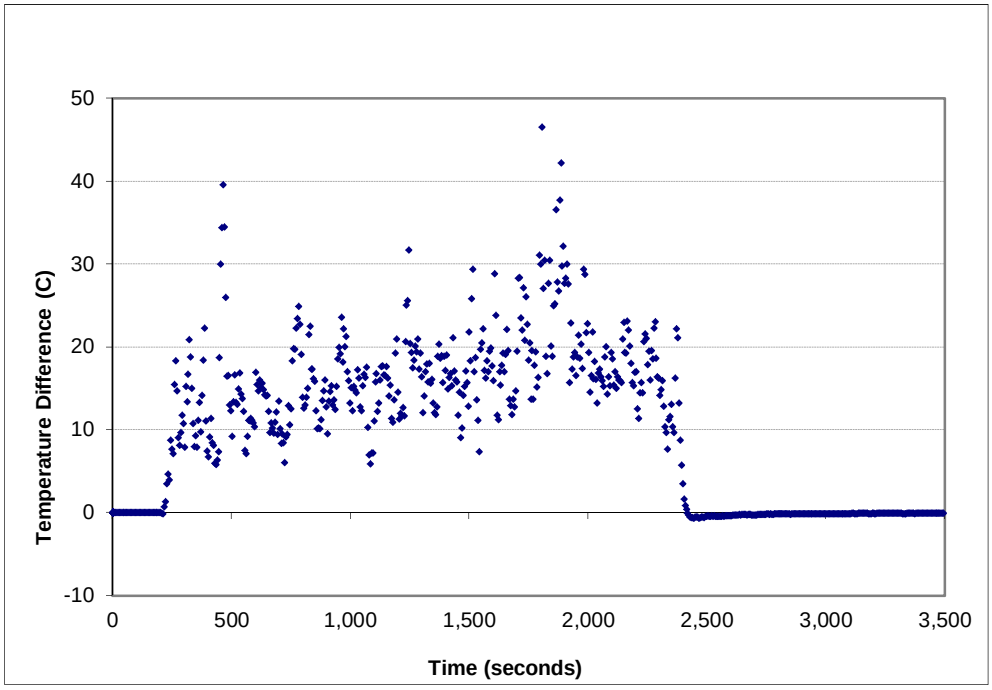

Figure A-50: Temperature error (layer 1) for the 1.0 g/s, ϕ_2 configuration

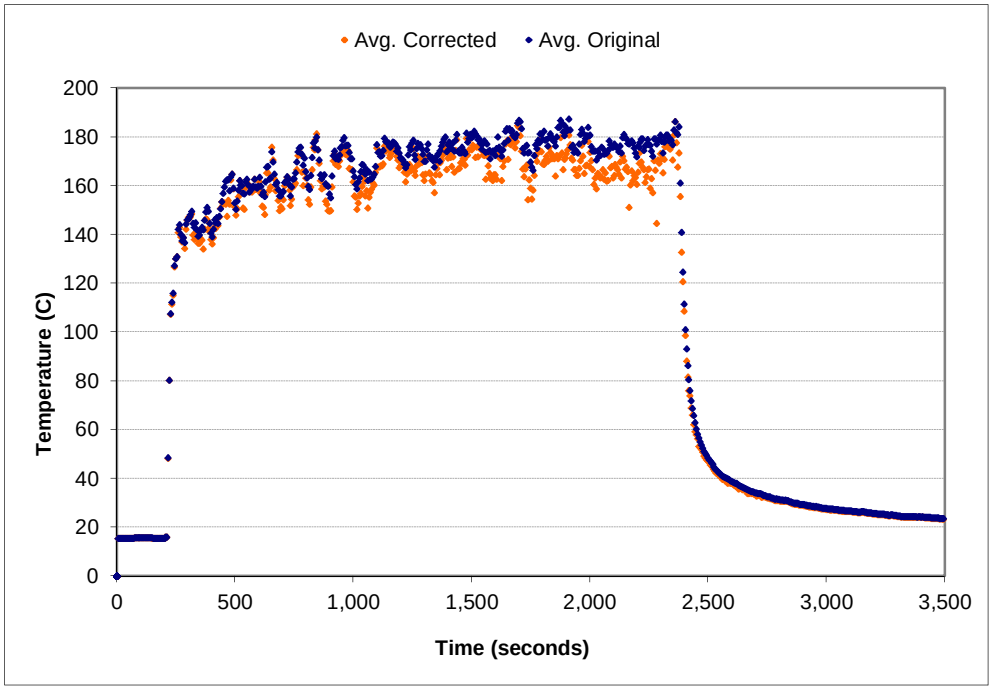

Figure A-51: Space-averaged (layer 2) temperature correction for the 1.0 g/s, ϕ_2 configuration

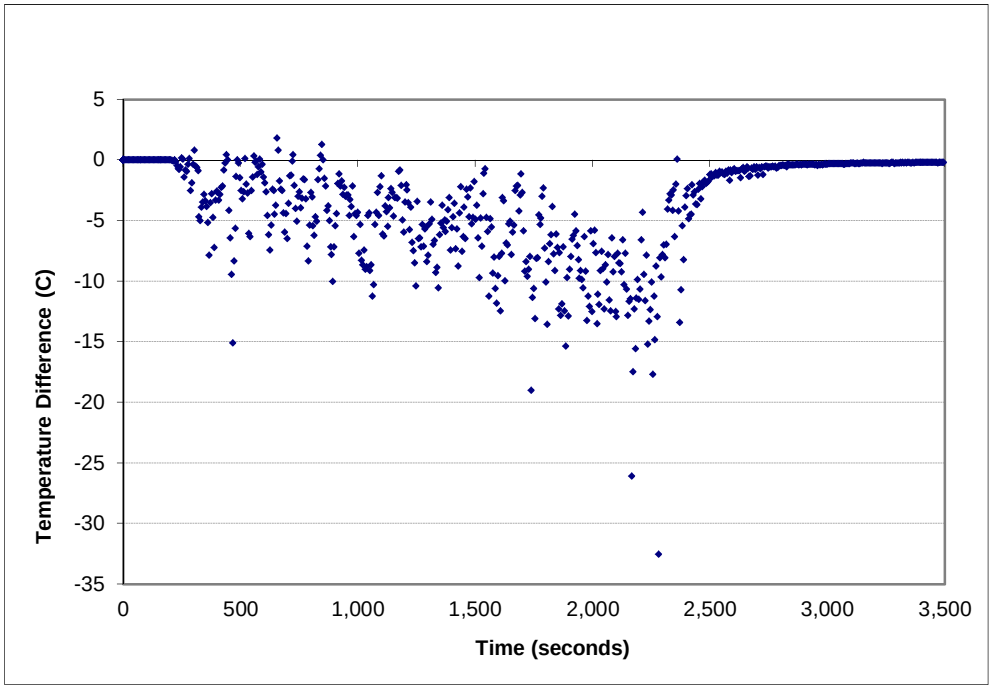

Figure A-52: Temperature error (layer 2) for the 1.0 g/s, ϕ_2 configuration

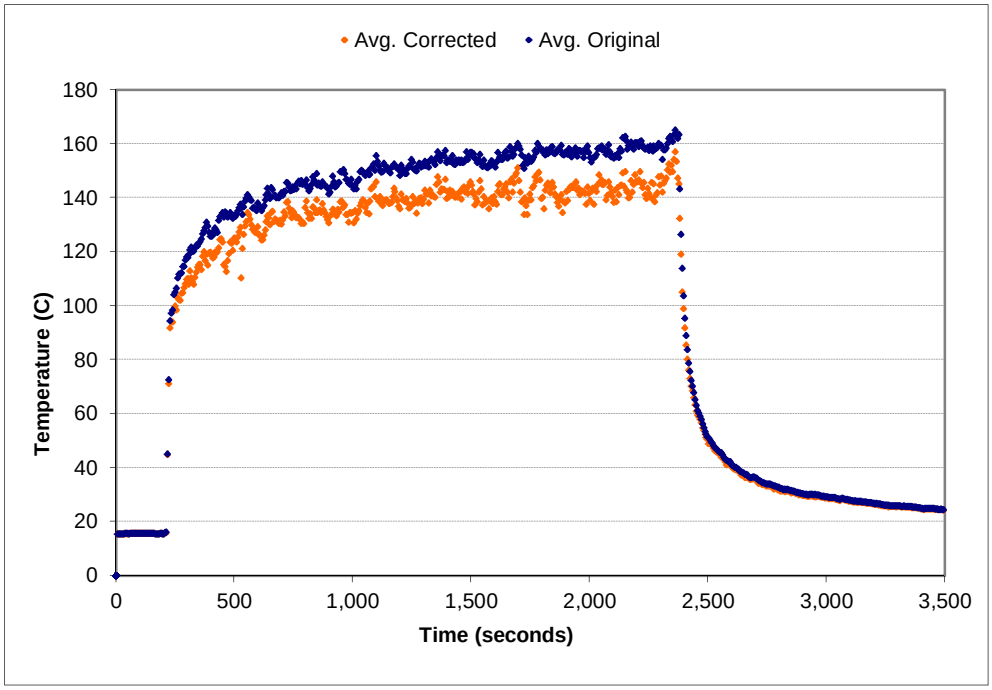

Figure A-53: Space-averaged (layer 3) temperature correction for the 1.0 g/s, ϕ_2 configuration

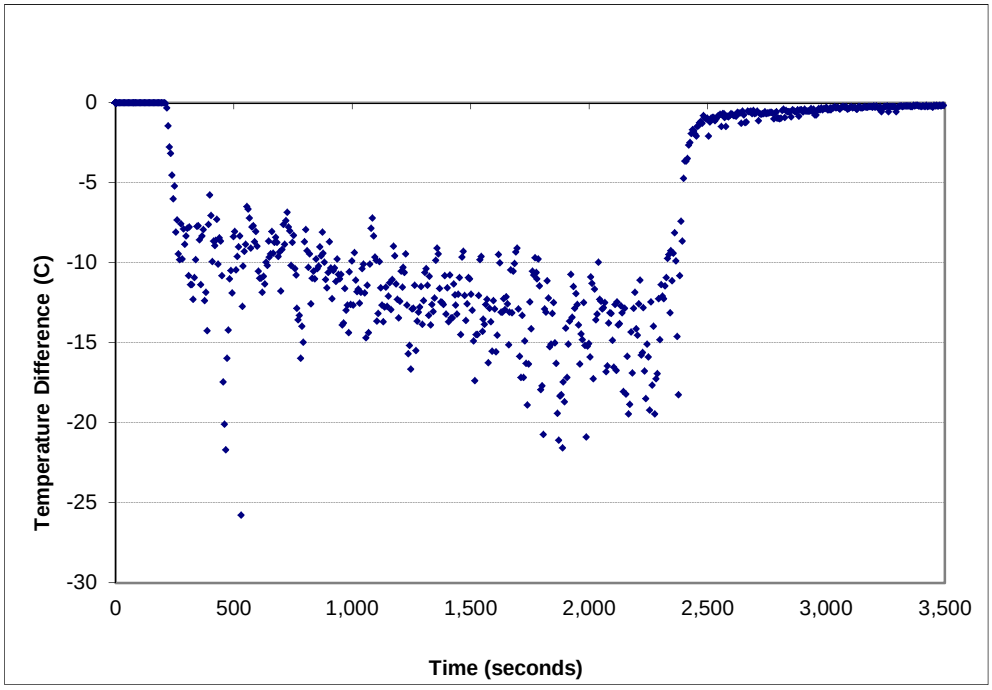

Figure A-54: Temperature error (layer 3) for the 1.0 g/s, ϕ_2 configuration

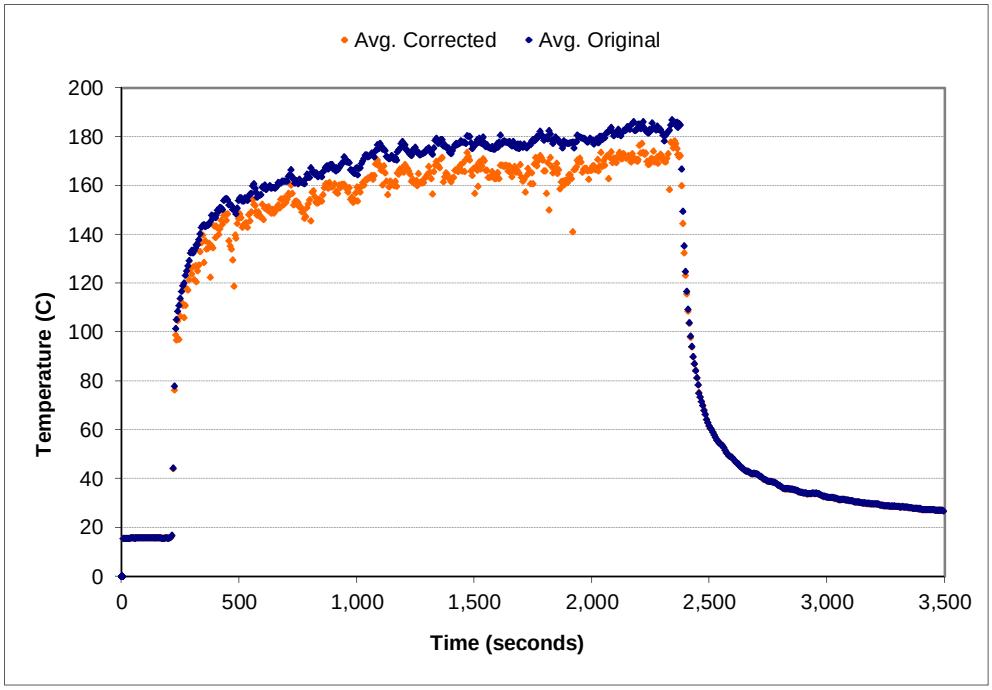

Figure A-55: Space-averaged (layer 4) temperature correction for the 1.0 g/s, ϕ_2 configuration

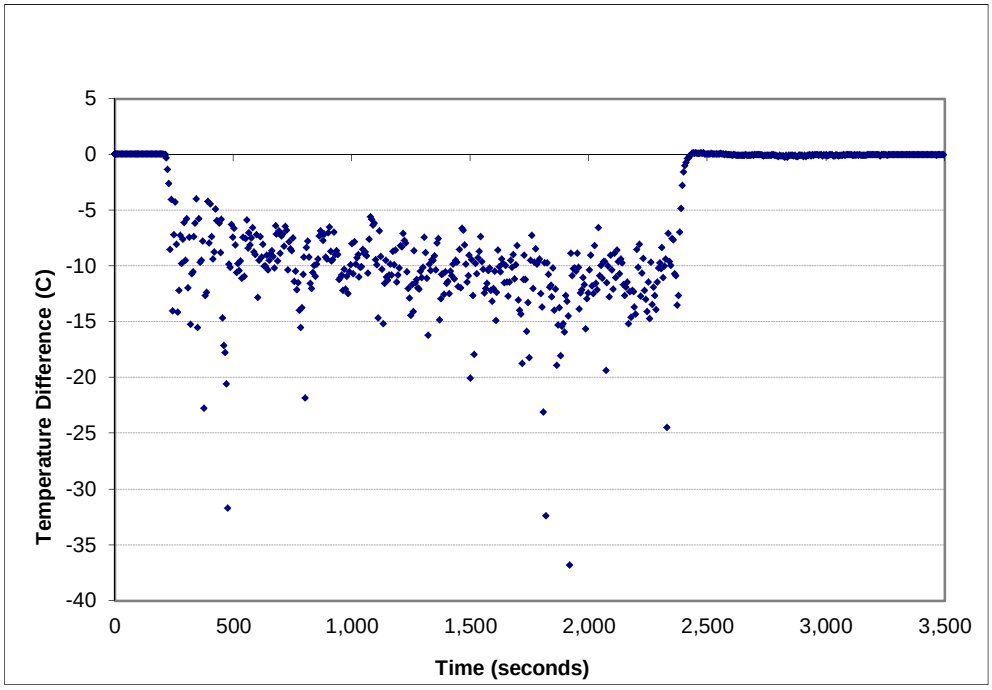

Figure A-56: Temperature error (layer 4) for the 1.0 g/s, ϕ_2 configuration

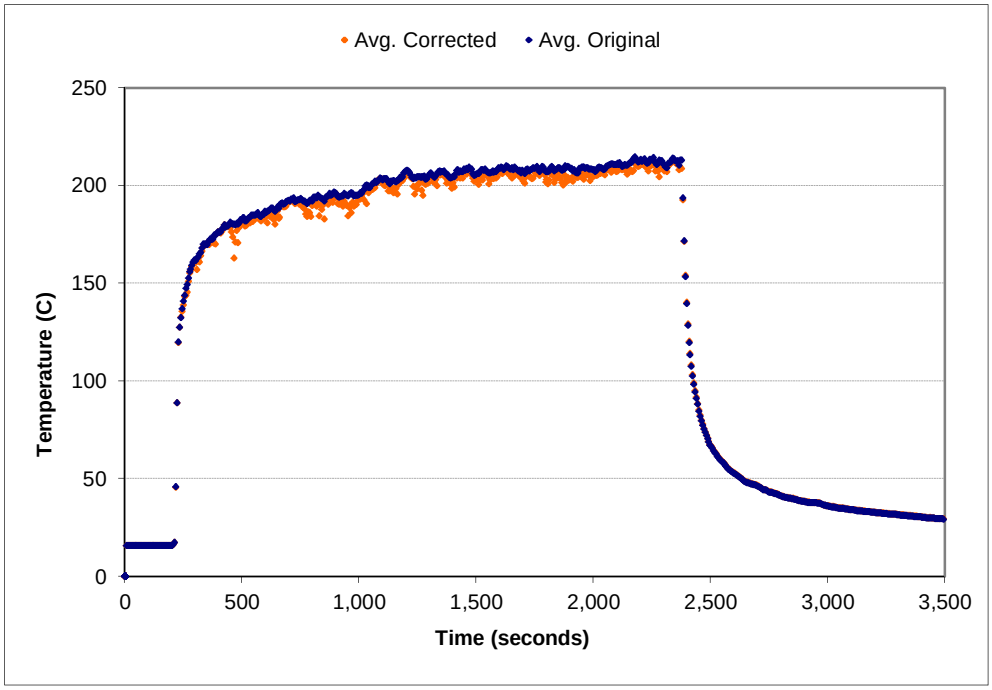

Figure A-57: Space-averaged (layer 5) temperature correction for the 1.0 g/s, ϕ_2 configuration

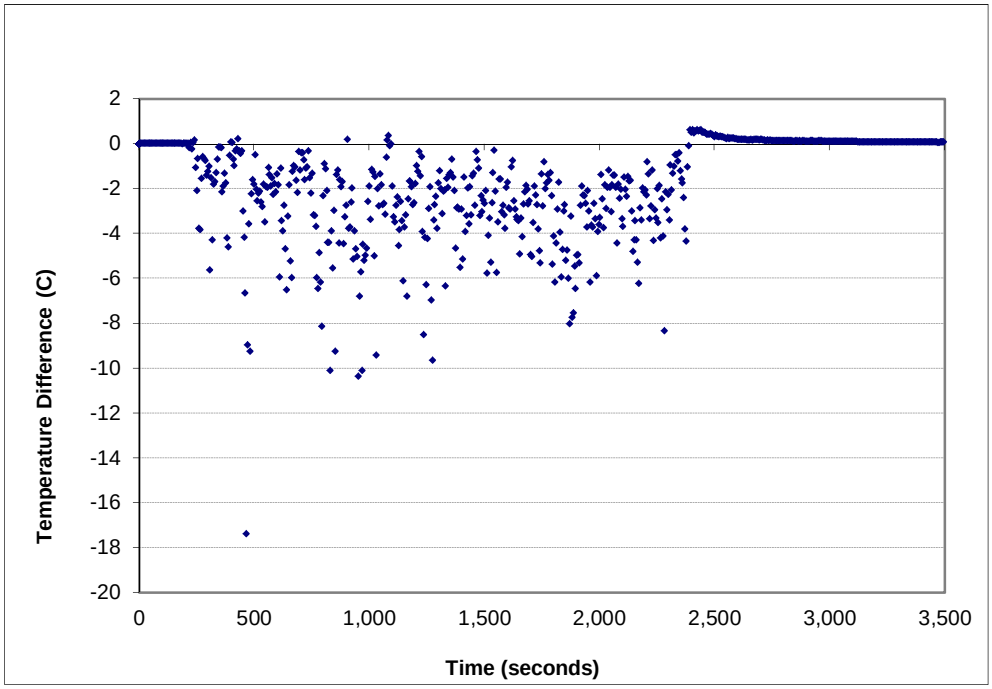

Figure A-58: Temperature error (layer 5) for the 1.0 g/s, ϕ_2 configuration

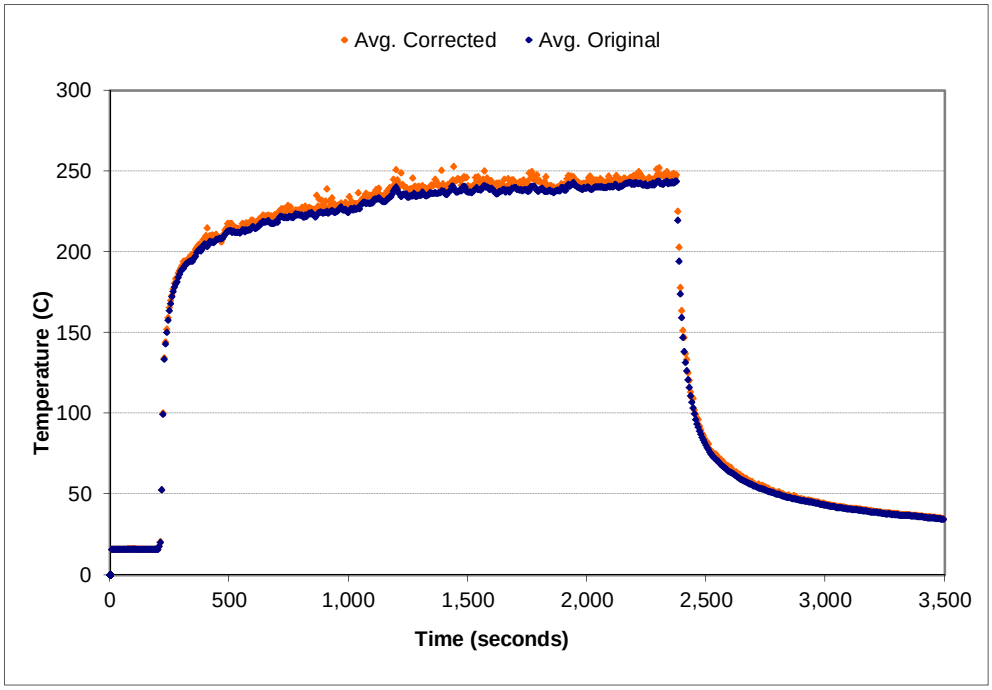

Figure A-59: Space-averaged (layer 6) temperature correction for the 1.0 g/s, ϕ_2 configuration

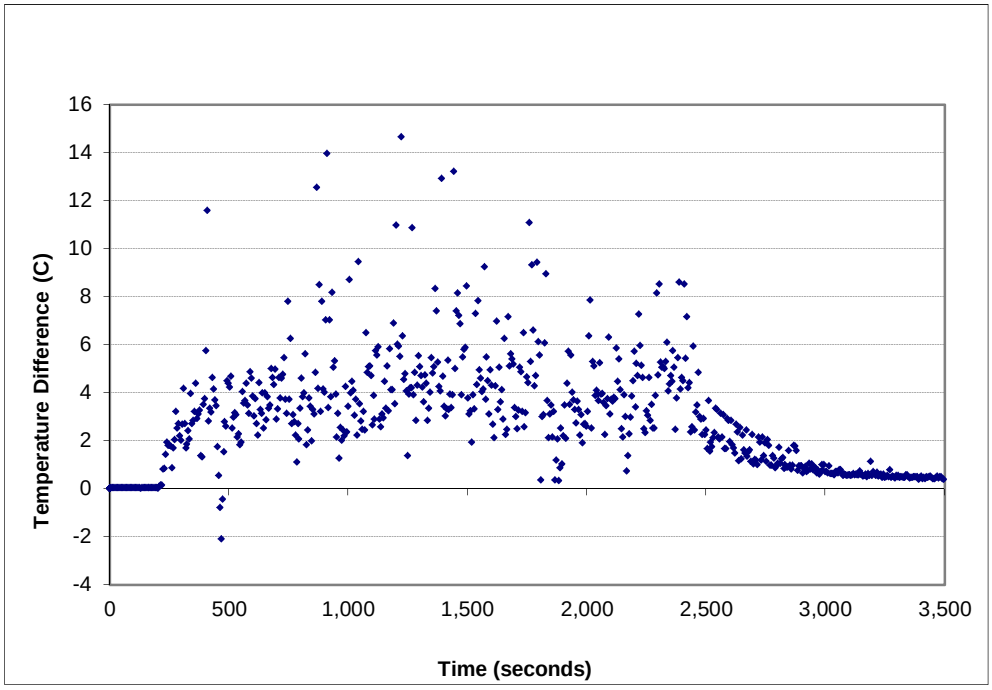

Figure A-60: Temperature error (layer 6) for the 1.0 g/s, ϕ_2 configuration

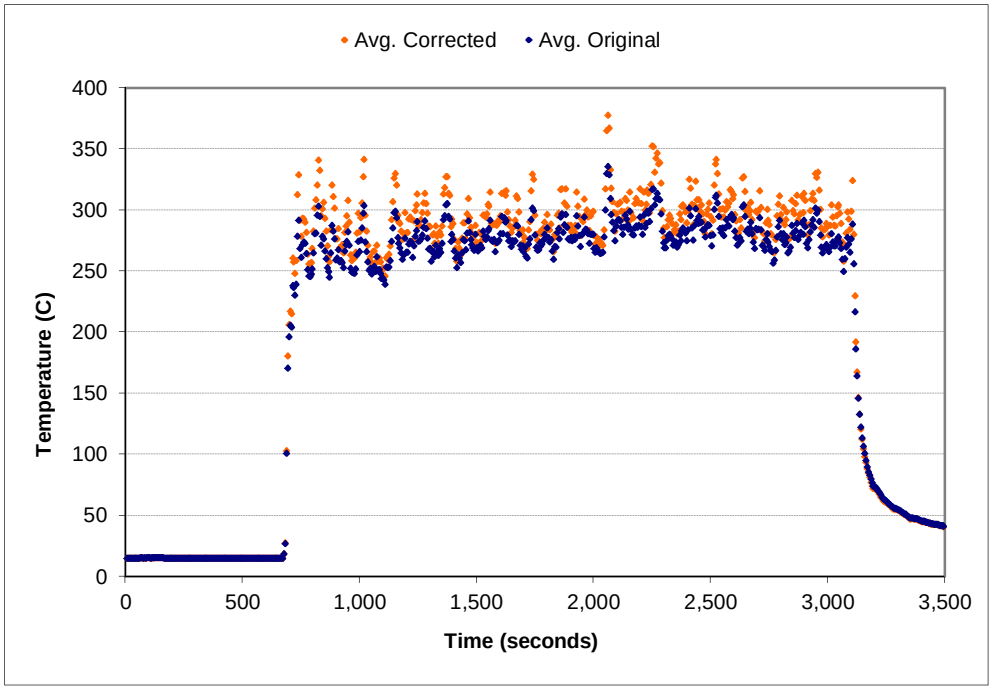

Figure A-61: Space-averaged (layer 1) temperature correction for the 1.5 g/s, ϕ_2 configuration

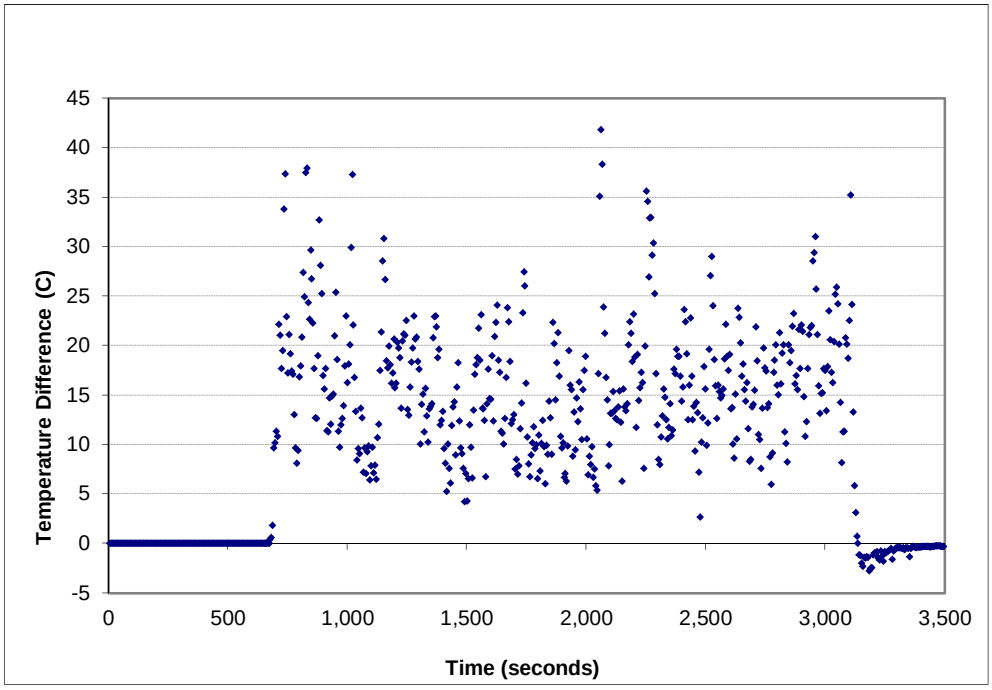

Figure A-62: Temperature error (layer 1) for the 1.5 g/s, ϕ_2 configuration

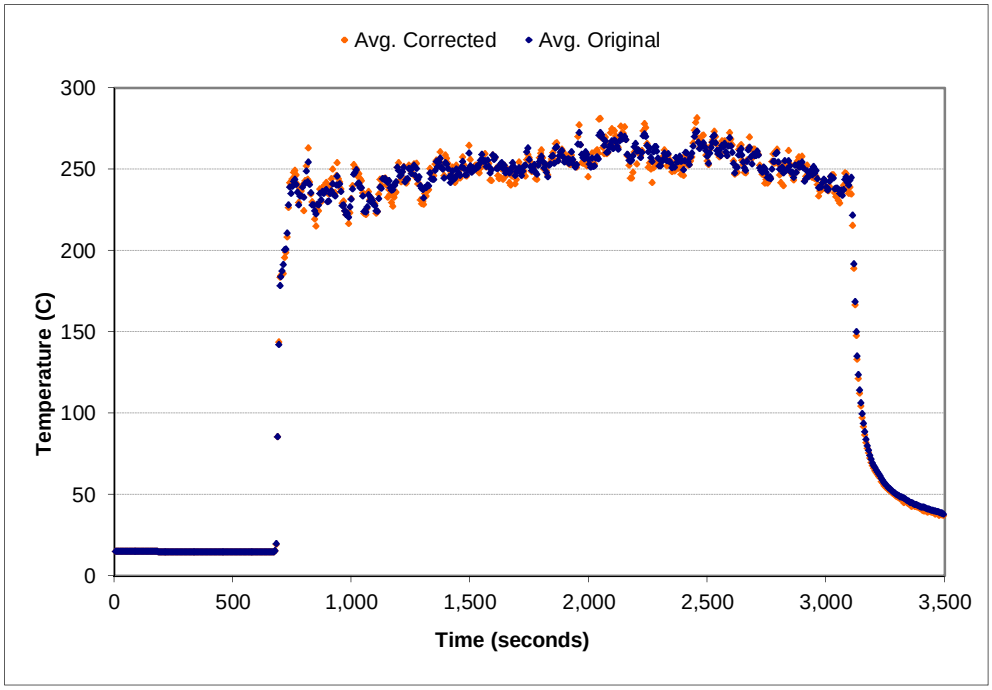

Figure A-63: Space-averaged (layer 2) temperature correction for the 1.5 g/s, ϕ_2 configuration

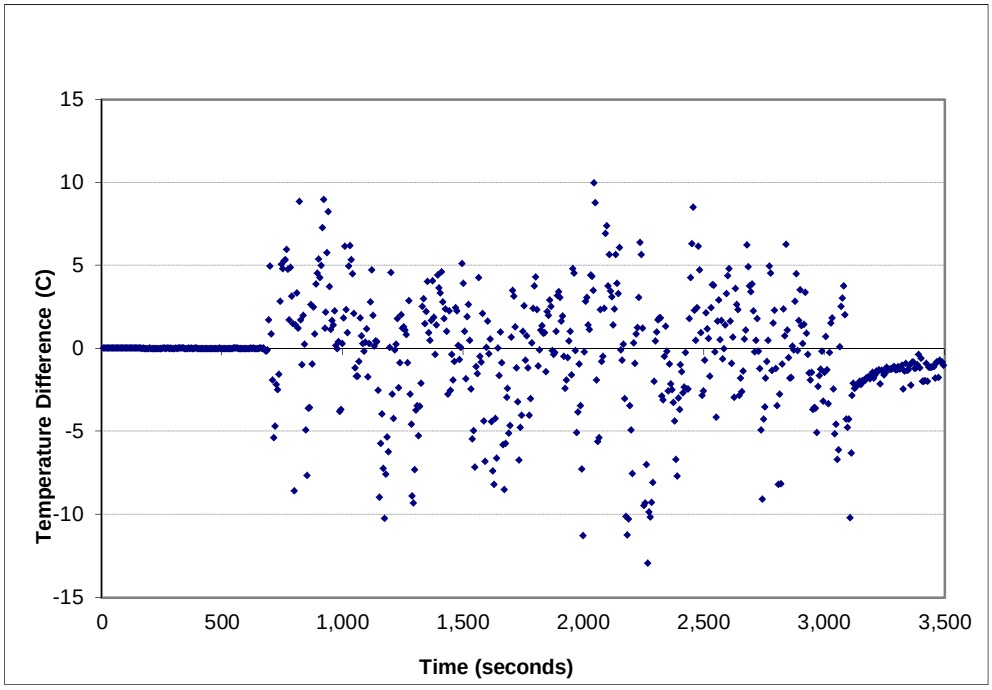

Figure A-64: Temperature error (layer 2) for the 1.5 g/s, ϕ_2 configuration

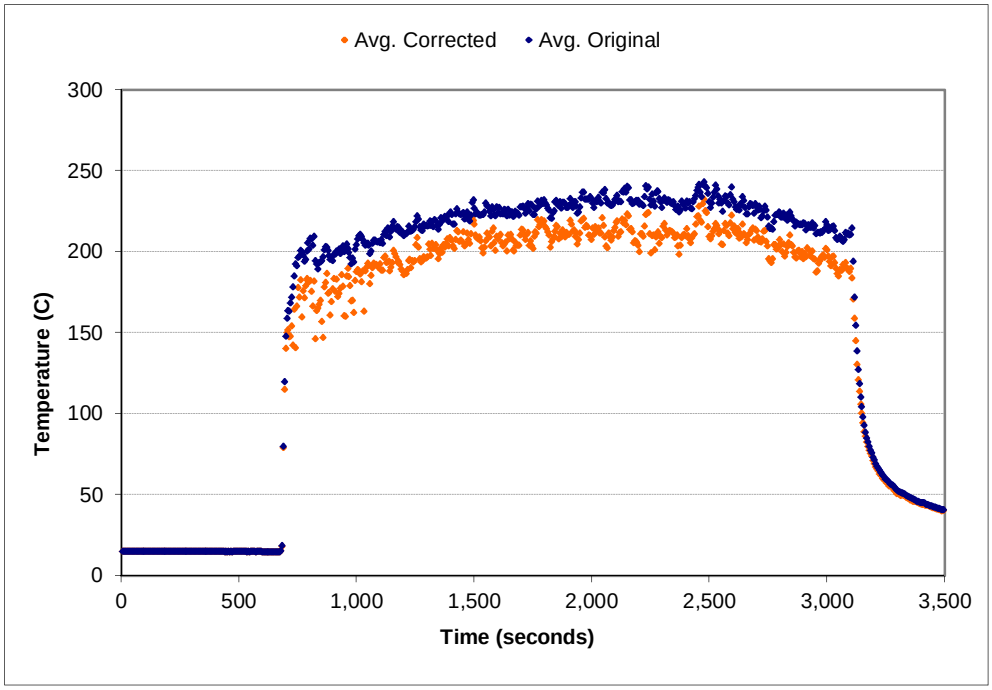

Figure A-65: Space-averaged (layer 3) temperature correction for the 1.5 g/s, ϕ_2 configuration

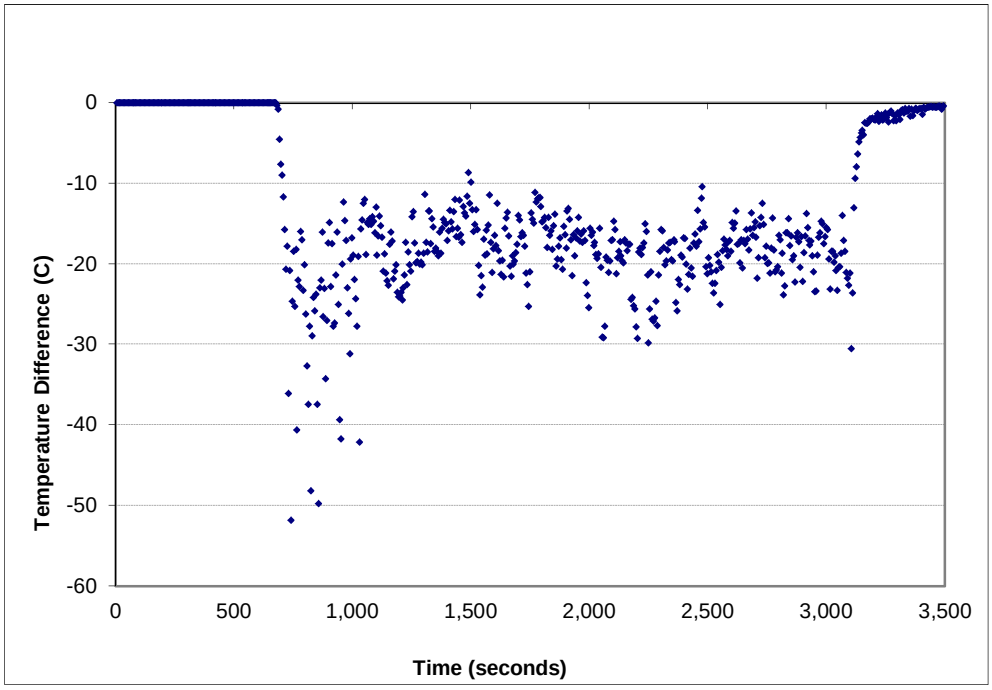

Figure A-66: Temperature error (layer 3) for the 1.5 g/s, ϕ_2 configuration

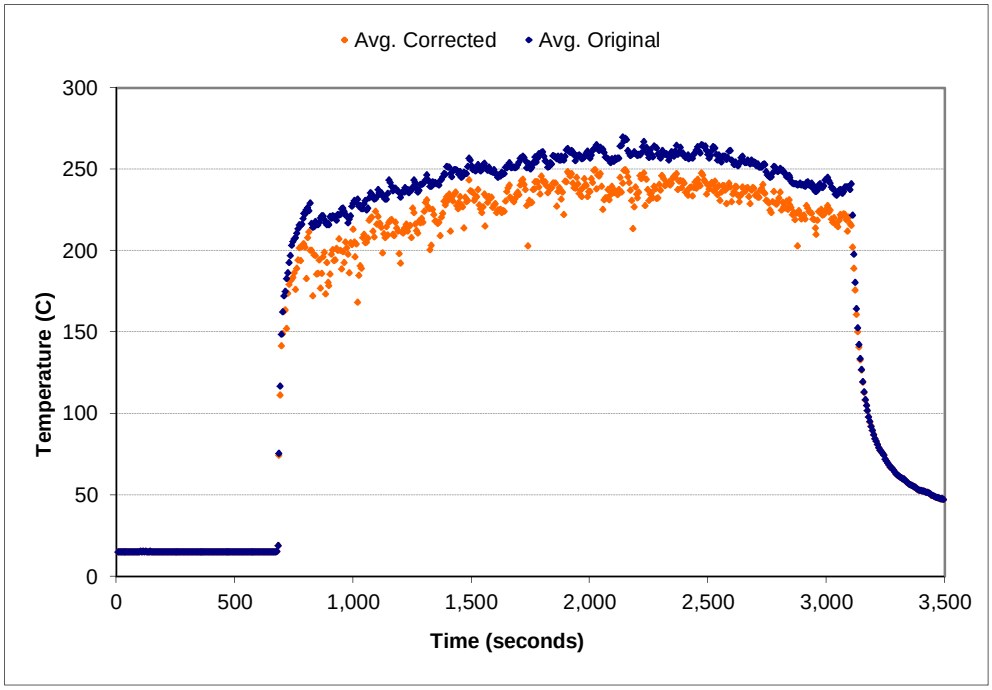

Figure A-67: Space-averaged (layer 4) temperature correction for the 1.5 g/s, ϕ_2 configuration

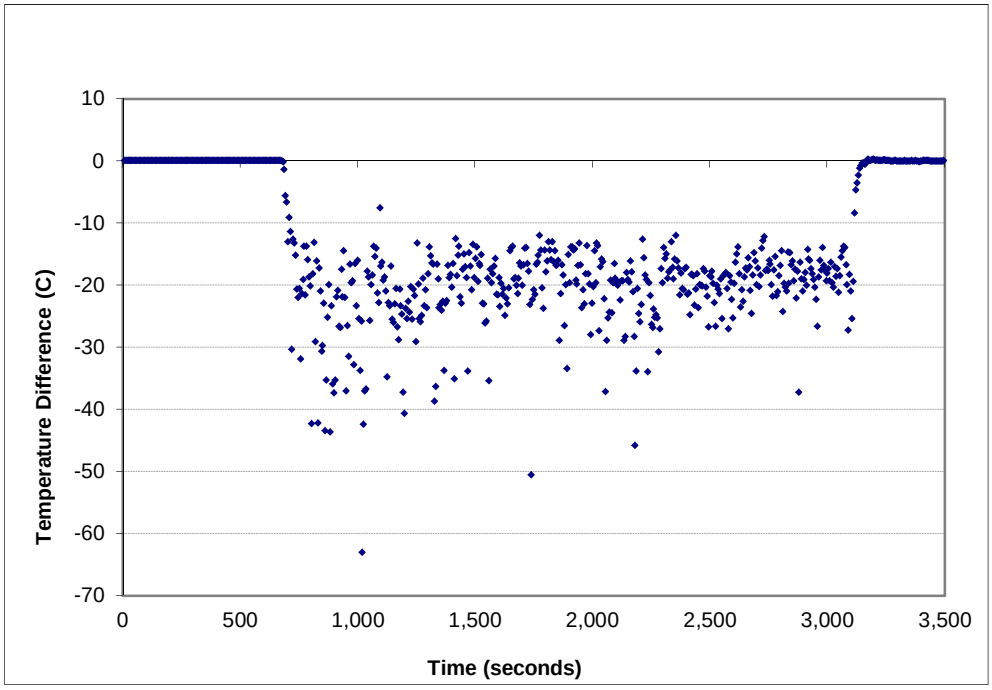

Figure A-68: Temperature error (layer 4) for the 1.5 g/s, ϕ_2 configuration

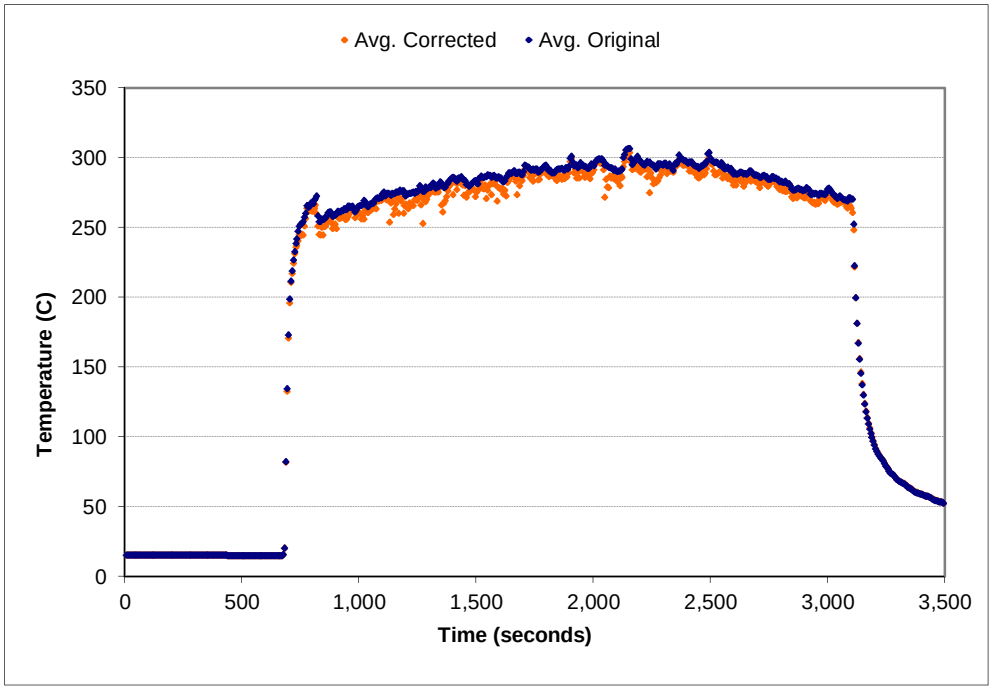

Figure A-69: Space-averaged (layer 5) temperature correction for the 1.5 g/s, ϕ_2 configuration

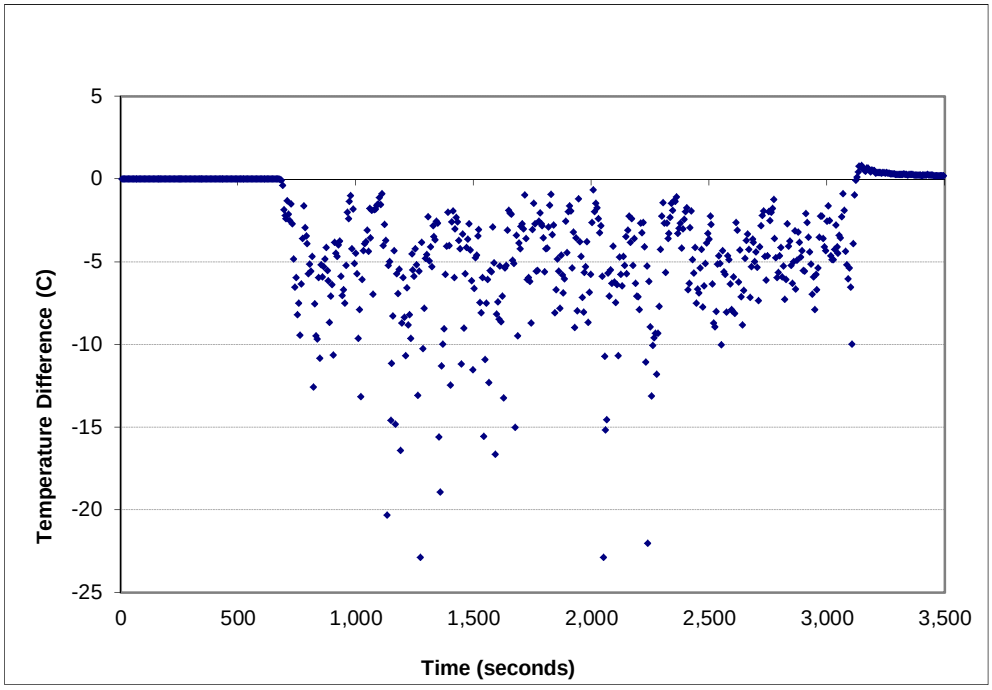

Figure A-70: Temperature error (layer 5) for the 1.5 g/s, ϕ_2 configuration

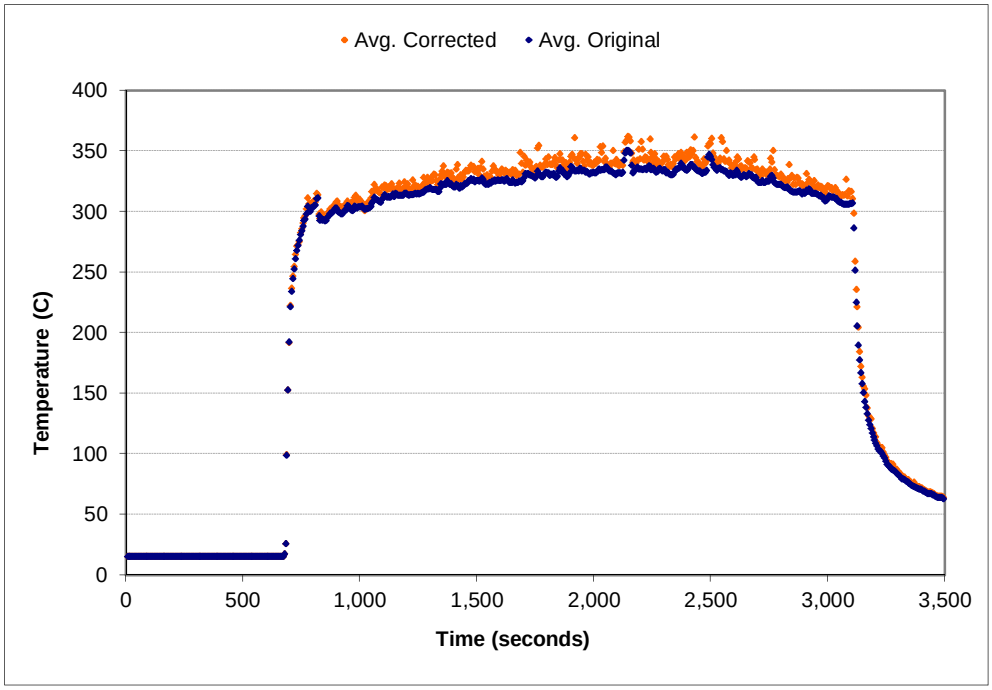

Figure A-71: Space-averaged (layer 6) temperature correction for the 1.5 g/s, ϕ_2 configuration

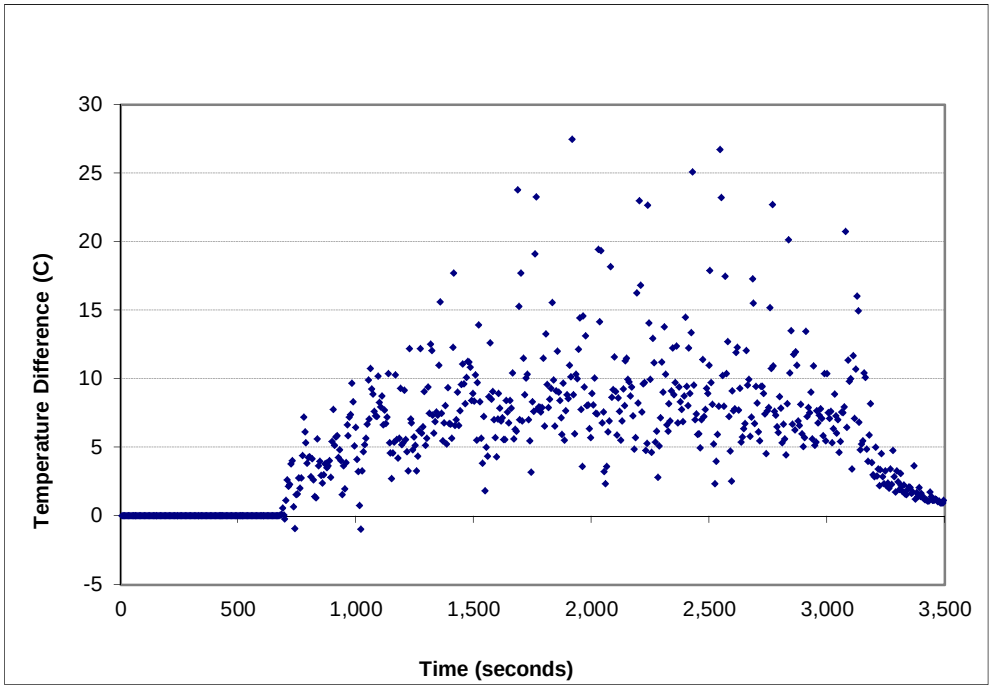

Figure A-72: Temperature error (layer 6) for the 1.5 g/s, ϕ_2 configuration

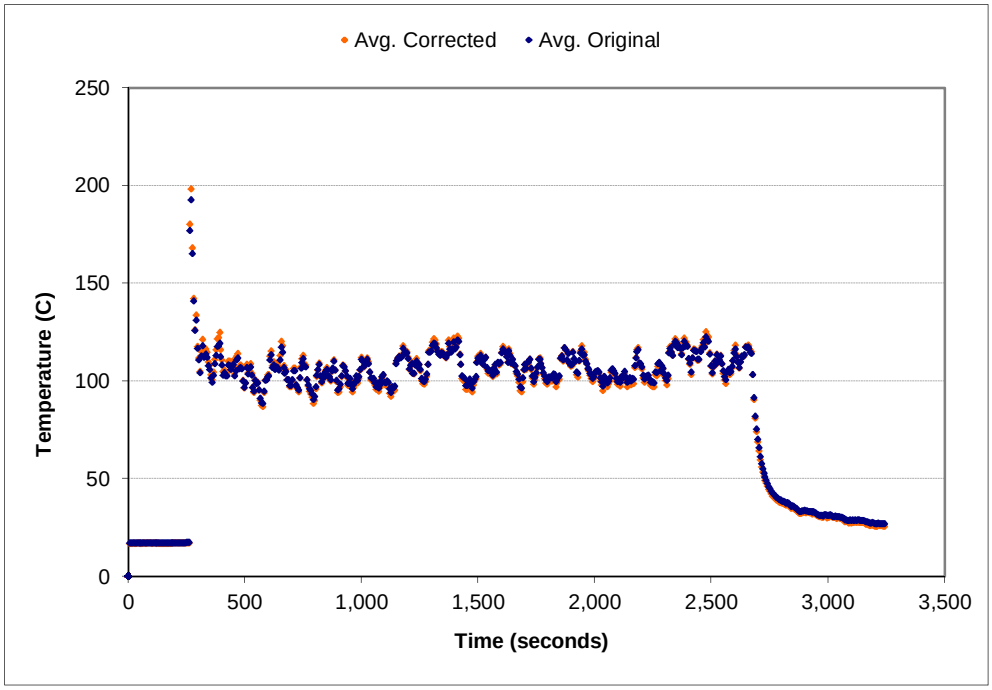

Figure A-73: Space-averaged (layer 1) temperature correction for the 0.5 g/s, ϕ_3 configuration

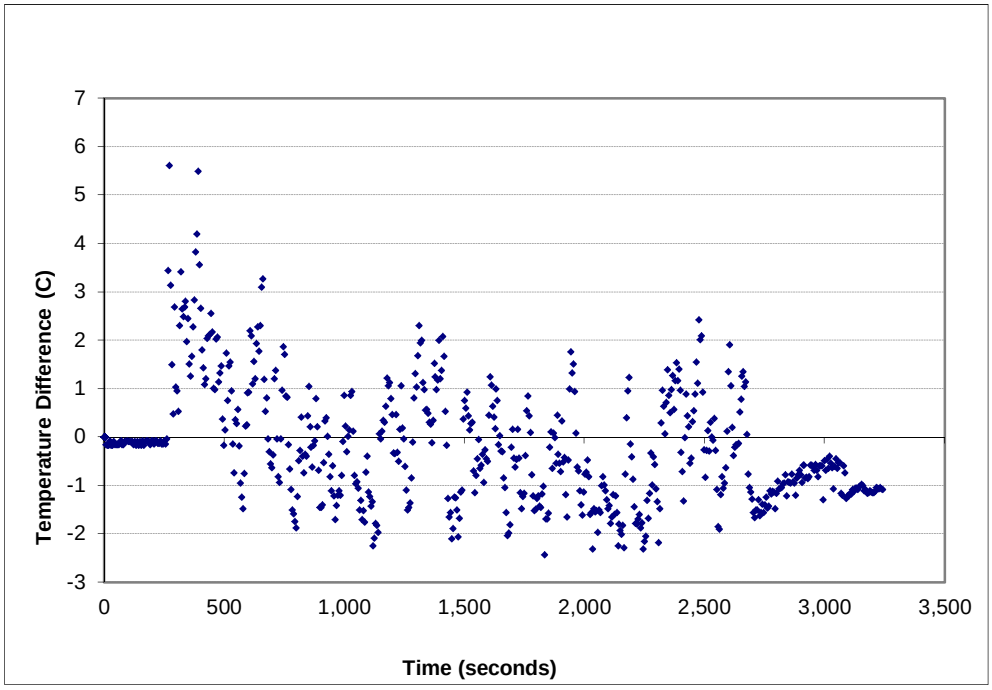

Figure A-74: Temperature error (layer 1) for the 0.5 g/s, ϕ_3 configuration

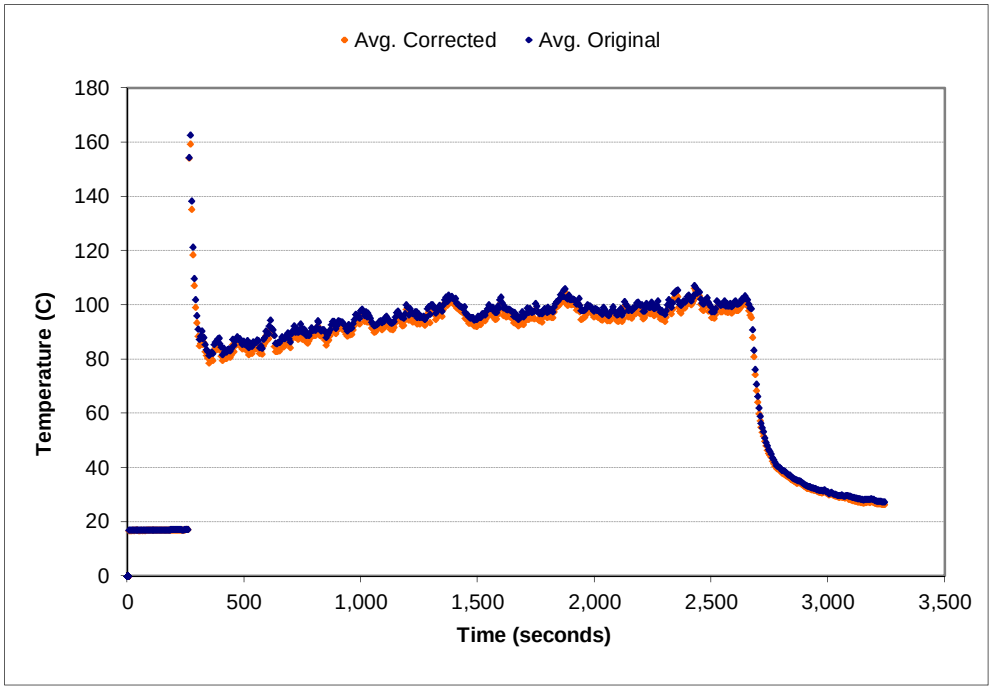

Figure A-75: Space-averaged (layer 2) temperature correction for the 0.5 g/s, ϕ_3 configuration

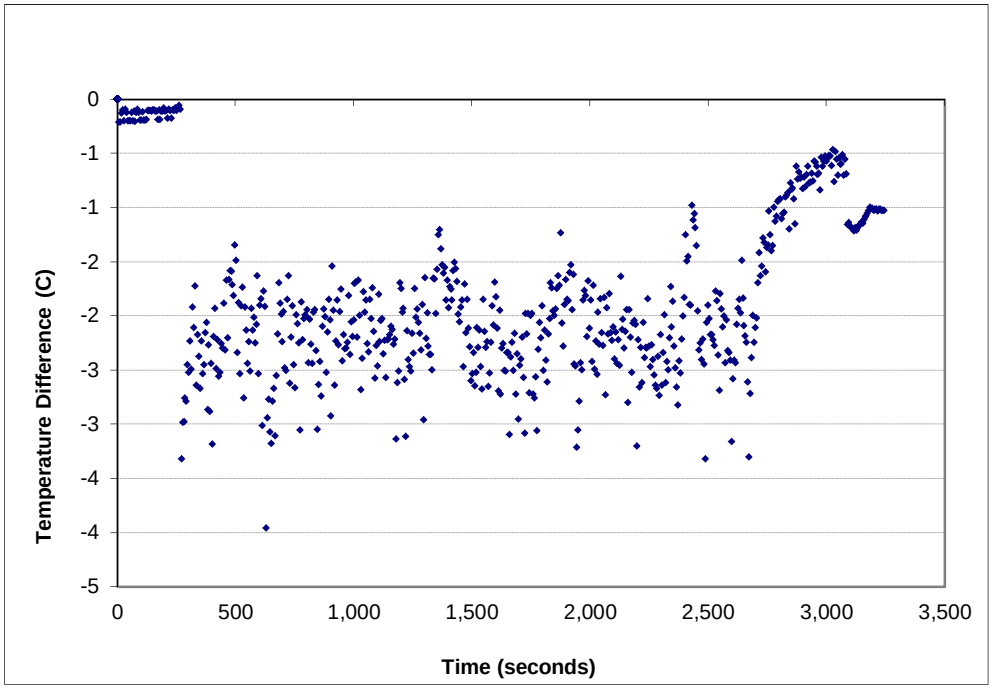

Figure A-76: Temperature error (layer 2) for the 0.5 g/s, ϕ_3 configuration

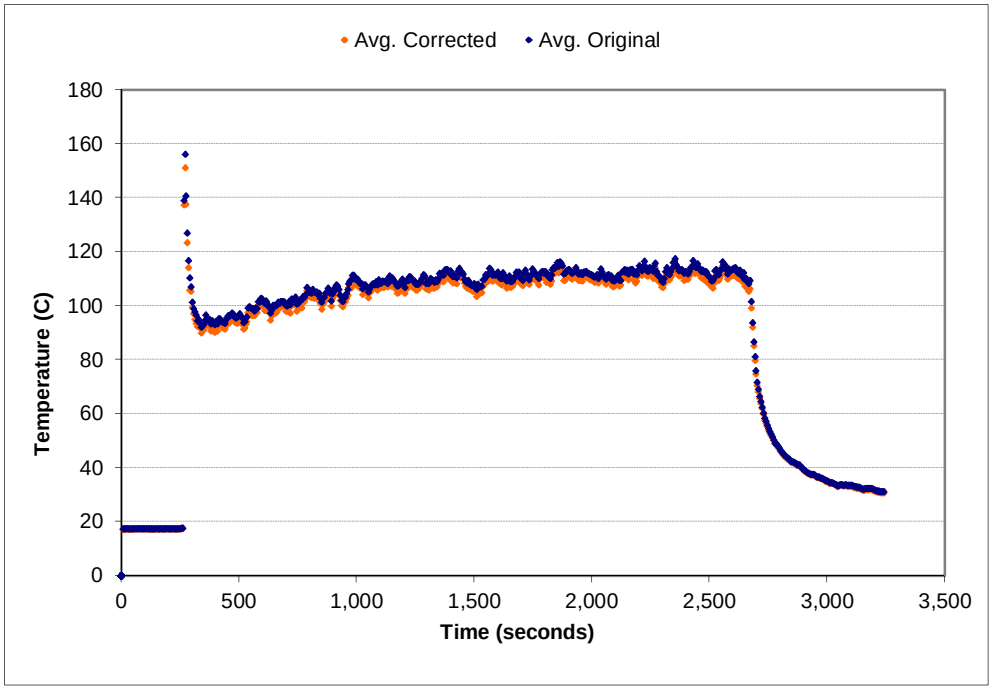

Figure A-77: Space-averaged (layer 3) temperature correction for the 0.5 g/s, ϕ_3 configuration

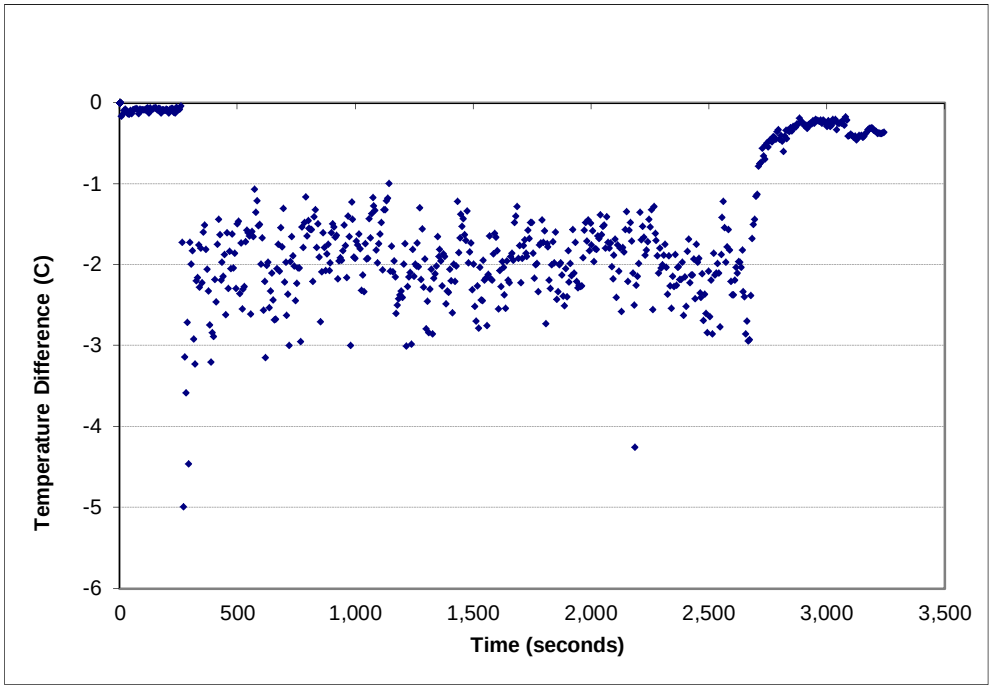

Figure A-78: Temperature error (layer 3) for the 0.5 g/s, ϕ_3 configuration

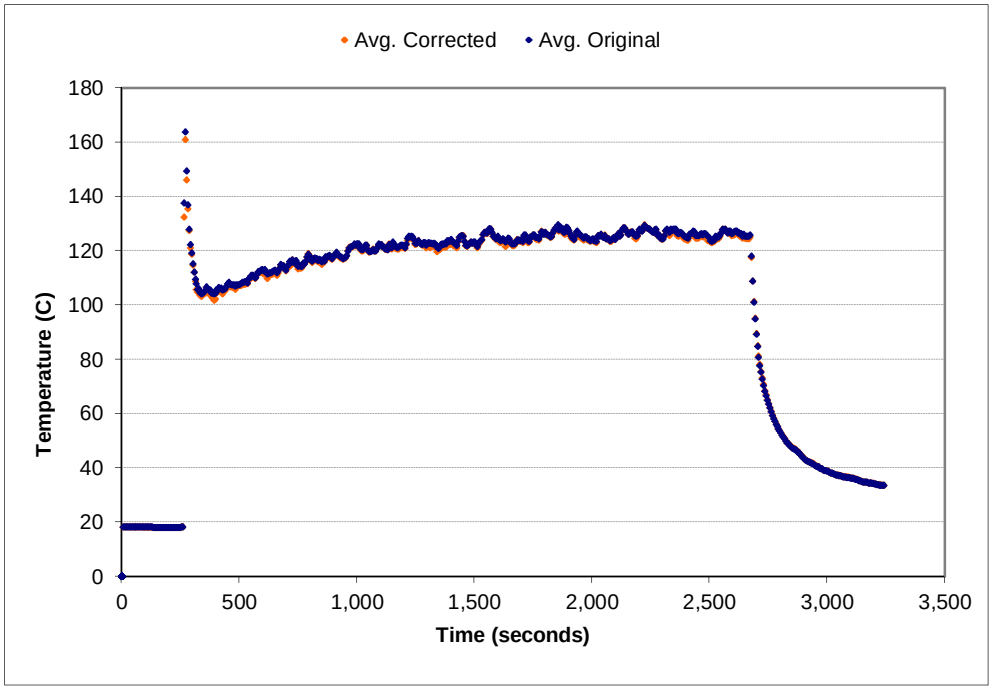

Figure A-79: Space-averaged (layer 4) temperature correction for the 0.5 g/s, ϕ_3 configuration

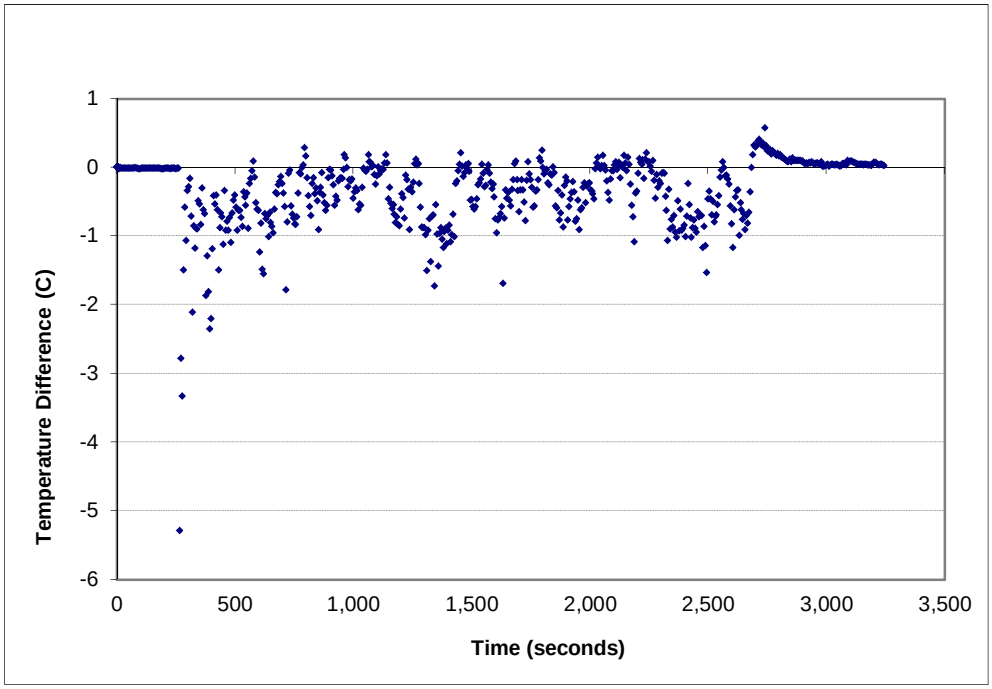

Figure A-80: Temperature error (layer 4) for the 0.5 g/s, ϕ_3 configuration

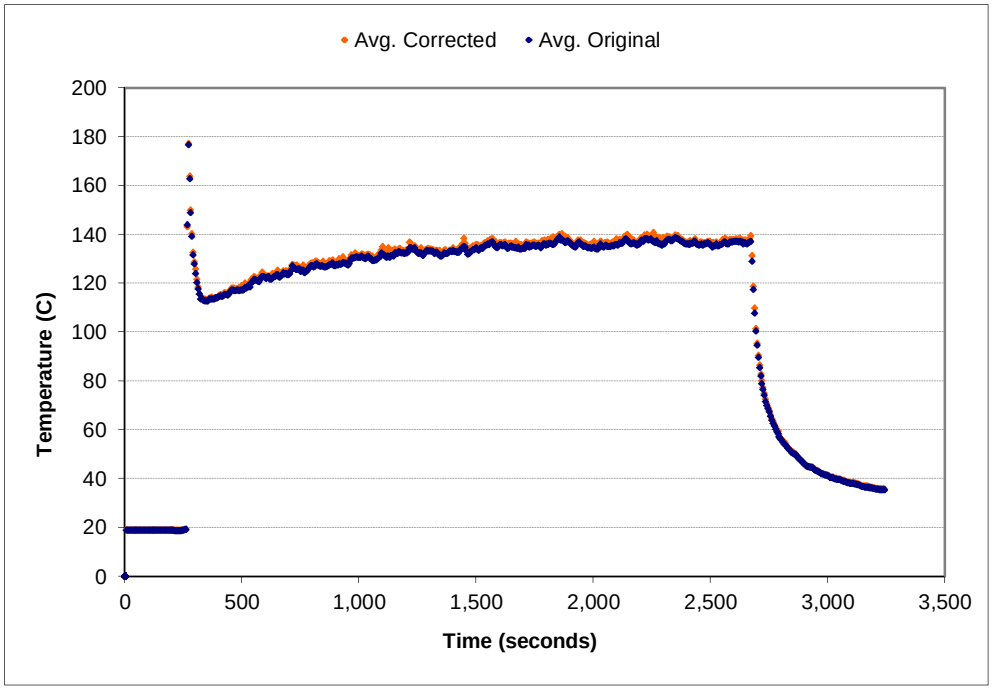

Figure A-81: Space-averaged (layer 5) temperature correction for the 0.5 g/s, ϕ_3 configuration

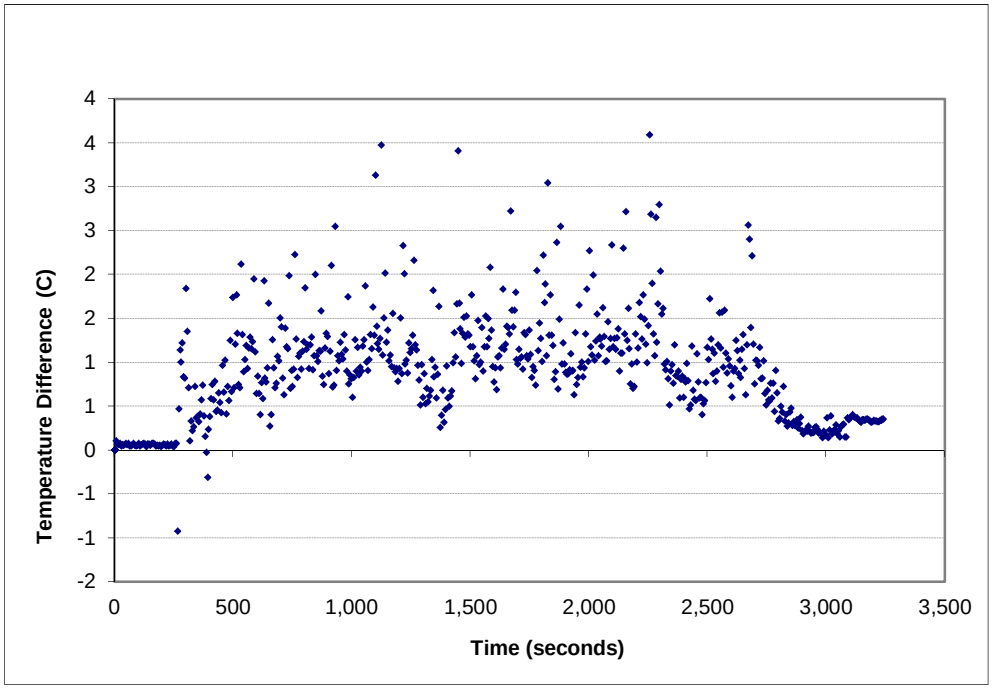

Figure A-82: Temperature error (layer 5) for the 0.5 g/s, ϕ_3 configuration

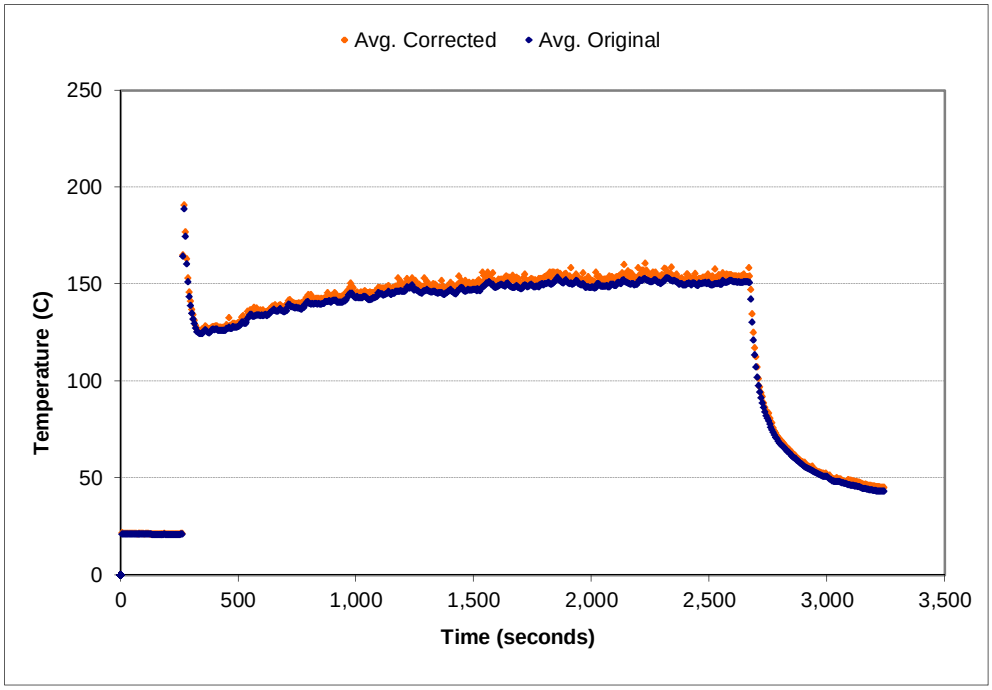

Figure A-83: Space-averaged (layer 6) temperature correction for the 0.5 g/s, ϕ_3 configuration

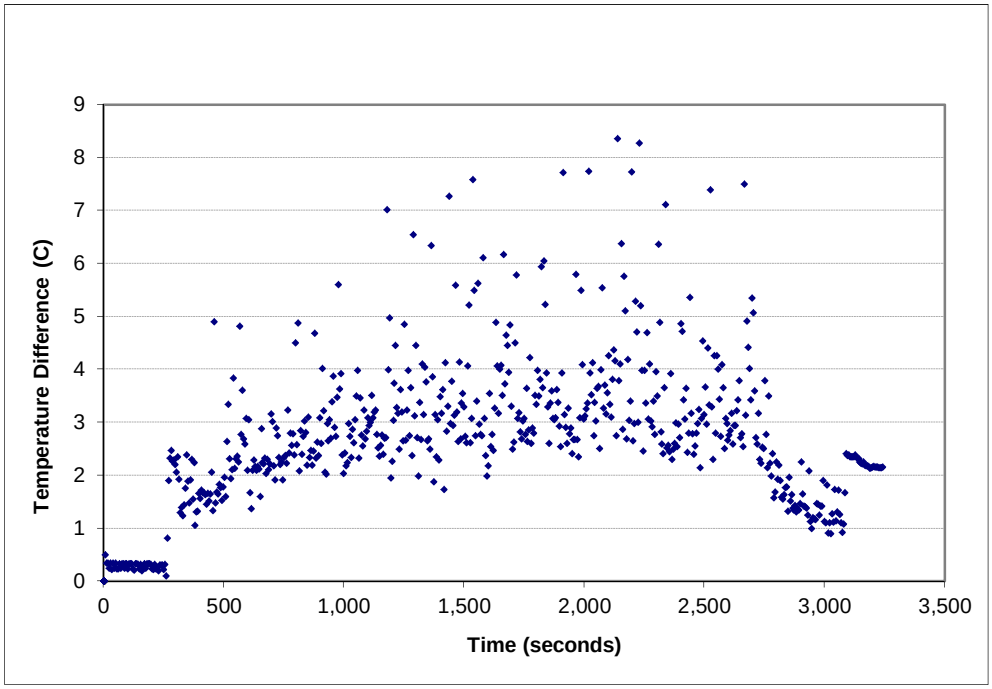

Figure A-84: Temperature error (layer 6) for the 0.5 g/s, ϕ_3 configuration

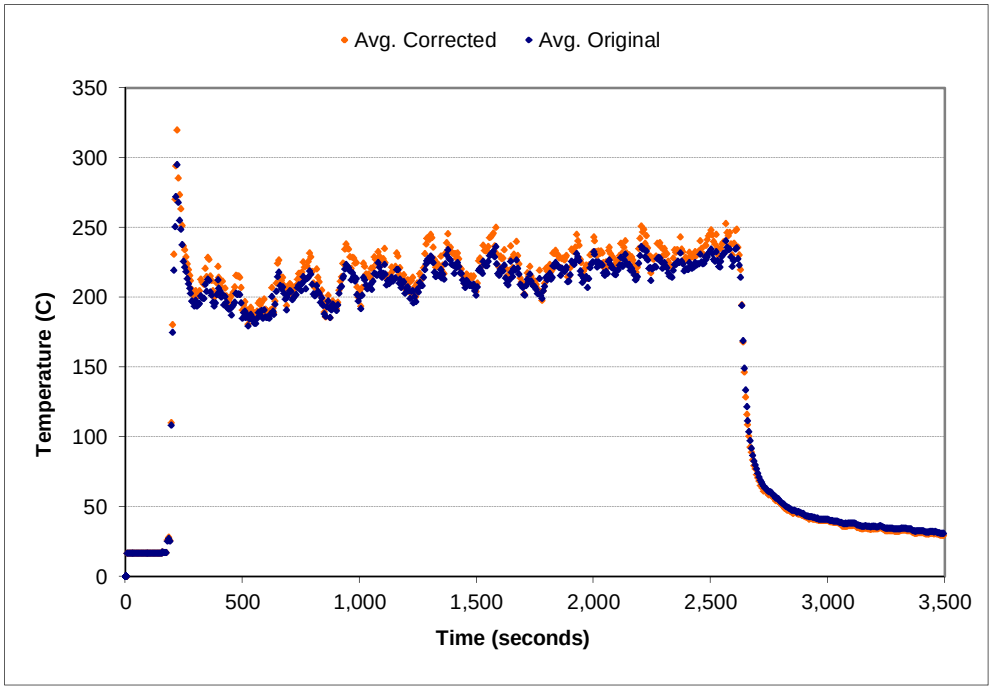

Figure A-85: Space-averaged (layer 1) temperature correction for the 1.0 g/s, ϕ_3 configuration

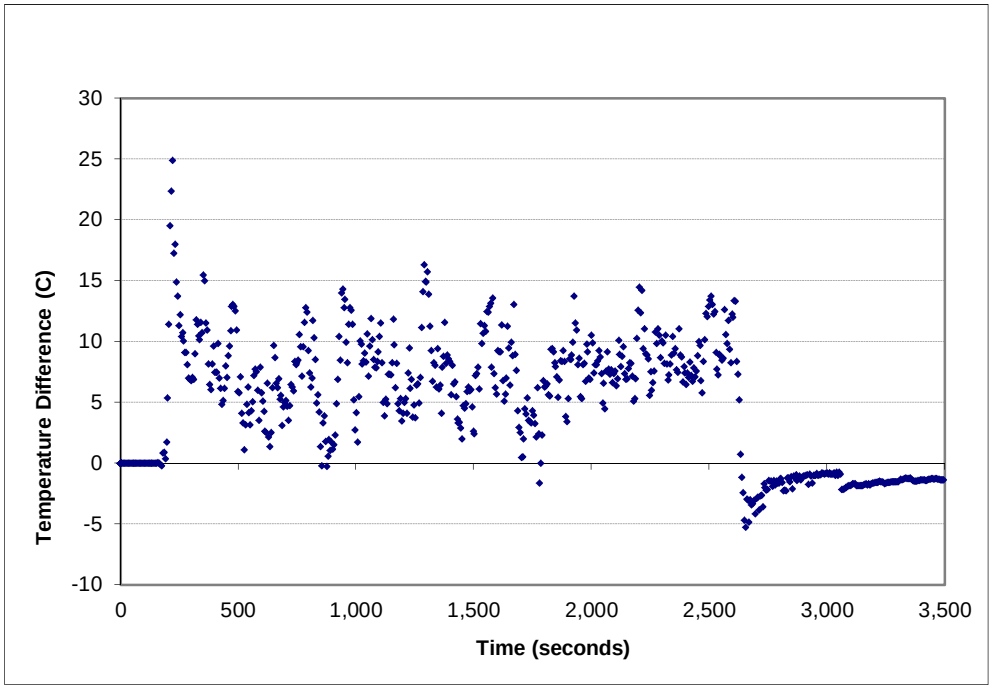

Figure A-86: Temperature error (layer 1) for the 1.0 g/s, ϕ_3 configuration

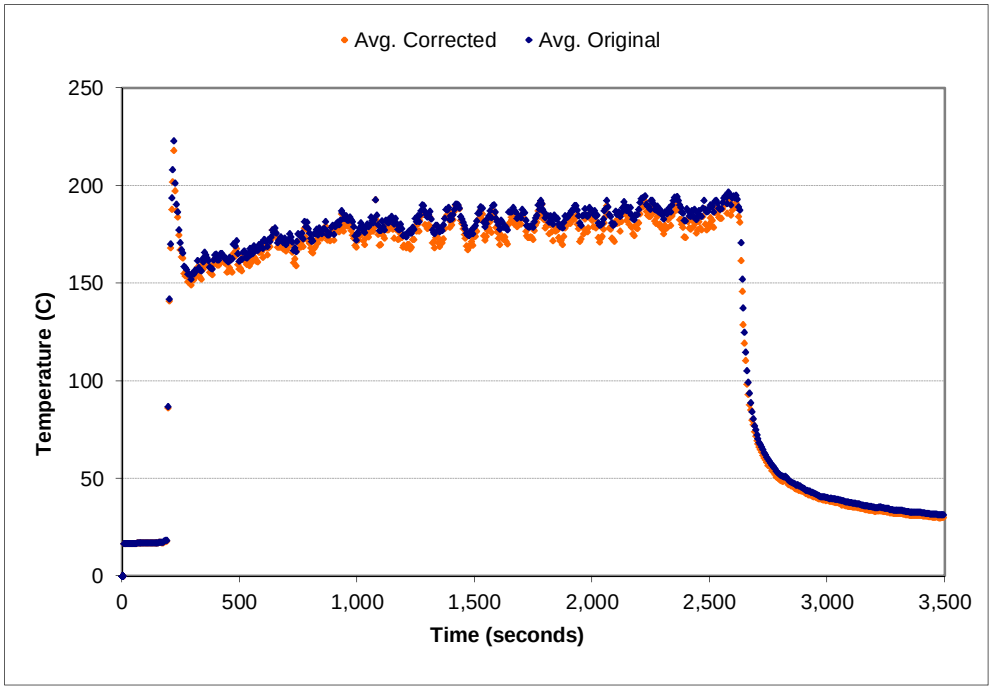

Figure A-87: Space-averaged (layer 2) temperature correction for the 1.0 g/s, ϕ_3 configuration

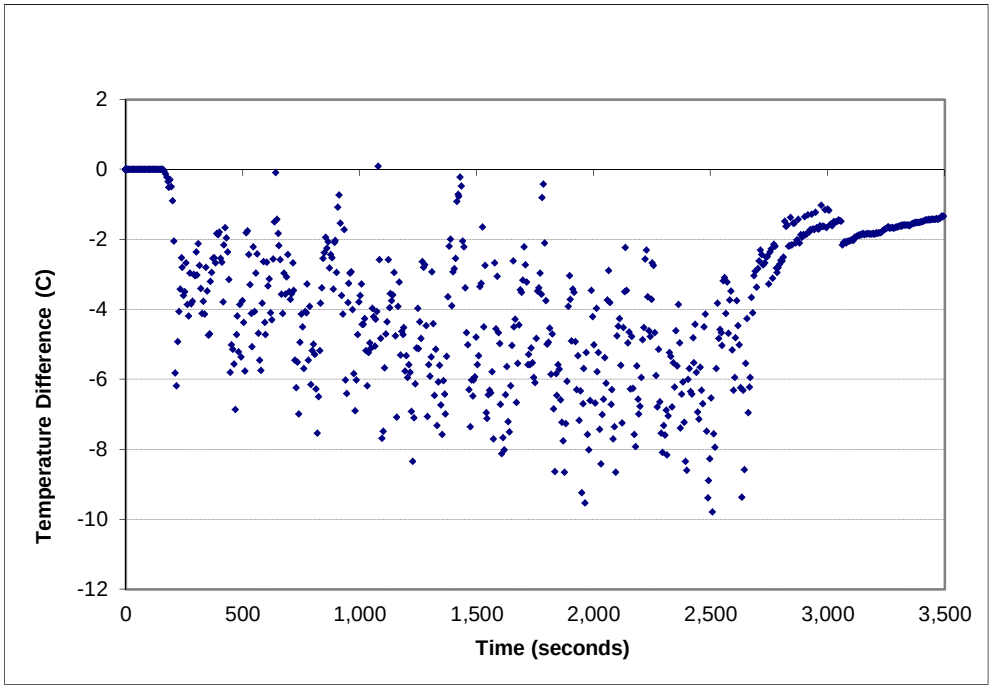

Figure A-88: Temperature error (layer 2) for the 1.0 g/s, ϕ_3 configuration

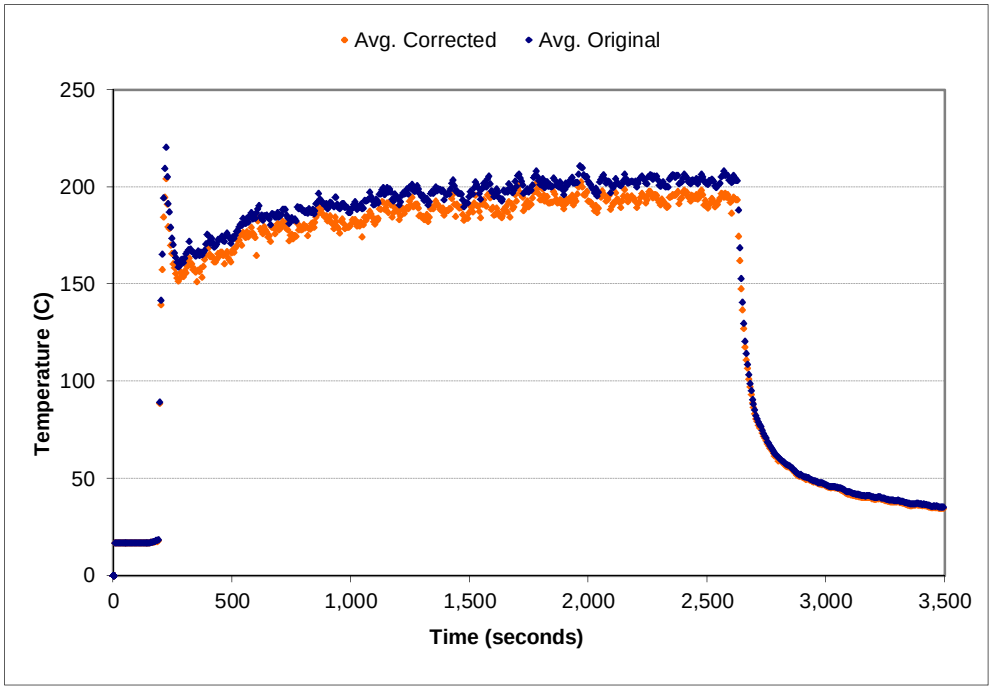

Figure A-89: Space-averaged (layer 3) temperature correction for the 1.0 g/s, ϕ_3 configuration

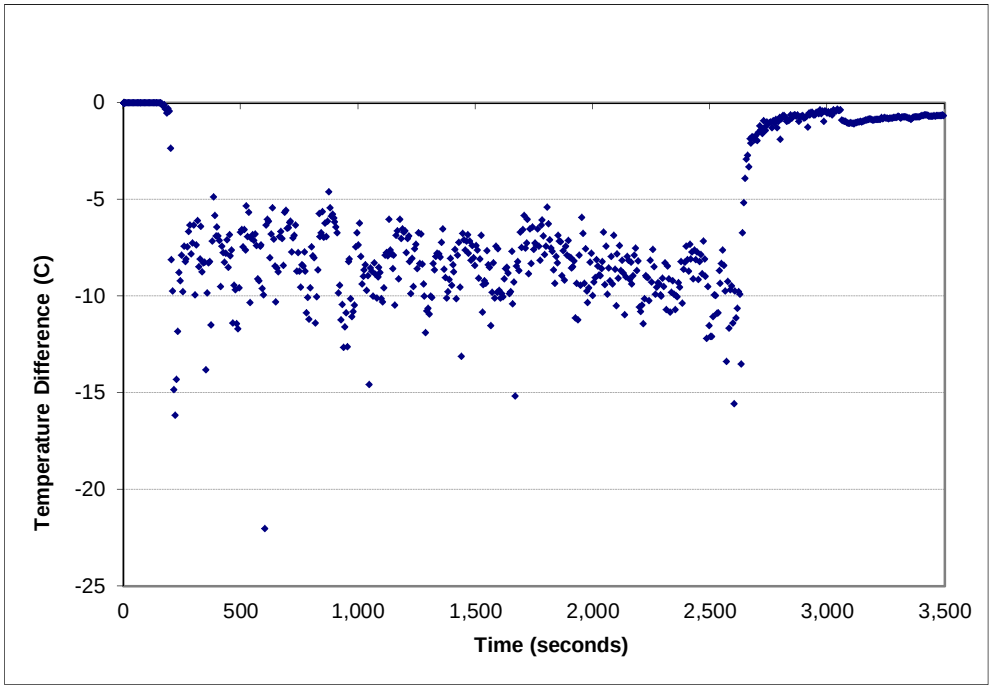

Figure A-90: Temperature error (layer 3) for the 1.0 g/s, ϕ_3 configuration

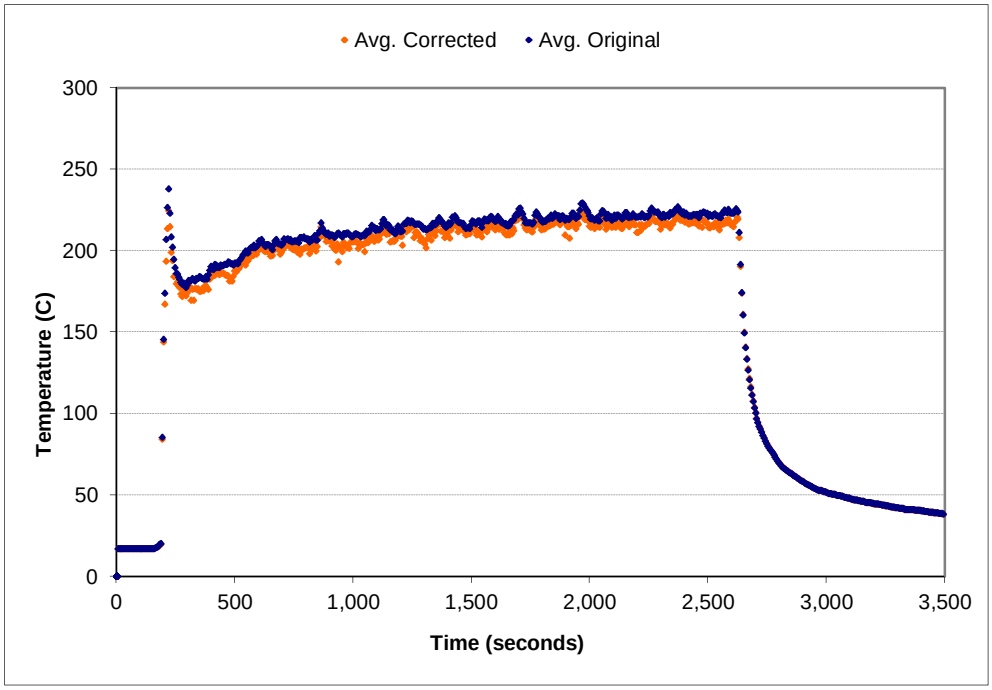

Figure A-91: Space-averaged (layer 4) temperature correction for the 1.0 g/s, ϕ_3 configuration

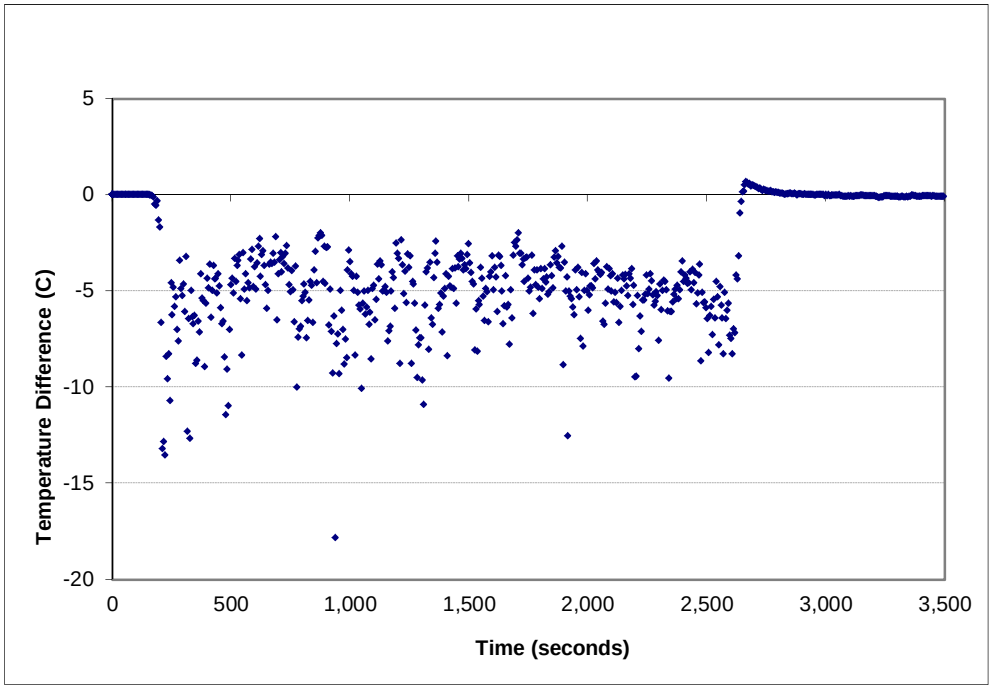

Figure A-92: Temperature error (layer 4) for the 1.0 g/s, ϕ_3 configuration

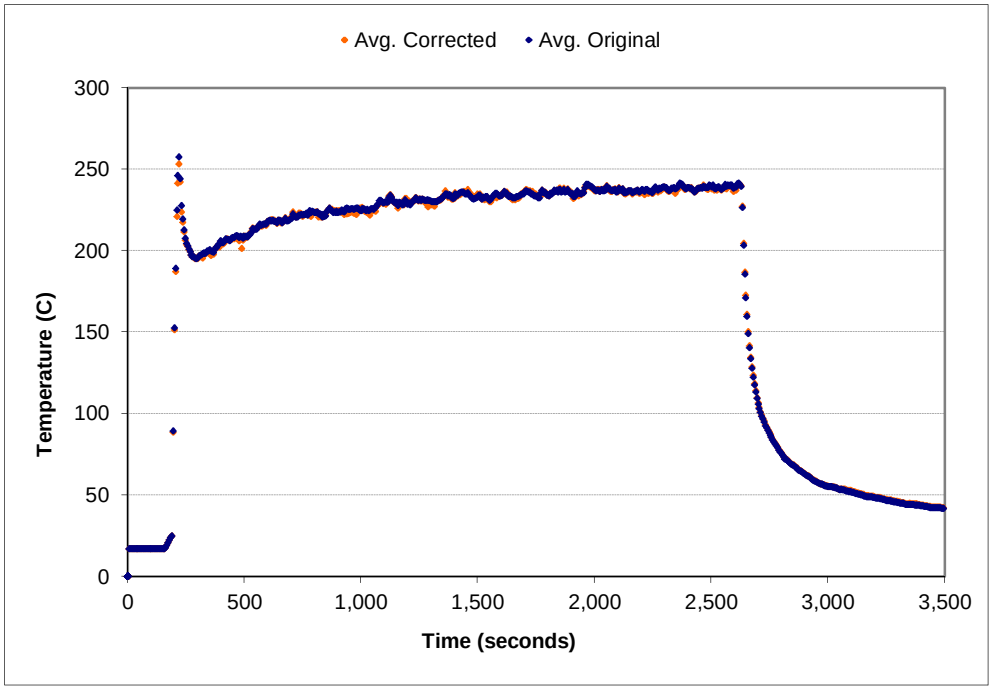

Figure A-93: Space-averaged (layer 5) temperature correction for the 1.0 g/s, ϕ_3 configuration

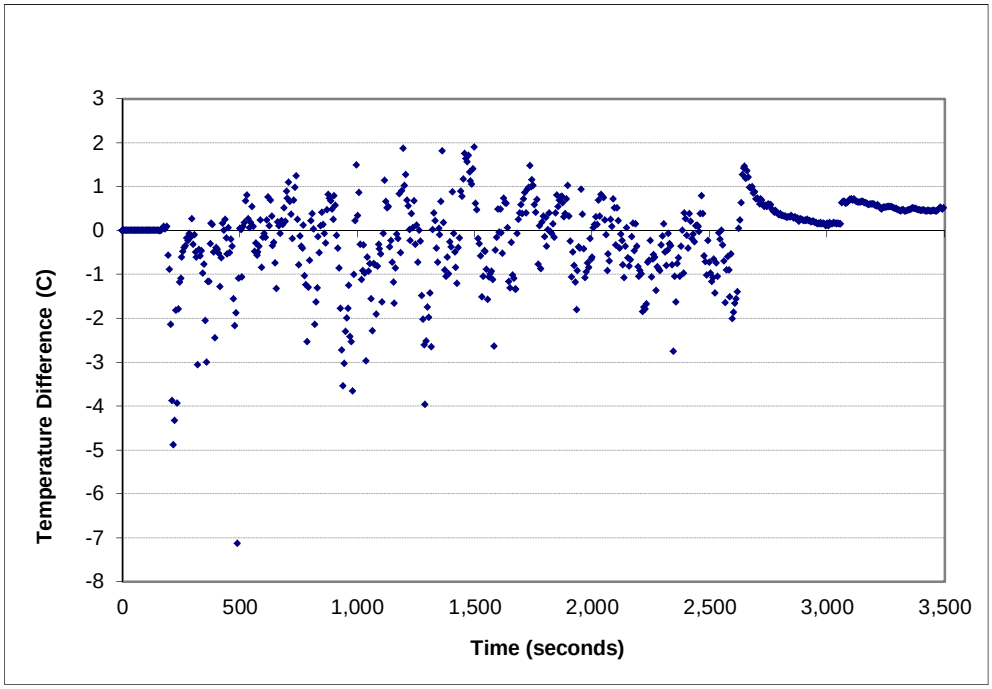

Figure A-94: Temperature error (layer 5) for the 1.0 g/s, ϕ_3 configuration

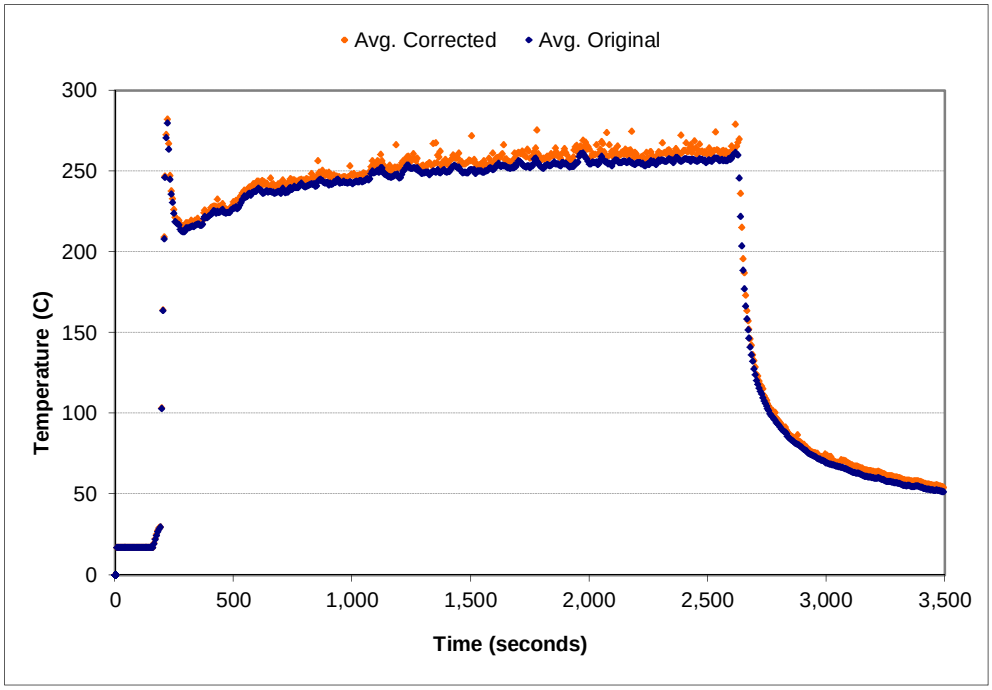

Figure A-95: Space-averaged (layer 6) temperature correction for the 1.0 g/s, ϕ_3 configuration

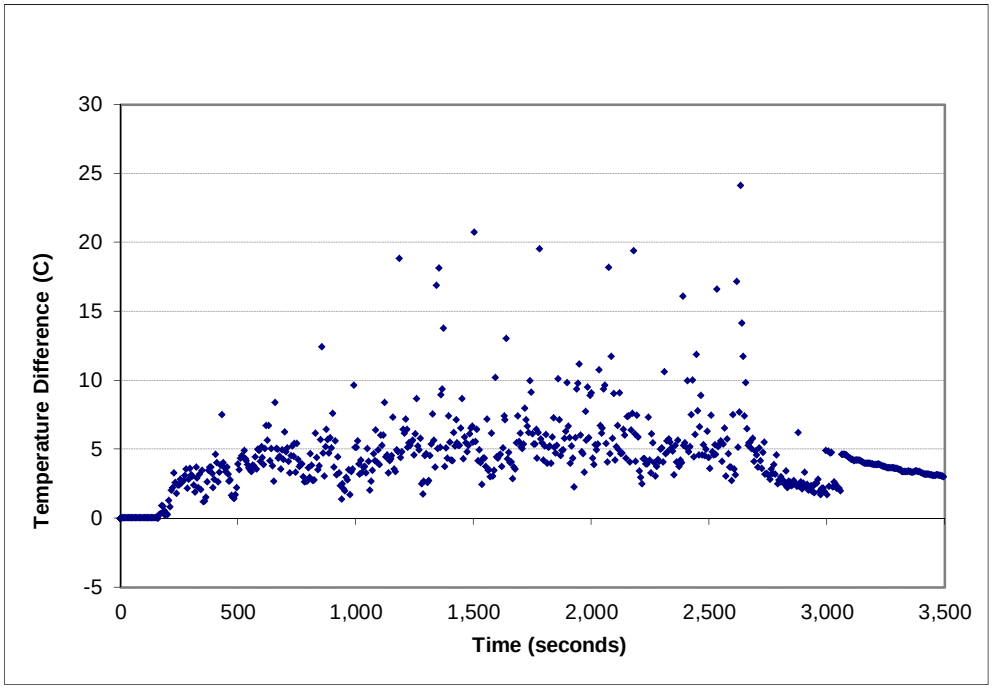

Figure A-96: Temperature error (layer 6) for the 1.0 g/s, ϕ_3 configuration

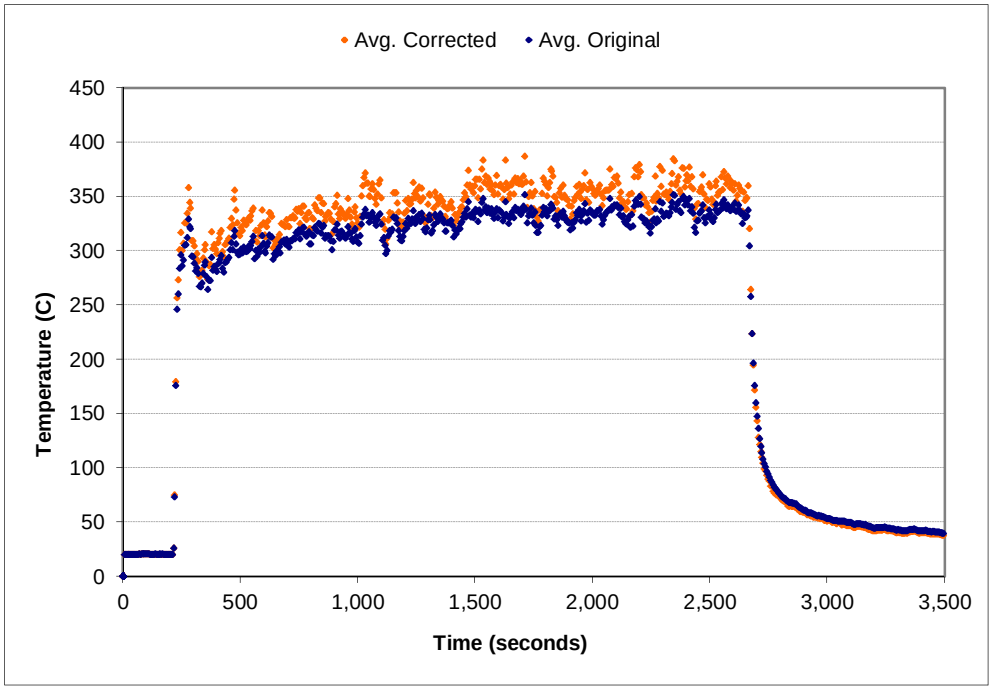

Figure A-97: Space-averaged (layer 1) temperature correction for the 1.5 g/s, ϕ_3 configuration

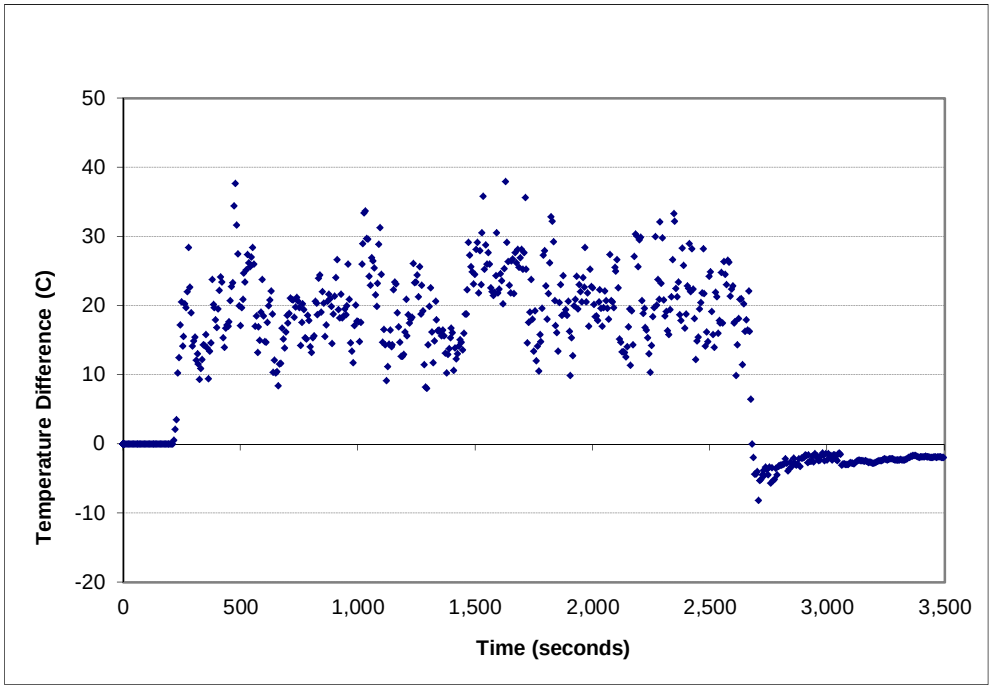

Figure A-98: Temperature error (layer 1) for the 1.5 g/s, ϕ_3 configuration

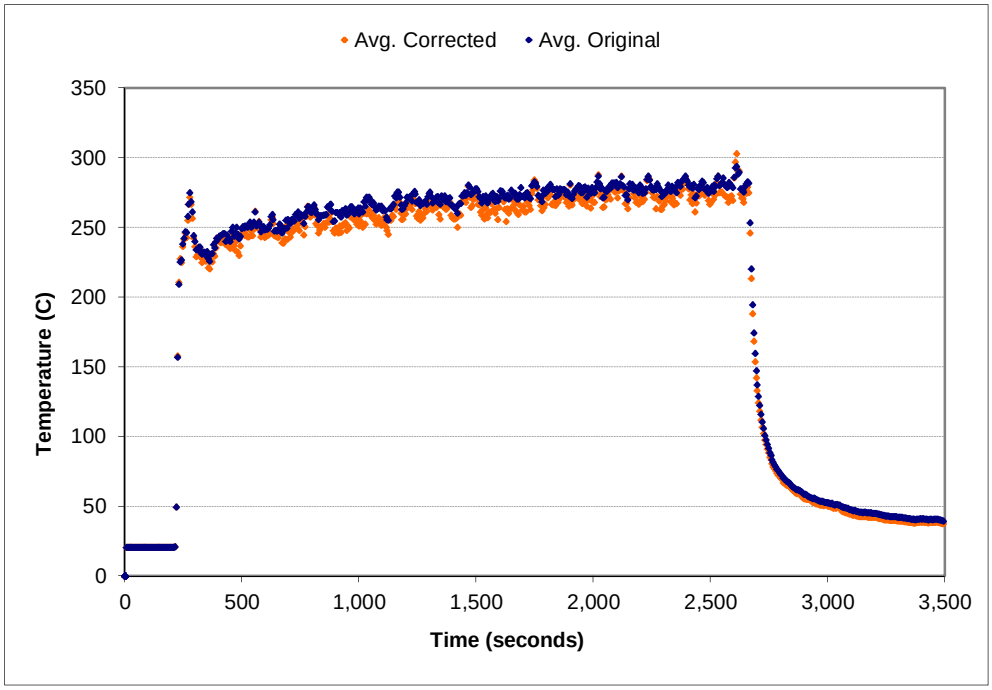

Figure A-99: Space-averaged (layer 2) temperature correction for the 1.5 g/s, ϕ_3 configuration

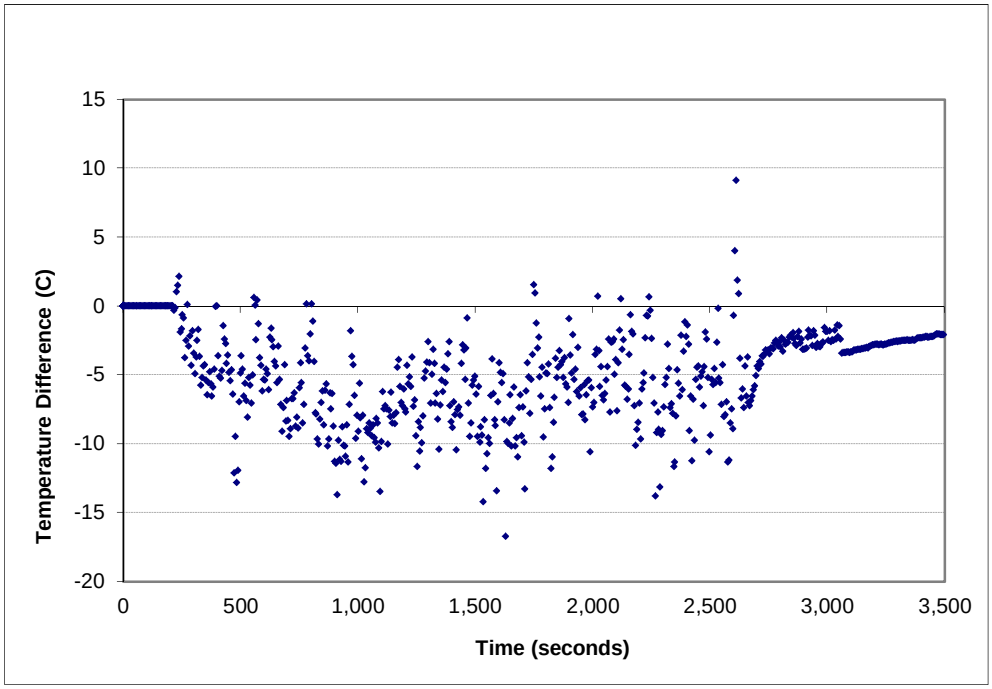

Figure A-100: Temperature error (layer 2) for the 1.5 g/s, ϕ_3 configuration

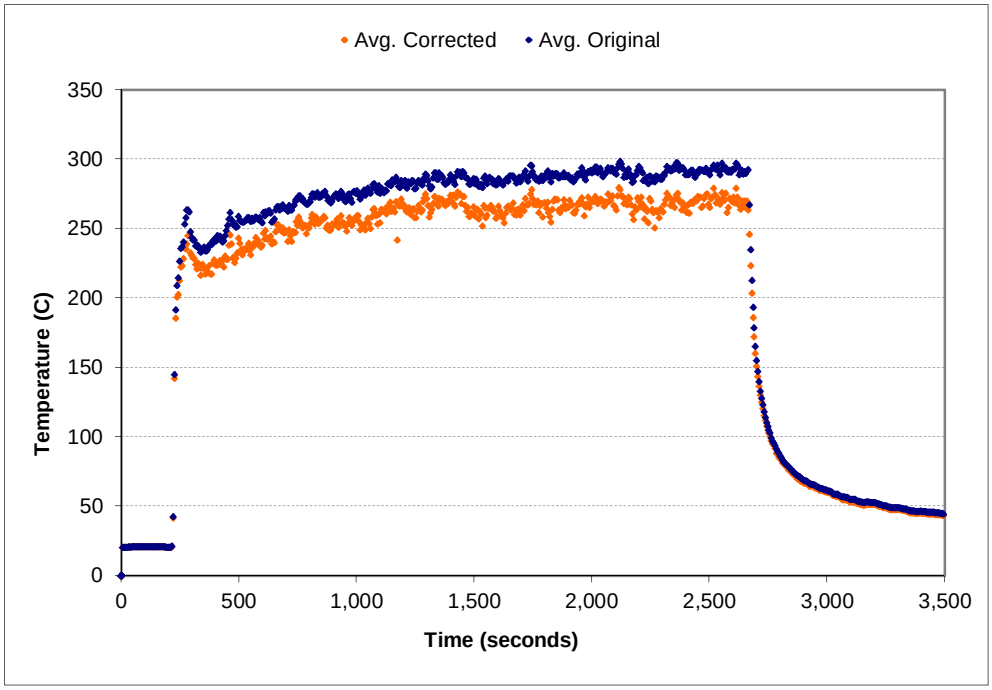

Figure A-101: Space-averaged (layer 3) temperature correction for the 1.5 g/s, ϕ_3 configuration

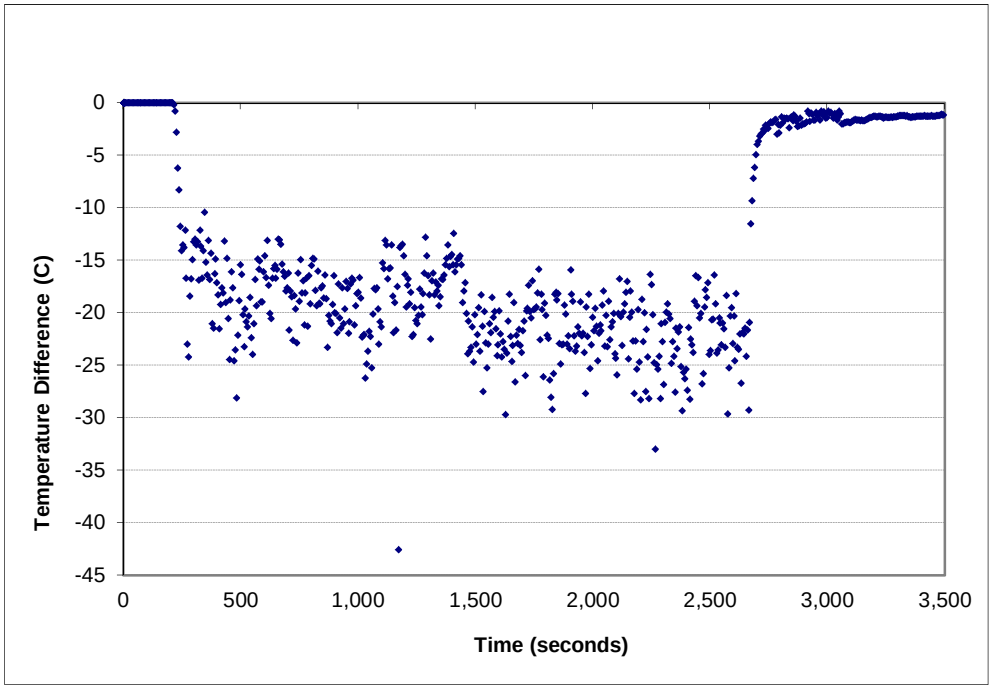

Figure A-102: Temperature error (layer 3) for the 1.5 g/s, ϕ_3 configuration

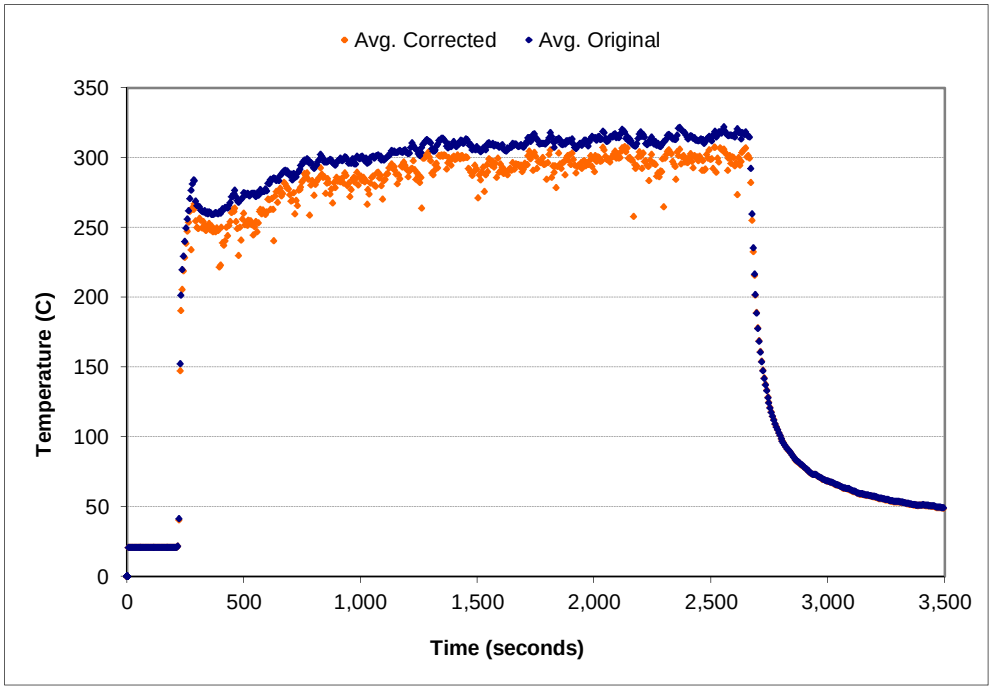

Figure A-103: Space-averaged (layer 4) temperature correction for the 1.5 g/s, ϕ_3 configuration

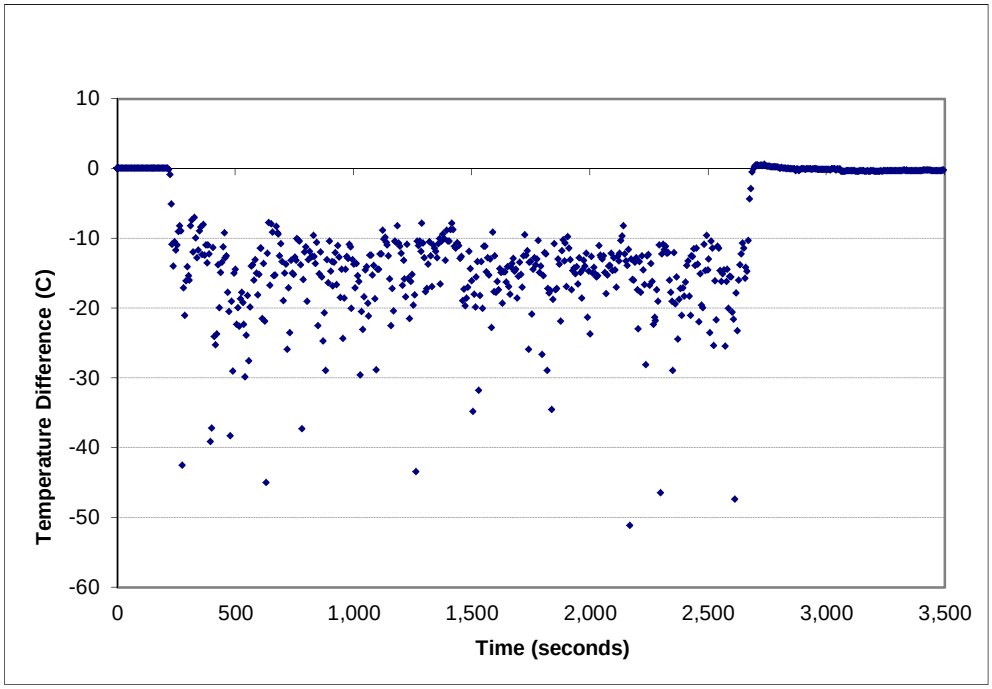

Figure A-104: Temperature error (layer 4) for the 1.5 g/s, ϕ_3 configuration

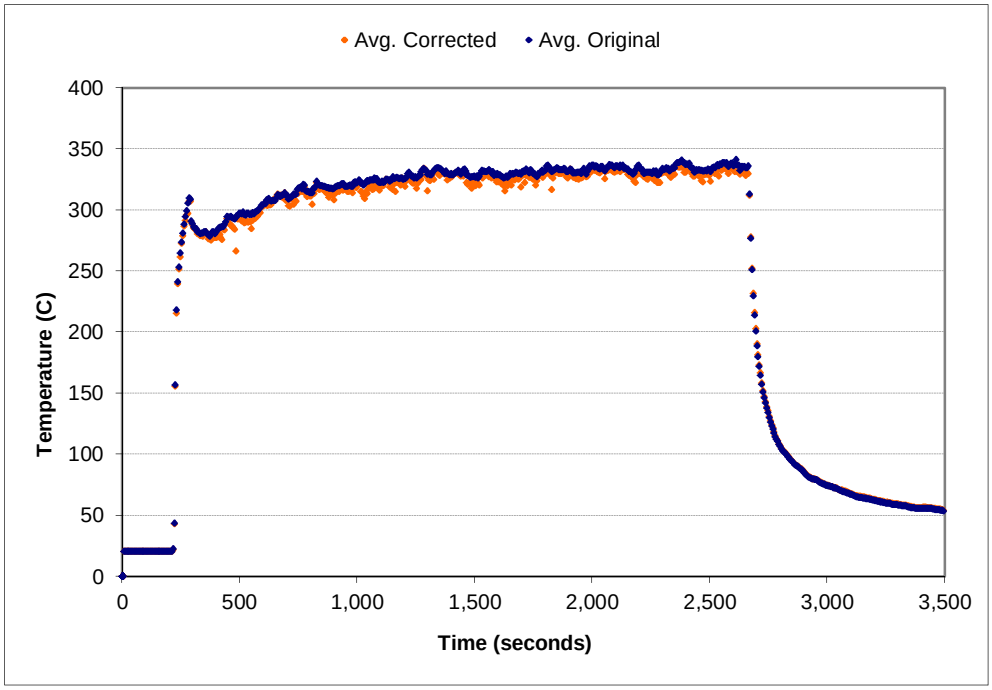

Figure A-105: Space-averaged (layer 5) temperature correction for the 1.5 g/s, ϕ_3 configuration

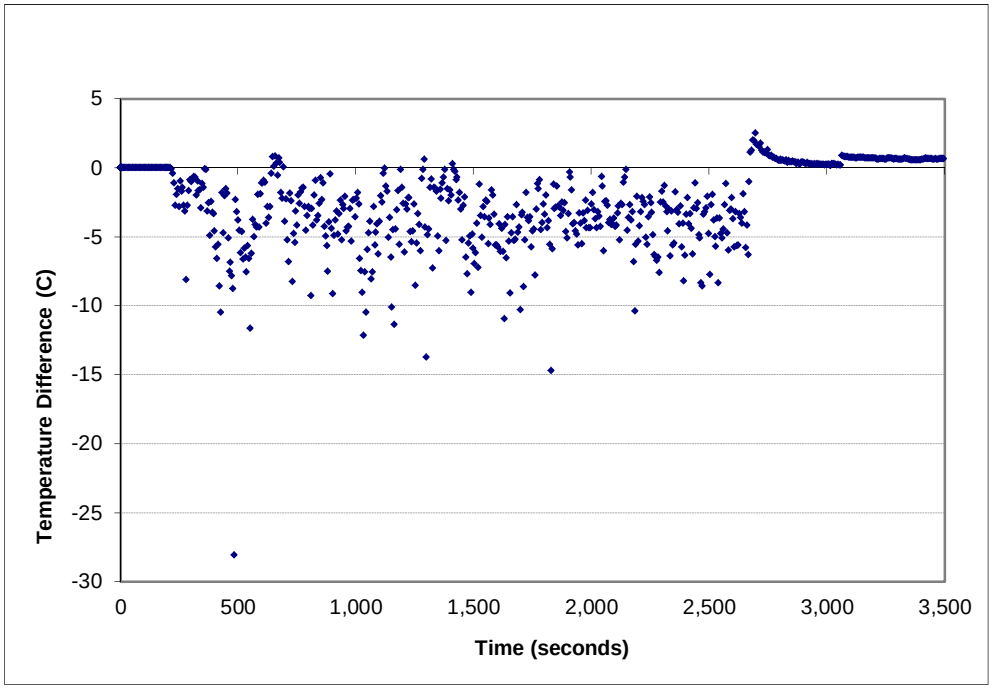

Figure A 106: Temperature error (layer 5) for the 1.5 g/s, ϕ_3 configuration

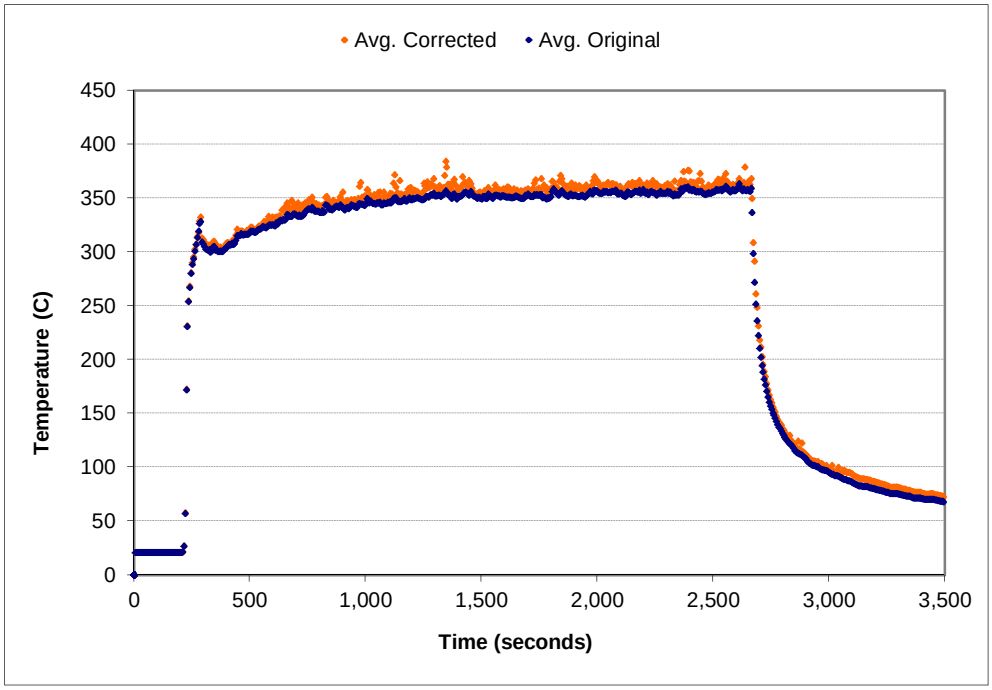

Figure A-107: Space-averaged (layer 6) temperature correction for the 1.5 g/s, ϕ_3 configuration

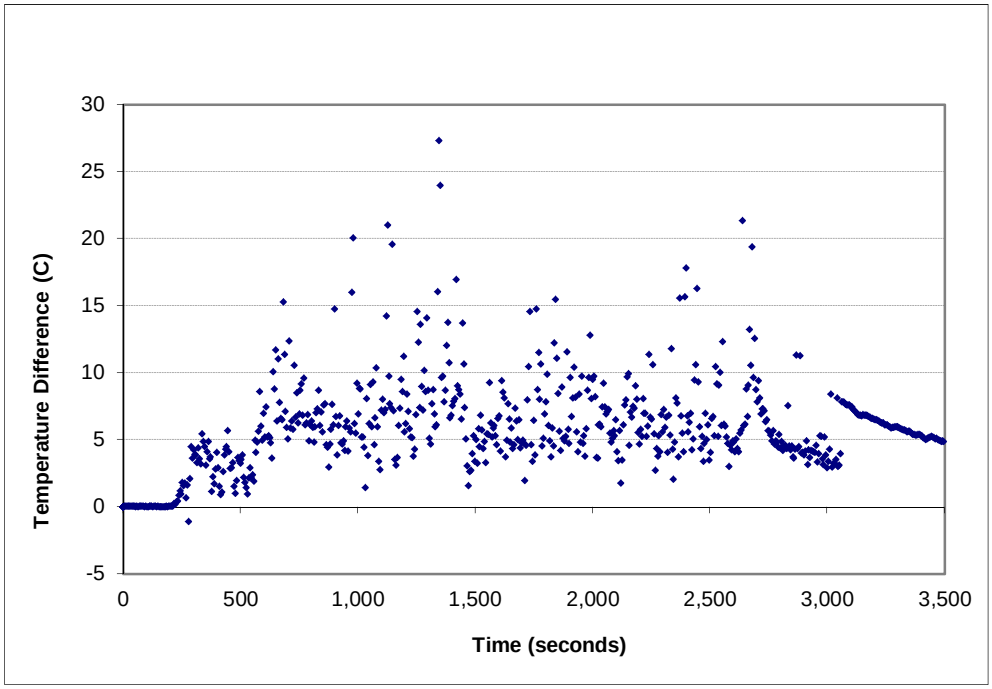

Figure A-108: Temperature error (layer 6) for the 1.5 g/s, ϕ_3 configuration

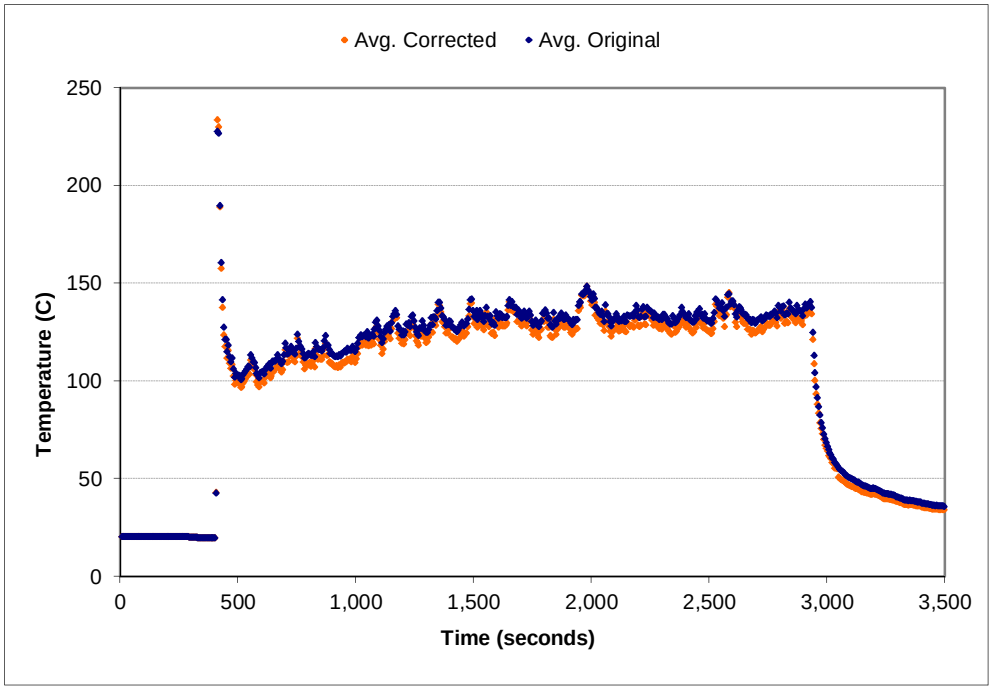

Figure A-109: Space-averaged (layer 1) temperature correction for the 0.5 g/s, ϕ_4 configuration

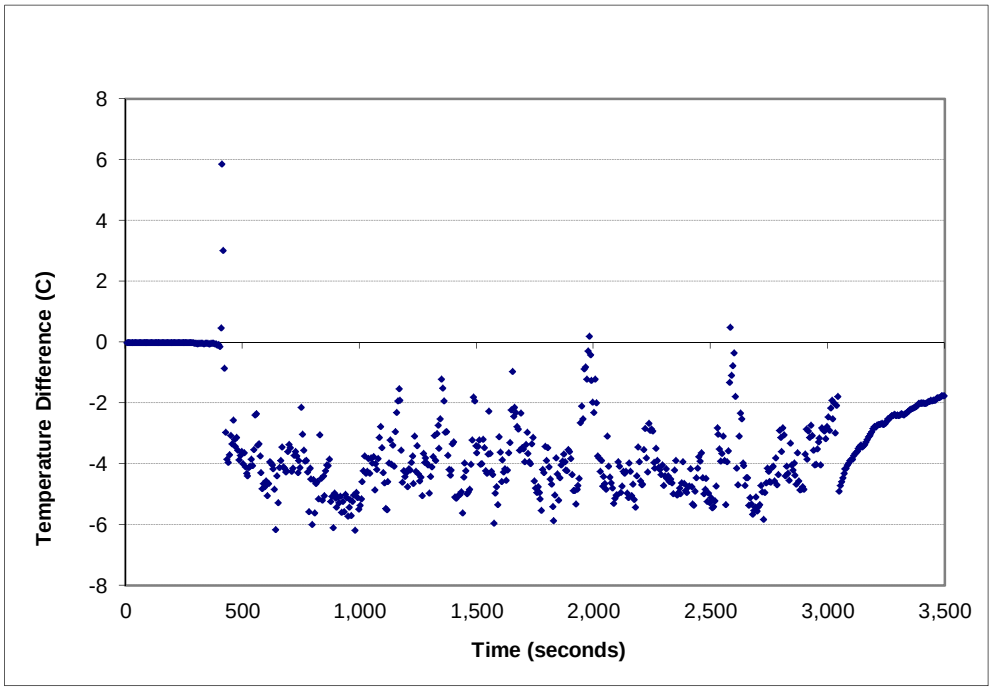

Figure A-110: Temperature error (layer 1) for the 0.5 g/s, ϕ_4 configuration

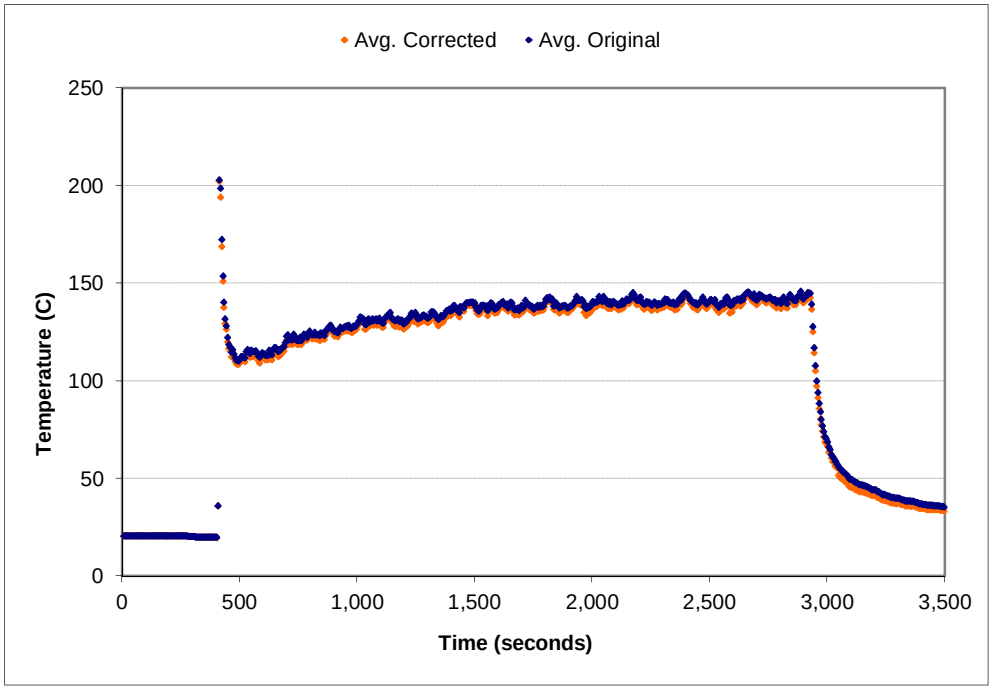

Figure A-111: Space-averaged (layer 2) temperature correction for the 0.5 g/s, ϕ_4 configuration

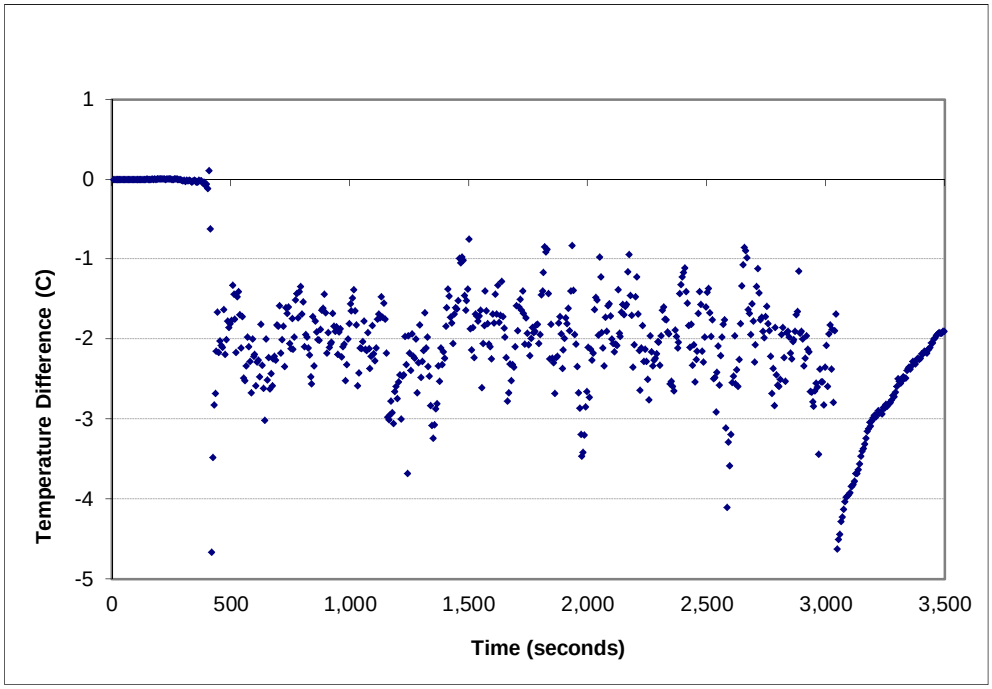

Figure A-112: Temperature error (layer 2) for the 0.5 g/s, ϕ_4 configuration

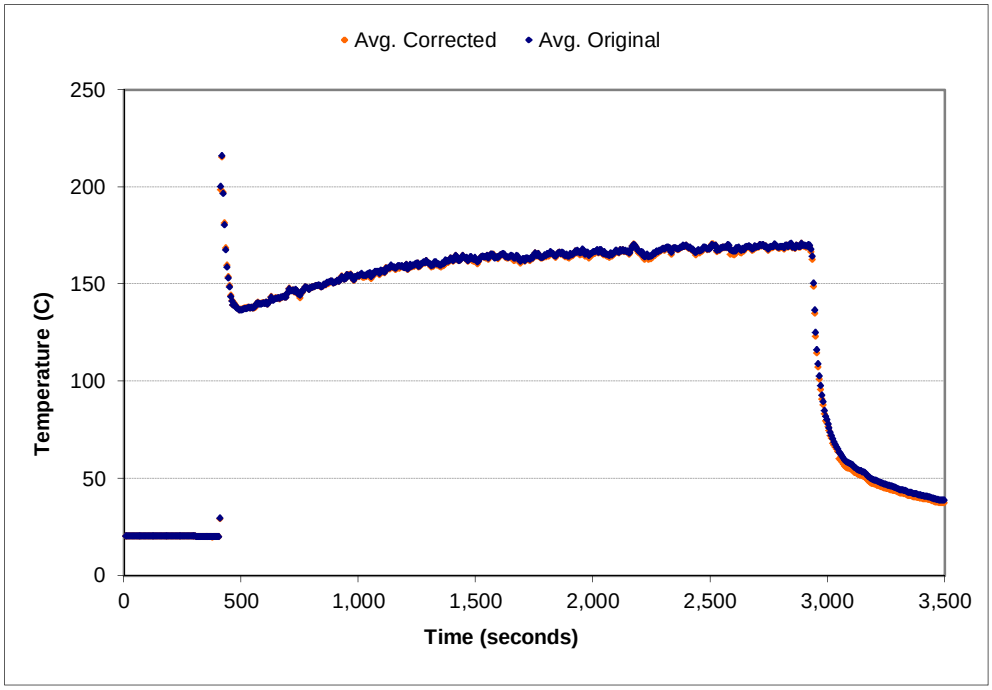

Figure A-113: Space-averaged (layer 3) temperature correction for the 0.5 g/s, ϕ_4 configuration

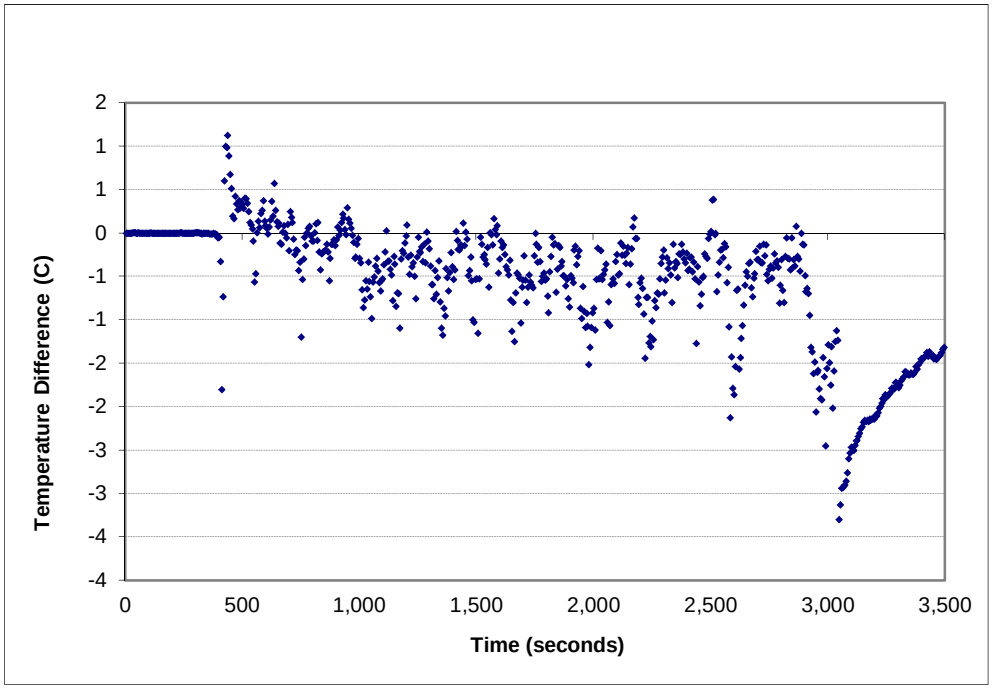

Figure A-114: Temperature error (layer 3) for the 0.5 g/s, ϕ_4 configuration

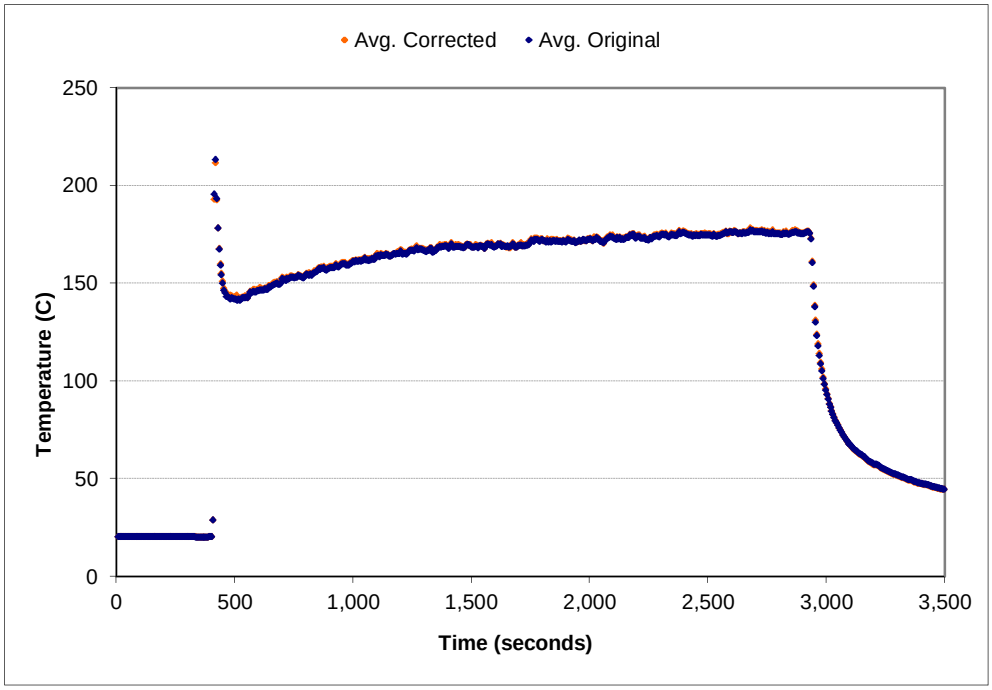

Figure A-115: Space-averaged (layer 4) temperature correction for the 0.5 g/s, ϕ_4 configuration

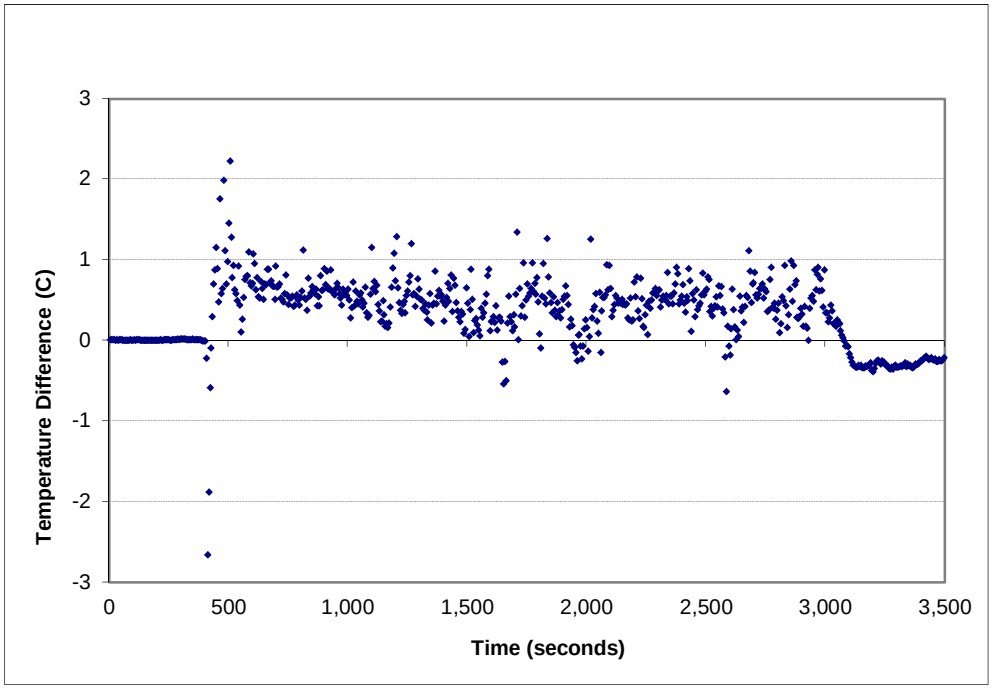

Figure A-116: Temperature error (layer 4) for the 0.5 g/s, ϕ_4 configuration

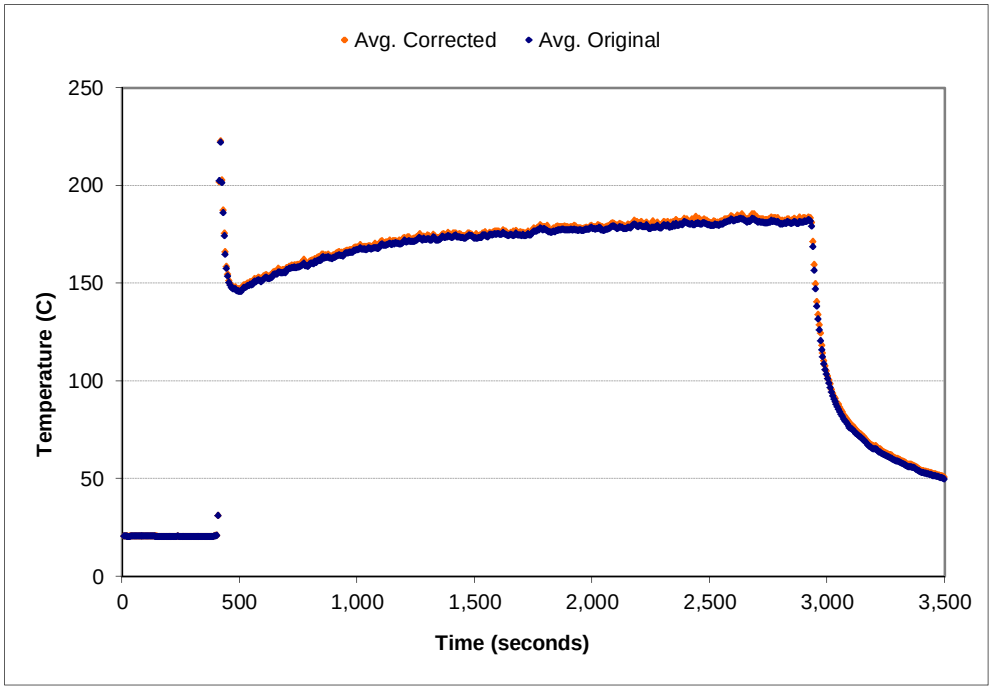

Figure A-117: Space-averaged (layer 5) temperature correction for the 0.5 g/s, ϕ_4 configuration

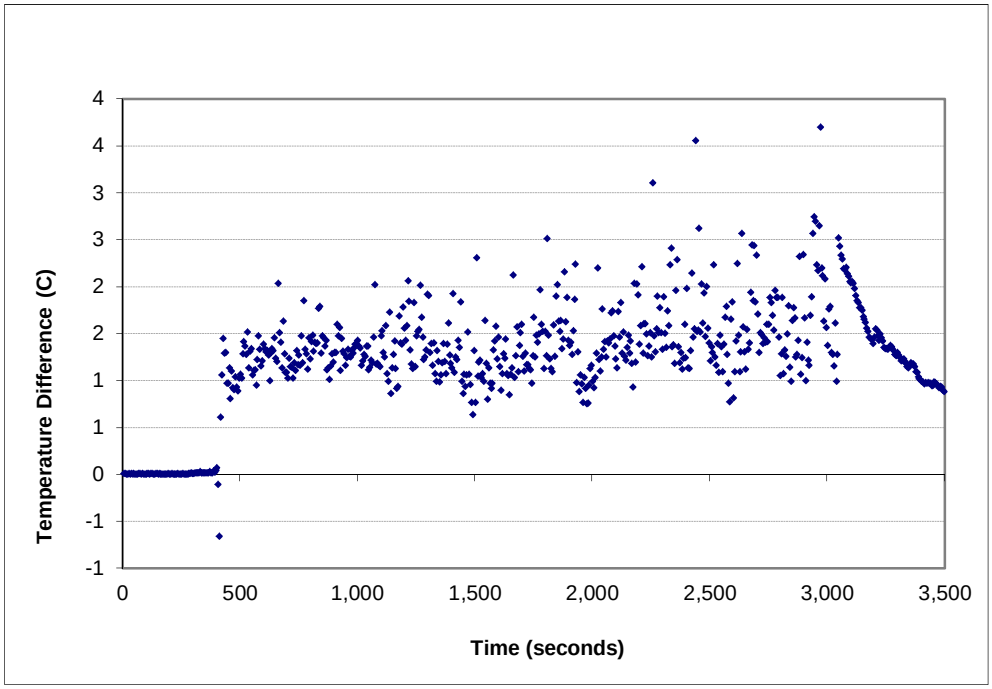

Figure A-118: Temperature error (layer 5) for the 0.5 g/s, ϕ_4 configuration

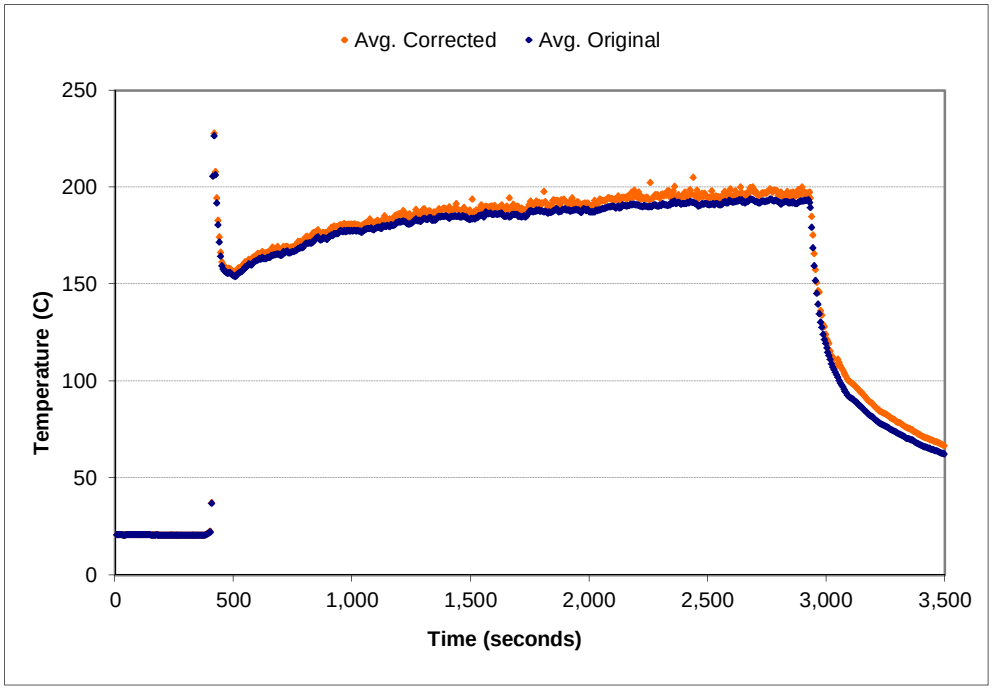

Figure A-119: Space-averaged (layer 6) temperature correction for the 0.5 g/s, ϕ_4 configuration

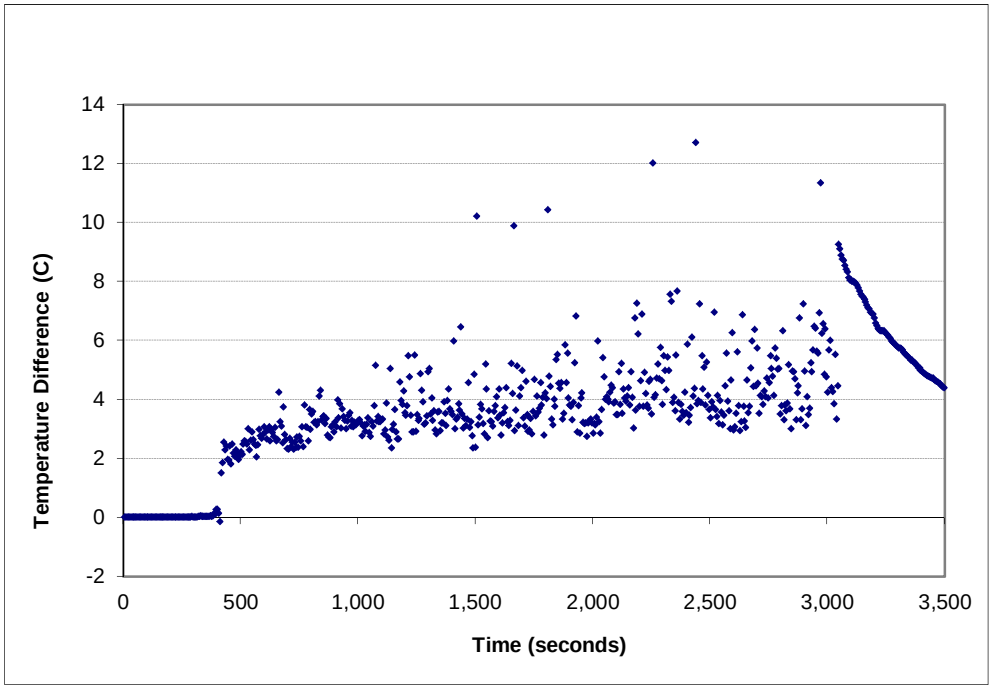

Figure A-120: Temperature error (layer 6) for the 0.5 g/s, ϕ_4 configuration

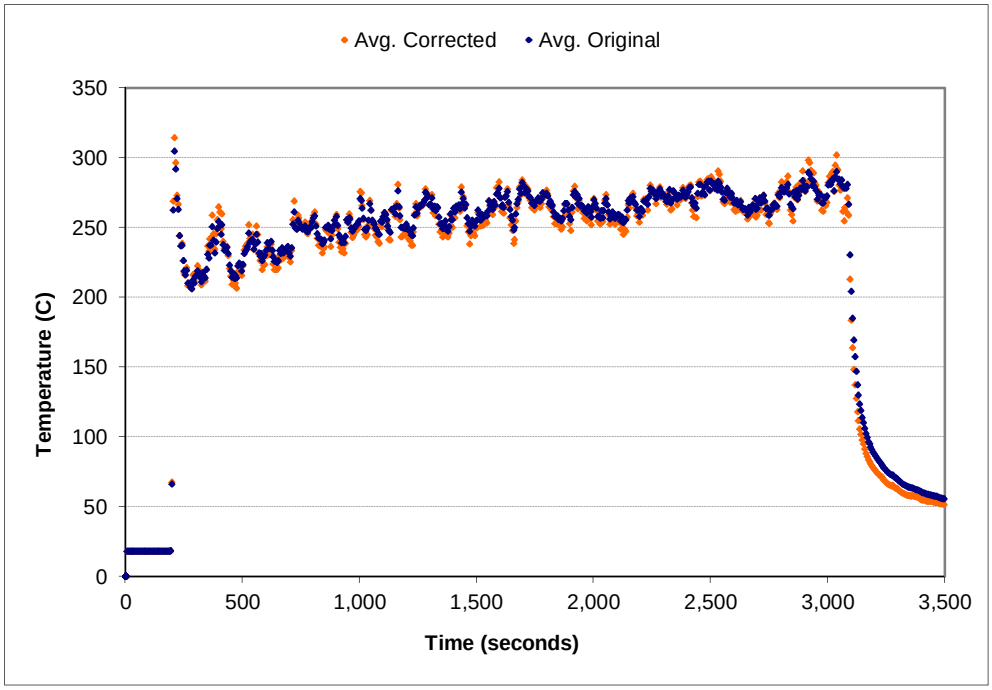

Figure A-121: Space-averaged (layer 1) temperature correction for the 1.0 g/s, ϕ_4 configuration

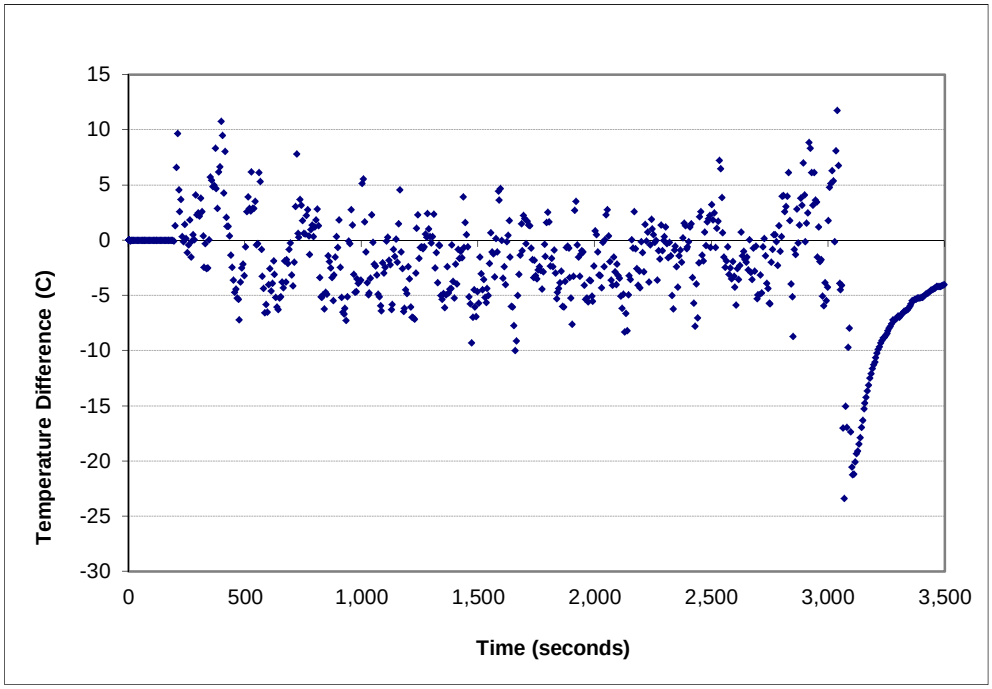

Figure A-122: Temperature error (layer 1) for the 1.0 g/s, ϕ_4 configuration

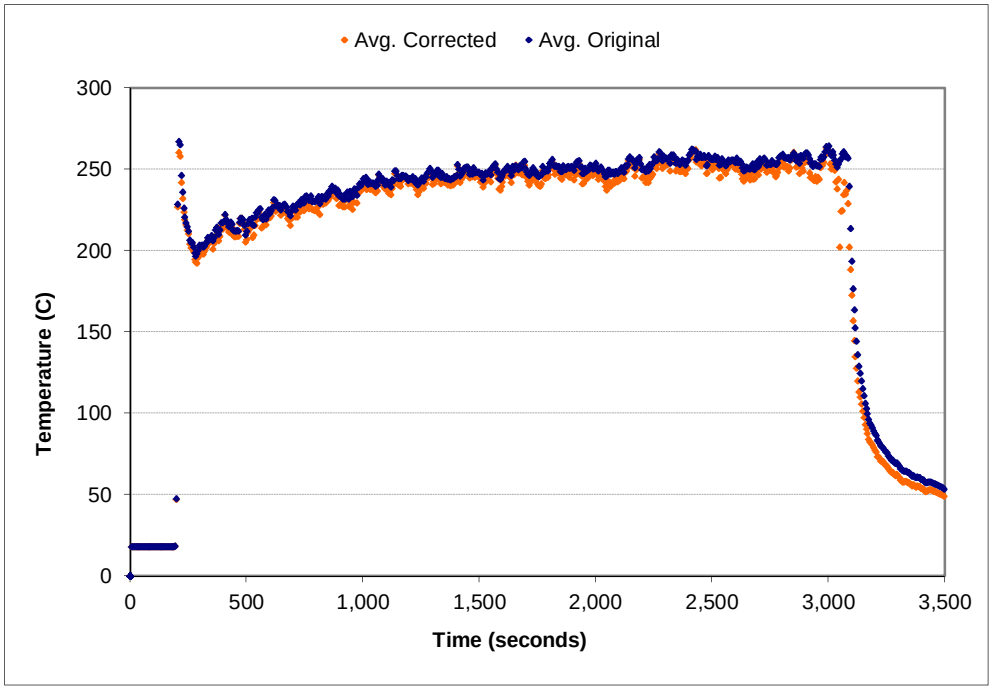

Figure A-123: Space-averaged (layer 2) temperature correction for the 1.0 g/s, ϕ_4 configuration

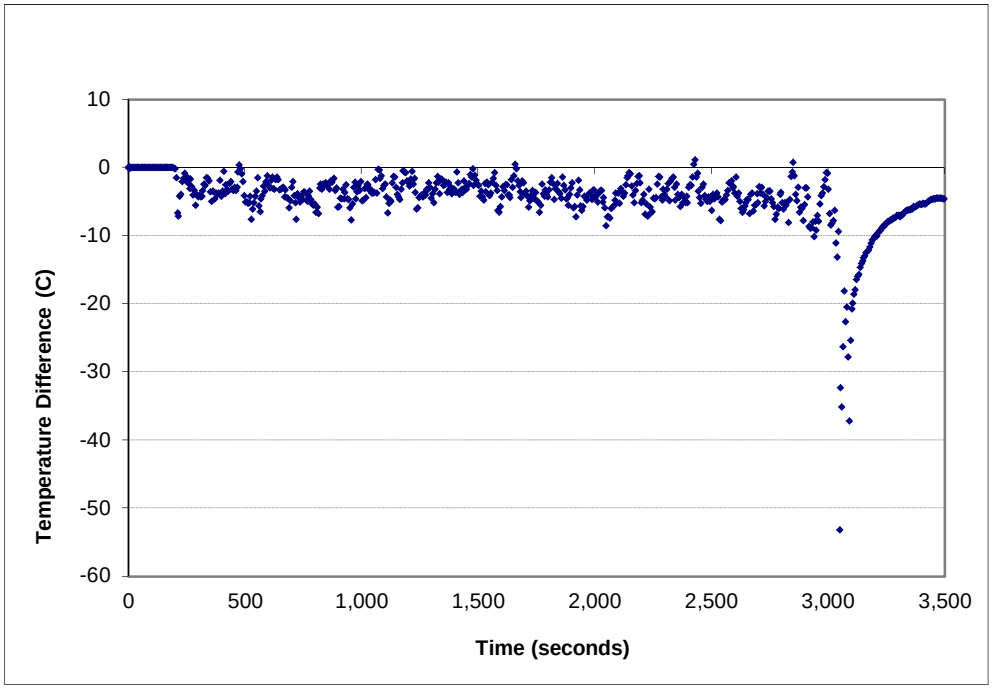

Figure A-124: Temperature error (layer 2) for the 1.0 g/s, ϕ_4 configuration

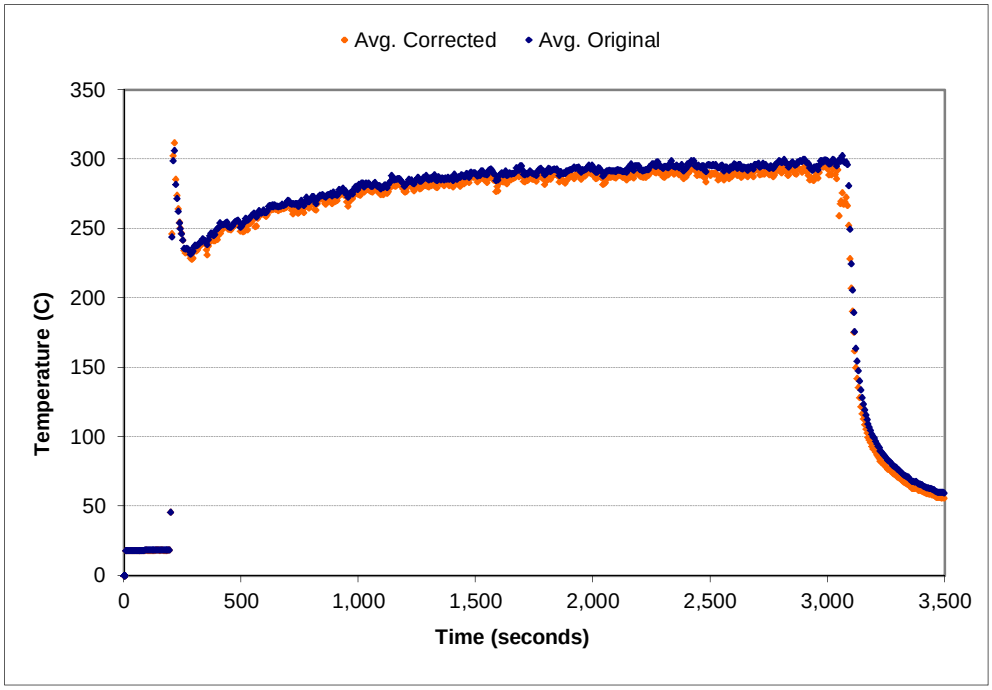

Figure A-125: Space-averaged (layer 3) temperature correction for the 1.0 g/s, ϕ_4 configuration

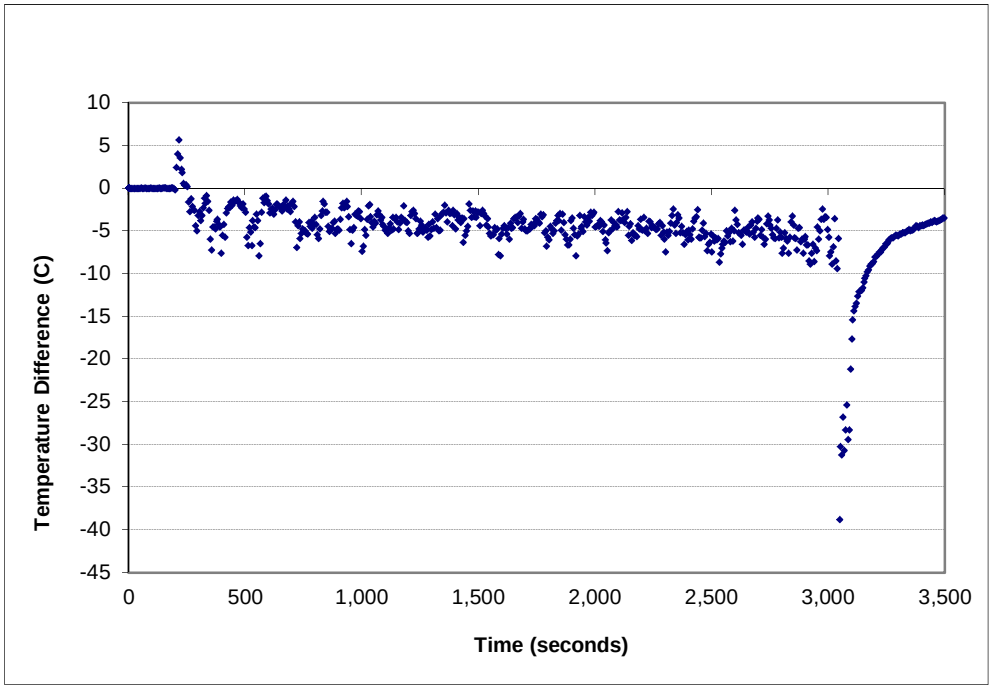

Figure A-126: Temperature error (layer 3) for the 1.0 g/s, ϕ_4 configuration

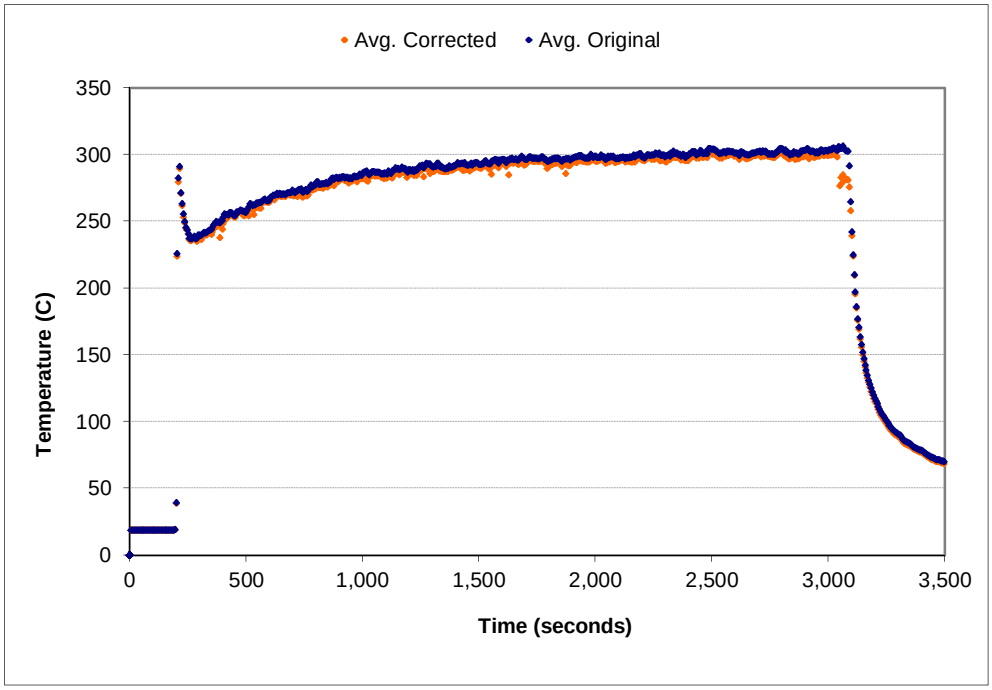

Figure A-127: Space-averaged (layer 4) temperature correction for the 1.0 g/s, ϕ_4 configuration

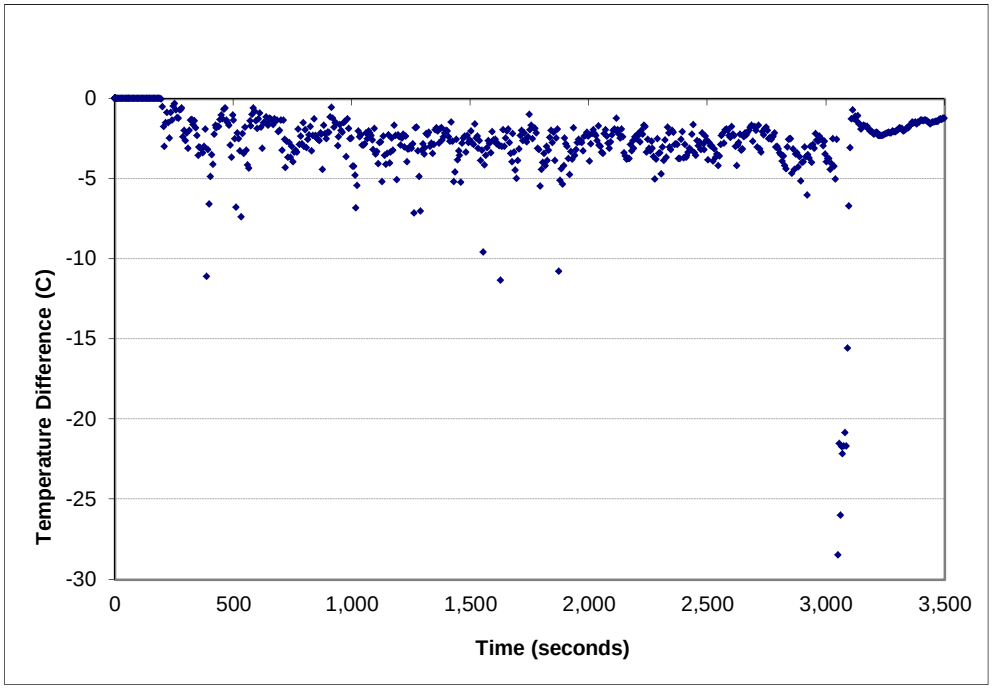

Figure A-128: Temperature error (layer 4) for the 1.0 g/s, ϕ_4 configuration

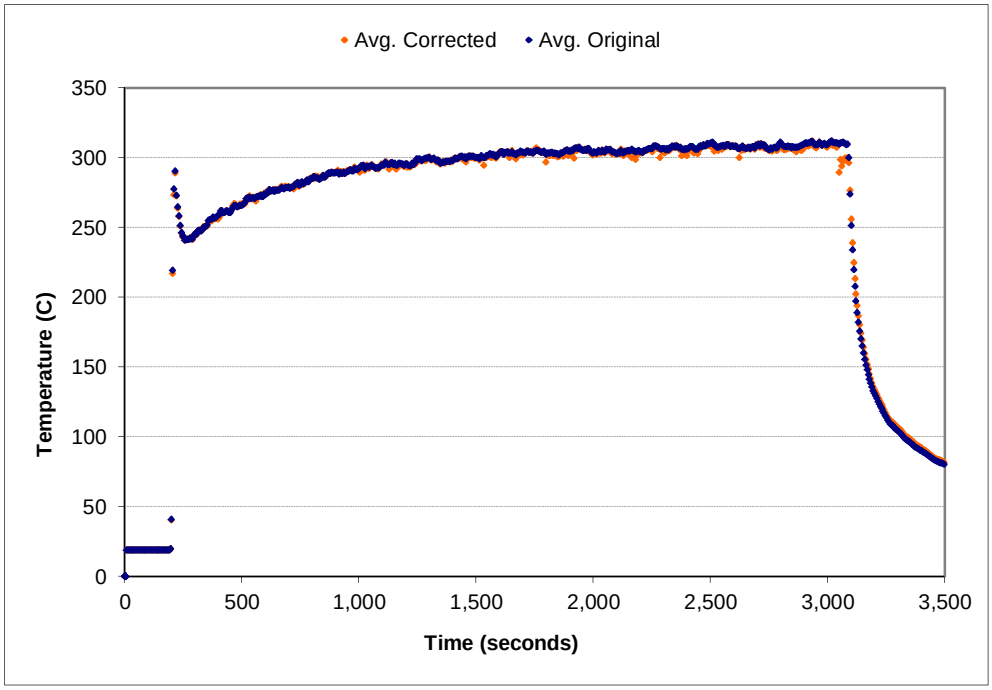

Figure A-129: Space-averaged (layer 5) temperature correction for the 1.0 g/s, ϕ_4 configuration

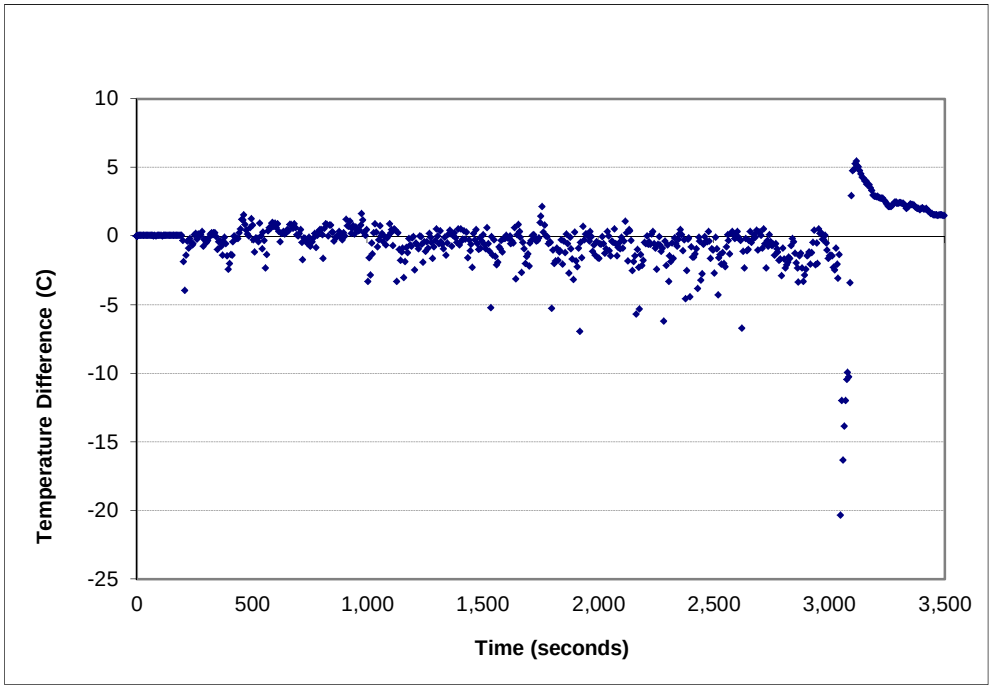

Figure A-130: Temperature error (layer 5) for the 1.0 g/s, ϕ_4 configuration

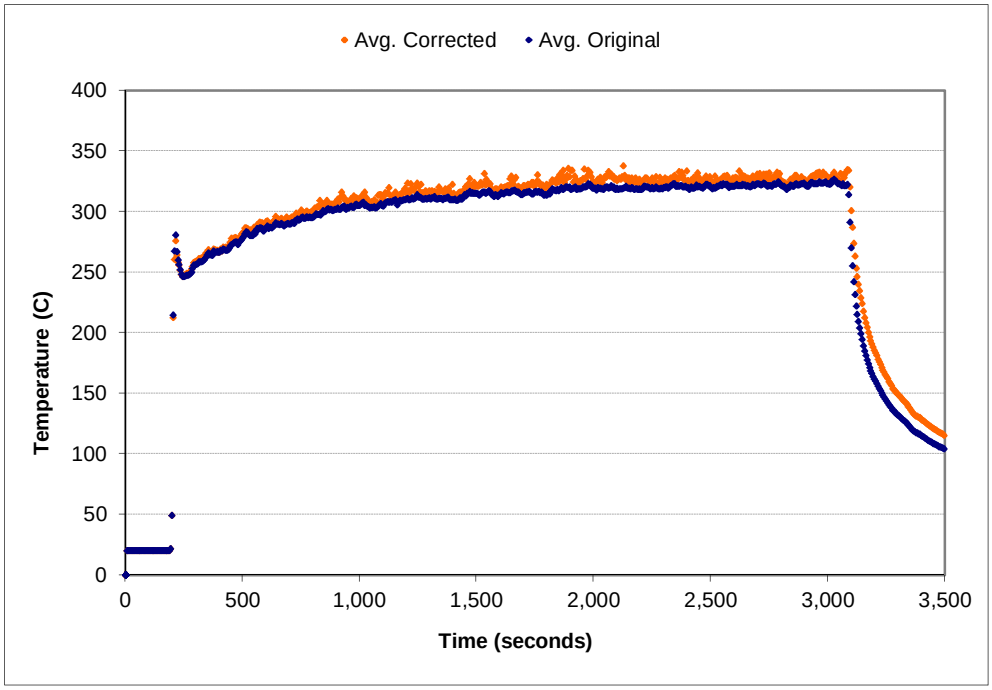

Figure A-131: Space-averaged (layer 6) temperature correction for the 1.0 g/s, ϕ_4 configuration

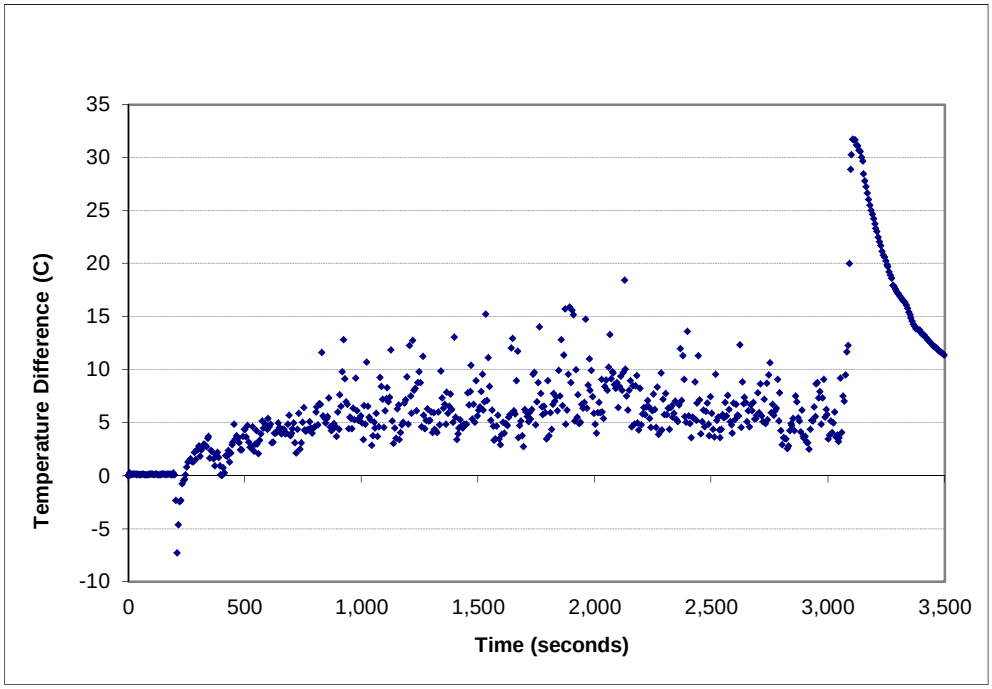

Figure A-132: Temperature error (layer 6) for the 1.0 g/s, ϕ_4 configuration

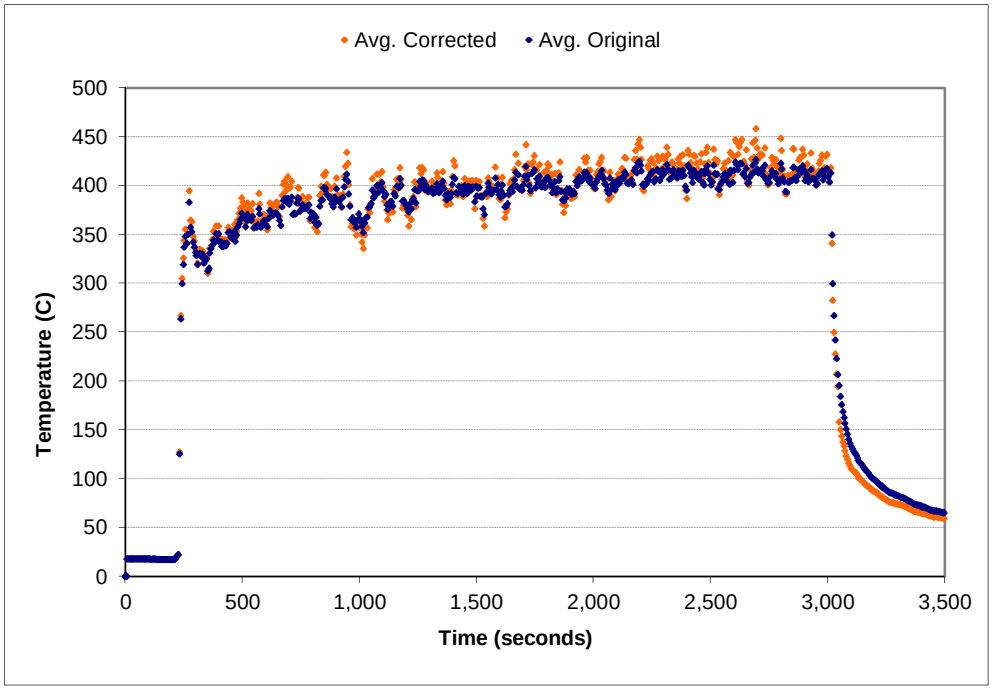

Figure A-133: Space-averaged (layer 1) temperature correction for the 1.5 g/s, ϕ_4 configuration

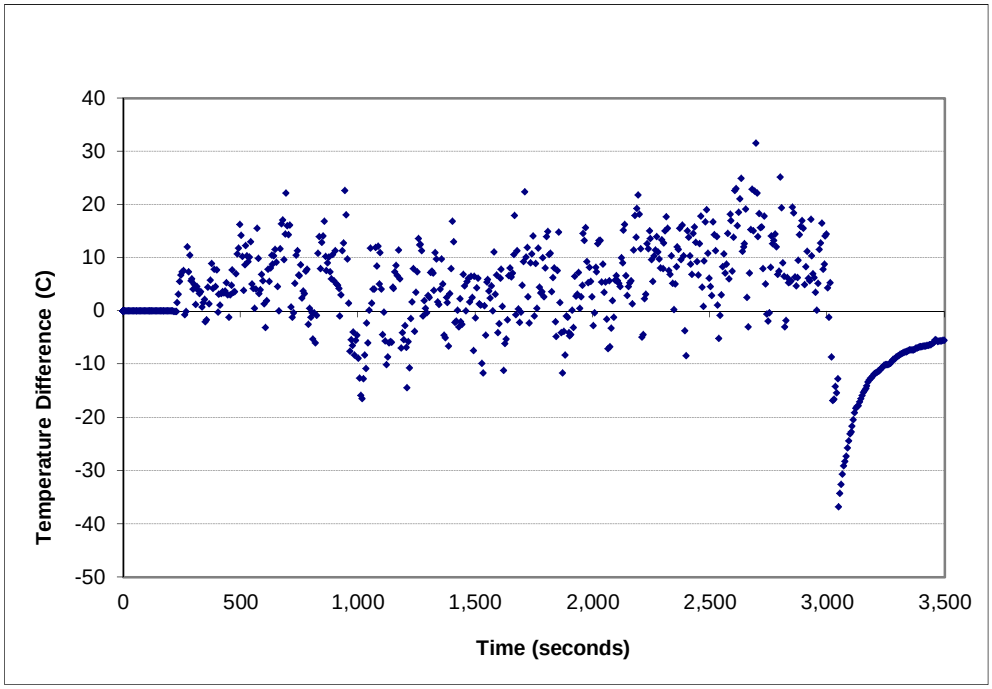

Figure A-134: Temperature error (layer 1) for the 1.5 g/s, ϕ_4 configuration

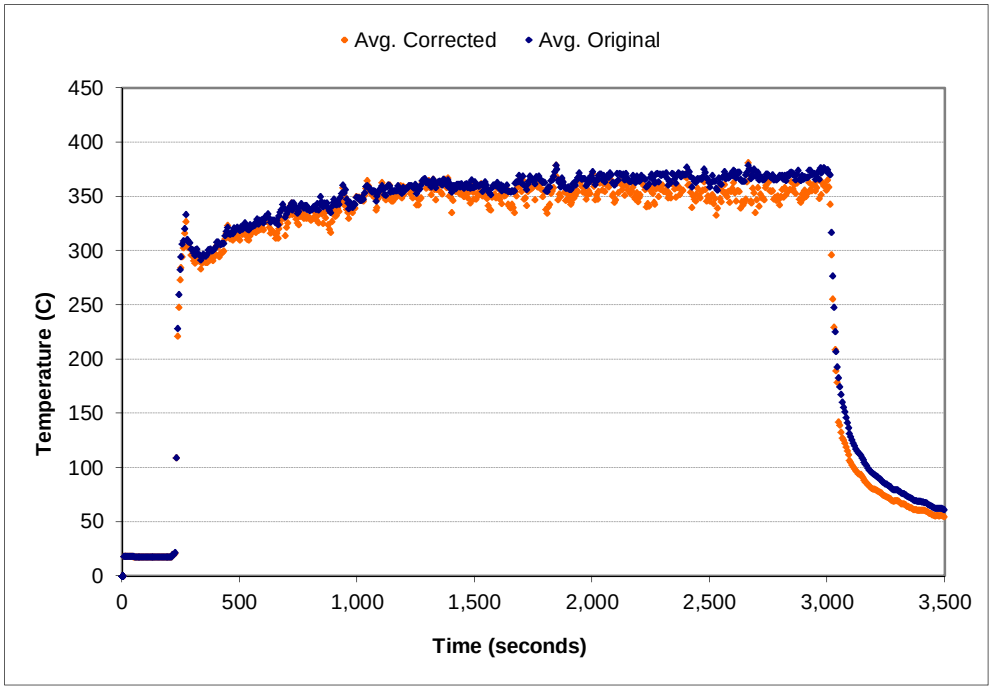

Figure A-135: Space-averaged (layer 2) temperature correction for the 1.5 g/s, ϕ_4 configuration

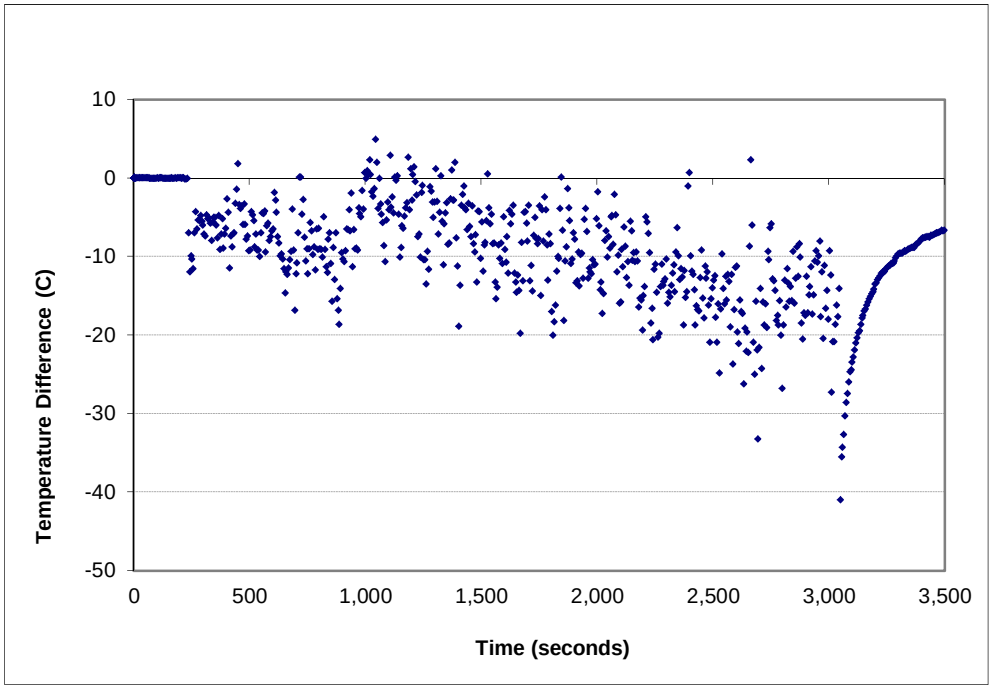

Figure A-136: Temperature error (layer 2) for the 1.5 g/s, ϕ_4 configuration

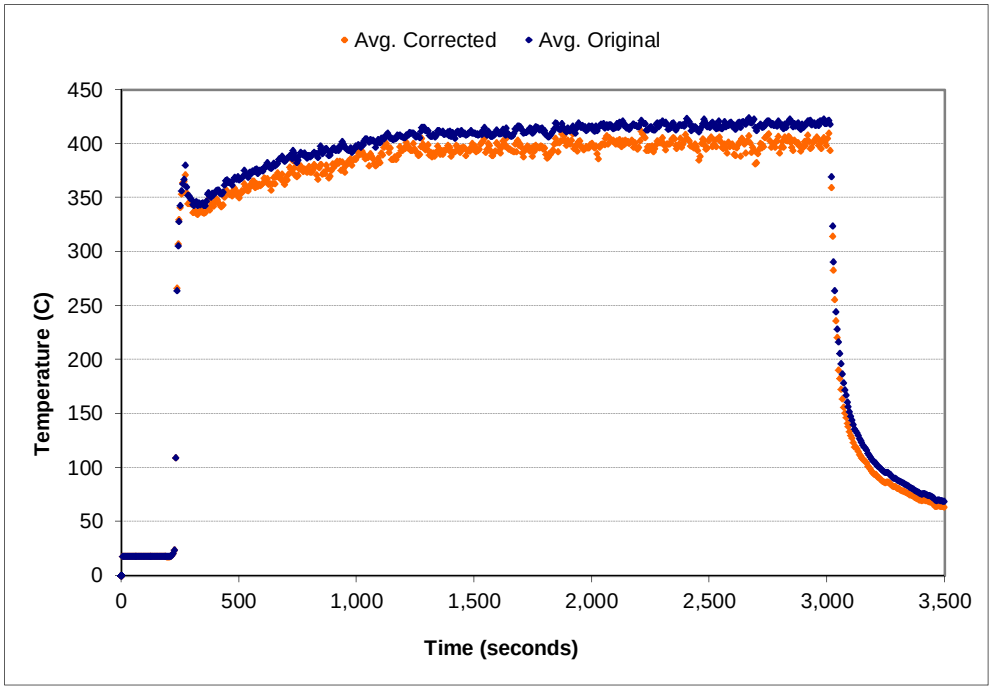

Figure A-137: Space-averaged (layer 3) temperature correction for the 1.5 g/s, ϕ_4 configuration

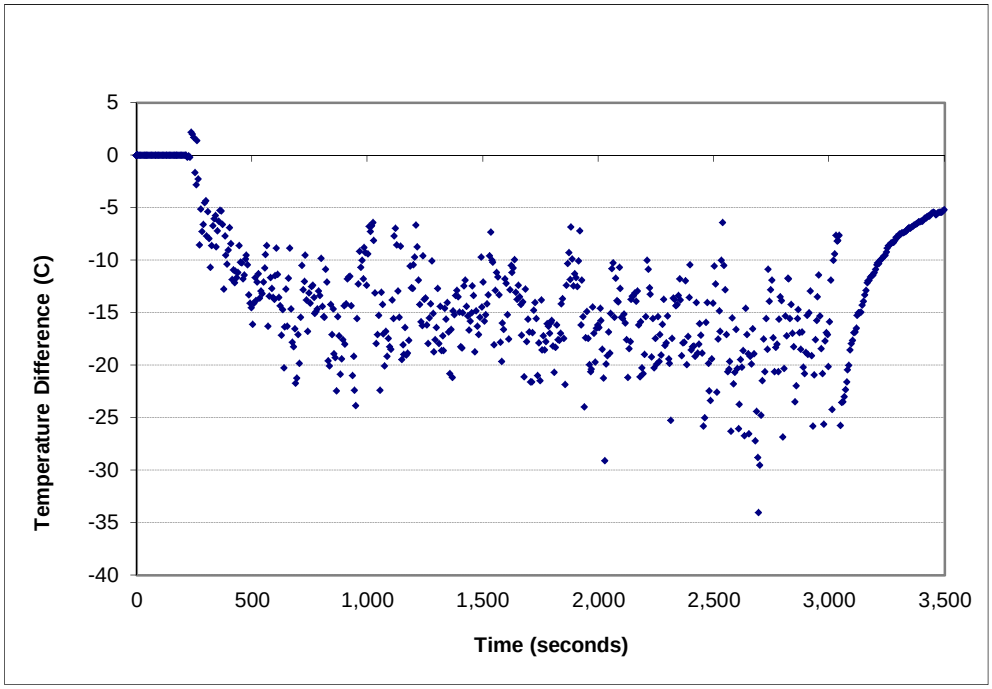

Figure A-138: Temperature error (layer 3) for the 1.5 g/s, ϕ_4 configuration

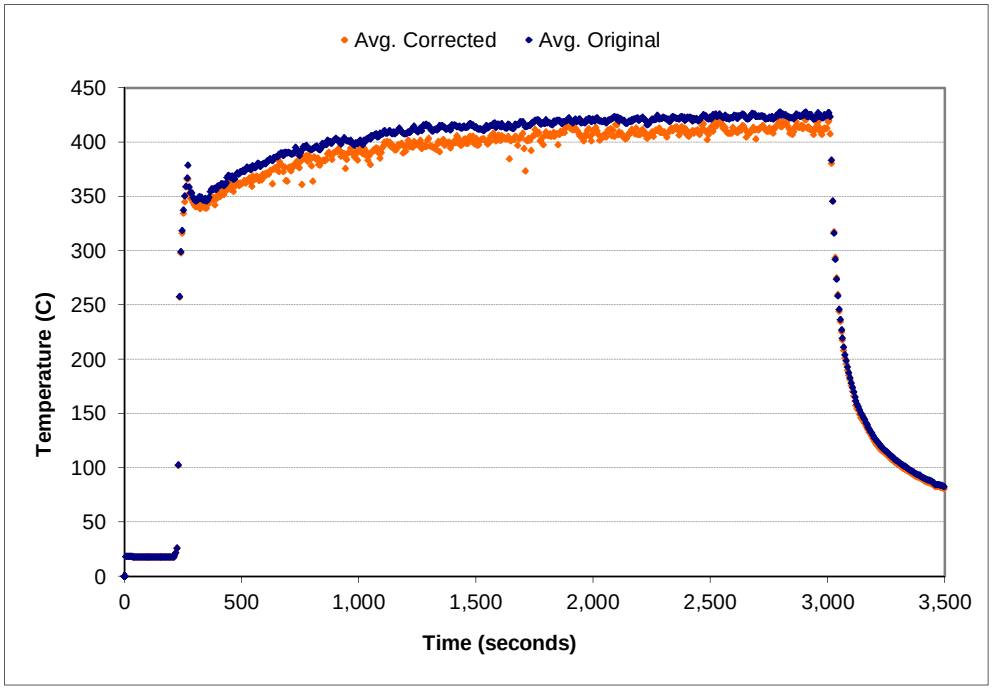

Figure A-139: Space-averaged (layer 4) temperature correction for the 1.5 g/s, ϕ_4 configuration

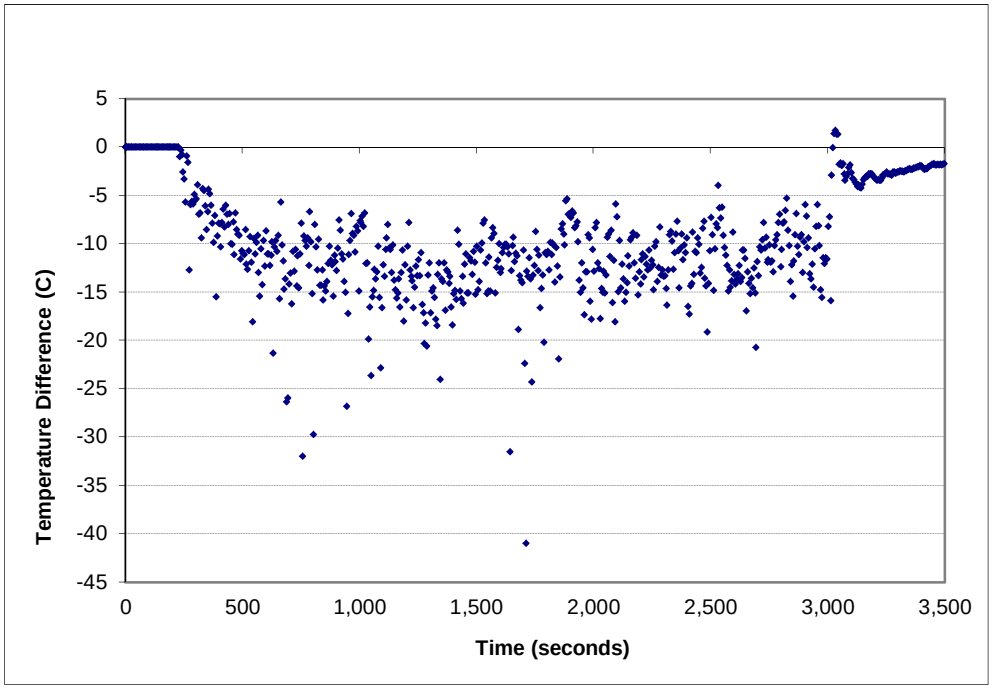

Figure A-140: Temperature error (layer 4) for the 1.5 g/s, ϕ_4 configuration

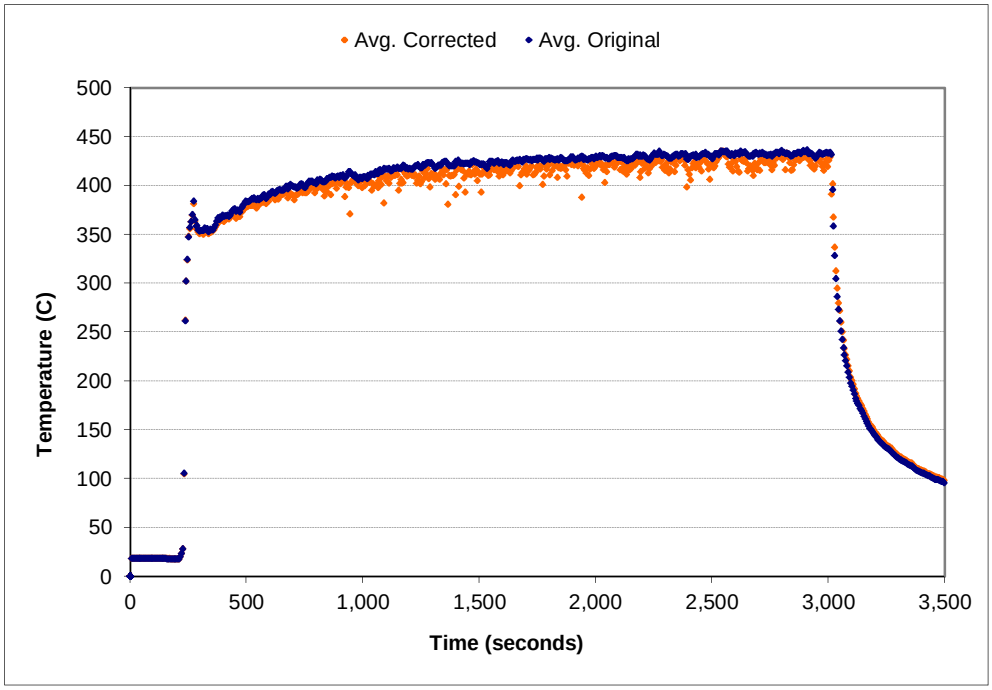

Figure A-141: Space-averaged (layer 5) temperature correction for the 1.5 g/s, ϕ_4 configuration

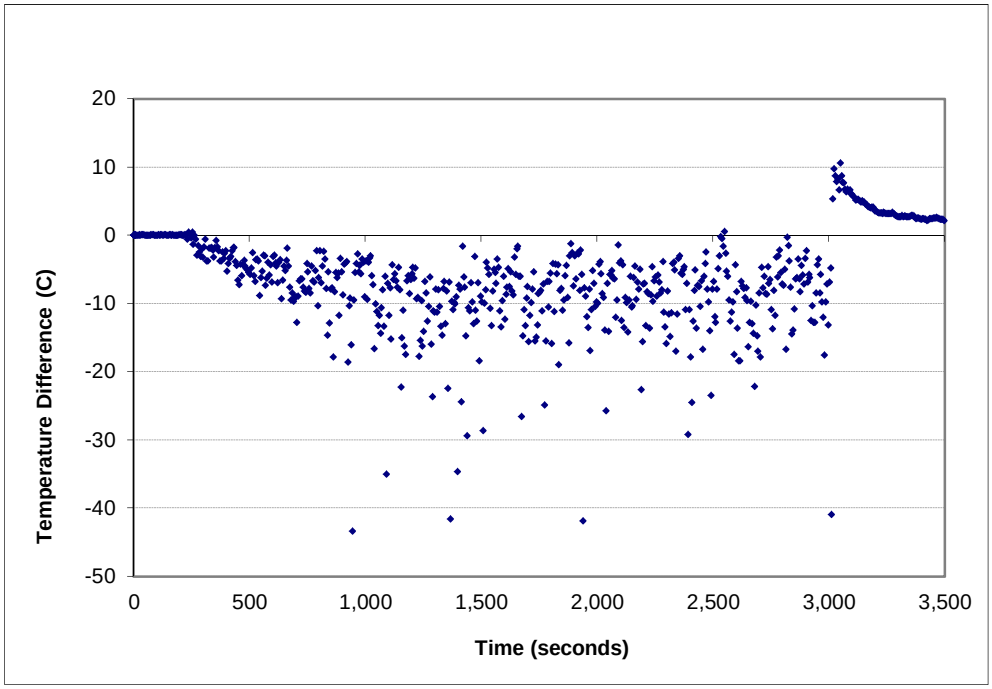

Figure A-142: Temperature error (layer 5) for the 1.5 g/s, ϕ_4 configuration

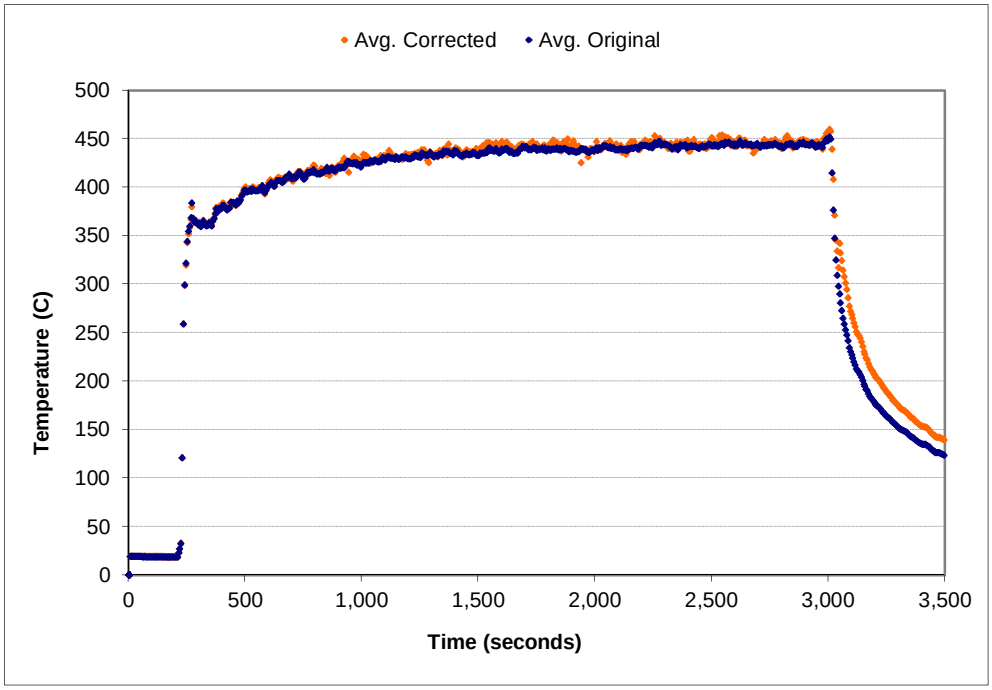

Figure A-143: Space-averaged (layer 6) temperature correction for the 1.5 g/s, ϕ_4 configuration

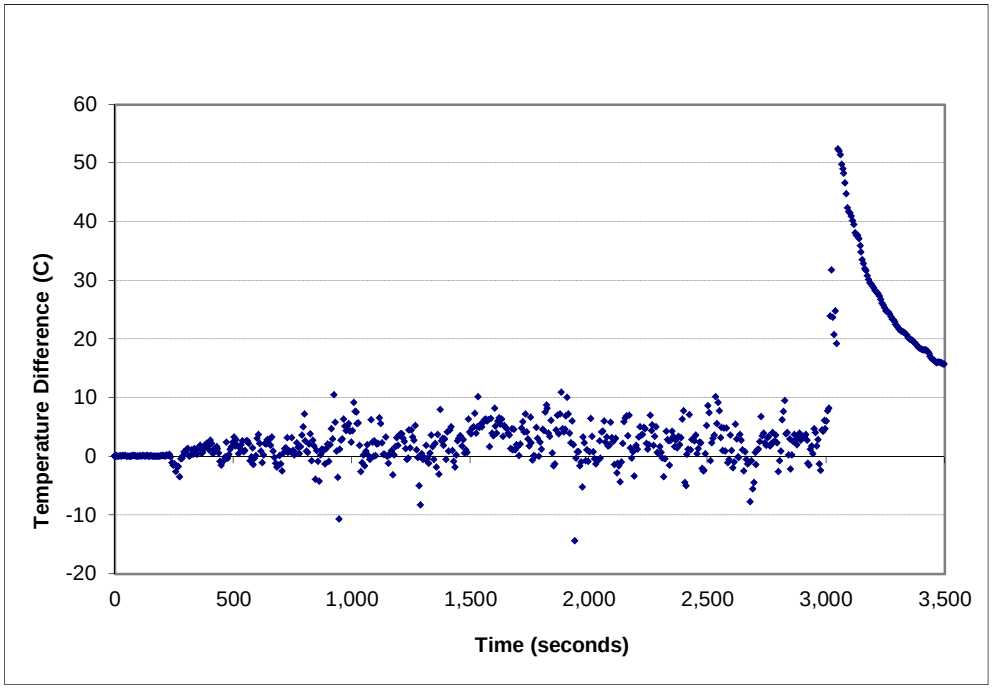

Figure A-144: Temperature error (layer 6) for the 1.5 g/s, ϕ_4 configuration

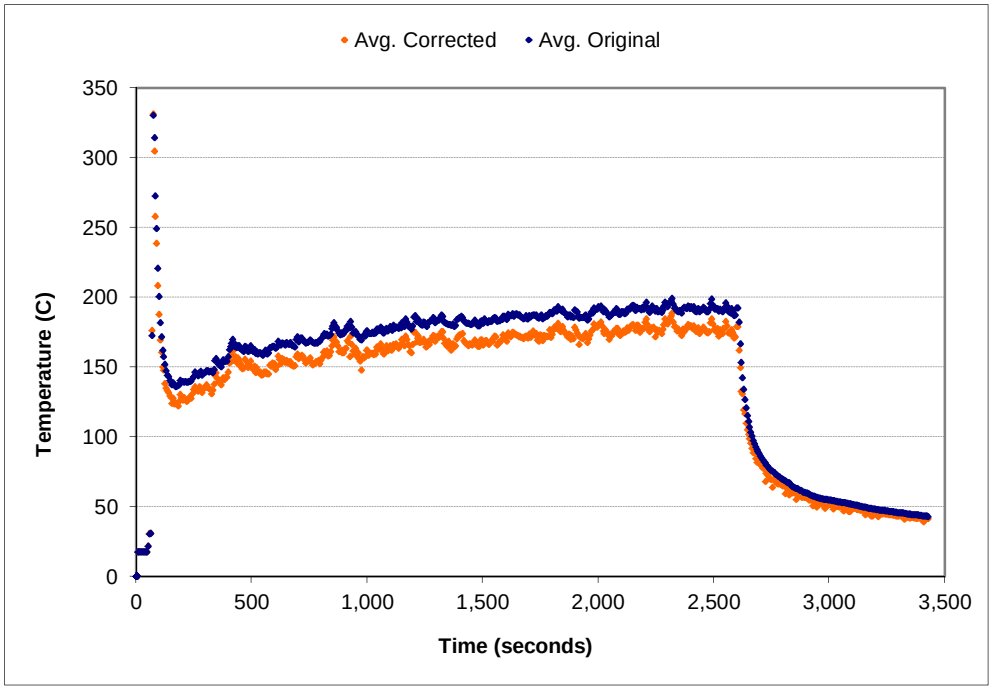

Figure A-145: Space-averaged (layer 1) temperature correction for the 0.5 g/s, ϕ_5 configuration

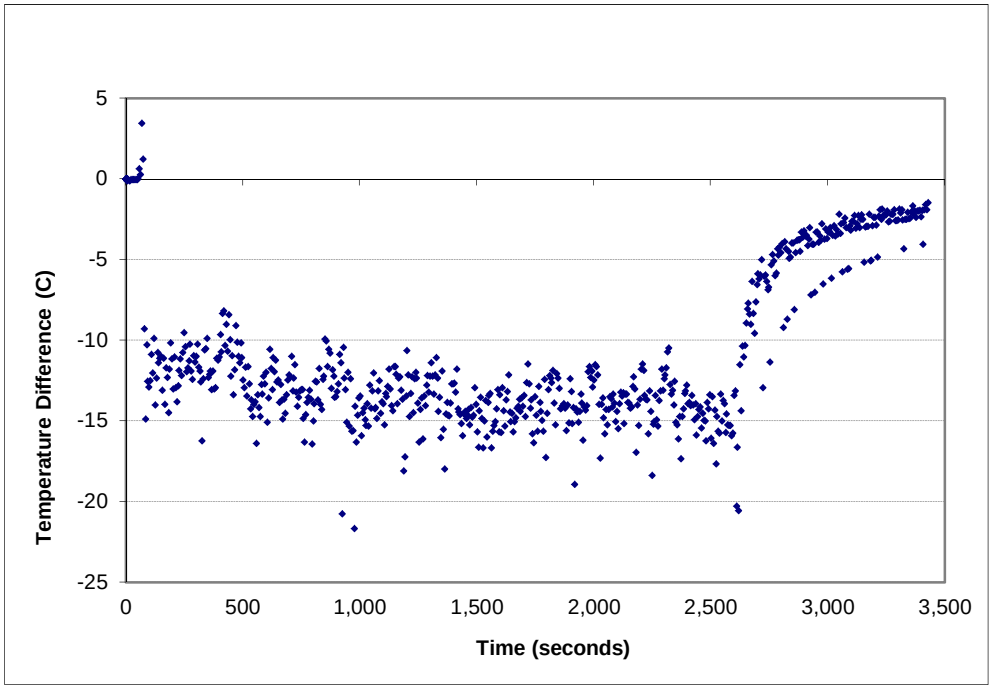

Figure A-146: Temperature error (layer 1) for the 0.5 g/s, ϕ_5 configuration

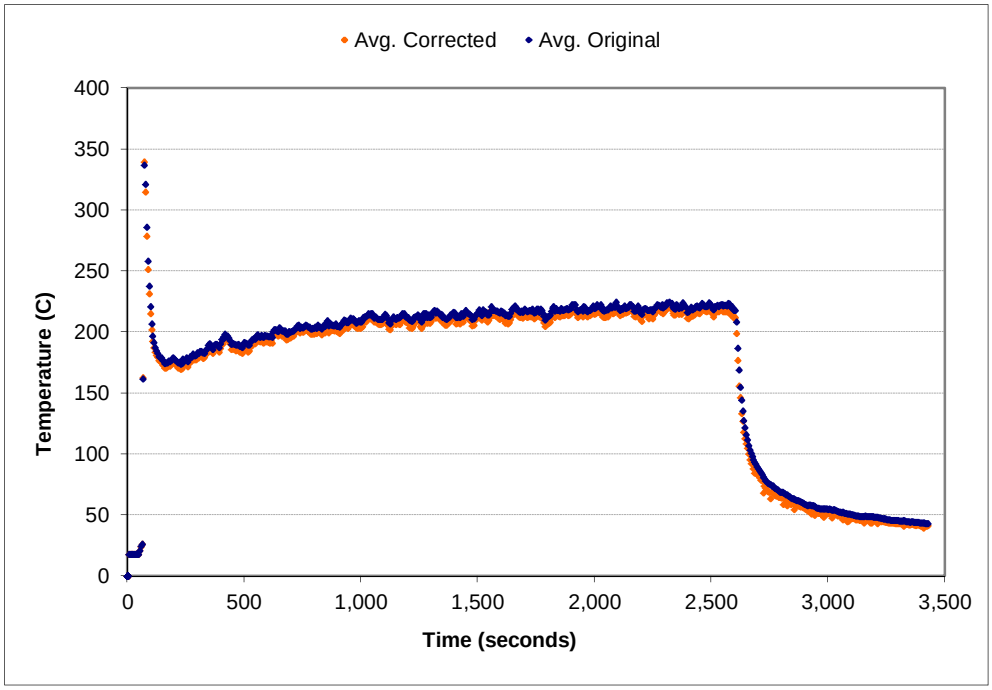

Figure A-147: Space-averaged (layer 2) temperature correction for the 0.5 g/s, ϕ_5 configuration

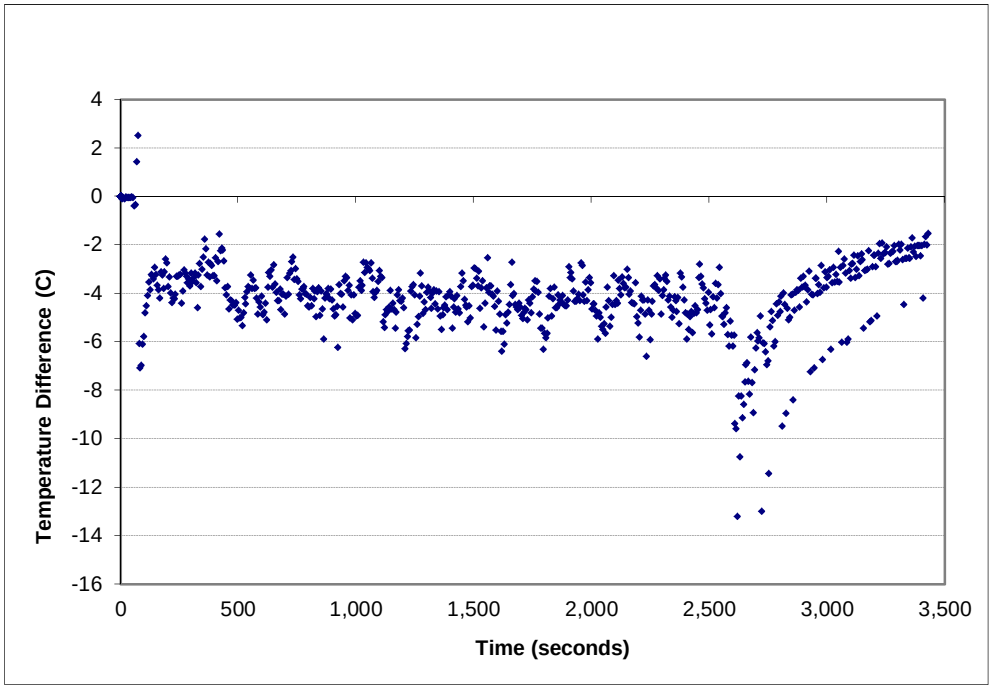

Figure A-148: Temperature error (layer 2) for the 0.5 g/s, ϕ_5 configuration

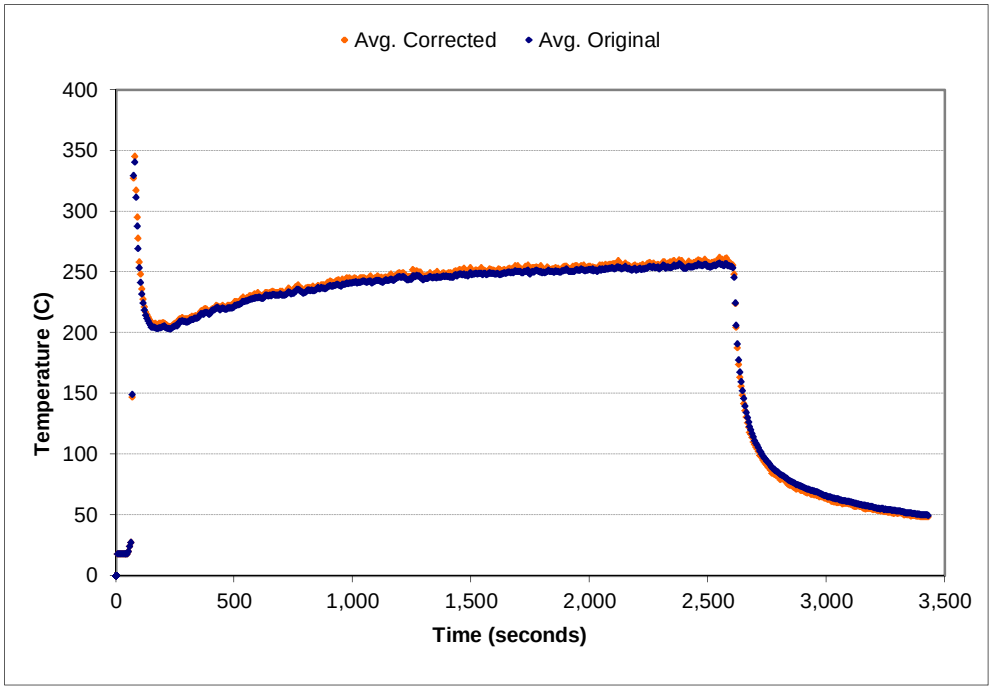

Figure A-149: Space-averaged (layer 3) temperature correction for the 0.5 g/s, ϕ_5 configuration

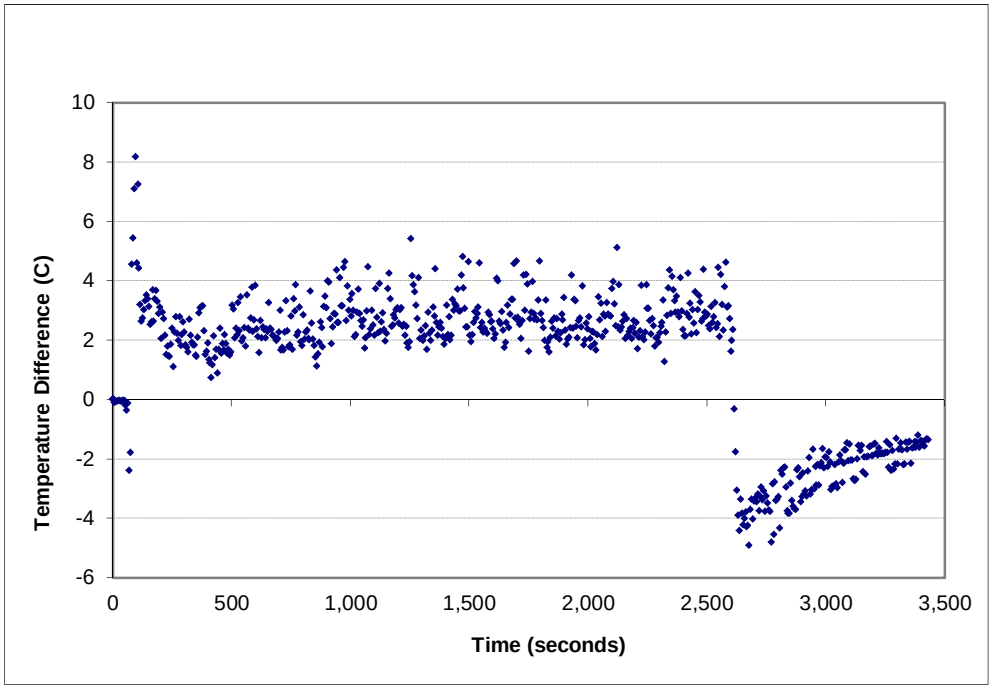

Figure A-150: Temperature error (layer 3) for the 0.5 g/s, ϕ_5 configuration

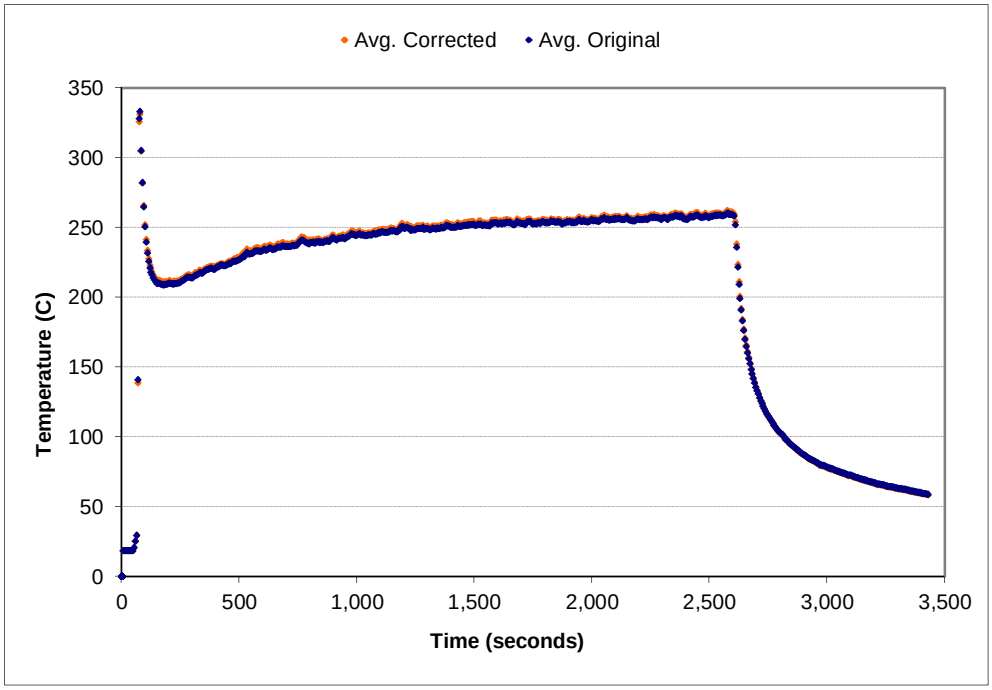

Figure A-151: Space-averaged (layer 4) temperature correction for the 0.5 g/s, ϕ_5 configuration

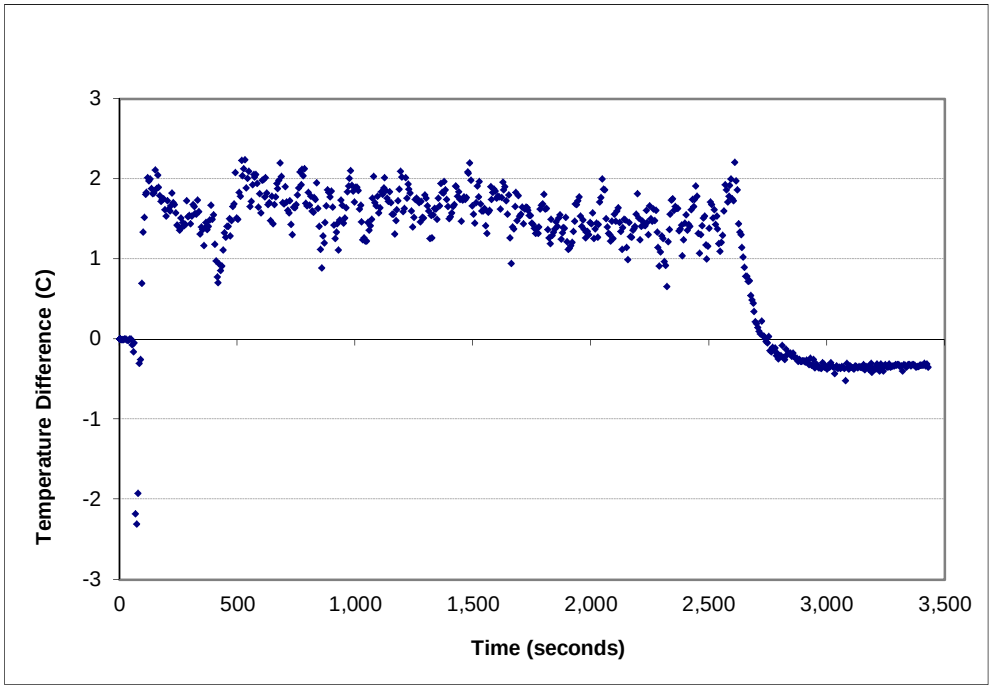

Figure A-152: Temperature error (layer 4) for the 0.5 g/s, ϕ_5 configuration

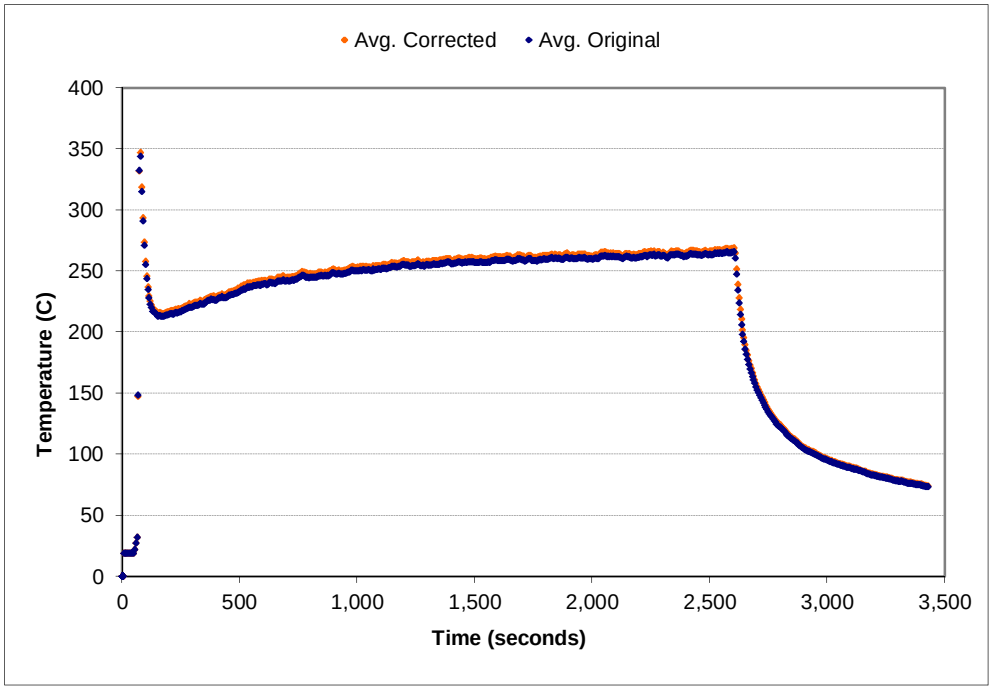

Figure A-153: Space-averaged (layer 5) temperature correction for the 0.5 g/s, ϕ_5 configuration

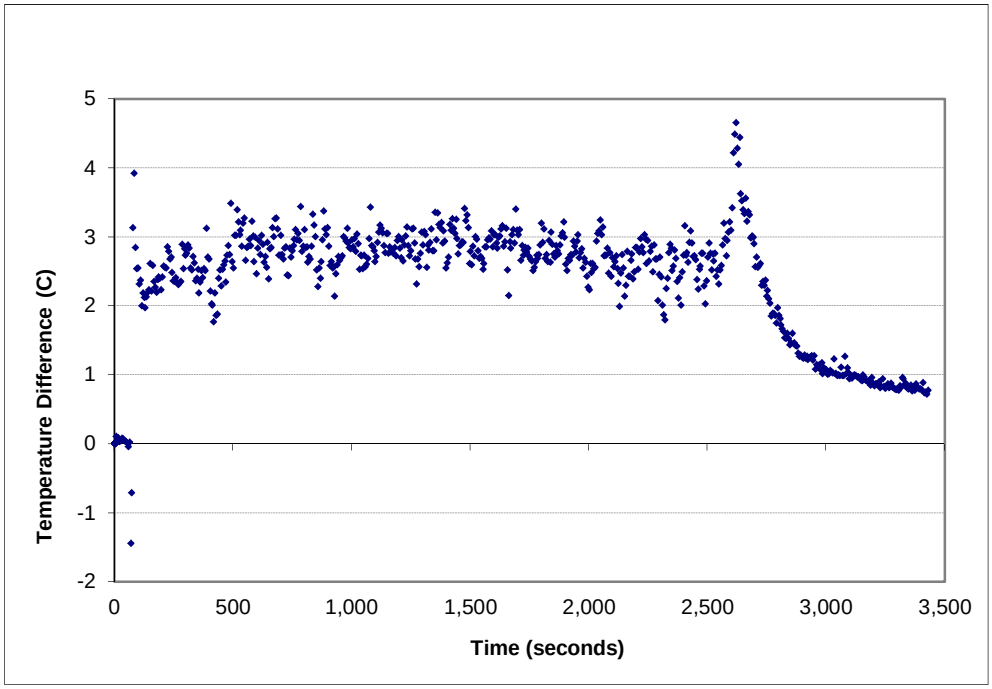

Figure A-154: Temperature error (layer 5) for the 0.5 g/s, ϕ_5 configuration

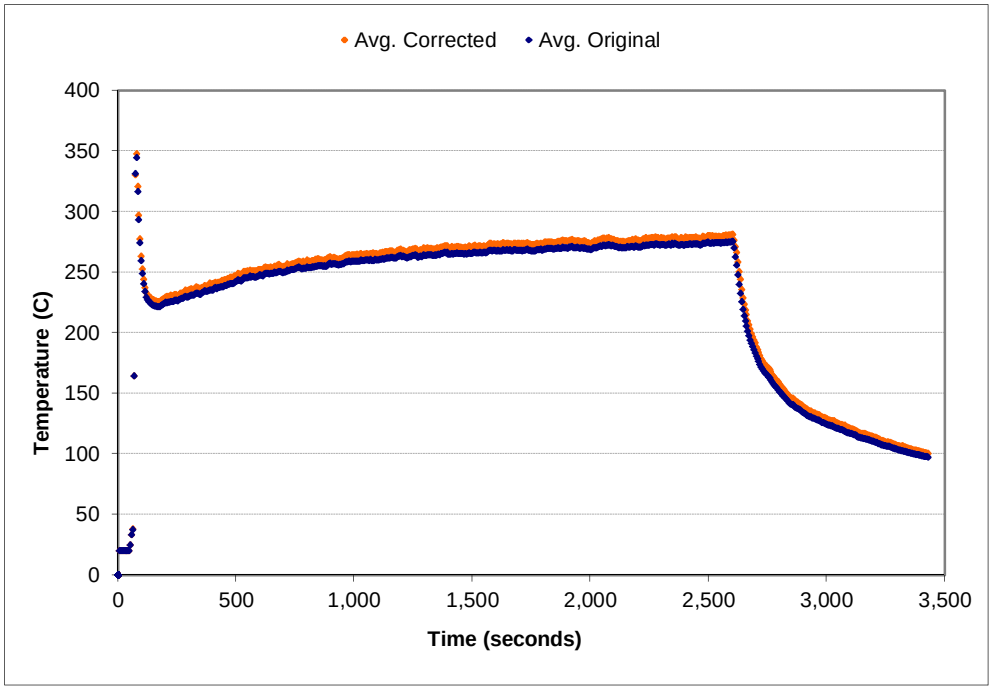

Figure A-155: Space-averaged (layer 6) temperature correction for the 0.5 g/s, ϕ_5 configuration

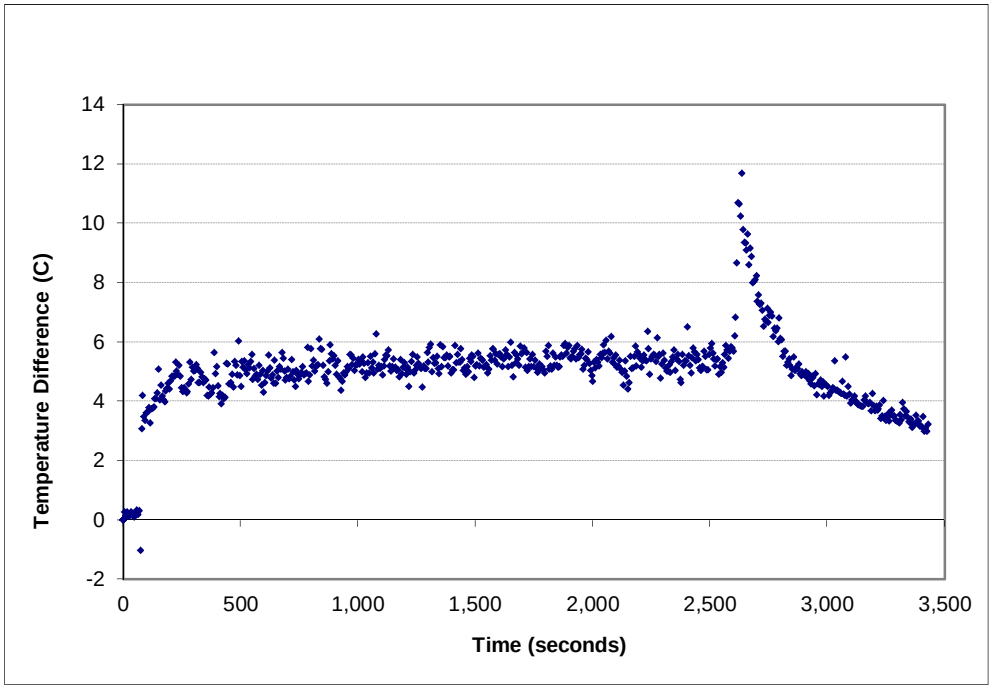

Figure A-156: Temperature error (layer 6) for the 0.5 g/s, ϕ_5 configuration

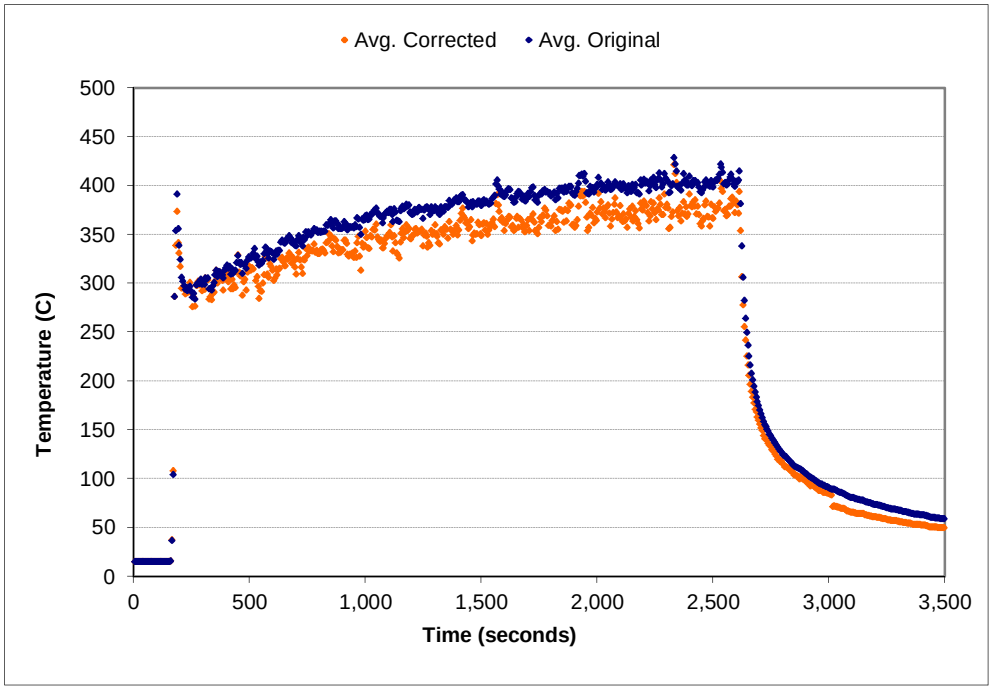

Figure A-157: Space-averaged (layer 1) temperature correction for the 1.0 g/s, ϕ_5 configuration

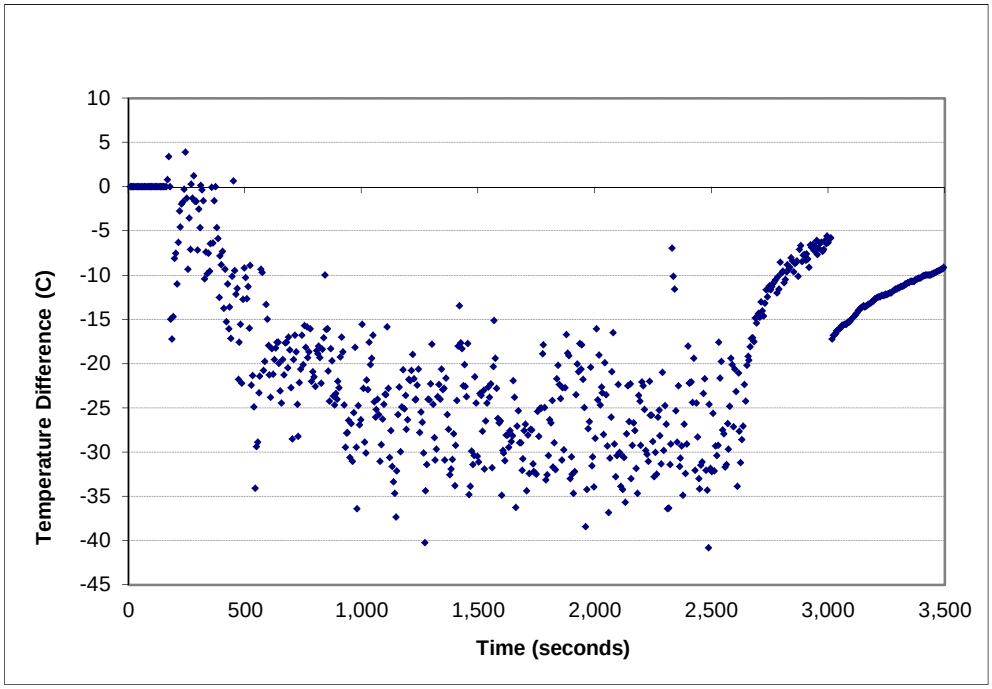

Figure A-158: Temperature error (layer 1) for the 1.0 g/s, ϕ_5 configuration

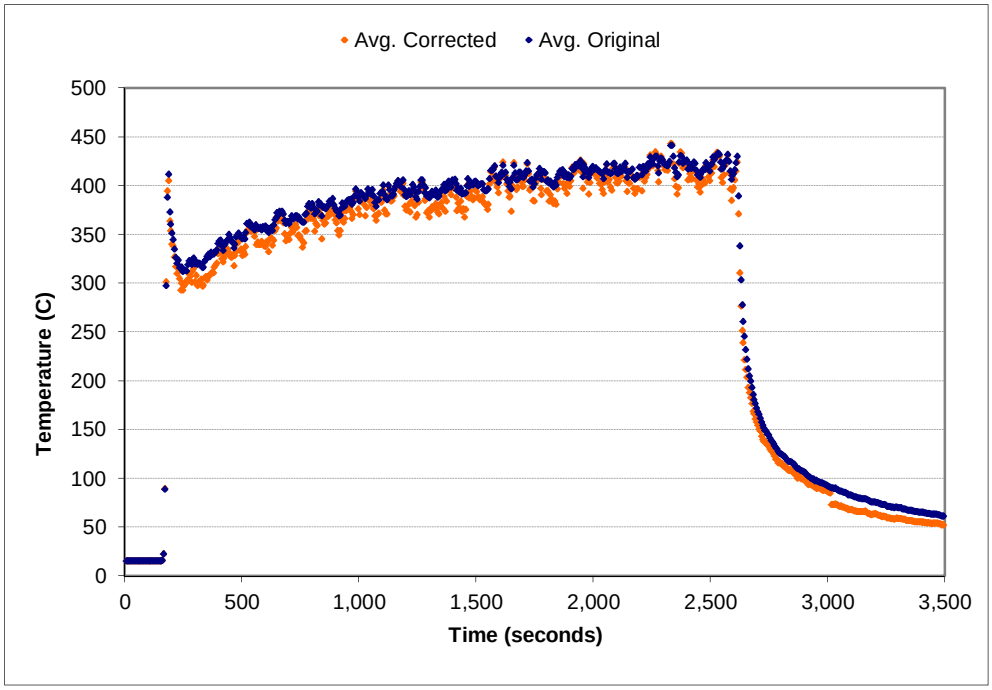

Figure A-159: Space-averaged (layer 2) temperature correction for the 1.0 g/s, ϕ_5 configuration

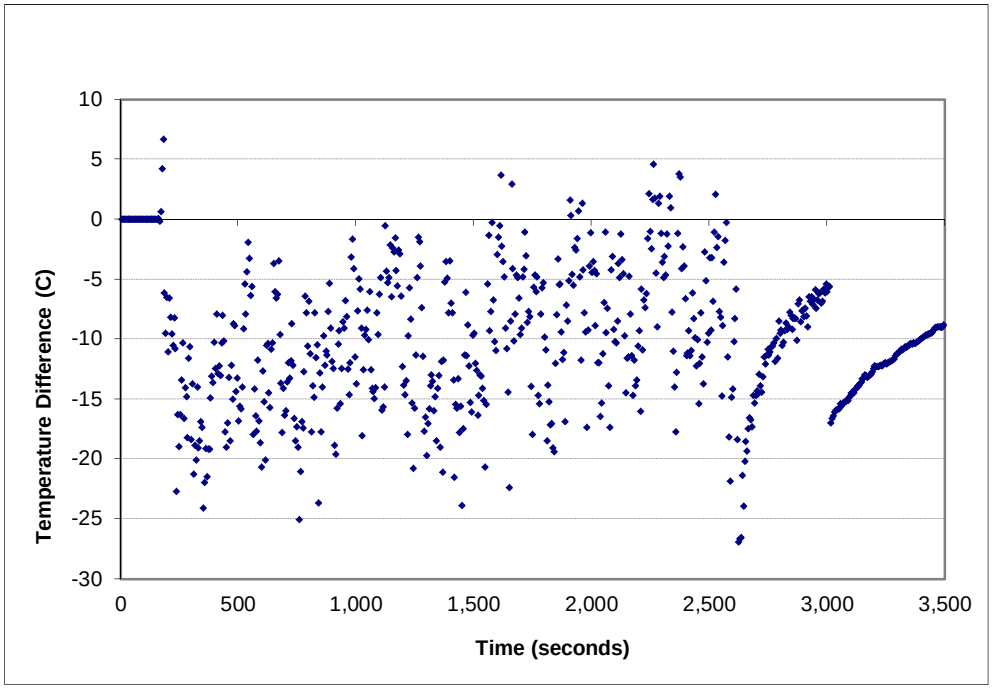

Figure A-160: Temperature error (layer 2) for the 1.0 g/s, ϕ_5 configuration

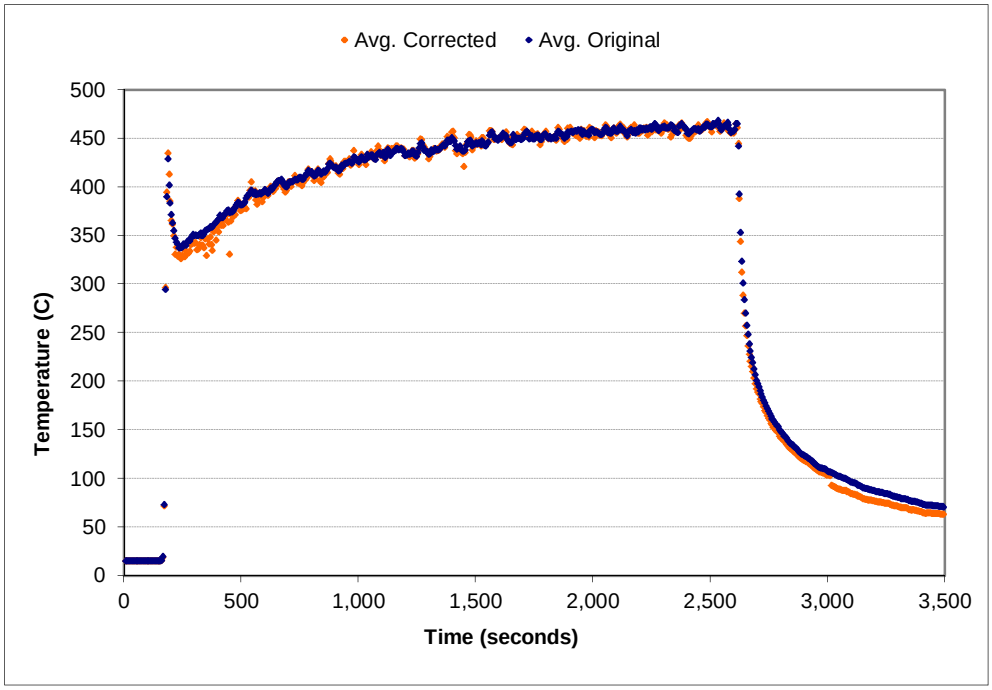

Figure A-161: Space-averaged (layer 3) temperature correction for the 1.0 g/s, ϕ_5 configuration

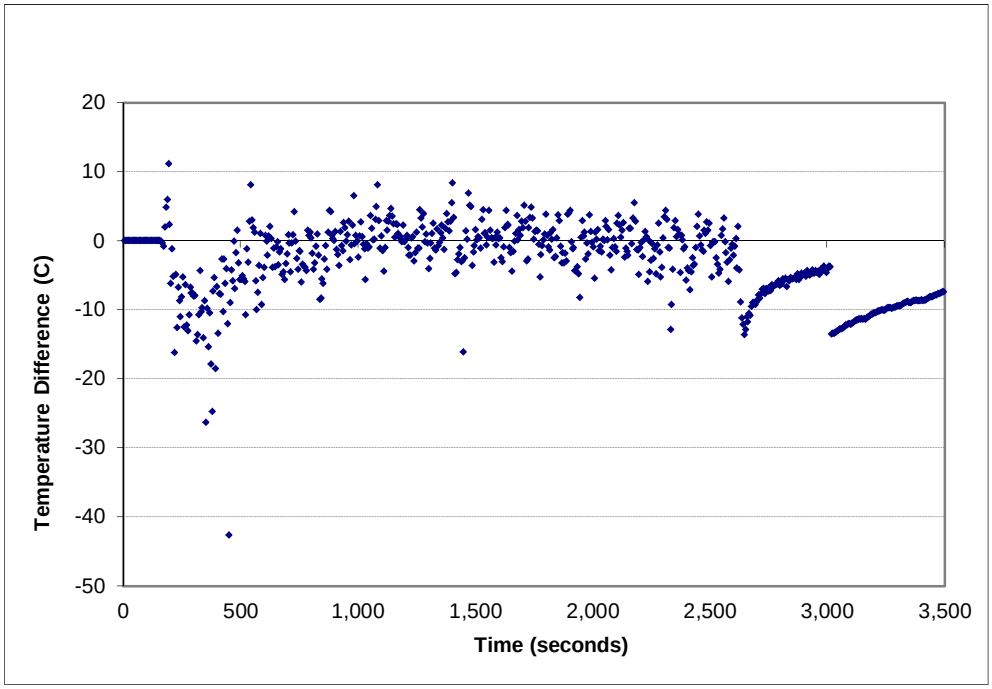

Figure A- 162: Temperature error (layer 3) for the 1.0 g/s, ϕ_5 configuration

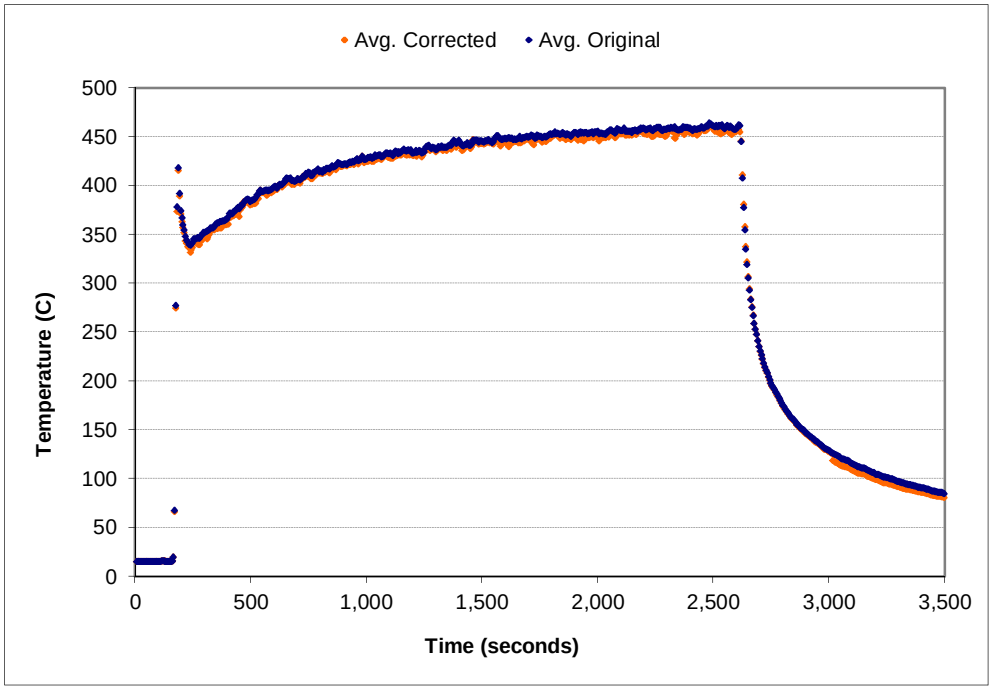

Figure A-163: Space-averaged (layer 4) temperature correction for the 1.0 g/s, ϕ_5 configuration

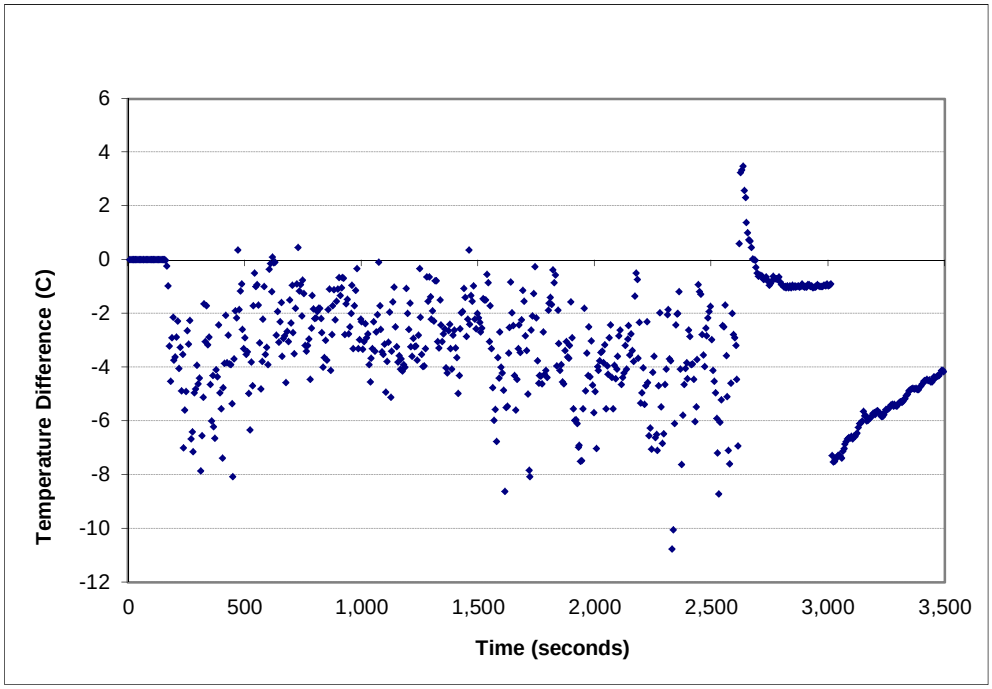

Figure A-164: Temperature error (layer 4) for the 1.0 g/s, ϕ_5 configuration

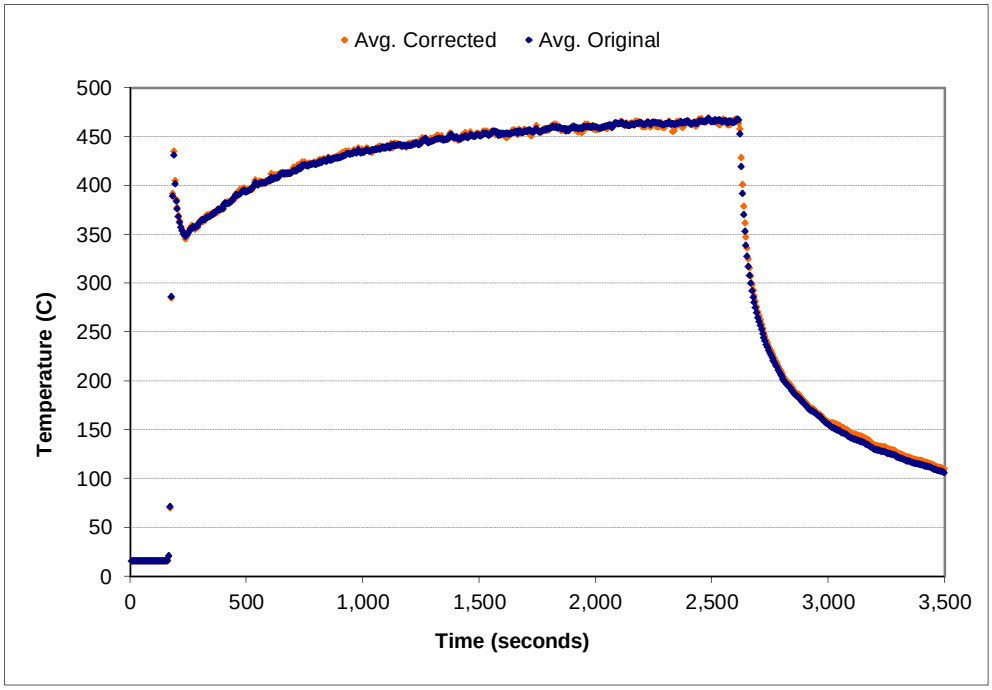

Figure A-165: Space-averaged (layer 5) temperature correction for the 1.0 g/s, ϕ_5 configuration

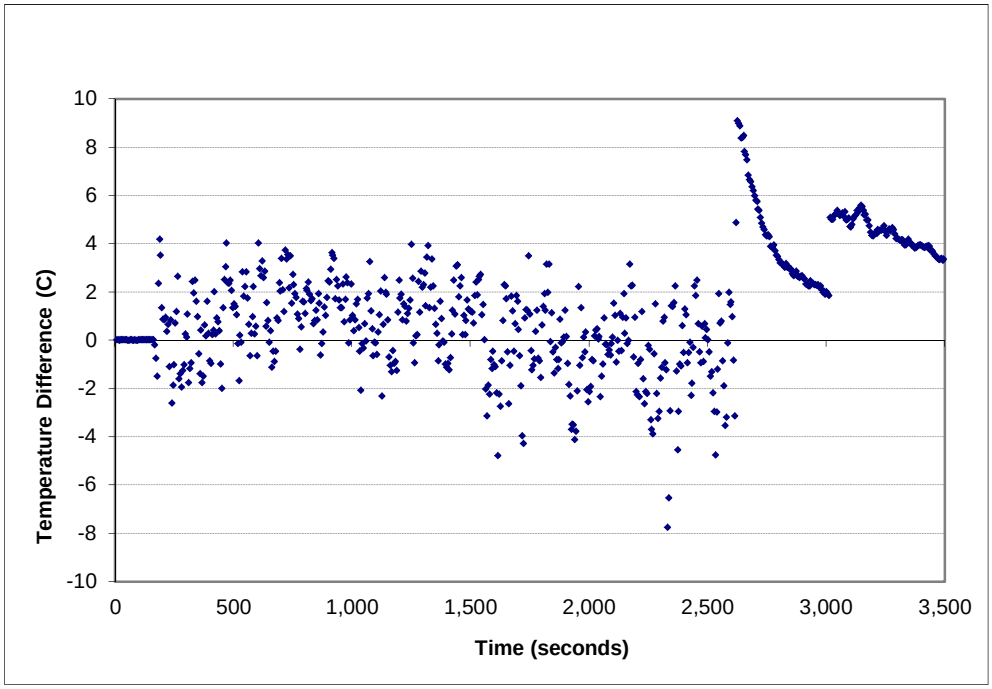

Figure A-166: Temperature error (layer 5) for the 1.0 g/s, ϕ_5 configuration

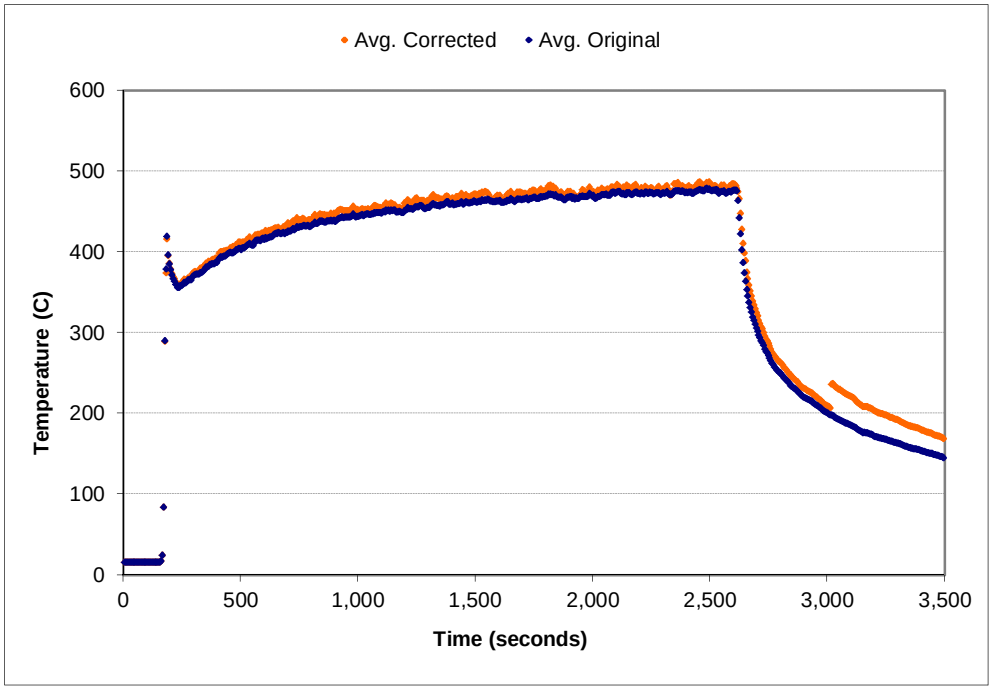

Figure A-167: Space-averaged (layer 6) temperature correction for the 1.0 g/s, ϕ_5 configuration

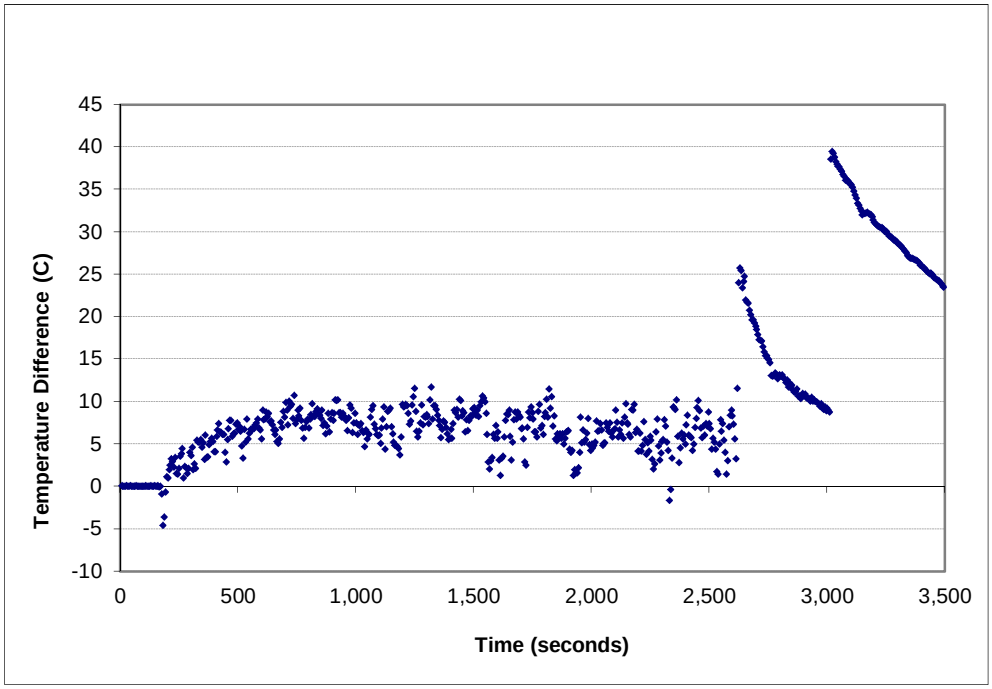

Figure A-168: Temperature error (layer 6) for the 1.0 g/s, ϕ_5 configuration

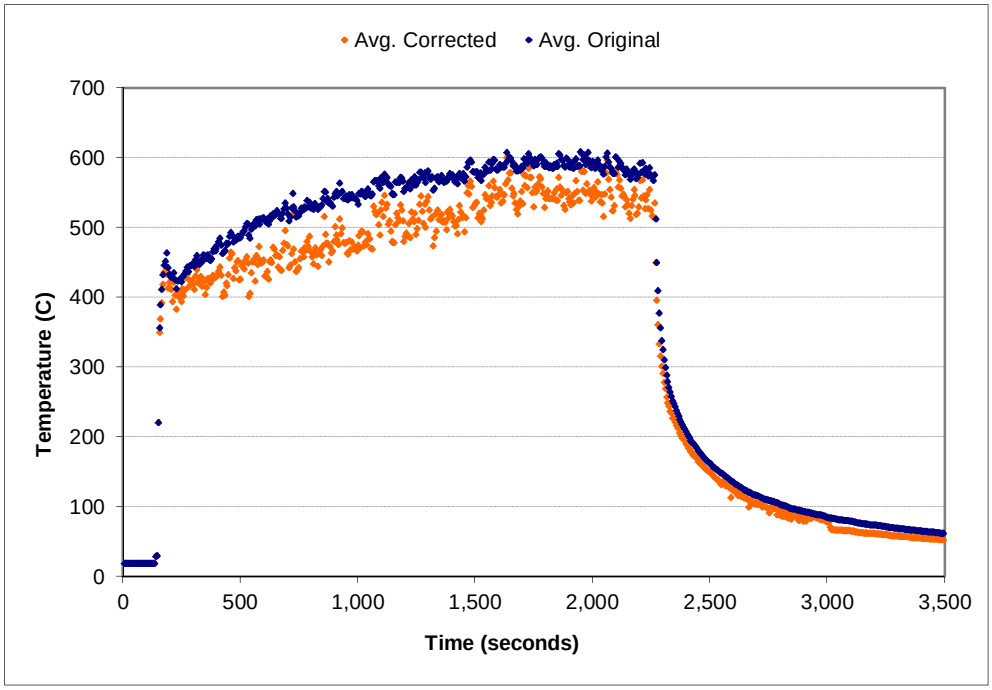

Figure A-169: Space-averaged (layer 1) temperature correction for the 1.5 g/s, ϕ_5 configuration

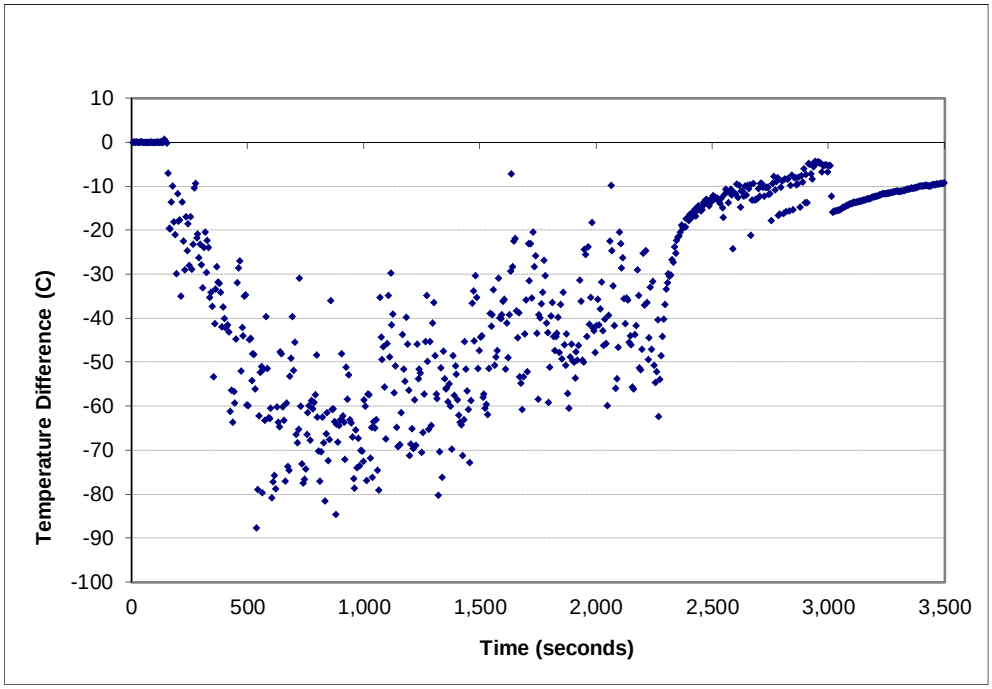

Figure A-170: Temperature error (layer 1) for the 1.5 g/s, ϕ_5 configuration

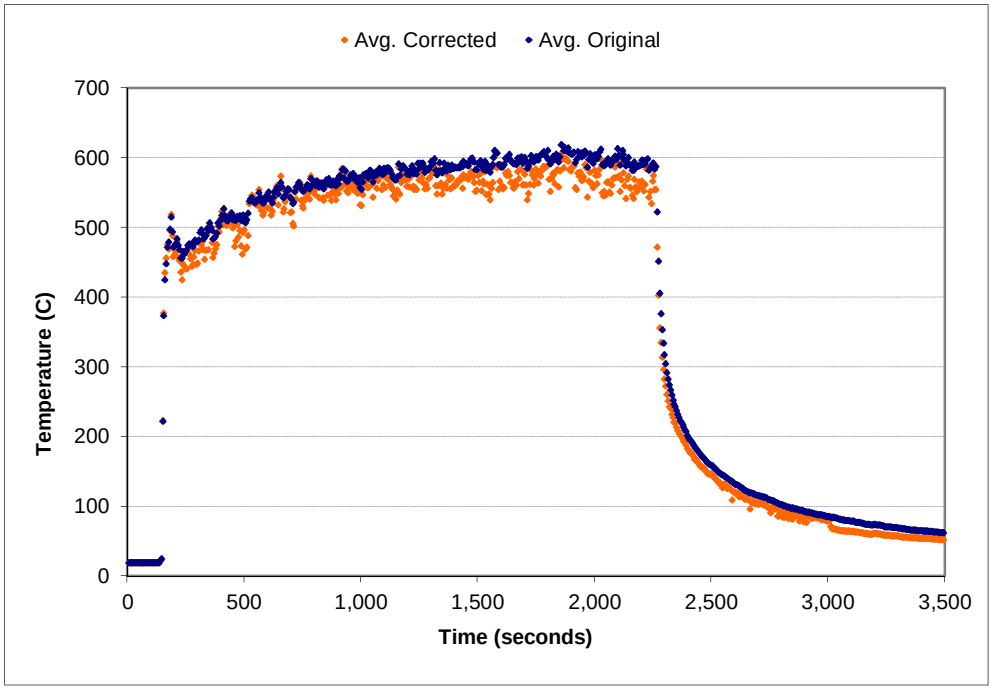

Figure A-171: Space-averaged (layer 2) temperature correction for the 1.5 g/s, ϕ_5 configuration

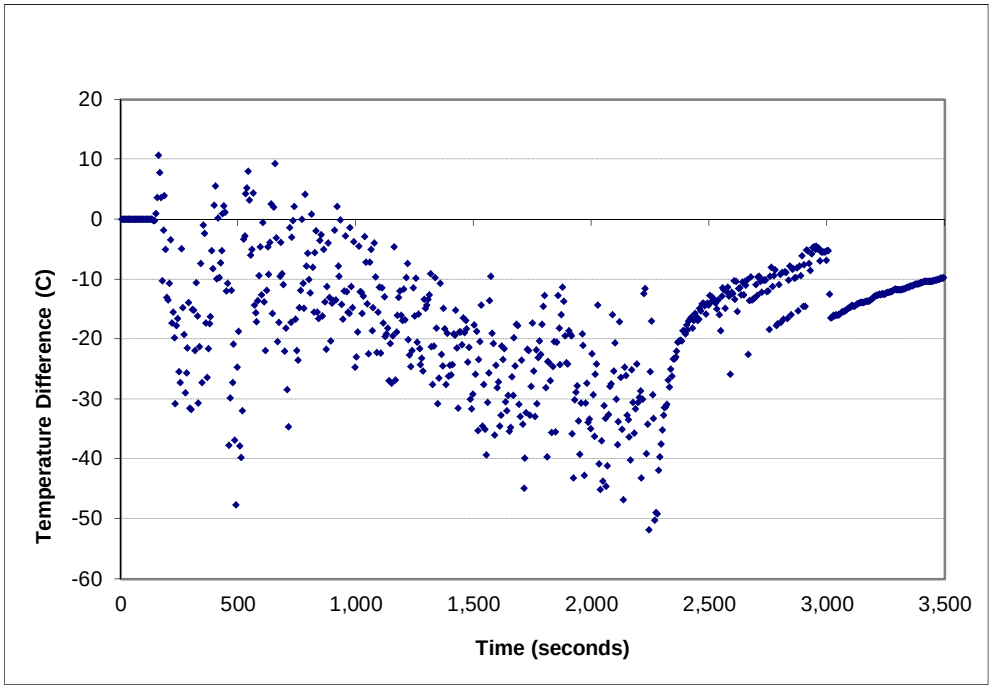

Figure A-172: Temperature error (layer 2) for the 1.5 g/s, ϕ_5 configuration

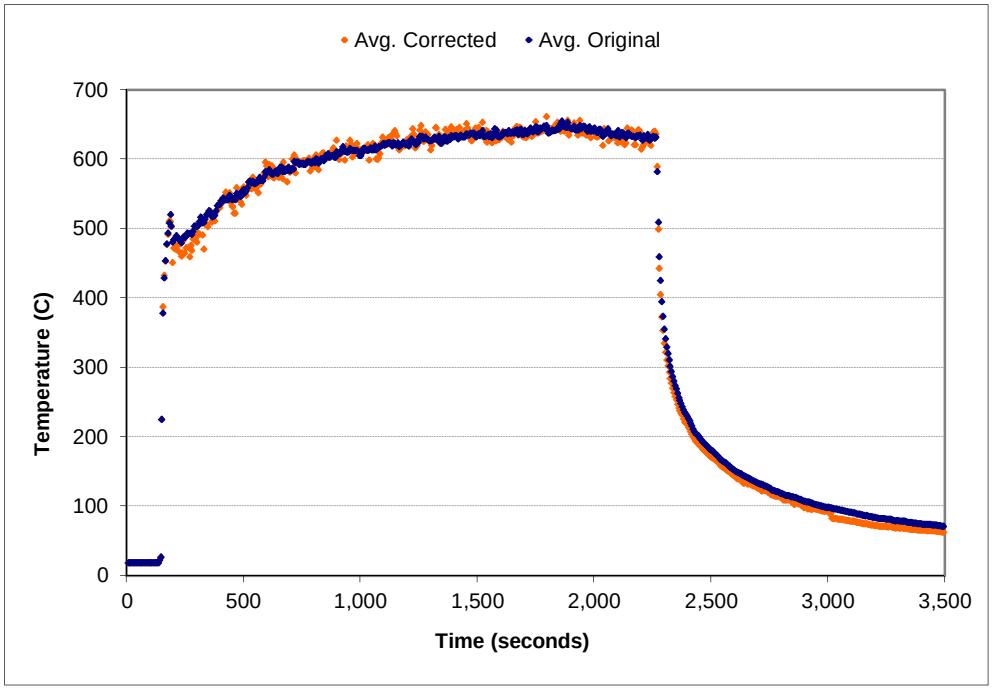

Figure A-173: Space-averaged (layer 3) temperature correction for the 1.5 g/s, ϕ_5 configuration

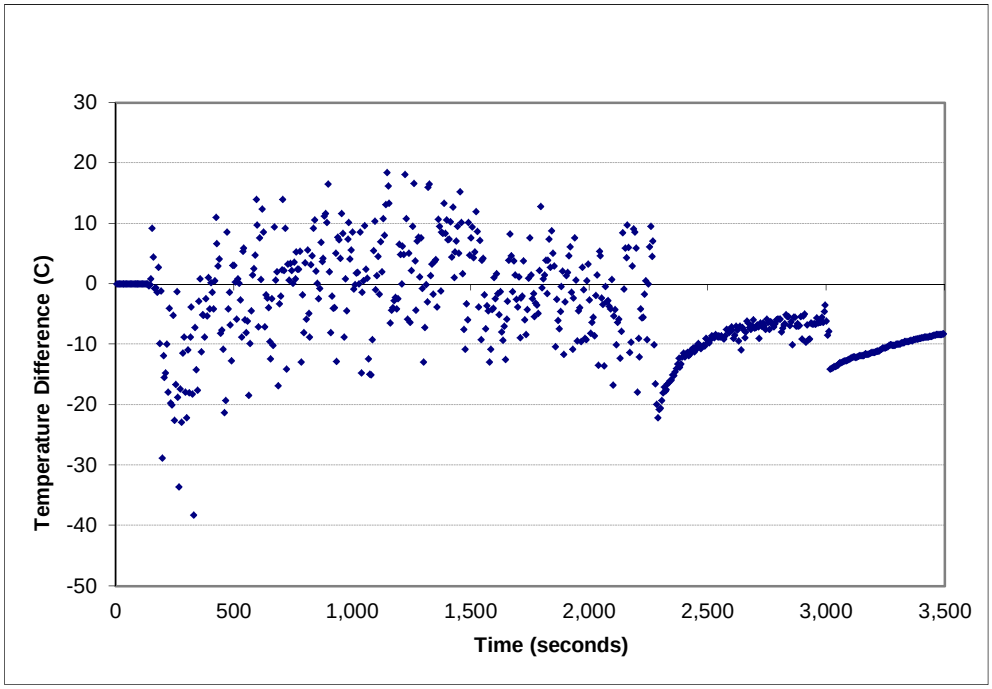

Figure A-174: Temperature error (layer 3) for the 1.5 g/s, ϕ_5 configuration

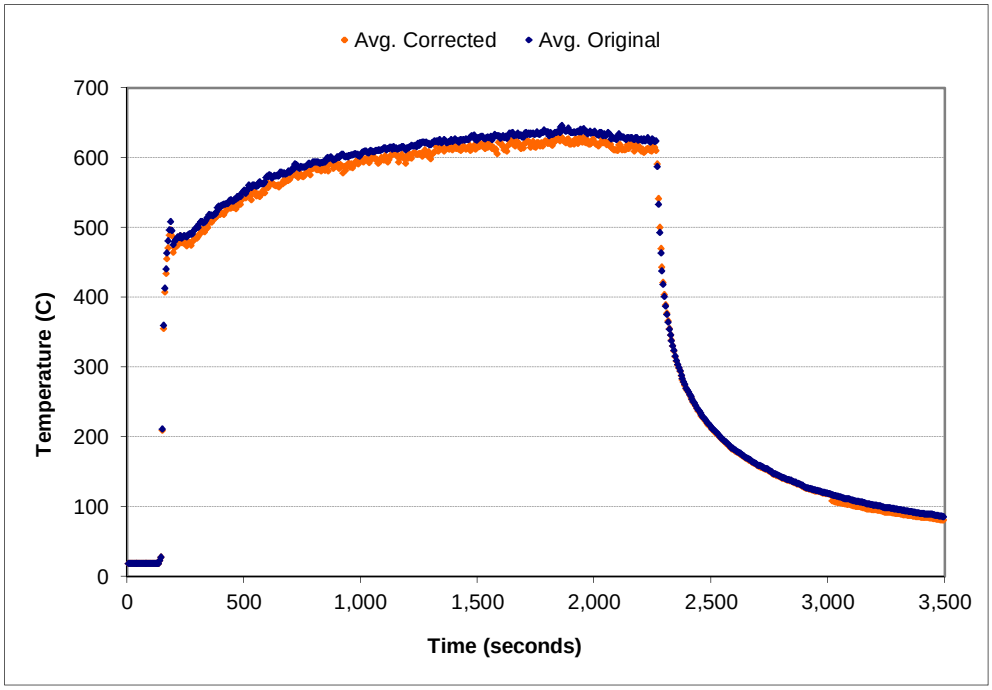

Figure A-175: Space-averaged (layer 4) temperature correction for the 1.5 g/s, ϕ_5 configuration

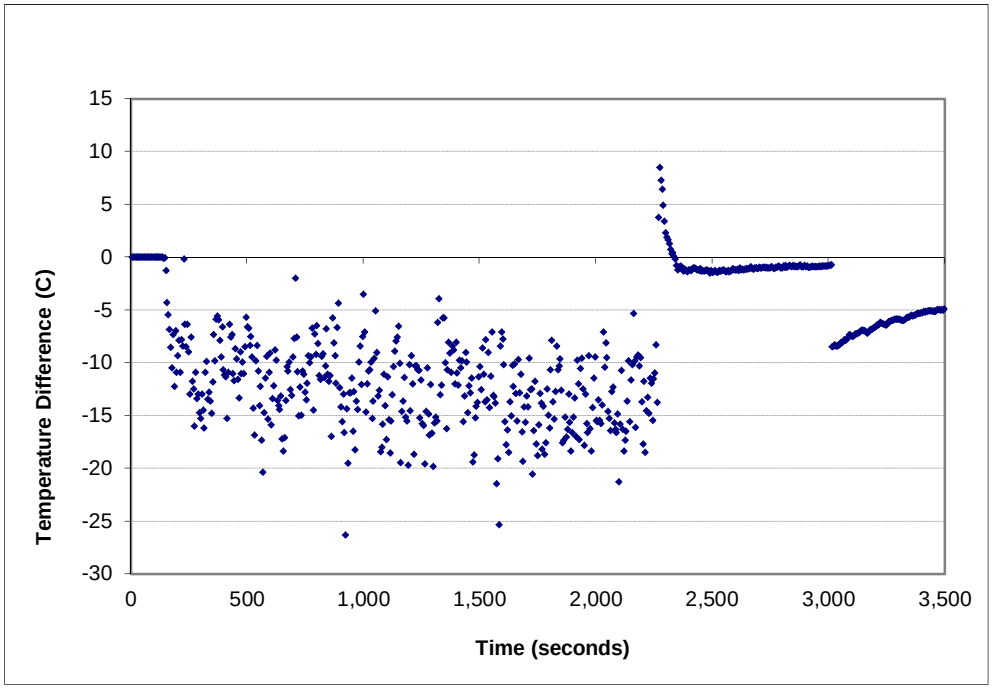

Figure A-176: Temperature error (layer 4) for the 1.5 g/s, ϕ_5 configuration

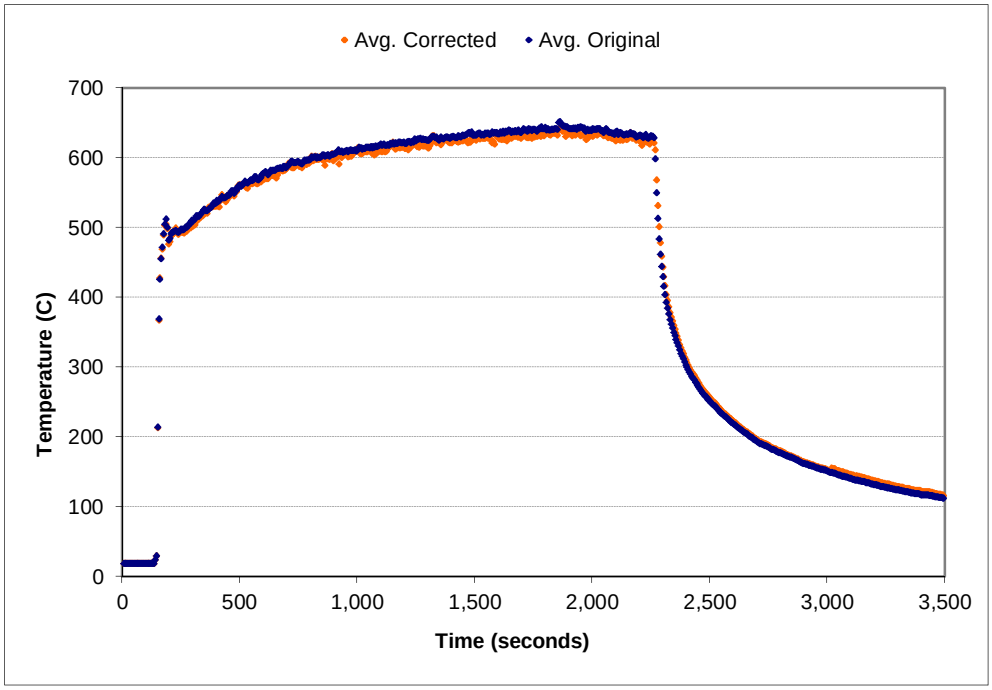

Figure A-177: Space-averaged (layer 5) temperature correction for the 1.5 g/s, ϕ_5 configuration

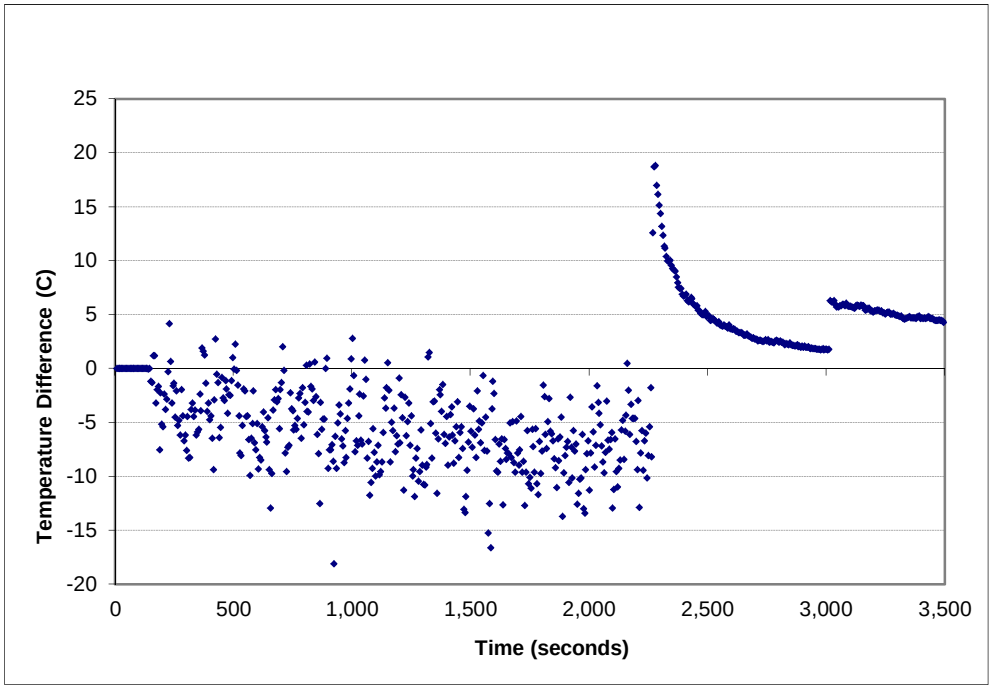

Figure A-178: Temperature error (layer 5) for the 1.5 g/s, ϕ_5 configuration

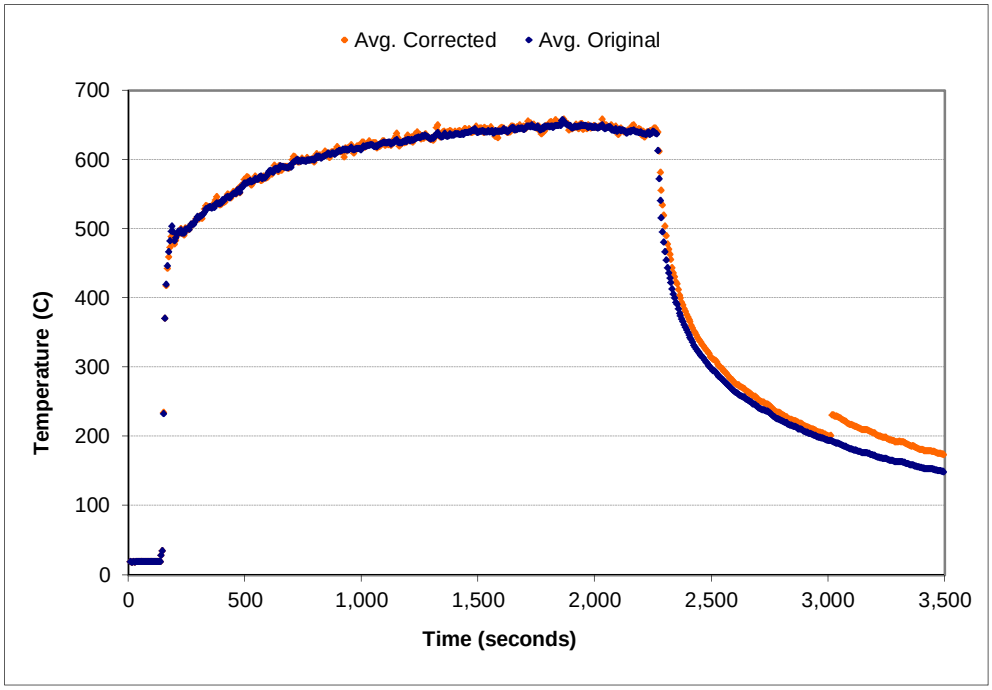

Figure A-179: Space-averaged (layer 6) temperature correction for the 1.5 g/s, ϕ_5 configuration

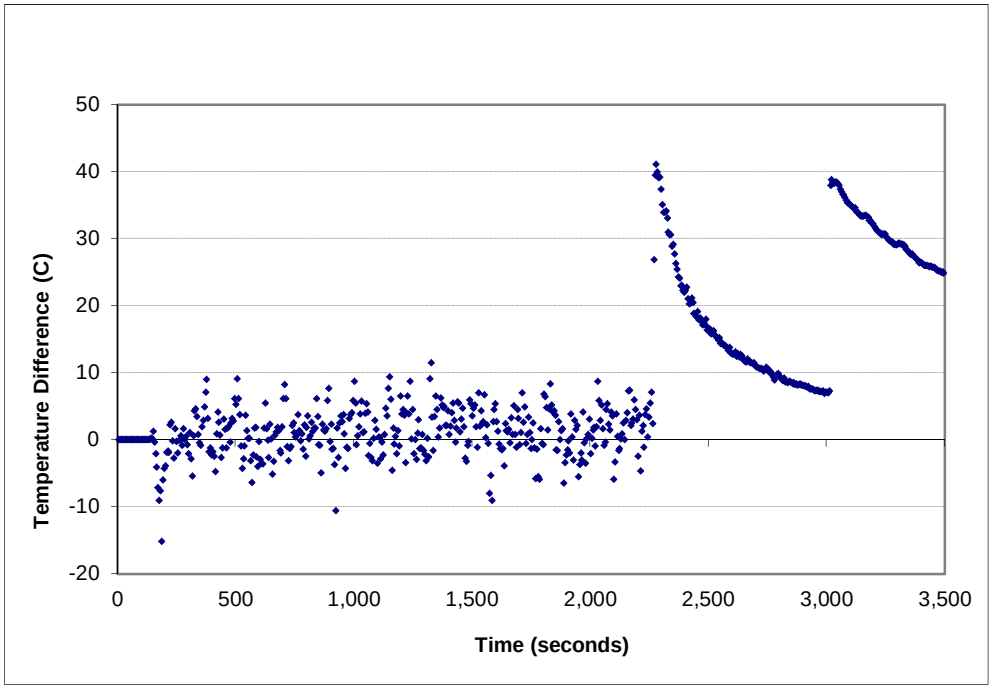

Figure A-180: Temperature error (layer 6) for the 1.5 g/s, ϕ_5 configuration

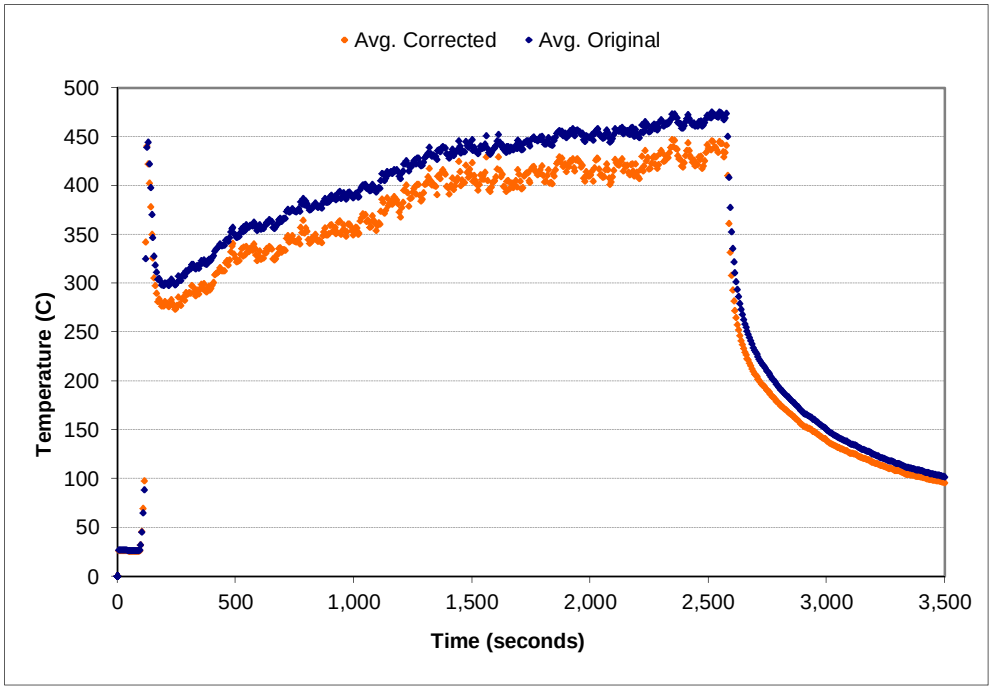

Figure A-181: Space-averaged (layer 1) temperature correction for the 0.5 g/s, ϕ_6 configuration

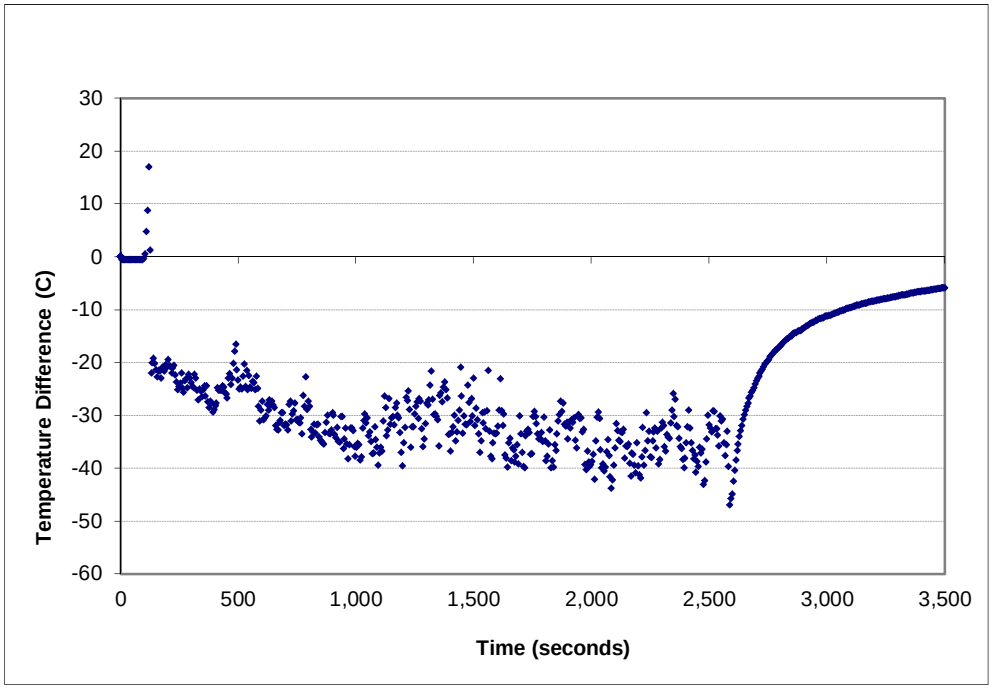

Figure A-182: Temperature error (layer 1) for the 0.5 g/s, ϕ_6 configuration

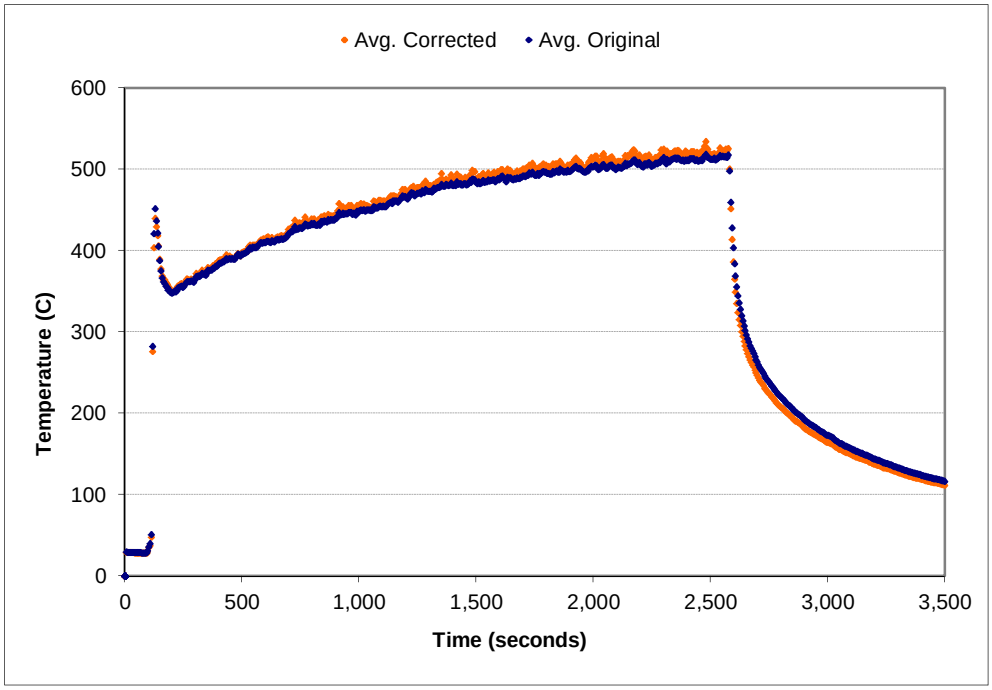

Figure A-183: Space-averaged (layer 2) temperature correction for the 0.5 g/s, ϕ_6 configuration

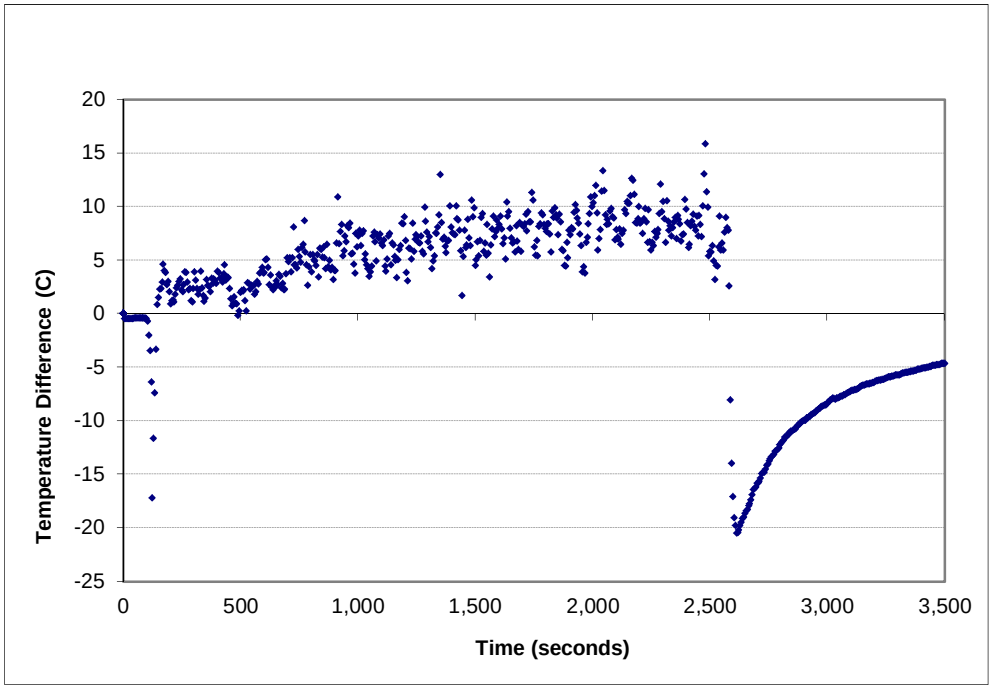

Figure A-184: Temperature error (layer 2) for the 0.5 g/s, ϕ_6 configuration

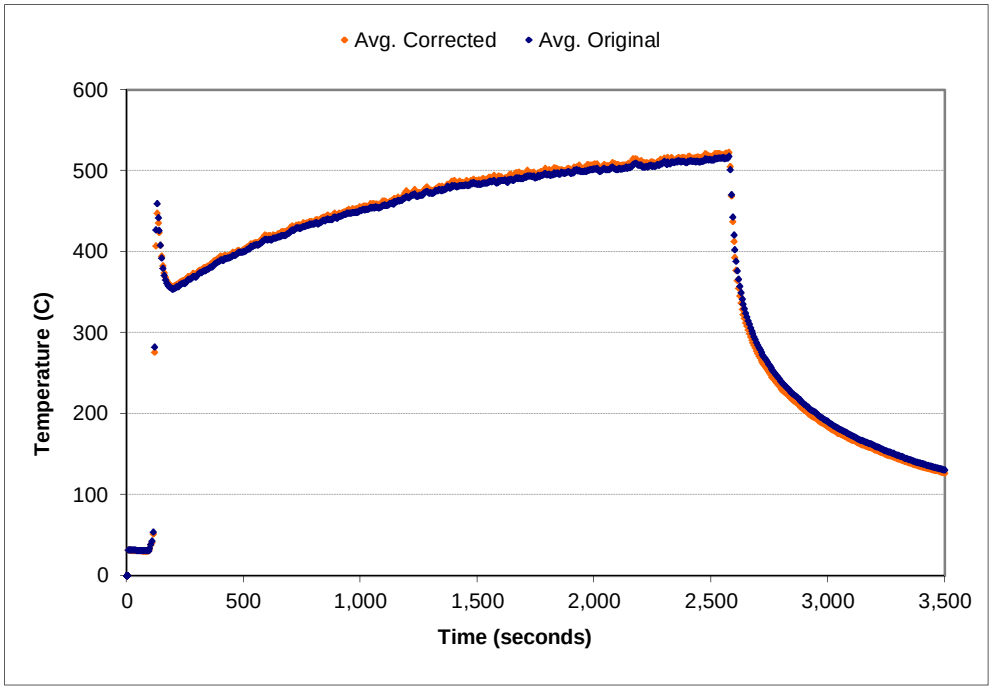

Figure A-185: Space-averaged (layer 3) temperature correction for the 0.5 g/s, ϕ_6 configuration

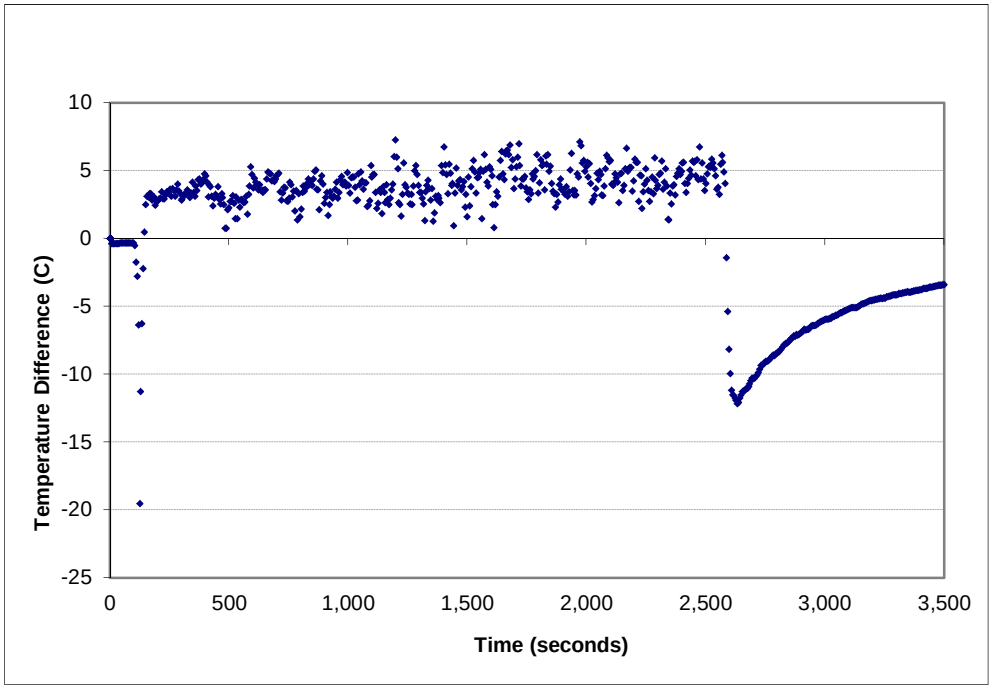

Figure A-186: Temperature error (layer 3) for the 0.5 g/s, ϕ_6 configuration

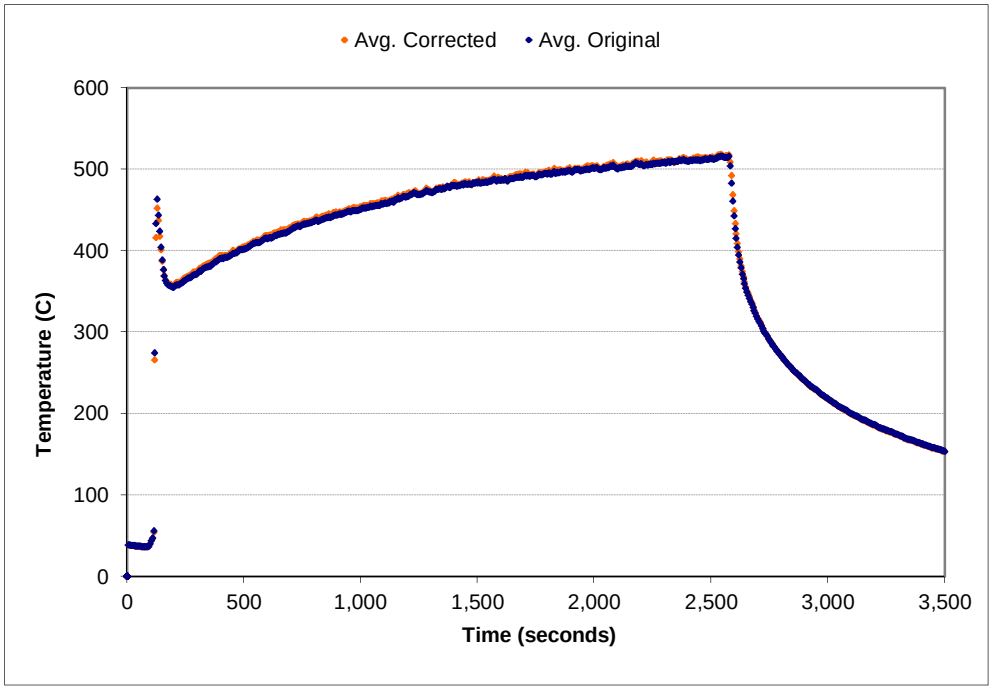

Figure A-187: Space-averaged (layer 4) temperature correction for the 0.5 g/s, ϕ_6 configuration

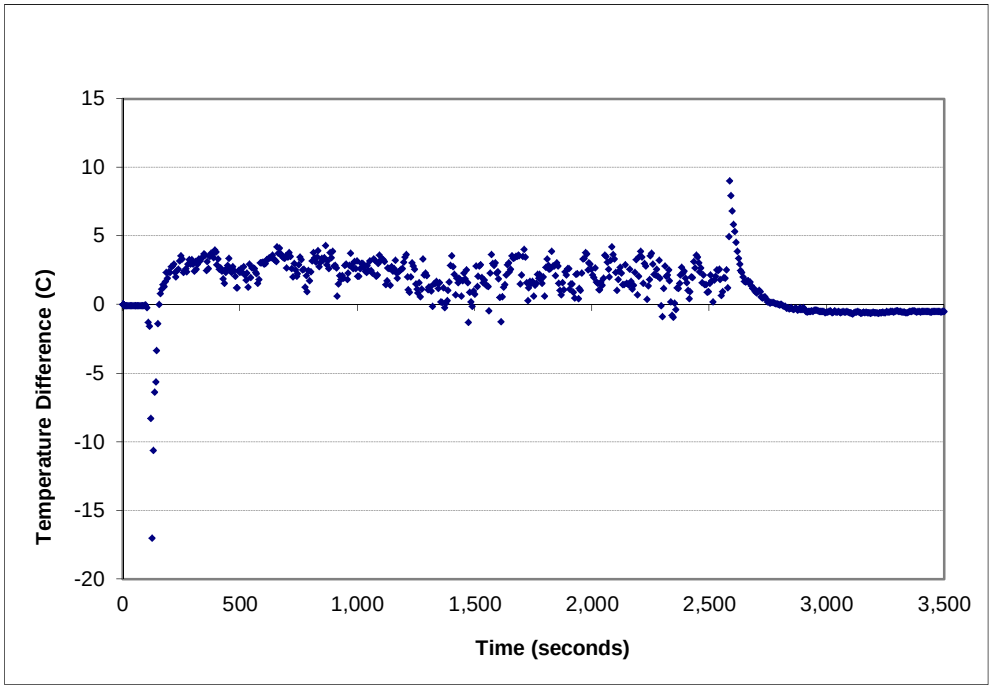

Figure A-188: Temperature error (layer 4) for the 0.5 g/s, ϕ_6 configuration

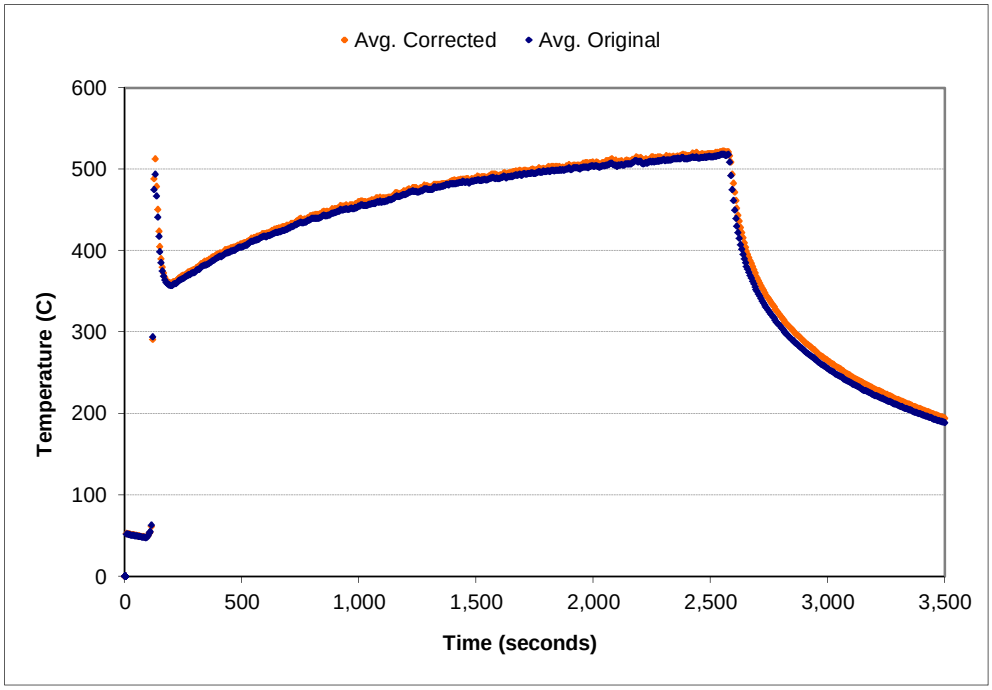

Figure A-189: Space-averaged (layer 5) temperature correction for the 0.5 g/s, ϕ_6 configuration

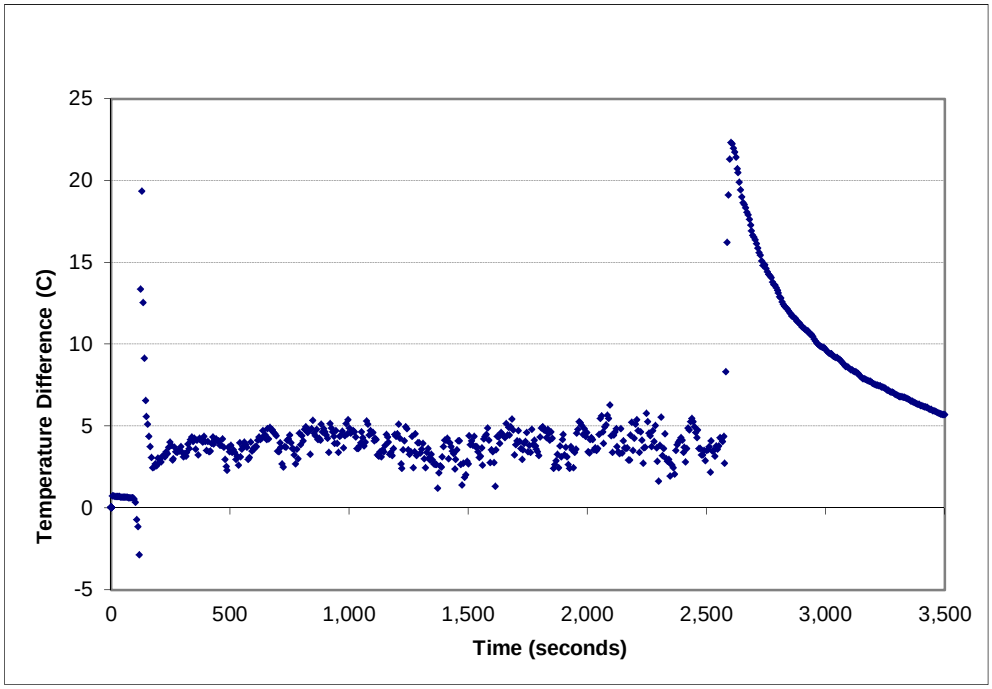

Figure A-190: Temperature error (layer 5) for the 0.5 g/s, ϕ_6 configuration

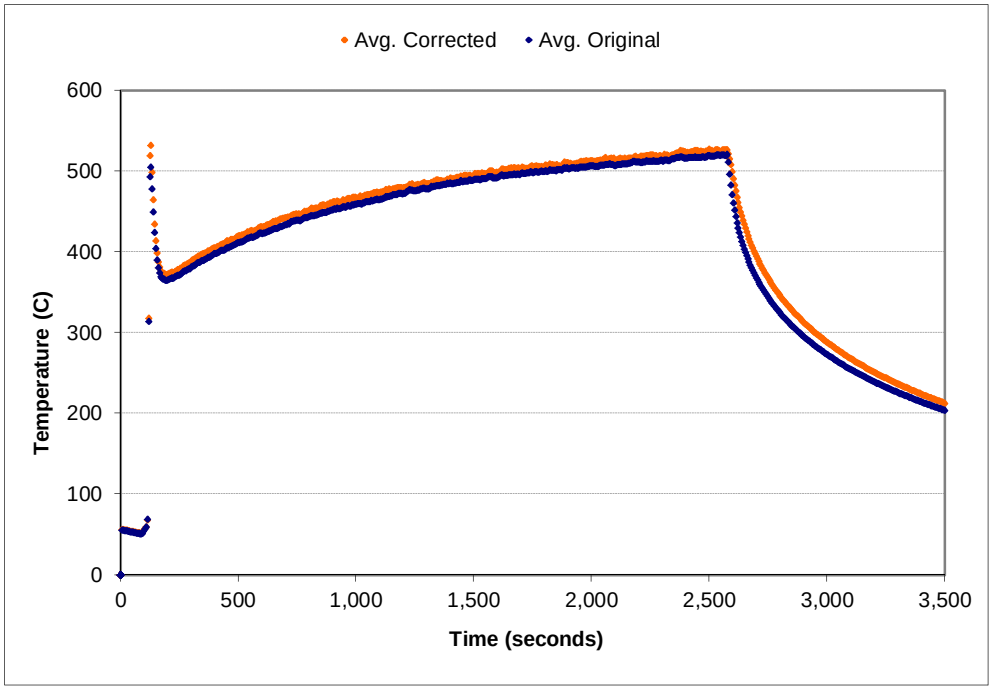

Figure A-191: Space-averaged (layer 6) temperature correction for the 0.5 g/s, ϕ_6 configuration

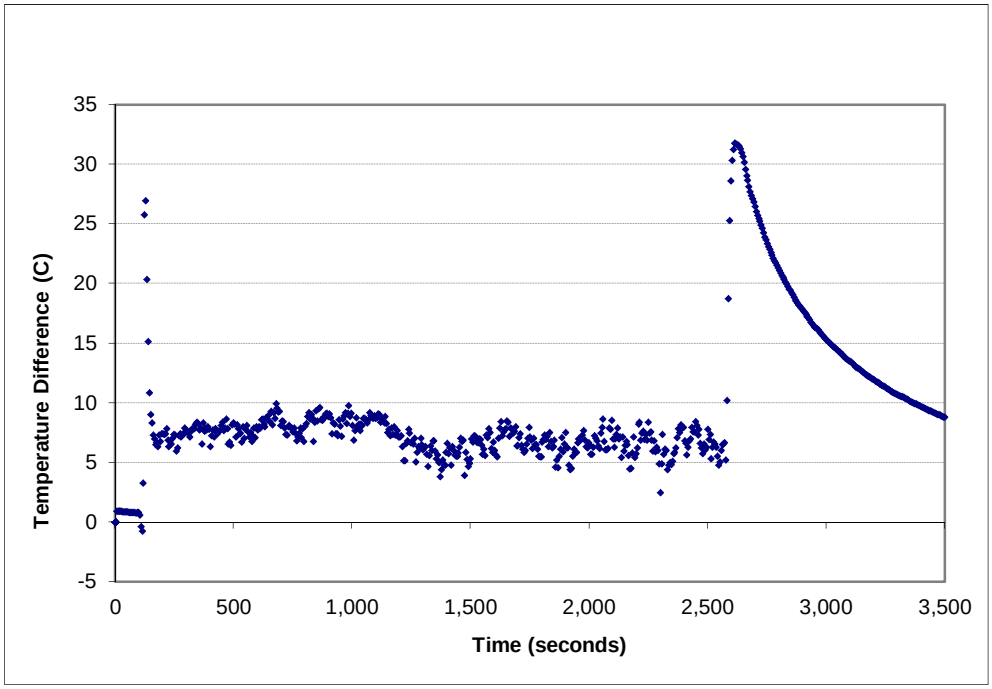

Figure A-192: Temperature error (layer 6) for the 0.5 g/s, ϕ_6 configuration

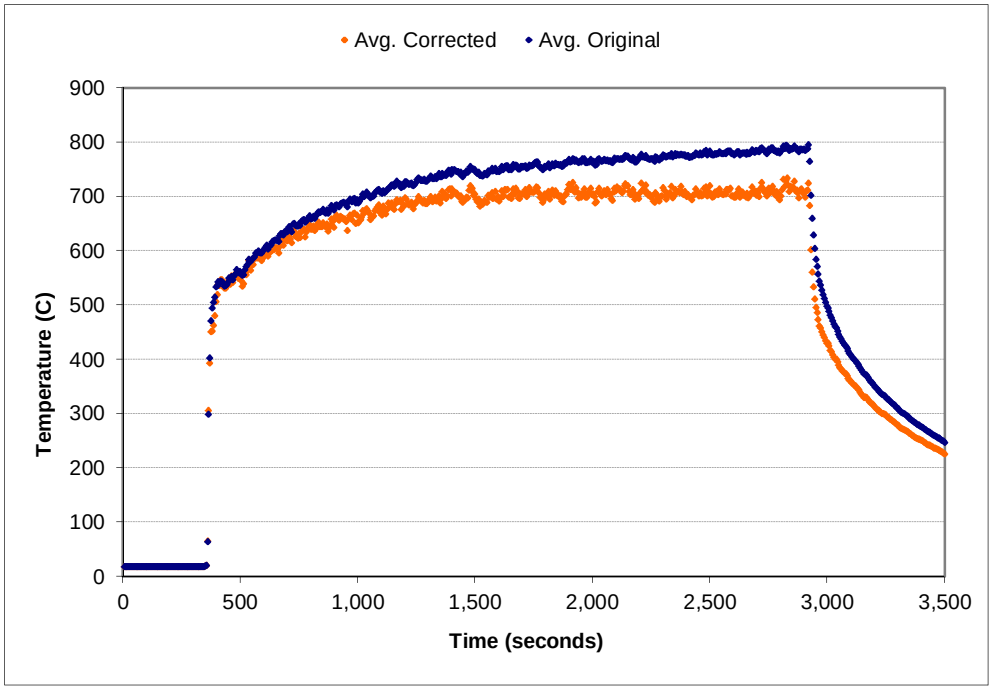

Figure A-193: Space-averaged (layer 1) temperature correction for the 1.0 g/s, ϕ_6 configuration

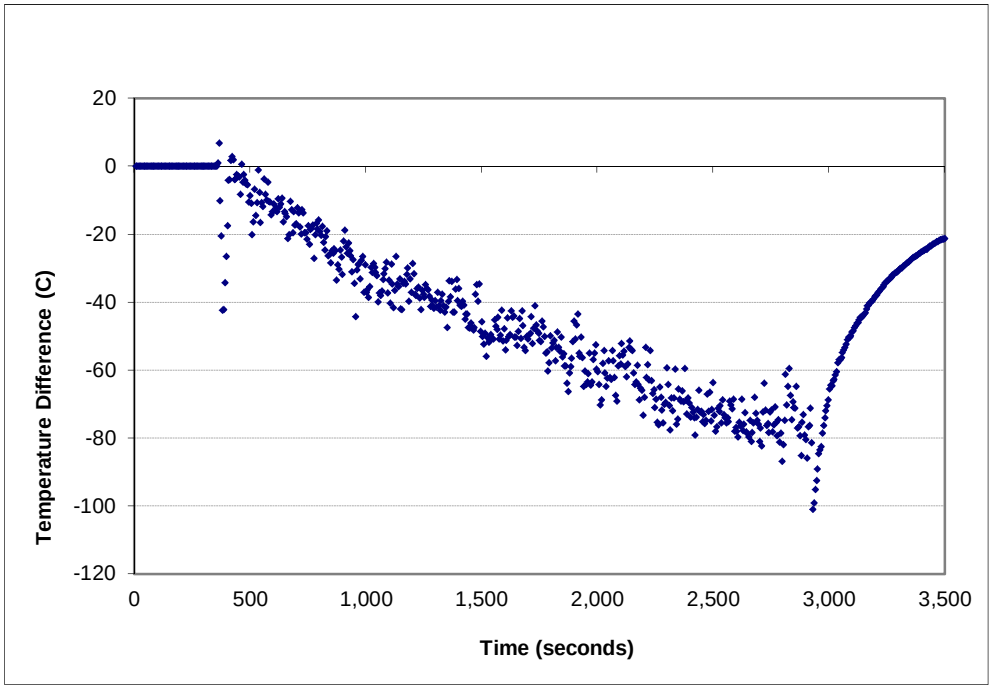

Figure A-194: Temperature error (layer 1) for the 1.0 g/s, ϕ_6 configuration

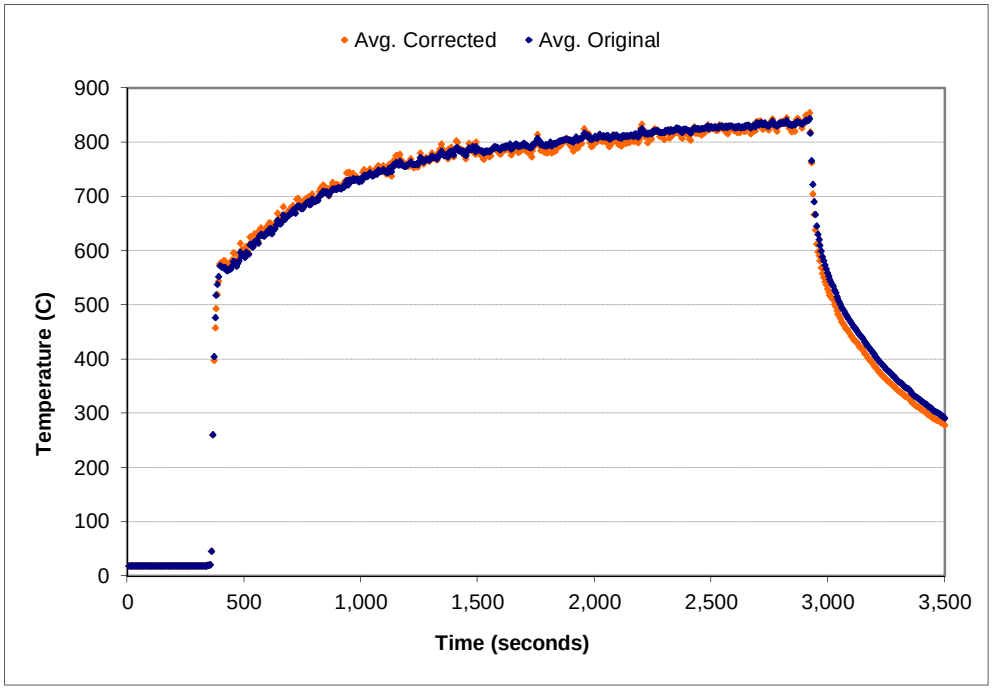

Figure A-195: Space-averaged (layer 2) temperature correction for the 1.0 g/s, ϕ_6 configuration

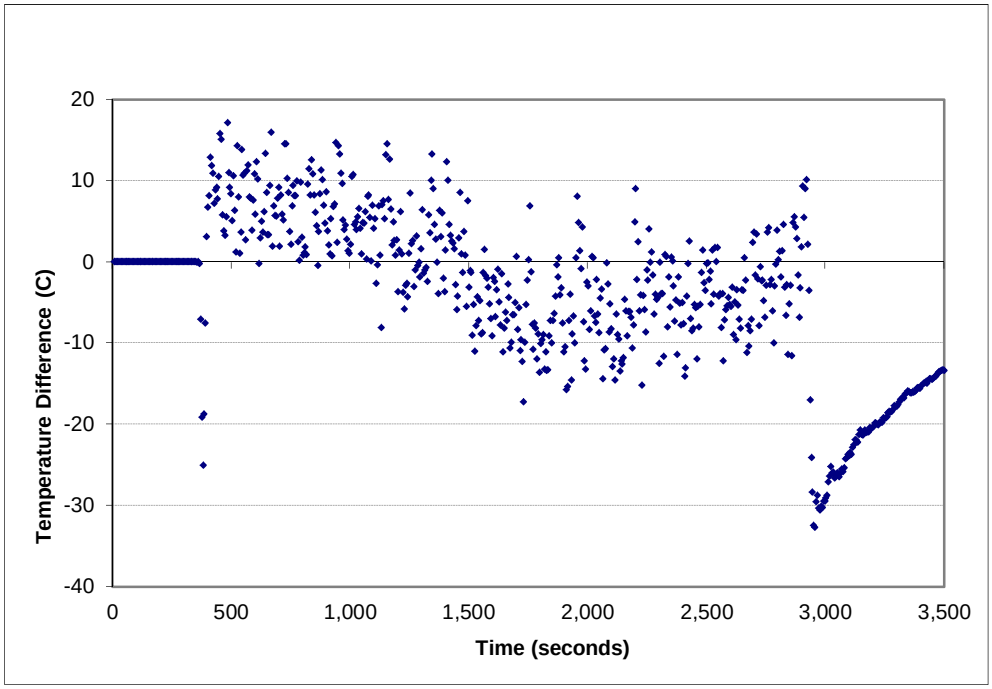

Figure A-196: Temperature error (layer 2) for the 1.0 g/s, ϕ_6 configuration

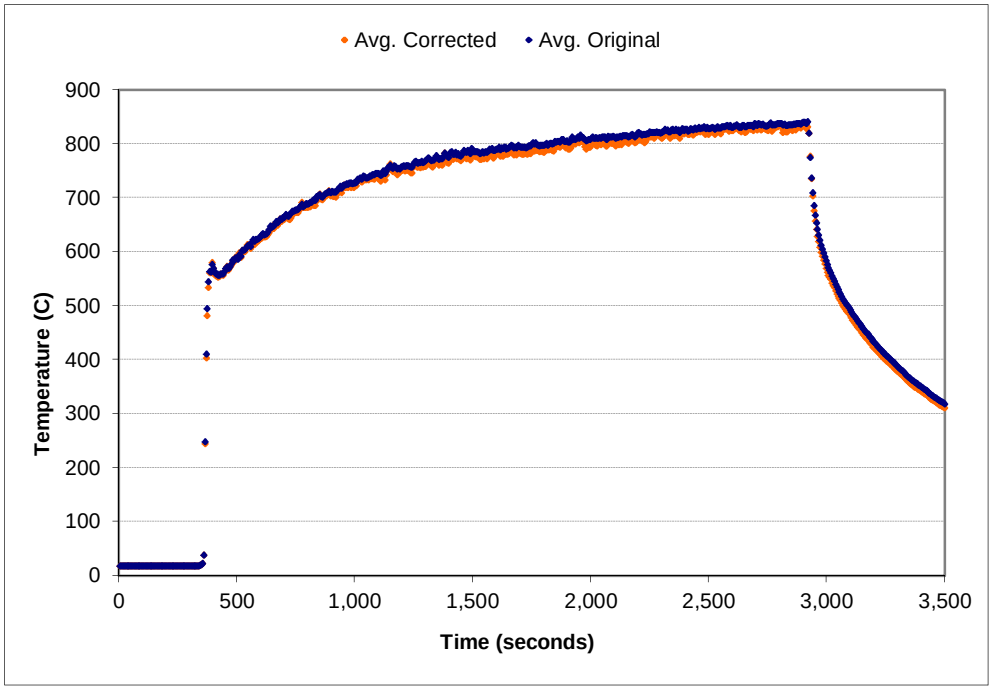

Figure A-197: Space-averaged (layer 3) temperature correction for the 1.0 g/s, ϕ_6 configuration

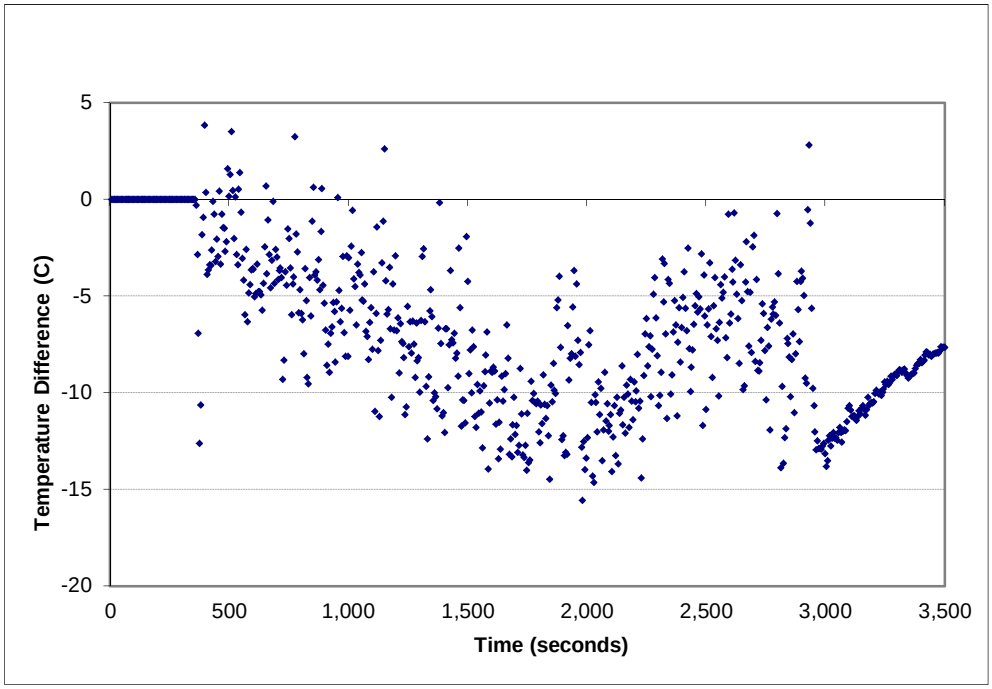

Figure A-198: Temperature error (layer 3) for the 1.0 g/s, ϕ_6 configuration

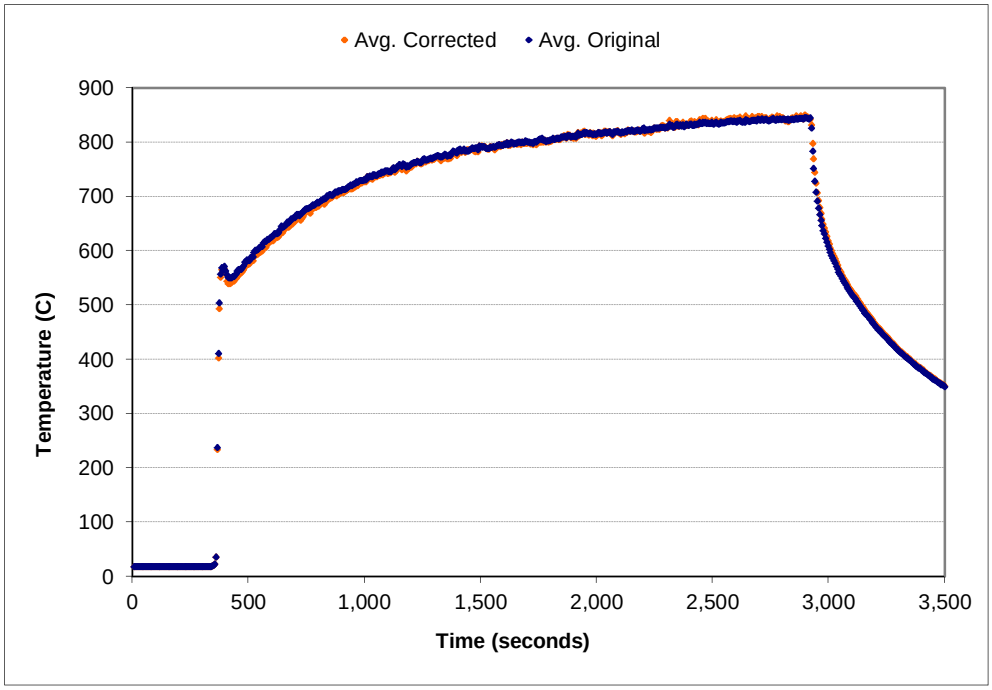

Figure A-199: Space-averaged (layer 4) temperature correction for the 1.0 g/s, ϕ_6 configuration

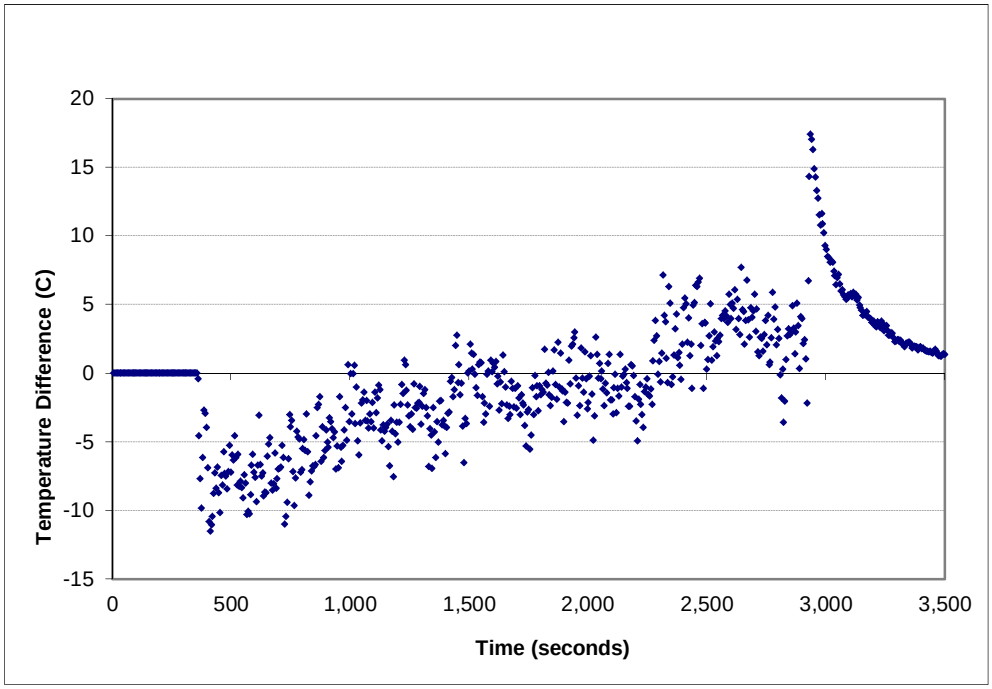

Figure A-200: Temperature error (layer 4) for the 1.0 g/s, ϕ_6 configuration

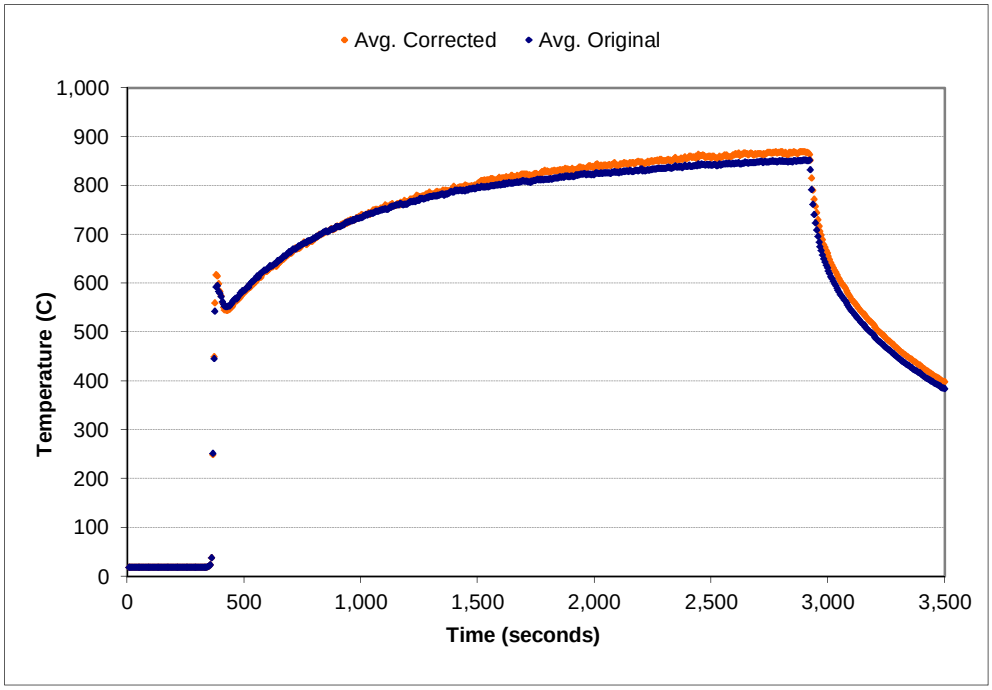

Figure A-201: Space-averaged (layer 5) temperature correction for the 1.0 g/s, ϕ_6 configuration

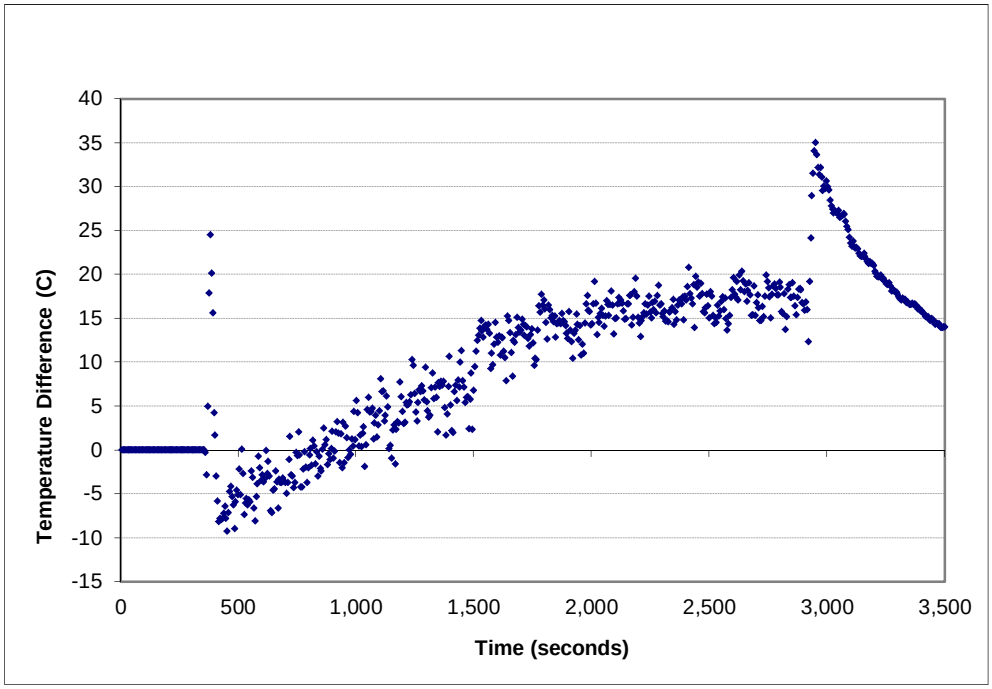

Figure A-202: Temperature error (layer 5) for the 1.0 g/s, ϕ_6 configuration

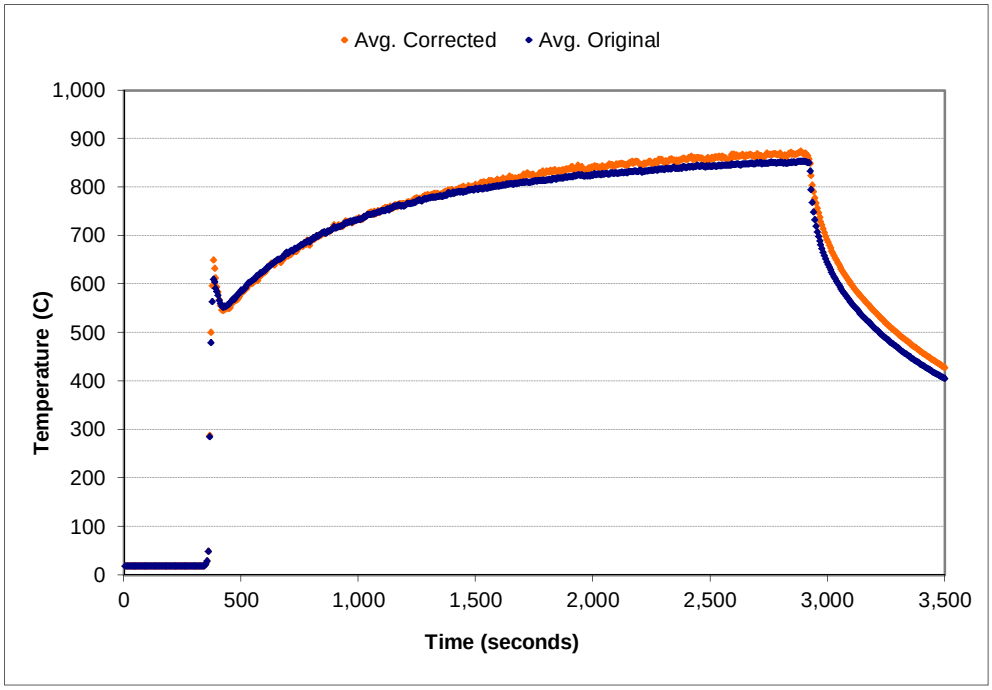

Figure A-203: Space-averaged (layer 6) temperature correction for the 1.0 g/s, ϕ_6 configuration

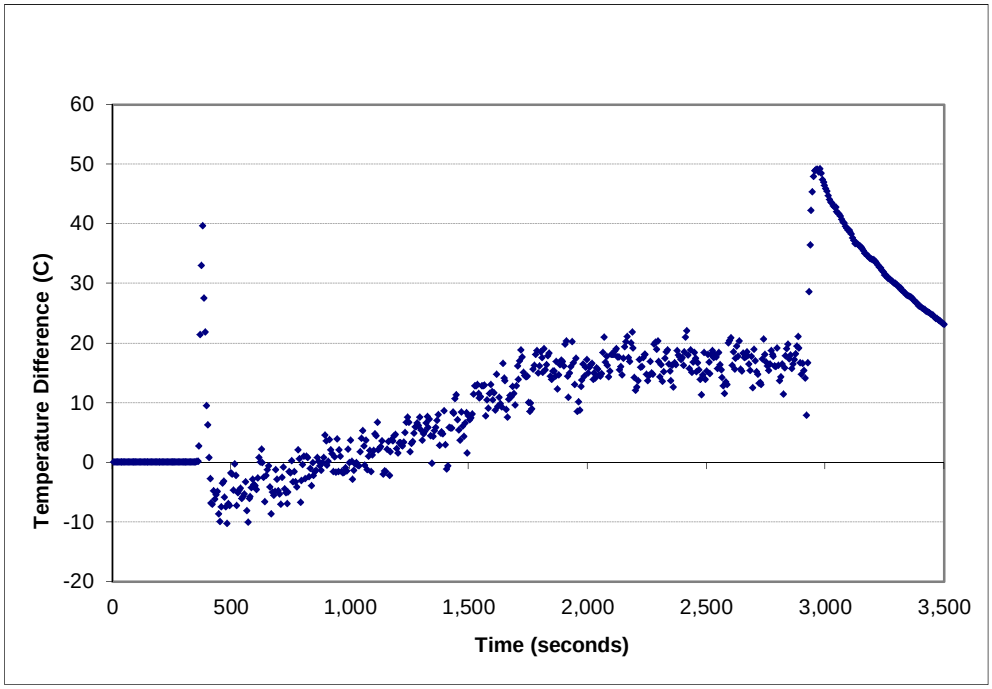

Figure A-204: Temperature error (layer 6) for the 1.0 g/s, ϕ_6 configuration

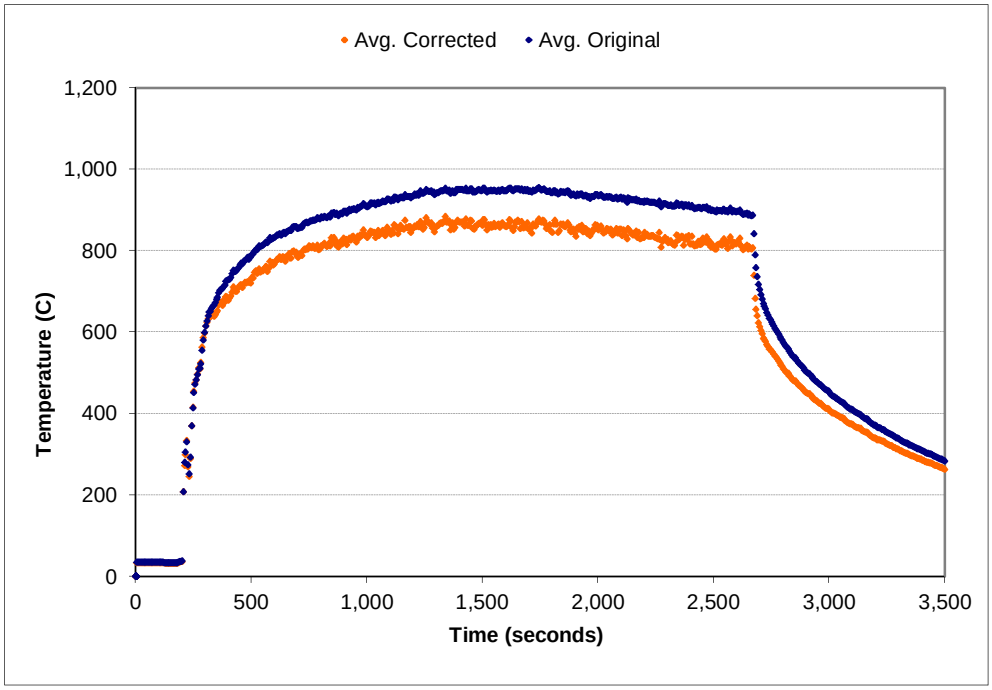

Figure A-205: Space-averaged (layer 1) temperature correction for the 1.5 g/s, ϕ_6 configuration

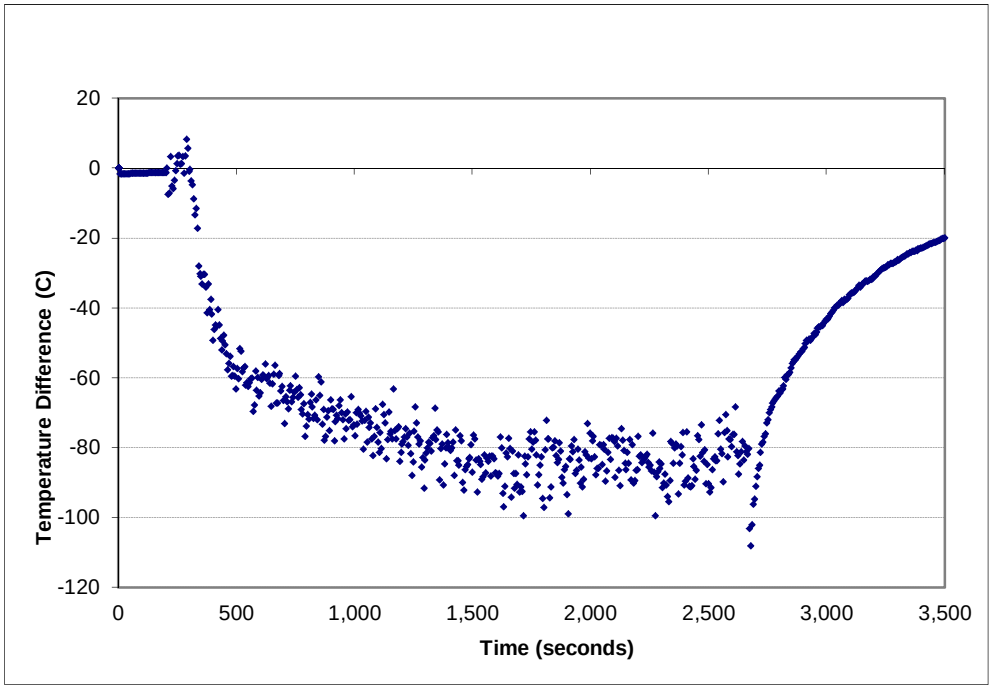

Figure A-206: Temperature error (layer 1) for the 1.5 g/s, ϕ_6 configuration

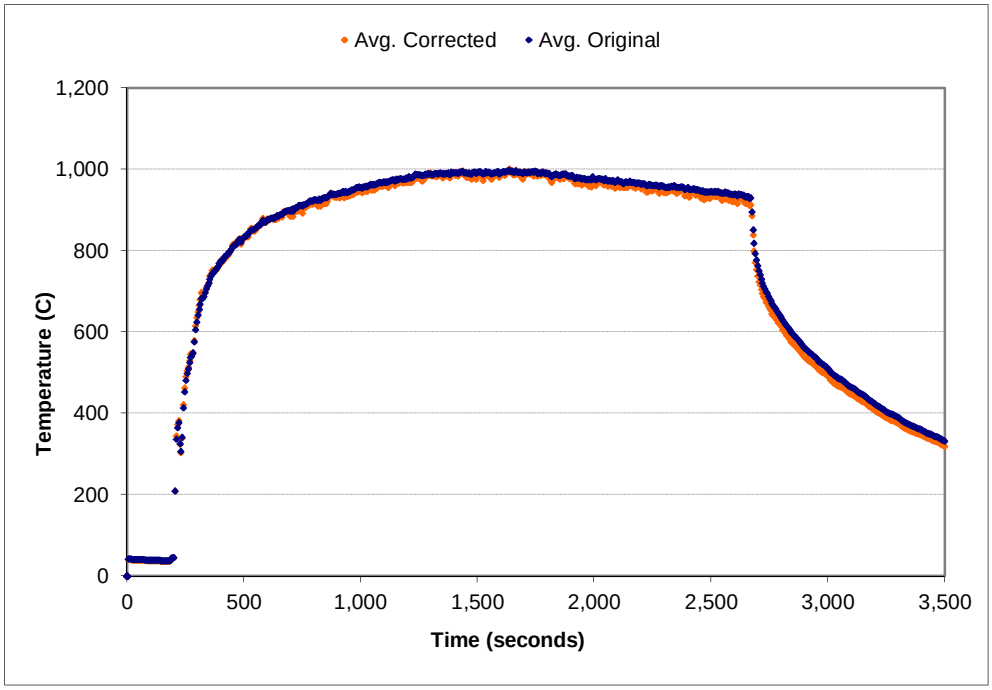

Figure A-207: Space-averaged (layer 2) temperature correction for the 1.5 g/s, ϕ_6 configuration

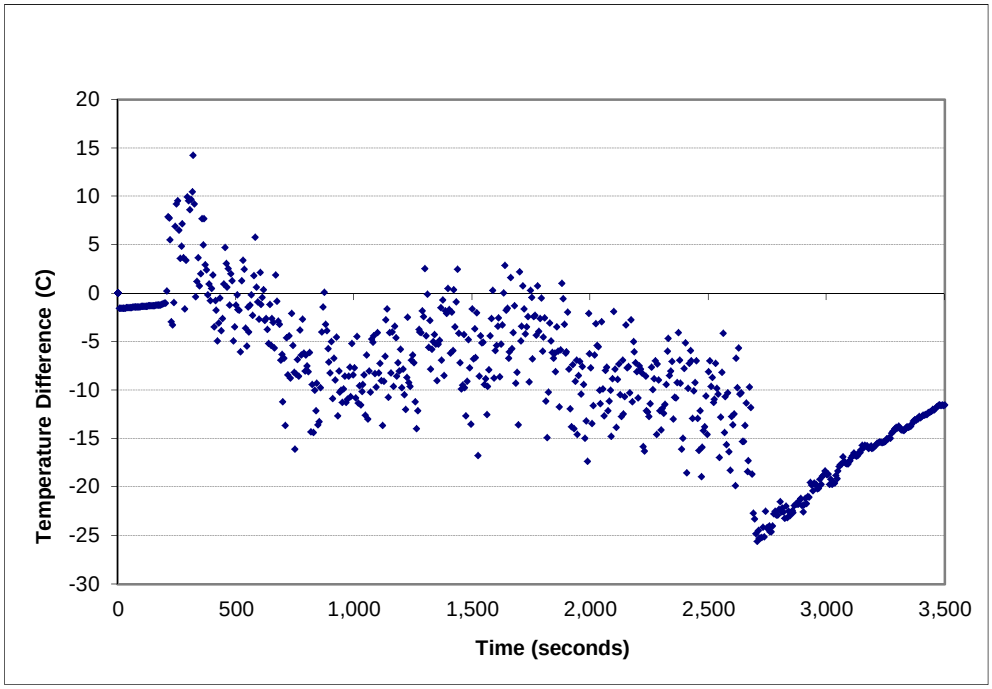

Figure A-208: Temperature error (layer 2) for the 1.5 g/s, ϕ_6 configuration

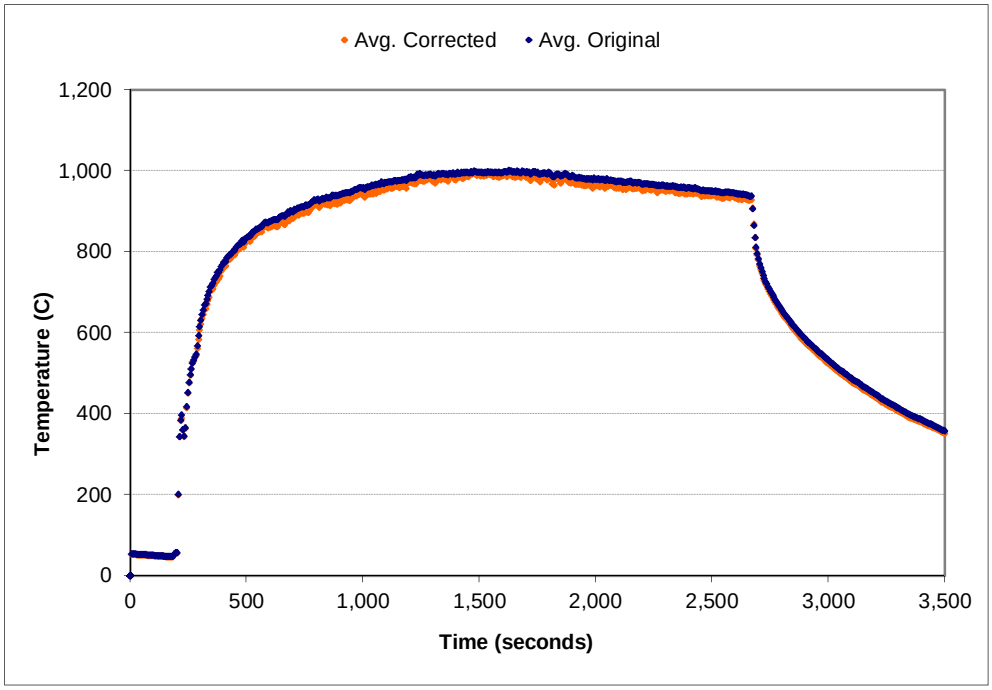

Figure A-209: Space-averaged (layer 3) temperature correction for the 1.5 g/s, ϕ_6 configuration

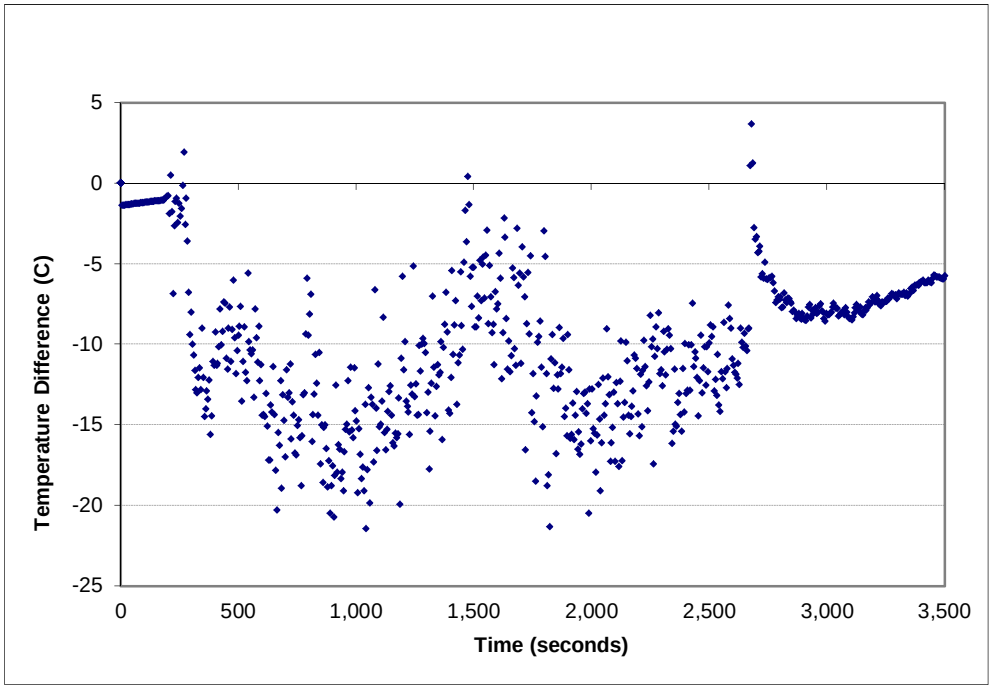

Figure A-210: Temperature error (layer 3) for the 1.5 g/s, ϕ_6 configuration

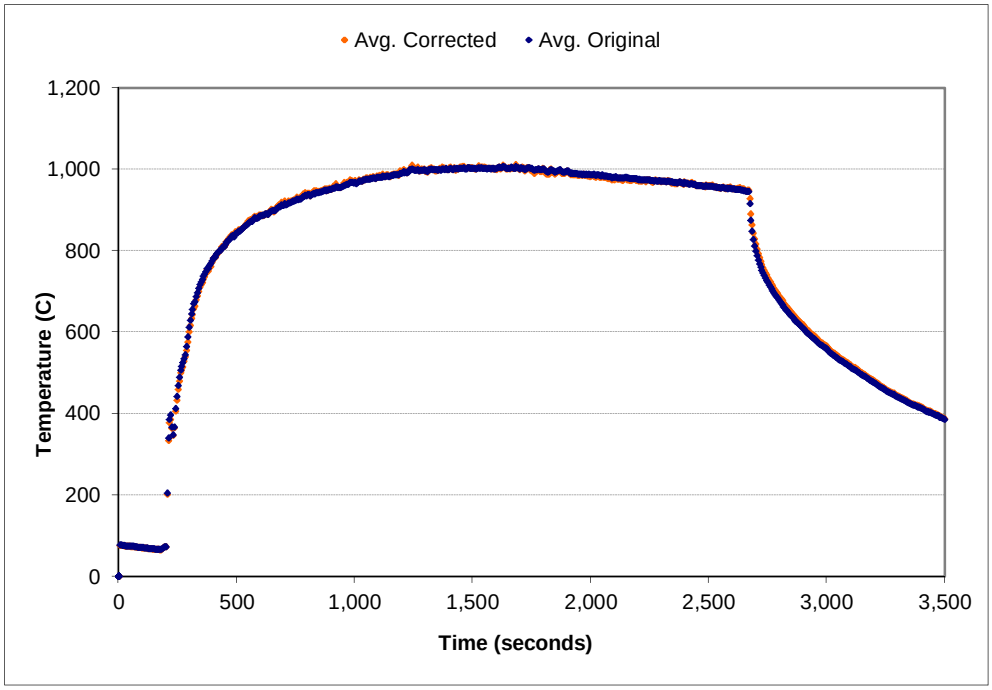

Figure A-211: Space-averaged (layer 4) temperature correction for the 1.5 g/s, ϕ_6 configuration

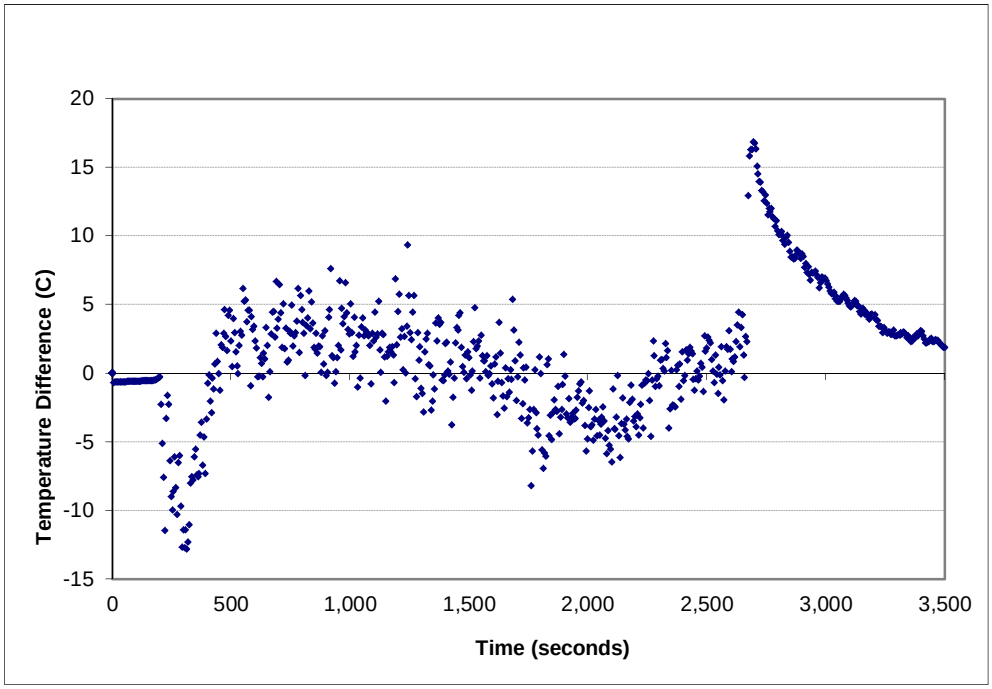

Figure A-212: Temperature error (layer 4) for the 1.5 g/s, ϕ_6 configuration

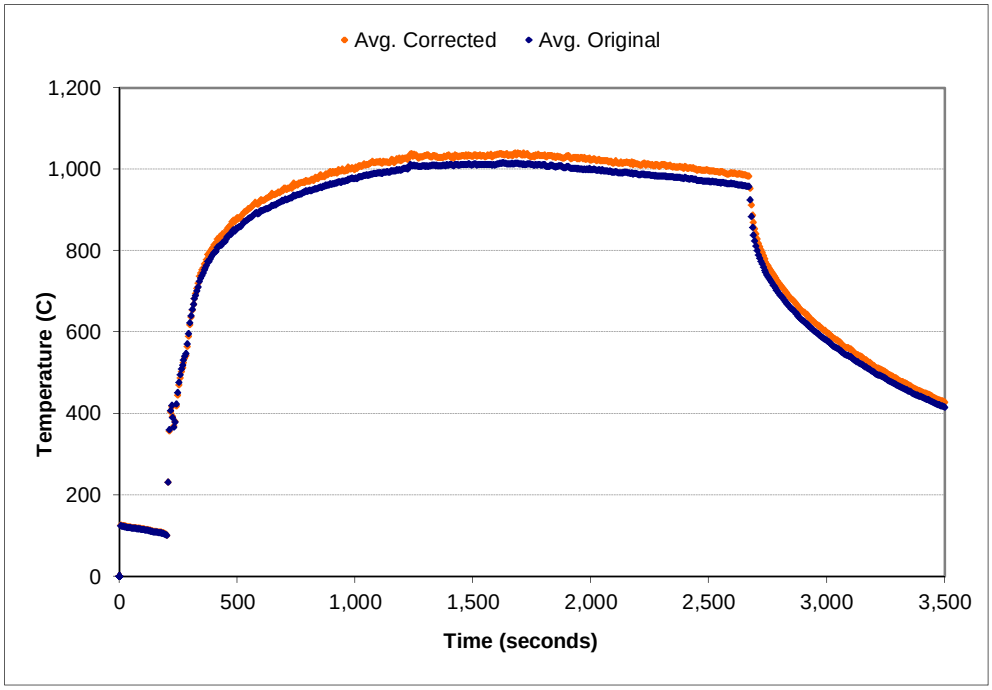

Figure A-213: Space-averaged (layer 5) temperature correction for the 1.5 g/s, ϕ_6 configuration

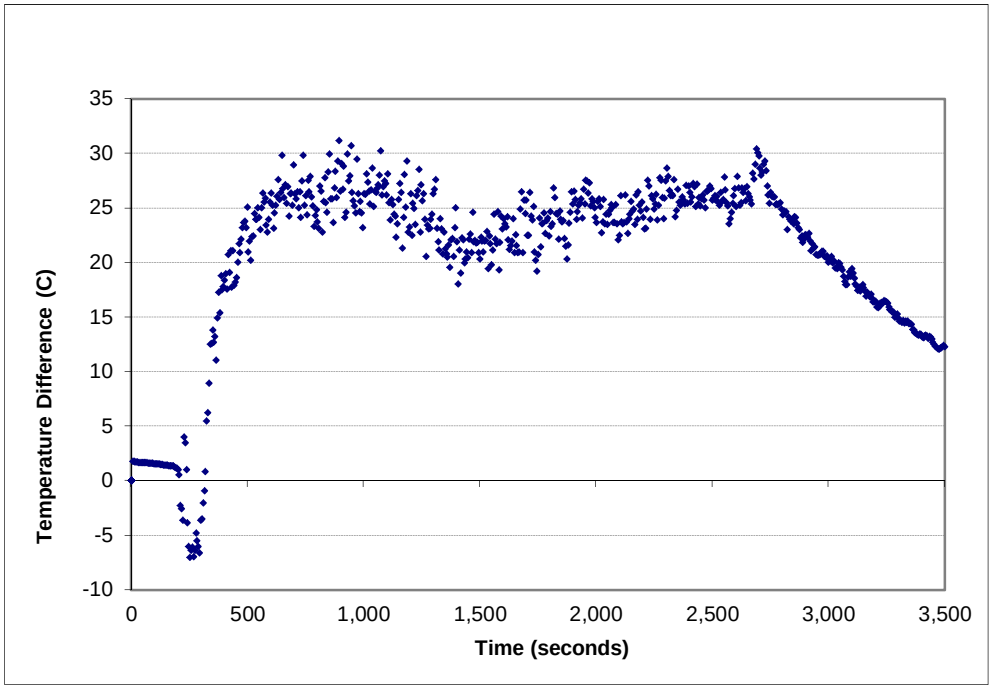

Figure A-214: Temperature error (layer 5) for the 1.5 g/s, ϕ_6 configuration

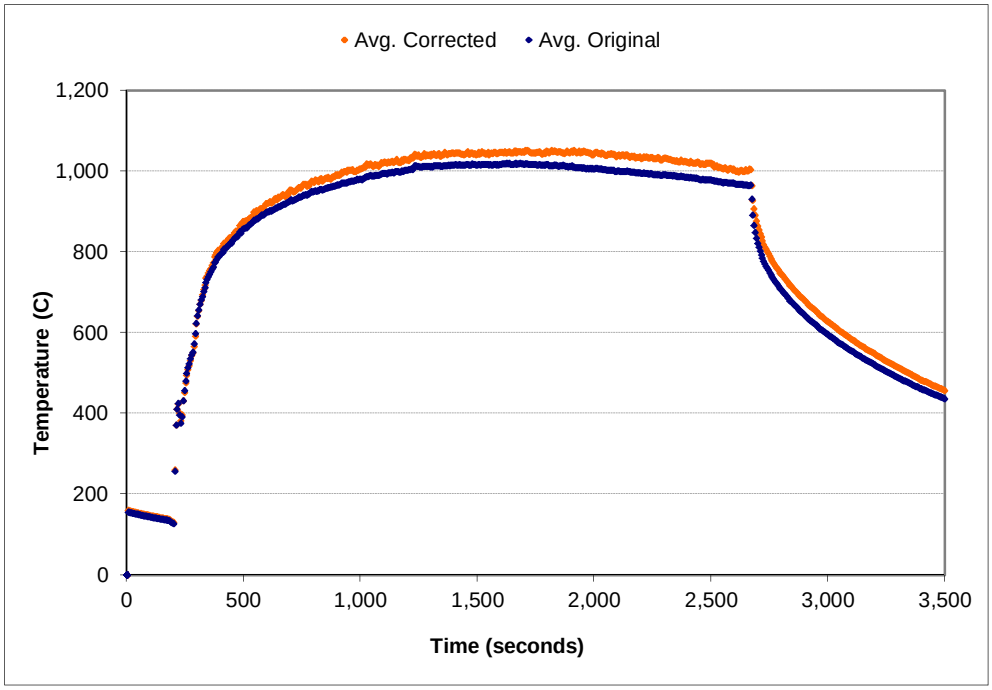

Figure A-215: Space-averaged (layer 6) temperature correction for the 1.5 g/s, ϕ_6 configuration

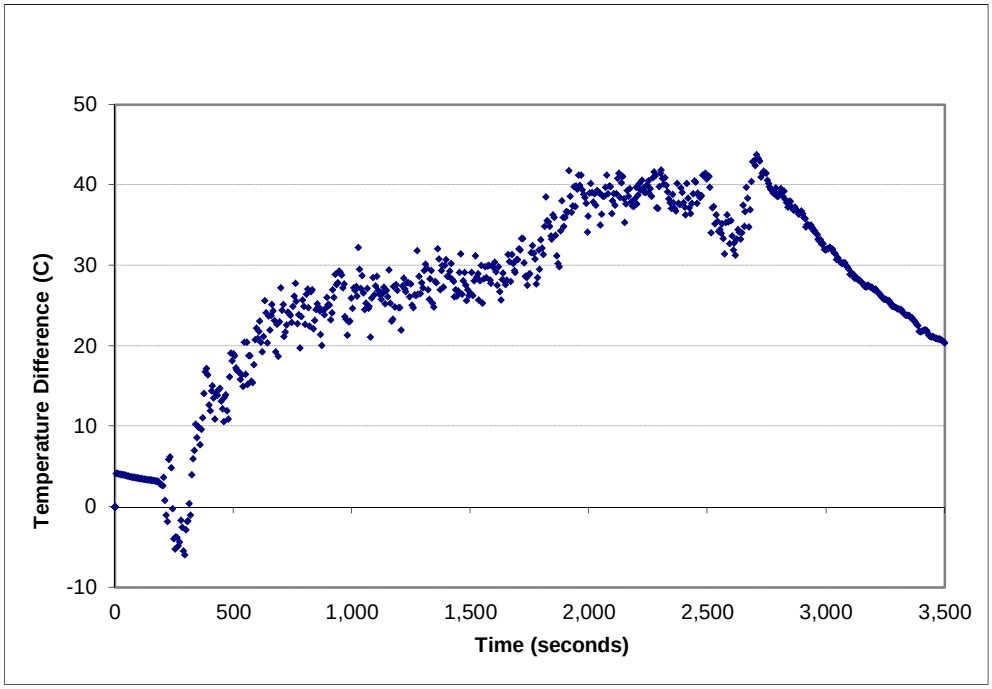

Figure A-216: Temperature error (layer 6) for the 1.5 g/s, ϕ_6 configuration

A.2 Pressure Probes Calibration Approach Selection

At a stagnation point the fluid velocity reduces to zero converting all its kinetic energy into pressure energy. Thus, the stagnation pressure, P_s, is equal to the free-stream hydrodynamic pressure, $P_{hydrodynamic}$ (i.e., kinetic energy per unit volume) plus the free-stream static pressure, P_i, (i.e., internal energy per unit volume). It is also equal to the total pressure, P_0, also called simple *Pitot* pressure since it is measured using a simple *Pitot* tube. So, from basic fluid dynamics it is known that a simple *Pitot* tube measures the total pressure, while a *Pitot-static* tube measures the hydrodynamic pressure. In equations,

$$P_{Pitot-Simple} = P_o = P_i + P_{hydrodynamic} \qquad \textbf{Equation A-1}$$

$$P_{Pitot-Static} = P_{hydrodynamic} \qquad \textbf{Equation A-2}$$

$$\Rightarrow P_{Pitot-Static} = P_o - P_i \qquad \textbf{Equation A-3}$$

$$\Rightarrow P_{Pitot-Static} = P_{Pitot-Simple} - P_i \qquad \textbf{Equation A-4}$$

A bi-directional probe works in the same way as a *Pitot-static* tube; i.e. it is designed to measure the hydrodynamic pressure difference at the opening of a compartment, where the hydrostatic pressure is converted to hydrodynamic pressure. The only difference between a *Pitot-static* tube and a bi-directional probe is that, given a set of conditions, the latter measures a slightly higher pressure than the former. The reason for this is that the positive end of the bi-directional probe – i.e., the end receiving the flow – measures the total pressure, while the negative end – i.e., the opposite end – measures a slightly lower pressure than the static due to a turbulence effect. Therefore,

$$\Delta P_{probe} = x\, \Delta P_{Pitot-Static} \qquad with \quad x > 1 \qquad \textbf{Equation A-5}$$

These pressure differences come from the definition of hydrodynamic pressure (refer to Chapter 2) and can be expressed as:

$$\Delta P_{probe} = \frac{1}{2} u_{probe}^2 \rho_i$$ **Equation A-6**

$$\Delta P_{Pitot-Static} = \frac{1}{2} u_{real}^2 \rho_i$$ **Equation A-7**

The velocity ratio would therefore be:

$$\frac{u_{probe}}{u_{real}} = \frac{\sqrt{2x\Delta P_{Pitot-Static} / \rho_i}}{\sqrt{2\Delta P_{Pitot-Static} / \rho_i}} = \sqrt{x} = K$$ **Equation A-8**

K is a factor function of the Reynolds number, *Re*, which – following McCaffrey [122]– has a theoretical suggested value of 1.08. The exact empirical value for this factor depends on the probe head geometry and must be obtained by calibration.

The unit tested used in these experiments was mounted 140 mm from the end of a wind tunnel with the head aligned perpendicular to the flow direction and was calibrated against a laser Doppler anemometer. When stabilized conditions were observed, the measurement conditions were recorded. The air velocity was adjusted to the next condition and, once steady state conditions were achieved, the results were again recorded, this procedure being repeated until the calibration was complete. The results are derived from the average of at least 10 readings, and are depicted in the following figures:

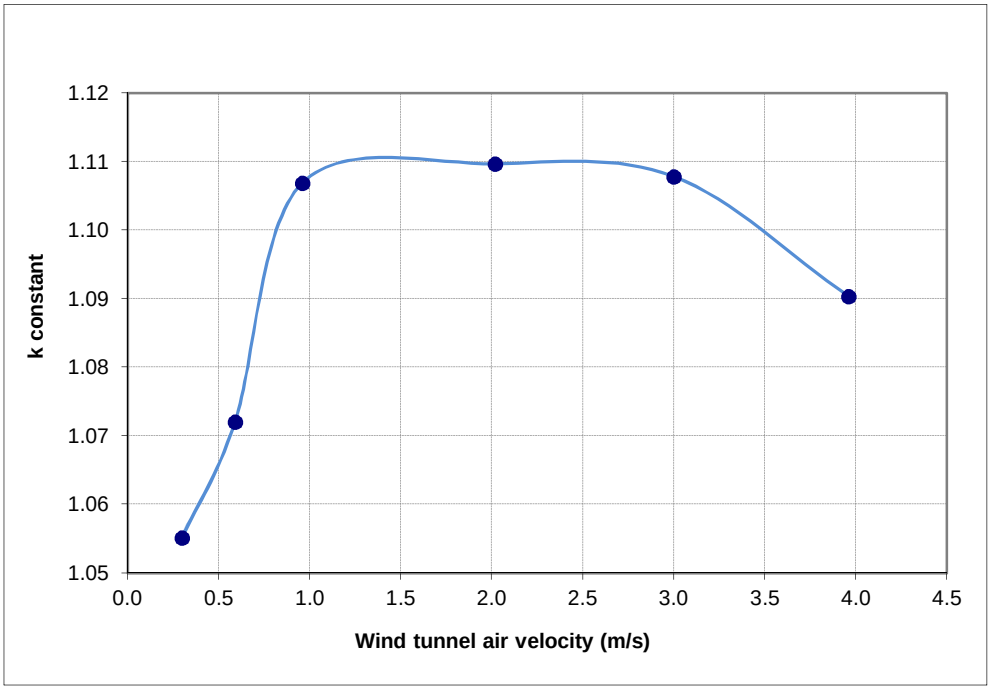

Figure A-217: Probe Response versus Wind Tunnel Velocity

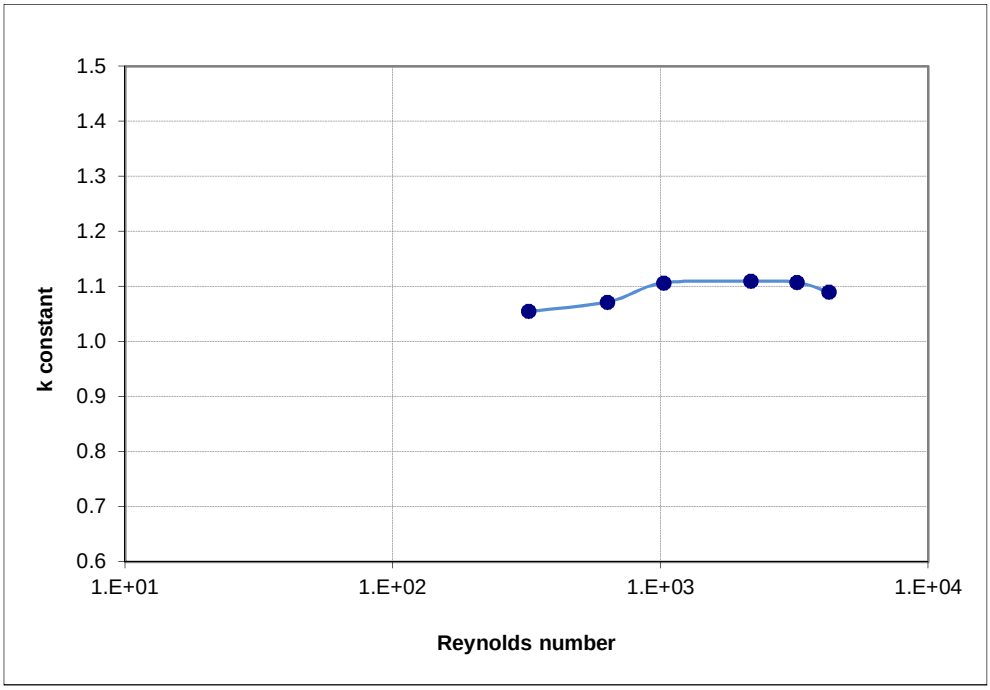

Figure A-218: Probe Response versus Reynolds number

The air temperature, atmospheric pressure, and relative humidity during the test were 27.8 to 28.1 C, 1011.0 to 1011.1 mbar, and 35.1 to 35.5% respectively.

It should be noted that for air velocities above 1 m/s, *K* tends to a fairly constant value. Given the uncertainty of the above velocity measurements (± 1.0% + 0.1m/s + instrument resolution), air density measurements (± 0.15%), and pressure measurements (± 0.3% + 0.6 Pa) under laboratory conditions (that gave as a result large positive error bars in the low velocity range of 0.3 to 0.6 m/s), the *K* value adopted in for these experiments was effectively taken as an average value equal to 1.10.

A.3 TSC Calibration Approach Selection

a. Introduction

Energy balances assuming three dimensional heat transfer mode in the calibration assembly and stainless steel thin skin calorimeter (TSC) plate were assessed to characterize the various factors – represented by the correspondent term in the conservation of energy equation – that influence the performance of these instruments in calibration and test situation, respectively [124][125].

For the *calibration* process, the heat transfer equation is:

$$\boxed{\boldsymbol{OUT\ from\ the\ radiant\ panel\ (total\ output) = IN\ to\ the\ TSC\ (stored + losses)}}$$

$$\rightarrow \boldsymbol{Incident = stored + conduction\ losses + reradiation\ losses + convection\ losses}$$

For the *tests* – or generally in any compartment fire situation – the heat transfer equation is:

$$\boxed{\boldsymbol{OUT\ from\ the\ fire\ (total\ output) = IN\ to\ the\ TSC\ (stored + losses)}}$$

$$\rightarrow \boldsymbol{radiative\ output + convective\ output = stored + conduction\ losses + reradiation\ losses}$$

The *Incident* term expresses the heat flux imposed by the radiant panel to the TSC embedded in and part of the calibration assembly, which in the calibration process is assumed to be equal to that imposed to and recorded by a calibrated Schmidt-Boelter radiometer set aside of the TSC.

The *conduction losses* term expresses in both situations – calibration and tests – the heat lost by conduction to the back and sides of the stainless steel plate. It strongly depends on the thermal properties of the structural element into which the TSC is embedded and is expressed as a fraction of the incident heat flux. During calibration and tests, the TSC was embedded in the same type and thickness of Ceraboard backing (W/m^2).

The *stored* term, $\rho_s \delta_s c_s$ (dT_s/dt), corresponds to the energy stored or heat build-up within the stainless steel plate over a discreet time step. This is calculated by multiplying the stainless steel density, ρ_s (in Kg/m^3), thickness, δ_s (in m), specific heat, c_s (in J/Kg·K), and the rate of change in temperature of the plate surface with respect to time, dT_s/dt (in K/s). This term expresses how quickly the plate heats up when the surrounding temperature (T_a or T_g) increases rapidly, assuming that the plate's temperature, T_s, remains uniform at every time step (low Biot number, no temperature gradients through and across the solid).

The *re-radiation losses* term, $\varepsilon_s \sigma (T_s^4 - T_a^4)$, corresponds to the radiation exchange between the stainless steel plate and the surroundings. It is calculated by multiplying the emissivity of the stainless steel plate, ε_s, and the *Stefan-Boltzmann constant*, σ, by the difference in temperature to the power of four between the plate and the surroundings, T_s and T_a, respectively, in units of energy per unit area (W/m^2).

The *convection losses* term corresponds to the convective portion of heat loss to the surroundings during calibration, h_c ($T_s - T_a$). This term is also in units of energy per unit area (W/m^2) and is calculated by multiplying an appropriate average convective factor, h_c – over the vertical length of the calibration assembly (TSC + Ceraboard), L – by the difference in temperature between the calibration assembly and the ambient, T_s (since the Ceraboard is assumed to be at the same temperature as the plate) and T_a, respectively.

The *convective output* term, h_c ($T_g - T_s$), corresponds to the convective portion of heat gain from the surroundings (T_g) during an actual fire or test. This term is also in units of energy per unit area (W/m^2) and calculated by multiplying an appropriate average convective factor, h_c – estimated over the vertical length of the TSC – by the difference in temperature between the TSC and the surrounding gas, T_s and T_g, respectively.

The *radiative output* term is equal to the incident radiation flux from the compartment fire to the stainless steel plate, which together with the convective flux

(convective output) are equal to the total incident flux from the fire to the TSC during the tests.

b. Calibration

There are two different ways of calibrating the TSC. The *simple* calibration is based on the TSC's material properties, while the *complex* or *empirical* calibration is otherwise based on a more accurate TSC's empirical constant.

In either method, the calibration tests comprised a sequence of experiments in which the thin skin calorimeter (TSC) was subjected to a series of known constant heat fluxes. The TSC was embedded in the same material (Ceraboard) used in the actual reduced-scale compartment tests (which has a very low thermal conductivity) and was set aside a calibrated *Schmidt-Boelter* radiometer that accurately recorded the incident heat fluxes.

The calibration assembly, together with the radiometer and radiant panel, are shown in the following Photos:

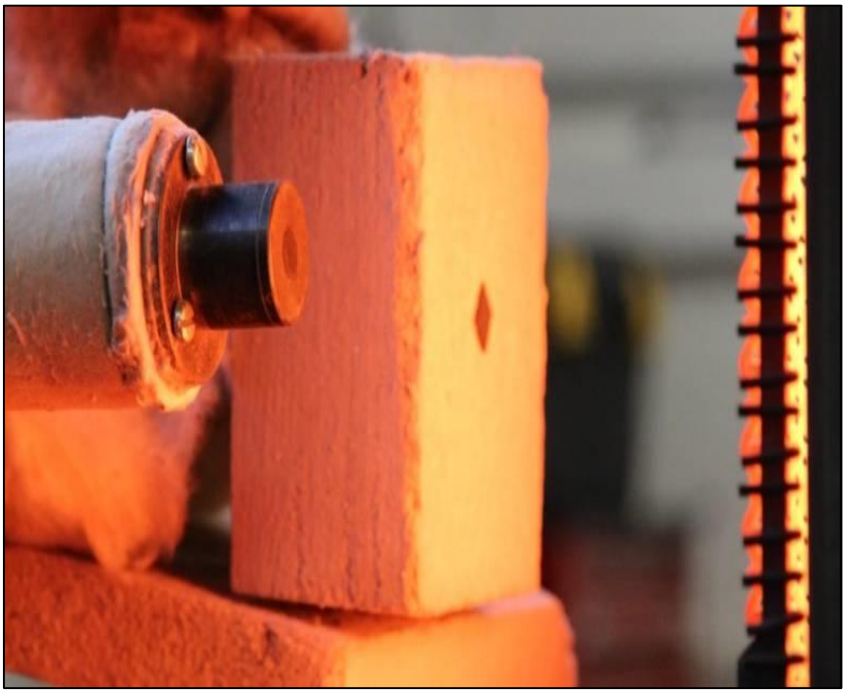

Photo A-1: Schmidt-Boelter radiometer set aside the calibration assembly

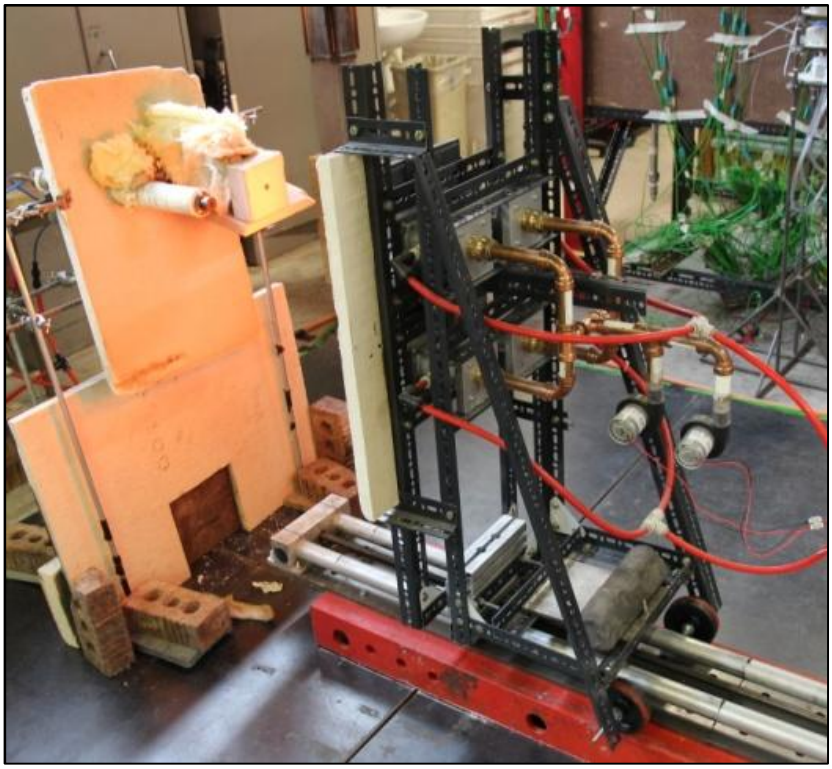

Photo A-2: Calibration arrangement using radiant panels

The emissivity was assumed to be about 0.9 after the stainless steel plate was blackened after previous thermal exposures (pre-tests) and by soot. The temperature of the plate was recorded over time with thermocouple wires type-K welded to the back of the plate. The error in the temperature reading depends on the system used to attach the wires to the stainless steel plate; thus, in order to reduce this error, these were joined using spot welding.

If conduction into the type-K thermocouple wire is ignored, then the initial response time – which is the time for the unexposed side of the TSC to attain within 1% of the exposed side's temperature - could be expressed by the following equation [126]:

$$t_f = 0.5\frac{\rho_s c_s \delta_s^2}{k_s}$$ **Equation A-9**

Where,

t_f is the initial response time, in seconds

ρ_s is the density of stainless steel AISI 304 = 7,900 Kg/m^3

c_s is the specific heat capacity of stainless steel AISI 304 = 477 J/Kg·K

δ_s is the thickness of the thin skin calorimeter = 0.0012 m

k_s is the thermal conductivity of stainless steel AISI 304 = 14.9 W/m·K

In this case, the stainless steel TSC initial response time was estimated as:

$$t_f = 0.5\frac{\left(7{,}900\frac{kg}{m^3}\right)\left(477\frac{J}{kg.K}\right)\left(1.2x10^{-3}m\right)^2}{\left(14.9\frac{W}{m.K}\right)} = 0.18\ s$$ **Equation A-10**

On the other hand, the *Biot number* defines the ratio of the heat transfer resistance inside and at the surface of a body giving, therefore, an idea of the temperature field uniformity within the body. In general, problems involving small *Biot numbers*

below a critic value much smaller than 1 are considered thermally simple, whereas problems with *Biot numbers* much larger than 1 represent more difficult solutions due to the non-uniformity of the temperature field within the object. In the stainless steel TSC's case, assuming an average characteristic convective coefficient ($h_{charact}$) of 25 W/m.K and a characteristic length ($L_{charact}$) – ratio of the solid's volume to surface area – equal to 1.2 x 10^{-3} m, the *Biot number* was estimated as:

$$B_i = \frac{h_{charact}\ L_{charact}}{k_s} = \frac{\left(25\frac{W}{m.K}\right)\left(1.2x10^{-3}m\right)}{\left(14.9\frac{W}{m.K}\right)} = 2.0x10^{-3} << 0.1 \qquad \textbf{Equation A-11}$$

Accordingly, taking advantage of the TSC's extremely fast initial response time and a low *Biot number*, the temperature gradients within the solid plate could be ignored and, hence, the plate defined as *thermally thin*, treating the transient part of the heat transfer problem within the TSC's plate by the *lumped thermal capacity analysis*; i.e., reducing the conduction part of the problem to a one dimension in the TSC's perpendicular direction. It is therefore important to note that the heat loss by conduction is assumed as that lost to the insulation backing (Ceraboard) and not within the metal plate.

i. Simple Calibration

The calibration procedure is done by subjecting the TSC to a series of known constant heat fluxes to establish the backside heat loss by conduction as a fraction of these known incident heat fluxes. In this particular case, heat fluxes between 10 and 80 kW/m^2 - at 10 kW/m^2 intervals – were imposed in time steps far beyond the TSC's initial response time, approximating the problem to a steady-state one by waiting until steady conditions were reached; i.e. a constant TSC temperature, T_s, for every constant heat flux imposed. This meant reducing the *stored* term to zero given that there is no temperature increase recordings on the plate surface (i.e., $dT_s/dt = 0$) during each time step [16].

Taking this into consideration, the TCS calibration was based on the following simplified equation:

$$\boldsymbol{Incident = stored + conduction\ losses + reradiation\ losses + convection\ losses}$$

with,

$$\rightarrow \boldsymbol{conduction\ losses = C\ x\ Incident}$$

$$\rightarrow \boldsymbol{stored = 0}$$

then,

$$\boldsymbol{Incident = (C\ x\ Incident) + reradiation\ losses + convection\ losses}$$

$$\boldsymbol{Incident = \frac{reradiation\ losses + convection\ losses}{1 - C}}$$

The mathematical equation for the incident term is:

$$Q''_{inc} = \frac{Q_{inc}}{A_s} = \frac{\varepsilon_s \sigma \left(T_s^4 - T_a^4\right) + h_c \left(T_s - T_a\right)}{1 - C} \quad [\text{W/m}^2] \qquad \textbf{Equation A-12}$$

Where,

$\dot{Q}_{inc}$ = incident heat flux to the TSC, assumed equal to that obtained with the heat flux gauge, in W

A_s = surface area of the stainless steel AISI 304 TSC = 10 mm x 10 mm = 100 mm^2 = 1.0 x 10^{-4} m^2 or the heat flux gauge, in m^2

ε_s = emissivity of the stainless steel TSC ≈ 0.9, dimensionless

σ = Stefan-Boltzmann constant = 5.670373x10^{-8} W/m^2.K^4

T_s = Temperature of the stainless steel TSC, in K

T_a = Temperature of the surroundings, in K

C = calibration corrective (or conduction) factor representing the proportion of incident heat flux that is lost via conduction through the back and sides of the stainless steel TSC into the insulation backing, dimensionless

h_c = average convective heat transfer coefficient along the characteristic length of the calibration assembly (stainless steel AISI 304 plate + insulation backing) , in W/m^2.K

So, the conduction loss term (or conduction factor *C*) is the only unknown in this equation, and could be determined at steady-state from recordings of the incident heat flux by the calibrated gauge, $\dot{Q}_{inc}$, stainless steel plate temperature recordings, T_s, taking an emissivity of 0.9, and estimating the average convective heat transfer coefficient, h_c, from free convection on vertical plate correlations (refer to note at the end of Appendix A). Working out the *C value* from the Equation A-12, it is found that:

$$(1-C)\,Q''_{inc} = \varepsilon_s \sigma\left(T_s^4 - T_a^4\right) + h_c\left(T_s - T_a\right) \quad [\text{W/m}^2] \qquad \textbf{Equation A-13}$$

$$(1-C) = \frac{\varepsilon_s \sigma\left(T_s^4 - T_a^4\right) + h_c\left(T_s - T_a\right)}{Q''_{inc}} \text{ [dimensionless]} \qquad \textbf{Equation A-14}$$

$$C = 1 - \left[\frac{\varepsilon_s \sigma\left(T_s^4 - T_a^4\right) + h_c\left(T_s - T_a\right)}{Q''_{inc}}\right] \text{ [dimensionless]} \qquad \textbf{Equation A-15}$$

Even though *C* was only experimentally calculated for TSC temperatures, T_s, up to 800°C (~1,100 K), its value can still be used up to 1,000°C (~1,300 K), approximating it over the whole range of temperatures by a curve-fitting mathematical method, which is represented by the following function:

- for 600 K < $T_s \leq$ 850 K

$$C = \begin{cases} +7.95189391975777x10^{-7}T_S^2 \ldots \\ \ldots -1.39275542079189x10^{-3}T_S \ldots \\ \ldots +77.53607948728248x10^{-1} \end{cases}$$

- for 850 K < $T_s \leq$ 1,300 K

C = 0.14

Graphically:

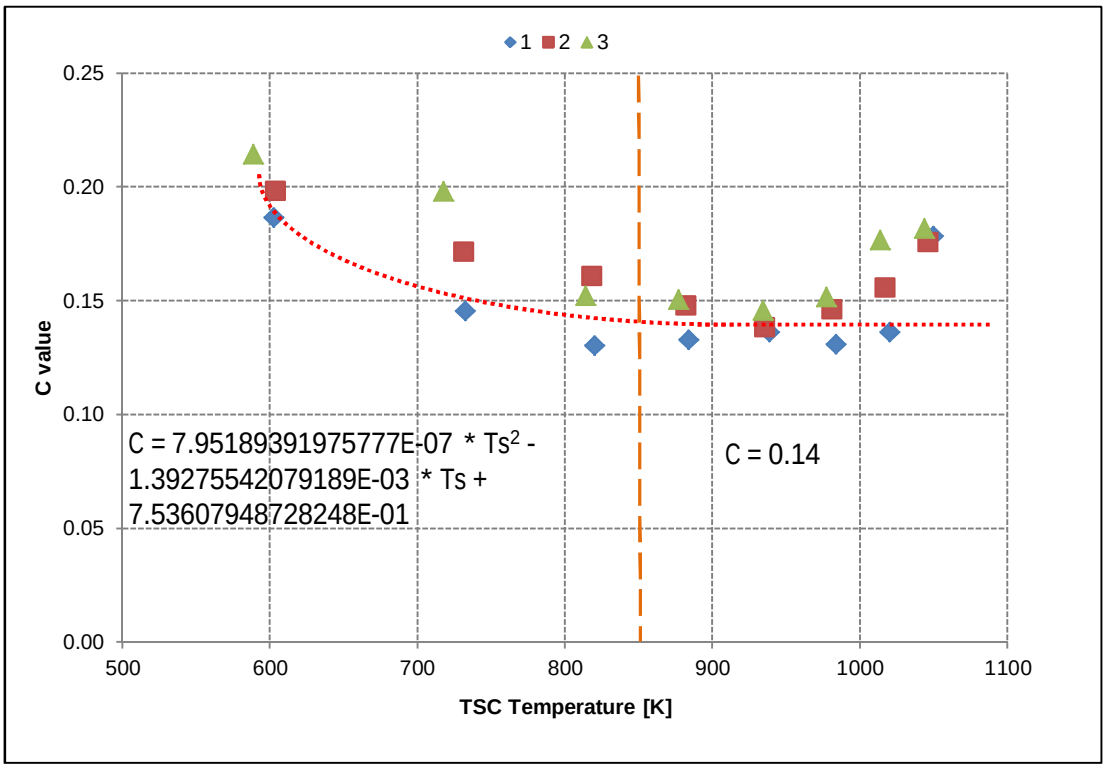

Figure A-219: Curve fitting to obtain the calibration corrective factor C for the TSC

Once these losses by conduction are estimated in the steady-state calibration process, because they are expected to be relatively small, they can be further applied in the transient (tests) process.

ii. Empirical Calibration

This calibration relies not only on the steady-state part of the tests, but also on the transient period of them [125]. From the steady-state calibration period (i.e., constant heat flux + constant T_s) a conductive coefficient could be worked out – based on the same assumptions taken in the previous calibration – by reducing the *stored* term to zero. This time, in a slightly different approach than in the previous case, the conduction losses are linearized with the temperature difference between the TSC and the ambient ($T_s - T_a$), instead of considering them proportional to the incident heat flux. The simplified equation would be:

$$\boldsymbol{Incident = stored + conduction\ losses + reradiation\ losses + convection\ losses}$$

with,

$$\rightarrow \boldsymbol{conduction\ losses = h_k(T_s - T_a)}$$

$$\rightarrow \boldsymbol{stored = 0}$$

then,

$$\dot{Q}''_{inc} = \frac{Q_{inc}}{A_s} = \varepsilon_s \sigma\left(T_s^4 - T_a^4\right) + h_c\left(T_s - T_a\right) + h_k\left(T_s - T_a\right) \quad [\mathrm{W/m^2}] \qquad \textbf{Equation A-16}$$

Where the terms, variables and constants are the same as those explained in the simple calibration, plus:

h_k = average conduction coefficient [W/m^2.K]

Knowing the steady state incident heat fluxes $\left(\dot{Q}''_{inc} = \alpha_m \dot{q}''_{inc}\right)$ and the T_s (= T_m) associated to them, the conductive coefficient could be worked out as:

$$h_k = \dot{Q}''_{inc} - \left[\frac{\varepsilon_s \sigma\left(T_s^4 - T_a^4\right) + h_c\left(T_s - T_a\right)}{\left(T_s - T_a\right)}\right] \quad [\mathrm{W/m^2}] \qquad \textbf{Equation A-17}$$

Depending on each situation, this value could be approximated either to a constant value or use a trend line function to estimate it later in both the transient calibration and actual tests for every time step.

After a series of three different calibration tests at eight different constant incident heat fluxes and in steady-state (i.e., wait until and record only constant T_s), the average conduction coefficient for this particular TSC in this setting was found not to be constant, but to follow an approximate second degree polynomial curve function of the incident heat flux. This is shown in the following graph:

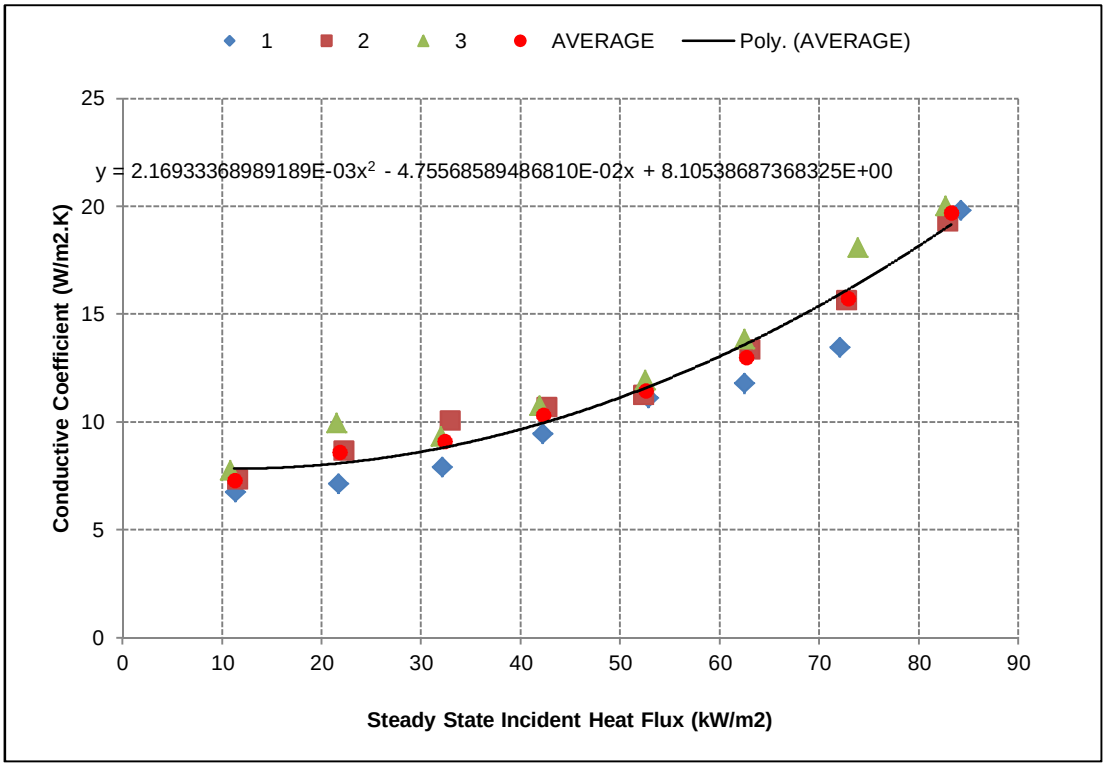

Figure A-220: Conductive loss coefficient (h_k) as a function of the incident heat flux

Therefore, the conductive coefficient was defined for these TSC as a function of the incident heat flux as:

$$h_k = \begin{cases} +\,2.16933368989189\text{x}10^{-3} Q''^{2}_{inc} \ldots \\ \ldots - 4.75568589486810\text{x}10^{-2} Q''_{inc} \ldots \\ \ldots + 8.10538687368325 \end{cases} \quad [\text{W/m}^2\text{.K}]$$

Because during an actual test the incident heat flux is not available (it is exactly the data looked after), the conductive coefficient needs to be also defined as a function of the TSC temperature, T_s. Thus, the best fit curve found to better represent this h_k evolution as a function of T_s was:

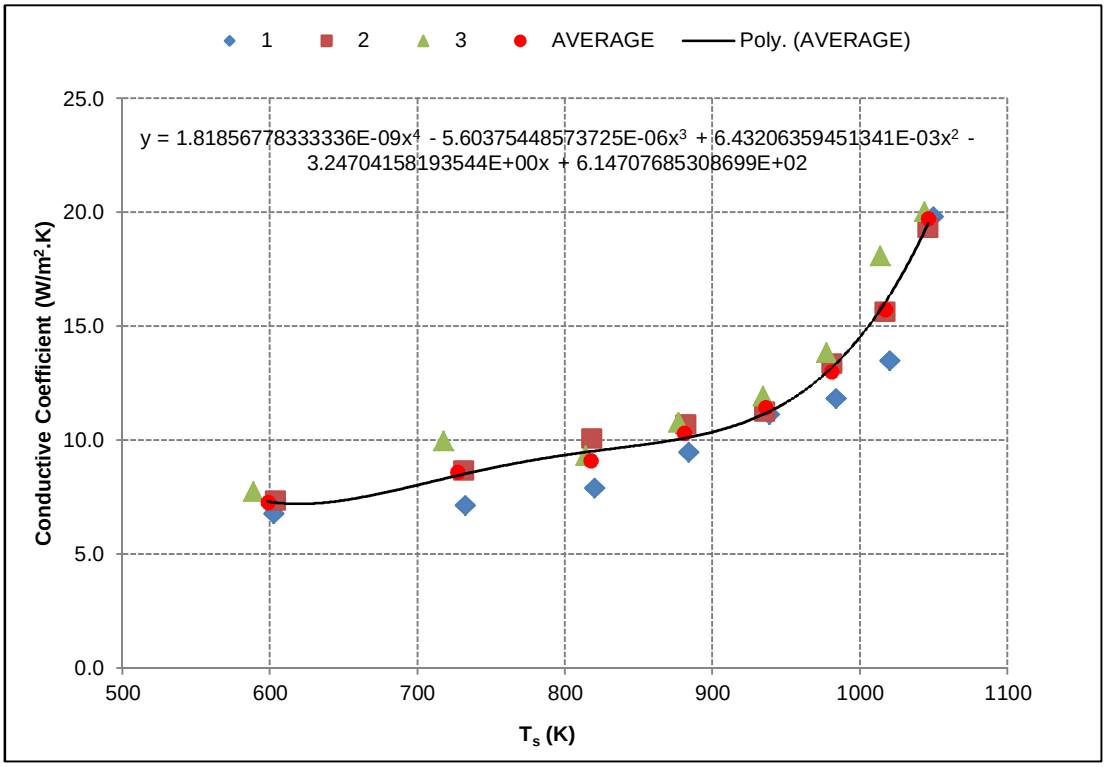

Figure A-221: Conductive loss coefficient (h_k) as a function of the TSC's temperature

- for 600 K < T_s

  h_k = 7.9 [W/m^2.K]

- for 600 K ≤ T_s ≤ 1,050 K

$$h_k = \begin{cases} +1.81856778333336x10^{-9}\ Q_{inc}^{"4}... \\ ...-5.60375448573725x10^{-6}\ Q_{inc}^{"3}... \\ ...+6.43206359451341x10^{-3}\ Q_{inc}^{"2}... \\ ...-3.24704158193544\ x10^{0}\ Q_{inc}^{"}... \\ ...+6.14707685308699x10^{2} \end{cases} \quad [\mathrm{W/m^2.K}]$$

- for T_s > 1,050 K

h_k = 19 [W/m^2.K]

Additionally, the transient part of the calibration test (constant heat flux + increasing T_s before reaching steady-state) could be approximated with the following simplified equation:

Incident = stored + conduction losses + reradiation losses + convection losses

Mathematically expressed,

$$Q_{inc}^{"} = \frac{Q_{inc}}{A_s} = \rho_s \delta_s c_s \left(\frac{dT_s}{dt}\right) + \varepsilon_s \sigma \left(T_s^4 - T_a^4\right) + h_c \left(T_s - T_a\right) + h_k \left(T_s - T_a\right) \ [\mathrm{W/m^2}]$$

Equation A-18

$$Q_{inc}^{"} = \frac{Q_{inc}}{A_s} = \frac{m_s c_s}{A_s} \left(\frac{dT_s}{dt}\right) + \varepsilon_s \sigma \left(T_s^4 - T_a^4\right) + h_c \left(T_s - T_a\right) + h_k \left(T_s - T_a\right) \ [\mathrm{W/m^2}]$$

Equation A-19

Where the terms, variables and constants are the same as those explained previously, plus:

m_s = mass of the stainless steel AISI 304 TSC [kg]

$\frac{m_S c_S}{A_S}\left(\frac{dT_S}{dt}\right)$ = energy stored term [W/m^2]

The re-radiation losses are treated in a similar way to the conduction losses by linearizing them with the temperature difference between the plate and the ambient.

Thus,

$$Q''_{inc} = \frac{m_s c_s}{A_s}\left(\frac{dT_s}{dt}\right) + h_{eff}\left(T_s - T_a\right) \text{ [W/m}^2\text{]} \qquad \textbf{Equation A-20}$$

Where h_{eff} is an effective heat transfer coefficient represented by:

$$h_{eff} = h_c + h_k + \varepsilon_s \sigma\left(T_s^2 + T_a^2\right)\left(T_s + T_a\right) \text{ [W/m}^2\text{.K]} \qquad \textbf{Equation A-21}$$

And which can be estimated with h_k, T_s, and h_c, for each time step. If we were in a steady-state situation, the actual TSC heat flux readings, q''_s, in each time step would have therefore been estimated as:

$$q''_s = \varepsilon_s \sigma\left(T_s^4 - T_a^4\right) + h_c\left(T_s - T_a\right) + h_k\left(T_s - T_a\right) = h_{eff}\left(T_s - T_a\right) \text{ [W/m}^2\text{]} \qquad \textbf{Equation A-22}$$

But, as we are in a transient mode, if we wish to derive the incident heat flux from this plate reading, we would need to 'correct' this q''_s reading by adding the missing *stored* term as follows:

$$Q''_{inc} = \frac{m_s c_s}{A_s}\left(\frac{dq''_s/dt}{h_{eff}}\right) + q''_s \text{ [W/m}^2\text{]} \qquad \textbf{Equation A-23}$$

$$Q''_{inc} = \frac{m_s c_s}{A_s h_{eff}}\left(\frac{dq''_s}{dt}\right) + q''_s \text{ [W/m}^2\text{]} \qquad \textbf{Equation A-24}$$

Here, the term embracing the coefficient of the derivate is defined as the time constant of the device, $t_{r,calibration}$, and can be obtained during the transient calibration test (for each time step) as,

$$t_{r,calibration} = \frac{Q''_{inc} - q''_s}{\left(dq''_s/dt\right)} \quad [\text{s}] \qquad \textbf{Equation A-25}$$

using the already estimated q''_s and the actual TSC heat flux reading time derivate $\left(\frac{dq''_s}{dt}\right)$ for each time step, and knowing the constant value of $\dot{Q}''_{inc}$ used during this transient part of the calibration process.

Finally, the $\left(\frac{m_s c_s}{A_s}\right)$ ratio can be derived not from the device's components (as it would have been done if following the simple calibration process approach) but empirically as:

$$\frac{m_s c_s}{A_s} = t_{r,calibration}\ h_{eff} = const. \quad [\text{J/m}^2\text{.K}] \qquad \textbf{Equation A-26}$$

This value is assumed as constant and related to the specific device (TSC).

The following graph shows the results of the average heat capacity per unit area of TSC, obtained after a calibration test with six different settings; i.e., six different and constant heat fluxes were imposed to the TSC with a radiant panel, and its temperature evolution recorded in time.

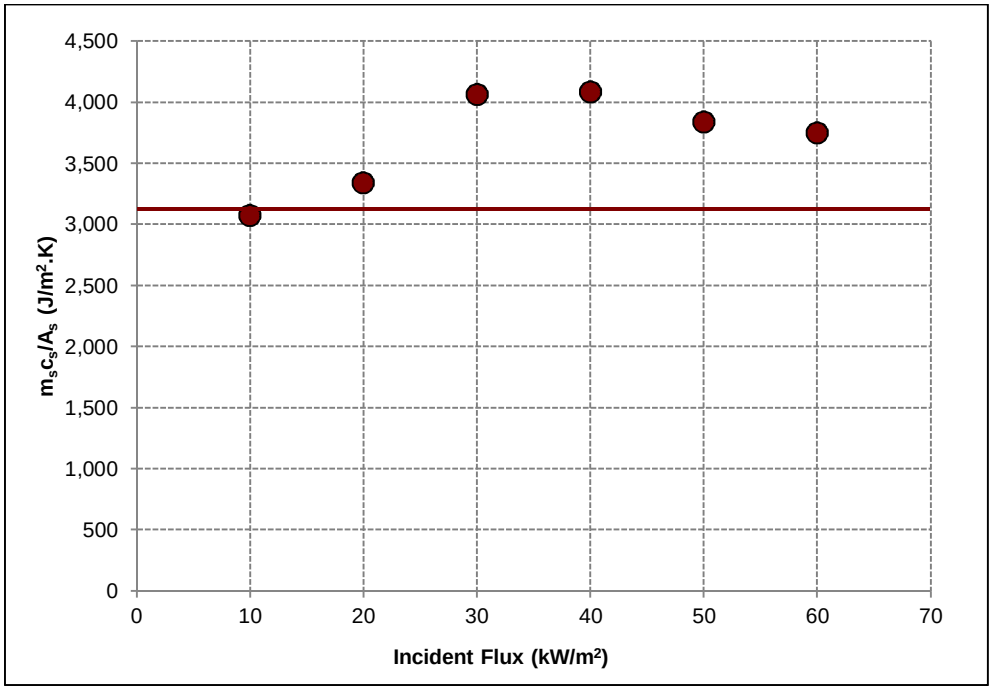

Figure A-222: Average $\left(\frac{m_s c_s}{A_s}\right)$ as a function of incident heat flux

After these results, a constant $\left(\frac{m_s c_s}{A_s}\right)$ value of 3.7 kJ/m^2.K was assumed for this particular TSC dimensions and backing arrangement.

c. Testing the calibration

In order to test the calibration results after the constants and functions obtained, a set of variable heat flux (transient) tests were ran, using the same boundary conditions as in the calibration process, assessing the evolution of the TSC reading against the heat flux vs. time curve obtain with the calibrated *Schmidt-Boelter* radiometer set aside.

i. Simple Calibration

In this testing calibration mode, the simple energy equation to be used after the *C value* was found during the steady-state calibration is the following:

$$\boldsymbol{Incident = stored + conduction\ losses + reradiation\ losses + convection\ losses}$$

$$\boldsymbol{\rightarrow conduction\ losses = C\ x\ Incident}$$

$$\boldsymbol{Incident = stored + (C\ x\ Incident) + reradiation\ losses + convection\ losses}$$

$$\boldsymbol{Incident = \frac{stored + reradiation\ losses + convection\ losses}{1 - C}}$$

The mathematical equation for the incident term is:

$$Q''_{inc} = \frac{\rho_s \delta_s c_s \left(\frac{dT_s}{dt}\right) + \varepsilon_s \sigma \left(T_s^4 - T_a^4\right) + h_c \left(T_s - T_a\right)}{1 - C} \quad [\mathrm{W/m^2}] \qquad \textbf{Equation A-27}$$

Where,

$(\rho_s \delta_s c_s)$ = taken from the device's components [$\mathrm{J/m^2.K}$]

$\left(\frac{dT_s}{dt}\right)$ = TSC temperature evolution in time [K/s]

h_c = average convective heat transfer coefficient along the characteristic length of the calibration assembly (stainless steel AISI 304 plate + insulation backing) [$\mathrm{W/m^2.K}$]

C = calibration corrective (or conduction) factor representing the proportion of incident heat flux that is lost via conduction through the back and sides of the stainless steel TSC into the insulation backing.

ii. Empirical Calibration

In this slightly more complex calibration mode, the simple energy equation to be used after the h_k and the $\left(\frac{m_S c_S}{A_S}\right)$ values were found during the steady-state and transient calibrations, respectively, is the following:

$$\boldsymbol{Incident = stored + conduction\ losses + reradiation\ losses + convection\ losses}$$

$$\rightarrow \boldsymbol{conduction\ losses = h_k(T_s - T_a)}$$

$$Q''_{inc} = \frac{m_s c_s}{A_s h_{eff}}\left(\frac{dq''_s}{dt}\right) + q''_s \quad [\text{W/m}^2] \qquad \textbf{Equation A-28}$$

Where**,**

$h_{eff} = h_c + h_k + \varepsilon_s \sigma\left(T_s^2 + T_a^2\right)\left(T_s + T_a\right)$ [W/m^2.K] (from **Equation A-21**)

h_k = either constant value or trend line function approximated from the steady-state portion of the calibration process [W/m^2.K]

h_c = average convective heat transfer coefficient along the characteristic length of the calibration assembly (stainless steel AISI 304 plate + insulation backing) [W/m^2.K]

$\left(\frac{m_S c_S}{A_S}\right)$ = constant value approximated from the transient portion of the calibration process [J/m^2.K]

$q''_s = h_{eff}\,(T_s - T_a)$ [W/m^2]

$\frac{dq''_s}{dt}$ = q_s reading evolution in time [W/m^2.s]

iii. Results & Comparison

The results of three calibration tests are shown in the following graphs:

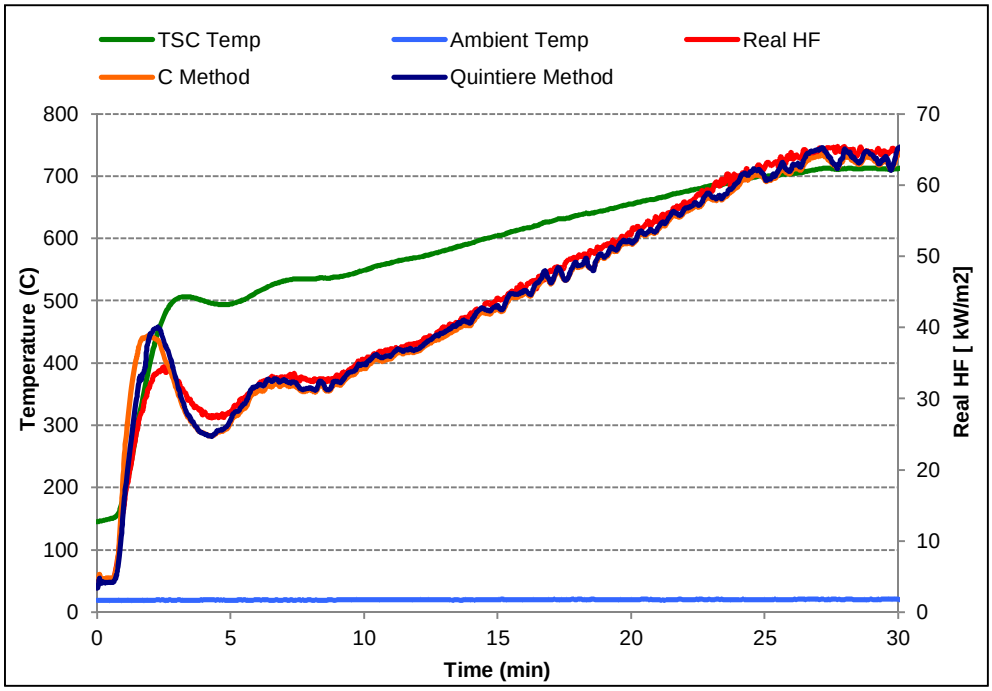

Figure A-223: Calibration test 1

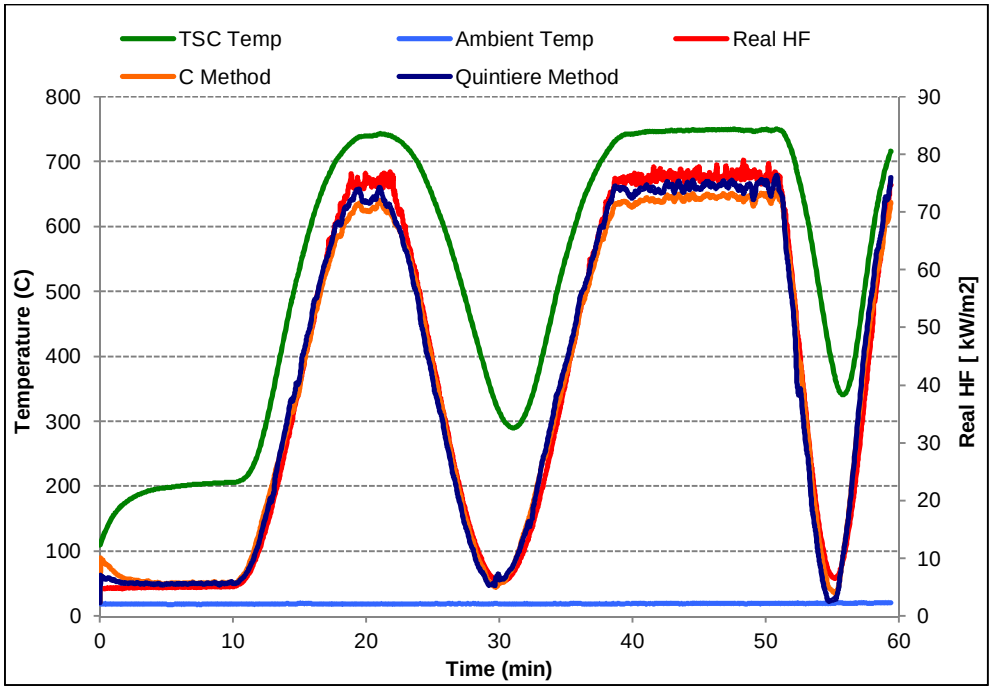

Figure A-224: Calibration test 2

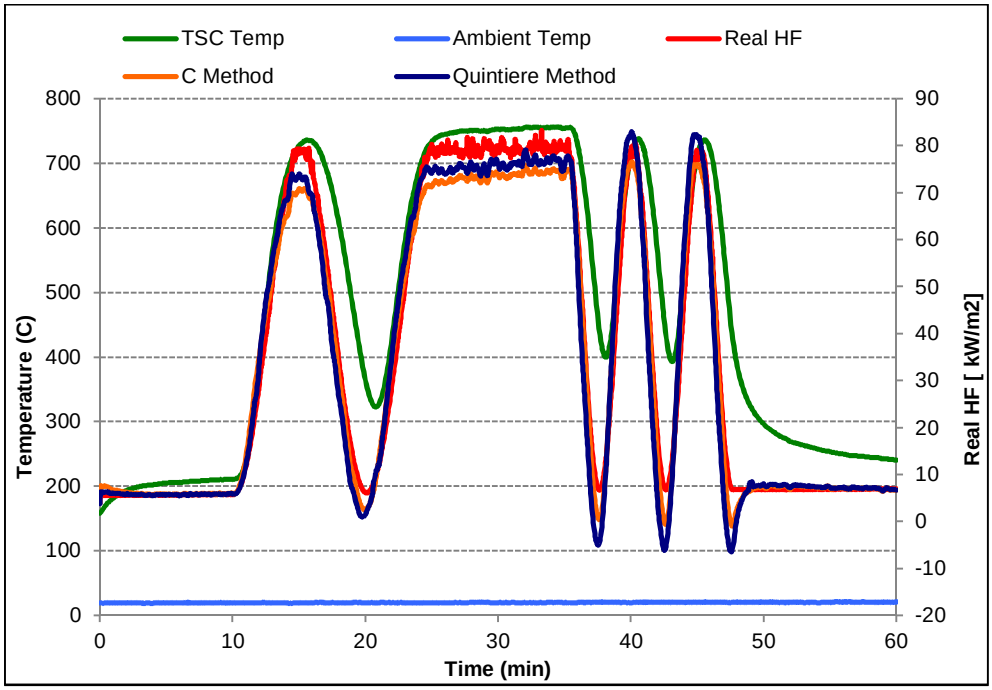

Figure A-225: Calibration test 3

After these results, it is clearly seen that the TSC calibrated following either approach – i.e. simple or empirical – reproduce quite accurately the real incident heat flux imposed by the radiant panel and recorded by the calibrated *Schmidt-Boelter* radiometer set aside the TSC. The only difference relies on the steady-state portion of the tests, were the empirical calibration approach seems to give better results.

Due to the fact that the reduced-scale compartment fire tests – subject of this thesis – were designed to approximate as much as physically possible to a steady-state condition, the empirical approach was found to be a better option and, thus, applied instead of the simple *C method* approach.

d. Application to Tests

Due mainly to the change in ventilation patterns, the situation of a TSC immersed in a compartment engulfed in flames is different to that of a TSC located in front of a radiant panel immersed in a quiescent atmosphere which is otherwise at rest (no air velocities far from the heated zone), as it was the case during calibration. In terms of the energy balance, this means that the convective loss term typically found in free convection situations (e.g. in calibration) will now be replaced by a convective gain term which will be considered in addition to the original incident heat flux (*incident*) towards a *total fire incident* heat flux.

So, the equation that characterizes the TSC total energy (or heat) balance for a compartment fire which accounts for both radiation and convection heat fluxes from the fire is:

$$\boxed{\boldsymbol{OUT\ from\ the\ fire\ (total\ output) = IN\ to\ the\ TSC\ (total\ incident = st.\ + loss.)}}$$

$$\rightarrow \boldsymbol{radiative\ output + convective\ output}$$
$$\boldsymbol{= stored + conduction\ losses}$$
$$\boldsymbol{+ reradiation\ losses\ (no\ convection\ losses)}$$

The total incident heat flux to the TSC is equal to the total incident radiation and convection heat flux from the compartment fire to the stainless steel plate; i.e.:

$$Q''_{fire} = Q''_{TSC}$$ **Equation A-29**

Replacing each term, the equation for the energy balance in the stainless steel plate can therefore be expressed, for the different calibration approaches as:

i. Simple Calibration

$$Q''_{rad} + h_{c,\,fire}\left(T_g - T_s\right) = \rho_s \delta_s c_s \left(\frac{dT_s}{dt}\right) + CQ''_{fire} + \varepsilon_s \sigma\left(T_s^4 - T_a^4\right) \text{ [W/m}^2\text{]}$$ **Equation A-30**

$$\left(1 - C\right) Q''_{fire} = \rho_s \delta_s c_s \left(\frac{dT_s}{dt}\right) + \varepsilon_s \sigma\left(T_s^4 - T_a^4\right) \text{ [W/m}^2\text{]}$$ **Equation A-31**

$$Q''_{fire} = \frac{\rho_s \delta_s c_s \left(\frac{dT_s}{dt}\right) + \varepsilon_s \sigma\left(T_s^4 - T_a^4\right)}{1 - C} = Q''_{TSC} \quad \text{[W/m}^2\text{]}$$ **Equation A-32**

Where,

T_g = Temperature of the gases around the stainless steel plate taken from thermocouples trees measurements in the proximity, and corrected from radiation error [K]

ρ_s = density of stainless steel AISI 304 = 7,900 kg/m^3

δ_s = thickness of the TSC's stainless steel AISI 304 plate = 1.2 x 10^{-3} m

c_s = specific heat capacity of stainless steel AISI 304 (temp. dependant) [J/kg.K].

The latter was obtained as a best-fit function after the following temperature dependent values found in the literature:

Table A-1: Specific Heat Capacity of Stainless Steel AISI 304 at various Temperatures [117]

Temperatures	K	100	200	300	400	600	800	1,000	1,200	1,500
	C	-172	-72	28	128	328	528	728	928	1,228
c_s [J/kg.K]		272	402	477	515	557	582	611	640	682

So the process to estimate Q''_{TSC} for every TSC installed in the compartment test would simply be to apply the previous equation (Equation A-32) using the *C value* obtained from the steady-state portion of the calibration process.

ii. Empirical Calibration

$$Q''_{rad} + h_{c,\,fire}\left(T_g - T_s\right) = \frac{m_s c_s}{A_s h_{fire}}\left(\frac{dq''_s}{dt}\right) + q''_s \quad [\mathrm{W/m^2}] \qquad \textbf{Equation A-33}$$

$$Q''_{fire} = \frac{m_s c_s}{A_s h_{fire}}\left(\frac{dq''_s}{dt}\right) + q''_s = Q''_{TSC} \quad [\mathrm{W/m^2}] \qquad \textbf{Equation A-34}$$

Where,

$h_{fire} = h_k + \varepsilon_s \sigma\left(T_s^2 + T_a^2\right)\left(T_s + T_a\right)$ [W/m^2.K] (i.e., no h_c, no convection losses)

h_k = either constant value or trend line function approximated from the steady-state portion of the calibration process [W/m^2.K]

$\left(\frac{m_S c_S}{A_S}\right)$ = constant value approximated from the transient portion of the calibration process [J/m^2.K]

$q''_s = h_{fire}\,(T_s - T_a)$ [W/m^2]

$\frac{dq_s^{"}}{dt}$ = q_s reading evolution in time [W/m^2.s]

T_g = Temperature of the gases around the stainless steel plate taken from thermocouples trees measurements in the proximity, and corrected from radiation error [K]

m_s = mass of the TSC's stainless steel AISI 304 plate [kg]

c_s = specific heat capacity of stainless steel AISI 304 (temp. dependant) [J/kg.K].

The latter – same as in the previous case – was obtained as a best-fit function after the temperature dependent values found in the literature (refer to Table A-1).

In this case, the process to estimate $Q_{TSC}^{"}$ for every TSC installed in the compartment test would be:

1. Using the previously found h_k we now estimate h_{fire} for each time step without accounting for the convection losses (because there's no cooling convection but heating convection from the hot gases) as:

$$h_{fire} = h_k + \varepsilon_s \sigma \left(T_s^2 + T_a^2\right)\left(T_s + T_a\right) \quad [\text{W/m}^2\text{.K}]$$

2. This effective coefficient, h_{fire}, is then used to obtain the actual (i.e., not corrected) TSC heat flux reading as:

$$q_s^{"} = h_{fire}\left(T_s - T_a\right) \quad [\text{W/m}^2]$$

3. With the calibration value $\left(\frac{m_s c_s}{A_s}\right)$ and the effective heat transfer for each time step, h_{fire}, the device's time constant is obtained, $t_{r,\,fire}$, for each time step as:

$$t_{r,\,fire} = \frac{\left(m_s c_s / A_s\right)}{h_{fire}} \qquad [s]$$

4. Finally, the actual TSC reading, $q_s^{"}$, can be 'corrected' to obtain the real incident heat flux ($Q_{fire}^{"} = Q_{TSC}^{"}$) in every time step by adding the correspondent *energy stored* term (actual reading derivate times time constant):

$$Q_{fire}^{"} = \frac{m_s c_s}{A_s h_{fire}} \left(\frac{dq_s^{"}}{dt} \right) + q_s^{"} = Q_{TSC}^{"} \qquad [W/m^2]$$

As seen previously,

$$Q_{fire}^{"} = Q_{rad}^{"} + h_{c,\,fire}\left(T_g - T_s\right) = Q_{TSC}^{"} \qquad [W/m^2]$$

$h_{c,fire}$ is only needed if we wanted to know how much of the total incident heat flux to the internal surface, $Q_{TSC}^{"}$, is convective ($h_{c,fire}\,(T_g - T_s)$) and how much is radiative ($Q_{rad}^{"}$). For this particular case, any value of the convective heat transfer, $h_{c,fire}$, falling between 25 W/m^2.K (typically assumed in a compartment fire) and Quintiere's 50 W/m^2.K [125] could be assumed to assess this comparative analysis.

Appendix A Note - Details on the average calibration heat transfer coefficient calculations.

Noticing that transition to turbulence never occurred on the TSC calibration assembly ($R_{aL} < R_{a,critic} \sim 10^9$) over the full range of temperatures acquired, the average convective heat transfer coefficient, h_c, over a surface of length L (TSC calibration assembly) was estimated – as said before – from the following correlations of free convection on a vertical plate [117]:

$$Ra_L = \frac{g\beta(T_s - T_a)L^3}{\alpha\nu}$$

$$Nu_L = 0.68 + \frac{0.670 Ra_L^{1/4}}{\left[1 + \left(\frac{0.492}{\mathrm{Pr}}\right)^{9/16}\right]^{4/9}} \qquad Ra_L \le 10^9$$

$$h_c = \frac{Nu_L\, k_a}{L}$$

The air properties were evaluated at the 'film' temperature, T_f, which is an average between the plate's surface temperature, T_s, and the ambient temperature, T_a, at the time of the calibration tests. Therefore, the C value was calculated using a temperature, T_s, dependant on the value of h_c averaged over the vertical length of the TSC calibration assembly.

Appendix B: Small-Scale Experiments Full Results

All the time averages shown in the graphs were calculated over a selected steady-state period – of around 10 minutes depending on each test configuration – representing the fully-developed or post-FO conditions.

The black-dotted horizontal lines at or near the upper and lower edges of the graphs represent the upper and lower edges of the opening plane, respectively. Additionally, the red-dotted horizontal line represents the estimated neutral plane position.

For image clarity and neatness, the first figure of this appendix (Figure B-1) is the only one that shows said nomenclature.

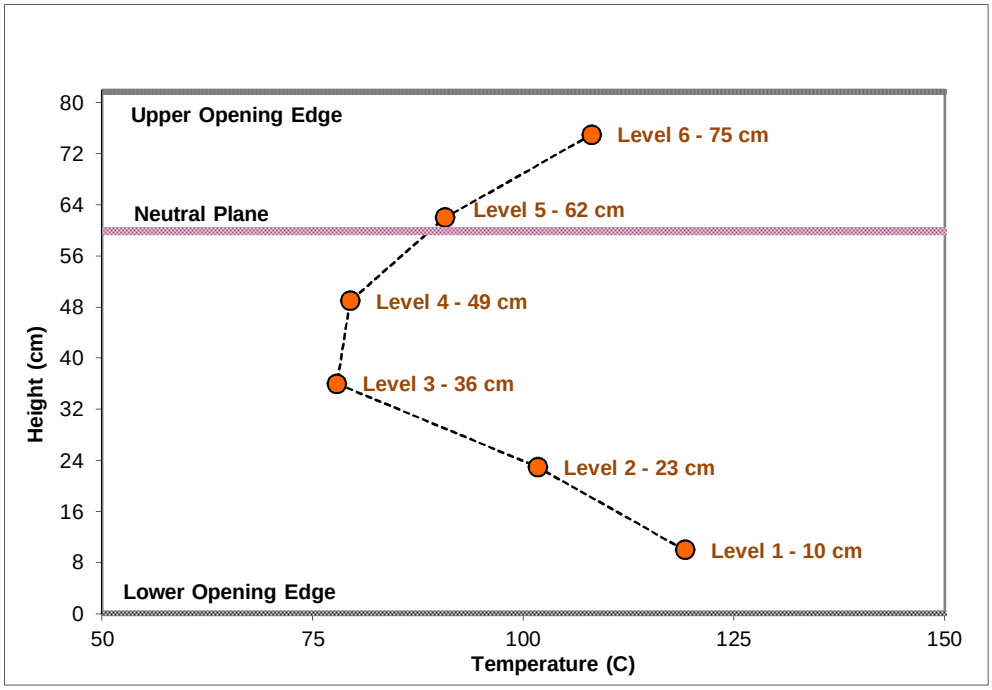

Figure B-1: Space-time-averaged layer temperatures for the 0.5 g/s, ϕ_1 configuration

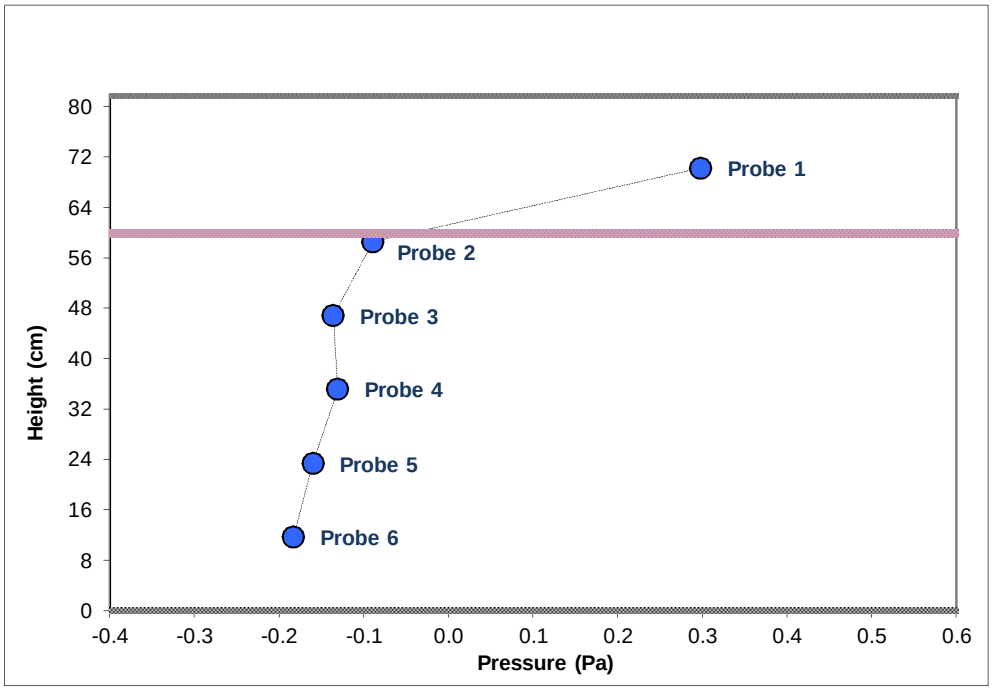

Figure B-2: Time-averaged pressure profile at the opening plane for the 0.5 g/s, ϕ_1 configuration

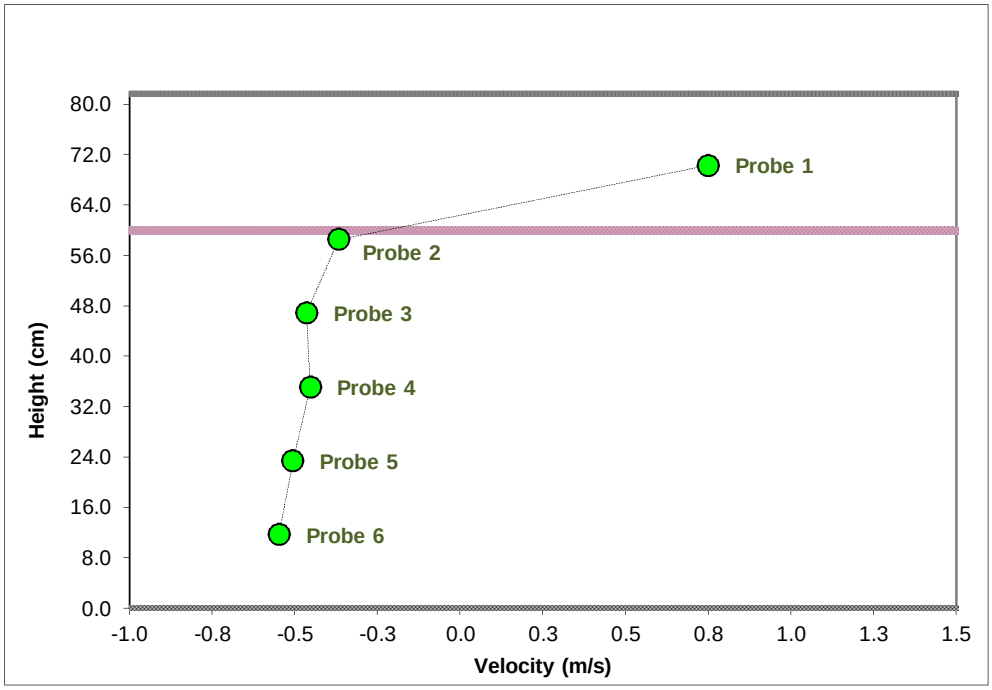

Figure B- 3: Time-averaged velocity profile at the opening plane for the 0.5 g/s, ϕ_1 configuration

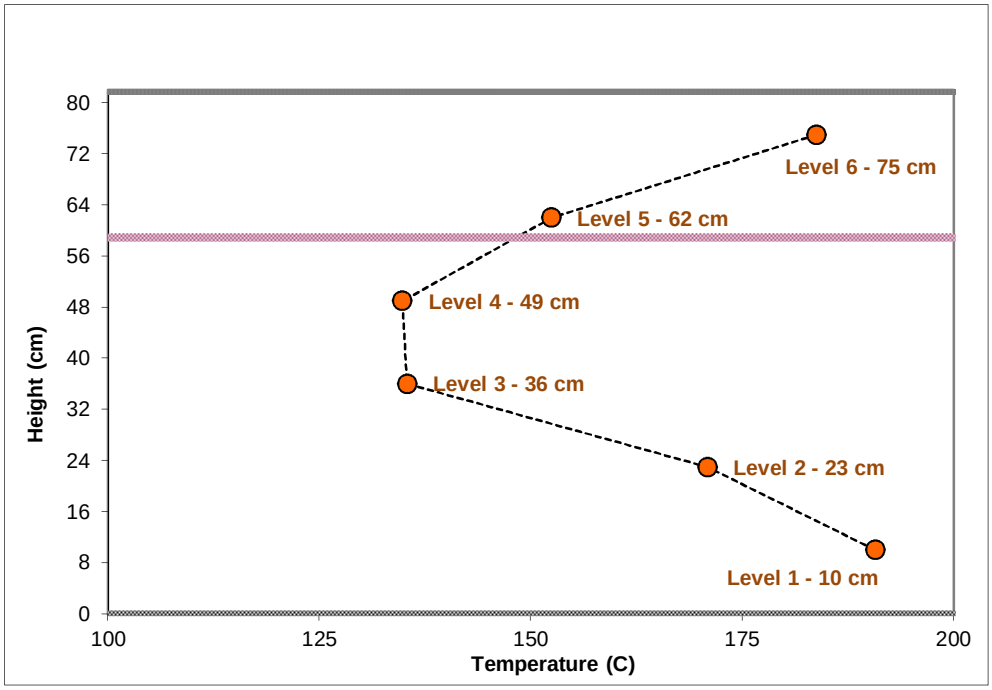

Figure B-4: Space-time-averaged layer temperatures for the 1.0 g/s, ϕ_1 configuration

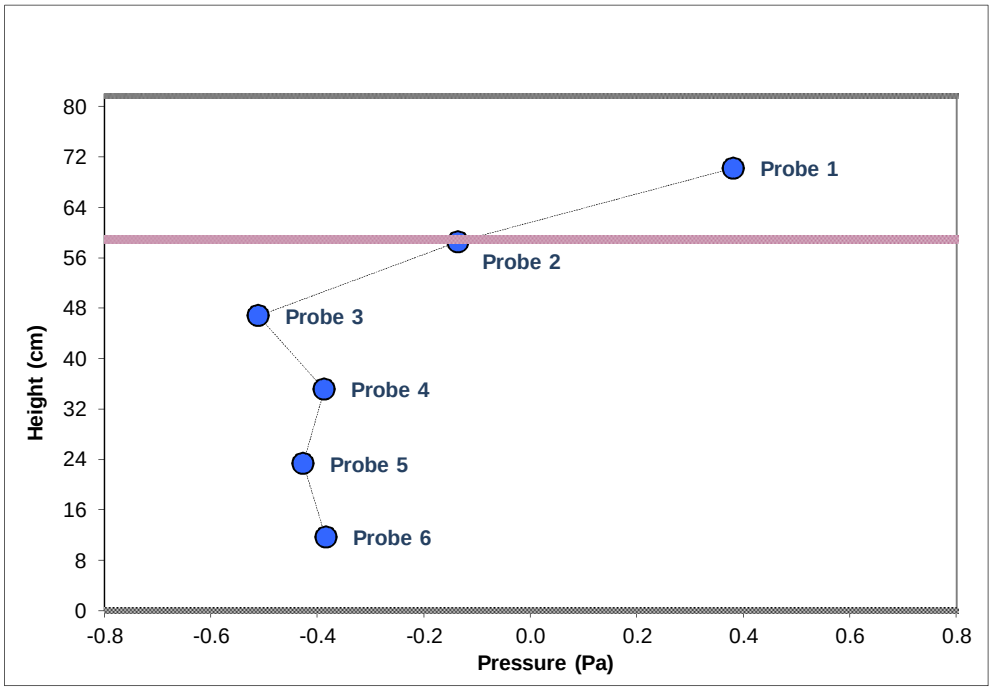

Figure B-5: Time-averaged pressure profile at the opening plane for the 1.0 g/s, ϕ_1 configuration

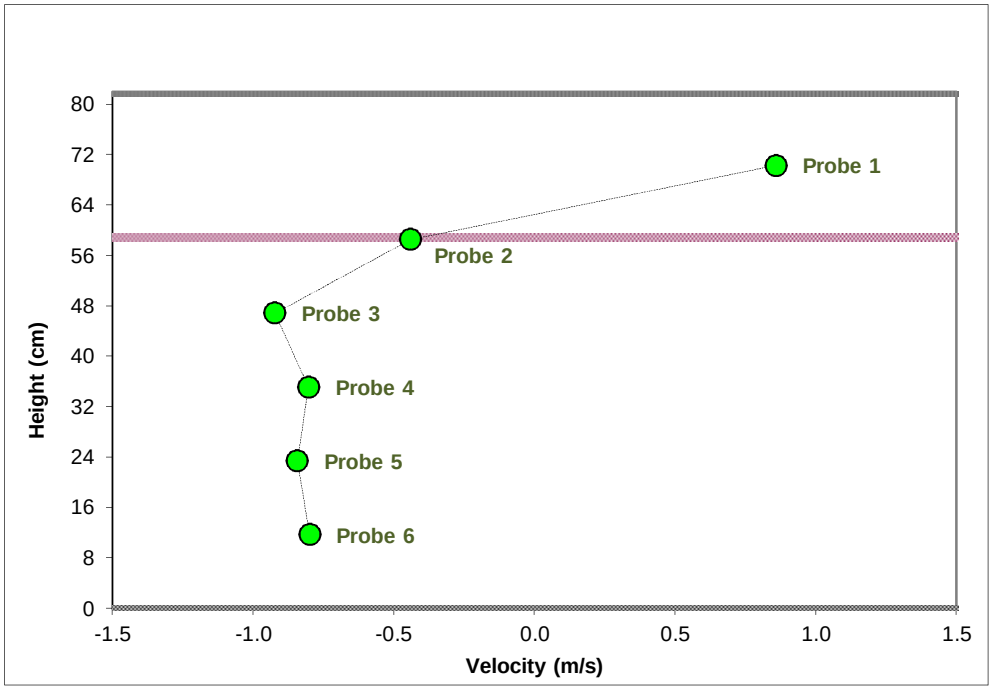

Figure B-6: Time-averaged velocity profile at the opening plane for the 1.0 g/s, ϕ_1 configuration

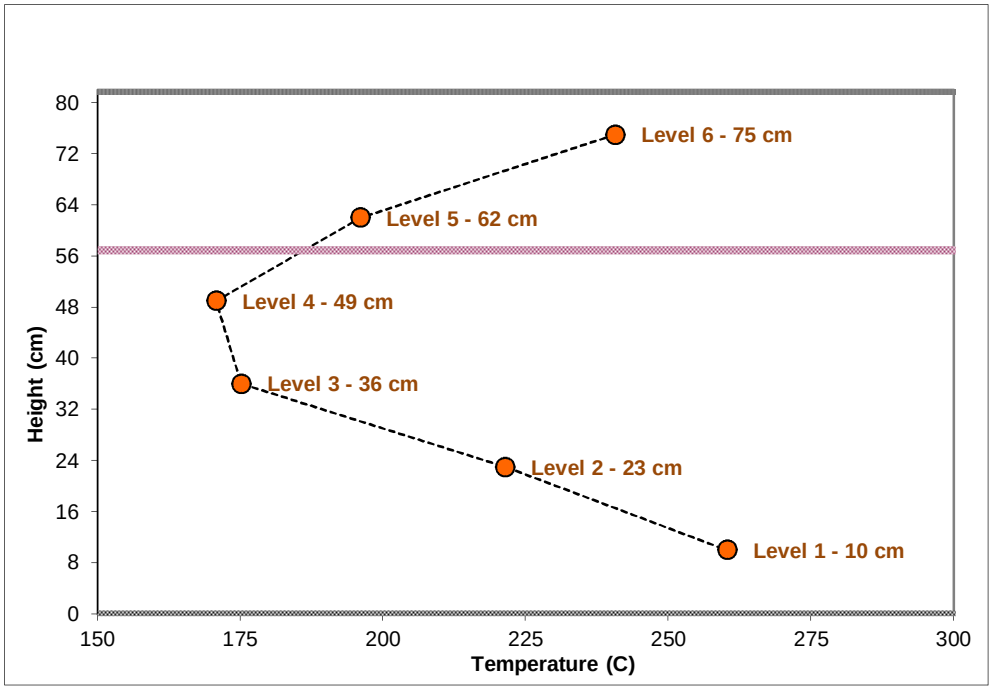

Figure B-7: Space-time-averaged layer temperatures for the 1.5 g/s, ϕ_1 configuration

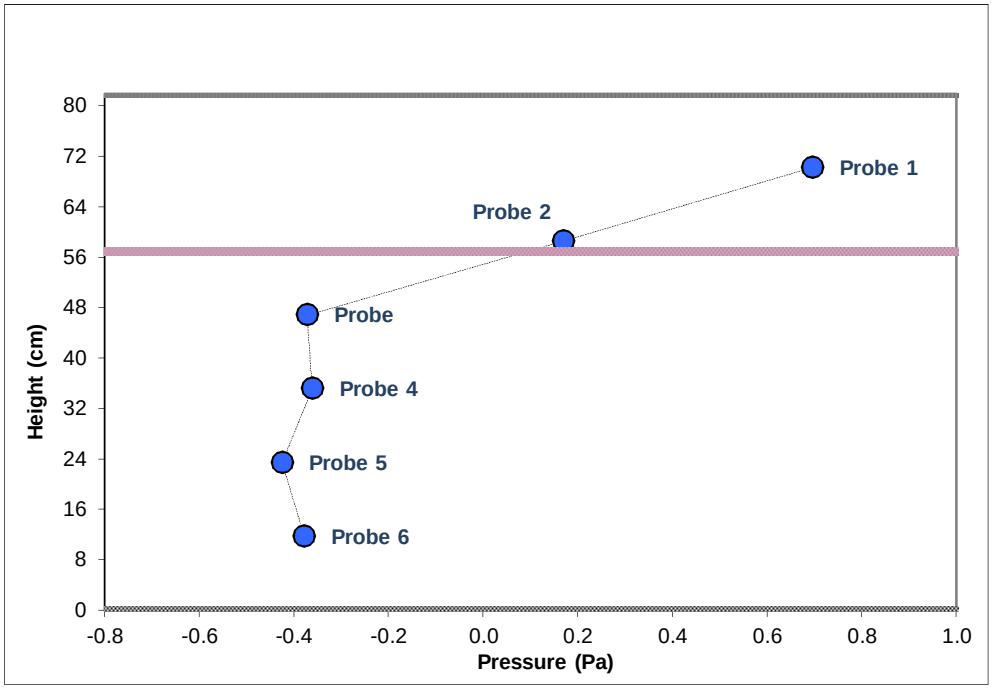

Figure B-8: Time-averaged pressure profile at the opening plane for the 1.5 g/s, ϕ_1 configuration

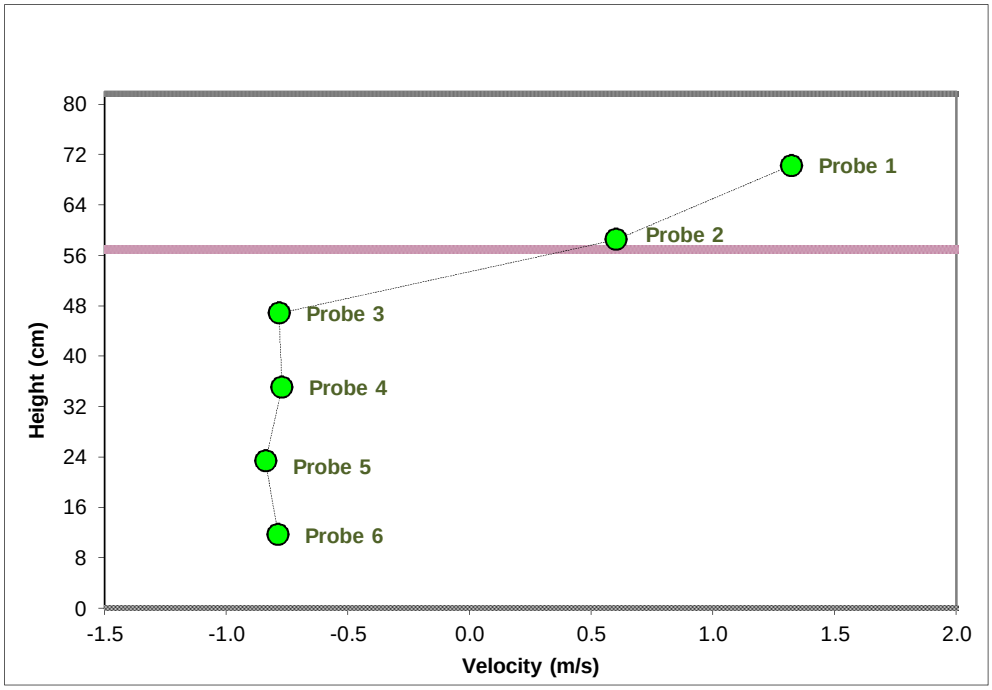

Figure B-9: Time-averaged velocity profile at the opening plane for the 1.5 g/s, ϕ_1 configuration

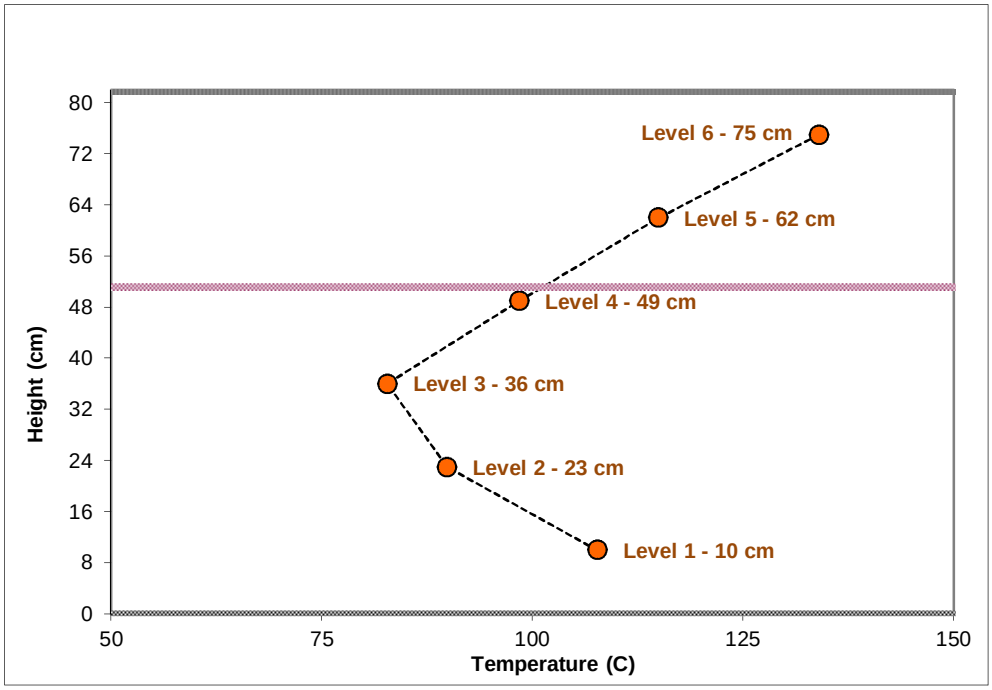

Figure B-10: Space-time-averaged layer temperatures for the 0.5 g/s, ϕ_2 configuration

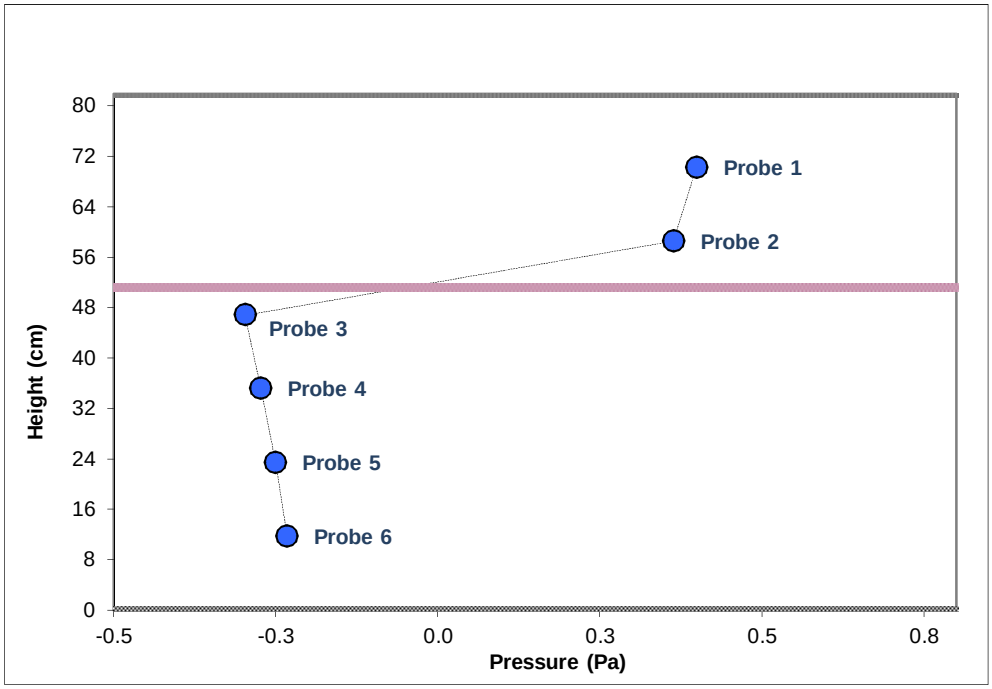

Figure B-11: Time-averaged pressure profile at the opening plane for the 0.5 g/s, ϕ_2 configuration

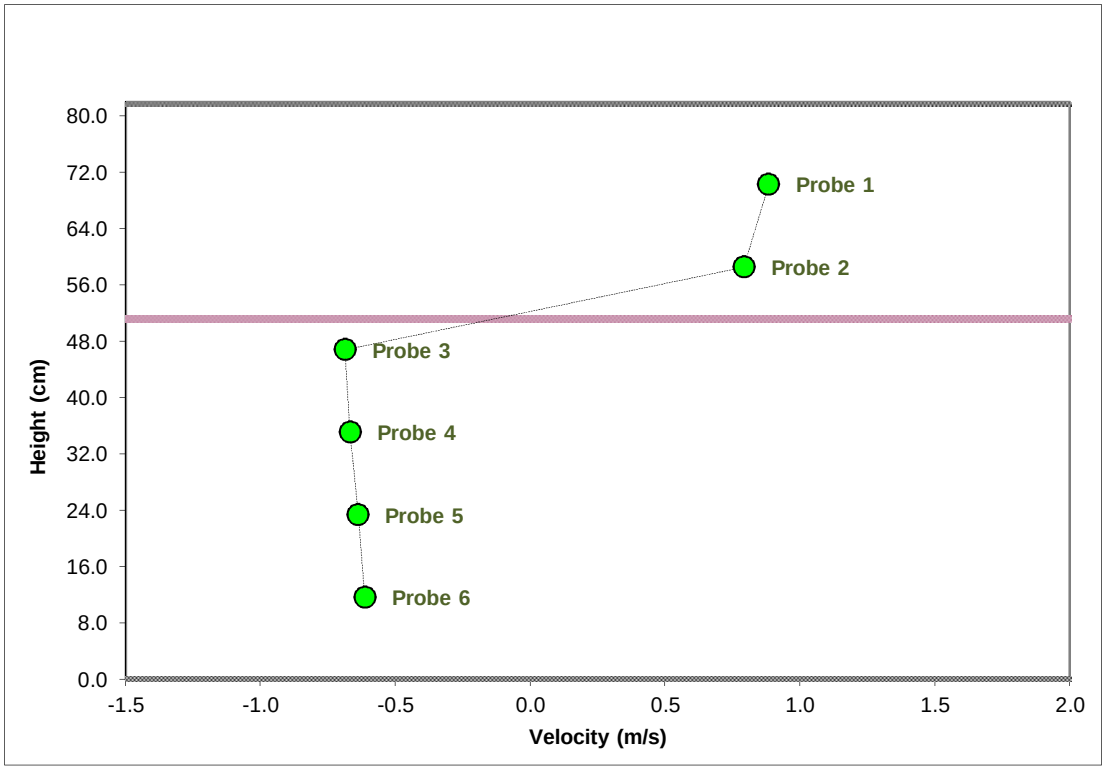

Figure B-12: Time-averaged velocity profile at the opening plane for the 0.5 g/s, ϕ_2 configuration

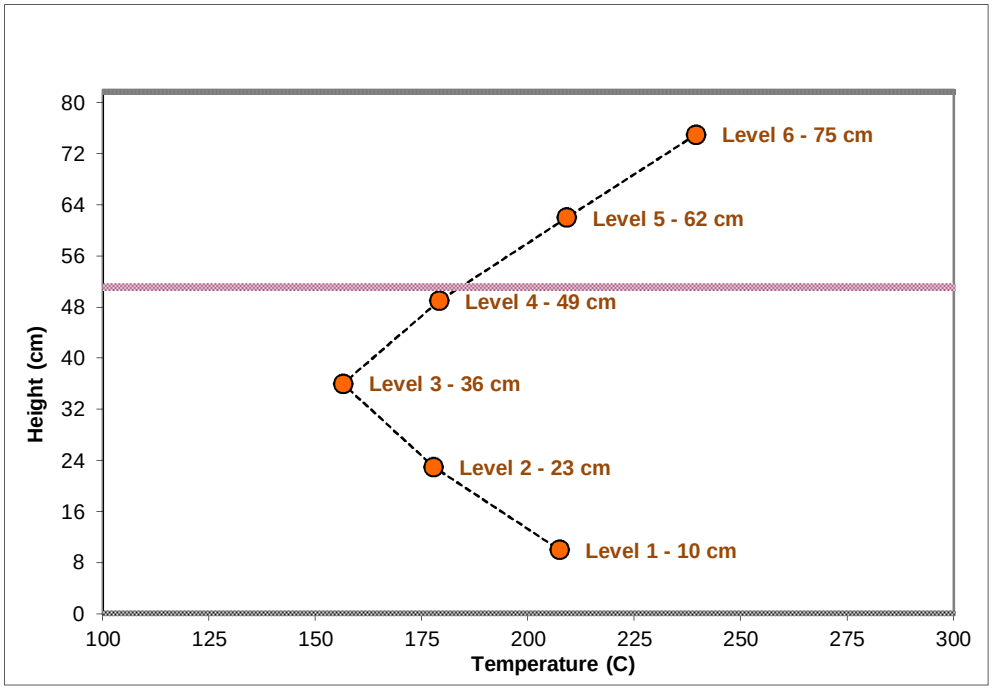

Figure B-13: Space-time-averaged layer temperatures for the 1.0 g/s, ϕ_2 configuration

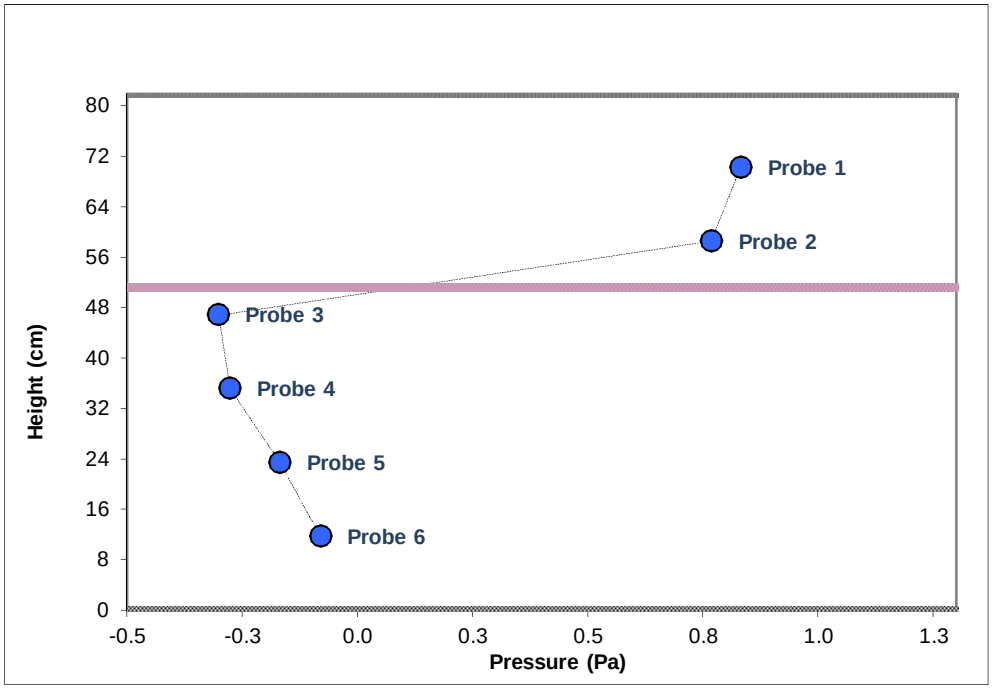

Figure B-14: Time-averaged pressure profile at the opening plane for the 1.0 g/s, ϕ_2 configuration

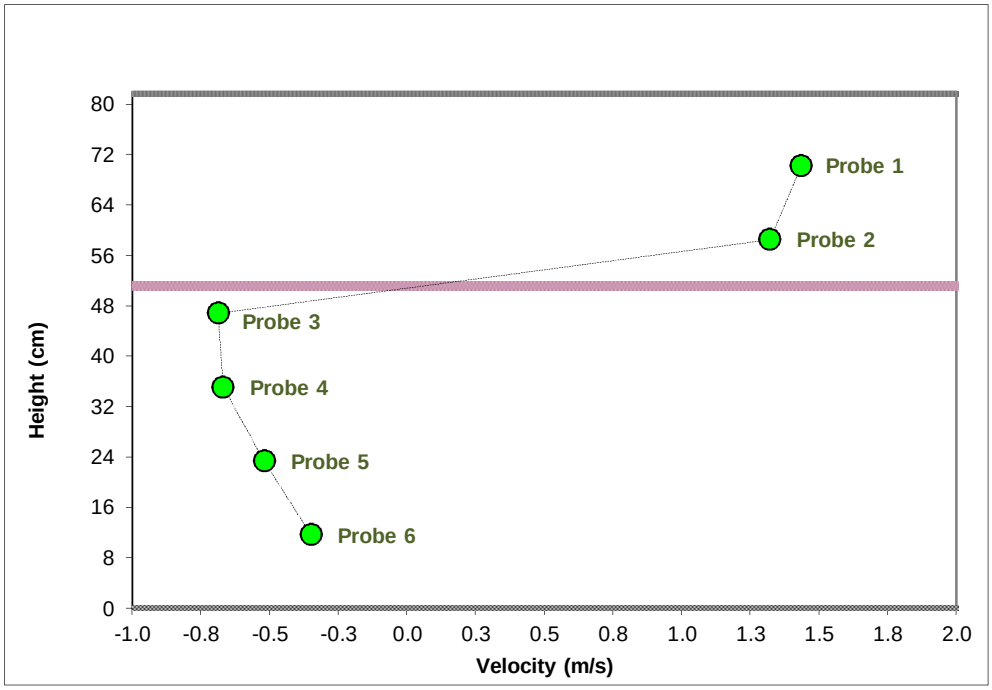

Figure B-15: Time-averaged velocity profile at the opening plane for the 1.0 g/s, ϕ_2 configuration

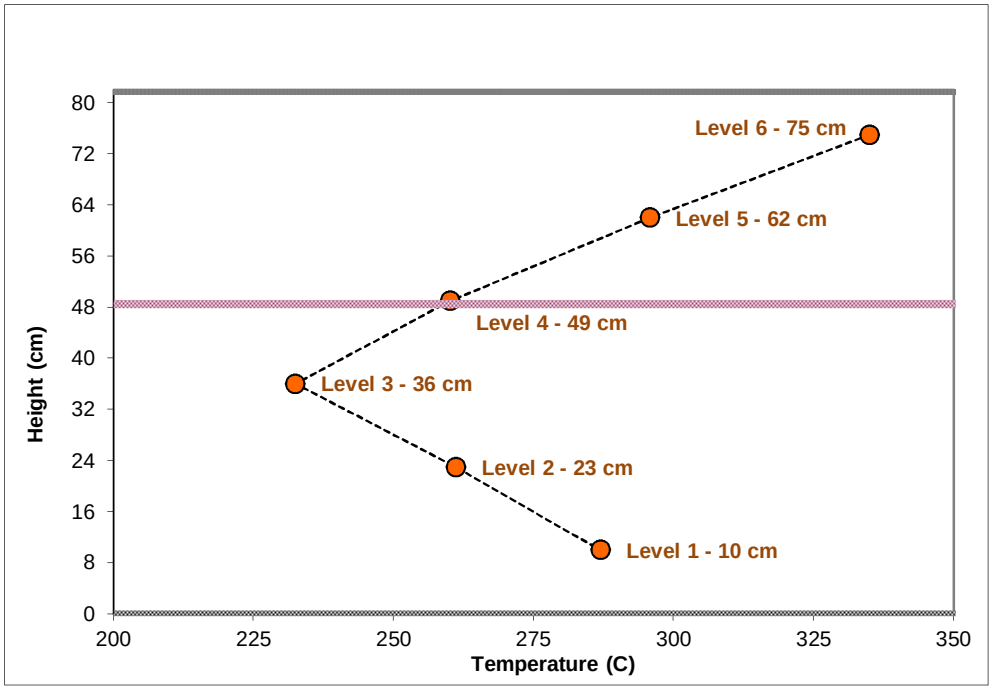

Figure B-16: Space-time-averaged layer temperatures for the 1.5 g/s, ϕ_2 configuration

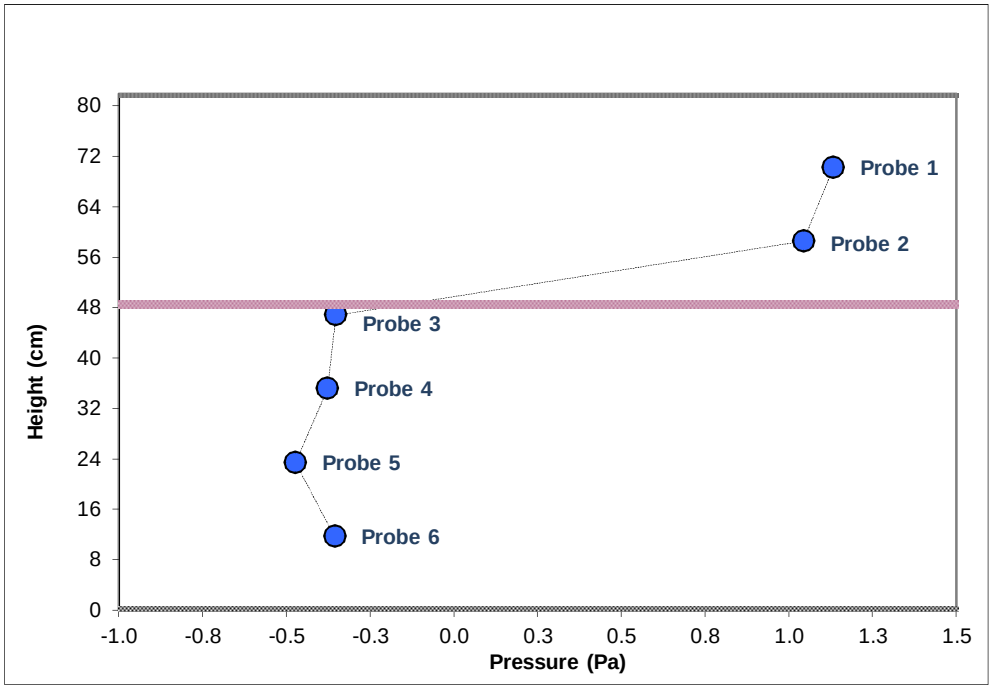

Figure B-17: Time-averaged pressure profile at the opening plane for the 1.5 g/s, ϕ_2 configuration

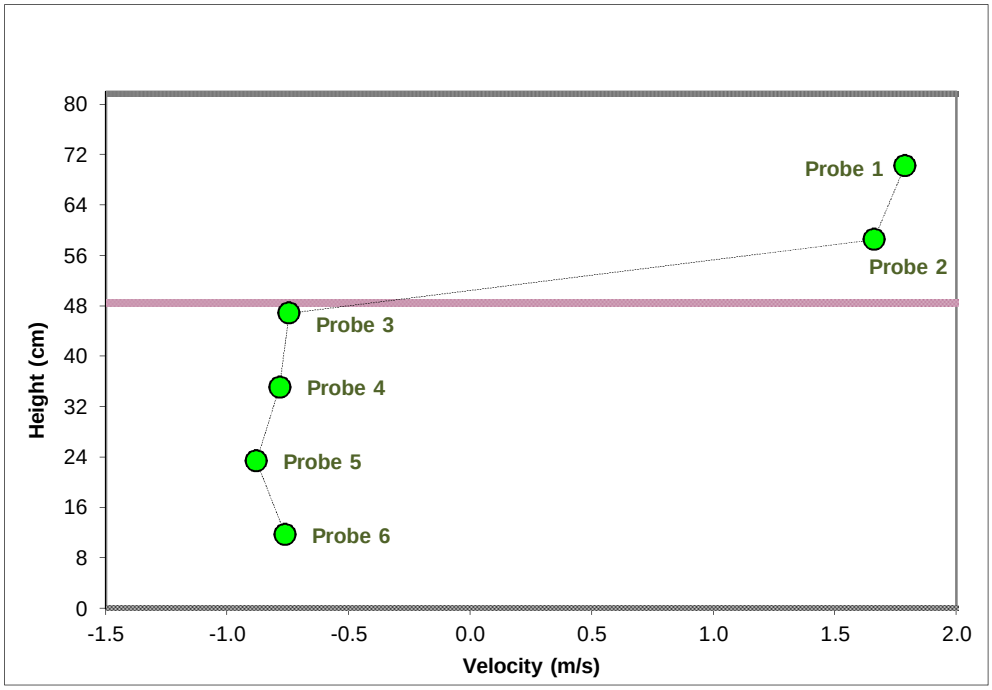

Figure B-18: Time-averaged velocity profile at the opening plane for the 1.5 g/s, ϕ_2 configuration

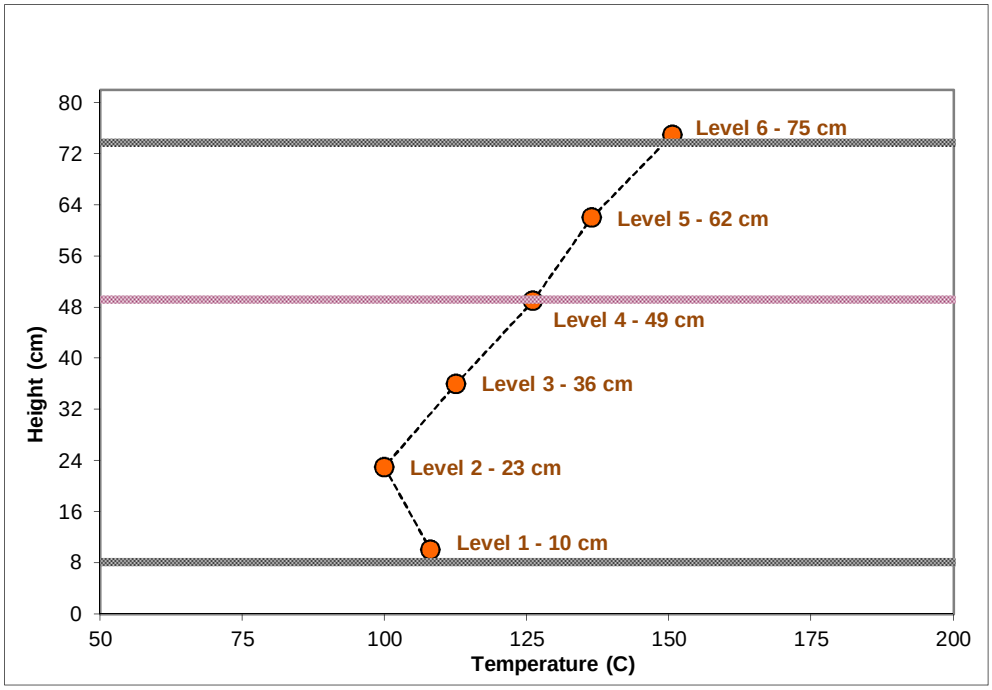

Figure B-19: Space-time-averaged layer temperatures for the 0.5 g/s, ϕ_3 configuration

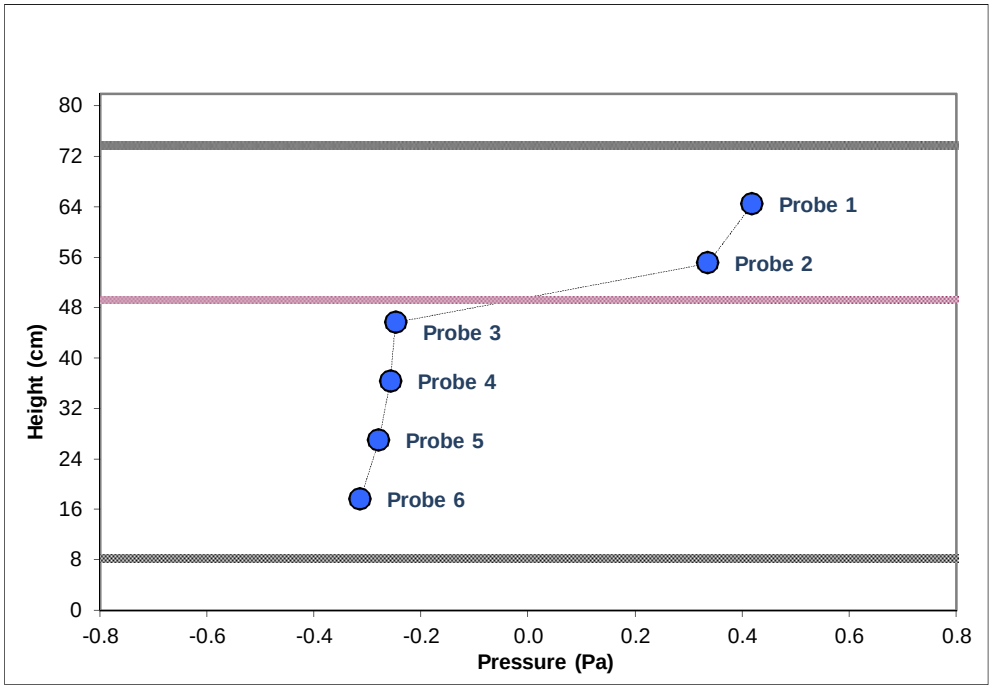

Figure B-20: Time-averaged pressure profile at the opening plane for the 0.5 g/s, ϕ_3 configuration

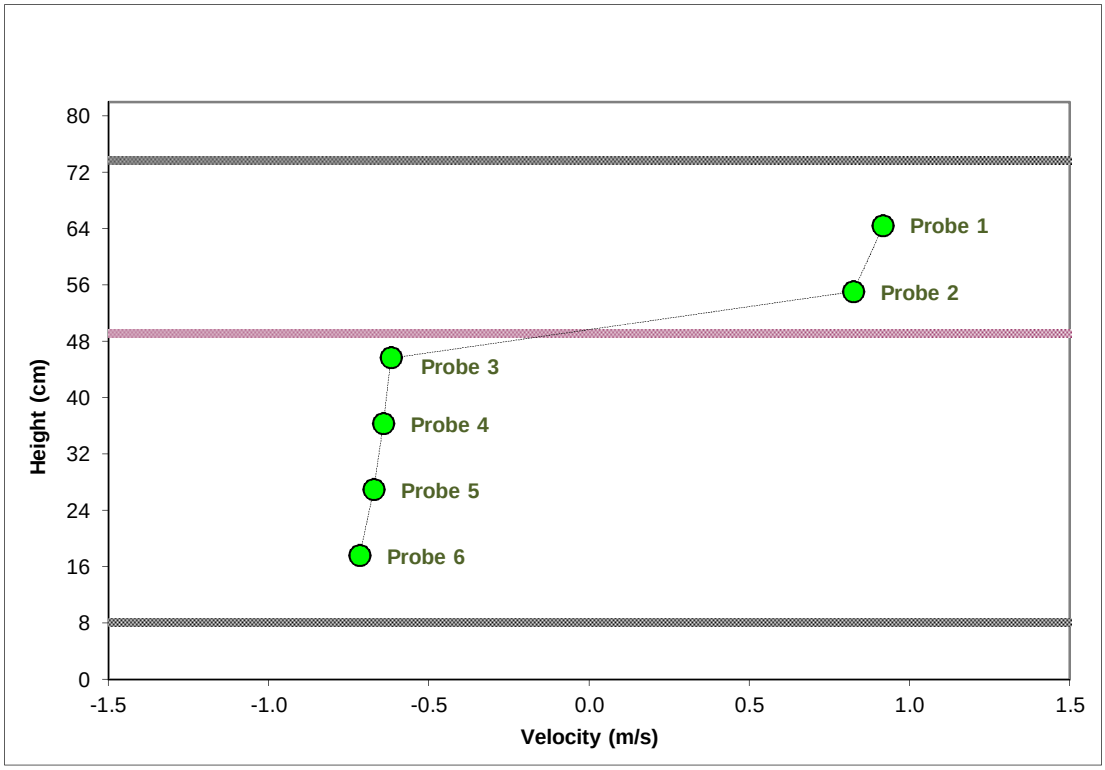

Figure B-21: Time-averaged velocity profile at the opening plane for the 0.5 g/s, ϕ_3 configuration

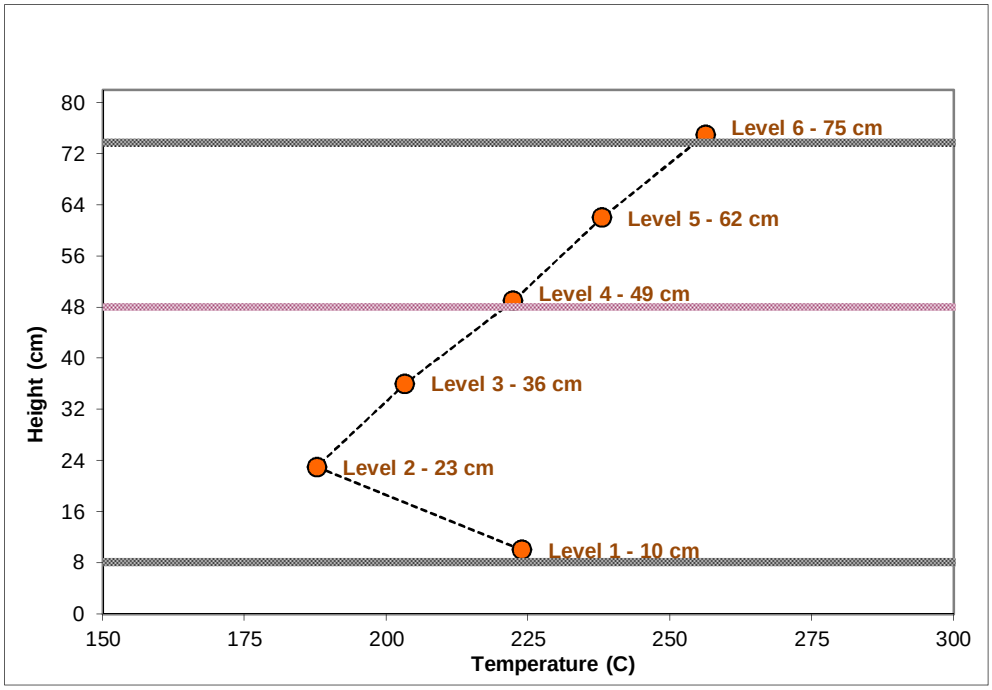

Figure B-22: Space-time-averaged layer temperatures for the 1.0 g/s, ϕ_3 configuration

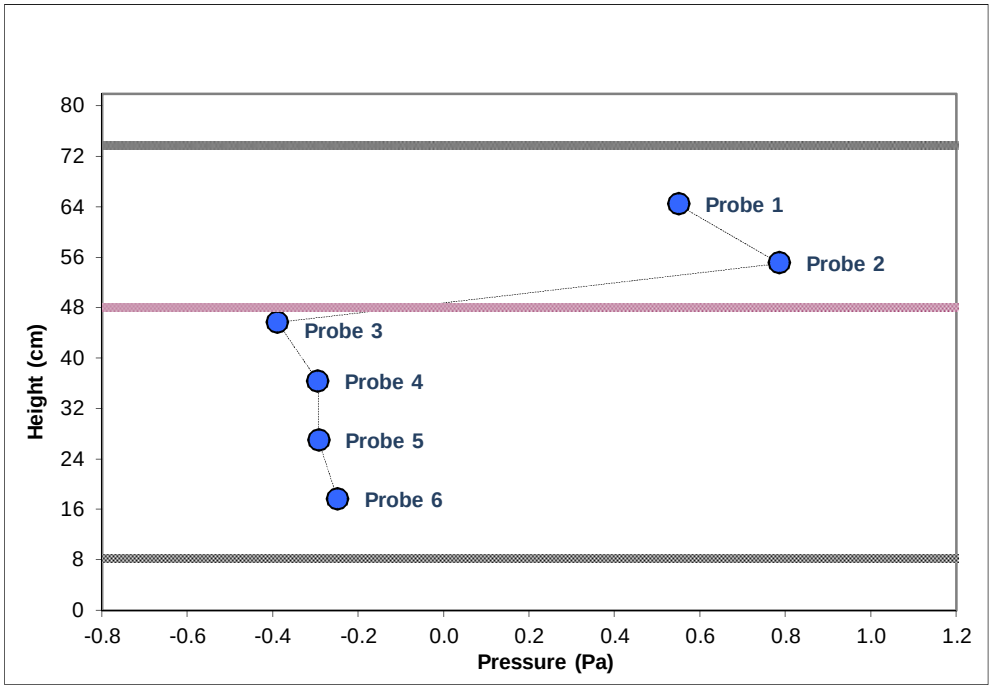

Figure B-23: Time-averaged pressure profile at the opening plane for the 1.0 g/s, ϕ_3 configuration

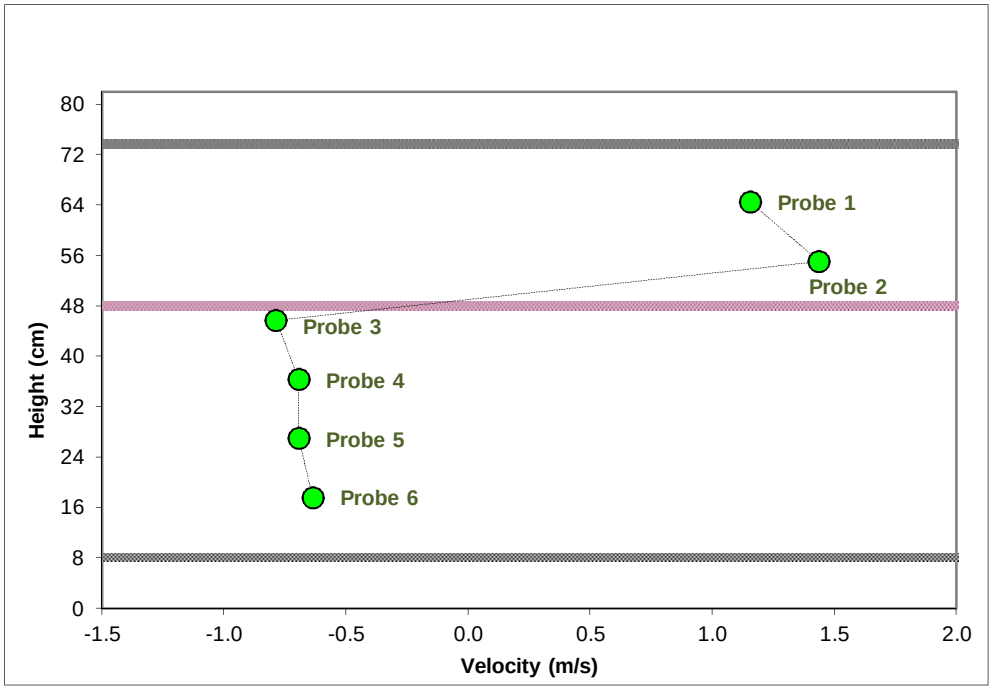

Figure B-24: Time-averaged velocity profile at the opening plane for the 1.0 g/s, ϕ_3 configuration

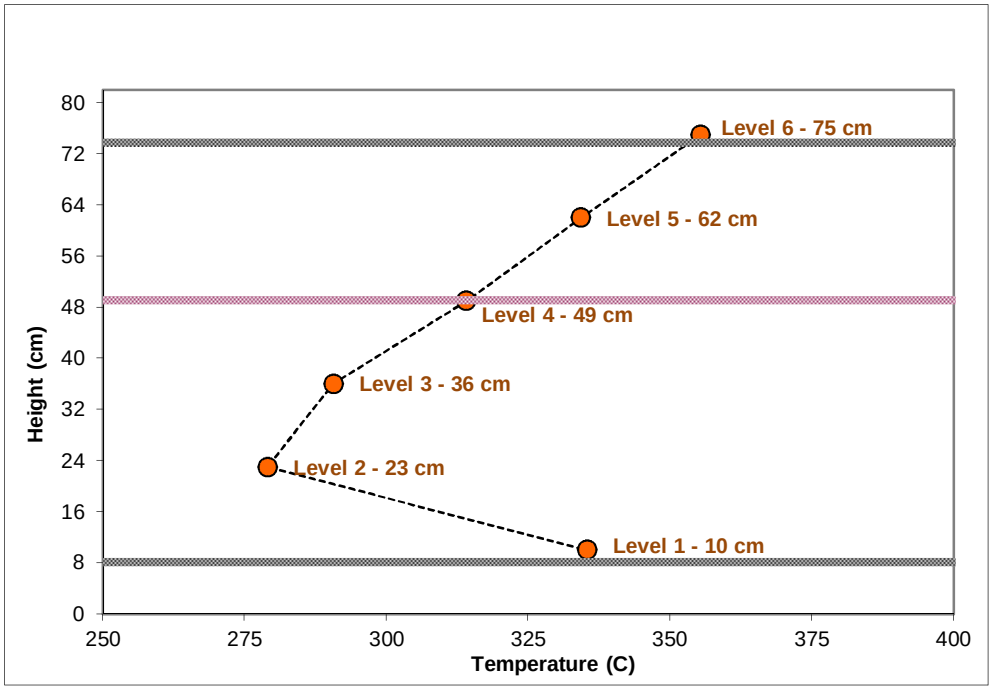

Figure B-25: Space-time-averaged layer temperatures for the 1.5 g/s, ϕ_3 configuration

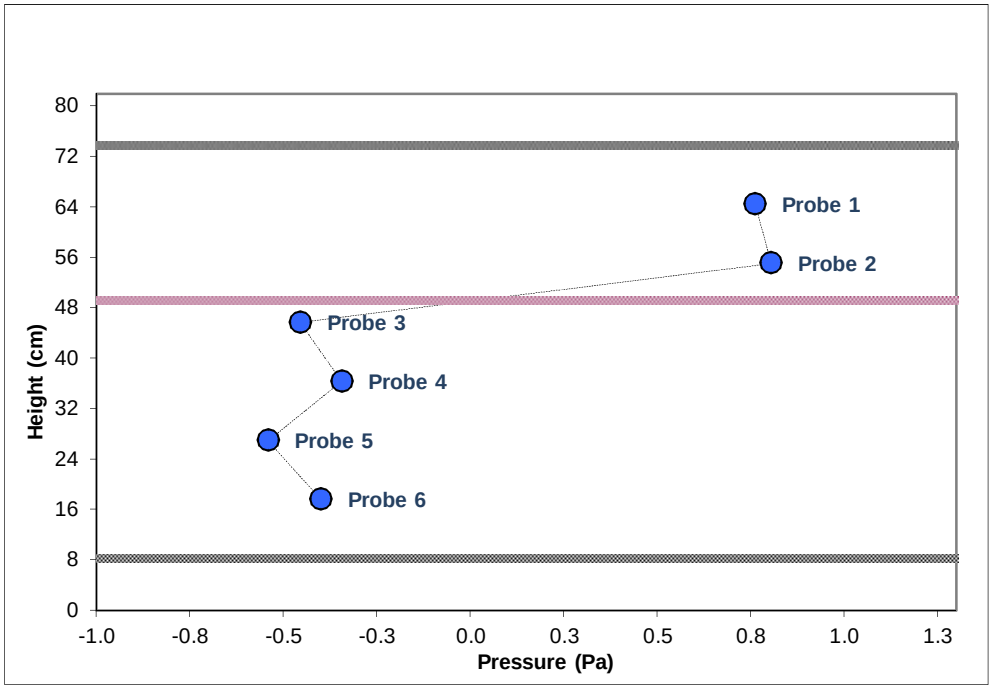

Figure B-26: Time-averaged pressure profile at the opening plane for the 1.5 g/s, ϕ_3 configuration

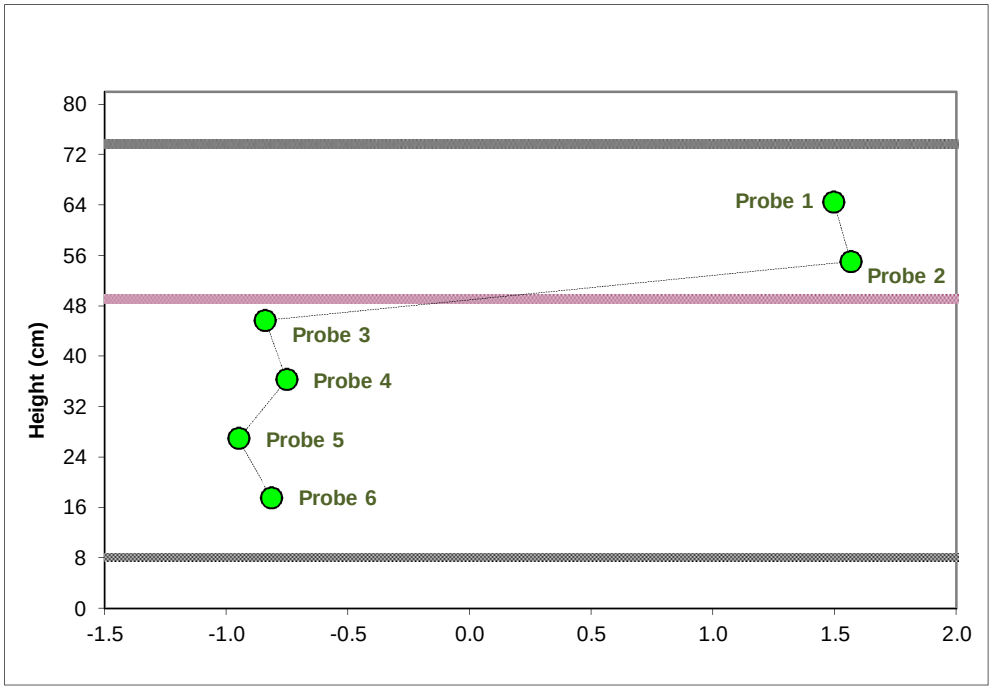

Figure B-27: Time-averaged velocity profile at the opening plane for the 1.5 g/s, ϕ_3 configuration

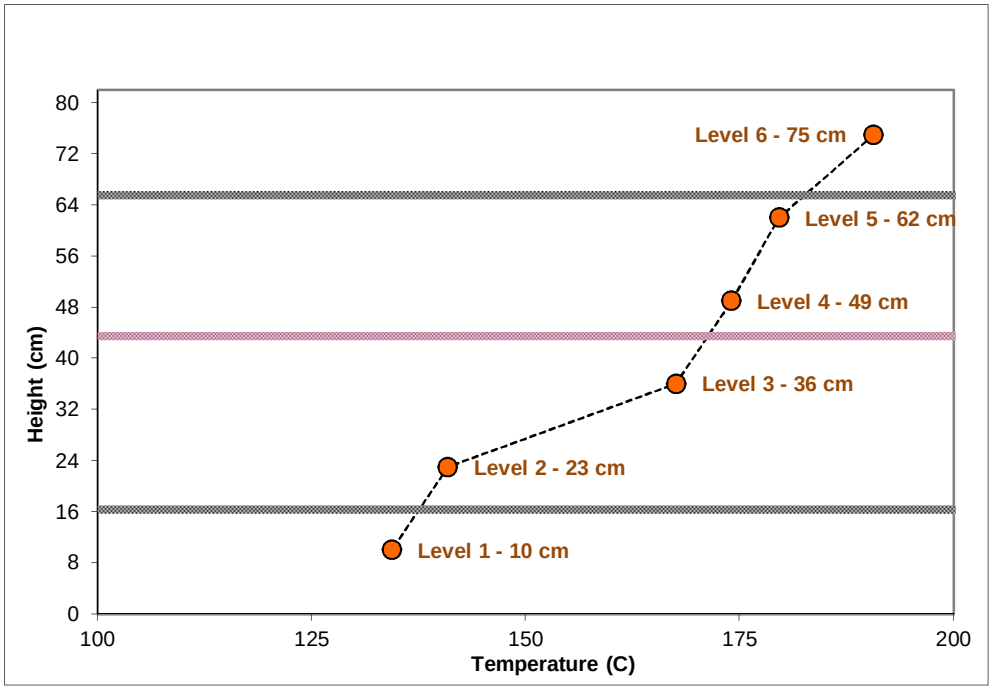

Figure B-28: Space-time-averaged layer temperatures for the 0.5 g/s, ϕ_4 configuration

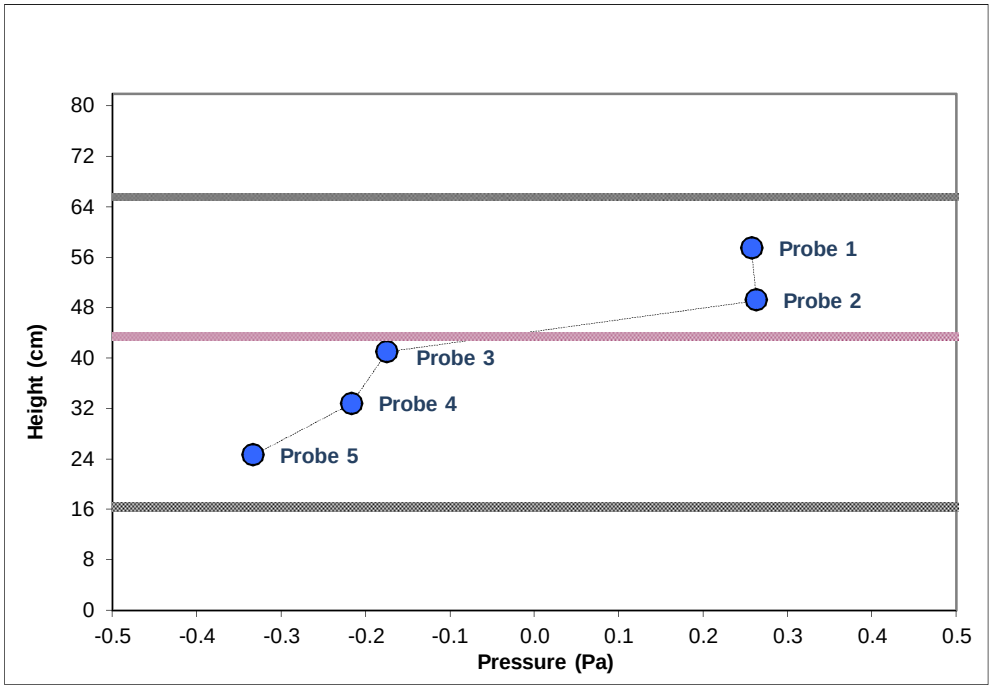

Figure B-29: Time-averaged pressure profile at the opening plane for the 0.5 g/s, ϕ_4 configuration

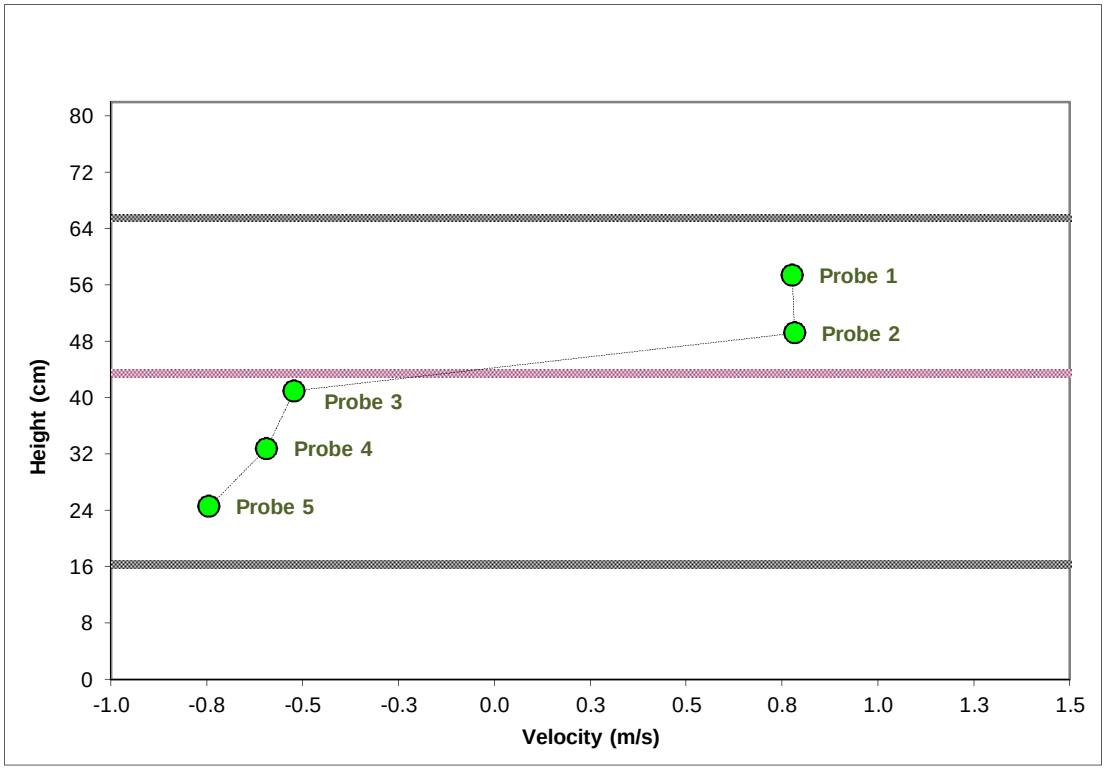

Figure B-30: Time-averaged velocity profile at the opening plane for the 0.5 g/s, ϕ_4 configuration

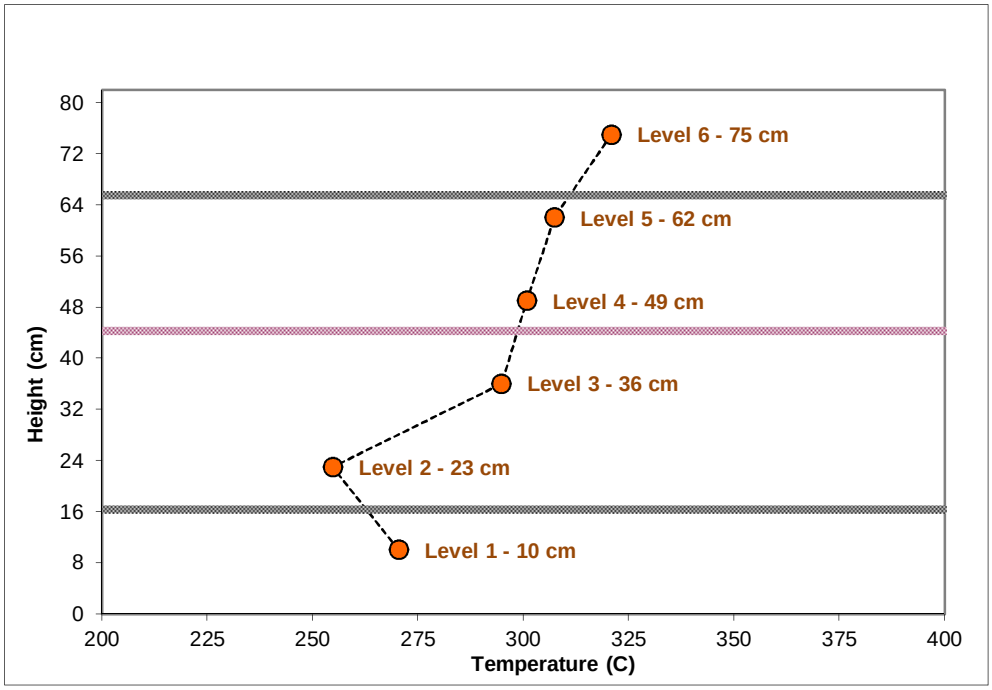

Figure B-31: Space-time-averaged layer temperatures for the 1.0 g/s, ϕ_4 configuration

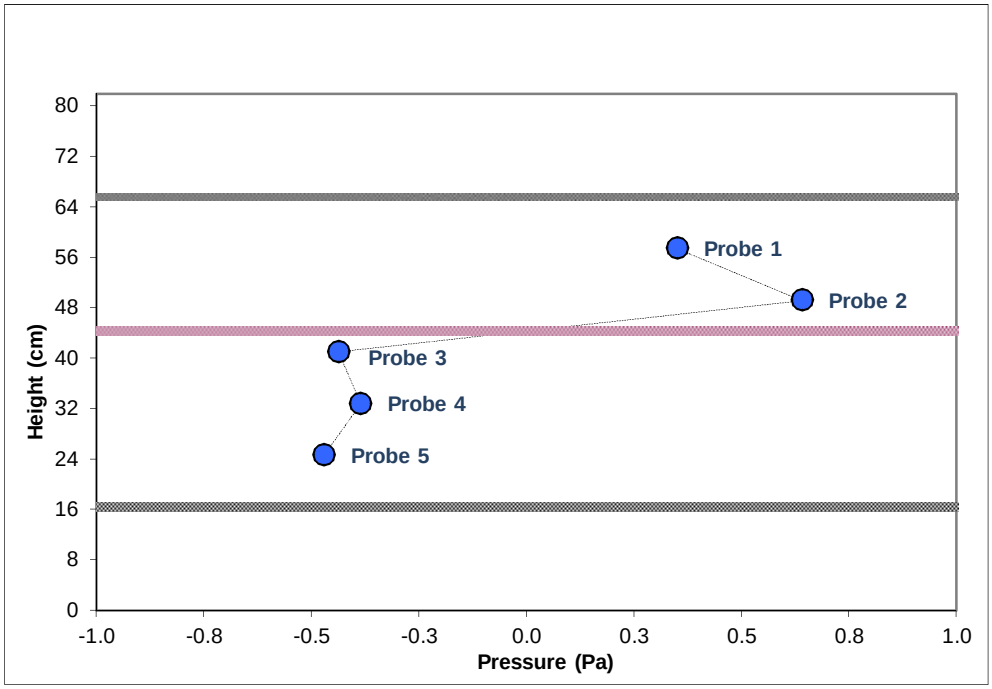

Figure B-32: Time-averaged pressure profile at the opening plane for the 1.0 g/s, ϕ_4 configuration

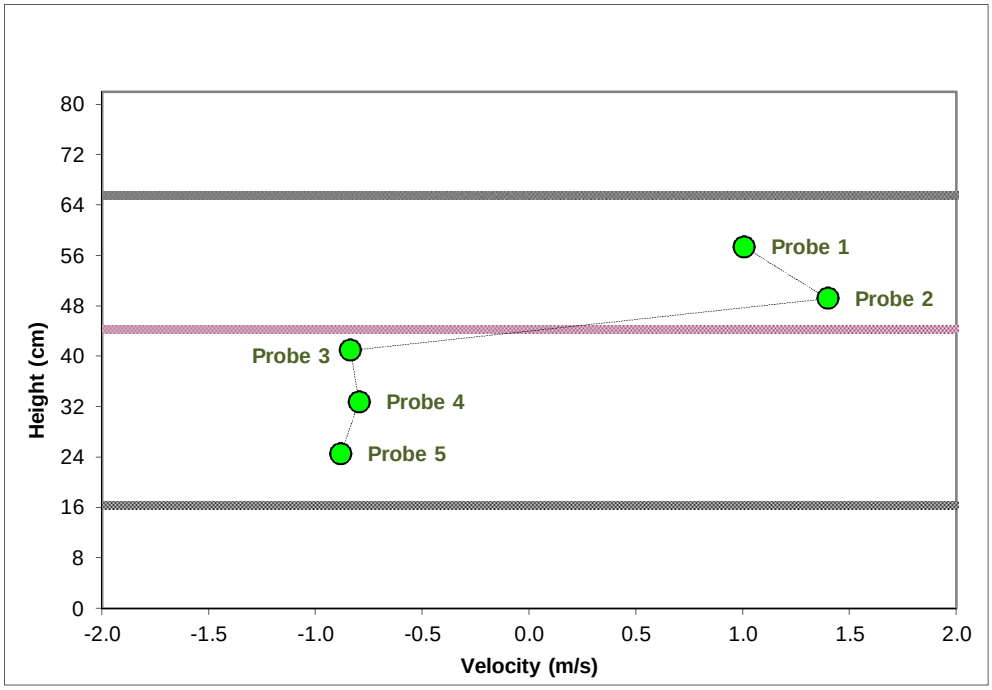

Figure B- 33: Time-averaged velocity profile at the opening plane for the 1.0 g/s, ϕ_4 configuration

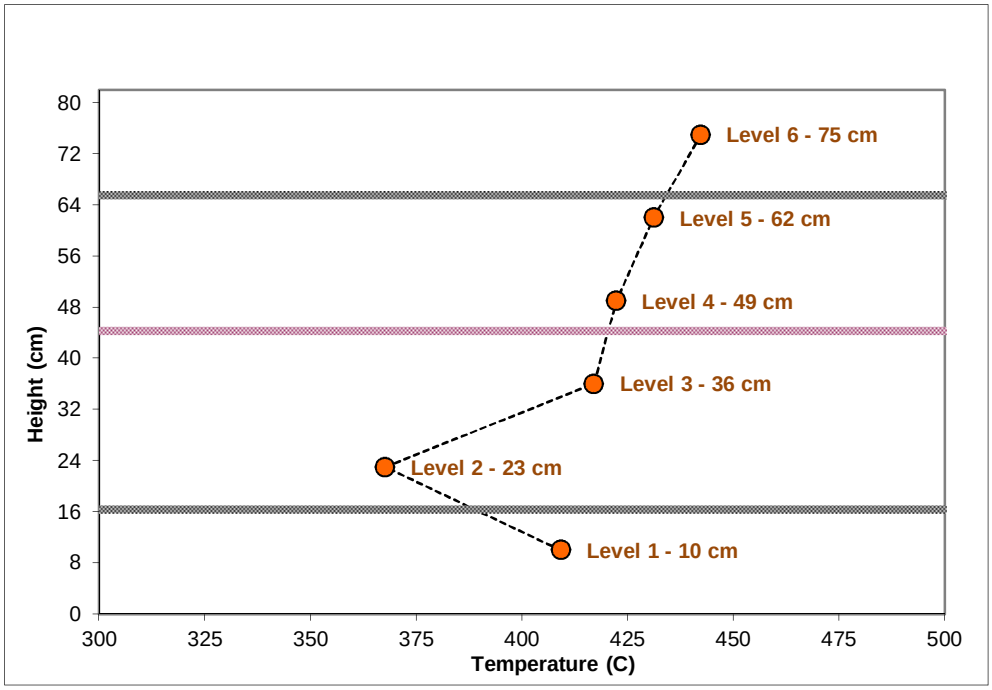

Figure B-34: Space-time-averaged layer temperatures for the 1.5 g/s, ϕ_4 configuration

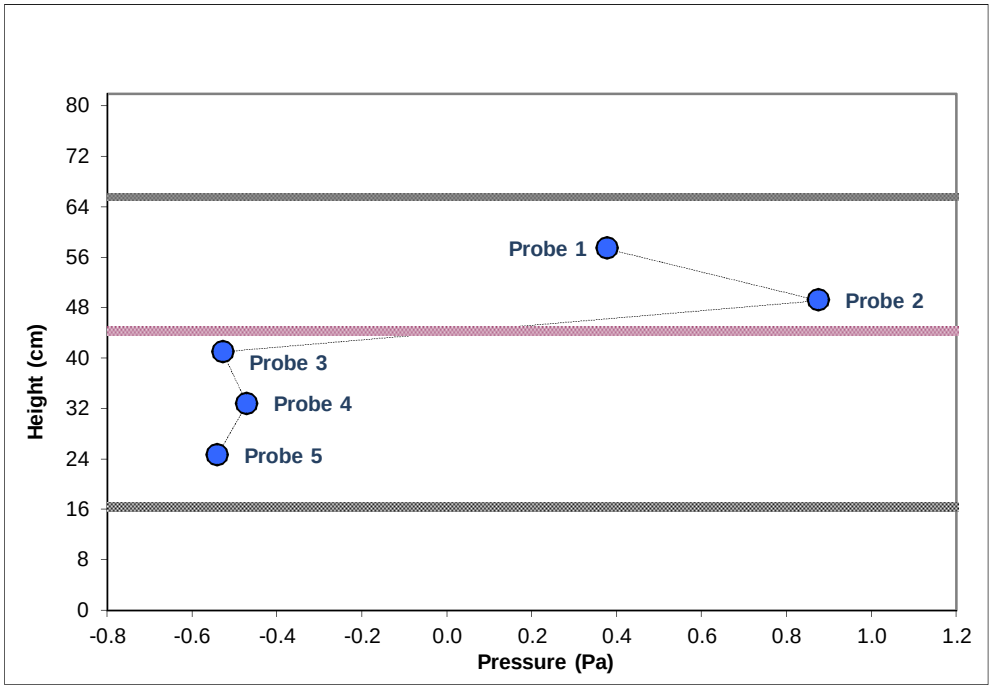

Figure B-35: Time-averaged pressure profile at the opening plane for the 1.5 g/s, ϕ_4 configuration

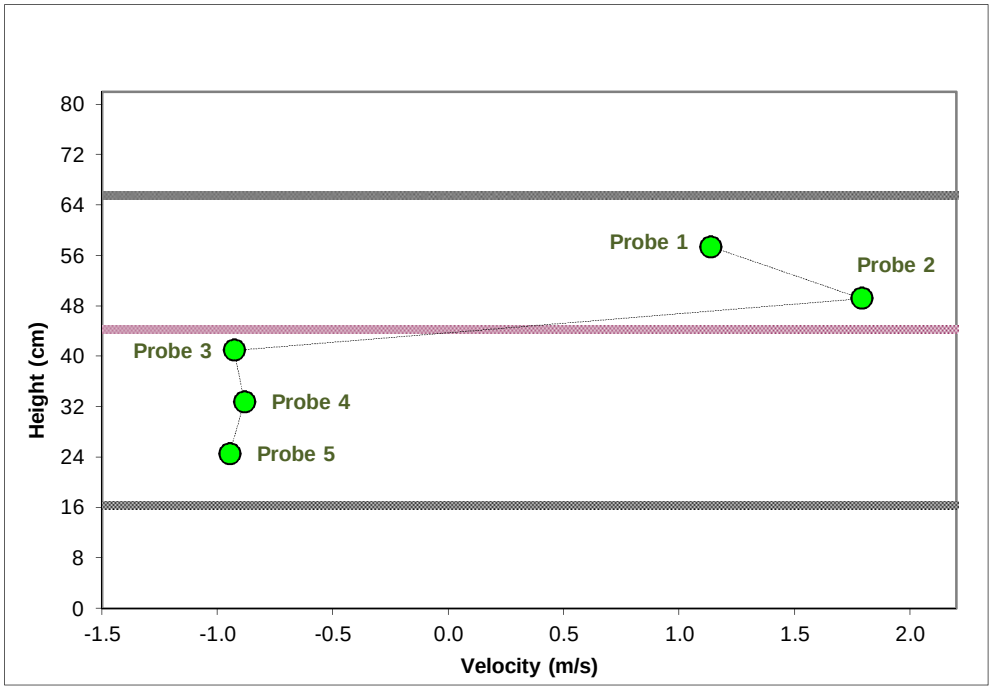

Figure B- 36: Time-averaged velocity profile at the opening plane for the 1.5 g/s, ϕ_4 configuration

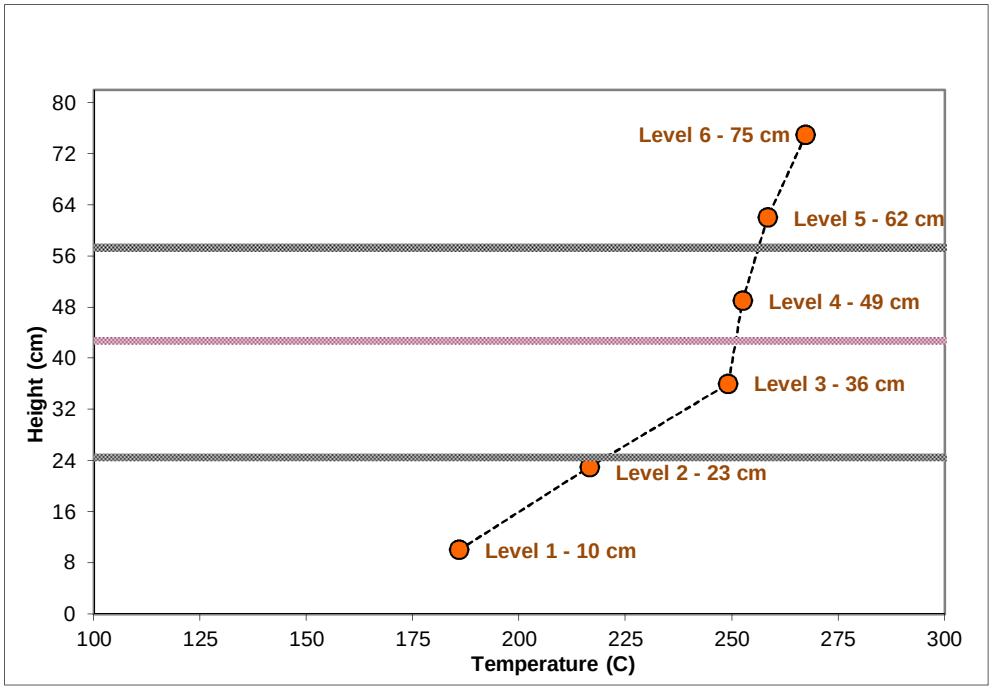

Figure B-37: Space-time-averaged layer temperatures for the 0.5 g/s, ϕ_5 configuration

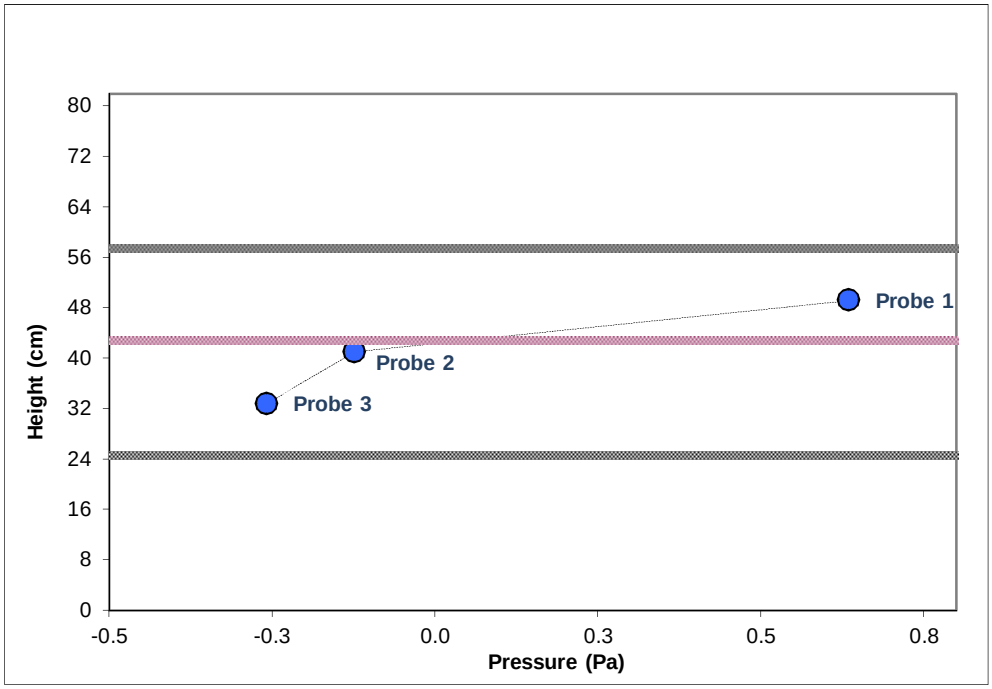

Figure B-38: Time-averaged pressure profile at the opening plane for the 0.5 g/s, ϕ_5 configuration

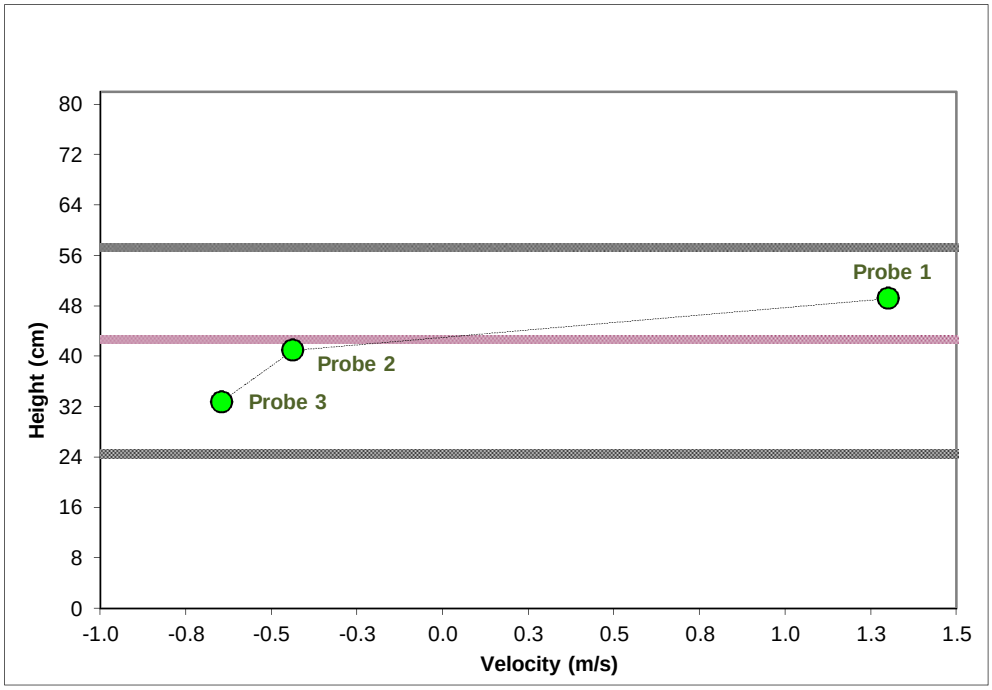

Figure B-39: Time-averaged velocity profile at the opening plane for the 0.5 g/s, ϕ_5 configuration

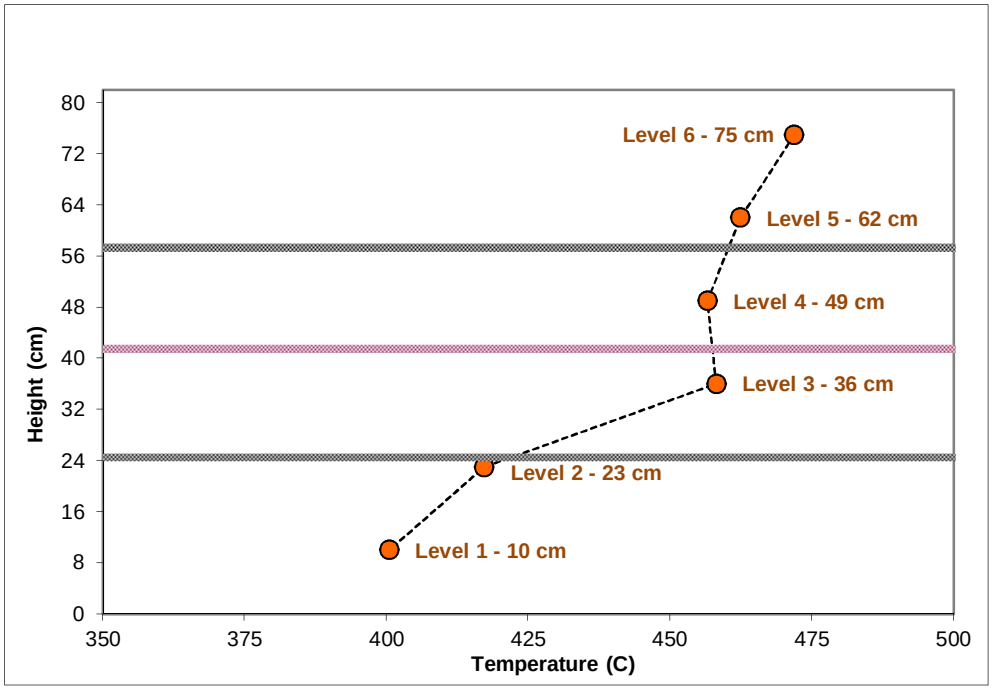

Figure B-40: Space-time-averaged layer temperatures for the 1.0 g/s, ϕ_5 configuration

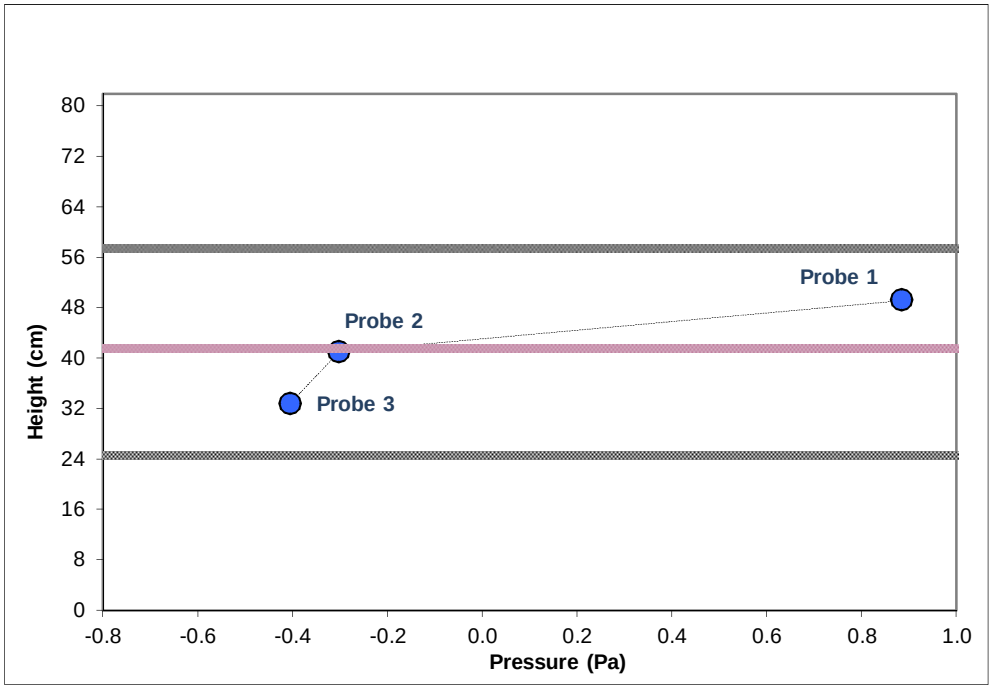

Figure B-41: Time-averaged pressure profile at the opening plane for the 1.0 g/s, ϕ_5 configuration

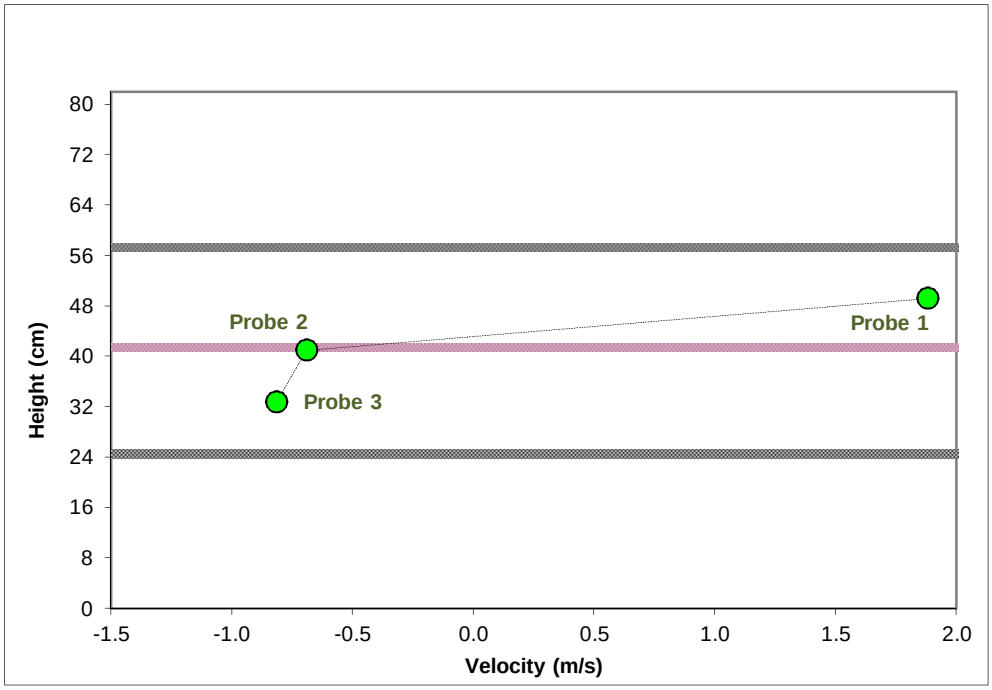

Figure B-42: Time-averaged velocity profile at the opening plane for the 1.0 g/s, ϕ_5 configuration

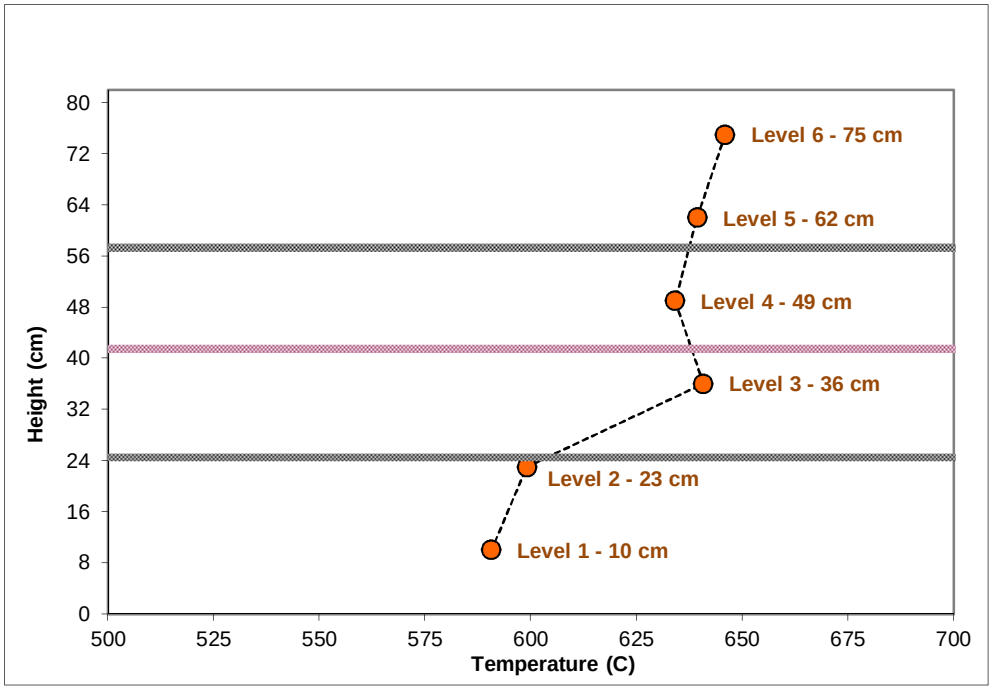

Figure B-43: Space-time-averaged layer temperatures for the 1.5 g/s, ϕ_5 configuration

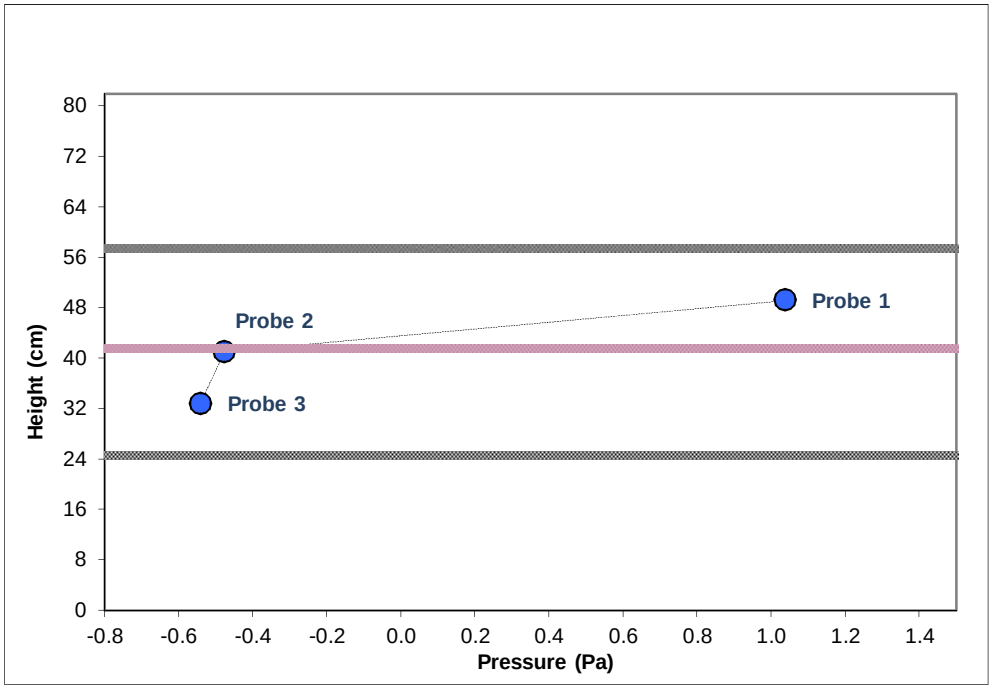

Figure B-44: Time-averaged pressure profile at the opening plane for the 1.5 g/s, ϕ_5 configuration

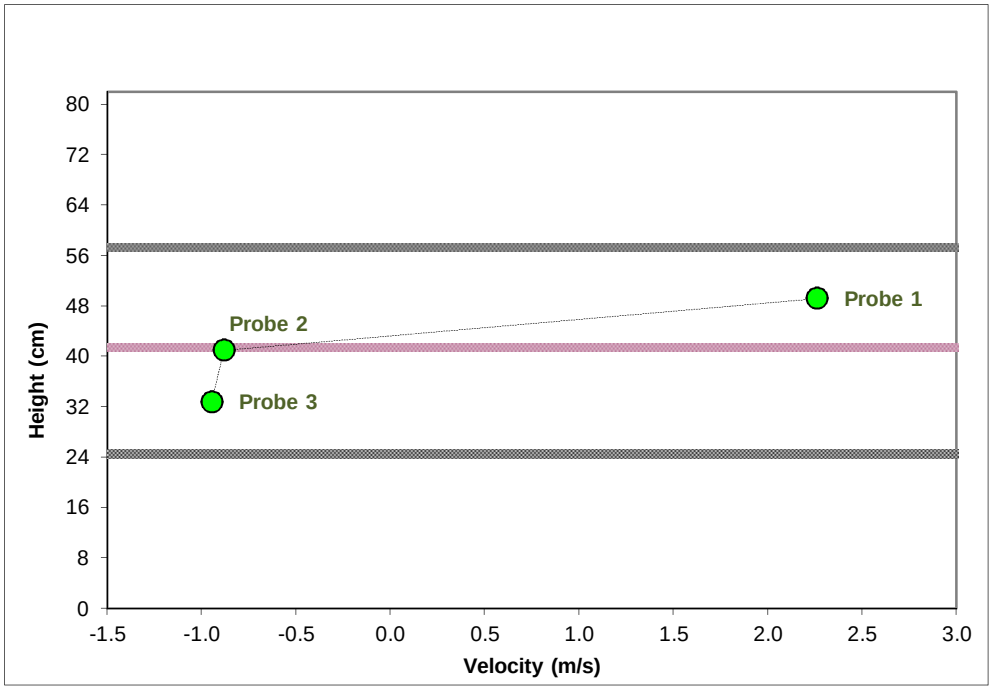

Figure B-45: Time-averaged velocity profile at the opening plane for the 1.5 g/s, ϕ_5 configuration

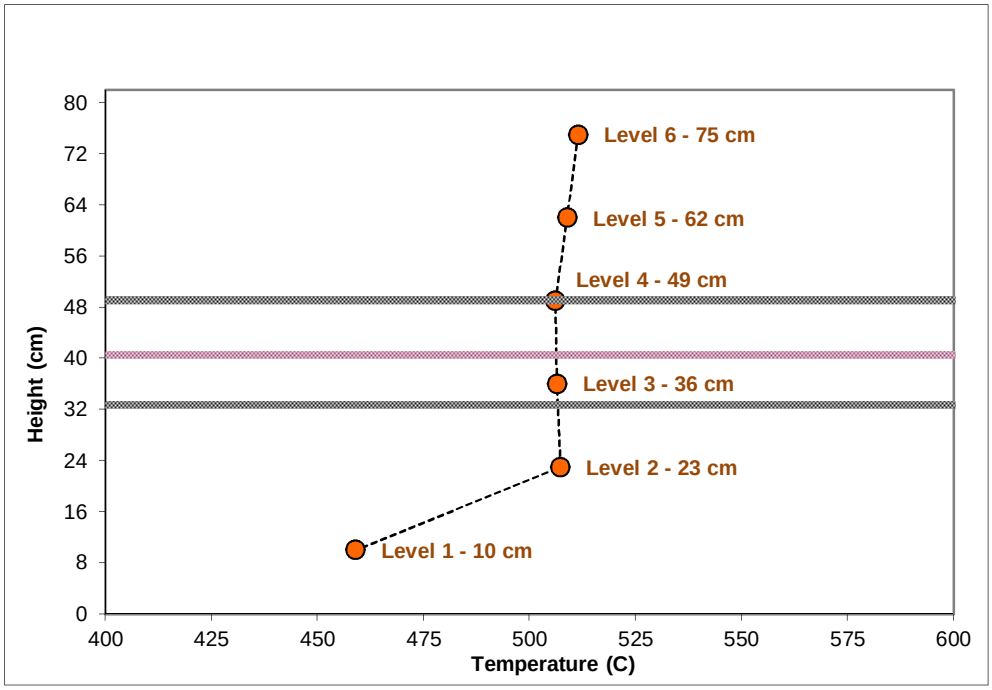

Figure B-46: Space-time-averaged layer temperatures for the 0.5 g/s, ϕ_6 configuration

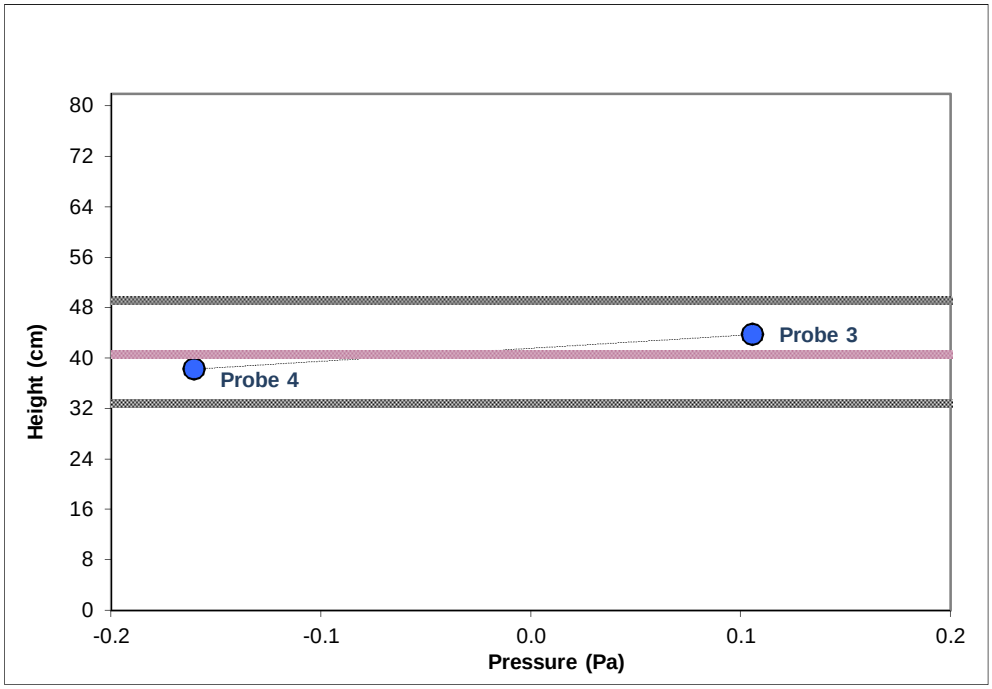

Figure B-47: Time-averaged pressure profile at the opening plane for the 0.5 g/s, ϕ_6 configuration

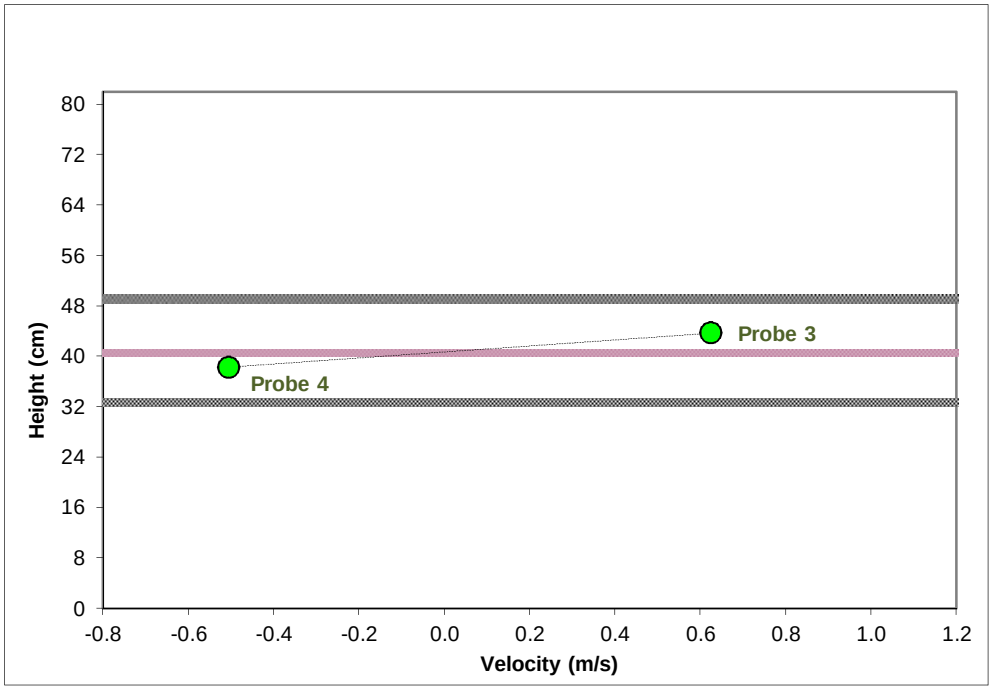

Figure B-48: Time-averaged velocity profile at the opening plane for the 0.5 g/s, ϕ_6 configuration

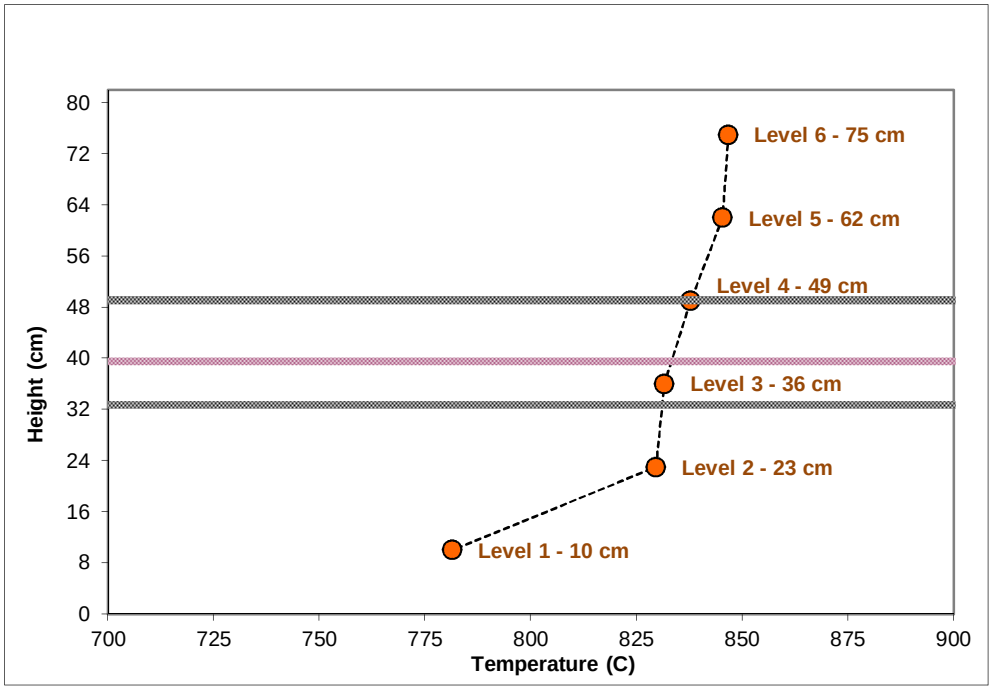

Figure B-49: Space-time-averaged layer temperatures for the 1.0 g/s, ϕ_6 configuration

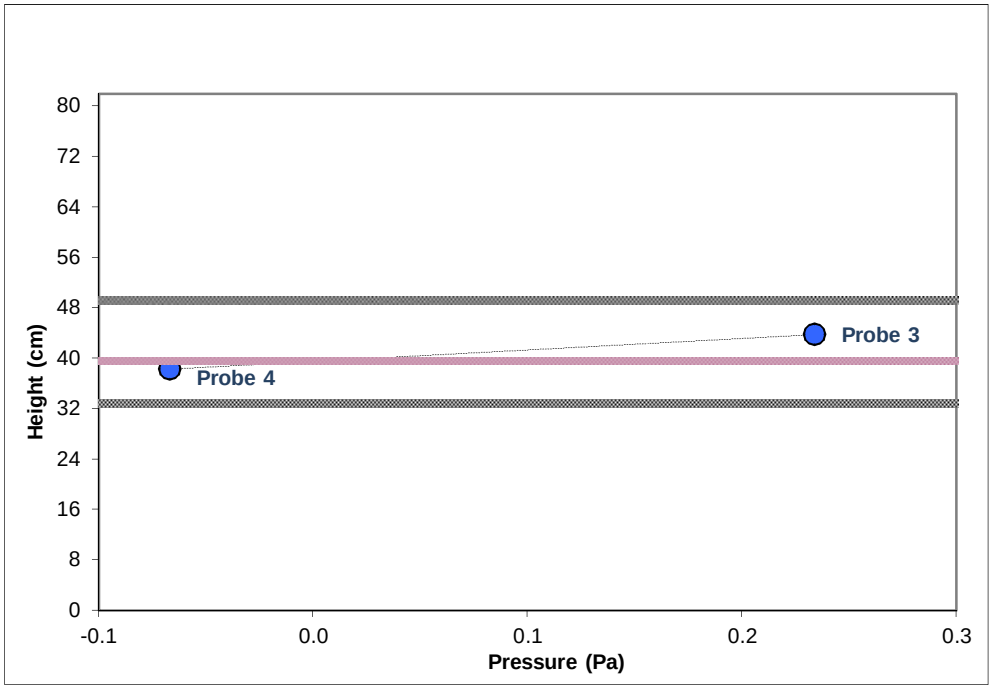

Figure B-50: Time-averaged pressure profile at the opening plane for the 1.0 g/s, ϕ_6 configuration

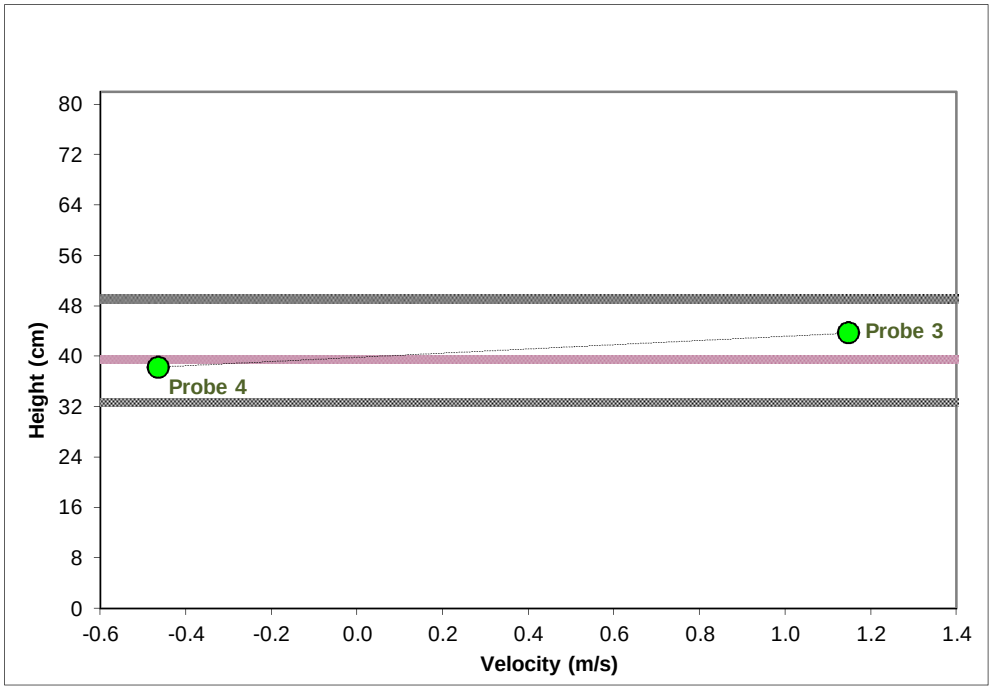

Figure B-51: Time-averaged velocity profile at the opening plane for the 1.0 g/s, ϕ_6 configuration

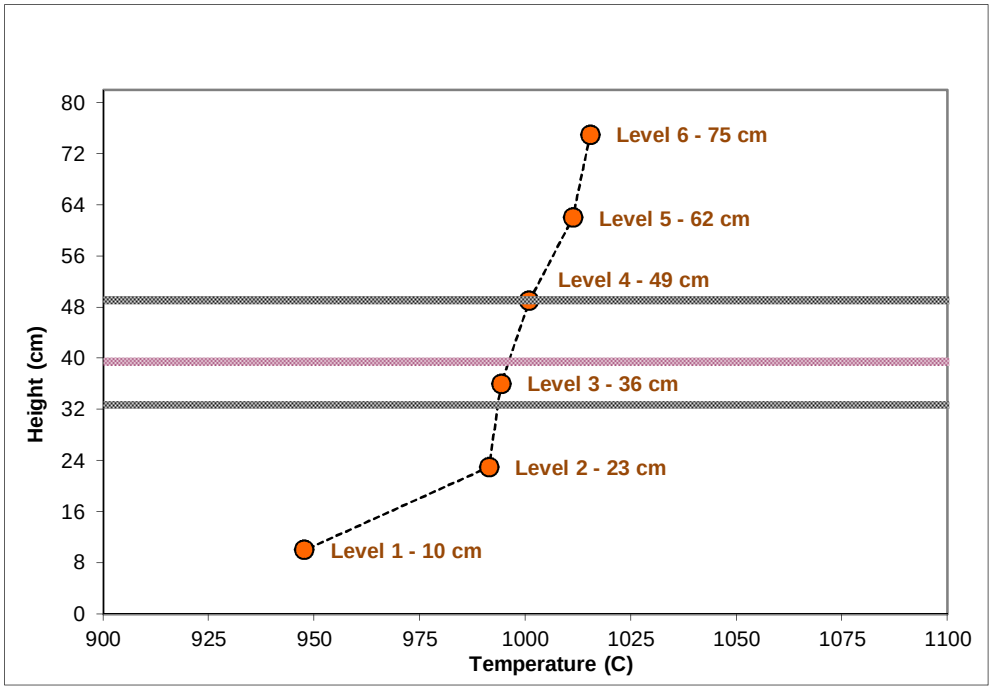

Figure B-52: Space-time-averaged layer temperatures for the 1.5 g/s, ϕ_6 configuration

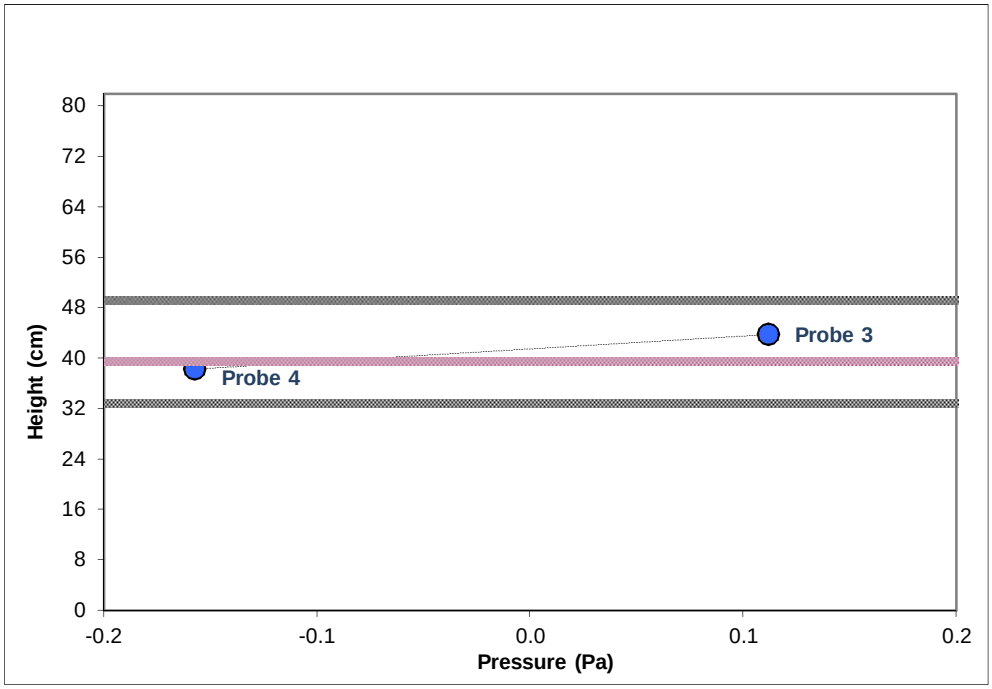

Figure B-53: Time-averaged pressure profile at the opening plane for the 1.5 g/s, ϕ_6 configuration

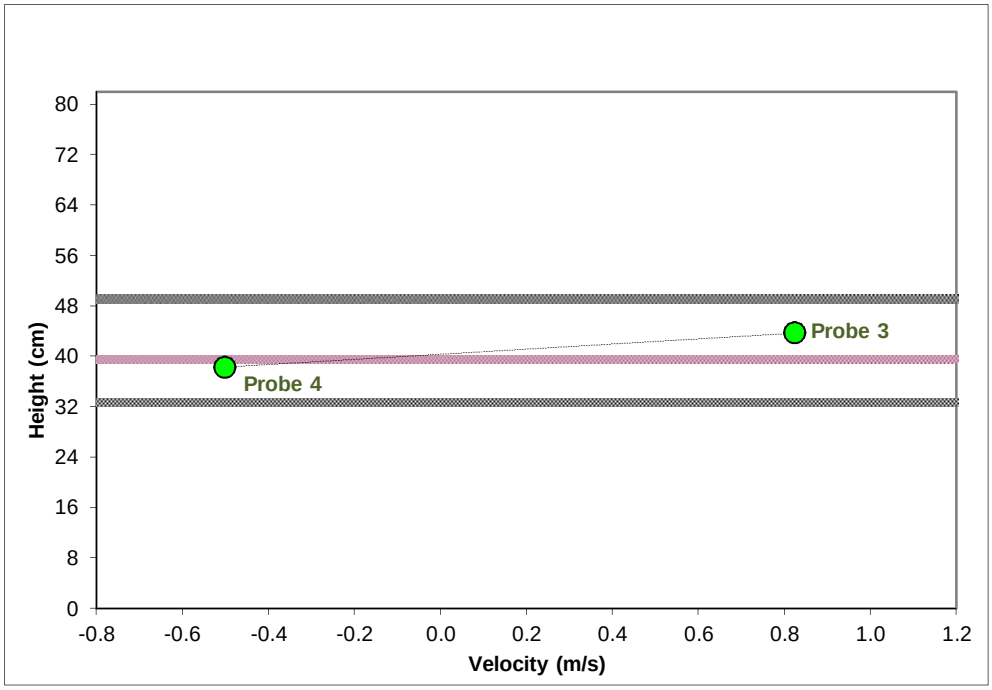

Figure B-54: Time-averaged velocity profile at the opening plane for the 1.5 g/s, ϕ_6 configuration

References

[1] T. Z. Harmathy, “Design of Buildings for Life Safety Part II,” *Fire Technol.*, vol. 12, no. 3, pp. 219–236, 1976.

[2] T. Z. Harmathy, “A New Look at Compartment Fires,” *Fire Technol.*, vol. 8, no. 3, pp. 196–217, Aug. 1972.

[3] M. Law, “Translation of Research into Practice: Building Design,” *Fire Saf. Sci.*, vol. 1, pp. 603–610, 1986.

[4] P. Schumacher, *The Autopoiesis of Architecture: A New Framework for Architecture*, 1st Ed. West Sussex: John Wiley & Sons, 2011.

[5] R. Mogosin, “Forensic Analysis of the VDL Research House I,” University of Edinburgh, 2012.

[6] T. Z. Harmathy, “Fire Severity: Basis of Fire Safety Design,” *Fire Saf. Concr. Struct.*, pp. 115–149, 1983.

[7] J. G. et al. Quintiere, “SFPE Guide to Fire Exposures to Structural Elements,” 2004.

[8] L. Bisby, J. Gales, and C. Maluk, “A Contemporary Review of Large-Scale Non-Standard Structural Fire Testing,” *Fire Sci. Rev.*, vol. 2, no. 1, p. 1, 2013.

[9] W. Pitts, “The Global Equivalence Ratio Concept and the Formation Mechanisms of Carbon Monoxide in Enclosure Fires,” *Prog. Energy Combust. Sci.*, vol. 21, pp. 197–237, 1995.

[10] Y. Utiskul, “Theoretical and Experimental Study on Fully-Developed Compartment Fires,” University of Maryland, 2006.

[11] I. S.H., “Ingberg, S.H. (1928). ‘Fire loads’. Quarterly Journal of The National Fire Protection Association, 22, 43-61.,” *Quaterly J. NFPA*, vol. 22, pp. 43–61, 1928.

[12] K. Kawagoe, “Fire Behaviour in Rooms - Report No. 27,” 1958.

[13] S. Rodak and S. H. Ingberg, “Full-Scale Residential Occupancy Fire Tests of 1939 - Report 9527,” USA, 1967.

[14] D. L. Simms, D. Hird, and H. G. H. Wraight, “The temperature and duration of fires. Part I. Some experiments with models with restricted ventilation - Fire Research Note No. 412,” 1960.

[15] D. L. Simms and H. G. H. Wraight, “The temperature and duration of fires . Part II. Analysis of some full-scale tests - Fire Research Note No. 413,” 1959.

[16] D. Drysdale, *An Introduction to Fire Dynamics*, 3rd Ed. West Sussex: John Wiley & Sons, 2011.

[17] K. Kawagoe and T. Sekine, “Estimation of Fire Temperature-Time Curve in Rooms,” 1963.

[18] K. Fujita, “Characteristics of fire inside a non-combustible room and prevention of fire damage - Report 2(h),” Tokyo.

[19] V. A. Ptchelintzev, “Study of the Thermal System of Fires in order to Determine the Limits of Fire Resistance Required by Structural Elements. Collected Information on Fire Resistant Building Construction.,” Moscow, 1958.

[20] D. Gross and A. F. Robertson, “Experimental Fires in Enclosures,” in *Thenth Symposium (International) on Combustion*, 1965, pp. 931–942.

[21] D. L. Simms, P. L. Hinkley, and A. M. Bisset, “Roof Venting of Burning Enclosures - Part I - FRN No. 390,” Borehamwood, 1959.

[22] D. L. Simms, P. L. Hinkley, and A. M. Bisset, “Roof Venting of Burning Enclosures - Part II - FRN No. 391,” Borehamwood, 1959.

[23] P. L. Hinkley, “Roof Venting of Burning Enclosures - Part IIIA - FRN No. 443,” Borehamwood, 1960.

[24] P. H. Thomas, D. L. Simms, P. L. Hinkley, and C. R. Theobald, “Roof Venting of Burning Enclosures - Part III - FRN No. 419,” Borehamwood, 1960.

[25] P. H. Thomas, “Studies of Fires in Buildings Using Models - Part I,” *Research*, vol. 13, no. February, pp. 69–71, 1960.

[26] P. H. Thomas, “Studies of Fires in Buildings Using Models - Part II,” *Research*, vol. 13, no. March, pp. 87–93, 1960.

[27] P. H. Thomas, “Some General Questions in the Study of Fires in Rooms - FRN No. 429,” Borehamwood, 1960.

[28] P. H. Thomas and A. J. M. Heselden, “Behaviour of Fully Developed Fire in an Enclosure,” *Combust. Flame*, vol. 6, no. 3, pp. 133–135, 1962.

[29] P. H. Thomas, A. J. M. Heselden, and M. Law, “Fully-developed Compartment Fires -Two Kinds of Behaviour,” Fire Research Technical Paper No. 18, 1967.

[30] P. H. Thomas and L. Nilsson, “Fully Developed Compartment Fires: New Correlations of Burning Rates - FRN No. 979,” Borehamwood, 1973.

[31] A. J. M. Heselden, “Some Fires in a Single Compartment with Independent Variation of Fuel Surface Area and Thickness,” Borehamwood, 1961.

[32] M. Law, “Private communication (with Thomas P.H.).” .

[33] T. Z. Harmathy, “Mechanism of Burning of Fully-Developed Compartment Fires,” *Combust. Flame*, vol. 31, no. 1, pp. 265–273, 1978.

[34] P. H. Thomas and A. J. M. Heselden, “Fully Developed Fires in Single Compartments - FRN 923,” Borehamwood, 1972.

[35] T. Z. Harmathy, “Effect of the Nature of Fuel on the Characteristics of Fully-Developed Compartment Fires,” *Fire Mater.*, vol. 3, no. 1, pp. 49–60, 1979.

[36] T. Z. Harmathy, “Design of Buildings for Fire Safety - Part I,” *Fire Technol.*, vol. 12, no. 2, pp. 95–108, 1976.

[37] P. H. Thomas, “Behavior of Fires in Enclosures — Some Recent Progress,” *Symp. Combust.*, pp. 1007–1020, 1973.

[38] P. H. Thomas, “Fires in Model Rooms: CIB Research Programmes - Current Paper 32,” Borehamwood, 1974.

[39] P. H. Thomas, “Some Problem Aspects of Fully Developed Room Fires,” in *Symposium on Fire Standards and Safety*, 1976, no. April.

[40] M. L. Bullen and P. H. Thomas, “Compartment Fires with Non-Cellulosic Fuels,” *Symp. Combust.*, pp. 1139–1148, 1979.

[41] P. H. Thomas and M. L. Bullen, “Burning of Fuels in Fully-developed Room Fires,” vol. 2, pp. 275–281, 1980.

[42] P. H. Thomas, “Fires and Flashover in Rooms - A Simplified Theory,” no. 3, pp. 67–76, 1980.

[43] M. L. Bullen, B. J. McCaffrey, P. H. Thomas, and J. G. Quintiere, “Flashover and instabilities in fire behavior,” *Combust. Flame*, vol. 38, pp. 159–171, 1980.

[44] P. H. Thomas, “Modelling of Compartment Fires,” *Fire Saf. J.*, vol. 5, pp. 181–190, 1983.

[45] A. Tewarson, “Some Obsevations on Experimental Fires in Enclosures - Part I - Cellulosic Materials,” *Combust. Flame*, vol. 19, no. 3, pp. 101–111, 1972.

[46] A. Tewarson, “Some Obsevations on Experimental Fires in Enclosures - Part II - Ethyl Alcohol and Paraffin Oil,” *Combust. Flame*, vol. 19, no. 3, pp. 363–371, 1972.

[47] O. Pettersson, S. E. Magnusson, and J. Thor, “Fire Engineering Design of Steel Structures,” Stockholm, Jun. 1976.

[48] J. Prahl and H. W. Emmons, “Fire-induced Flow Through an Opening,” *Combust. Flame*, vol. 25, pp. 369–385, May 1975.

[49] B. J. McCaffrey and J. A. Rockett, “Static Pressure Measurements of Enclosure Fires,” *J. Res. Natl. Bur. Stand. (1934).*, vol. 82, no. 2, pp. 107–117, Sep. 1977.

[50] M. Law, “A Relationship between Fire Grading and Building Design and Contents - FRN No. 877,” Borehamwood, 1971.

[51] M. Law, “Designing Fire Safety for Steel – Recent Work,” *Proc. ASCE Spring Conv. …*, pp. 135–150, 1981.

[52] M. Law, “A Basis for The Design of Fire Protection of Building Structures,” *Struct. Eng.*, no. February, pp. 25–33, 1983.

[53] T. Tanaka, “A Mathematical Model of a Compartment Fire - BRI Research Paper No. 70,” Tokio, Japan, 1977.

[54] T. Tanaka, “A Model on Fire Spread in Small Scale Buildings - 1st Report - BRI Research Paper No.79,” Tokio, Japan, 1978.

[55] T. Tanaka, “A Model on Fire Spread in Small Scale Buildings - 2nd Report - BRI Research Paper No. 84,” Tokio, Japan, 1980.

[56] T. Tanaka, “A Performance Based Deding Method for Fire Safety of Buildings - NISTIR 4449,” 1990.

[57] T. Tanaka, “Simple Formula for Ventilation Controlled Fire Temperatures - NISTIR 6030,” 1997.

[58] E. G. Butcher, T. B. Chitty, and L. A. Ashton, “Temperatures Attained by Steel in Building Fires - Fire Research Technical Paper No. 15,” 1966.

[59] E. G. Butcher, G. K. Bedford, and P. J. Fardell, “Further Experiments on Temperatures Reached by Steel in Buildings,” in *Symposium held at Fire Research Station*, 1967, no. January 1967.

[60] C. T. Webster and M. M. Raftery, “The Burning of Fires in Rooms. Part II. Tests with cribs and high ventilation on various scales - Fire Research Note No. 401,” 1959.

[61] C. T. Webster, P. G. Smith, and M. M. Raftery, “The Burning of Well-Ventilated Compartment Fires. Part III. The effect of the wood thickness - Fire Research Note No. 474,” 1960.

[62] S. E. Magnusson and S. Thelandersson, “Temperature-Time Curves for the Complete Process of Fire Development. A Theoretical Study of Wood Fuel Fires in Enclosed Spaces - Acta Polytechnica Scandinavica - Bulletin No. 65, CIB/CTF/72/46,” Stockholm, 1970.

[63] S. E. Magnusson and S. Thelandersson, “Comments on Rate of Gas Flow and Rate of Burning for Fire in Enclosures - Bulletin No. 19, CIB/CTF/72/48,” Lund, 1971.

[64] S. E. Magnusson and O. Pettersson, *Brandteknisk Dimensionering av Stalkonstruktioner (Fire Engineering Design of Steel Structures)*. Lulea: Norrbottens Jarnverk AB, 1972.

[65] W. J. Christian and T. E. Waterman, “Characteristics of Full-Scale Fires in Various Occupancies,” *Fire Technol.*, vol. 7, p. 205, 1971.

[66] T. Z. Harmathy and I. Oleszkiewicz, “Fire Drainage System,” *Fire Technol.*, vol. 23, no. 1, pp. 26–48, 1987.

[67] P. H. Thomas, “The Building Fire Problem - Keynote Paper,” in *7th Internatinal CIB (Council for Building Research) Congress*, 1977.

[68] P. H. Thomas, “The Fire Resistance Required to Survive a Burn-out - FRN No. 901,” Borehamwood, 1970.

[69] R. Baldwin and P. H. Thomas, “Passive and Active Fire Protection - The Optimum Combination - FRN No. 963,” Borehamwood, 1973.

[70] P. H. Thomas, “Recent Developments and Trends in Fire Testing for Fire Growth in Buildings,” *Combust. Sci. Technol.*, vol. 40, no. 1–4, pp. 153–165, Aug. 1984.

[71] J. R. Mehaffey and T. Z. Harmathy, “Assessment of Fire Resistance Requirements,” *Fire Technol.*, vol. 17, no. 4, pp. 221–237, Nov. 1981.

[72] T. Z. Harmathy, “The Possibility of Characterizing the Severity of Fires by a Single Parameter,” *Fire Mater.*, vol. 4, no. 2, pp. 71–76, 1980.

[73] T. Z. Harmathy, “Fire Resistance versus Flame Spread Resistance,” *Fire Technol.*, vol. 12, no. 4, pp. 290–302, Nov. 1976.

[74] T. Z. Harmathy, “Performance of Building Elements in Spreading Fires,” *Fire Saf. J.*, vol. 1, no. 2, pp. 119–132, Sep. 1977.

[75] T. Z. Harmathy, “Designers Option: Fire Resistance or Ventilation,” in *6th CIB Congress - The Impact of Research on The Built Environment*, 1974, no. 436, pp. 277–282.

[76] T. Z. Harmathy, “Flame Deflectors - Building Research Note no. 96,” Otawa, 1974.

[77] T. Z. Harmathy, “Overview of Impact of Energy Conservation on Fire Safety,” *Fire Technol.*, vol. 19, no. 1, pp. 31–56, Feb. 1983.

[78] T. Z. Harmathy, “Extensible Flame Deflector,” *US Pat. 4,635,729*, no. 10, p. 4635729, 1987.

[79] T. Z. Harmathy, “The Role of Thermal Feedback in Compartment Fires,” *Fire Technol.*, vol. 11, no. 1, pp. 48–54, 1975.

[80] P. H. Thomas, “Old and New Looks at Compartment Fires,” *Fire Technol.*, no. 1, pp. 42–47, 1975.

[81] M. Law, “Fire Resistance Requirements of Buildings - A New Approach - Paper No. 2 of Symposium No. 5,” *Symp. held Fire Res. Stn.*, p. 1971, 1971.

[82] E. E. Smith and T. Z. Harmathy, *Design of Buildings for Fire Safety, ASTM Special Technical Publication (STP) 685 - A symposium sponsored by ASTM Committee E05*, no. June. Boston, Massachusetts: ASTM Committee E05, 1978, p. 1978.

[83] J. Kenneth Richardson, “SFPE Engineering Standard on Calculating Fire Exposures to Structures,” 2011.

[84] A. Buchanan, “The Challenges of Predicting Structural Performance in Fires,” *Fire Saf. Sci.*, vol. 9, pp. 79–90, 2008.

[85] J. Franssen, “Structures in Fire: yesterday, today and tomorrow,” *Fire Saf. Sci.*, vol. 8, no. December 2004, pp. 21–35, 2005.

[86] M. Law, “A basis fo r the design of fire Pr otecti on of building structures,” no. February, pp. 25–33, 1983.

[87] T. T. Lie, *Structural Fire Protection*. New York: ASCE (American Society of Civil Engineers), 1992, pp. 137–158.

[88] A. H. Buchanan, *Fire Engineering Design Guide: Report of a Study Group of the New Zealand Structural Engineering Society and the New Zealand National Fire Protection Association*, 1994th ed. 1994.

[89] "Eurocode 1 : Actions on structures — General Actions — Part 1-2: General Actions – Actions on Structures Exposed to Fire," *Communities*, vol. EN 1991–1-, no. CEN Brussels.

[90] DiNenno et al., *SFPE Handbook of Fire Protection Engineers*, 3rd Ed. Quincy, Massachusetts: (NFPA), National Fire Protection Association, 2009.

[91] M. J. Peatross and C. G. Beyler, "Ventilation Effects on Compartment Fire Characterization," in *Fifth International Symposium Fire Safty Science*, 1997, p. 1997.

[92] R. M. N. Kumar and S. K. Sharma, "Compartment Fires: CALTREE and Cross Ventilation - CST 06-04-12," 2006.

[93] H. R. Baum, "Simulating Fire Effects on Complex Building Structures," *Fire Saf. Sci.*, vol. 8, pp. 3–18, 2005.

[94] K. B. McGrattan, "Fire Modeling: Where are we? Where are we going?," … , *Int. Assoc. Fire Saf. …*, vol. 8, pp. 53–68, 2005.

[95] G. Rein, X. Zhang, P. Williams, B. Hume, A. Heise, A. Jowsey, B. Lane, and J. L. Torero, "Multi-Storey Fire Analysis for High-Rise Buildings," in *11th Interflam Conference*, no. September.

[96] A. Jowsey, S. Welch, and J. L. Torero, "Heat and Mass Transfer for Modeling of Structures in Fire," in *Transport Phenomena in Fire*, WIT Press., B. Sunden and M. Faghri, Eds. UK, 2008.

[97] A. H. Majdalani and J. L. Torero, "Compartment Fire Analysis for Modern Infrastructure," in *Congresso Ibero-Latino-Americano em Seguranca Contra Incendios*, 2011.

[98] X. C. Zhou and J. P. Gore, "Experimental Estimation of Thermal Expansion and Vorticity Distribution in a Buoyant Diffusion Flame," *Symposium (International) on Combustion*, vol. 27. pp. 2767–2773, 1998.

[99] F. M. White, *Fluid Mechanics*, 7th Ed. 2011.

[100] B. Karlsson and J. G. Quintiere, *Enclosure Fire Dynamics*, 1st Ed. Boca Raton: CRC Press, 2000.

[101] T. Z. Harmathy, “Ventilation of Fully-Developed Compartment Fires,” *Combust. Flame*, vol. 37, no. 1, pp. 25–39, 1980.

[102] G. M. E. Cooke, “Tests to Determine the Behaviour of Fully Developed Natural Fires,” Watford.

[103] G. M. E. Cooke, “The Severity of Fire in a Large Compartment with Restricted Ventilation,” in *Fire Safety on Ships (IMAS 94)*, 1994, no. May.

[104] B. R. Kirby, D. E. Wainman, and T. L. Tomlinson, “Natural Fires in Large Scale Compartments,” Rotherham, 1994.

[105] B. R. Kirby, D. E. Wainman, and T. L. Tomlinson, “Natural Fires in Large Scale Compartments,” *Int. J. Eng. Performance-Based Fire Codes*, vol. 1, no. 2, pp. 43–58, 1999.

[106] G. et al. Rein, *The Dalmarnock Fire Tests: Experiments and Modelling*. Edinburgh, 2007, p. 211.

[107] J. Stern-Gottfried, G. Rein, L. A. Bisby, and J. L. Torero, “Experimental Review of the Homogeneous Temperature Assumption in Post-flashover Compartment Fires,” *Fire Saf. J.*, vol. 45, pp. 249–261, 2010.

[108] G. C. Clifton, “Fire Models for Large Fire cells - HERA Report R4-83,” Manukau City, New Zealand, 1996.

[109] G. W. Shorter and J. H. McGuire, “St. Lawrence Burns Summary Report,” Otawa, 1959.

[110] J. Gales, “Travelling Fires and the St. Lawrence Burns Project,” *Fire Technol.*, Nov. 2013.

[111] J. Stern-Gottfried and G. Rein, “Travelling Fires for Structural Design -Part II: Design Methodology,” *Fire Safety Journal*, vol. 54. pp. 96–112, 2012.

[112] C. Huggett, “Estimation of Rate of Heat Release by Means of Oxygen Consumption Measurements,” *Fire Mater.*, vol. 4, pp. 61–65, 1980.

[113] A. J. M. Heselden, “Supplementary Reports of Work for the CIB International Co-operative Research Programme on Fully-Developed Fires - FRN No. 923 (Appendix),” Borehamwood, 1972.

[114] J. L. Torero, A. H. Majdalani, C. Abecassis-Empis, and A. Cowlard, “Revisiting the Compartment Fire,” in *IAFSS 11th International Symposium on Fire Safety Science*, 2014.

[115] “BS 9999:2008 - BSI British Standards - Code of practice for fire safety in the design, management and use of buildings,” 2008.

[116] A. S. Usmani, J. M. Rotter, S. Lamont, A. M. Sanad, and M. Gillie, “Fundamental Principles of Structural Behaviour Under Thermal Effects,” *Fire Saf. J.*, vol. 36, pp. 721–744, 2001.

[117] F. P. Incropera, D. P. DeWitt, T. L. Bergman, and A. S. Lavine, *Fundamentals of Heat and Mass Transfer*, vol. 6th. John Wiley & Sons, 2007, p. 997.

[118] S. R. Turns, *An Introduction to Combustion - Concepts and Applications*, 2nd Ed. Mc Graw Hill, 2000.

[119] J. M. Kay and R. M. Nedderman, *An Introduction to Fluid Mechanics and Heat Transfer*, 3rd Ed., vol. 55, no. 9. Cambridge: University Press, 1974.

[120] T. Lennon and D. Moore, “The Natural Fire Safety Concept—Full-Scale Tests at Cardington,” *Fire Saf. J.*, vol. 38, no. 7, pp. 623–643, Nov. 2003.

[121] S. Welch, A. Jowsey, S. Deeny, R. Morgan, and J. L. Torero, “BRE Large Compartment Fire Tests —Characterising Post-Flashover Fires for Model Validation,” *Fire Saf. J.*, vol. 42, no. 8, pp. 548–567, Nov. 2007.

[122] B. J. McCaffrey and G. Heskestad, “A Robust Bidirectional Low-Velocity Probe for Flanle and Fire Application,” *Combust. Flame*, vol. 26, no. 1, pp. 125–127, 1976.

[123] R. G. Rehm and H. R. Baum, “The Equations of Motion for Thermally Driven, Buoyant Flows,” *Res. NBS*, p. 11, 1978.

[124] A. Amundarain, “Assessment of the Thermal Efficiency, Structure and Fire Resistance of Lightweight Building Systems for Optimised Design,” The University of Edinburgh, 2007.

[125] J. G. Qunitiere and P. S. Veloo, “Convective Heat Transfer in Compartment Fires,” in *MCS 7*, 2011.

[126] C. T. Kidd, “Thin-Skin Technique Heat-Transfer Measurement Errors Due to Heat Conduction into Thermocouple Wires,” *ISA Trans.*, vol. 24, no. 2, 1985.